PhD Thesis

Development of a Novel Toner for Electrophotography based Additive Manufacturing Process

By : Soumya Banerjee

Student ID : P02287244

LIST OF ABBREVIATIONS

AM	Additive manufacturing
RP	Rapid prototyping
RM	Rapid Manufacturing
SLA	Stereolithography
SGC	Solid Ground Curing
LOM	Laminated Object Manufacturing
SLS	Selective Laser Sintering
SLP	Selective Laser Printing
IR	Infrared
COV	Coefficient of Variation
ERP	Electrophotography based Rapid Prototyping
FCA	Flow Control Agent
CCA	Charge Control Agent
RAM	Radiation Absorbing Material
HSS	High Speed Sintering
OPC	Organic Photo Conductor
CAD	Charged Area Development
DAD	Discharged Area Development
VOC	Volatile Organic Compound
SSSP	Single Station Single Pass
MSSP	Multiple Station Single Pass

Acknowledgements

First of all I would like to thank my supervisor Professor David Wimpenny for his active support , advice and guidance to complete this project in time.

A big thank also to all my coworkers in the university including Dennis Waldron, Paul Dean and Keith Harrop for their active support and assistance.

I would like to express my gratitude to my family members, parents and wife for their active support and encouragement to complete this project.

LIST OF FIGURES

List of Tables:

ABSTRACT

This thesis is intended to conduct feasibility study of producing 3D objects by printing thermoplastic elastomer using electrophotography technique and thereafter sintering the whole layer using infrared light source instead of incrementally "rastering" the slice using a laser for example. The term Selective Laser printing (SLP) has been coined by the author for this new process.

Research has been conducted in the field of electrophotography linked to Additive Manufacturing (AM) for almost 20 years. Electrophotography has been utilised successfully, albeit indirectly to generate a mask in several commercial AM techniques, including the Solid Ground Curing and SpeedPart processes, for example. However, the use of laser printing for the direct deposition of build or support material has yet to be exploited commercially. Unfortunately, the standard toners for laser printing are based on very brittle polymers which precludes their use for the manufacture of 3D objects. Moreover, there are some significant hardware challenges which must be overcome to enable effective deposition of multiple layers. In this thesis potential solutions to these hardware "problems" are presented and the basic feasibility of the SLP process based on a simple tackyfication approach for final transfer of toner is clearly demonstrated. The research on hardware development was conducted by the author in parallel with the toner materials and process development which forms the basis of this PhD study.

The aim of this project is to investigate and develop a new experimental toner based on an engineering polymer suitable for the manufacture of functional parts by the SLP process. Initial scoping trials were conducted using HDPE experimental toner. Later Somos 201 – a thermoplastic Elastomer was selected instead of HDPE due to its more favourable electrical characteristics. One of the major challenges faced in this work was to generate powder of the appropriate particle size. It proved extremely difficult to efficiently grind tough polymer powder to form particles below 20μm. To overcome this problem smaller particles of Somos 201 were separated from larger particles using a laboratory classifier. These particles were then surface coated with fumed silica to provide a better flow to enable printing. Having established a method for the generation of an experimental toner based on Somos 201 which can be laser printed the key question addressed in this thesis is if this material can be fused to form functional parts. In particular the influence of the silica coating on the mechanical properties has been studied.

Trials were undertaken using IR radiant heaters to thermally fuse layers of toner to form tensile test samples. Experimental toner with a range of particle sizes and level of silica coating was exposed to different intensities and duration of IR radiation and the mechanical properties of the samples were then measured.

Although it was found that mechanical strength of uncoated samples was comparable with laser sintered samples (SLS), the addition of silica has an adverse affect on the mechanical properties of the samples (tensile modulus, UTS and elongation to failure). In addition, the particle size of the toner was clearly shown to affect the properties of the samples. Finer particle size (around 17µm) toner was found to give significantly higher mechanical strength compared to larger particle sizes such as 30µm. To understand the role of silica in the fusing process further trials using a convection oven were used to sinter toner samples coated with increasing levels of silica. The results of these trials clearly indicate that silica acts as interparticle barrier rather than adversely affecting the infrared absorption of the powder.

This thesis represents a significant step forward in the development of the SLP process. It provides a clear route for the production of experimental toner using engineering thermoplastics for the production of functional parts using both monocomponent and dual component print engines. Moreover, the work undertaken provides a crucial insight into the influence of toner parameters on the mechanical properties of parts produced by the SLP process.

1.0 Chapter 1 - Introduction

Standard laser printers work on the principle of electrophotography, where fine polymeric toner powder is picked up and precisely deposited on a substrate, usually paper, using electrostatic forces. Laser printing offers several key advantages for layer manufacturing applications; it can process dry powders at high speed, offers excellent resolution and it is capable of forming functionally graded structures through the deposition of several materials simultaneously. Once the toner has been deposited it is fused to form a solid layer, typically by contact with heated rollers or via infrared radiant heating. Laser printing is, in principle, highly adaptable to a range of toner materials based on thermoplastics, cermics and metallic powders. The potential application of laser printing in layer manufacturing has been recognized by several researchers (Bynum.K.D 1992, Grenada 2001, Kumar 2000, 2003 ,2004, Cormier 2002 and Banerjee 2006,2007).

Unfortunately, although Electrophotography has been utilised successfully, albeit indirectly to generate a mask in several commercial AM techniques, including the Solid Ground Curing and SpeedPart processes, the use of laser printing for the direct deposition of build or support material has yet to be exploited commercially.

At least two fully functional toners are required to enable complex 3D objects with overhanging features to be formed ; a tough toner for the build material and the other a support material which can be easily removed from the finished object. Standard commercial toners for laser printing are based on very brittle polymers and this precludes their use for the manufacture of 3D objects.

There are two basic forms of toner; either mono-component or dual component. Mono-component toner is very popular for desktop applications whereas dual component toner is more common for industrial printers. Dual component toner is generally comprised of magnetic carrier particles (30 to 300 μm) and fine toner particles (5 to 15 μm). Dual component systems have an advantage that the carrier particles “do most of the work” in terms of electrostatic transfer and this makes them more flexible in terms of toner formulation. In addition dual component printers is capable of offering much higher printing speeds, increased layer thickness and better resolution than mono-component machines. In this PhD study toners for both monocomponent and dual component print engines have been investigated.

Previous research groups have generally focused on addressing the challenges related to depositing multiple layers of material through development of innovative hardware solutions. In particular the final transfer of the polymeric toner using electrostatic forces presents a problem as successive layers of toner are deposited to increase the Z height of the object, the field strength which forces the transfer

of the toner reduces. This leads to very poor printing efficiency after just 1-2mm of material has been deposited. Despite the significant body of research undertaken this problem remains unresolved. In this thesis potential solutions to these hardware "problems" are presented and the basic feasibility of the SLP process based on a simple tackyfication approach for final transfer of toner is clearly demonstrated. The research on hardware development was conducted by the author in parallel with the toner materials and process development which forms the basis of this PhD study.

1.1 Aims & Objectives of the work

The aim of this research project is to investigate the development of a toner based on an engineering polymer for the manufacture of functional parts by the SLP process.

To achieve the overall aim three main elements must be addressed within the experimental programme;

1. Develop manufacture route for experimental toners based on a range of engineering polymers.
2. To investigate the suitability of the experimental toners (produced in Trial 1) in the laser printing process.
3. To evaluate the mechanical properties of parts formed using the experimental toner.

This project represents a significant step towards the development of a commercial RM based on electrophotography by providing a clear route through to the manufacture of toners suitable for functional polymeric parts.

In terms of novelty there are several unique elements to this project;

- Development of a suitable dual component toner for the SLP process based on Somos201 (PBT based material – see appendix for details).
- Development of a flexible manufacturing route for tough toners.
- Investigation of the properties of dual components toners developed for the SLP process.

1.2 Experimental approach

Initial scoping trials were conducted using a range of thermoplastic polymers (PE, Nylon) These materials were selected based on their mechanical properties in order to generate toners which are suitable for the manufacture of functional 3D objects.

In the scoping trials the following stages were undertaken;

- A mechanical milling method for the production of fine thermoplastic toners was investigated.

- To provide the appropriate properties trials were conducted to establish if it possible to apply surface coatings of FCA/CCA directly to the surface of polymer particles (rather than integrate CCA inside the toner particle as with conventional toner production).

Based on the results of the scoping trials a tough rubber like thermoplastic materials Somos 201 was selected for the subsequent main trials due to its charge characteristics and mechanical properties. In the main trials the following steps were undertaken;

- Detailed particle size analysis was performed on this selected material including; particle characterisation by sieving and laser diffraction method. A range of mechanical milling techniques were assessed to reduce the particle size of the off-the-shelf Somos 201. Classification methods were used to remove the oversized and undersized particles to leave material which is suitable for laser printing.
- Charge to diameter (q/d) trials were undertaken to assess the polarity/tribocharging characteristics on the uncoated Somos 201 powder. To provide the appropriate flow control properties surface coating trials were performed with an industry standard FCA. Further Q/D tests were performed on the coated Somos201 powder to ensure that the application of the FCA has not adversely affected its polarity/tribocharging characteristics.
- Printing trials were then conducted using both mono-component (HP LaserJet4) and dual component print engines.
- Trials were undertaken using IR radiant heaters to thermally fuse layers of toner to form tensile test samples. Experimental toner with a range of particle sizes and level of silica coating was exposed to different intensities and duration of IR radiation and the mechanical properties of the samples produced were then measured.

1.3 Structure of the Thesis

The thesis is comprised of 16 chapters. Following on from this introduction five chapters cover the information gathered from the literature. Chapter 6 provides an oveveiw of the trials undertaken by the author to develop the SLP process in the EU funded Custom-Fit project. The methodology, experimental work, results, discussion, conlusions, furtherwork and recommendations are presented in

Chapters 3-7. In addition to the main thesis an appendices containing the experimental data and supporting information is provided. The details of each chapter is described in the Table 1.

Chapter	Title	Description
1	Introduction	
2	Literature Survey : Rapid prototyping process	This chapter provide a background to rapid prototyping and some of the current commercial systems. This should help to provide context to the project and enable the results of the work to be compared against known commercial benchmarks.
	Electrophotography principles(Hardware)	This chapter provides the generic information of laser printer.
	Toner	This chapter provides the generic information of laser printer.
	State of art of electrophotography and Rapid prototyping	This chapter decsribes the research work in Additive Manufacturing(AM) where laser printers were used to develop to produce the engineering product/object.
	EU- Frame 6 –Custom-Fit project	Background to the research presented in the thesis in respect of Hardware development undertaken by the author within the EU funded Custom-Fit project.
3	Experimental Methodology	Focussed on aim and objective with experimntal methodology to produce tough toner for SLP process.
4	Scoping trial	To assess the processing of different thermoplastic polymers for the production of toners; this includes an assessment of grinding, surface coating and printing.
5	Main Trial I –Printing with Somos 201	Assessing the printing feasibility using Somos 201 powder.
6	IR sintering-stand-offdistance between sorce and target	To determine the appropriate distance from the source to the samples to sinter the powder samples without any hot spots from the bulbs.
	Particle size & IR sintering	To determine the ideal particle size for the toner, which balances the needs of printing and sintering.
	IR sintering –surface coated Somos 201 powder	To assess the effect of fumed silica on mechanical strength of parts produced after multiple prints for SLP process.
	Oven sintering –coated and uncoated Somos 201 powder	As heat transfer in the oven does not rely on IR radiation if the silica is found to affect the mechanical properties of sintered samples then this can only be attributed to its forming a barrier to effective sintering rather than any change in IR absorption
7	Conclusions,recommendations and future work	

Table 1 Structure of Thesis

2.0 Chapter 2: Literature Survey

Aim of the chapter is to provide a background to rapid prototyping and some of the current commercial systems. This should help to provide context to the project and enable the results of the work to be compared against known commercial benchmarks.

Rapid prototyping is commonly known as layer manufacturing and is a solid freeform fabrication process of producing 3D objects using Additive Manufacturing technology. The process involves:

1. Receiving Data from CAD model
2. Transform the data into thin virtual cross-section of each layers (slices)
3. Deposits the liquid/powder material in layers
4. Creates cross section of each layer according to the geometry of each layer as per the CAD model
5. Process is repeated until the 3D Object is completed

The materials commonly used in rapid prototyping are plastics, ceramics or metals. Historically Stereolithography was first commercially available RP machine developed by Charles Hull (Hull 1986). Stereolithography was defined as a method and apparatus for making solid objects using a vat of UV curable photopolymer resin by successively "curing /printing" thin layers of resin one on top of the other with laser/light beam. The light beam draws the object onto the surface of the liquid layer by layer, causing polymerization or crosslinking to produce solid layers.

Figure 1a) Bench-top machine developed by Hull and (b) Commercial SLA machine

Since then there are around 32 commercial processes developed but this chapter will focus on methods which employ thermal fusing of powder and electrophotography. Although in last 10 years various research groups have shown interests on infrared sintering and electrophotography, the use of electrophotography dates back to the early 1990's with the Solid Ground Curing (SGC) system, developed by Cubital, Israel and Laminated Object Manufacturing (LOM) process, developed by KIRA.

2.1 Solid Ground Curing – Cubital –Israel

Solid Ground Curing was also known as the Solider Process, developed by Cubital Inc. of Israel(see Figure 2). It was patented by Scitex Corporation- Israel. Patent was approved on 2nd October 1990 (Pomerantz ,1990).

This process also used electrophotography technique to print mask and cured the entire layer at once without any hatching /laser scanning. Although this process was developed more than 15 years ago the original machine concept is still being applied (even today) while developing new generation RP machines for various other applications. The similar masking and selective fusing ideas were adopted by Speed part, SIS processes.

Figure 2 Typical SGC machine

This SGC process was similar to stereolithography (SLA) as ultraviolet light was used selectively to harden the photosensitive polymers. But unlike SLA, the SGC process cures the entire layer at a time. The Steps of SGC process are as follows:

- First, photosensitive resin sprayed on top of the build platform.
- Then the machine develops a photomask (like a stencil) of the layer to be built. This photomask is printed on a glass plate above the build platform using an electrostatic process similar to that found in photocopiers /electrophotography (Laser printers). The mask is then exposed to ultraviolet light which then allows to pass the radiation through the transparent portions of the mask selectively to cure the shape of the current layer.

- After the layer is cured, the machine vacuums up the excess liquid resin. Wax is sprayed in its place to support the 3D model during the build.
- The top surface milled flat, and then the process repeated to build the next layer.
- When the part is complete, the parts were de-waxed by immersing it in a solvent bath. SGC machines distributed in the U.S. by Cubital America Inc. of Troy, MI.

The machine was quite big and was able produce large models. Large parts with dimensions 500 × 500 × 350 mm could be fabricated using this machine. The process was unique when it was introduced, as the build speed is independent of the number of parts being produced. However, the process was very complex (see Figure 3 below) and thus the machines suffered from very poor reliability.

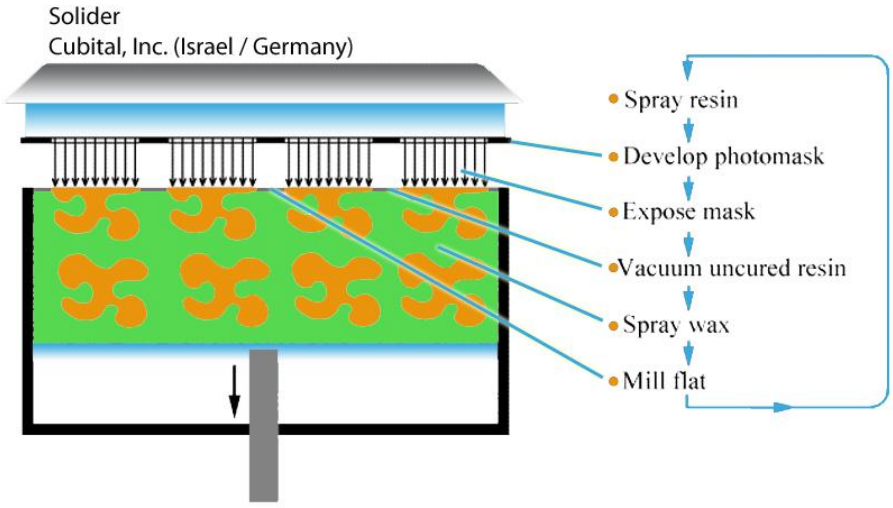

Figure 3 Schematic of SGC process (Cubital)

2.2 Laminated Object Manufacturing (LOM) /KIRA process

The original LOM process introduced in 1986 by Helisys used paper as the build material, which was unwound from a feed roll onto the stack. The first layer of paper first bonded to the previous layer using a heated roller, which melted the plastic (Polyethylene) coating on the underside of the paper. The profiles (inside and external perimeter of the slice) are then traced by laser optics system that is mounted to an X-Y stage. Material around the model is hatched to enable manual removal at the end of the build process. The method is self-supporting for overhangs and undercuts. The process produces wood like models which were very popular with traditional patternmakers but unfortunately the machines tended to be unreliable and were prone to catching fire. This basic laminating principle is also being used by several other processes, including Kira's Paper Lamination Technology (PLT)

where a rotating knife is used to cut each layer (instead of a laser) and adhesive is selectively applied using the xerographic process to bond layers. Resin powder in the form of toner is printed onto plain paper using a typical laser stream printer commonly known as Xerography process. The following five steps describe the process:

1. **Hot press:** The individual sheets of paper are used to create a block as the sheets are printed and then fed onto the table. The bonding process achieved by a hot pressing process each time a new sheet of paper is fed to the table. The temperature-controlled hot press (175°C), melts the toner (resin powder), which adheres the sheets together.

2. **Cutting the contour:** The paper is cut accurately along the contour of the sectional data, and parting lines are cut at the same time.

3. **Completed block:** Printing, hot pressing, and cutting are now complete.

4. **Removal:** Excess material is easily removed.

5. **Completion:** The complete three-dimensional form is revealed.

This KIRA process was sold exclusively in the Pacific including US and Japan but later did not, with a total of 18 systems sold as of December 1995.

Figure 4 Schematic of SGC process (Cubital)

2.3 Powder sintering using Laser

'Laser sintering' (LS) process is one of the most popular and well-established RP processes. The LS process was first developed and patented by Dr. Carl Deckard at the University of Texas at Austin under sponsorship of DARPA (Deckard 1989).This process was later commercialized by DTM Corporation which was subsequently bought out by 3D Systems. The LS process uses the heat from a CO_2 laser to sinter/ melt the powder build materials. LS can produce parts from a relatively wide range of commercially available powder materials including polymers (nylon, also glass-filled or with other fillers, and polystyrene), metals (steel, titanium, alloy mixtures, and composites) and green

(resin coated) sand (see Figure 5,6). A major benefit of the process is that the unfused powder provides support for the object being built and this also enables the full volume build chamber to be filled with components

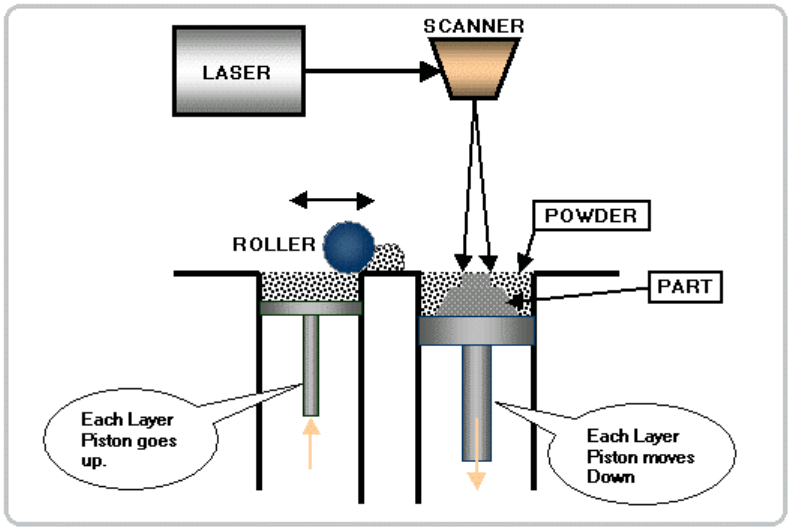

Figure 5 Schematic of typical SLS process

Figure 6 Typical SLS (Schematic) for Plastic developed by EOS

Since its inception research work to develop the LS process and the associated build materials has continued unabated. This has resulted in significant improvements in part quality, production speed as well as a widening the range of materials and end-use applications.

2.4 Infra-Red (IR) & Masking Systems

There is significant interest in improving the process speed for 'Rapid Manufacturing' (RM) process. The processing speed for laser based processes like SLA /SLS becomes slower depending on the number of parts being produced.

To overcome this problem researcher explored the feasibility of developing new technologies using alternate heating sources to fuse the polymer powder. Several processes such as 'Speed Part', 'Selective Inhibition Sintering' (SIS), 'High Speed Sintering' (HSS) use masking and IR heating as an alternative to laser sintering to produce 3D plastic object. Infrared light sources were used instead of laser to fuse the polymer powder for all these processes. The infrared light source was selected due to its high process speed and less running cost.

One of the critical factors is the distance between the infrared heat source and the powder particles. The intensity of energy decreases as the distance between infrared source and the object increases. The amount of radiation passing through a specific area is inversely proportional to the square of the distance of that area from the energy source. This 'Inverse Square Law' is described in the equation below:

$$\text{Intensity} \propto 1/d^{2}$$

where **I** is the intensity of the radiation at unit distance and **d** is the distance between source and target

Polymer & Infrared absorption: The energy associated with electromagnetic radiation in the infrared range (above the visible range in wavelength) is normally sufficient to excite vibrations of chemical bonds for polymers. A transition from a lower energy level to a higher energy level with the transfer of electromagnetic energy to the atom or molecule is called absorption. If the frequency of the radiation matches with the frequency of vibration then radiation will be absorbed which will cause a change in the amplitude of molecular vibration. The change of molecular vibration can occur either by changing atomic distance along bond axis (e.g covalent bond) called stretching or by changing the angle between the bonds known as bending.The vibrations or rotations within a molecule must cause a net change in the dipole moment (which is the product of the net partial charge difference between the two bonded atoms and the distance between them) of the molecule to absorb IR. The IR absorption involves the oscillating electric field changing the charge distribution so that a dipole is enhanced or diminished.

If a vibration is IR active then there will be a change in the sum of the (charge*distance) vectors. For a symmetric stretch of O=C=O (linear molecule) the movement of the left O is offset symmetrically by the movement of the right O so there will be no net change in the (charge * distance) vector which implies no change in the dipole moment so this is not IR active. For a non-linear molecule like HOH (shaped like a V) there is a change in the dipole moment for a symmetric stretch so the vibration is IR active.High temperature emitters are normally better in converting electrical energy to IR radiation (Carr etal., 1999). Figure 7 shows that Near Infra-Red (NIR) lamps are high temperature emitters

(Lamp temperature =2950K) whereas Medium Wave IR lamps are said to be low temperature emitters (Lamp temperature =1750K).

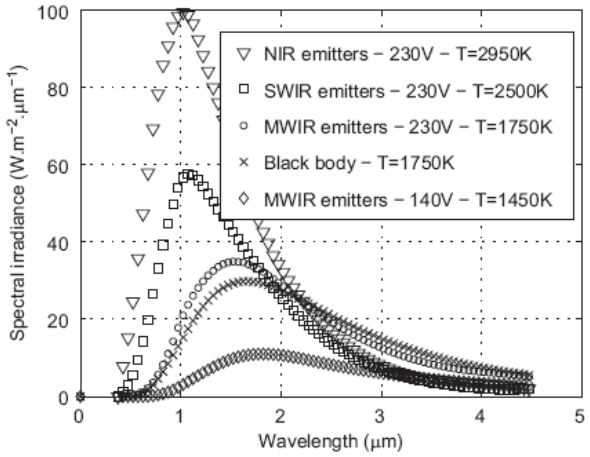

Figure 7 Emitter's spectral irradiance as a function of wavelength, emitter type and emitter bulb temperature

The infrared absorption by top surface of the polymer is a function of wavelength of emitter as well, which can be expressed as (Bombard 2009):

$$\alpha_p (T_{surf}) = [\int_0^\infty E(\lambda).\ \alpha_{\alpha p} (\lambda, T_{surf}) .\ d\lambda] / [\int_0^\infty E(\lambda)d\lambda\ ] \text{.....Eq(1)}$$

$\alpha_p (T_{surf})$ is absorption coefficient , $E(\lambda)$ is the spectral irradiance of emitters and $\alpha_{\alpha p} (\lambda, T_{surf})$ is spectral absorption coefficient at top surface as a function of wavelength of emitter lamps

The effective thermal radiation on top of the surface (target) can be expressed as:

$$\phi_{ir} (t) = FF \int_0^\infty E(\lambda)d\lambda \text{.....Eq(2)}$$

where $\phi_{ir} (t)$ is thermal radiation arriving on top surface and FF is the form factor between emitter (bulbs) and samples which is primarily the distance between them.

The infrared absorption characteristics depend on the type of material, the particle size, colour, and the surface finish. For example, a rough, black object will absorb more infrared energy than will a smooth white object which reflects more energy. Strong IR absorption bands generally occur for polar groups such as OH, Cl, and the C=O bond. Figure 8 shows the different IR absorption characteristics of polymer such as PS coated with different colour pigments (such as white, blue, transparent). Standard polymers mostly absorb infrared radiation in the region of medium wavelength, which helps to sinter the polymer powder within few seconds

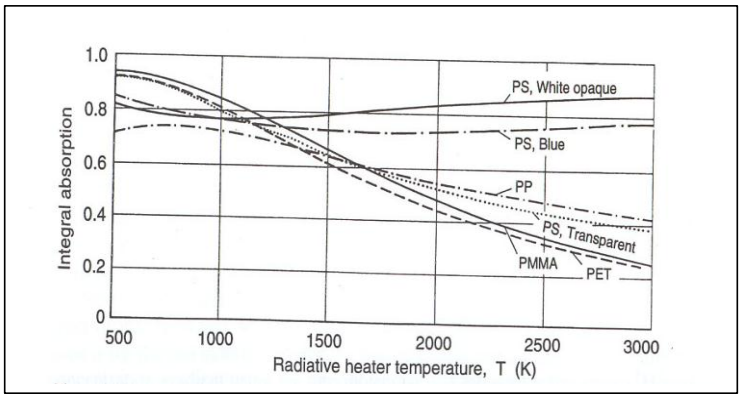

Figure 8 Infrared absorption characteristics of different polymers [Oswald,Menges1995]

The following table shows also the absorption wavelengths for various polymer groups:

Polymer group	Wavelength (µm)
O-H	2.74
N-H	3.00
C-H	3.36
C-O	9.67
C-C	11.49
C=O	5.80
C=N	5.94
C=C	6.07
C=S	6.57

Table 2 Infrared absorption characteristics of different polymers

There are various other factors including particle size, particle shape and surface roughness, which affect IR absorption of polymers. Polymer powder more readily absorb infrared in the short wavelength region if the powders are coated with sinter promoting agents/dark coloured pigments/ radiation absorbing material. Other coating agents may also inhibit absorption of IR radiation (as described in section 2.4.2).

Figure 9 shows the relationship between the IR absorption (as defined by Peak Area on the Y axis) and the particle diameter (X axis) of polystyrene powder for different IR wavelengths (1=1.14, 2=1.19 and 3=2.16µm) respectively (Ventura, Papini1999). It shows that polystyrene powder particles of more than 100 µm diameter are more IR sensitive towards shorter wavelength of IR radiation.

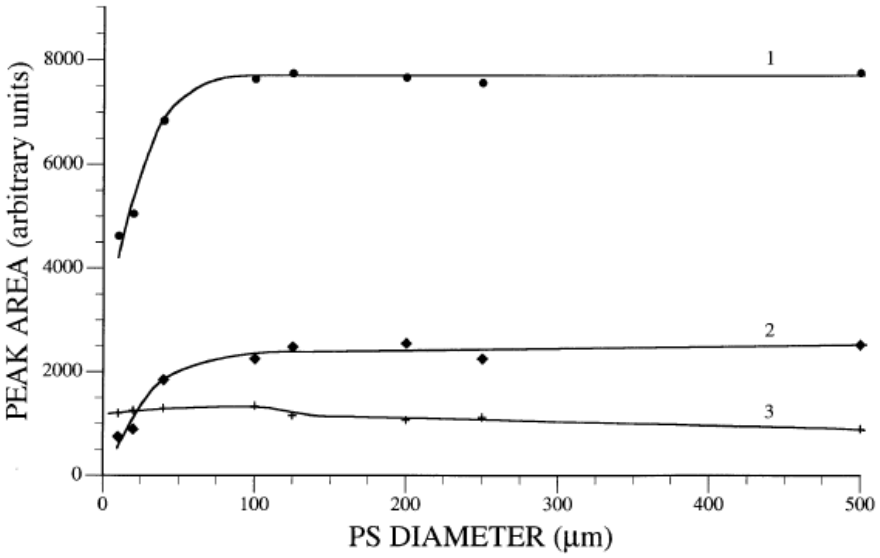

Figure 9 #1 #2 # 3 corresponds to 1.14, 1.19 and 2.16 µm IR wavelength respectively w.r.t particle size of PS powder. This represents the transition from shortwave to medium wave radiation.

2.4.1 SPEED PART –Sweden

Speed Part RP was originally a rapid prototyping company in Sweden but was taken over by German service bureau and technology provider- Sintermask FIT GmbH in 2008. The company is continuing the development of Selective Mask Sintering technology (SMS) which had been in beta test for several years.

Ralf Larson was the inventor for Speed-Part process. US Patent 6531086 for 'Speed Part' process was approved on 11th March 2003. The inventive step was to use a heat medium, such as infrared radiation to fuse the powder layer through the negative masks printed under glass plate (see Figures 10,11). A negative image of the slice of the desired object is printed using an electrophotographic process, on the underside of a quartz glass plate with an IR reflective toner to form the mask. Only the clear (unprinted) areas of the glass will allow IR radiation to reach the surface of the polymer (typically glass filled nylon) powder placed beneath the mask. This causes the powder to be selectively sintered. The powder deposition technique with a roller is very similar to conventional powder deposition process used in laser sintering machines. The printed image on the glass is then removed and replaced for each layer of the object.

Conventional toner is unsuitable to form the mask because it would adhere to the masking plate. Aluminium oxide powder, with a high melting temperature, was used as the IR reflective toner for creating the mask. According to the patent (Figure 10), the masking device (9) would be arranged to print masking pattern in accordance with the information available from the CAD- unit for each layer.

An electromagnetic radiation source (8) preferably infrared to be arranged /led over the masking device (9), whereby the particles which were not covered by the masking pattern would be exposed under infrared radiation. Therefore the exposed powder particles would be sintered due to the heat coming from the radiation. According the patent the operating window of the wavelength of infrared radiation would be selected according to the absorption sensitivity of the polymer powder so that the sintering between the adjacent particles can take place effectively.

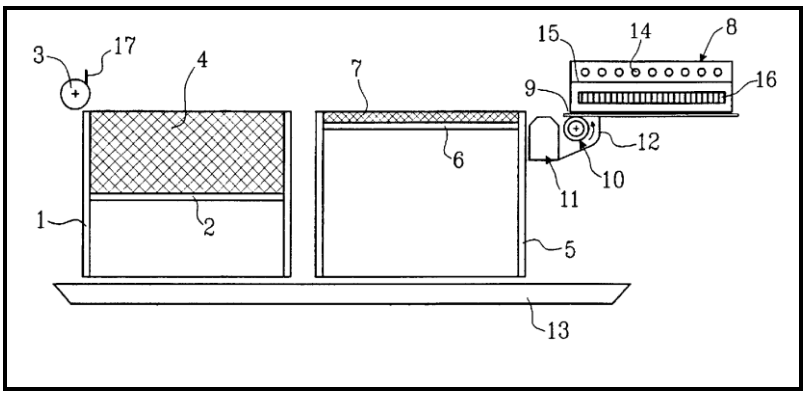

Figure 10 Typical schematic arrangement (Larson, 2003)

The sintering of each layer (0.1mm) only takes about 1-2 seconds but other aspects of the process increases the process time for each layer to around 10 seconds (20 – 35 mm/hour). This extended duration is primarily due to cleaning and cooling cycles required to complete one cycle and does not depend on the size, complexity or number of parts being produced The current, commercially available machine has a build volume of 300 x 210 x 500 mm and the claimed resolution in the range of 0.1mm.

Steps of 'Speed Part' process are schematically shown below:

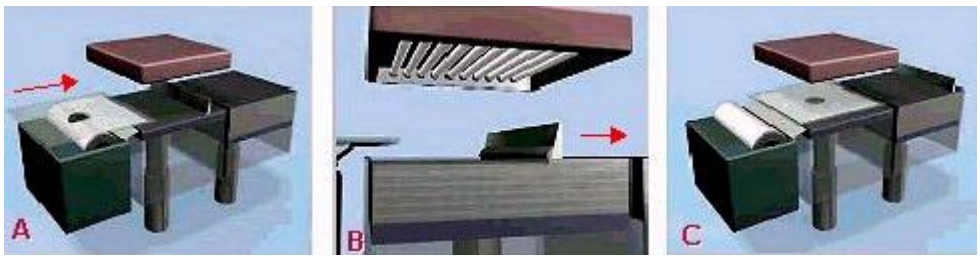

A. Laser printing of negative mask **B.** Powder deposition **C**. Moving Mask plate on top of powder bed

D. Switch on Infrared **E.** Radiation through masking plate **F.** Removal of masking powder Layer

Figure 11 Typical schematic arrangements –Speed Part Process

2.4.2 Selective Inhibition Sintering (SIS)

It is a layered fabrication process, essentially based on the inhibiting the fusing of selected areas of the powder bed. University of southern California patented this 'Selection Inhibition process' (SIS) and Professor Khosnevish was main inventor for this process (Khoshnevish 2003). The primary claim was to produce a 3-D object providing a layer of powder material and selectively depositing bonding inhibitor as per the geometry of each layer and promoting the bonding of uninhibited areas of the said layer using electromagnetic heat source (preferably infrared heat source) and repeating the process until said 3-D object is formed (see Figure 9).

As with 'Speed Part' the processing time for one layer of SIS process is fast compared to Selective Laser Sintering (SLS) process as sintering of the entire powder layer can take place at once. The SIS process is also lower to run compared to SLS as no laser running cost is involved for this process.

Although 'Speed Part' and SIS use infrared heat source and masking techniques to produce 3D objects but the approach of producing mask is different for the two processes. Speed Part prints a negative mask using dry powder underneath of a plate positioned above the powder bed where as SIS prints sintering inhibitor directly on powder particles in the form of liquid droplets.

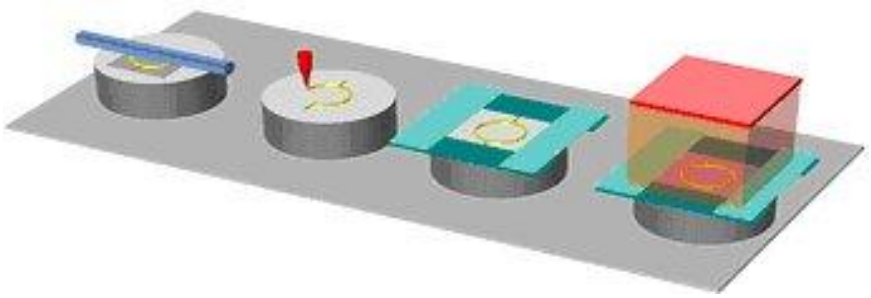

Figure 12 Schematic of SIS process

Each layer of SIS process completes in four steps as shown below;

1. **Laying thin powder layer:** This uses a similar kind of powder spreading mechanism as the LS and 3DP process. The recoating unit sweeps a horizontal surface slightly above the previous layer and brings the powder material in front while rotating in a manner so that the front surface makes an upward motion.

2. **Deposition of sintering inhibitor:** Inhibitor deposition is very critical for this process. Printing of inhibitor is carried out using raster printing using a multi nozzle inkjet printer, or vector printing with a single printing nozzle. This inhibitor liquid is deposited on selected areas according to the geometry of each layer.

3. **Minimizing radiation frame:** This step is used for powder conservation. In addition to printing inhibitor liquid, reflective plates are recommended to prevent sintering of entire layer. These plates prevent the radiation to pass through so that no sintering can take place for the unwanted areas of powder bed and selectively allows the radiation through the exposed areas only according to the geometry of CAD model for each layer. This would help to reduce the wastage of powder preventing the unwanted area of powder sintering, as unwanted powder if sintered cannot be reused.

4. **Sintering by thermal radiation:** Sintering would be carried out by bringing the heat source, preferably an electrical infrared heat source, to sinter the selected areas of the powder layer. After all layers have been sintered, the parts would be removed from powder bed.

Inhibition of sintering using different liquids including water, isopropyl alcohol, silicone, and salt water were carried out during the feasibility stage of this process. Different theories also put together by researchers regarding this inhibition process mentioned below (Khoshnevis 2003).

a) **Macroscopic mechanical inhibition:** Droplets released from the print head can have sufficient velocity to penetrate into the powder layer. Due to this impact force the powder particles at the point of impact will be displaced and adjacent powder particles can no longer stay in proximity to each other. Therefore no coalescence and inter-particular bonding will occur.

b) **Microscopic mechanical inhibition:** The explanation of inhibition could be further explained due to natural flow of inhibitor liquid across the surface as droplets would spread through the voids between powder particles. This will not disturb/displace the powder surface due to impact but will not allow any adhesion between the adjacent powder particles and droplets and therefore no sintering can occur.

c) **Thermal inhibition:** This can occur as droplets of inhibitor liquid penetrate the powder layer and coat the powder surface without disturbing or displacing the powder particles. The water

content of the inhibitor liquid coats the powder particles. No powder sintering occurs unless the water from powder surface is vapourised. Additional heat would be required to vapourise the water from the top surface of the powder particles. The water particles protect the powder from the direct heat of infrared radiation and restrained the particles from sintering.

d) **Chemical inhibition:** Another possibility is that due to chemical resistance, which might develop while powder, surfaces are coated with inhibitor liquid. This would not allow any sintering between the adjacent powder particles.

Temperature control of the entire powder bed to avoid unnecessary sintering of coated powder particles is a big challenge for this SIS process. This temperature control is important to reduce powder waste as powder particles once sintered can not be reused. Research was conducted to improve the uniformity of heating of infrared heating systems.

A feasibility study using modular and reconfigurable heaters was undertaken to improve the uniformity of temperature distribution across the powder bed for SIS process (Asiabanpour, Wasik, Cano 2005). Simulation software (AGI32) was used to study the temperature distribution on powder bed assuming heat is transferred predominantly by radiation. The effect of conduction and convention were not included into this study as their effects are very minimal for this sintering process.

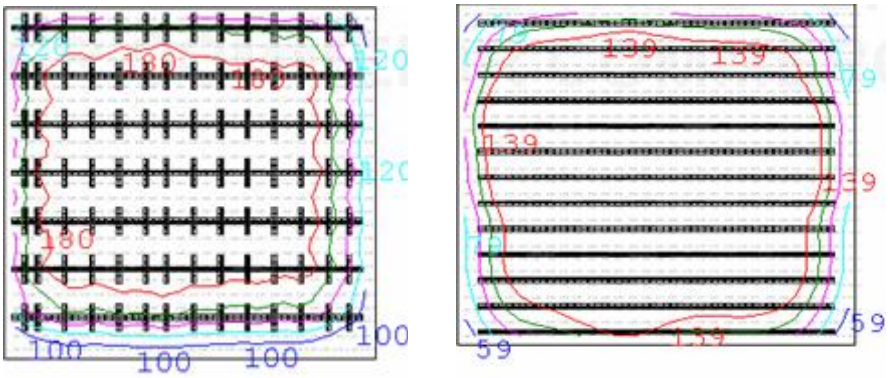

Figure 13 Pattern of heater used in simulation (Ag 312) to study thermal distribution

The preliminary patterns were determined by running the simulator programmes. The heater prototype models were then built based on the square configurations shown above (see Figure 13). The prototype of heater models consisted of two types of base material: ceramic and fibre composites. The results of heat distributions are shown below (see Figures 14,15, 16). Samples with a commercial heater show the best thermal distribution compared to other two.

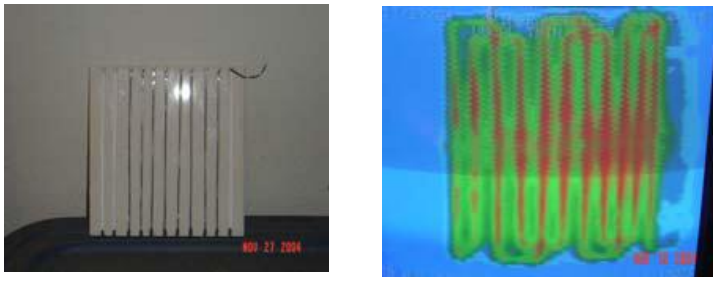

Figure 14 Nichrome with ceramic board (left) and corresponding thermal image (right)

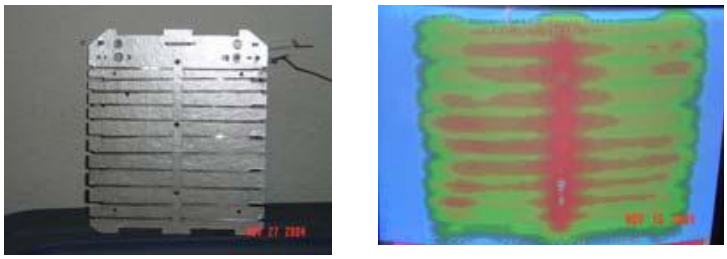

Figure 15 Nichrome with fibre composite board (left) and corresponding thermal image (right)

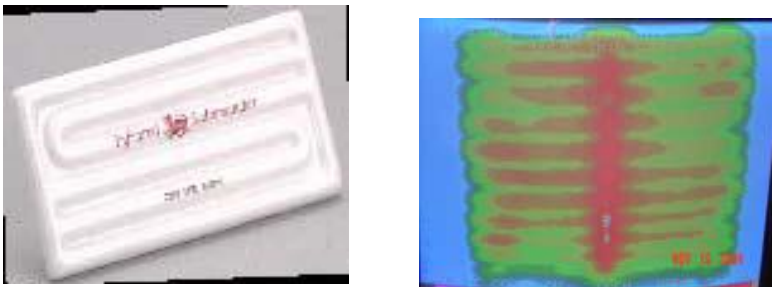

Figure 16 Commercial ceramic heater (left) and corresponding thermal images (right)

Research on several masking arrangements was conducted to save the waste of powder material. Qualities of un-sintered powder with different mask arrangements were assessed. Few masking arrangements are primarily used to selectively block the radiation so that no sintering can occur for powder particles on which inhibitors were printed (see Figure 17).

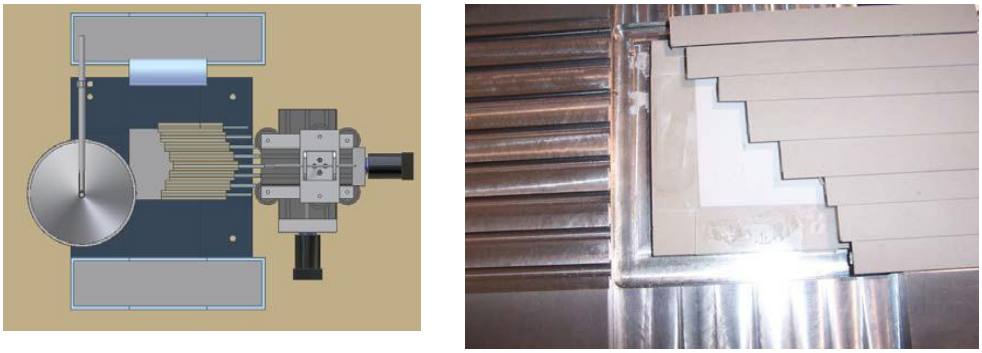

Figure 17 Finger Mask concept and prototype (Typical)

New patent was filed on 19th December 2003 by University of Southern California about selective heating systems (Khoshnevis 2007). The main objective of the patent is the use of 'Selective Heating Elements' to reduce the waste of powder material by restricting the area of the powder bed, which is exposed to the IR radiation. In this patent the infrared heating unit (342) coupled with shutter arrangements(560) is mentioned to selective fuse the powder layer (see Figure 18).

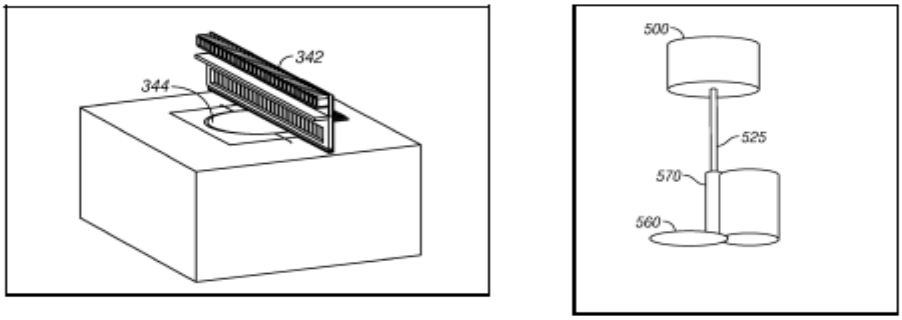

Figure 18 Schematic of typical Heating element (342) and with shutter (560)-(Khoshnevis 2007).

Although this SIS process is still under development at Southern University at California but this process is well recognised within various research groups and RP industry (Wohlers Report 2007)The test bed was also developed at university of southern California (see Figure 19).

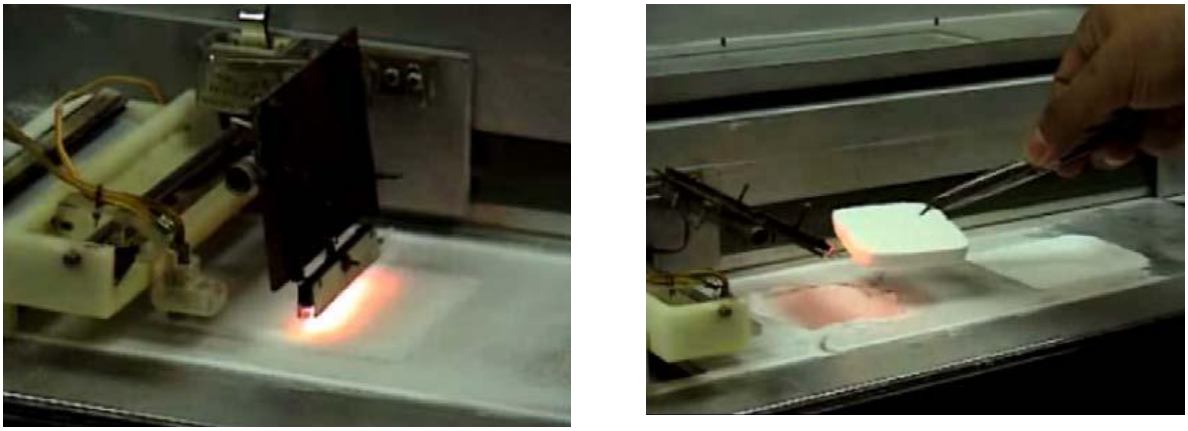

Figure 19 (a) & (b): Lab scale test rig (SIS) at University of Southern California

2.4.3 High Speed Sintering (HSS)

High Speed Sintering is another novel Rapid Manufacturing process developed to produce 3D plastic part using infrared heat source to sinter the polymer powders. This process was patented (WO 0180957) by Loughborough University on 17th August 2006 (Hopkinson 2006). Patent revealed about a process of varying the absorption properties of powder bed by printing 'Radiation Absorbing

Material'. The IR bulbs(12) are placed on top of powder bed(20 and 22) and the Radiation absorbing Material is printed using the device (30) integrated with roller (28) and controller (See Figure 20).

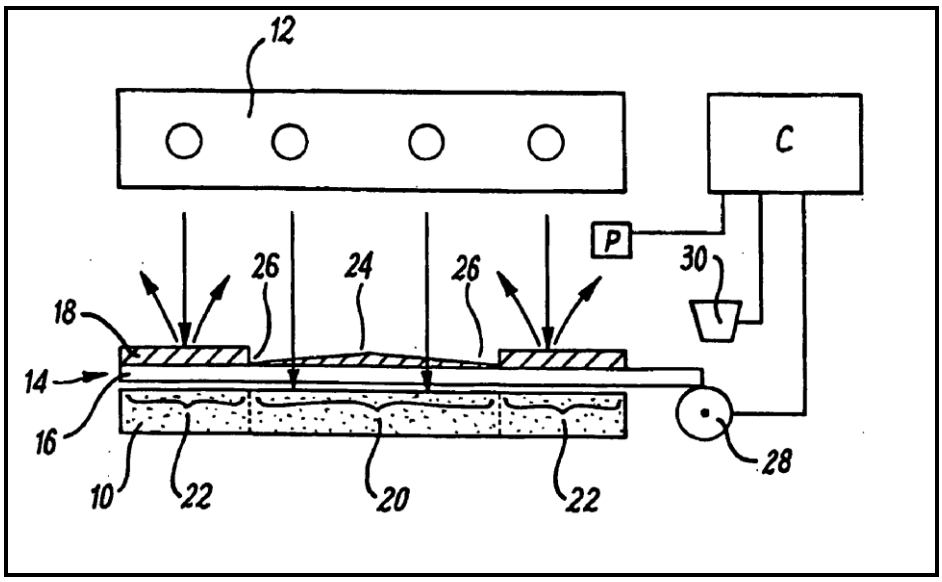

Figure 20 Schematic of Patent by Loughborough university with Infrared heat source(12)

The wavelength of infrared heat source was selected matching with the infrared absorption sensitivity of Radiation Absorption Material (RAM). The fundamental principle of this process is based on the sharp difference of absorption sensitivities, which exists between the dark (coated) object and light coloured object. This feature verified by the author using white and black colour (coated with ink) of Nylon and polyethylene powder samples as shown below (Banerjee 2006).

The test bed was made using powder deposition mechanism based on a LS machine from 3D Systems. Later it was integrated with an inkjet printing device to deposit radiation-absorbent material on powder bed (see Figure 21). Xaar UK developed the Print head for this process. Black ink is printed on to the powder according to the 2D geometry of each layer from the CAD model. An infrared bulb is then switched on. The pigments in the ink absorb more infrared energy, which would finally help to sinter the adjacent powder particles (such as nylon). The build platform then moves downwards according to the thickness of each layer and a fresh layer of powder from the powder storage bin would be deposited onto the build area. The geometry of next layer was then printed and fused thereafter-using infrared. The process would be repeated until the 3D part is finished.

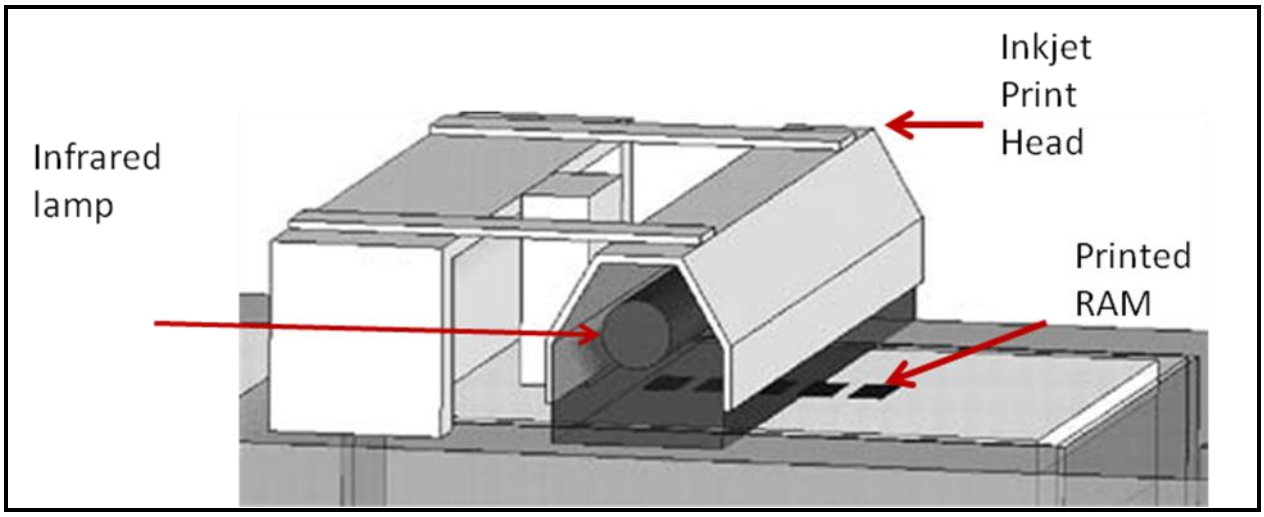

Figure 21 Typical machine concept of HSS at Loughborough University

Similar to Speed Part and SIS, this process in principle can have high process speed as sintering can take place all across the powder bed simultaneously without any laser hatching.

Although the infrared heat source was common for all 3 processes (Speed Part, SIS and HSS) mentioned above but there are subtle differences among all these 3 processes. For HSS the sintering is enhanced by printing Radiation Absorbing Material (RAM) whereas for SIS the sintering of unwanted areas are inhibited by printing the inhibitor as droplets on top of the powder bed. The challenges regarding the uniform heat distribution across the entire powder bed using infrared heat source would be similar for both SIS and HSS processes.

Research work conducted at De Montfort university revealed that short wavelength of infrared radiation would be absorbed more by black/coated powder particles compared to white/uncoated powder material (see Figure 22). So coated powder material would absorb more heat, which will effectively sinter the coated powder faster leaving the loose white powder without any inter-particle bonding. Poor edge definition across the boundaries of 3D part for HSS is another major concern. This poor edge definition was primarily due to the scattering effect of the infrared radiation (see Figure 23). The coherent nature of laser radiation would improve the temperature gradient between the sintered and unsintered powder particles across the boundaries for each layer. De Montfort University has patented this process where author as inventor explicitly mentioned about the use of laser to improve the edge definition while producing 3D parts from HSS process (Wimpenny, Banerjee 2005).

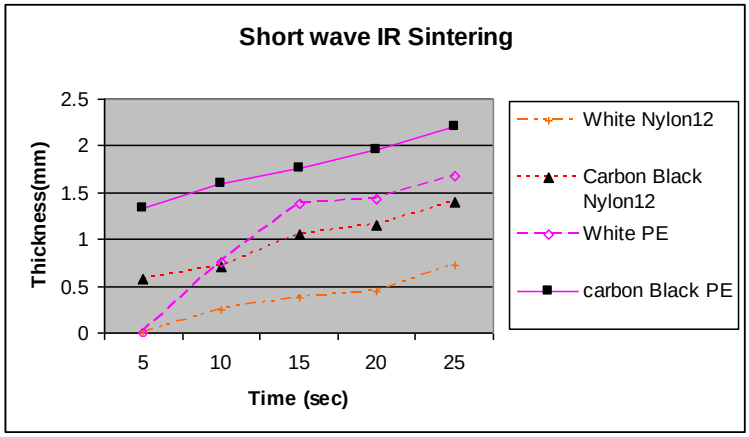

Figure 22 Increased layer thickness for black ink coated PE/ Nylon compared to white PE/Nylon for same duration of IR (Banerjee 2006)

Another concern regarding this process was the contamination of Radiation Absorbing Material (like carbon black present in ink) with the adjacent powder particles along the boundaries of printed images (see Figure 24). This happens as ink flows across the powder bed through the voids normally present in any powder layer. This is a normal for ink flow due to gravity and difficult to control. Further research on ink rheology and modelling of ink flow would be required to understand this process better.

The power / intensity of the infra-red bulb units and the maximum achievable layer thickness of single-layer parts using the HSS process was investigated by the researchers at Loughborough university (Odyue. Thomas, Hopkinson, 2008). It was earlier expected that higher layer thickness could be achieved by increasing the intensity/power level of infrared radiation. However, test results had indicated that there is a maximum layer thickness above which no further layer thickness could be increased even with the increasing the intensity of infrared radiation. On the contrary results revealed a slight decrease in the layer thickness at higher levels of IR radiation. Researchers proposed several possible explanations for this behaviour. It seems that the heat transfer was more effective in the XY plane compared to the heat transfer-taking place along Z direction. This could be achieved when the temperature powder particles would attain a certain temperature where the neck formation of adjacent powder particles would take place. One of the explanation was the reduction of inter particular gaps due to this neck formation which would further attenuate the infrared radiation to penetrate through powder bed along the Z direction. As a result more heat would be available in XY plane and this heat would finally help to achieve better heat transfer and inter particular bonding across XY plane for each layer (Odyue. Thomas, Hopkinson, 2008).

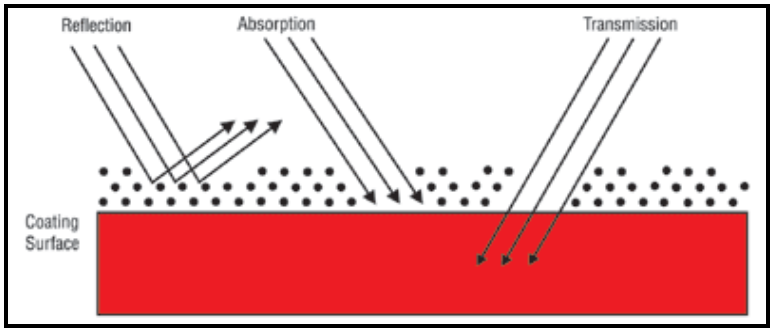

Figure 23 Interaction between IR radiation and a substrate

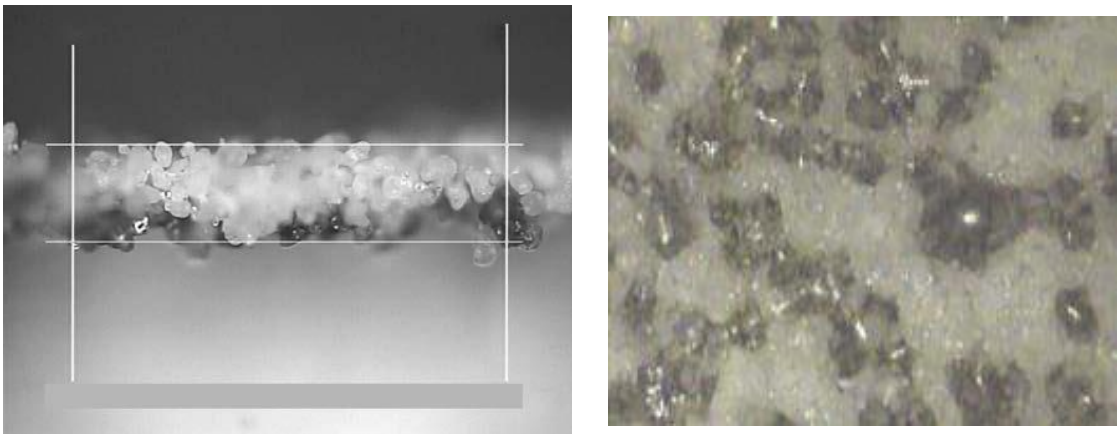

Figure 24 a) optical microscopy -sintered parts & b) Distribution of ink on powder

2.4 Selective Laser Printing (SLP)

Laser printing as a direct method of dry powder deposition has been recognised by earlier researchers because of its high printing speed (200 ppm) and resolution of printed image. Similarly, the interest of using infrared (IR) radiation as a heat source instead of laser units has increased among various research groups. This is primarily because of the capital cost and running cost of lasers is very high compared to infrared heat bulbs 'Selective Laser Printing' (SLP) is one option based on electrophotography (the fundamental principle of Laser Printing) and infrared sintering technique which forms the core of the research presented in this thesis. Laser printers and the RP processes based on electrophotography are described later of this chapter in details.

2.5 Introduction: Electrophotography principles

Electrophotography is a collective term of many processes process where an image can be reproduced using light and electricity.

2.5.1 History of Electrophotography & Laser Printing

In 1938 Chester Carlson invented electrophotography, which later became the foundation technology for laser printing and later it was patented on 6th October 1942 (Carlson,1942). Carlson found that some materials /photoconductors release their charges while exposed under light and the property of these materials could be used to form an electrostatic image to develop a copying device by developing this image with dry powder and finally it was possible to transfer the powder on a standard paper. Carlson carried out few experiments with plates of amorphous sulpher by casting molten sulpher on a base with conductive metal. Carlson then charged the plate by rubbing the plate with cloth and later plate was exposed under light and image was developed with fine powder on plate. Based on above preliminary research, Battelle Memorial Institute, Columbus, Ohio began research in 1944 with the funding received from Haloid Company (Later known as Xerox Corporation) and US Army Signal Corporation. In 1950 feasibility of the new 'Xerography' process (from the Greek term which means 'Dry printing'), was successfully demonstrated which still forms the basis for many printing and reprographic techniques.

The original laser printer called Electronic Alto Research Character Generator Scanned Laser Output Terminal (EARS) was developed at the Xerox Palo Alto Research Center in 1969 and was finally completed in November, 1971. Xerox Engineer, Gary Starkweather modified a Xerox copier by adding a laser beam to it thus giving the laser printer. The Xerox 9700 Electronic Printing System, the first xerographic laser printer product, was released in 1977. This printer was large in both size and cost.

During the early eighties, personal computers started gaining popularity in business and in the home. In the year 1984, Hewlett Packard came to market with the "LaserJet" printer (8 pages per minute) with 300 dpi. Apple Computer releases the Apple LaserWriter laser printer in 1985. In 1992, Hewlett-Packard released the popular LaserJet 4, the first 600 by 600 dpi resolution laser printer. QMS introduced the ColourScript Laser 1000 colour laser printer, costing $12,499 in 1993.

Today there is a vast array of laser printers each with a specific printing characteristic (speed, first-page-out-time, resolution, accuracy and duty cycle) targeted at particular segments of the market. The speed of most laser printers varies from 8 to 24 ppm for desktop personal laser printers costing $300-1,000. However, high production laser printers can print more than 700 ppm and the cost in excess of

$100,000. The standard resolution for most laser printers today is 600 dpi, however printers with a resolution of 2400 dpi are also available.

2.5.2 Basic principles Electrophotography /Laser Printing

Electrophotography is a powder printing technology where powder is picked up and deposited using electrostatic forces which is commonly known as Laser printing .The core component of the laser printer /LED based electrophotography is photoreceptor**,** typically a revolving drum or belt. This is made out of a **photoconductive** material which can be charged by exposure to an electrical field and then parts of the surface selectively discharged by exposure light (laser beam or LED array). In the laser printing process, an electrostatic image is produced on the photoreceptor by charging and selective discharging. The surface of the drum is then coated with a fine layer of powdered toner material, depending on the charged area, and then this latent image is transferred to the paper and fused to form the printed text/image (see Figure 21).

The laser printing process requires five stages to complete one printing cycle:

1. Charging of photoconductor drum
2. Exposure of photoconductor drum with light
3. Development of latent image on photoconductor
4. Image Transfer from photoconductor on substrate/paper
5. Fusing & fixing of toner on paper/substrate

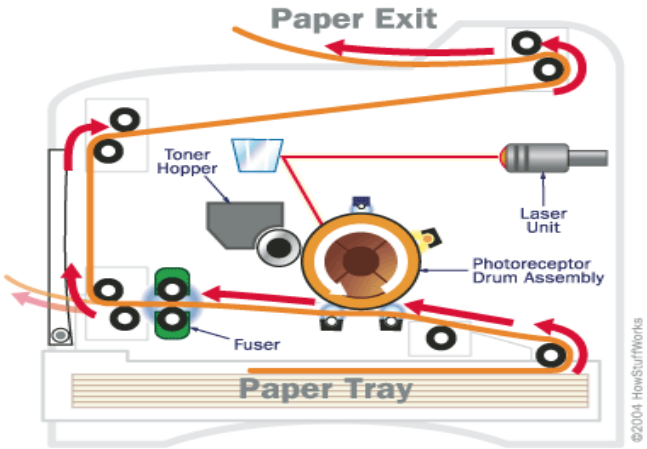

Figure 25 Schematic diagram of the laser printing process

Laser printing is governed by electrostatic force which can be expressed as;

$$F = QE$$

where F is the force on pigment particle, E is the local electrostatic field acting the particle charge Q.

By differentiating the above equation:

$$\delta F = Q\delta E + E\delta Q$$

where δE is the variation of electrostatic field and δQ is the variation in charge on the pigment particle.

The equation suggests that either charge (Q) on pigment particle is fixed and image information appears on image wise field variation (δE). Alternatively electrostatic field is fixed (E) is fixed and image appears on image wise variation of charge. However the vast majority of system operates on 'Field variation concept' (Q δE) .The relationship of exposure, photoconductor, development system, image development density can be shown with the help of 'Photo-induced Discharge Curve' (PIDC) and hence the shape of PIDC is a critical xerographic parameter (see Figure 26). The output density of the printed image depends on the geometry of the printed image. It is shown that for the same exposure, the output density of lines is much higher compared to the solid area.

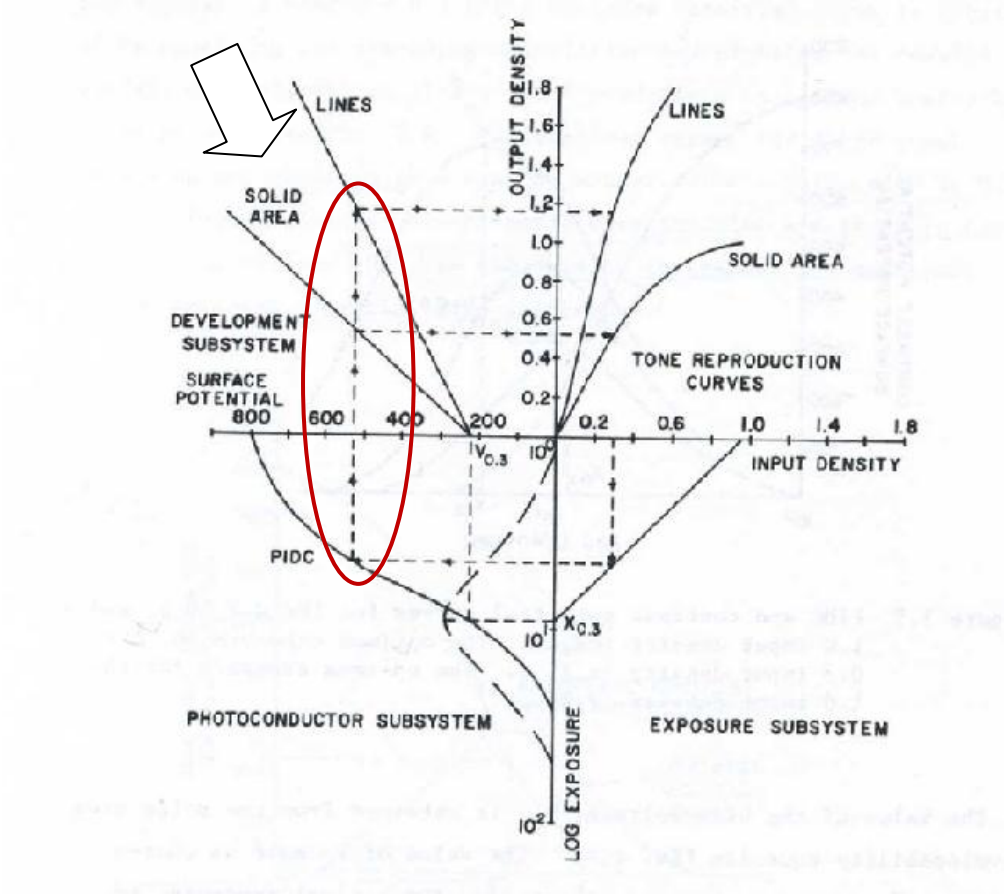

Figure 26 PIDC for Electrophotography(Scharfe-1984)

A. Charging the photoconductor: Carlson used simple friction to achieve electrostatic charge on top surface of photoconductor. In today's printer, a high voltage device (corona) which consists of a fine wire held close to photoconductor is used. When high voltage 6 Kv is applied on wire with the photoconductor base is grounded, the wire causes ionization of air and charged gaseous molecules are attracted towards photoconductor at a constant velocity due to the presence of applied field. In some cases scoritron is applied which had a grid wire between corona wire and photoconductor surface. More uniform charge distribution on photoconductor surface could be achieved by applying a small voltage is on that grid .In some cases high voltage leads to production of ozone and nitrogen oxides which might damage the photoconductor surface. These gases are undesirable due to emission of odour and adverse environmental issues. Straughan and Mayer mentioned about using conductive rubber rollers to apply uniform charge on photoconductor surface which used direct contact method with photoconductor with much lower voltages[Gregory 1996].

B. Exposure to light: The charged surface is exposed to a light source of a suitable wavelength (laser/arrays of LED) selectively discharging areas of the photoreceptor. If the geometry of photoconductor is flat and placed on a flat plate/surface, then the exposure could be done on a single flash. This feature was very common early days. In modern printers, exposure time is controlled very fast for high throughput speed using optical arrangement using either lens and/or mirrors. In some cases photoconductor is available in form of belt or and in other cases photoconductor are wrapped around top surface of a drum and the image is focused by controlling the focal distance without any damage/distortion of image using careful mechanics an optics. This type of method commonly known as indirect exposure method using either Laser/LED light source.

i) Laser beam: A laser beam and scanner assembly is used to "draw" a latent image on the photoreceptor. The laser beam is converted into scanning line of laser light by reflecting it off rotating polygon mirror. The laser light is switched on and off to form the required image (see Figure 27 below). The maximum resolution which could be achievable via laser one is 2400 dpi or more.

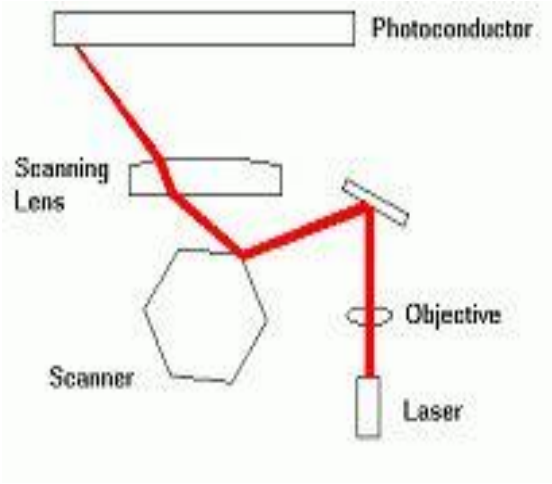

Figure 27 Laser Scanning Process

ii) LED printers:

LED printers, developed by Oki, Panasonic, Oce use an array of very small **L**ight **E**mitting **D**iodes to form the latent image. Because no laser or scanner is required LED technology offers some potential advantages over lasers based systems (cost, compactness, and simplicity). The critical issue is the integration of the 2400 diodes (A4 format with 300 dpi) into a staggered or single row, along with lens arrays for focusing the LED emission onto the photosensitive surface. The maximum resolution currently using LED arrays is 1200 dpi

C. Photoconductor and Charging Mechanism:

One of the key components in conventional electrophotography is photoconductor as it transforms the optical input image to an electrostatic latent image on the surface of photoconductor**,** hence the charging and discharging mechanism of photoconductor has an important role for this process (see Figure 28).

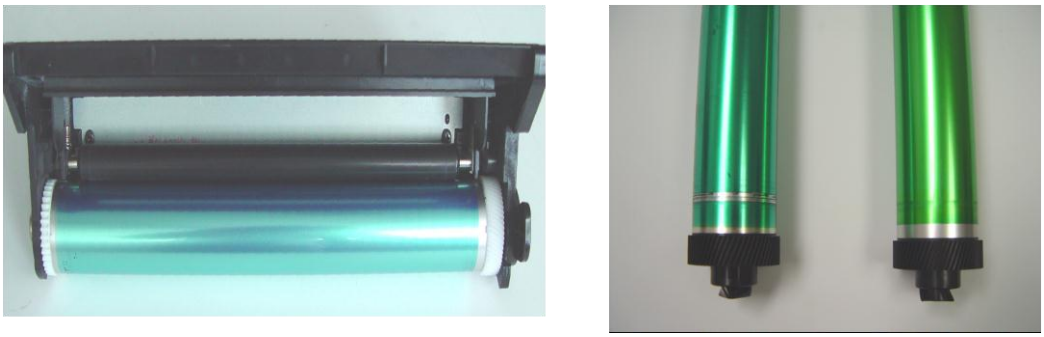

Figure 28 Photoconductor/ OPC roller

Once the charged photoconductor is exposed to light source to produce latent image,this exposure creates holes and electron pair where the holes and electrons flow through the bulk of photoconductor until they reach the correct charged surface so that they could neutralize the surface charge and form latent image. Figure 29 shows the photogenerated electrons flowing to the top surface to neutralize the positive charge and holes move through the bulk of material to the substrate to neutralize with negative charge. These processes are known as photogeneration and subsequent charge transport. The photogeneration depends on wavelength of input radiation, internal electric field of photoconductor and the temperature. The charge generation materials (CGM) selected on spectral response and are highly conjugated aromatic compound (dyes/pigments)like bis-azo pigments, Perylenes (derived from perylene 3,,9,10 tetracarboxylic acid), Squaryliums (from squaric acid and substituted anilines),Phthalocyanines etc. For charge transport materials (CTM) there are popular hole-transport materials (like triarylamines, Hydrazone etc) and for Electron transport with low molecular weight aromatic compounds which have electron withdrawing substituent like cyano groups.

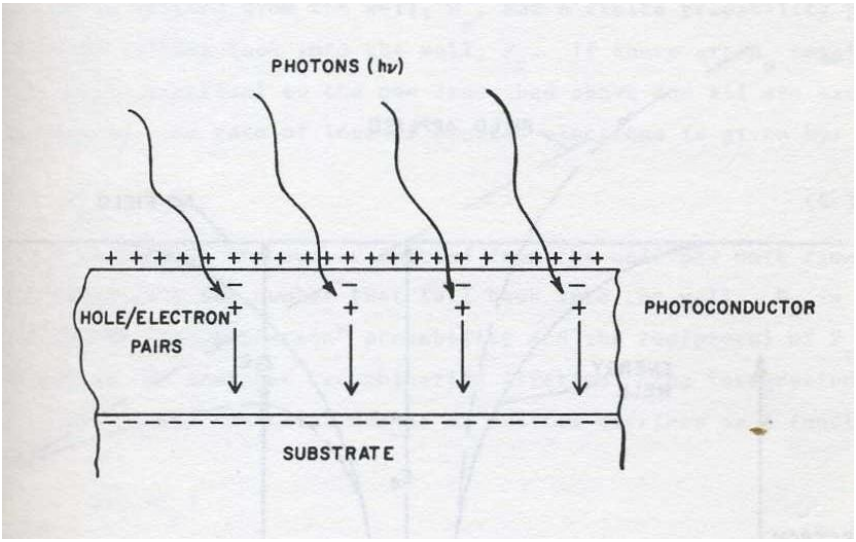

Figure 29 Photogeneration (Scharge-1984)

These processes of Photogeneration and 'Charge Transport' largely depend on following properties of photoconductor:

- ***Surface Trap Density*** helps to hold the charge (either electron or hole) so that the trapped hole or electron cannot be emitted into a band and transported through the photoconductor before the image has been developed.
- ***Effective Blocking Substrate*** does not allow a charge to be transferred from the conductive substrate to the photoconductor surface (see Graph 6) as this could neutralize the surface trapped charge on the photoconductor.

- ***Low Bulk Dark Decay*** prevents a thermally generated carrier in the bulk of the material of the photoconductor from developing. 'Bulk dark decay' produces a thermally generated carrier if the energy state of the conduction band and the forbidden energy gap in photoconductor is very close and the temperature is high enough during the process (see Figure 30).

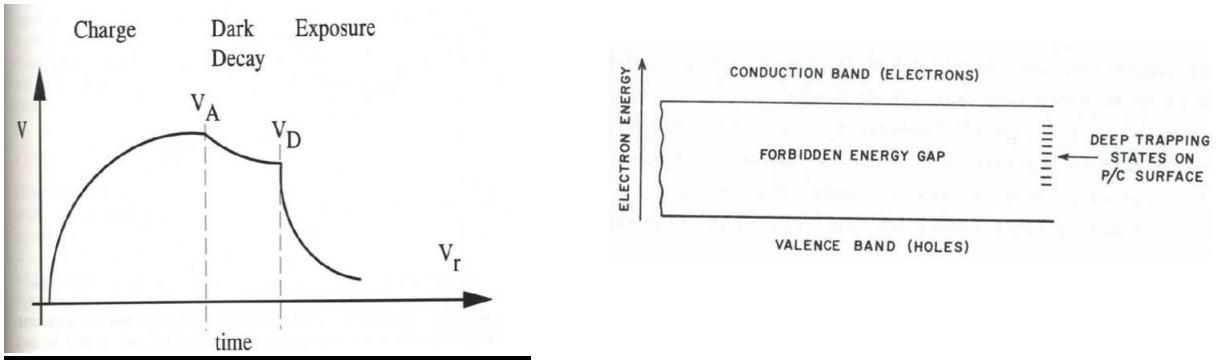

Figure 30 a) Charge, Dark decay and exposure of OPC vs time & b) Energy Gap (Scharfe 1984)

D. Development Basics : Once the electrostatic image is formed, this has to be transformed into real physical image using dry powder toner. This is achieved using electrostatic force of attraction between charged toner particle and uncharged spots on photoconductor (see Figure 31). This "image development" depends on the electrostatic field across the photoconductor, the size of toner particles, the optical density of toner particles as well as the charge on the toner particle. As toner particles are charged, the movement of toner particles is dictated by Maxwell's equations. .

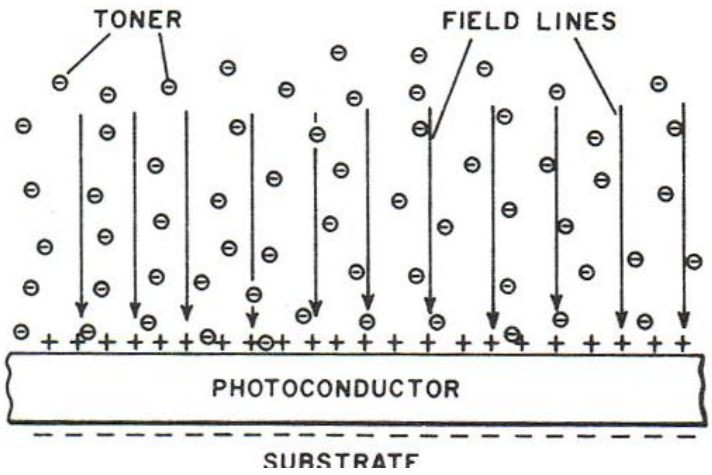

Figure 31 Schematic of Development on Photoconductor [Scharfe 1984]

Photoconductor produces electric field as a result the toner current flow is achieved which is presented as:

$(d\sigma_t / dt) = cE$ …(1) where σ_t is charge of toner and E is electrostatic field.

When toner touches the photoconductor surface the electric field is reduced and expressed by the equation as follows: $dE/ dt = - b_1 (d\sigma_t / dt)$ ….(2)where b_1 is 'Neutralisation Constant' .

As toner accumulates, the density of toner image on photoconductor increases and expressed as:

$dD/dt = b_2 (d\sigma_t / dt)$ ……(3) where D is the density of toner image on photoconductor and b_2 is a constant depends upon toner size, toner optical density.

Differentiating Equation(1) and substituting with Equation(2):

$d^2\sigma_t / dt^2 = -c\, b_1 (d\sigma_t / dt)$ …..(4)

Solving the above equation : $\sigma_t = A_0 e^{(-k_1 t)} + A_1$……..(5) where k_1, A_0 and A_1 are all constants

From Equation (5) the Equation (5a) can be derived: $(d\sigma_t / dt) = A_0 (-k_1) e^{(-k_1 t)}$ ….(5a)

From Equation (5a) the Equation (5b) can be derived : $d^2\sigma_t / dt^2 = A_0 (-k_1) (-k_1) e^{(-k_1 t)}$

$= A_0 (k_1)^2 e^{(-k_1 t)}$ ….(5b)

Putting the values calculated of Equations (5a) and (5b) in Equation (4) to give Equation (6);

$A_0 (k_1)^2 e^{(-k_1 t)} = - c\, b_1 A_0 (-k_1) e^{(-k_1 t)}$

or; $A_0 (k_1)^2 e^{(-k_1 t)} = c\, b_1 A_0 k_1 e^{(-k_1 t)}$

or; $k_1 = c\, b_1$ ……..(6)

Using the boundary condition at t=0 , $(d\sigma_t / dt) = cE_0$ ……(6) where E_0 is electric field at t=0

Putting this value into Equation(1) gives Equation(7): $(d\sigma_t / dt)$ at t=0 => cE_0……(7)

Putting this value into Equation(5a) gives Equation(8);

$cE_0 = A_0 (-k_1)$ as t=0;

and $cE_0 = A_0 (- c\, b_1)$

or $A_0 = - E_0 / b_1$……(8)

Putting the value of k_1 from Equation (6) and A_0 from Equation(8) in Equation(5) gives Equation (9):

$\sigma_t = (-E_0 / b_1) e^{(-cb_1 t)} + A_1$….(9)

As at t=0 => σ_t =0 (σ_t is the toner charge) and hence putting the value in Equation (9) to give Equation (10)

$A_1 = (E_0 / b_1)$……..(10)

Value of A_1 (from Equation10); A_0 from Equation(8) and k_1 from Equation (6) can be rewritten within Equation (5) to give Equation (11);

$\sigma_t = A_0 e^{(-k_1 t)} + A_1$

or; $\sigma_t = (- E_0 / b_1) e^{(-c b_1 t)} + (E_0 / b_1)$

or; $\boldsymbol{\sigma_t = (E_0 / b_1)(1- e^{(-c b_1 t)})}$ ……(11)

The above equation shows that surface charge ($\boldsymbol{\sigma_t}$) density grows exponentially in time and the constant factor.

$\boldsymbol{c b_1}$ which indicates that maximum amount of toner charge is limited by the initial field E_0 and neutralisation co-efficient b_1.

Density is directly proportional to toner charge σ_t and by integration Equation(3) and using Equation (11):

$D = (b_2/b_1) E_0 (1 - \boldsymbol{e^{(-c b_1 t)}})$ and this shows that Development proportional to initial development field E_0 and Development also depends on b_1 (i.e Neutralisation constant) as well as b_2 (which is a function of toner size, toner shape, toner optical density) etc.

Development system:

This could be classified as 'Discharged Area Development (DAD)' and 'Charged Area Development (CAD)'.

Discharged Area Development: In this case the charge of toner is having similar polarity with the charge developed on the top surface of photoconductor. While laser is tracing the photoconductor , traced areas is being discharged through the ground of photoconductor and toner is only being

attracted to the discharged area due to higher voltage bias and the similar charge present on photoconductor repels the toner particles . Typically the surface potential of photoreceptor has an applied potential of -1000 V and after exposing with light source (e.g Laser/LED) it then has a discharged potential of -100 V (see Figure 32). While typically a DC polarity of -800 V is applied on the development roll. This gives a development potential (bias) of + 700 V between the development roller and the photoreceptor which enables the physical image of negative polarity toner to be developed. The Non-image background will have a development potential of -200 V and thereby repel the negatively charge toner. This process is called as 'Write Black' as the laser is writing/tracing only the black printed areas of the paper.

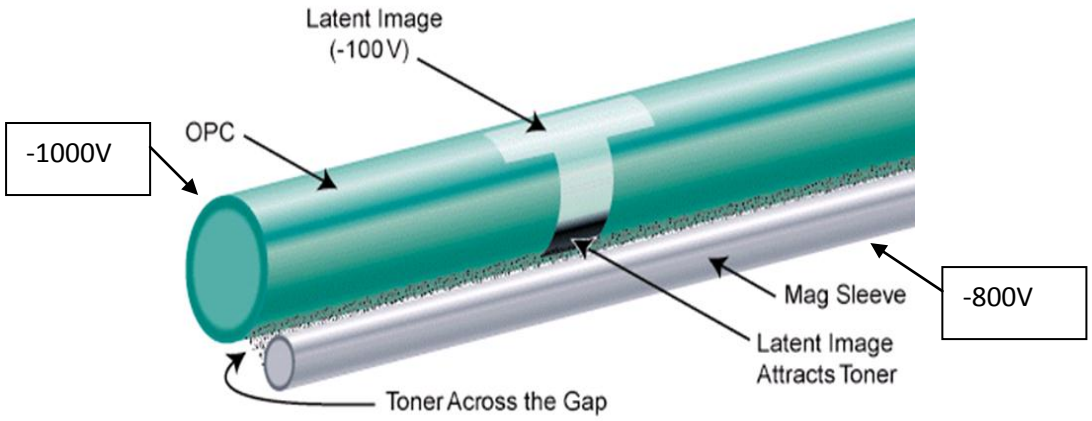

Figure 32 Schematic of voltage difference

Charged Area Development:

Toner is charged with opposite polarity with the charge of photoconductor. The Laser traces the negative image on the photoconductor and hence the charged region of the photoconductor is having higher voltage bias to attract the oppositely charged toner particles. This process is known as 'Print White' as Laser is tracing the white regions of paper.

For both the CAD /DAD systems, charged powder (toner) is brought close to the photoconductor and it adheres selectively on the discharged areas of the surface. Hence by using this process fine 'Line details' can be reproduced easily. However, for large areas, there is a possibility of a reduced field of contrast in some places and thus the attraction forces between toner particles and photoconductor would be poor not sufficiently strong enough in some places. To combat this problem separate development electrode is used connected to the earth conduct of photoconductor, positioned close to

photoconductor surface which helps to maintain uniform field contrast in large charged areas to ensure even toner distribution.

There are various types of 'Development System' available among which very well known systems are known as follows:

- Powder cloud development
- Electrophoretic development
- Dual component(Two component) magnetic brush development

Powder Cloud Development: It is a simplified system compared to other development system where aspirator creates turbulence with air to disturb settled toner and toner is uniformly deposited over the entire grid where the grid voltage is biased at some potential (see Figure 33). When toner approaches the region over the grid area the image development electrostatic force (QE) attracts the toner and finally toner are being transported towards the top surface of the photoconductor. The important criterion is to minimise the effect of turbulence on toner particles as they pass through the grid (screen with an applied potential).

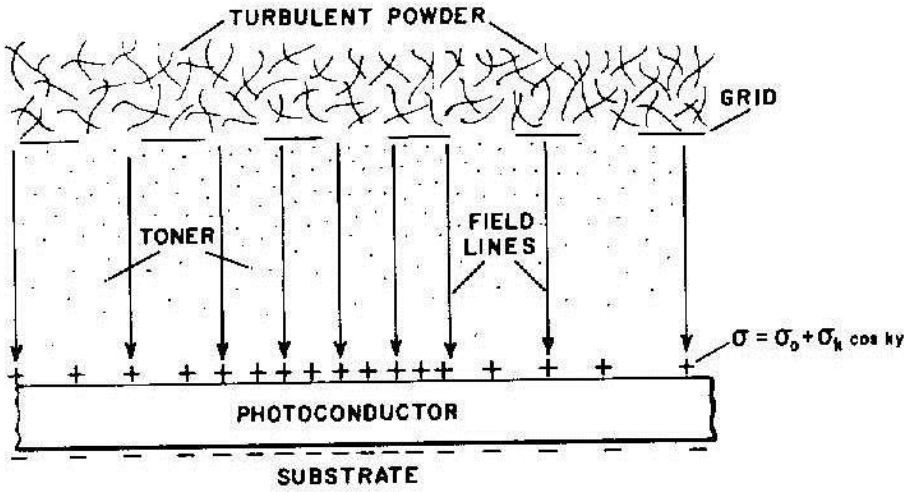

Figure 33 Schematic of Powder cloud development

Electrophoretic Development: In this case liquid developers are suspended in a liquid hydrocarbon where liquid hydrocarbons act as carrier and help to bring forward the toner particles towards the

surface of the latent image of photoconductor (see Figure 34). Toner particles are charged during dispensing process and due to electrostatic charge it is possible to maintain the dispersion. Photoconductor is immersed in the liquid and toner is attracted due to image driving electrostatic force of attraction and finally the development occurs via electrophoretic migration of the toner particles through the hydrocarbon and finally towards the electrostatic image. This type of development not very common but sometimes used for high resolution printing applications.

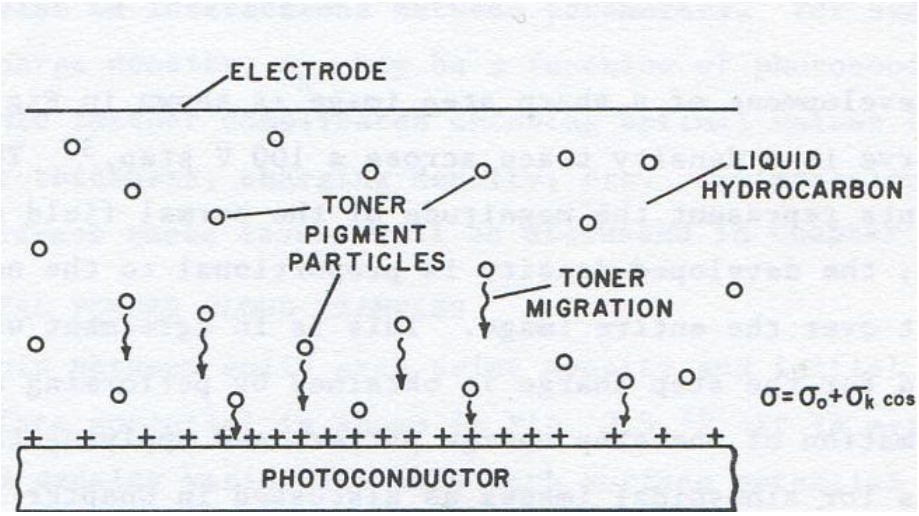

Figure 34 Electrophoretic development [Scharfe 1984]

Both the 'Powder Cloud' and 'Electrophoretic development' are having limited practical application as free powders are difficult to control and contain for 'Powder cloud system' and handling of liquid developers needs special care for the development process.

Magnetic Brush Development: Magnetic Brush Development is a very common approach. Young patented this type of development in 1957. Brush fibers are replaced with ferromagnetic particles and a similar effect is observed as to when iron particles are attracted towards a magnet. Particles align themselves in direction of magnetic field and appears as a "fibre like" magnetic brush and friction between toner and coated ferro-magnetic particles cause tribo-charging effect and helps to hold the toner with ferromagnetic particles unless the toner will transfer on photoconductor due to high electrostatic force between photoconductor and toner particles. The driving electrostatic force (QE) must be sufficient enough to break the bond between toner and carrier particles to transport the toner towards the image.

This kind of magnetic brush development could be two types:

- *Insulative Magnetic Brush Development* where individual carriers are coated with insulating layer so that carrier beads cannot make any electrical contact between adjacent particles.

- *Conductive Magnetic Brush Development* where adjacent carrier makes electrical contacts either due to no coating on the top surface of the particles or partial coating of the carrier particles. Conductive magnetic brush development was a major step forward and one of the most successful forms of two-component development. The major change is that the carrier is now composed of irregular particles that were more capable of transmitting current across the development gap. This means much more powder can be transferred (Kasper and May 1978). This lead to darker lines and text, and more regular solid area development

Dry Cascade Development : Fine dry toner powder(10 µm) are mixed with bigger carrier (50-150 µm) which is made from iron/iron oxide and sometimes surface coated with different polymer coating to have better tribocharging effect between carrier and toner. During agitation inside toner hopper the friction between toner and carrier develop electrostatic charge and the charge on the top surface of carrier is opposite with the charge on toner particle which helps to coat the carrier with even distribution of small toner particles (see Figure 35). When developer is allowed to cascade over photoconductor, the toner particles are attracted towards photoconductor where sufficient field strength existed between toner and charging state on top surface of photoconductor so that toner can be removed from the carrier bead.

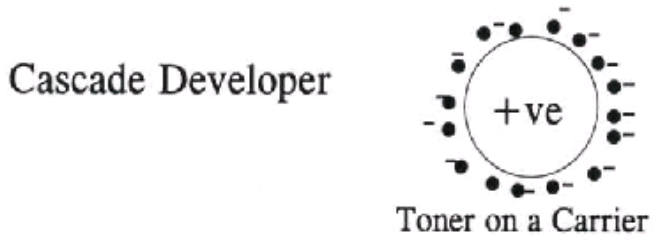

Figure 35 Schematic of Cascade develoment

Fur brush development: Bolton and Goetz described this development process (REF), where carrier is replaced with a fine fur brush and certain types of fur can produce correct polarity of charge. The fibres of the fur hold the toner particles unless the correct and sufficient field strength between toner and photoconductor causes the toner particles to release on photo conductor (see Figure 36).

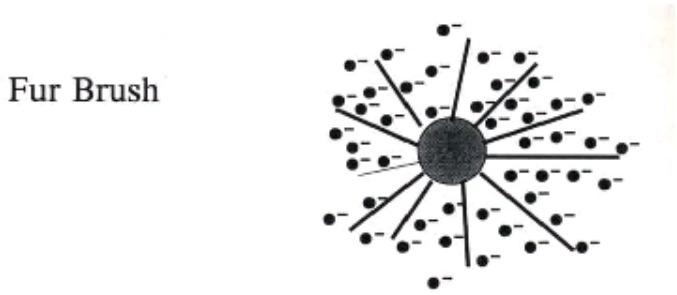

Figure 36 Schematic of fur brush development

Adhesive forces in the magnetic brush development**:**

Magentic brush development is widely used for development. The most important factor for magnetic brush development is to break the adhesive force between toner and carrier with the help of electrostatic force while development occurs. The adhesive force between toner and carrier is primarily due to short range 'Van der Waals' force and also columbic electrostatic force due to charge exchange between toner and carrier (see Figure 37). The total adhesive force can be mathematically expressed as:

$$F_a = F_v + \infty Q^2 / 4 \pi €_0 r^2$$

Where F_v short range Van der Waals force, Q is charge of toner, r is radius of toner particle, $€_0$ permittivity of free space and ∞ is constant that depends on dielectric constant of toner particle. The charge and polarity of the toner is an important factor and dictates the polarity and magnitude of charge on photoconductor so that sufficient electrostatic force is exists to overcome the adhesive force between the toner and the carrier.

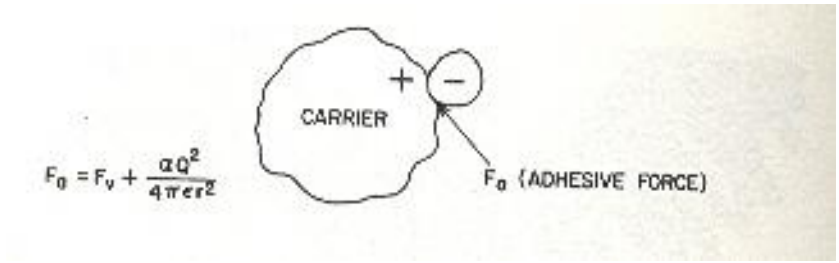

Figure 37 Force balance between toner and carrier

The development would occur for the insulative magnetic brush development when:

F (electroststic) > F (Adhesive)

$QE > F_v + (\alpha Q^2 / 4 \pi \varepsilon_0 r^2)$

For the equilibrium condition; $E = (F_v / Q) + (\alpha Q / 4 \pi \varepsilon_0 r^2)$…..(a)

Differentiating equation w.r.t Q :

$dE/dQ = - (F_v / Q^2) + (\alpha / 4 \pi \varepsilon_0 r^2)$….(b)

For optimization of the field and charge Q ; we need to put dE/dQ= 0;

or; $(F_v / Q^2) = (\alpha / 4 \pi \varepsilon_0 r^2)$

or; $Q^2 = (F_v 4 \pi \varepsilon_0 r^2) / \alpha$

or; $Q = (F_v 4 \pi \varepsilon_0 / \alpha)^{1/2} . r$…….(c)

Substituting the value of Q in equation (c) on to equation (a):

$E = [(F_v / (F_v 4 \pi \varepsilon_0 / \alpha)^{1/2})] .(1/r) + (\alpha . (F_v 4 \pi \varepsilon_0 / \alpha)^{1/2} . r) / 4 \pi \varepsilon_0 r^2)$

or; $E = (F_v \alpha)^{1/2} / (4 \pi \varepsilon_0)^{1/2} + [(F_v \alpha)^{1/2} / (4 \pi \varepsilon_0)^{1/2}] .(1/r)$

or; $E = 2. [(F_v \alpha)^{1/2} / (4 \pi \varepsilon_0)^{1/2}] .(1/r)$……(d)

From equation (d) it is observed that minimum development field varies directly with the square root of short range of Van der Waal force and inversely varies with toner particle size. Hence for the same amount of adhesive force the development field varies inversely with the toner size i.e. with less toner size the development field will increase while other parameters remain unchanged. This shows that the smaller the particle size the larger the development field (i.e. increase in bonding to the carrier particle- see Figure 38).

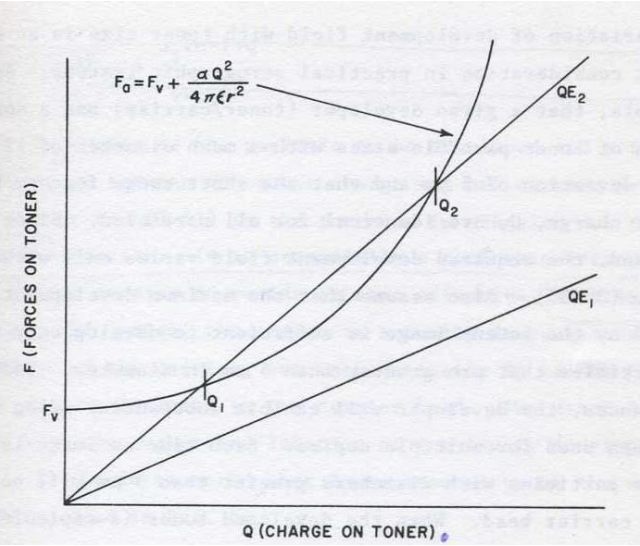

Figure 38 Force balance between Carrier and toner (Scharfe 1984)

Finally the 'Toner development' is a complex process and it largely depends on various parameters including 'Image surface potential' of photoconductor, size of toner, thickness of photoconductor, dielectric characteristics of carrier etc. This process could be mathematically expressed as:

$$D= b_2 (vr/vp)(L/2r) [(4 \pi \varepsilon R^2/ \alpha_1 Q)[(f_0+ p(z) f_k) (\Delta Vc /2)-f_0 (V_b-V bg)] +(4 \pi \varepsilon R^2/ \alpha_1 Q^2)[Fp-Fv] +[((\alpha_2 Qp^2 – \alpha Q^2)R^2)/(\alpha_1 Q^2)r^2)+1]$$

where D is the developed density , V is the image surface potential , V_b is the bias potential. γ_0 is the constant which depends on toner delivery rate , size of toner, its dielectric constant, thickness of photoconductor and developer etc. and V_{bg} is the background potential i.e magnitude of the surface potential under the exposed background area.

It shows that development is proportional to the electric field [f_0, ΔVc, p(z)]; the adhesive force between toner, carrier and photoconductor (Q, R, Fp parameters),delivery rate of carrier/toner to the image (vr/vp , L) and finally b_2 is the functional relationship between total number of developed particles and the final output image.

E. Image Transfer:

The image is either being transferred directly on to the standard paper/ substrate or in some cases it is transferred indirectly on paper (which is more common for monochrome printer) via an intermediate belt, which is more common for colour laser printers.

There are four principle methods of achieving image transfer;

1. Electrostatic corona
2. Charge roller
3. Cold pressure transfix
4. Hot pressure transfuse

Electrostatic corona & charging roller: Dielectric property of substrate (paper) is one of the important parameters for this type of toner transfer process. The paper is charged either by electrostatic corona or by direct contact with a charged roller. The toner from the drum is attracted onto the paper by the stronger electrostatic force. Some HP laser printers work with this kind of image transfer mechanism. This is a non–contact process and hence there is less probability of contamination and/or smudging of the printed image.

Cold pressure transfix/hot pressure transfuse: This method relies on the application of pressure and, in the case of hot pressing, heat to adhere the toner to the surface of the paper. Some Oce and Lexmark laser printer use this approach.

There are various types of xerographic process configurations which can be selected to produce full colour images. The four colour images can be accumulated either on the standard substrate (like paper), or on an intermediate surface or on photoreceptor. Each method has its advantages and disadvantages. Sequentially transferring the colour images on top of the paper is relatively simple but presents challenges in maintaining registration of the different colour images. Accumulating the colour images on an intermediate roll or belt before transfer to paper provides a more stable surface for registration but requires two image transfer steps which can degrade the image quality. Building the colour images on the photoreceptor before transfer to paper provides a stable substrate and only requires one transfer of the full image to paper. However, the photoreceptor needs to be sequentially recharged, exposed and developed in the presence of previously developed colour images. This presents challenges in the design of the charging and development systems.

In general image transfer is a very complicated processes where electrostatic force and different cohesive and adhesive forces between particles and substrate, the particle size, shape as well as surface roughness of substrate play in important role while the toner is being deposited on a substrate. Various mathematical models developed to explain the pheneomenon. Hays and Shefil of Xerox corporation also carried out mathematical modelling to understand this process. The electrostatic adhesion between a uniformly charged dielectric sphere and conductive substrate can be described by an electrostatic image force given by (Hays, Sheflin 2005):

$Fi = \alpha (k, f_m) * [Q^2 / (16 *\pi*\varepsilon*R^2]$

If any non-electrostatic adhesion component is present such as Van der Waals force F_{NE} then the particle adhesion would be;

$Fad = F_{NE} + \alpha (k, f_m) * [Q^2 / (16 *\pi*\varepsilon*R^2]$….1)

The applied force on charged particle would be due to external electric field E as

$Fa = \beta(k, f_m) QE - \gamma(k, f_m) \pi*\varepsilon*R^2* E^2$……2)

where $\beta(k, f_m)$ and $\gamma(k, f_m)$ are polarization correction factors

As per the two equations the particle detachment would occur when $Fa \geq Fad$

As per the model hexagonal arrays of dielectric spheres with fractional area coverage $0 \leq f_m \leq 1$(monolayer) and dielectric constant $1 \leq k \leq 6$ the coefficients are considered and the polarization correction factors would be as follows:

$\alpha (k, f_m)= 0.75+2.7 f_m+ 4.64 f_m^2 -2.47 f_m^3+ 0.22 k+0.35 f_m k-0.08 f_m^2 k +0.12 f_m^3 k+0.012 k^2+ 0.0038 f_m k^2+0.066 f_m^2 k^2 -0.057 f_m^3 k^2$……3)

and $\beta(k, f_m) = 0.85+0.15 f_m-0.11 f_m^2 +0.018 f_m^3+ 0.14 k - 0.18 f_m k +0.16 f_m^2 k -0.042 f_m^3 k+0.0099 k^2+ 0.0097 f_m k^2 -0.029 f_m^2 k^2 + 0.014 f_m^3 k^2$……4)

and $\gamma (k, f_m)= -0.056-0.19 f_{m-+} 0.48 f_m^2 -0.26 f_m^3-0.024 k +0.33 f_m k -0.55 f_m^2 k +0.26 f_m^3 k+0.066 k^2- 0.14 f_m k^{2\ +} 0.10 f_m^2 k^2 - 0.021 f_m^3 k^2$……5)

Putting $k=3$, $f_m=0$ (isolated particle) as per equation 3 ,4 and 5 the $\alpha\ \beta\ \gamma$ are equal to 1.52,1.36 and 0.47 respectively.

Similarly $k=3$ $f_m=1$(monolayer in a hexagonal array) the $\alpha\ \beta\ \gamma$ would be equal to 7.67 ,1.18 and 0.07 respectively

The adhesive force between substrate and toner found critical for toner deposition. Different substrates found significantly different physical and electrical properties which affected the quality of toner deposition on different substrates. The properties of different substrates are also an important factor for SLP process to find out the most suitable substrate considering the physical and electrochemical properties of different substrate.

Measurements of adhesion forces of toner and polymer particles to various substrate aluminium /PTFE substrates were also carried out by various researchers (Takuechi 2006) applying various types of detachment methods (like centrifugal, detachment field and microelectrode typed) . The factors which affect the adhesion force between substrate and polymer are as follows:

- The adhesion forces of toner particles depends on particle size / particle charge.

- The adhesion force of an irregularly shaped toner is larger compared to spherical toner having same particle size and same particle charge.

-The electrostatic forces found predominant for the moderately charged particles deposited on the PTFE sheet at a low relative humidity.

Similarly, the influence of electrostatic interactions and the influence of surface roughness between particles and substrates on adhesion was studied (Zohu, Gotzinger(2003). This is an important parameter to understand the toner transfer mechanism on different substrates. From theoretical modelling it was found that Van der Waals adhesion force would be significantly reduced if the surface profile is rough and the peak-to-peak between the roughness peaks is also in the right order so that density between the two adhering partners is minimised. The control of adhesion force between particle and substrate could be carried out either by electrostatic or Van der waal forces or both.

F. Fusing of Toner:

The toner is subsequently fused thermally to fix it on the paper.

Toner fusing methods include;

1. Cold pressure fusing
2. Hot roll fusing
3. Radiant fusing
4. Flash fusing
5. Vapour fusing

Cold pressure fusing does not require any thermal input. The image transferred from the drum with high pressure with the help of rollers and it is suitable for relatively soft toners.

Hot roll fusing is also a relatively simple process but slower than cold fusing. Less pressure (5 to 6 bar) is required than cold fusing but the substrate is subjected, albeit briefly, to a hot roller at 170^{o}C and the thickness of deposited toner is limited due to thermal transfer requirements. This process is

best suited to toners which melt rapidly and flow - recently low temperature fusing polyester toners has been introduced.

Radiant heating fusing typically requires halogen lamps which heat the entire substrate to melt and thermally fuse the toner.

Flash fusing employs high intensity IR lamps which provide more rapid heating of the substrate and toner. IR heating is more effective for dark (IR sensitive) toners on a white substrate.

Vapour fusing is limited to certain toner and substrate materials. It involves passing the substrate and toner through a solvent bath which chemically "melts" the toner. This system is particularly suitable for thermally and pressure sensitive substrates which cannot be processed using the alternative fusing methods.

G. Toner Transfer Mechanism and Machine architecture:

Several machine architectures can be used for producing full colour copies or prints. For Multiple Station, Single Pass (MSSP) systems, separate xerographic stations for major colours e.g cyan, magenta, yellow and black are arranged in tandem (see Figure 39).For paper in the form of sheets, a belt transports the paper to each station where the colour image is transferred with a charging device. MSSP systems have the advantage that the printing speed of monochrome and full colour images is the same. However, the multiple stations increase the size and cost of a MSSP full colour system. The challenge is to reduce the size and cost of the xerographic subsystems while maintaining high performance in image quality, speed and reliability.

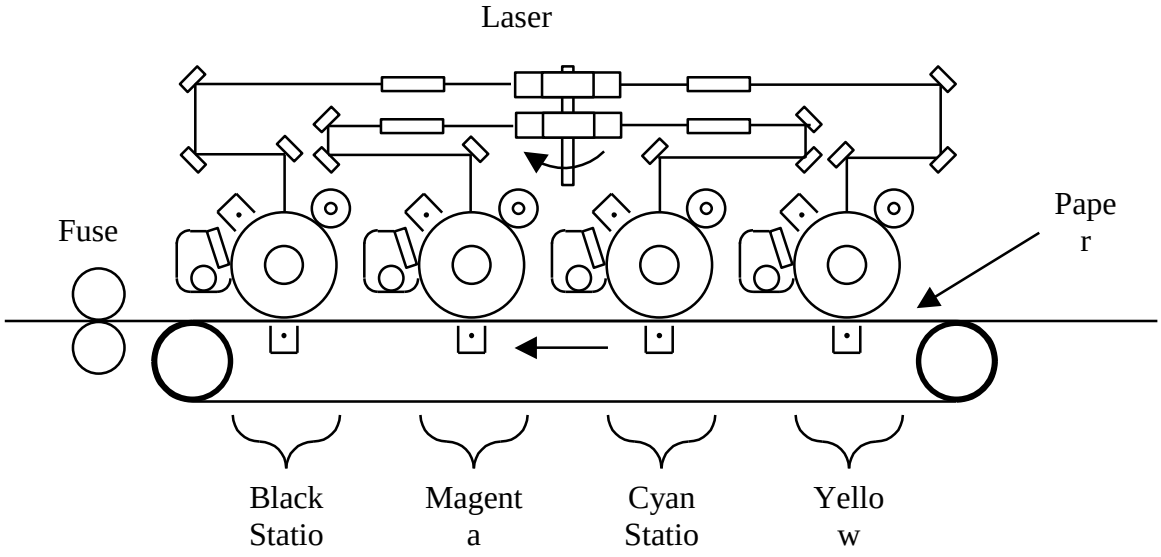

Figure 39 Multi station single pass-Type 1 (schematic)

An architecture variation of a Multiple Station, Single Pass (MSSP) system is also shown below where colour images accumulated on the photoreceptor (see Figure 40). The photoreceptor is charged, exposed and developed for each colour toner. Wavelength of the laser is selected so that the light is not strongly absorbed by the secondary colour toners previously deposited on the photoreceptor. The full image electrostatically transferred to paper and fused.

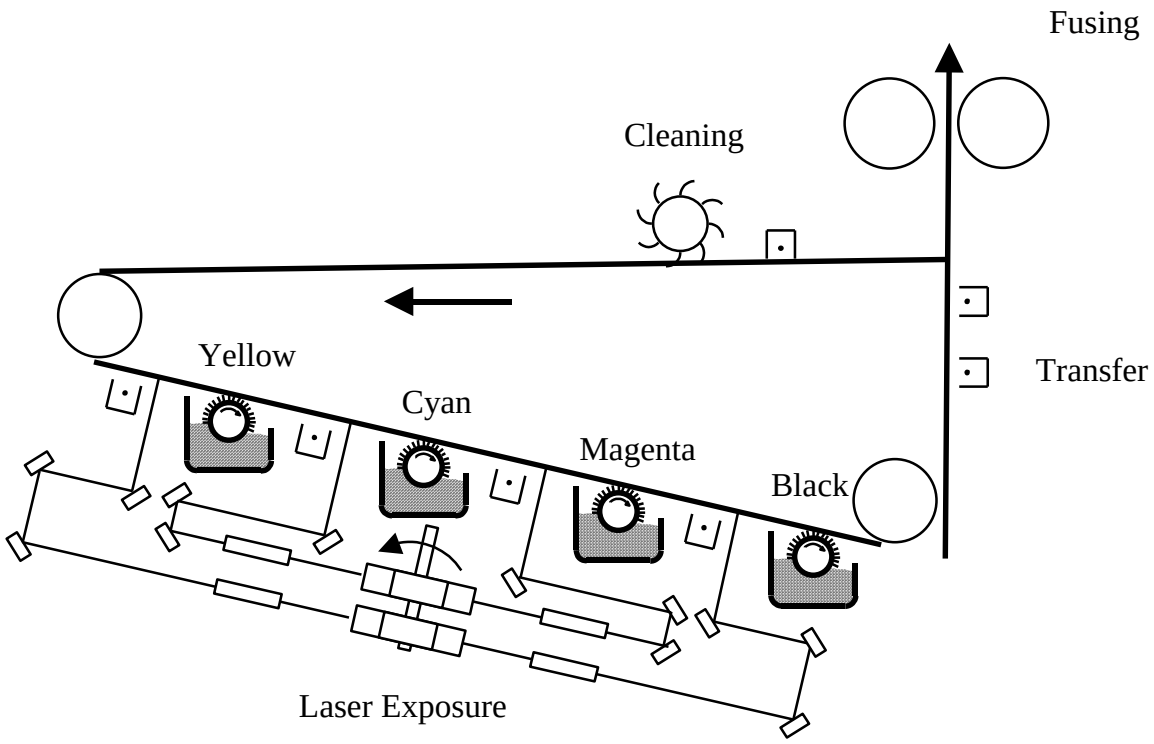

Figure 40 Multi station single pass- Type 2 (schematic)

A machine architecture, which reduces the size and cost of full colour copying and printing, uses a Single Station, Multiple Pass (SSMP) paper path. SSMP system is similar to the xerographic system shown before except four colour development systems are configured around the photoreceptor. For each colour imaging cycle, the appropriate development system is engaged to develop the electrostatic image. Each colour image can be transferred to either paper transported with a transfer drum or belt, or an intermediate transfer belt which is subsequently transferred to paper. If the colour images are

accumulated on the photoreceptor, the last three of the four development systems must be designed to not disturb or contaminate previous developed images as they are engaged for development of the appropriate image. After the full colour image is transferred to paper, the cleaning system is engaged to remove residual toner. Although the size and cost of a full colour xerographic copier and printer is reduced with the SSMP architecture, the printing speed is only 25% of the monochrome speed.

Xerographic machine can be configured also as a Single Station, Single Pass (SSSP) system if only two-colour printing (e.g black plus a highlight colour like magenta) is desired; This type of colour laser printer is similar to the xerographic system shown earlier but with several modifications. A second development system is required which has a different colour toner charged to the opposite polarity of the first system. To create two electrostatic images in a single pass, the photoreceptor is either fully discharged as in normal monochrome printing, or partially discharged to an electrostatic potential midway between unexposed and fully exposed photoreceptor potentials. This is achieved by modulating the laser beam intensity and two electrostatic images are possible having perfect registration. Each Development system would have DC voltage on the development roll which is set at the midway potential so that no development is obtained in these non-image areas. The charged area is developed with a development system which has positive charged toner on unexposed regions of the negative charged photoreceptor. In fully discharged areas, the other development system generates images on the discharged areas with a negative charged toner of a different colour. The important thing is to electrostatically transfer both polarities of toner to paper and in some cases the toner layer on the photoreceptor is corona charged to one polarity prior to the transfer zone to achieve this goal. There are wide range of choices available to select machine architecture regarding configuration (e.g in terms of exposure, type of substrate/paper, exposure, development, image registration ,accumulation, number of stations and number of passes) full colour xerographic copiers and printers. Such diversity helped to develop a larger market for colour copying and printing starting from the markets range of desktop publishing to centralized production for short run colour printing as well. Each market segment is designed to have a particular set of system requirements which guides the technology choices.

2.6 Toner for Electrophotography

Standard toner is a dry pigmented powder consisting of particles typically in the size ranges 8-12 micrometer. Bulk of the standard toner is a resin matrix (between 40 to 95%) composed of either polyester or styrene based polymers like styrene co-polymers i.e acrylates, methacrylates and butadienes including other basic components as mentioned below(see Figure 41):

- Colourant (Pigments e.g Carbon black)
- Charge Control Agent (CCA)
- Flow Control Aadditive (FCA , e.g. fumed silica)
- Wax to assist with fusing and prevent sticking to the fusing roller.

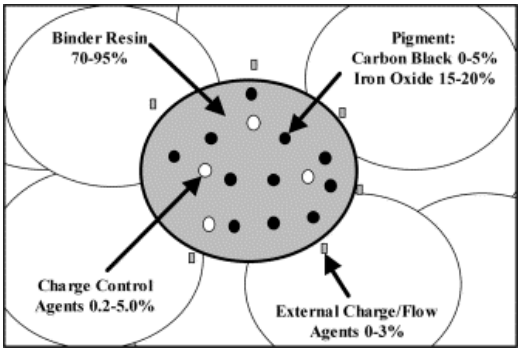

Figure 41 Typical composition of toner for 'Laser Printer'

The following parameters are important for toner development:

2.6.1 Standard toner and its properties:

A) Thermal Properties:

- Glass transition temperature- to measure the heat softening properties of toner particles
- Melt viscosity- to measure melt and flow characteristics for toner fixing on substrate/standard paper

- Thermal stability- to determine whether polymer is decomposed during fusing or processing of toner

B) Mechanical Properties:

The impact strength including adhesive and cohesive strength is a very important factor. This is very important factor particularly for mechanical processed toner where grinding of toner particles to an

acceptable particle size distribution is very critical. Additionally as the electrophotography requires numerous frictional steps, the mechanical integrity of toner is important factor.

C) Electrical Properties:

The resistivity and dielectric constants of toner are defined by resin. Triboelectric charging of the toner material is a critical parameter as this dictates the efficiency of electro-photographic printing. Triboelectric properties depend on resin type and nature of carrier as well as influenced by the polymer type, particle size, pigments and other additives. Typical surface additives are silicas, titanias, inorganic oxides; organo-metallic salts (zinc stearate etc).

Styrene & Polyester based Toners**:**

Styrene acrylics and styrene –butadienes are very common in toner industry. Polyesters are very popular in full-colour applications because they have many desirable properties including pigment dispersibility which is an important parameter to develop colour toner. Polyester based toners allow lower temperature fusing than conventional styrene based toners. This enables faster print speeds while providing excellent print quality/adhesion and shortening the printer warm-up time. Polyester toners are also proven to be more environmentally friendly as they do not contain styrene or benzene volatile-organic-compounds (VOCs). Unsaturated polyester toners have a cross linked structures and are thermosetting (once thermally fused they cannot be re-melted). Polyester based toners are relatively weak and tend to be brittle. Styrene based toners have a faster jetting rate and lower humidity sensitivity.

Surface Additives:

Particle coating is an effective method for surface modification of powder particles to improve flow-ability and dispersibility, chemical stability, electrical or thermal conductivity, and mechanical strength. Particle coating is used in various applications including pharmaceuticals , toners and the development of advanced materials .When two different kinds of materials contact each other, charges transfer through the interface [10, 11] and polarization will occur even in coated particles. Various models are still being developed to understand the effect of the polarization on the electrostatic forces between the coated particles (Matsusaka 2003).‘Charge control Agent’ and ‘Flow Control Agent’ are very common surface additives required to develop a fully functional toner applied to improve the performance of toner.

Charge Control Agent (CCA):

There are two types of additives added to basis toner particle during toner development which are known as internal additives and external additives. Internal additives are added to the material prior to compounding where as external additives are added during post processing during toner manufacturing.

Toner particles are charged either positively or negatively depending upon the characteristics of the print engine. The chemical composition of toner controls the charge produced on toner particle. Charge control agents controls the rate of charging, charge amount and polarity of charge for the toner particle.

Charge control agents (CCA) are added in 1-2 % (Typical) on the surface of each particle to keep the charge of each toner particle at a desired level. The CCA must be selected to give either negative charge toner or positive charge toner depending on printer type. The first charge control agents were designed by Japanese to create negative polarity on toner particles.

Negative charged toners are more common for desktop printing applications. CCA for negative charged toners are using a special organic metal complex made from Oxy carboxylic Acid Zn complex. There are also various types of CCA available for negative charged toners which are produced from Azo-metal complex Cr / Oxy carboxylic Acid Al complex.

CCA for positive charged toners are based on Nigrosine which is based on Azine compound. Orient chemicals is a very well known for developing CCA .For negative charged toners , Orient produces E-series /Bontron S series like E-84,E88, S34 and for positive charged toners the products are known as under N series(N-01,N-04) /P series(P51).

Flow Control Agent (FCA):

Flow control agent (FCA) is a surface additive agent which helps to prevent any blocking/coalescence of toners and improves the image quality during toner formulations. FCA is normally applied to the surface of the toner particles by mechanical mixing. FCA prevents toner particles from sticking together and adhering to the photoreceptor as they flow through the photocopying machine/laser printer. In some cases magnetic additive is blended into the toner material to control machine ‘dirt’ caused due to loose bonding between polymer and additives due to low charge on toners .The toner particle size distribution helps easy dispersion while blending toner with FCA.

The FCA is selected based on the hardware which will be finally used for printing and the characteristics of the toner material. The most common type of FCA is Fumed silica, also known as

micro silica (between 100 to 150 ηm) is a non-crystalline, fine-grain, low density and high surface area silica. Fumed silica, typically 0.5 -1.5 % (by weight), is applied by blending to improve the flow characteristics of the dry toner and minimise the electrostatic charge variation at extreme conditions. The hydrophilic nature of the fumed silica also helps to absorb water off the surface of the particles, preventing caking. This also helps to control the electrical resistivity of the toner.

Performance enhancements in terms of printing resolution and clarity have driven an increased usage of fumed silica due to greater difficulties in maintaining good flow and controlling charge for finer particle sized toner (Tadahiro, 2005).

TG -308F, TG 810 G developed by Cabot corporation are common fumed silica based FCA where TG-308F used for negative charge toners and TG-820F used for positive charge toners.TG-308F improves the transfer properties to paper by reducing the magnitude of the adhesive forces between the toners and the photoconductor during printing. Its highly hydrophobic surface helps in providing stable tribo-electric charging characteristics during toner formulation for a wide range of temperature and humidity conditions.

Big particles are sometimes produced due to agglomeration while blending toner particles with fumed silica using industrial scale mixers. This was due to heat generated during the blending process due to friction presents between blade and powder particles. Various measures are taken in toner industry to avoid any agglomeration during blending as a single large particle can completely block the aperture between developing roller and doctor blade and stops printing. Thermocouples are normally located on the industrial mixer which controls the speed and movement of the blades of mixer along the z-axis while blending. The location of the blade is controlled moving the shaft up and down to avoid any localised heating

Colourant & Wax :

Colourants also have a very important role other than the visual effect. Low molecular weight wax (like polyethylene/polypropylene based) added to toner composite to reduce the amount of toner adhesion to the heated roll during fusing. They also able to disperse into the resin during the formation of toner and must have the capacity to hold the charge either positive or negative depending upon the toners. Although organic pigments provide colour and exhibit also certain triboelectric properties depending on their chemical composition and solid state properties (see Figure 42). Normally organic pigments provide colouristic properties along with low electrostatic influence (Baur, Macholdot 1997)

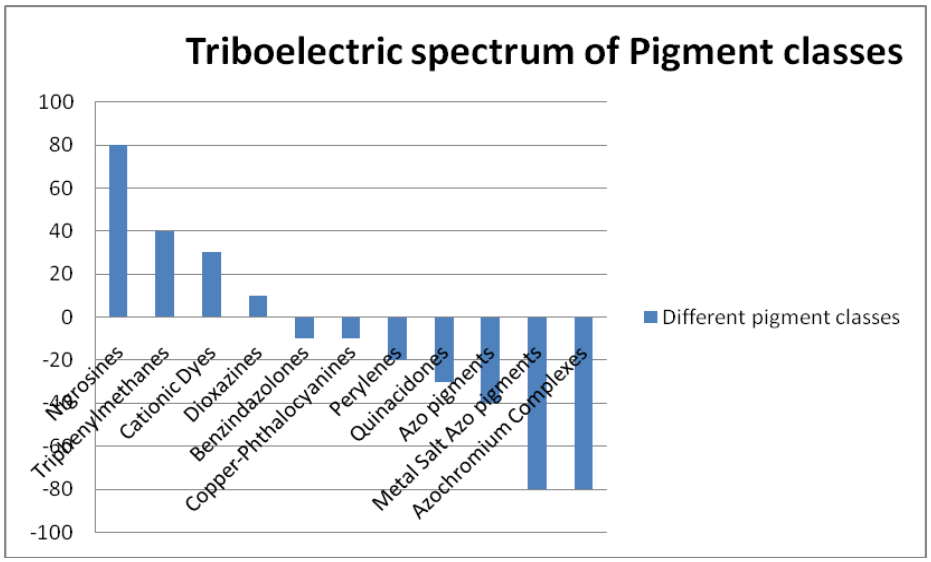

Figure 42 Triboelectric spectrum of pigments

Ingredients of a typical colour toner and their influences on tribo-electric charging and colour as shown below (Baur , Macholdot 1993, 1997,2001):

Ingredients	**Approximate Concentration (%)**	**Function**	**Triboelectric Influence**	**Colouristic Influence**
Resin	90	Polymer-matrix	+	+
Pigment	5	Colour	++	+++
CCA	2	Friction Charge	+++	+
Wax	3	Fusing	(+)	0
Flow Agents FCA(External)	0.5	Flowability	++	0

Table 3 Triboelectric spectrum of pigments/Cca/Wax/Flow Agents

- High/ Dominating Influence : +++ or ++, Certain Influence : +

Little influence: (+), No influence : 0

From the table it is evident that that friction charge of particles is controlled by CCA and FCA as well.

2.6.2 Toner Types

Development system could be of two types depending upon the toner:

- '**Mono-Component'** and
- '**Dual Component'** systems.

Mono component toners:

This can be broadly classified as:

-Resistive magnetic toner (HP/Canon type-except HP 4600) and

-Resistive non-magnetic type (for example Lexmark).

Magnetic toners have a relatively high proportion of iron-oxide additive (30-60%). The printed layer formed with magnetic toners is relatively brittle compared to pure non-magnetic toners and also magnetic toners are dark in colour thus limiting their use to black toner. Generally non-magnetic toners are transferred from drum on to the paper via direct contact method. The commercial desktop printers are mostly using mono-component toners.

Dual component toners:

This consists of fine toner particles and larger diameter carrier beads (commonly known as developer- see Figure 43). These toners are generally used in high speed (dual component) laser printers. Toner particles are fine pigment polymer powders of approximately 5-30 μm in diameter and carrier beads are usually larger magnetic particle of size 30-200 μms in diameter. The toner particles are "carried" to the photoreceptor by the larger magnetic carrier beads, which then fall away from the charged, drum and are recycled (see Figure 44). The advantage of dual component toners is that the toner is relatively simple to formulate and the carrier beads do most of the "work" while printing (in terms of charge and flow of toner particles).

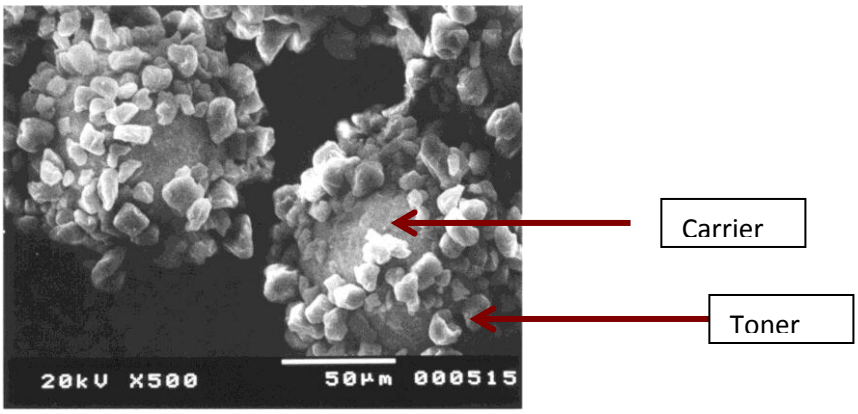

Figure 43 Typical dual component toner with carrier

Generally, toner particles of dual components toners are charged quickly due to larger contact surface between carrier and toner particles. Dual component toners are more common for high-speed industrial applications as large amount of charge is required to be distributed on each toner particles in less time. This dual component is very useful while developing the toner with high non-conductive toners like polymers as the charge on each toner particle is mostly taken care by carrier bead hence charging the non-conductive powder is not very critical. In many cases the carrier is coated with a polymer, which can deliver the correct amount of charge with same polarity on each toner particles. This tribocharging phenomenon depends on 'work function', intrinsic resistivity and dielectric constants of polymers.

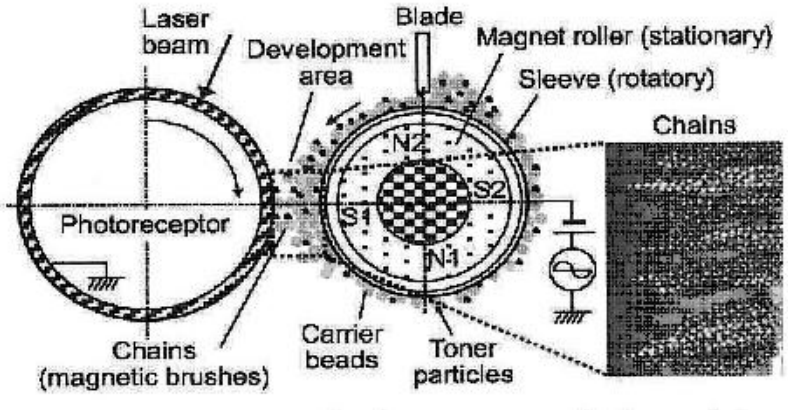

Figure 44 Printing with dual component toner

Toner charging is an important process for laser printing. Carrier particles are also coated with polymers to provide right tribocharge with right polarity required for the toner development (see Figure 45).

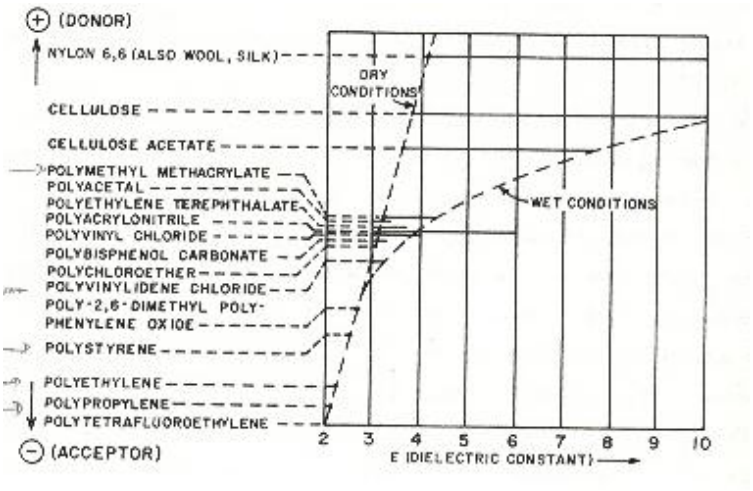

Figure 45 Tribocharging series for various polymers

Toner development of dual-component system is described by two theories known as low density and high density surface state theory respectively. Both of these theories can account for the dependence of Q/M on carrier and toner diameter and toner concentration C (the ratio of toner mass to carrier mass). But the theories are very different conceptually.

In the first theory known as low-density surface state theory, it is mentioned that the toner and carrier have surface states that exchange charge until their surface 'work functions' are equilibrated. In this theory, it is assumed that there are N t (N c) states per unit energy per unit area on the toner (carrier) and that charge is exchanged to fill the states between the carrier 'work function' (φ c) and the toner 'work function'(φ t)After equilibration, it can be shown that the inverse of the charge-to-mass ratio M/Q is given by

$$[M/Q] = RC[\rho_c]/[3\Delta\varphi_e N_c] + r[\rho_t]/[3\Delta\varphi_e N_t]$$

where R is the carrier (+toner) radius and $\Delta\varphi_e$ is the difference between carrier and toner 'work functions' and c and t are referred as carrier and toner respectively. This equation suggests that a measurement of M/Q plotted against C will be a straight line with a slope proportional to R and an intercept proportional to r.

As per second theory, the electric field theory, sometimes called the high-density surface state theory, the charge is exchanged until an electric field is created at the surface of the toner particle to offset the difference in 'work functions' at the interface $\varphi_c - \varphi_t$. Based on this model the M/Q would be represented as

$$[M/Q] = (RC[\rho_c]/[3\varepsilon_0 Ee]) + (r[\rho_t]/[3\varepsilon_0 Ee])$$

This equation also predicts the M/Q plotted against C will be a straight line with a slope proportional to R and an intercept proportional to r like earlier one (Schein 1999).

2.6.3 Toner Charging

Charging mono-component toner could be carried out as following:

- Induction/Injection charging
- Contact charging
- Corona charging

Induction Charging :

This charging method is used to charge the magnetic /non-magnetic toner by applying voltage on the top surface of developing roller. For magnetic toner, the developing roller is having a magnetic core which is surrounded with a concentric insulative sleeve .The voltage is applied outside the sleeve with a brush arrangement so during rotation of developing roller , toner particles are charged due to applied voltage.

Contact Charging :

This method is used to charge primarily insulative toner and no separate high voltage source is connected with the sleeve of the developing roller. The top surface of the developing roller could be coated with a another separate layer to assist in charging with the help of triboelectric charging while the toner particles are coming out from the aperture between doctor blade and developing roller.

Corona Charging :

The most direct system of charging corona charging. This method has striking similarity with corona charging of the photoconductor. The corona charging method has few drawbacks. One of the problems of corona charging is that corona wire may sometimes become coated with toner particles, which makes it difficult to operate.

2.6.4 Printer hardware for magnetic/non-magnetic toner

Printer hardware is also designed according to the toner type. For example the HP LaserJet4 was designed for negatively charged magnetic toners. Magnetic toner is normally used for standard HP LaserJet 4 printer. The developing roller selected for this printer was magnetic which helps to coat the magnetic toner particles on top of it while printing. The gap between the developing roller and doctor blade was slightly more compared to the normal gap found in recent cartridges. The bigger gap between developing roller and doctor blade of HP LaserJet 4 printer helps larger particles to pass through the aperture between doctor blade and developing roller while printing. The top surface of the roller is coated with toner particles due to magnetic attraction force between toner and the magnetic developer roller. This magnetic force helps to improve toner coating on developing roller by reducing any unnecessary toner leakages inside the cartridge while printing.

Toner particle size of this printer was slightly higher (15 to 20 μm) compared to the sizes of recent toner. The standard print cartridge of HPLaserJet4 Printer is integrated with toner hopper, developing roller, cleaning roller and OPC drum. The position of toner hopper inside the HP Laser Jet 4 printer was placed in an angle (not perfectly horizontal rather slightly inclined approximately at an angle of 20 degree). This inclination was to assist the toner flow towards developing roller /OPC drum due to gravity.

Printing using non-magnetic print engines is more challenging. There is no magnetic force available to hold the toner particles on developing roller for print engines using non-magnetic toners. The non-magnetic print engines require accurate control of charge and flow compared to magnetic toner print engines. The amount of gap between the developing roller and doctor blade is normally less compared to the gap for magnetic print engines (HP LaserJet4).The average particle sizes of conventional nonmagnetic toner are less compared to the particle size of standard magnetic toner.

2.6.5 Toner Performance

Toner shape/ size and tribocharge of toner are very critical for electrphotography process.

Toner shape /size and Flow Characteristics:

Toner size and shapes are key parameters for Laser printing. Average particle size of toner is between 5 to 10 µm. The size of the toner particles is extremely important to achieve the correct charge-to-mass ratio for effective laser printing. The mobility of the toner in the supply reservoir mechanism, the transferability of toner on substrate /paper, the property of peeling from the drum and the fusing characteristics are all affected by toner particle size, shape and material properties.

Advantages of smaller particle size toners:

- Less material added to substrate/ medium
- More prints could be taken from same amount of toner (in weight) compared to bigger toner particles, hence consumables cost is reduced.
- High resolution images could be developed especially for fine lines/geometries.
- As effectively less polymer is to be fused while printing, hence lower energy is required to fuse the toner
- Toner **t**ransfer efficiency from photoreceptor/intermediate carrier on substrate is higher for toners having a more spherical surface. This feature is more relevant while printing via intermediate carriers /transfer belts.

2.6.6 Toner Manufacturing Processes

Toner manufacturing processes are characterised according to their ability to produce toners with more precise shape and size distributions. Three are 'Standard Measurement Techniques' to characterise the size and shapes of toner particles. 'Circle equivalent diameter' is one of the very commonly accepted approach used in toner industry to measure the average dimension/ size of toner particles which is defined as the diameter of a circle that has the same area as the projected particle image. Various irregularly shaped particles can be evaluated on the basis of a single consistent measure using this diameter as a standard of reference. Shape is characterized using circularity – which is defined as the ratio between the perimeters of the projected particle image with the circumference of the area-equivalent circle which numerically represent the shapes of complex particle shapes (see Figure 46).

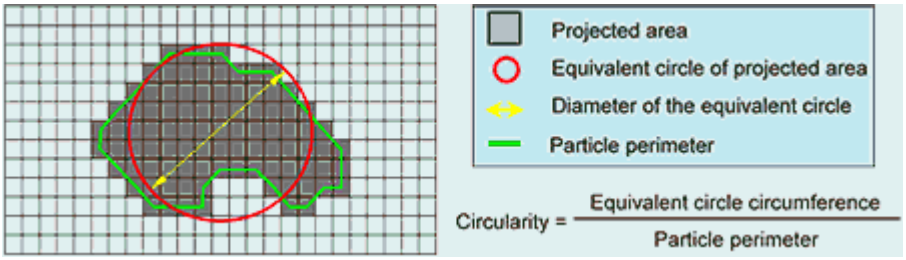

Figure 46 Circularity

Circularity of 0.95-0.96 is optimum particle size for toner. Toner particles with a lower than this value would as act as an abrasive which will eventually reduce the lifetime of printing mechanism components. Similarly toner particles with a higher than this optimum circularity (i.e. perfect spheres with a circularity of 1.00) act as a lubricant and do not transfer properly on to the substrate during printing Optimized image quality depends to a great extent upon achieving both a narrow size distribution (centered around a mean diameter of 8-10 µm) and a narrow shape distribution (centered around a mean circularity of 0.95-0.96). Toners can be produced by the conventional mechanical milling process or by the relatively new chemical polymerization process.

2.6.6.1 Pulverizing Process: Grinding

Grinding is common to many process industries and this process is well known for inorganic substances including and minerals. Grinding of organic materials including polymers/toners is found more complicated and research still being carried out to understand the grindability of different polymers including tough polymers for producing toners using conventional milling process (Tanaka 2008).The grindability of tough polymer was investigated using different milling techniques. The challenge of grinding tough material is due to material hardness, modulus of elasticity and material toughness.

Grindability is numerical indication of the capacity of a material to be ground. This could be explained mentioning rate of grinding for a particular milling process meeting a particular specification in unit time (e.g kg/hour passing through 100 meshes). The fineness to which material is ground and the toughness of the material increases the specific energy and has adverse effect on production rate.

Various attempts have been made to formulate "laws" of grinding, but they are largely empirical. These "laws" are all based on a general differential equation $dE = - C\, dX/X^{n}$ where E is the work done , X is the particle size and C and n are constants. **Kick's law** is expressed considering n=1 and the equation becomes $E = C \log (X_F / X_P)$ where X_F is the particle size and X_P is the product size and (X_F / X_P) is the size reduction ratio. This implies that a constant quantity of energy is required when

reducing the particle size in a given ratio. It has been found more applicable to coarse grinding. **Rittinger's Law** considers n>1 and the solution becomes as shown below:$E = (C/n-1)[(1/((X_P)^n - 1) - (1/ ((X_F)^n - 1)]$

Rittinger's law considers n=2 and says that the energy consumed in grinding is proportional to the amount of new surface produced. This relationship has been found to be more applicable to fine grinding. Another factor of fine grinding is to analyse the plastic deformation of finer particles. It has been found that plastic deformation increases the resistance of brittle materials. This further endorsed by Gane (1972) as plastic deformation in a magnesium oxide crystal of 0.2 to 0.4 μm particle size with average strength of the fine particles 180 kg/mm^2 found 15 times stronger than large magnesium oxide crystal This suggests more energy would be required for finer grinding and fine grinding of tough polymers would be more challenging.

The traditional mechanical milling (pulverizing) process involves blending of resin, charge control agent, wax, pigment and iron oxide. This blended material is then heated until the polymer is fully melted, extruded and when sufficiently cooled is then granulated. The basic polymer and few additives like pigments and others are mixed and extruded via special typed of twin screw extruder. The extruded product is crushed into smaller particles. Then granulated material (3-5mm diameter) is ground by air jet milling to produce fine particles which are then passed through a classifier unit which controls the size of the toner particles. Finally the particles are blended in a mixer fitted with a special kind of surface mixing blade to add the surface additives (e.g fumed silica) on the surface of each polymer particle. This process largely depends upon efficient grinding /pulverizing and hence this process is very effective while producing toners formulated with toners which are very brittle and have low molecular weight.

2.6.6.2 Chemical Process

Wet chemical toner processes, such as suspension polymerization and emulsion polymerization, are used to produce toners particles directly without any milling. This chemical process provides much better control of the size and shape of the toner particles (see Figure 47). This uniform distribution of powder size and shape helps to improve the powder flow characteristics giving better transfer efficiency from drum to the paper and improved image quality.

In any of the chemical processes, the final outcome is smaller and uniform particles. Canon uses suspension polymerization whereas Xerox/Konica uses emulsion polymerization techniques. Unfortunately, each of this process requires significant capital expenditure and is limited to only few

polymer types and thus present much higher risk while developing toners with new materials/polymers.

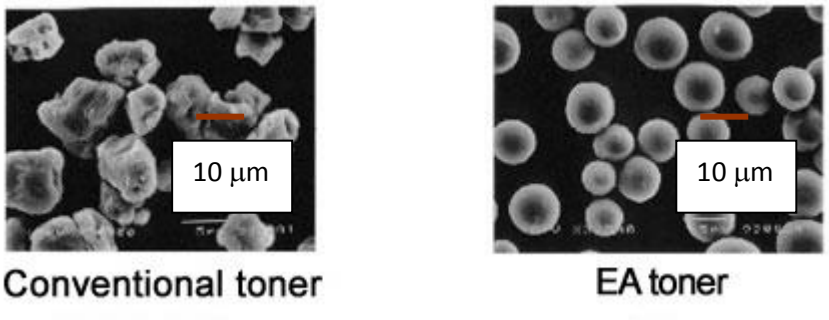

Figure 47 a) conventional and b) Chemical Toner

Description	Value
Particle size	9 ~7 micron(commercialised) ~5 micron (if required)
Polymer Tg	63 ^{o} C (usually) but variable
Triboelectric Charge	+100 ~ (-)110 µm(controllable)
Electric Resistance	10.5~12.0 log (Ω - cm)
Flowability	> 50 (Zeon's method)

Table 4 Typical properties of polymerized toner (Hasegawa, Yanegida 1999)

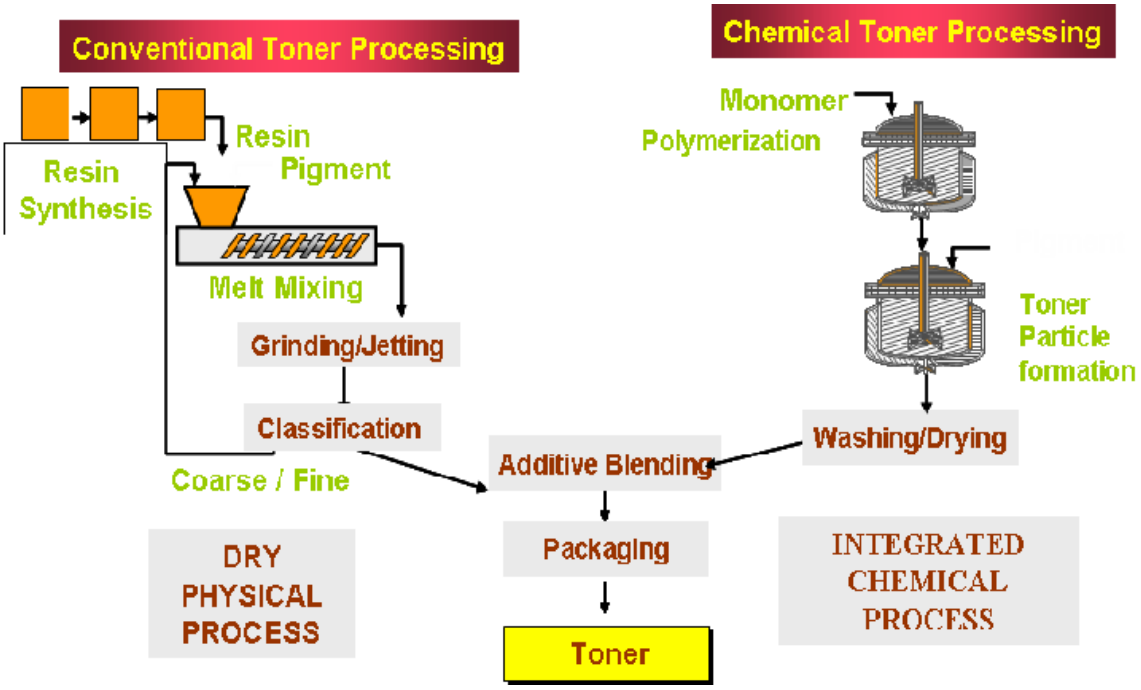

Figure 48 Schematic of both the conventional and chemical toner manufacturing process

Chemical toners and its advantages: Chemical processes generates finer toner sized particles (particle size of 5 µm or less) with narrow particle size distribution.

- Chemical processes toners are eco-friendly compared to conventional toner particle as it produces less waste with fewer fines than conventional toners of same mean particle size.
- The surface geometry of chemical toners are having almost spherical or spherical shape without any flat "fractured".
- The release agents like wax for fuser release could be readily incorporated into formulation in chemical toner.
- Toner developed/ deposited on photoreceptor/substrate shows better definition of the latent image with rounded chemical toner (Hopper,2004)- see Figure 49.

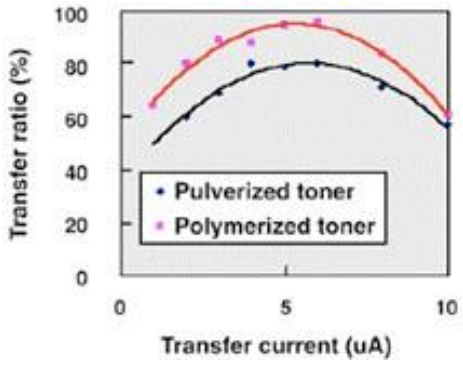

Figure 49 Improved toner transfer using polymerized toner

- Polymerised toner has better flow characteristics compared to conventional mechanically milled toner particles (see Figure 50).

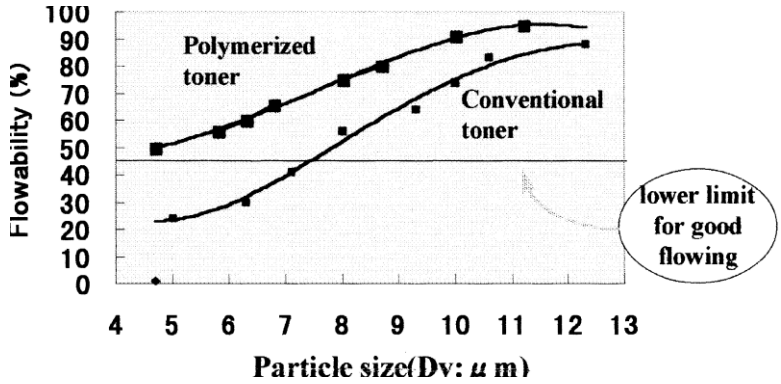

Figure 50 Flowability comparisons between polymerized and conventional toner (Hasegawa. Yanagida 1999)

- In the pulverization process, various chemicals are dispersed to binder resins through kneading. For polymerization process, chemicals are added to binder resins during the monomer phase. So adding fixed charges to particles would be easier and the electrical charge performance of each particle should be identical. This helps to achieve uniform electrical charge distribution resulting in a higher-quality printed image.
- For conventional toner the particle size is controlled by a classifier and to produce finer toner particles the resin has to be designed to be easily pulverized. Unfortunately, this also results in a greater proportion of fines (particle size <1μm)and larger particle size distribution (see Figure 51). These unnecessary fines are difficult to classify and are usually mixed into the product. For suspension polymerization process, since particle diameter is determined by the monomer solution bead size while particles are being manufactured, the particle size can be readily controlled by the quantity of dispersant and volume of particle production.

Consequently, this process is well suited for the manufacture of toner with smaller particle sizes. Concerning the particle size distribution with the suspension polymerization process, there is basically no problem with the smaller particle sizes causing increased occurrences of fines.

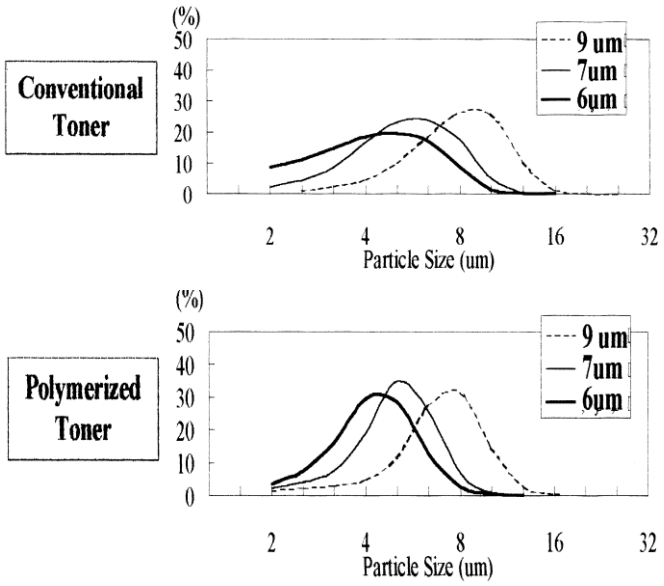

Figure 51 Particle sizes of Conventional toner are widely distributed compared to chemical toner

Figure 52 a) Deposited conventional toner b) and deposited Chemical toner

2.6.7 Few common Standard tests for material characterization of toners:

Various tests are normally carried out to find out the characteristics of each toner particle (these are listed in the appendix). The few important tests are mentioned as below:

- Complete microscopy testing using 'Scanning electron microscopy' (SEM)- to study the shape and size of the particles followed by a zoom in to the surface to look for modifications and surface treatment. Finally 'Energy Dispersive X ray' analysis (EDAX) is normally carried out to check for major elements - for example chromium or titanium. This normally would be followed by embedding the toners in resin and cutting this into 50ηm slices. Then toner particles would be examined by transmission electron microscopy (TEM) to look at the internal morphology for example pigment or wax distribution.

- 'Differential scanning calorimeter' (DSC) study - this looks at the melting profile and Tg of the polymer and gives information on behaviour.

- Mass spectrometry – It helps to analysis the core component of each toner particle with other additive agents as well. Normally high resolution probe EI or EI using Finnigan MAT 900 is recommended. This would identify many additives present for example many charge control agents. Alternatively MALDI-TOF is also used for material characterization.

- Pyrolysis GC (gas chromatography)/ MS (mass spectrometry). This would give information on the resin composition - the technique breaks the polymer into fragments which can usually be related back to the polymer.

- The diffuse reflectance infrared Fourier transform spectroscopy (DRIFTS) is also used to analyze toners. This method looks experimentally simple, rapid and reliable and has 100 times as sensitive than traditional infrared spectroscopy.

- STXM provides simultaneous observation of the spatial distributions of wax, resin and carbon black in toners, and also provide chemical information about the wax and the resin components and their micro environment. The strength of the STXM technique is the strong

functional group, local bonding and orientation sensitivity of NEXAFS spectroscopy, which can reveal extensive chemical information at high spatial resolution using multiple energy image sequences (Iwata, Tani 2006).

- Characterization of toners size and charge distribution has been carried out by a number of techniques:
  - Faraday cage blow off method

  - Electrical mobility spectrograph analysis

  - The Laser based system called electrical –single particle aerodynamic relaxation time (E-SPART) analyzer is also used to measure the aerodynamic size and electrostatic charge distribution of particles in real time

  - The q-test charge-spectrometer measures charge per diameter distribution and gives more information about the charging characteristics, as amount of oppositely charged portion and relation of low and high charged material (width of the curve)

2.7 Electrophotography & RP- Patent & Current Research

Over the last 10 years several research groups has shown interest in the feasibility of laser printing technology for the direct deposition of layers of material to form a physical object (different from printing a single layer of ink / toner on a standard piece of paper or use of electrophotography as an intermediate process). Although laser printing has been used to produce a mask in commercial RP systems, to date the direct deposition of material by laser printing has not been commercially exploited. Some of these developments are summarized in the bullet points shown below;

- Research to develop an electrophotography based Additive Manufacturing process for prototype and low volume engineering components.
- Feasibility of developing new toner from metal /ceramic composites for electronic / electrical application (e.g manufacturing of printed circuit board using laser printing technology) is becoming popular.
- Research work is also being conducted to print peptide arrays using adapted laser printers to produce functional surfaces for bio-technology applications.

This chapter is split in the following sections:

1. The first section describes the key patents in this relating to the use of electrophotography for the manufacture of 3D objects and 2 ½ D (pseudo 3D) features.
2. The second section describes the academic /commercial research carried out by several research groups

2.7.1 US PATENT 5088047- Automated Manufacturing System using thin sections

This is the first patent in which the concept of utilizing electrophotography as a means of selectively depositing toner material to generate 3D objects in layers is explicitly described (see Figure 53). In the proposed process, one latent image is formed on the rotating drum (26) and then the image is transferred on to the conveyor. The image is tackified by some form of heating device (58) and finally the image is transferred from the conveyor on to a substrate via solenoid valves (64) which is pressing against the back plate (62). Finally all of the layers are consolidated in layers (60) to form a 3D object. This patent was filed on 16th October 1989 and would normally be valid until Oct'2009 (20 years duration). However, although the maintenance fee was paid the 4th and 8th year from the date of filing no information was found about the payment of the maintenance for the 12th year, which may indicate that the patent was allowed to lapse before the end of its term. Apart from the filing of the patent there appears to have been no additional work to pursue the development of the process by the inventor. This tackification approach is novel and could be applied to build 3D Objects.

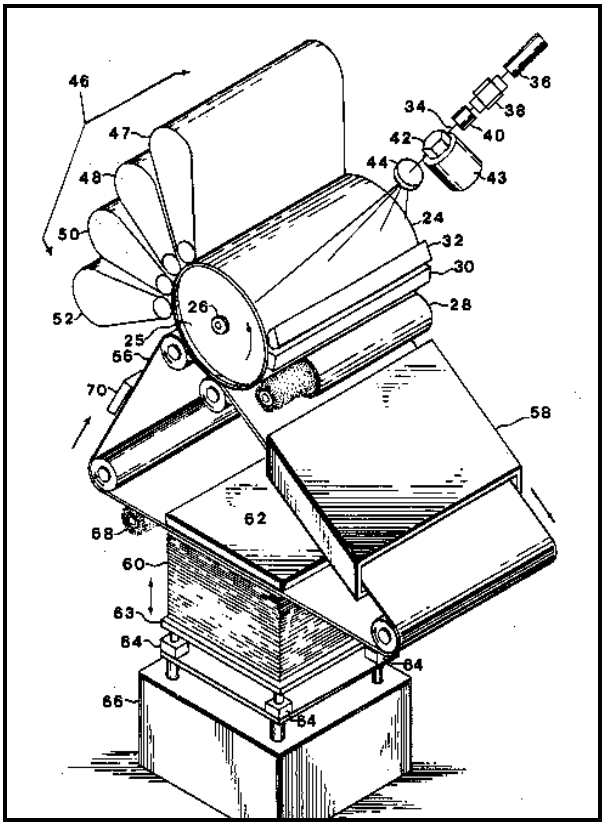

Figure 53 Schematic of the process - Bynum patent (Bynum 1989)

Claim	Key innovations
"Deposition of multiple layers of non-conductive toners from the Organic Photoconductor (OPC) drum on to the final substrate (build platform) via intermediate belt where the material is finally transferred on substrate (build platform) by tackification of each layer by some form of heating device" .	• Use of an OPC to develop the image • Transfer to the substrate via a intermediate belt • Use of thermally induced tackification.
Exposure of charged electrophotographic element (OPC) can be carried out via any kind of ELECTROMAGNETIC RADIATION. Any type of radiation, whether emitted by a laser or LED or any other type of light source, would be covered by this patent. The patent covers all generic in terms of light source which normally required to develop image on OPC drum for electrophotography process.	• Any source of electromagnetic radiation can be used to expose the OPC.

Table 5 Claims and key innovations of US patent 5088047

2.7.2 US PATENT 6066285 - Solid freeform fabrication by powder deposition

This patent was filed by Ashok .V Kumar, University of Florida in 11th December 1998. Patent was granted on 23rd May 2000. Patent is valid till Oct 2018and research group headed by A. V. Kumar, is still actively working on this idea.

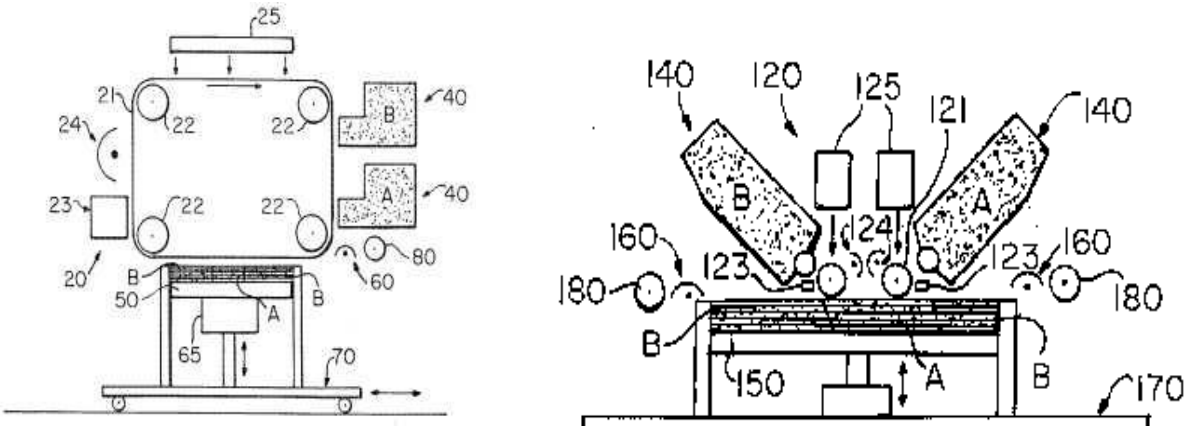

Figure 54 (a) and b) - 2 different embodiments and charging method (Kumar 1998)

Two different embodiments were discussed in the patent (see Figure 54). The first one relates to the use of a continuous photoconductor belt where electro-photographic powder deposition was carried out using photorecepting belt (21) . The belt was coated with a coating of photoreceptive material. The belt is cleaned with each pass using a belt cleaner device (23), which discharge the belt by exposing it to a bright light and which removes any residual particles by brushing or scrapping means. The belt is charged after each cleaning on each pass by a charging device (24). The build platform (50) is lowered incrementally for each layer, so that the uppermost layer is always at the correct distance from the belt. Two methods of charging were mentioned for the embodiment shown in figure (a). If the powder is conductive then the opposite polarity of charge could be inducted using the charging device (65) connected underneath to the build platform. If is nonconductive the opposite charge could be applied by the charging rollers (60) which could be rolled over the earlier deposited layer to induce opposite charge.

In an alternative design shown in figure b) the electro-photographic powder deposition (120) comprises a pair of photoreceptor or photoconductor rollers or drums (121) were used instead of photoconductor belt, each associated with separate image projectors (125), charging devices (124) and powder delivery devices (140), one for material A and the other for material B. Similar to the earlier embodiment if the powder is conductive a proper voltage to the platform (150) would be provided and for nonconductive powder the surface would be charged using a charging roller (160) and fusion/compaction would be carried out rollers (180). Each successive loose powder layer is deposited directly onto the previously deposited powder layer, which has been compacted or fused to its

underlying layer. After all powder layers have been deposited the green part is further processed such that the part compositional powder is fused to create a high-density part while the support powder is easily removed".

Claim	Key innovations
"Powder deposition by providing means to charge said deposited powder layer such that said deposited powder layer is charged opposite to said another transferable powder layer, and charging said deposited powder layer"	• Use of electrostatic transfer by charging the top surface of the earlier printed layer with opposite polarity for non conductive toner/powder • For conductive powder the charge could be applied below build platform and for non-conductive powder the charge would be applied on the top surface of the printed layer using charging rollers .
The invention could be applied utilizing a Photoreceptor belt or an alternative embodiment was proposed using photoreceptor rollers.	• Use of photoreceptor belt or drum.
This patent also proposed an alternative design system (other than photoreceptor belt design) where the 2 print engines (one for build and other for support powder) are designed to deposit on a movable build platform. But charging the top surface of deposited layer using corona was mentioned for this process as well.	• Build and support print engines

Table 6 Claims and key innovations of US patent 6066285

2.7.3 WO 200403746- Method and apparatus for rapid manufacturing of metal, ceramic and metal-ceramic products

This patent filed by SINVENT on 6th May 2004 and described the process of generating 3-D metal-ceramic parts via the electrophotography process where each printed layer would be carried away to a sintering die by a transporting device where final consolidation of layers would be carried out by applying pressure and sintering (see Figure 55). Sintering would be carried out by microwave / electrical heating or by both. This patent focuses on the deposition of metal & ceramic powder image, which is transported into a sintering die (21) where is it fused either by heat and/or pressure. This patent described primarily two types of embodiment. In the first embodiment the material would be deposited on a conveyor belt and finally transported to the sintering chamber 21.The particles of a single layer would be sintered using heat and pressure inside sintering chamber. The belt would be rigid so that powder deposited on conveyor would be not displaced. The second embodiment

mentioned about an additional transporting device (112-116) which is not a continuous belt type but rather sequentially receives powder from a powder receptor (101).

The difference between the two embodiments is the introduction of a transporting device (112- 116) which is not based on a continuous conveyor belt, but rather having absorption elements (112) that sequentially receive powder from powder receptor (101). Finally the loose powder would be transported to sintering chamber where heat and pressure would be applied to sinter the metallic powder.

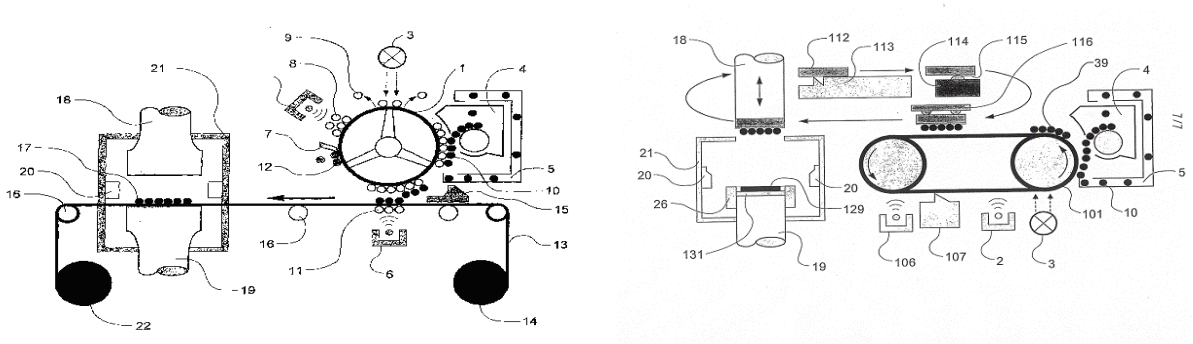

Figure 55(a) & (b) 2 Different embodiments proposed by SINTEF (WO 200403746 –2004)

Claim	Key innovations
A process of printing and transporting metal ceramic layer into sintering die to consolidate each layer which is very close to the ionography process. *	Use of electrostatic material deposition and conveying the material towards a separate sintering station/die.

*****deposition might have some infringements with Grenda patent covered later.

Table 7 Claims and key innovations of patent WO200403746

2.7.4 WO 2007073206: Method and device for manufacturing a powder layer for in layer production of objects

This patent was further extension of earlier patent filed by SINVENT and published on 28th June 2007 using an adhesive material to keep the powder particles in position without any distortion after deposition. This process described a method for manufacturing a layer of a work piece (see Figure 56).

The work-piece includes an object and the method comprising of:

a) Forming at least a first pattern on a printing face of at least a first part of the layer of the work piece to be manufactured.
b) The at least first pattern being constituted by an adhesive material.
c) Developing the first pattern by arranging/depositing a first powder material onto the adhesive material. An apparatus for implementing the method is also described.

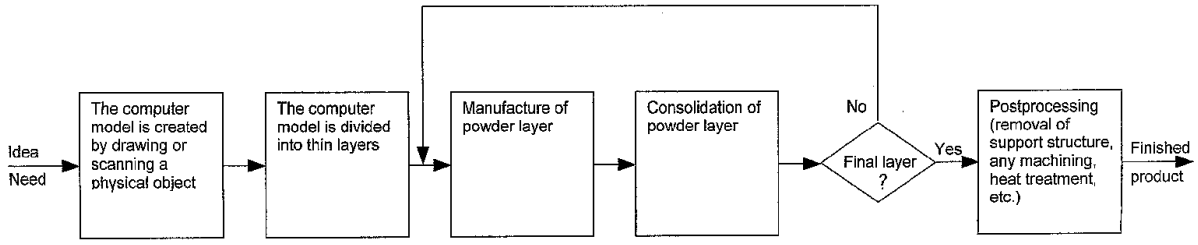

Figure 56 Process flow diagram of MPP process (WO 2007073206**)**

This process was further extension of earlier patent to minimize any distortion while conveying using an adhesive material, which would help to keep the powder particles in position without any distortion. In a first aspect, the invention provides a method for manufacturing a layer of a work piece, where the first pattern on a printing face of the work-piece would be produced, and first pattern would be constituted by an adhesive material, and developing the first pattern by arranging/depositing a first powder material onto the adhesive material. In an another embodiment method further includes of forming a second pattern on the printing face of at least a second part of the layer of the work piece to be produced, the second pattern being constituted by a dielectric solid material, and developing the second pattern by arranging/depositing a second powder material onto the dielectric solid material.

In a further embodiment, the device may comprise a second application device for applying a dielectric solid material onto the printing face to form a second pattern of at least a second part of the layer of the work piece to be produced, and a second developing device for arranging/depositing the second powder material onto the dielectric solid material. Also included may be a second application device for applying an adhesive material onto the printing face in order to form at least a second pattern of at least a second part of the layer of the work piece to be produced, and a second developing device for arranging/depositing a second powder material onto the at least second pattern of an adhesive material.

As described in the patent the first and second application devices could be an ink-jet print head. The first and second developing devices mentioned earlier could be a developing station, in which the powder material would be arranged /deposited by electrostatic attraction between the powder material and the printing face, so that the powder material is transferred to the printing face. The developing device could also be a developing station of the powder bed, conductive magnetic mono-component, or toner hopper type. A developing station in which the powder material is arranged using a conductive magnetic brush, aerosol, cascade, isolating magnetic brush, or isolating non-magnetic mono-component, may also be used.

Patent also disclosed about the adhesive material, which could be wax, viscous paraffin wax, or any type of viscous material. The first powder material may be a metal building powder, a metal alloy, an electrically conductive ceramics, or a metal mixture containing ceramics. The dielectric solid material may be a thermopolymer, or a material selected from the group consisting of animal wax (e.g. beeswax, stearine), vegetable wax (e.g. candelilla wax, castor wax), mineral wax (e.g. ozocerite wax), petroleum wax (e.g. paraffin wax), synthetic wax (e.g. polyethylene wax), photo- polymer, or be a mix of several wax types, such as sealing wax, for example. The second powder material may be a support powder of ceramics, in which case the support powder may be aluminum oxide.

Claim	Key innovations
A process of printing and transporting metal ceramic layer into sintering die to consolidate each layer which is very close to ionography process using an adhesive material to keep the powder particles in position without any distortion	Use of electrostatic material deposition and thereafter holding the deposited material printing adhesive material like wax

Table 8 Claims and key innovations of patent WO2007073206

2.7.5 US PATENT 6206672 - Apparatus of fabricating 3 dimensional objects by means of electrophotography, ionography or a similar process

The patent was filed by Edward Grenada filed on 31st march 1994. Patent was granted on 27th March 2001. This process described the apparatus includes ion-generating equipment for sequentially creating latent ion images of layers of an object to be fabricated (see Figure 57). Developing apparatus is provided for adhering at least one object building substance to the sequential latent ion images to create a series of laminae. Thereafter, the series of laminae are assembled to fabricate the object.

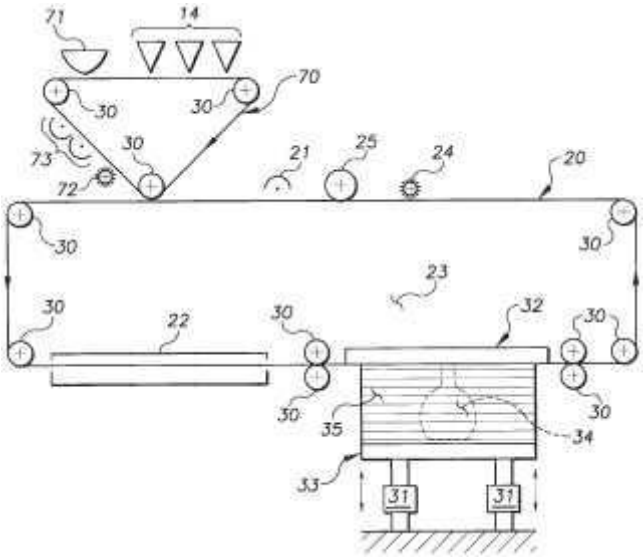

Figure 57 Schematic of the process proposed (Grenada 1994)

The charge was directly written on to a rotating drum (10) using ion discharge elements (19) and finally the latent image was produced on the drum through the developing station (14) where various object-building substances in a powder form were deposited on the drum. The image was electrostatically transferred onto the conveyor and tackified by heat source (22). Finally the tackified lamina was transferred on to the substrate by solenoids which apply a pressure against the back-up plate (32).The layers (35) are then consolidated, as shown in the figure above.

Claim	Key innovations
Apparatus for sequentially electrostatically propelling particles of an object building substance toward a support to create sequential particle images on the support of layers of an object to be fabricated and apparatus for assembling the sequential particle images to fabricate the object	This process is explicitly related to ionography / Electrophotography

Table 9 Claims and key innovations of US patent 6206672

Patent is valid till Oct 2014 and maintenance fee need to be till 2013 respectively.

2.7.6 US PATENT 6157789 – Electrophotographic apparatus

This patent mentioned about the circuit developing technique via electrophotography based RP technique by Murata Manufacturing company ltd, Japan. This process described about an electrophotographic apparatus to produce printed circuit board using a photosensitive member, a corona charger for charging a surface of the photosensitive member; a circuit-forming/chargeable

powder supplying device for supplying circuit-forming/chargeable powder to a latent image pattern on the photosensitive member; a transferring device for transferring the circuit-forming/chargeable powder on the latent image pattern onto a ceramic green sheet (see Figure 58).

This patent is focused on accuracy and minimization of any shift of the circuit patterns while using electrophotography as a power deposition device. According to the embodiment of the present invention, the electrophotographic apparatus is provided with detecting means for detecting the position of a circuit pattern on a print material. The detecting means generates a signal to control the circuit pattern forming position. Therefore, individual circuit patterns can be precisely formed.

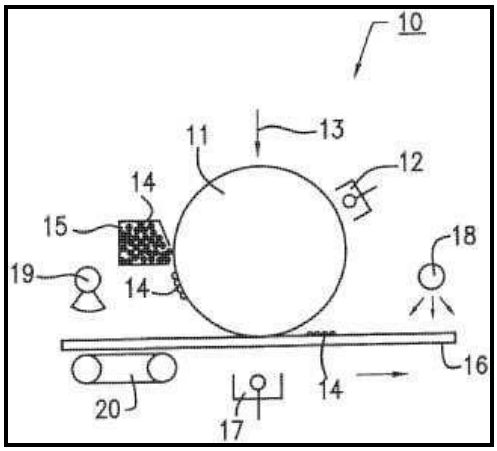

Figure 58 Schematic of the process with CCD Camera (Akihiko 2000)

The flash lamp (18), serving as fixing means, is used to fix the chargeable powder onto the ceramic green sheet (16) in order to form a circuit pattern (not shown) on the ceramic green sheet (16). The circuit pattern recognizing camera (19) is used to detect a circuit pattern forming position on the ceramic green sheet. The electrophotographic apparatus uses laser beams (13), serving as exposing means, to form a predetermined latent image pattern on a surface of the photosensitive member.

Claim	Key innovations
An electrophotographic apparatus for forming a circuit pattern by an electrophotographic method and detecting X and Y position and the angle (theta) at which the circuit pattern would be located on the print material. This detecting mechanism would also generate signal to control the X, Y and theta for the circuit pattern location positions.	This process is focused on the accuracy of printer circuit pattern using feedback from camera while depositing material to produce printed circuit board

Table 10 Claims and key innovations of patent WO2007073206

Patent was filed in March 1999 and normal valid period of the patent is up to Oct 2019. The maintenance fee needs to be paid until 2012.

2.7.7 US 6487386/ WO 00/25182: Device for applying decors and/or characters on glass, glass ceramics and ceramics products

This patent published on 4th May 2000 by Michael Zimmer ,W.Weinberg of Schott Glass Germany. This patent described of printing on glass using electrophotography technique where electrostatically layer is first deposited on a chargeable photoconductor layer (5) where photo-exposure assembly (6) is used to generate the electrostatic image corresponding to the pattern .The toner from the container (8) is first transferred on transfer roller (7) and there after using the corona (9 and 10) the image is finally transferred on the substrate/product (2).One heating device also arranged to fuse the deposited loose toner (see Figure 59) .

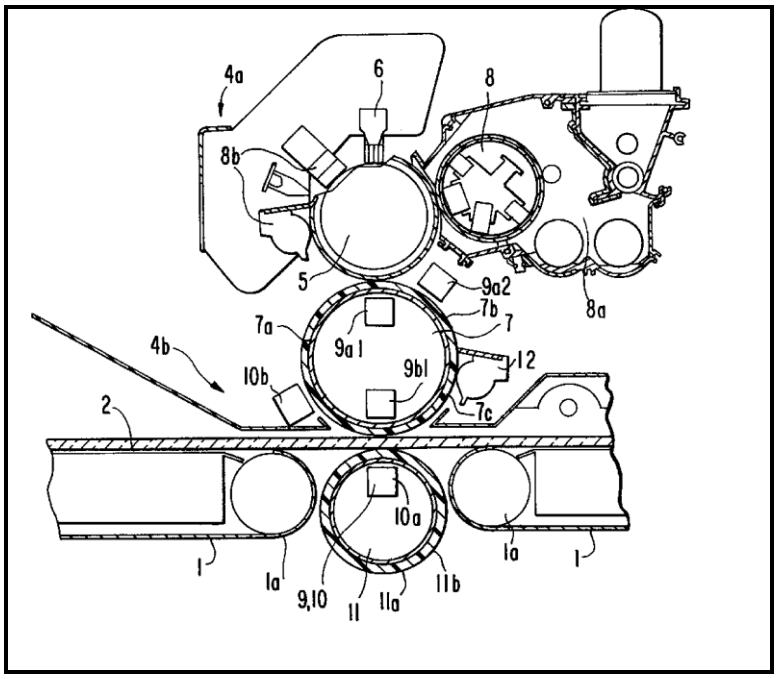

Figure 59 Schematic of toner deposition mechanism (Zimmer 2000)

This method discloses an electrostatic copying method to decorate glass/ceramics / other work pieces using corona in two stages where image is first transferred onto an intermediate roller and then from intermediate roller on to the image belt applying electrostatic force of repulsion. The electrostatic charge of same polarity is applied on the image, which finally repels the image on to the belt/substrate.

Claim	Key innovations
The second corona (10a) is arranged in an interior of the counterpart roller (11). The first corona (9a1, 9a2) on said transfer roller (7) is arranged in a region of contact of the transfer roller (7) with the image roller (5) and has an electrical potential that is opposite in sign to a charge of the toner image on the image roller (5); and wherein said third corona (9b1, 10b) has an electrical potential of opposite sign from that of the first corona (9a1, 9a2) and the second corona (10a) and is arranged on the transfer roller (7) in the vicinity of the zone of contact of the transfer roller (7) with the product (2).	Unlike with conventional laser printing where final transfer is achieved using electrostatic force of attraction this process an electrostatic force of repulsion is generated using a corona having same polarity of toner particles to repel the toner from roller to deposit it on the substrate.

Table 11 Claims and key innovations of US patent 6487386

This electrostatic force of repulsion is one of the potential solutions for 'Z height problem' while depositing non-conductive powders in layers to produce 3D objects. This ''Z height problem' is described in the next section of this chapter.

2.7.8 Research work by A.V. Kumar at the University of Florida

The research team at the University of Florida headed by Professor Ashok Kumar commenced investigations in to the use of electrophotography based Additive Manufacturingaround 1998. A test bed was developed using Hewlett Packard LaserJet4 print engine having a 600 dpi resolution. Standard black magnetic toner, average particle size 10 to 15 µm, was selected for the trials. The print engine was integrated with two axis build platform where the toners are deposited on to a build platform and later fused with radiant heater. Much of the printer hardware was removed so that build platform would have an access to the photoconductor drum. The sensors integrated with printer were bypasses /controlled so that it could simulate the normal printer operations. The heating system was replaced with compaction plate which was PTFE coated and heated by a mica strip heater.

The system was equipped with a digital motion controller to drive the servomotors, which activates the two axis of motion (X and Z direction) of the build platform. Galil control system was used to actuate motors and acts as an interface between printer and its several controls. The servomotors were used to get feedback regarding the position of build platform while trials are being carried out. The test bed was designed so that it could directly print layers from the photoconductor drum onto the build platform. Solid slicer programme was developed in Java to read CAD files of model and divides them into cross sections to automate the whole process.

The build platform was placed on a spring mounted platform to help during transfer by pressing against photoconductor drum and lessens the risk of damaging the printed part (or final transfer roller) if the platform is not perfectly horizontal (see Figure 60 and 61). The linear speed of the build

platform in x- axis needs to matched precisely to the linear (circumferential) speed of rotating photoconductor drum. After printing of each layer the build platform lowers by one layer so that the next layer can be printed on top of it. The gap between the photoconductor surface and top surface of the printed layer of the build platform would be maintained by monitoring the z axis movement of the build platform. The voltage of opposite polarity was applied underneath of the build platform to transfer the toner from OPC drum on to the top surface of build platform.

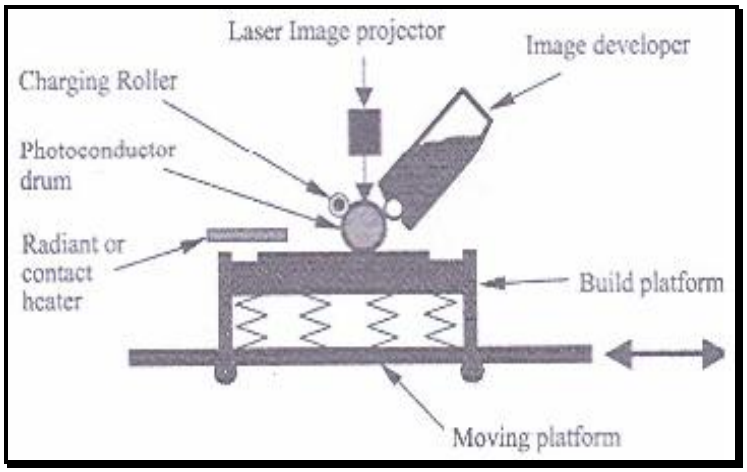

Figure 60 Schematic diagram of test bed (Kumar 2003)

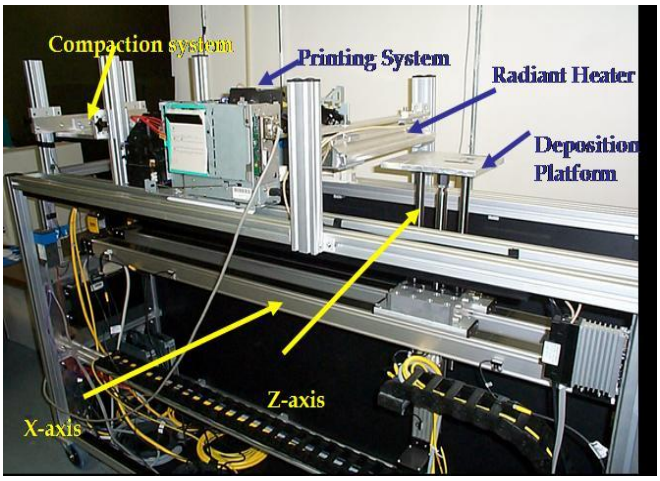

Figure 61 Actual test equipment developed by University of Florida, US

Initial experiments revealed the following points:

- The printing system used for the test was capable of printing 12 pages per minute with a resolution of 600 dpi. However, the test bed was only able to print 5 times per minute with an average print layer thickness of 20µm. This was due to the additional time required to move the platform under compaction platform for fusing and compacting of the multiple layers. It

was also found that best print was obtained while maintaining no print gap between the photoconductor drum and build platform and maintaining the voltage of build platform at 1000V (+ve).

- One of the most important finding was that powder deposition efficiency falls sharply after few layers of printing. It was found that there was negligible toner deposition after 40 to 45 layers using the approach of charging the build platform, as the strength of electric field between build platform and photoconductor drum drops significantly as the part height increases (Figure 63). The maximum part height initially obtained using this approach was only 2mm. The standard toners are primarily nonconductive and made from styrene based polymers as mentioned earlier. In standard laser printing application the electrostatic charge with opposite polarity (positive) is applied underneath of paper so that negative charged toner is attracted off the OPC drum. Unfortunately, when multiple layers are deposited the charge beneath the build platform is depleted. Maintaining the same amount of charge for non-conductive powder represents a major challenge when printing multiple layers due to this 'Z height problem'.
- Kumar at university of Florida while printing multiple layers using standard polymeric toner to build 3D objects earlier cited this Z height problem. The charge depletion phenomenon could be explained further using standard Gauss's law and static electric field as shown in Figure 50.

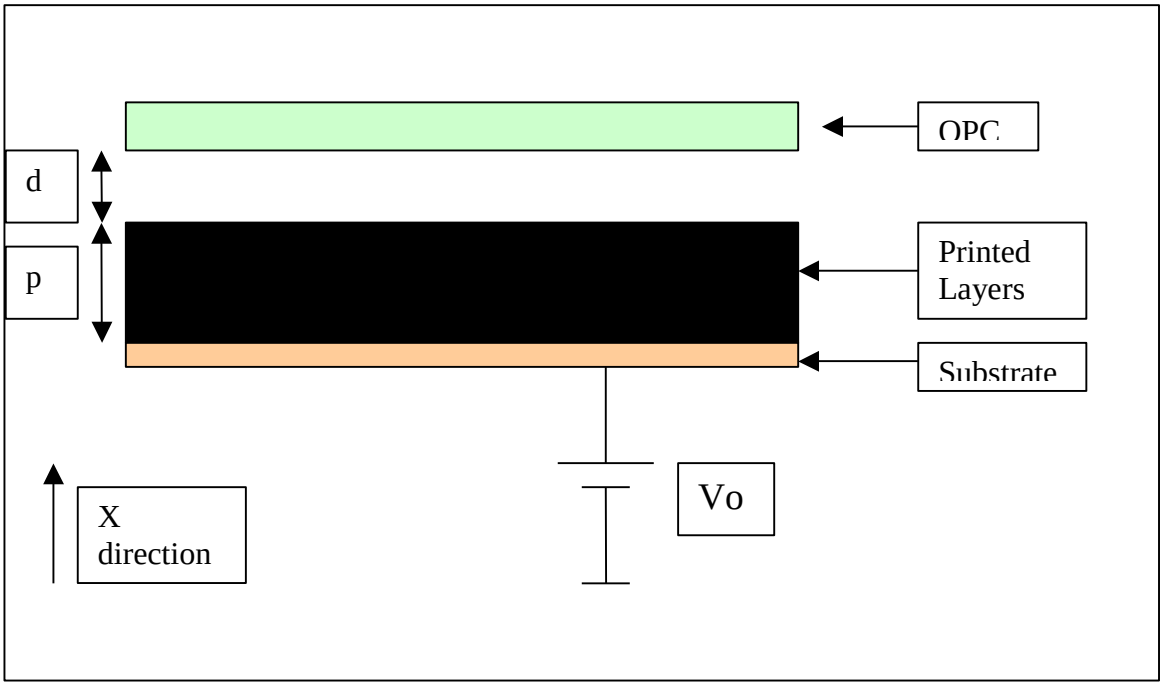

Figure 62 Electrostatic deposition of toner (schematic)

According to Gauss' law the electric field in the printed layers (p) at a distance x from the substrate/from top surface of build platform :

$$\mathbf{E_p = (\sigma_b + \rho_1 x)/ (K_p \varepsilon_0)} \quad \text{.....(1)}$$

Where $\sigma_{b \text{ is charge}}$ per unit area at the interface between build platform and previously printed layers; ρ1 is charge per unit volume in the printed layers, Kp is the relative permittivity of the printed layers and ε0 is the permittivity of free space. Similarly the electric field between in the fresh toner of the OPC drum can be written as $\mathbf{E_d = (\sigma_b + \rho_1 p + \rho_2(x-p)) / (K_f \varepsilon_0)}$ .....(2)

where ρ_2 is the charge per unit volume in fresh toner layer and K_f is the relative permittivity of the fresh toner and layer.

Now the voltage drop from the top of build platform to the photoconductor can be expressed as :

$V_0 =$

$$\int_0^p (\mathbf{E_p\, dx}) + \int_p^{p+d} \mathbf{E_d\, dx} \quad \mathbf{.....(3)}$$

Substituting the values of Ep and Ed from equation 1 and 2 into the equation (3) :

$$V_0 = \mathbf{(\sigma_b\, p/}\, K_p\, \mathbf{\varepsilon_0) + (\rho_1\, p^2 / 2}\, K_p\, \mathbf{\varepsilon_0) + (\sigma_b\, d/ K_f\, \varepsilon_0) + (\rho_1\, pd/ K_f\, \varepsilon_0) + (\rho_2 d^2) \ldots\ldots\ldots (4)}$$

Putting the derived value of σb in the equation 2 we get the value of Ed as :

$$\mathbf{E_{d \text{ at } x=p}} = K_p/ (\mathbf{K_f\, p} + K_p d)[V_0 + (\mathbf{\rho_1\, p^2/ 2\, \varepsilon_0}\, K_p) - (\mathbf{\rho_2 d^2/ 2\, K_f\, \varepsilon_0}) \ldots\ldots\ldots (5)$$

Plotting the value of Electric field function (Ed) vs printed layer (p)

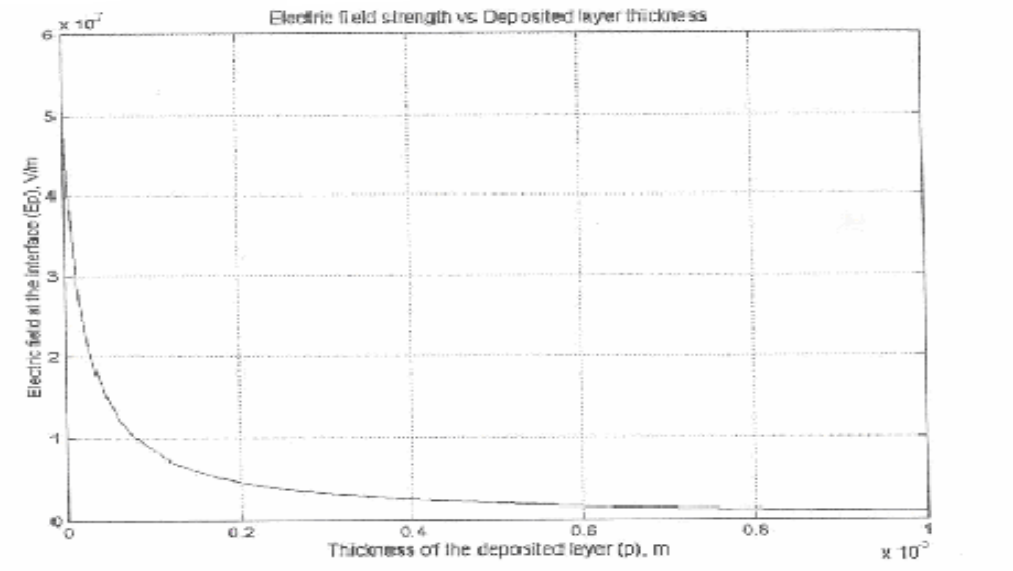

Figure 63 Electrostatic field strength (Y axis) vs. multiple prints (Thickness in x axis) with polymers(non-conductive)(Kumar 2003)

The graph shows that value of the electrostatic field decreased almost exponentially after few printed layers of nonconductive polymers. This problem is more acute for nonconductive polymeric powder compared to conductive toners.

- To overcome this charge depletion (i.e the charge depletion and the reduction of field strength after a few mm distance for nonconductive powder) due to nonconductive toner printed on build platform, Kumar applied charge on the top surface of each deposited layer to maintain sufficient electrostatic attraction force between the toner on the photoconductor drum and the top surface of the printed layer on the build platform. It was found that part height increased up to 3mm after printing 575 layers using this charging mechanism. No result was shown about the powder deposition above 3 mm of part height using this method. Graph 14 shows the plot of part height versus number of prints where corona charging device is used to charge the top surface.

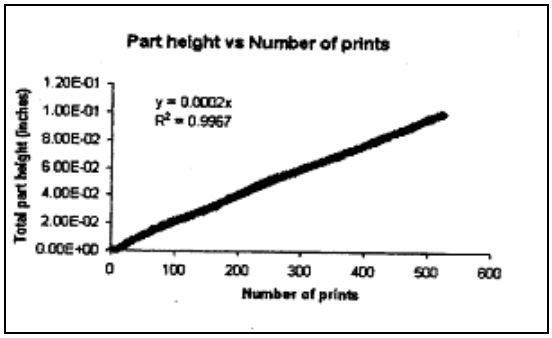

Figure 64 Electrostatic field strength vs. multiple prints with polymers with charge applied on top surface

Research work was also carried out by Kumar to understand the effect of charging and the importance of discharging the printed surface model. Theoretical model of printing is shown below considering the fused powder has surface charge and residual volumetric charge and fresh toner only has volumetric charge. The model was built assuming an initial layer of powder on the photoconductor drum of thickness d_1, which was transferred with efficiency η. An air gap was introduced between the photoconductor drum and the part to simulate irregularities in the part surface shown below. The fused powder has both a surface charge and residual volumetric charge, and the fresh toner transferred during printing which has only a volumetric charge of density ρ_1 .Assuming d as layer of thickness, k is relative permissivity of material, σ is surface charge density of layer, ρ is volume charge density of the layer and η is the toner transfer efficiency and the efficiency of the printing was expressed as;

$$\eta = \frac{\varepsilon_0 V_{platform} + C_1 V_{Corona} + C_2 E_c + C_3 \rho_l + C_4 \rho_c + C_5 \rho_t}{C_6 \rho_l}$$

C1 , C2 , C3 , C4 and C5 are constants and the charge density □1 is very complex to predict for fresh toner but it is related to both numerator and denominator of the formula mentioned above.

The programme was run in Matlab to understand the residual volumetric charge on fused toner as shown below:

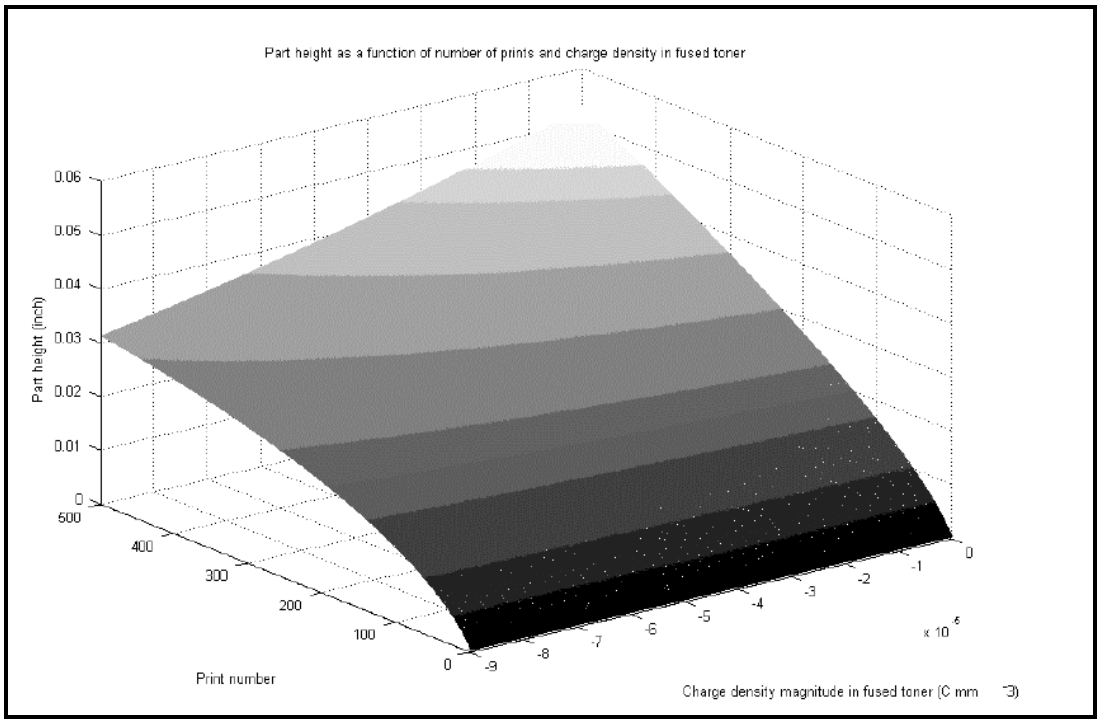

Figure 65 Electrostatic field strength and charge density vs. multiple prints with polymers

- It was found that initial build rate was faster and then falls sharply as the voltage reduced on top of the build platform has a major influence. For full discharge this fall off is minimal and if discharge rate is minimal then it has significant influence on powder deposition.

- Another interesting result, which was observed for all of the trials conducted, was that the boundary of the printed parts had higher material deposition resulting in a raised edge across the borders of the printed images. This is largely due to higher potential gradient near the edges of the printed images This phenomenon was further investigated using theoretical modelling and carrying out experiments. Potential solutions to minimize this 'Edge effect' were discussed. One of the solution which was discussed controlling the image quality across borders/ edges of the printed layer in software using halftone /grey scale images printing to control the resolution of the images across the border of the printed images.

Another approach related to electrophotography based layer manufacturing was investigated by Kumar where binder (in the form of a dry toner) power was deposited /printed onto a powder bed, akin to the 3 Dimensional printing process developed by MIT but using a dry binder rather than

printing a liquid binder [Kumar 2004]. In a subsequent step the binder powder was thermally fused to bind the part powder to form 3D objects. Polystyrene based binder powder was printed on a alumina (ceramic) powder bed where the part powder bed of ceramic was created by spreading the ceramic powder uniformly.

- The deposition of binder powder on top of the electrically conductive metallic powder (build) was difficult as this conductive powder can be electrically charged very quickly and forms a powder cloud which inhibits the smooth deposition of binder powder on top of the powder bed. For the nonconductive ceramic part powder, the top surface of the powder bed also needs to be charged by some sort of charging device (like a corona wire/bar) so that binder powder has sufficient electrostatic attraction force to deposit on top of the non-conductive part powder.
- It was also found that part powder was easily transferred to the charged portions of the photoconductor drum and this led to contamination of the next layer of deposited binder. This reverse printing not only adversely affects the deposition efficiency and can result in defects in the deposited layer (see 'white spots' in Figure 66) but has the potential to damage the photoconductor drum.

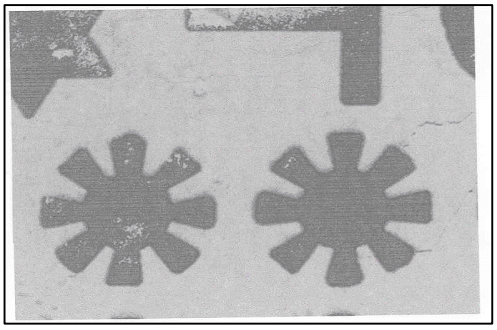

Figure 66 White spots due to reverse printing (Kumar 2004)

2.7.9 Research Work –by Cormier-North Carolina State University

In August 2000, the news came on US magazine of "Engineering News at NC state " (21st July, 2000) that a research group headed by Denis Cormier (Assistant Professor) of NC state university with his colleagues Jim Taylor and Harvey West were developing a rapid prototyping process based around a desktop Laser printer. It was also announced that they had applied for a patent for the new process but this was subsequently rejected, primarily due to the David Bynum's patent.

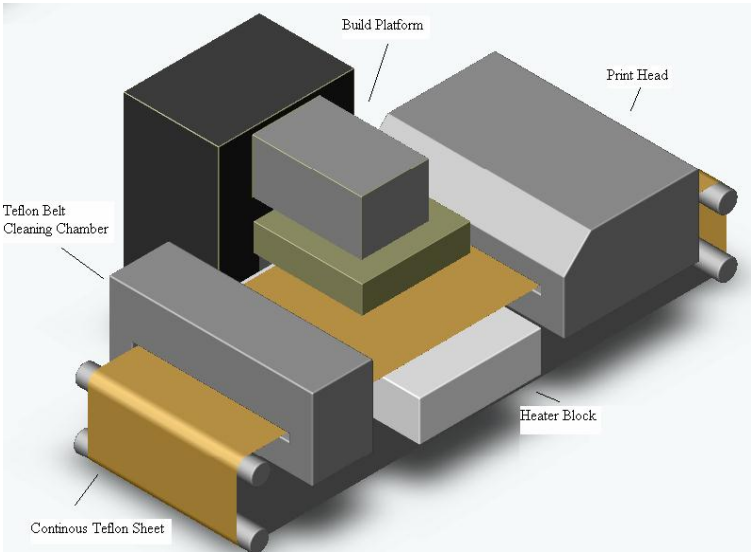

Figure 67 Concept model of Electrophotography based RP process developed at North Carolina University (Cormier 2003)

The toner transfer mechanism used by the researcher at North Carolina University was very similar to the tackification approach described by Bynum earlier where material is deposited in layers and consolidated thereafter using heat and pressure (see Figure 67). The image would be first deposited on a Teflon coated belt. The printed image would be then moved forward and placed below the build platform. The build platform would be lowered .The printed images would be pressed against the build platform and hot plate placed below the Teflon coated belt. The pressure applied by the build platform and temperature of the hot plate help to form a continuous layer. Process would be repeated until the 3D object is produced. This transfer mechanism was mechanical transfer and not electrostatic transfer.

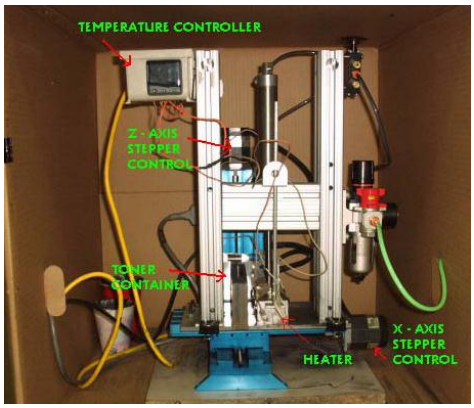

Figure 68 Test rig at North Carolina state university

Test rig was further developed to assess this tackification mechanism, retrofitting the standard CNC engraving machine (see Figure 68). The tool spindle was replaced with a container that could hold the polymer/toner and deposit/spread the powder while moving across x-axis. The testing station was made with heater connected with resistive heater elements. The heaters could be moved up and down along z axis pneumatically. The toner was deposited on a paper substrate which was glued on a metallic surface to avoid any sort of shift of deposited toner layer during the fusing process (see Figure 69). The trials were conducted to produce samples having each layer thickness 25.4µm using a heater temperature of 95^{o} C under 0.4 bar of contact pressure.

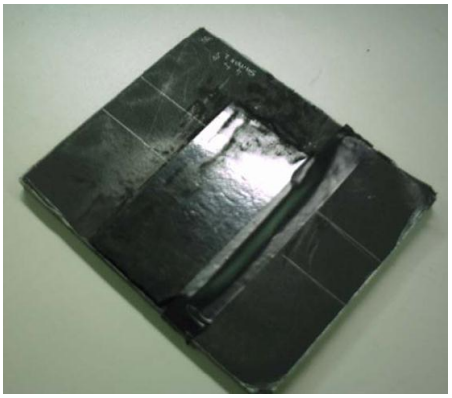

Figure 69 Specimen produced after 74 layers

Cormier conducted experiments to study the feasibility of depositing toner from standard engineering polymer such as high density polyethylene (HDPE) using HP LaserJet4 printer. Trials were carried out using HDPE powder (10µm particle size), which are very common for rotational moulding. The fine powder then coated with carbon black and cartridge was then filled with HDPE powder coated with carbon black. HDPE powder found deposited on standard paper. There was no information available about the image quality with HDPE powder.

There is no evidence earlier which had shown the feasibility of developing 3D plastic objects using HDPE / Standard engineering polymers other than styrene based toner which is very brittle and not feasible to build 3D objects. No 3D part samples were made using HDPE powder on this occasion by Cormier but this was the first feasibility study to develop 3D plastic objects using tough Polyethylene for electrophotography process.

2.7.10 Printing Metal /Ceramic Powder using Electrophotography

SINTEF/NTNU at Norway was developing Metal Printing Process (MPP) with high-speed photocopier to produce three-dimensional metallic objects from powder material since 1993. Some other work described here was conducted under the auspices of the 'Custom-Fit' project is also described in this section. This process was similarly based upon the commercially proven xerography process (see Figure 70). Photoconductor was exposed using 'Light Emitting Diodes' (LED) instead of a laser to develop the latent image on photoconductor. The loose toner of the printed image including build material and support material was transferred from the photoreceptor to a punch by electrostatic forces of attraction. The printed image would be then moved towards the consolidation system (CS) where loose powder layers are converged into useful engineering components by compaction and sintering in a heated die. The sintering, and thus the formation of metallic bonds in the parts, relies on the combined effects of the compression and elevated temperature inside die. The consolidation unit consists of the previously mentioned punch and a die surrounded by an induction coil. The die is heated and held at a constant temperature during the entire build time (Boivie, Karlsen 2006).

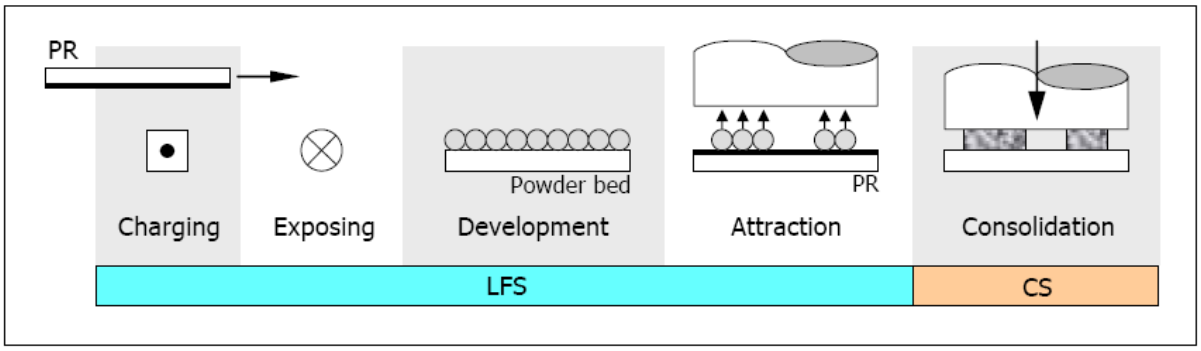

Figure 70 Schematic of Metal printing Process at SINTEF base on Laser Forming system(LFS) and Consolidation System (CS)

The powder used extensively during the development of the Metal Printing Process was Höganäs ASC200 iron powder of 200mesh (see Figure 71). Powder of other materials, like aluminium and copper, were also used while developing this process.Powder is printed using test rig and the performance of the deposited layer as a function of contact pressure was also plotted (see Figures 71, 72 , 73 and 74).

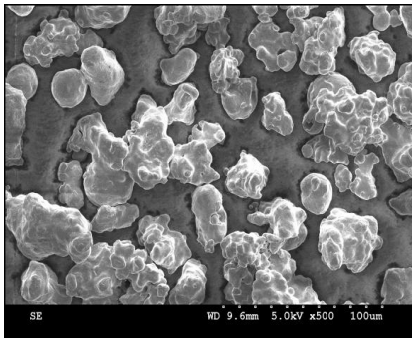

Figure 71 SEM of ASC200 iron powder

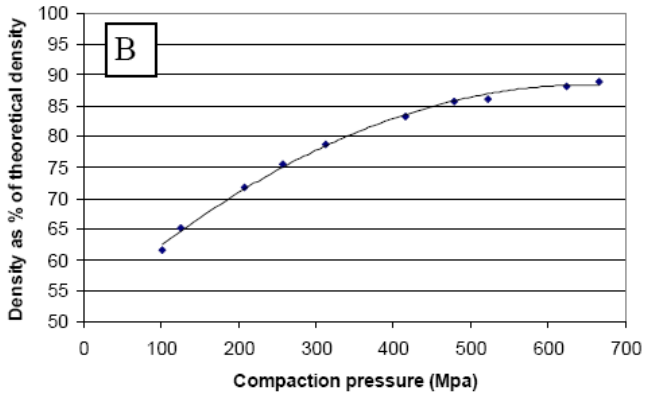

Figure 72 Density of the printed layer against compaction pressure

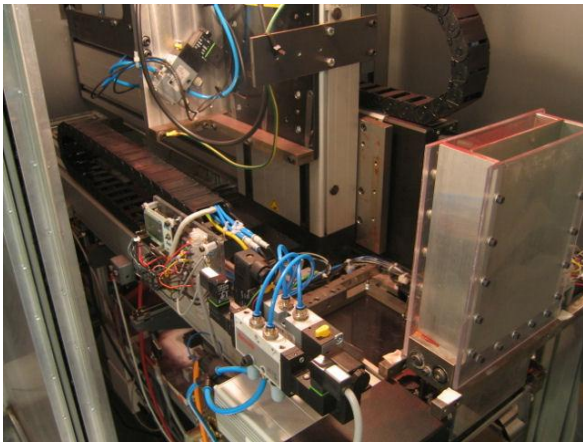

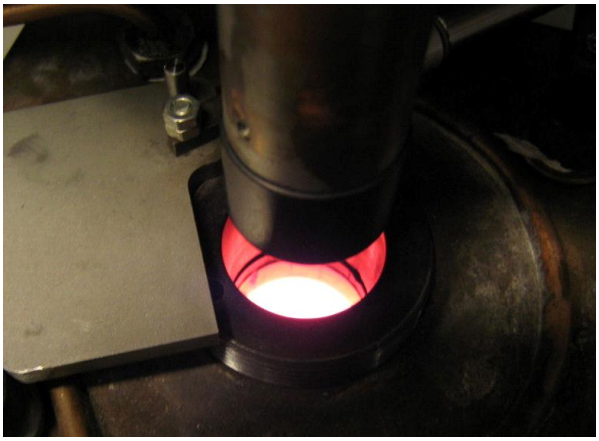

Figure 73(a) Demonstration Test rig MPP & (b) Sintering die

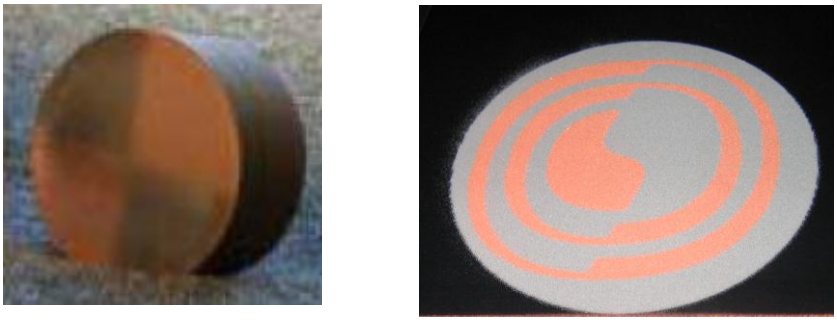

Figure 74(a) Multi-material component Iron and copper & (b) Deposited iron powder

The challenge was to sinter the metal powder without any material degradation and cracks, which might generate due to thermal stress if not controlled properly. Special care was also considered to inhibit any oxidation during consolidation process of metallic powder. The punch and the external walls of the consolidation unit were water cooled to control the temperature during sintering. Researchers at SINTEF are actively working on it to develop this process further.

2.7.11 Printed Circuit Board Manufacturing using Electrophotography at Hitachi Corporation

The following papers relate specifically to the use of electrophotography in electronics application these papers provide important information with respect to the development of non standard toners (albeit that these are conductive materials)

Hideo Aoki of Hitachi Corporation, Japan conducted a feasibility study of mask-less manufacturing of printed circuit boards using electrophotography to deposit toner /material [Aoki,Yamaguchi,2004] to form a conductive pattern which is then over-plated. Firstly the tracks were printed onto a PCB substrate using a "seed" toner (toner including metal particles) using the electrophotography technique. The binder resin of the "seed" toner was epoxy resin with high a glass transition temperature (to enable downstream soldering processes if required) with copper (Cu) particle filler. Copper was selected due to its compatibility high catalytic activity electroless plating.

Electroless plating was found to yield similar levels of track resistance and adhesion strength to the substrate to conventional PCB manufacturing methods. The Tribocharging characteristic of copper filled toner was also investigated and it found that lower copper content toner gives better charging characteristics (see Figure 75). The quality of electroless plating was observed by measuring the resistance of the plated tracks. It was found that shape of copper particle filler influences the resistance of the tracks formed with higher resistance for spherical particles to flat flake (see Figure

59b). It was also found that the resistance of the track is proportional to the amount of copper in the original toner.

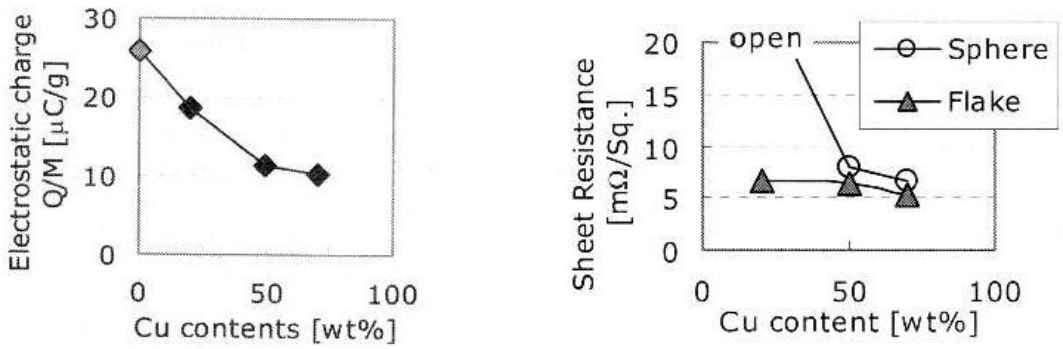

Figure 75(a): Triocharging vs Cu content & (b): Influence of particle shape on resistance

For this feasibility study the toner was formulated by grinding the copper filled epoxy resin to produce powder which was then mixed with a ferrite carrier to produce a dual component toner. Printing trials were conducted using dual component engine with a 600dpi resolution. The formulation of the toner particles and the carrier was optimised to make it more negative charging (see Figure 76).

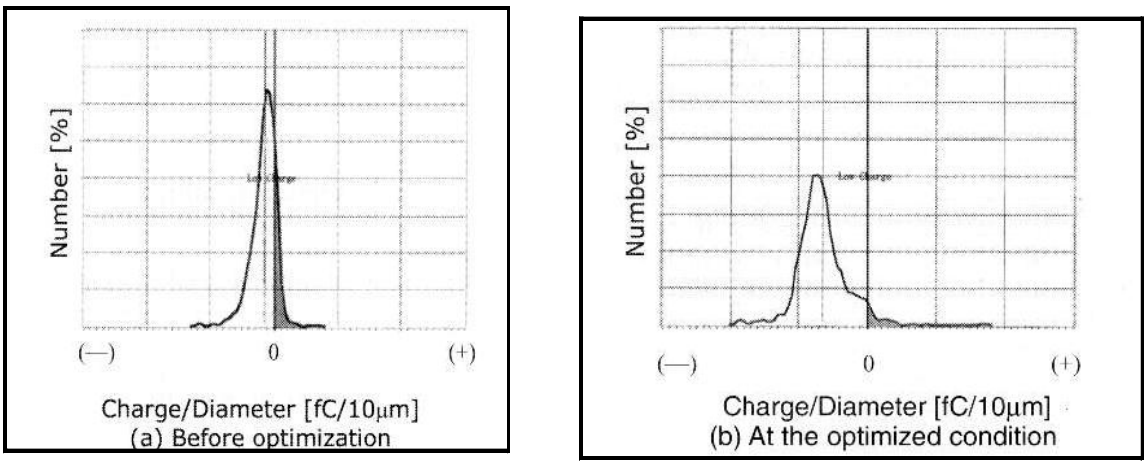

Figure 76 Electrostatic charging of seed toner, before (a) and after (b) optimisation

It was also observed that the flatness of the printed toner was improved when fused at 160^{o}C (Ra 0.6μm) compared to fusing at 100^{o} C (Ra 2.3μm).

The potential to generate multilayered PCB's and the subsequent soldering ability were also investigated and it was concluded that; Lines with 0.3mm pitch with 0.12mm width could be printed

using optimised charged seed toner using a 600dpi print engine. After applying electroless copper plating the resistance of the tracks was found to be 2mΩ/cm using this process. A connection between two copper layers was also generated which demonstrates the capability of the process to generate multilayer structures.

2.7.12 Research on Laser Printing of Ultra-Fine Solder at Georgia Institute of Technology

Anthony Walker at Georgia Institute of Technology carried out a feasibility study to assess the potential to deposit solder using Laser printing technology (Xerography) – see Figure 77. This paper compared the advantage of xerography process compared to standard stencil printing based approach which suffers from non-uniform printing, lack of repeatability particularly for ultrafine pitch applications. Several scoping trials were conducted coating the solder particles with dielectric material to enable them to be printed. The tribo-charging characteristics of the solder toner developed was analysed further and induction charging was also applied to produce an electrical field for this process.

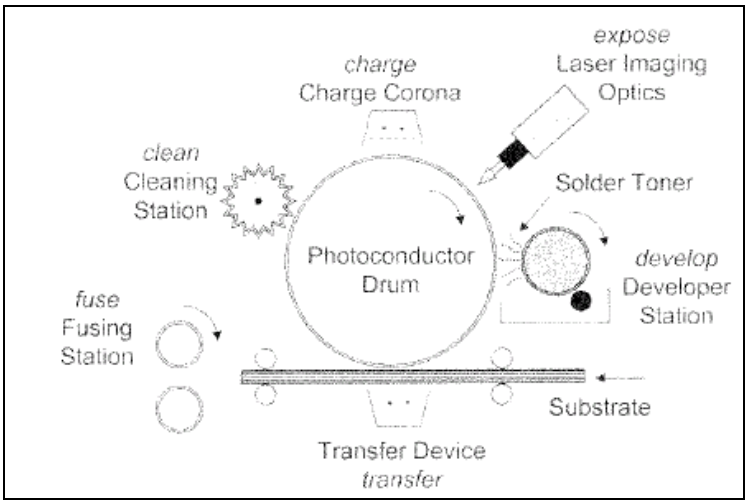

Figure 77 Schematic of xerography process using solder toner

The trials conducted successfully demonstrated the potential of this process to achieve very fine pitch prints compared with conventional stencil printing and the results indicated significantly better volume of deposited material across the substrate. It is proposed to use a laser printer to deposits the ultrafine pitch solder in the form of dry powder and then a stencil printer would be used to deposits solder paste on the remaining bond sites. The challenges associated with coating metallic toner particles with dielectric material was to provide a complete uniform coating as any exposed conductive material prevents effective printing due to discharging. Uniformity of thick dielectric coating is very important and the coating should have sufficient strength to withstand the contact force

while mixing in the hopper. It was also mentioned that final charge transfer from OPC drum on to the substrate (PCB) using standard electrostatic charge transfer should be investigated (this research employed hot tack transfer).

The potential of this process to achieve very fine pitch prints compared with stencil printing and had significantly better volume control over the substrate. Laser printer deposits the ultra-fine pitch in the form solid brick and stencil printer then deposits the bulk solder on the remaining bond sites. The paper mentioned the challenges associated with dielectric coating of metallic toner as with small amount of exposure of metallic toner, the particle would be discharged very quickly.

2.7.13 Biomedical Research Work - Amino Acid Toner Printing

Research group headed by Dr Stefan Guttle at Fraunhofer Institute Manufacturing (Germany) developed a novel manufacturing technique to produce peptide arrays for an advanced biomedical research by printing amino acid toner particles using standard laser printer [Guttle 2008]. The peptides are synthesized layer by layer from amino acid building blocks on a glass slide. The amino acid toner first printed on a coated glass substrate and thereafter heated up to 90^{o}C. After the heating the second layer of amino acid toner is allowed to print on top of the earlier solid amino acid layer using the test rig (see Figure 78). Process is repeated to form peptide arrays. This process found more flexible compared to the current standard process available to form peptide arrays.

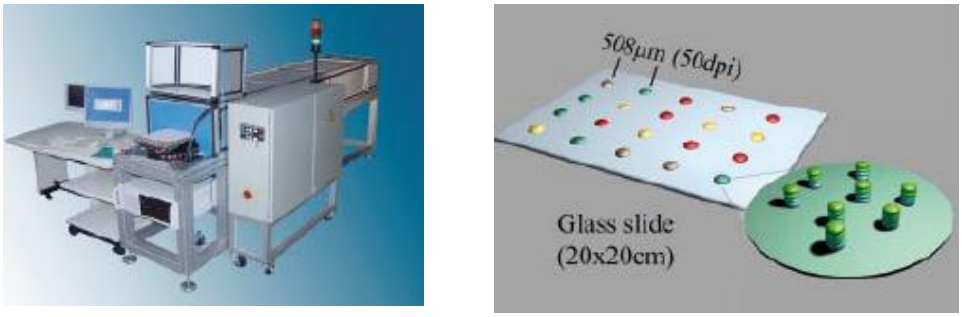

Figure 78 (a) Test rig at IFAM Germany & (b) Peptide arrays on plate (Schematic)

Laser printer was used as an efficient micro-dispensing tool to form peptide arrays with the help of toner particles that contain chemically activated amino acid building blocks within the toner matrix. These amino acid particles inside toner matrix have similar physical properties compared to commercial colour toners which helped them to print on glass substrate. The spots of different toners were printed in an array pattern onto a coated glass slide and each single spot found well separated from others.

Then the slide was removed from the printer and the plate was heated up to about 90°C. The toner particles then melted and turned into a solvent. The embedded amino acids are released from the matrix to diffuse and couple to the coating of the support. The toner matrix and excessive reagents washed away, and the coupled amino acids are deprotected and finally single layer of all different amino acids is immobilized on the glass slide. The complete cycle of synthesis is shown below (see Figure 79).

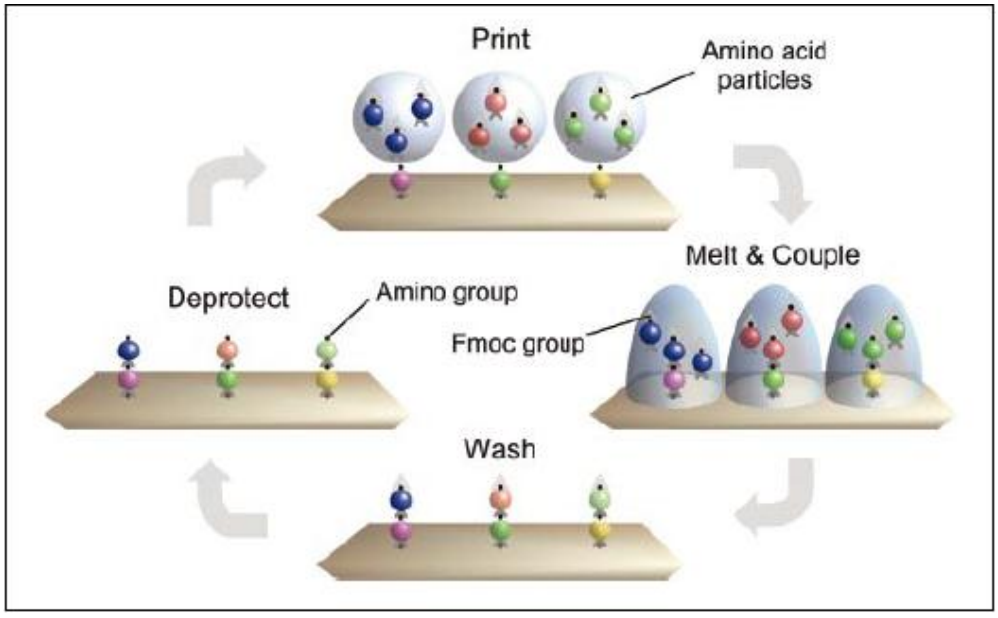

Figure 79 Cycle of synthesis includes printing of the amino acid toners (a),coupling of the amino acids by melting (b), washing (c), and deprotection

During printing, the amino acid particles are processed in a dry state preventing any undesired premature chemical reaction. The coupling reaction is initiated in a controlled manner by heating the printed support which was outside the printer.

After first cycle of synthesis, the glass slide is to be placed into the printer to print next layer .Second layer of amino acid toner is then printed exactly on top of the first. Again the cycle of coupling, washing, and deprotection to be carried out and finally it would result in chains of two amino acids coupled onto the glass slide. After printing and coupling for 12–20 times, more than 155,000 individual peptides of the corresponding length can be synthesised in parallel on a glass slide of 20 by 20cm. Compared to the current state of art, laser printed peptide arrays have a much higher density, i.e. they contain significantly more different peptides and thus have significant structural diversity in a given area.

2.8 Introduction: EU Frame 6- Custom-Fit Project

The aim of this chapter is to explain the background of the research presented in the thesis in respect of hardware development undertaken by the author within the EU funded Custom-Fit project. The results of the work help explain the machine concept and the link to the materials and processing experimental work conducted in the PhD trials.

2.8.1 Overview of the Project

'Custom–fit' (EU FP6 Integrated Project Number 507437) was a four and half year research project (Sept 2004 to March 2009) funded by the EU to develop new systems for the production of individually customised products. The aim of the project was to create a fully integrated system including scanning, design, production and supply of individualized custom fitting products. As part of this project several new Additive Manufacturing machine concepts were developed. One of these new methods, the Plastic Powder Printing (PPP) process, was based on the selective deposition of thermoplastic powder by laser printing, which is then fused using a radiant infrared heat source. Initial research was conducted at DeMontfort University and then MTT Technologies Ltd and CTG Gmbh joined the Custom-Fit project to develop a commercial process based on the PPP approach, this was later renamed Selective Laser Printing (SLP).

2.8.2 Development of the Selective Laser Printing Process

2.8.2.1 Print Engine Selection

The strategy of the project was to develop the lab scale test rig first. Later this test rig would be scaled up to provide a demonstration test rig if the initial test results proved to be promising. Selecting appropriate printer hardware was the first important step for the SLP machine development. Printer hardware and toner material must be closely matched (for example magnetic/nonmagnetic, mono/dual component, positive/negative polarity) and the fusing method.

Hewlett Packard developed the first generation 'Laser jet' printers where the print cartridge was integrated with photoconductor drum, toner hopper and cleaning rollers, all located inside the cartridge. Work undertaken by Cormier had already demonstrated that polyethylene toner can be deposited using a LaserJet 4 printer and on this basis early material development in the Custom-Fit project utilized LaserJet 4 printers. However, for the development of the test rig it was decided to select a printer (Lexmark C510) with a more flexible architecture, which had an intermediate transfer belt and OPC belt thus avoiding direct contact between the moving substrate and OPC surface thereby reducing the risk of mechanical and thermal damage as shown in Figure 80.

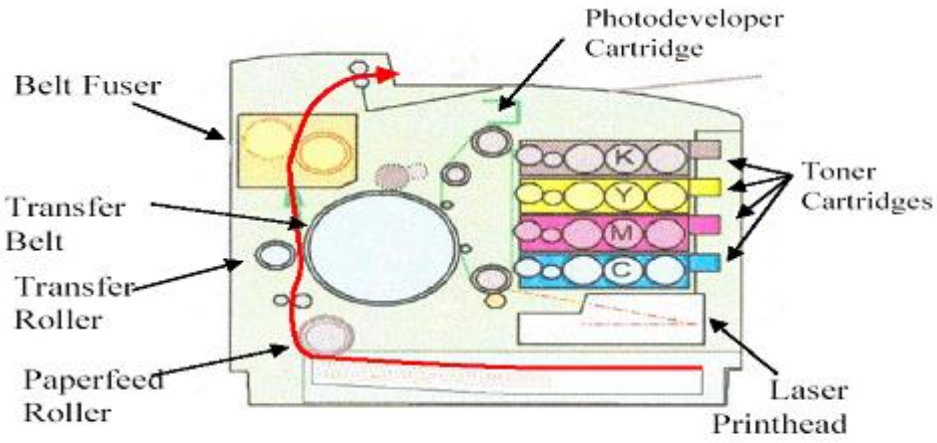

Figure 80 Schematic diagram of Lexmark C510 image transfer mechanism with intermediate transfer roller

The paper feed and thermal fusing unit was completely removed from the printer to give direct access to the transfer roller. Figure 81 shows the fuser unit which was externally connected with printer hardware. The printer was rotated through 90^{o} to allow a build platform to move in a linear path below the unit and make contact with the transfer roller. Another major element of work undertaken was to isolate the internal sensors that control the printing process, either by disconnecting them or providing a "dummy" input signal which simulates the printing operation under normal conditions. The motion controller for the build platform was integrated with the printer controller to enable the printing and build motion to be properly sequenced.

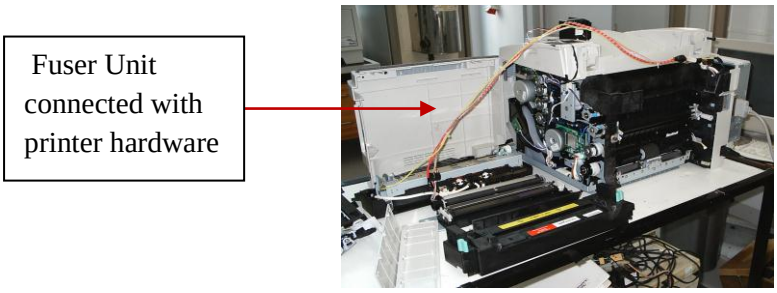

Figure 81 Lexmark C510 printer after removal of fuser unit and , intermediate rollers

2.8.2.2 Motion Control

The build platform motion was achieved through an electro-pneumatic system. The velocity of the build platform was controlled through adjustment of the air pressure to match the circumferential velocity of the transfer belt. This speed adjustment was important to avoid any distortion of images while printing on a movable build platform /substrate. An SMC Pneu-Alpha controller (ECC-PNAL-20MR-A) was used to control the motion of the build platform, operating as a slave to the printer which was selected as the master controller. Proximity sensors, triggered by the motion of the build platform were incorporated to provide the key input to the SMC controller.

2.8.2.3 Infrared Heating System

An infrared radiant heating unit was used to heat and thermal fuse the loose powder layer deposited on the build platform. A medium wavelength infrared unit was selected for the test rig development as shown in Figure 82. Medium wavelength was selected as this should provide more efficient heating and fusing of a polymer powder compared to shortwave IR radiation. The duration of exposure of the loose powder to the infrared heat source was controlled via the SMC controller.

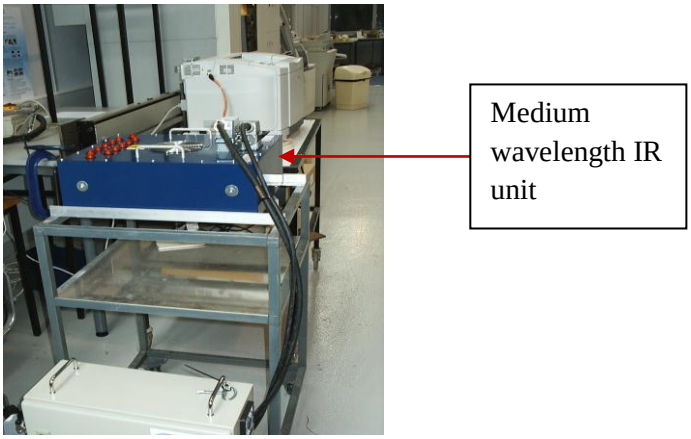

Figure 82 Infrared units for toner fusing

This approach provides a very flexible heating method and avoids direct contact (and possible back transfer/contamination) using a conventional heated fuser roller.

2.8.2.4 Levelling Roller

The top surface of the printed layers needs to be smooth and flat while depositing multiple layers using SLP process. The levelling roller was required to smooth and flatten the top surface of the deposited powder layer using heat and pressure prior to infrared sintering. The standard fusing roller from the Lexmark C510 printer was removed and placed between the print engine and infrared heating unit. This roller was selected as it had a non-stick coating, which would not pick up any

powder particles as shown in Figure 83. The temperature of the outer surface of roller was controlled (reduced below the conventional toner fusing temperature) using a thermostat. The roller was rotated using a small geared dc motor directly connected to the roller .The speed and direction of rotation of levelling roller was adjusted to match that of the build platform.

Figure 83 Heated levelling roller for Test Rig

The schematic arrangement of the machine concept was developed by author as shown in Figure 84 where the kinematics of the test rig is shown in arrows in sequence starting from step number 1 to 4 .

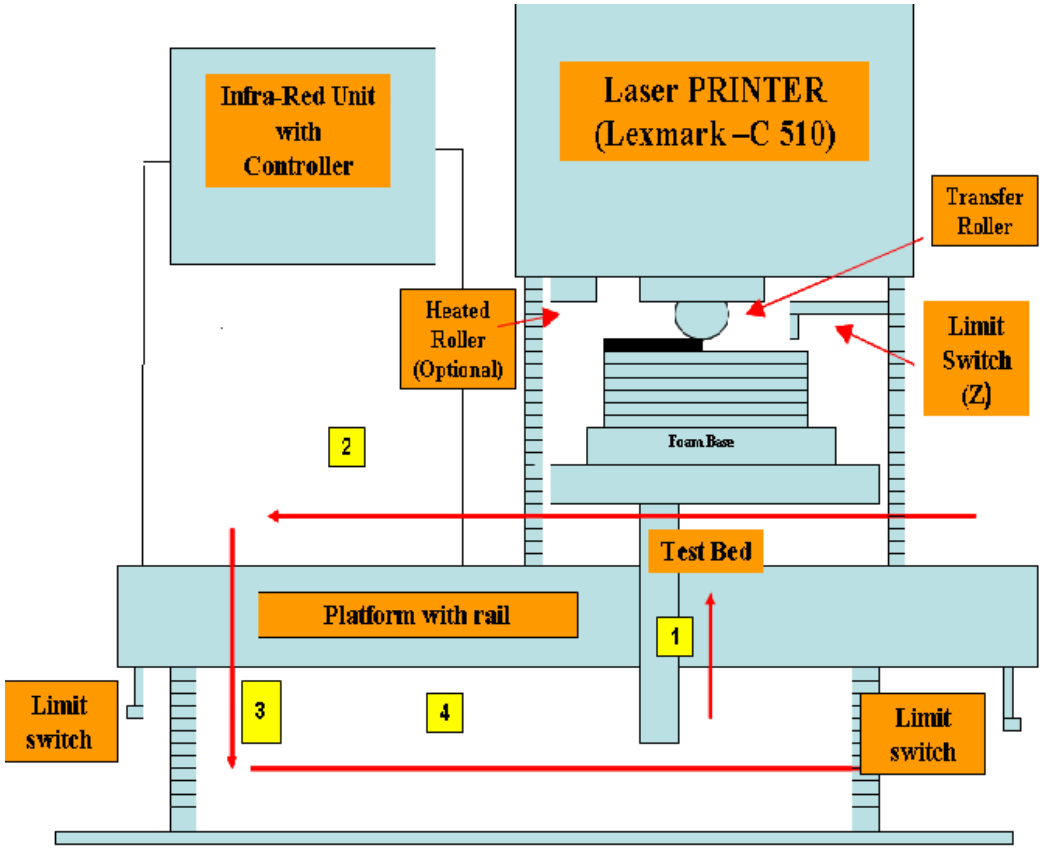

Figure 84 Arrangement with Lexmark printer and build platform

Kinematics shown in steps (highlighted with red arrow) from step number 1 (home position) to step number 4

2.8.2.5 Build Platform

In conventional printing using the C510 the paper substrate is normally pressed against spring-mounted rollers to provide the desired contact pressure with the transfer roller. The build platform for the test rig was designed to replicate this "cushioning" effect using a series of foam pads mounted on the platform. Initial test showed very poor toner transfer efficiency in the absence of the cushioning layer.

2.8.3 Single Layer Printing (Transfer)

Initial testing was conducted using conventional (80g/m^2) plain white paper mounted onto the top of the build platform using the test rig developed by author as shown in Figure 85. In the first trials transfer of the toner via contact alone (ie no electrostatic or tackyfication) was evaluated. As expected there was very limited toner transfer via van-der-walls forces/ mechanical adhesion (through pressing of the toner into the texture of the paper). A sheet of aluminium foil was then placed beneath the paper substrate and a positive charge was applied using a Brandenberg 477 high voltage source. The positive polarity charge attracted the negatively charged standard black toner onto a sheet of paper, as in conventional laser printing.

Figure 85 First Test rig at DMU on SLP

2.8.4 Multiple layer prints and 'Z Height Problem'

The aim of the second trial was to replicate trials conducted by Kumar and confirm that the efficiency of toner transfer using a charged substrate depends upon the number of printed layers deposited. A printed solid square (50x50mm) was printed onto the substrate using conventional black toner. The weight of toner deposited for every 10 printed layers was measured. In addition the weight of an unprinted "dummy" paper substrate was measured throughout the trials, in order to compensate for the effect of moisture loss in the paper (drying due to thermal fusing) on the weight measurement. It was found that after less than 20 layers of prints, the weight of the toner reduced almost exponentially

(see Figure 86). The cumulative weight of toner also recorded and a sharp decrease in weight also recorded. This was expected and results were found similar to the earlier observations made by Kumar.

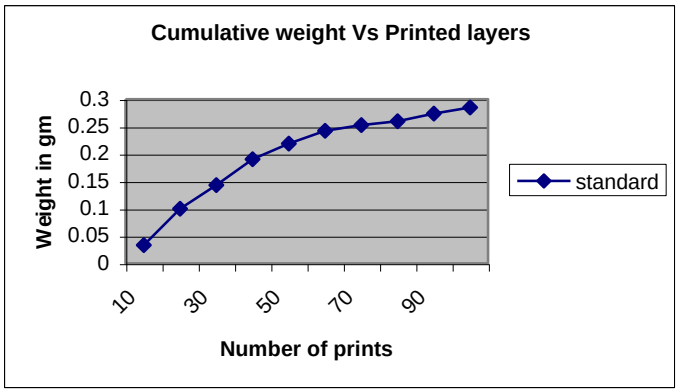

Figure 86 Cumulative Weight vs. Number of Prints

2.8.5 Methods explored to overcome the 'Z height' problem

Although trials by Kumar have shown that charging the top surface of the deposited toner layer helped to improve the toner deposition efficiency it was not possible to completely resolve the problem of charge depletion and the maximum height of sample produced using this approach was only 2.5mm. Two alternative approaches were investigated in the Custom-Fit project; the use of an electrostatic force of repulsion on the final transfer roller and tackyfication.

2.8.5.1 Electrostatic Repulsion

Using an electrostatic force of repulsion on the final transfer roller/belt instead of an electrostatic force of attraction beneath the substrate was considered to overcome the z height problem (Zimmer, Waldemar, Auchter, Jung ,2002). Using the repulsion technique, the toner particles would be pushed using electrostatic force (using a static charge with same polarity of toner particles) from the surface of the transfer roller and is deposited onto the substrate. There is no information in the public domain on the results of trials utilising the repulsion approach.

In order to apply an electrostatic charge to the final transfer belt adaptation to the test rig was required. The transfer belt runs on a large drum(A) is in contract with the OPC and then a small roller (B) is in contact with the paper as shown in figure 87 . A third spring-loaded roller (C) is used to maintain the tension on the belt. The roller which is normally in contact with the paper/substrate was insulated with two nylon bush so that any repulsion charge could not be dissipated through the frame of the printer as shown in figure 88 .

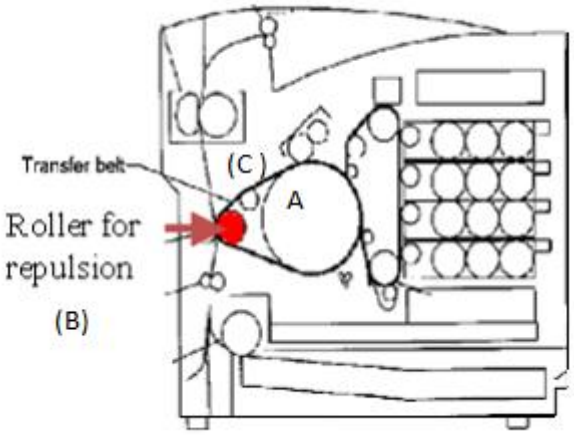

Figure 87 Schematic standard transfer roller

Figure 88 standard transfer roller fitted with Nylon bush (non-conductive) around the main shaft

The static charge of negative polarity (-2kV) was injected on to the transfer roller via Brandenburg 477 series of static charge unit as shown in figure 89 below. This would create an electrostatic force of repulsion as standard toner was negatively charged as well. The magnitude of the voltage was controlled using Brandenburg 477 series up to -3kV for this experiment.

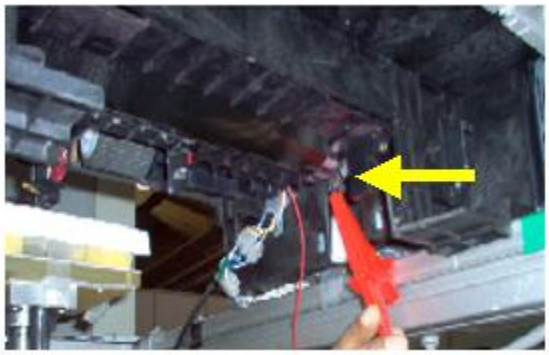

Figure 89 Voltage injection on supporting roller using Brandenberg 477 series voltage source

The layer thickness with standard toner of Lexmark C510 is 5 – 7µm. 'Bmp' image of rectangular block of 30 x 70 mm size was printed using repulsion mechanism applying 1.8 to 3 kV voltages on the transfer roller with negative polarity. Total 150 numbers of prints (multiple layers) were carried out and the weight of each successive 10 prints was recorded. The weight loss due to moisture vaporization was corrected using a dummy substrate. The weight of each successive 10 printed layers was recorded, as shown below (see Figure 90). The graph shows the weight of printed surface against the number of printed layers for both standard attraction (pulling effect) and repulsion principles (pushing effect).

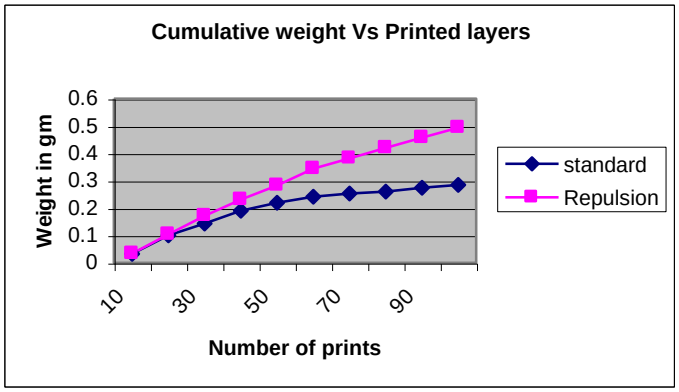

Figure 90 Weight of deposited toner against the number of prints using standard and repulsion approach

Figure 90 as shown above shows a slight improvement in deposition efficiency while printing multiple layers with repulsion mechanism compared to standard electrostatic attraction mechanism of toner transfer. After 50 printed layers there was only a 20% drop in transfer efficiency compared to 33% for the standard arrangement using an electrostatic force of attraction. This difference is more clearly shown when the cumulative weight of 150 printed layers is compared, where there is a 40% difference in the values for the two arrangements. Indeed the graph of weight versus number of printed layers for the electrostatic repulsion is almost linear.

Although the electrostatic repulsion method showed significant promise, further work is required to perfect this approach and it was decided due to lack of time to pursue an alternative approach based on tackyfication.

2.8.5.2 Alternative Solutions: Bynum Approach (Tackifying)

David Bynum mentioned about the tackifying method to overcome this Z height problem. This tackifying process is combination of heat and pressure while depositing multiple layers (US 5088047). There is no evidence that Bynum pursued any research work or commercial exploitation of the process.

Although this approach was mentioned earlier but no proper experiment was cited using this method. Test rig was used to study the feasibility of Bynum approach to solve the 'z height problem'. The test rig based on the Lexmark C510 was found to be unsuitable for the tackyification trial.

It was decided to undertake all further laser printing trials using a commercial dual component printer as this provides increased flexibility in terms of toner type and moreover the thickness of the deposited layer is much greater (~30µms compared to just 5 µms for the Lexmark C510). Tackifying experiments were conducted to print multiple layers by applying heat and pressure using a dual component print engine (CTG 900) incorporated into an industrial glass-coating unit developed by CTG GmBH. A 10 mm thick ceramic substrate was selected for the printing trials. The ceramic substrate was heated to approximately 160^{o}C inside an oven. The preheated substrate was then removed from the oven and the temperature of the top surface was monitored. At the point where the temperature of the surface was precisely 150^{o}C the printing command was given to deposit toner onto the substrate. The contact pressure between transfer roller and top layer of printed surface was adjusted by controlling the gap between the top surface of the substrate and the transfer roller. After the printing of first layer of powder, the preheating process was a repeated and further layer of toner deposited.

Using this approach a 2mm thick tensile test samples were produced, without any appreciable drop in toner deposition efficiency after 50 prints as shown in figure 91. This trial indicates that the tackyfication process provide a viable method of producing 3D objects (albeit that the samples produced were only 2mm thick). The potential to use an infrared heat source instead of oven to raise the temperature of the printed polymer powder/toner should be considered (Banerjee, 2006).

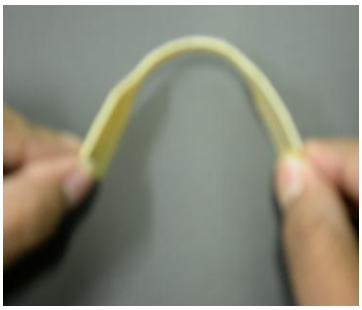

Figure 91 Laser Printed Tensile Specimen with Somos 201 Powder

2.8.5.3 Demonstration Test rig

The results of the initial trials using the 'Bynum approach' were encouraging. A more sophisticated demonstration rig was designed and manufactured in collaboration with MTT Technologies Ltd and CTG Gmbh as shown in Figure 92 and 93. This rig was developed to undertake further trials in the Custom-Fit project. The demonstration rig is equipped with two industrial laser duel component print engines (based on an CTG 900), one for build and the other for support material, and two medium wave infrared radiant heating units, one to fuse the deposited toner layer and the other to preheat the deposited layer to the appropriate tackyfication temperature prior to printing the next layer. The print engines were developed specifically by CTG for the demonstration unit. They have the same architecture CTG900 heads used in the initial tackyfication trials but are narrower (450mm rather than 900mm) and the units were designed with unique features (requested by the author whilst employed by De Montfort University) such as externally controllable voltage setting at every stage of the image development and toner transfer process. In addition, a conditioning roller (intermediate between the OPC and developing roller) was incorporated to help deposit a thick uniform powder layer on the top surface of OPC drum. This conditioning roller was patented by CTG to enhance the powder deposition on final substrate providing uniform layer thickness across the OPC drum. The basic design/engineering work for the test rig, including drive selection, specification of the IR radiant heaters and process logic for the control of the sequencing were finalised.

TPE (Somos 201) powder were formulated and deposited using this demonstration test rig. Deposited powder particles were fused using infrared heat source as shown below (See figure 92 and 93). The demonstration unit was used to produce demonstration components for the Custom-Fit project based on the previously developed Somos201 toner powder.

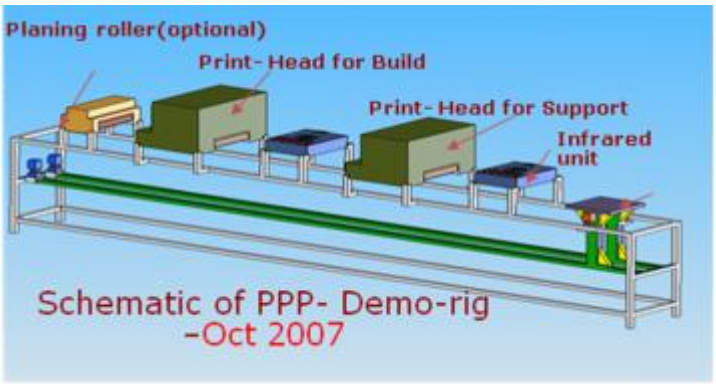

Figure 92: Demonstration Test rig (Schematic-Design Stage)

Figure 93 Demonstration Test rig (SLP Process)

The hardware development (critical to demonstrate the feasibility of the SLP process) was conducted in parallel with the toner materials and process development research. The conceptual test rig was prepared based on initial trials as described in section number 6.2 (see Figure 92). Later the Demonstration test rig was prepared (see Figure 93). The focus of the attention in this thesis will be on the materials and process research, which successfully led to the development of the Somos 201 toner. This is described is in detail in Chapter 3 under experimental methodology.

3.0 Chapter 3 : Experimental Methodology

The hardware development described in Chapter 6, was conducted in parallel with the toner materials and process development research which is the focus of this PhD study.

3.1 Contribution to the Body of Research:

Although the potential of electrophotography in Additive Manufacturing has been recognised by several research groups, to date, limited progress has been made with respect to the development of a technically viable process for the production functional 3D parts. Polymers commonly used for toner manufacture are extremely brittle. This property is useful for conventional toner manufacturing as rapid grinding can take place to produce fine powders as explained in earlier chapter .Unfortunately, conventional toner is not suitable for the production of 3D objects in layers as this material is prone to cracking due to the accumulation of thermally and mechanically induced stresses (Figure 94).

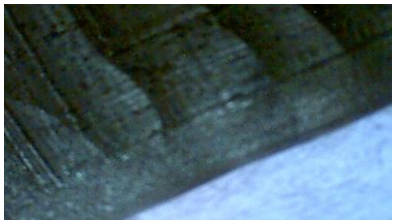

Figure 94 Surface cracks after 15 prints with standard non-magnetic toner (Lexmark C510)

This project represents a significant step towards the development of a commercial Additive Manufacturing process based on electrophotography by providing a clear route through to the manufacture of toners suitable for functional polymeric parts.

In terms of novelty there are several unique elements to this project;

- Development of a suitable dual component toner for the SLP process based on Somos201 (PBT based polymer – see appendix for details).
- Development of a flexible manufacturing route for tough toners.
- Investigation of the properties of dual components toners developed for the SLP process.

3.2 Overview of the Experimental Methodology:

Scoping Trials	
Description of trial	**Objective of trial**
Grinding trial	Assess the feasibility of producing fine powders suitable for the development of experimental toners from a range of tough engineering polymers.

Surface coating trial	Establish if suitable flow and charge properties could be obtained by surface coating flow /charge control agents onto the surface of polymer particles.	
Main Trials (SOMOS 201)		
Analysis	**Description**	**Objective of trial**
Particle size analysis	Particle size characterisation	To assess the particle size distribution of off-the- shelf Somos 201 powder.
	Grinding trial	Assess the feasibility of using a range of mechanical milling methods for producing fine powders suitable for the development of experimental toners using Somos 201. The following mechanical milling techniques : • Ball milling • Cryogenic milling • Airjet milling • Impact milling
	Classification trial	To assess the efficiency of separating particles of the appropriate size from off –the-shelf Somos 201 powder
Flow & charge analysis	Charge measurement of **uncoated** Somos 201	Assess the polarity/tribocharging characteristics of off-the-shelf Somos 201 powder.
	Surface coating trials	Establish if surface coating using FCA can improve the flow characteristics of Somos 201 particles.
	Charge measurement of **coated** Somos 201	Assess the polarity/tribocharging characteristics of surface coated Somos 201 powder
Printing trials	Initial trials using HP LaserJet 4	Assess the most appropriate particle size and surface additive concentration for printing the experimental Somos 201 toner
	Dual component print engine trials	Fine-tune the particle size and FCA coating (fumed silica) for an industrial dual component print engine
Fusing & mechanical property trials	IR set-up optimisation	To establish the most appropriate stand-off distance between the IR radiant heat source and surface of Somos 201 powder layer.
	Effect of particle size of IR fusing	Assess the influence of particle size on the thermal fusing of uncoated Somos 201 powder using the IR radiant heat source by comparing the tensile properties of sintered samples
	Effect of surface coating on IR fusing	Assess the influence of surface coating of FCA (fumed silica) on 17 and 30μm sized particles of Somos 201.
	Oven sintering trials	Establish if the FCA is affecting fusing by changing the IR sensitivity or by acting as a barrier to fusing between the Somos 201 particles

Table 12 Experimental methodology (Approach**)**

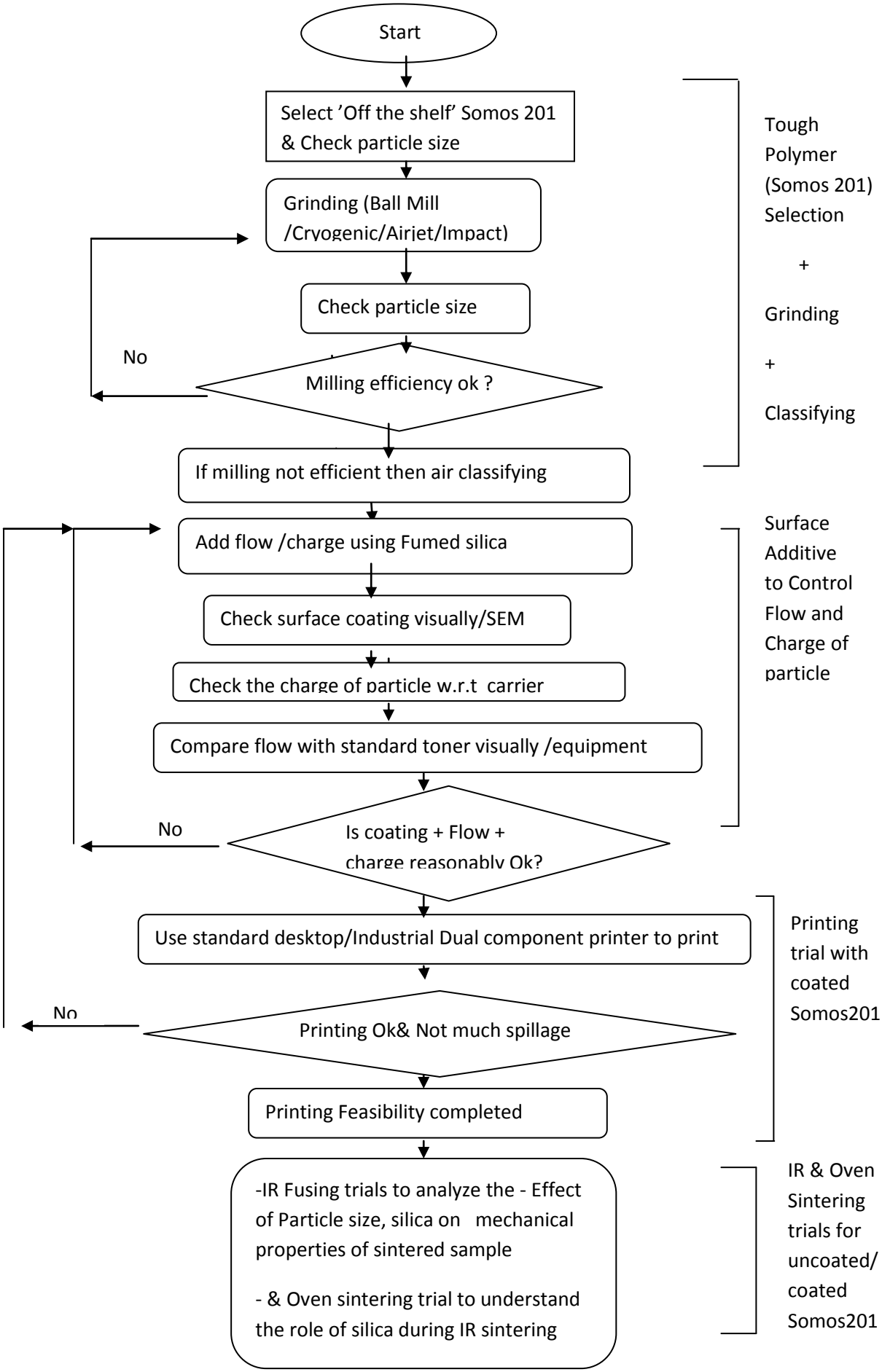
Start
Select 'Off the shelf' Somos 201 & Check particle size
Grinding (Ball Mill /Cryogenic/Airjet/Impact)
Check particle size
No
Milling efficiency ok ?
If milling not efficient then air classifying
Tough Polymer (Somos 201) Selection
+
Grinding
+
Classifying
Add flow /charge using Fumed silica
Check surface coating visually/SEM
Check the charge of particle w.r.t carrier
Compare flow with standard toner visually /equipment
No
Is coating + Flow + charge reasonably Ok?
Surface Additive to Control Flow and Charge of particle
Use standard desktop/Industrial Dual component printer to print
No
Printing Ok& Not much spillage
Printing Feasibility completed
Printing trial with coated Somos201
-IR Fusing trials to analyze the - Effect of Particle size, silica on mechanical properties of sintered sample
- & Oven sintering trial to understand the role of silica during IR sintering
IR & Oven Sintering trials for uncoated/ coated Somos201

3.3 Justification & Description of Methodology

3.3.1 Scoping Trial

Initial scoping trials were conducted using a range of thermoplastic polymers (PE, PP). These materials were selected based on their mechanical properties in order to generate toners which are suitable for the manufacture of functional 3D objects. Previous work has shown that conventional toner materials are too brittle for the production of multilayer objects (Figure 75). The production of experimental tough toners for this project using the chemical production method is not feasible due to the process complexity, the significant capital investment required and the very limited range of polymers presently available. Moreover, chemically produced toners are more suited to the production of very fine powder particles which although suitable for conventional printing applications will result in a lower production speed for the SLP process due to the thin layers. The production of conventional toners using a milling process is well established, simple and relatively efficient. Unfortunately, conventional toner materials are brittle so there was concern that it would not be possible to generate fine powders using tough toners. To establish the degree of difficulty, mechanical grinding trials using a range of methods including cryogenic grinding, will be conducted.

To provide the appropriate properties trials will be conducted to establish if it possible to apply surface coatings of FCA/CCA directly to the surface of polymer particles (rather than integrate CCA inside the toner particle as with conventional toner production). This will also provide a novel, low cost and extremely flexible method of generating experimental tough toners for the SLP process.

In addition to establishing the most favourable material/surface coating agents to employ in the main trials, these trials also provided a robust methodology for experimental toner material development, which was applied in subsequent trials.

3.3.2 Main Trials

Based on the results of the scoping trials a tough rubber like thermoplastic materials Somos 201 was selected for the subsequent main trials due to its charge characteristics and mechanical properties (see Appendix G). Detailed particle size analysis will be performed on this selected material including; particle characterisation by sieving and laser diffraction method. A range of mechanical milling techniques will be assessed to reduce the particle size of the off-the-shelf Somos201. Then classification methods will be used to remove the oversized and undersized particles to leave material which is suitable for laser printing.

Charge to diameter (Q/D) trials will be undertaken to assess the polarity/tribocharging characteristics on the uncoated Somos 201 powder. To provide the appropriate flow control properties surface coating trials will be performed with an industry standard FCA. Further Q/D tests will be performed

on the coated Somos 201 powder to ensure that the application of the FCA has not adversely affected its polarity/tribocharging characteristics.

Printing trials would be conducted using both mono component (HP LaserJet4) and dual component print engines. This HP LaserJet4 magnetic print engine was selected as Denis Cormier used this particular type of printer while printing HDPE powder particles (Cormier 2002). The HPLaserJet4 is the first generation HP printer and was designed for larger particles (average particle size up to 12 to 15 μm) as a result of which the gap between doctor blade and developing roller is relatively large compared to modern laser printers. This large gap between doctor blade and developing roller provides the potential to print larger diameter toner particles which makes it more appropriate for SLP trials due to increased layer thickness. The architecture of the printer (15^{o} inclination from the toner hopper to developing roller) also seems to encourage the transfer of toner (even with relatively poor flow properties) towards the developing roller (see Chapter 4).

Subsequent trials will be undertaken on an industrial dual component laser printer due to the greater flexibility with respect to charge and particle size as well as providing more robust platform for the production of commercial SLP machine.

After established the printability of TPE powder next stage of the trials will be to optimise the particle size, degree of surface coating with fumed silica FCA and the stand-off distance between powder bed and infrared heating unit based on the mechanical strength of the parts produced for SLP process.

To assess the mechanical properties of the experimental Somos 201 toner, trials will be undertaken using a simple aluminium mould which was manually filled with the toner and heated to fuse the toner to produce tensile test specimens. Heating of the mould will be undertaken using an IR radiant heating unit which emitters primarily in the medium wavelength range (5 to 25 μm) as, in general, polymers absorb medium wavelength IR radiation more effectively. An infrared source with 12 emitters (bulbs), each having capacity of 1 kW, will be used infrared heat source for SLP process and these trials. The intensity of IR radiation is adjusted by feeding a square wave dc voltage into the lamps to provide different on-off times. It was decided not to laser print the samples at this stage due to the complexity and time associated with developing several toners to cover all of the parameters required to support this trial. Moreover SLP hardware development was being conducted in parallel with the trials and changes to the architecture of the equipment would have introduced variation in the samples produced.

Trials will also be conducted to establish the ideal stand-off distance from the IR heating units to the surface of the polymer during fusing. A balance must be reached between a small stand-off distance which would result in very rapid fusing of the layer (and thus high production speed of the SLP unit)

with the need to ensure even heating of the entire powder layer which would be achieved with the larger stand-off distance (thus reducing the influence of individual bulbs). As the intensity of infrared radiation decreases with the square of the distance (as per square law) the 3 distances are selected to assess the effect of radiation such as longer distance (228 mm from infrared source), minimal distance (128 mm from infrared source) and the balance between the two which would be 178 mm from infrared source.

After optimising the distance between infrared heat source and powder particle the next stage of the trial will be conducted to understand the effect of different particle sizes and level of surface coating (using FCA) to improve the mechanical strength of the sintered parts. Particle size plays a vital role in determining the printability of toners but also it is known (Scharfe 1984) that particle size can influence the ability to sinter polymer powders. For this reason trials will be conducted to establish the influence of particle size on the mechanical (tensile) properties of IR sintered Somos 201 samples. Material with a particle size between 17 and 30µm has been selected to as this representative of material which can be laser printed. Powder with an average particle size greater than 30µm is difficult to laser print due to difficulties to apply sufficient charge (ie charge to mass ratio) and also mechanical limitations of the laser print engines (i.e gap between the doctor blade and developing roller). Below 17µm it becomes increasingly difficult to obtain sufficient material (from Somos 201 feed stock) .Separating this Somos 201 material from the very fine particles (sub 5µm) is difficult and this leads to contamination of print engine as well. Moreover, the build speed of the SLP process will be undermined by the small layer thickness resulting from very fine toner deposition.

In addition to trials on uncoated powder, particles of Somos 201 will be mechanically surface coated using FCA. Two industry standard Fumed Silica FCA such as HDK30TX, TG308F were used for these trials as they are very common in toner industry. They will be applied in concentrations from 0.3 and 1.2% level, which represent upper and lower limits employed within the toner industry.

Oven trial will be used to establish if the surface coatings (FCA) inhibit fusing of the Somos 201 powder (by changing the IR absorption characteristics of the powder) or if FCA coating acts as a barrier to interparticle bonding.

The fused samples produced from all of these trials (coated/uncoated IR and oven sintered) will be subjected to tensile testing to establish the effect on mechanical properties.

4.0 Chapter 4 - Scoping Trial

The initial scoping trial was conducted to assess the processing of different thermoplastic polymers for the production of toners; this includes an assessment of grinding, surface coating and printing.

4.1 Grinding Trial:

The aim of this trial was to assess the ease with which thermoplastic materials can be mechanically milled/ground to produce particles of the desired size for toner production (between 10 to 25 µms). In the first grinding trial three common engineering thermoplastics were evaluated; Nylon (polyamide12), High Density Polyethylene (HDPE) and Polypropylene (PP). The results for these polymers were compared to a conventional toner material (styrene based polymer).

As air jet milling is the standard process of grinding for conventional toners, the first approach was to conduct tests with air-jet milling to produce 10-20µm particles size (which is close to conventional toner particle sizes accepted in toner industry). The milling trials were conducted at 'British Rema UK' using a laboratory scale air jet mill. The airflow for grinding was maintained at 135m^3 / hour, at a constant pressure of 6 bar, with a rotor speed of 11,500 rpm (these are the settings used for conventional toner and were employed to produce a benchmark comparison). Each sample was subjected to the grinding environment for approximately 30 minutes. Samples were analysed after each grinding trials. It was found that only 24% had been ground below 10µm for HDPE materials (see Figure 95) .

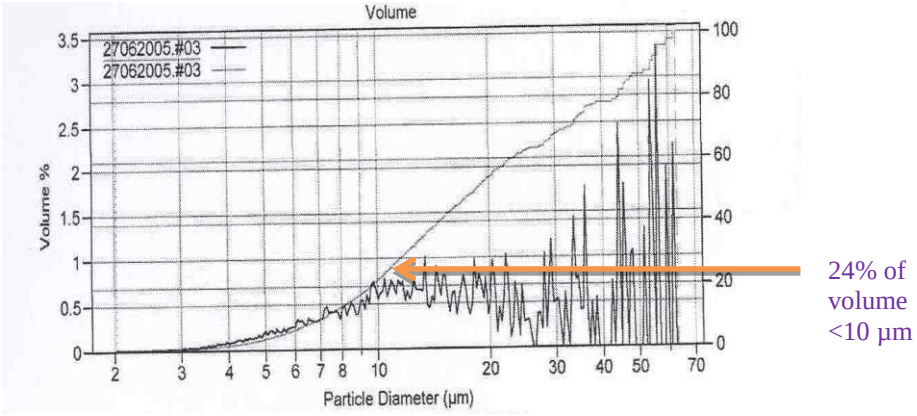

Figure 95 Air jet milling performance with HDPE pellets (57% volume under 20 µm)

Very poor grinding efficiency is found compared to that of standard brittle polymers used in the toner industry, which typically give a grinding efficiency of greater than 80% under the same conditions (see Figure 96).

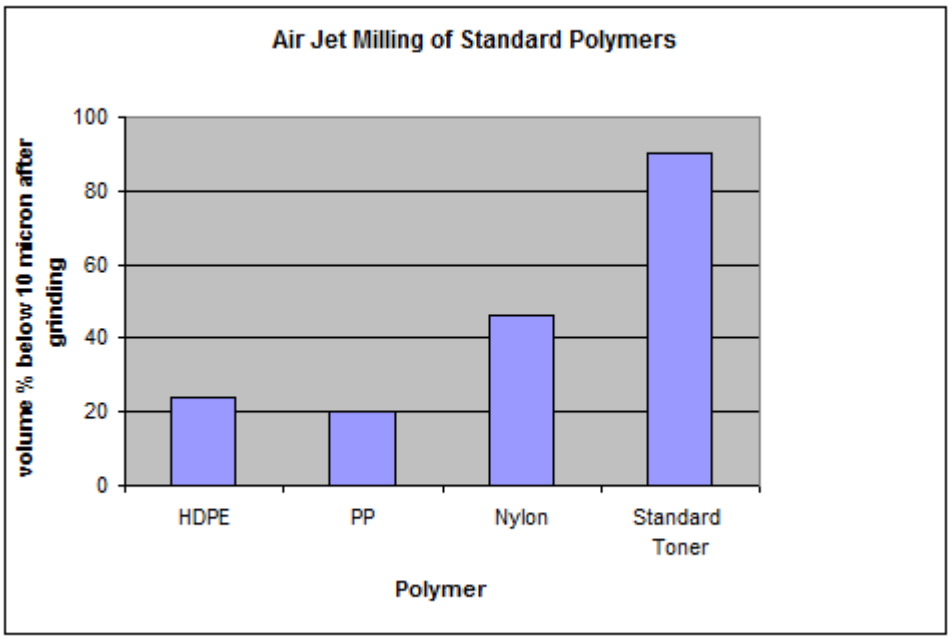

Figure 96 Air jet milling performance with different polymers

4.2 'Off-the-shelf' finer tough polymer

An investigation was conducted to see if it is possible to purchase standard engineering polymers as fine powder (under 20µm) "off-the-shelf" which could then be surface coated to provide the desired printing properties. Samples of low density & high-density polyethylene, nylon and polystyrene powder were sourced for the trial (Equistar chemicals US and EOS GmbH).

Sr No	Sample	Code	Particle size
1	HDPE (caking)	FA700	20 µm
2	HDPE (caking)	FARD3718	12 µm
3	HDPE (caking)	FARD3712	8 µm
4	Nylon (Polyamide 12)	Polymon 12/11	10 µm
5	Polystyrene	EOS-PS	50-90µm

Table 13 Materials and particle distribution

Melt Index (MI) is an indirect measure of mechanical strength (Lower the Melt Index, better the mechanical strength). The HDPE and PP selected for the trials are having reasonable melt index so that toner developed for SLP process can have better mechanical strength.

Polymer	Melt - index	density	Peak Melting temp (^{o} C)
HDPE	10	0.952	134
PP	35	0.909	163

Table 14 Melt index, density, Peak melting temp of polymers used for the trials

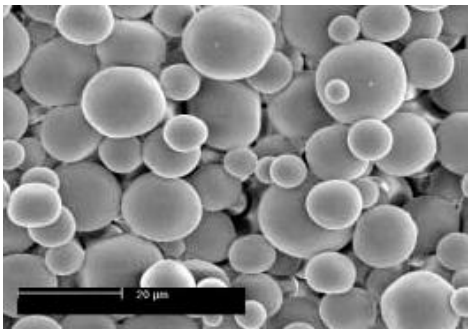

Figure 97 Microthene Powder

4.3 Surface coating of tough polymer

Surface coating is an important and highly specialised aspect of conventional toner manufacturing. It is based on controlled mixing of the additives and polymer powder to provide the desired level of surface coating, without mechanical or thermal degradation of the material. In this experiment several standard surface additives were investigated (charge control and flow control agents). Fumed silica, particle size 0.170 to 0.250µm, was selected as a main flow control agent. Fumed silica was selected primarily as it can control the flow as well as charge for conventional toner.

An Eiger Torrance laboratory scale mixer (model CKL Multi Mix) was used to coat the surface of the polymer particles by mechanical mixing. This mixer is commonly used in the toner development industry, as it provides precisely controlled mixing conditions.

HDPE, LDPE, Nylon and PS powder were coated with fumed silica TG308F (Cabot UK). The rotational speed and geometry of mixing blades carefully selected to encourage uniform coating of the entire powder sample. Special care was taken during the trials to avoid excessive heating of the powder during mixing, particularly at the higher mixing speed (>1500 rpm), as this can lead to coagulation of the particles

Trials were conducted with 1 - 2% fumed silica (TG308F/ HDK 20TX) to determine the optimised mixing parameters to achieve best coating on powder particles. This 1-2 % typical percentage of silica is used as this percentage of silica is not very uncommon in toner industry while developing conventional toner. Different mixing blades assessed and it was found that the "paddle type" blades gave better mixing efficiency than "shear type" mixing blades (see Figure 98). This is due to resultant vector of three velocity components in the horizontal and vertical plane while rotating, which encourages circulation of the entire powder samples through the mixing area. A rotational speed between 1500-2000 rpm was found to be the most appropriate to induce circulation of the powder to ensure even coating but without overheating. SEM photographs of coated particle have shown uniform surface coating as shown below (see Figure 99).

Figure 98(a) Lab scale mixer & (b) Paddle type mixing blade

Samples were then tested under surface electron microscope (SEM) to check coated polymers.

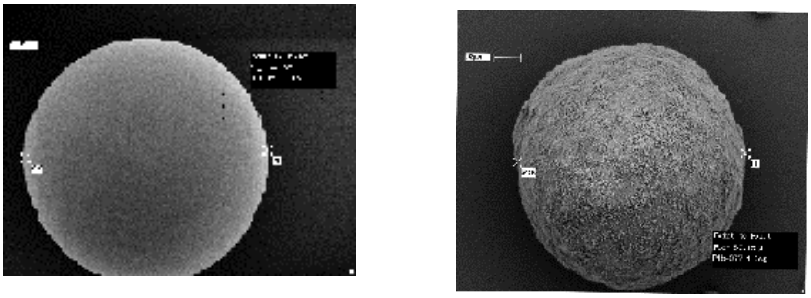

Figure 99 a) Uncoated polystyrene (b) Surface coated polystyrene powder particle coated with fumed silica

4.4 'q-test' with the surface coated polymer

The charge to mass ratio (q/d) and its polarity (+ve/-ve) are important factors to determine the printing characteristics of the toner particles. The q/d ratio of surface coated polymer samples was measured using Epping (Germany) charge measurement device and the values compared with standard toner material (Lexmark C510 yellow). The charge distribution of surface coated polymer samples (Nylon, PS, and HDPE) and conventional toner particles is shown in Figure 100.

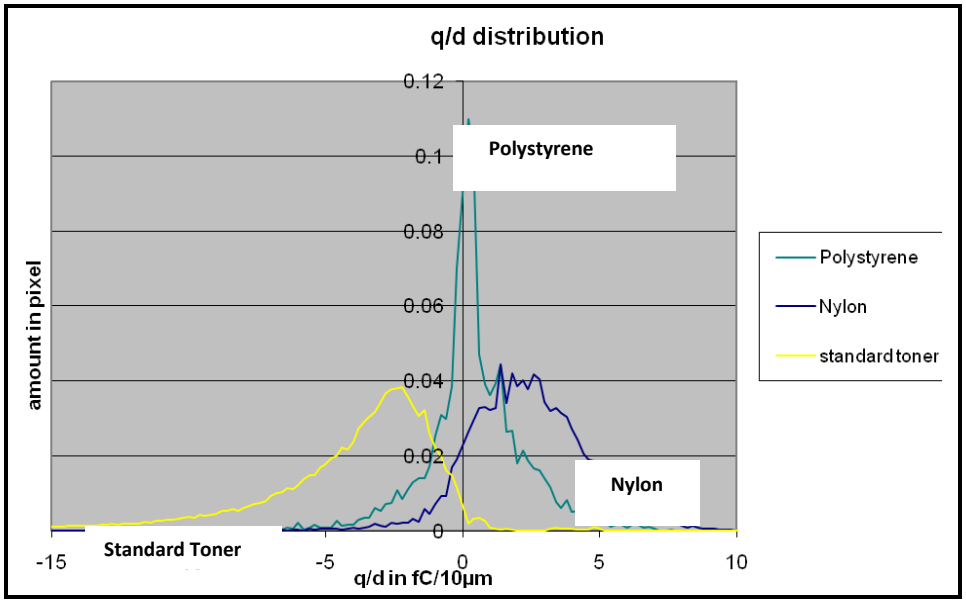

Figure 100 Charge distribution of Lexmark C510 toner, coated Nylon and Polystyrene

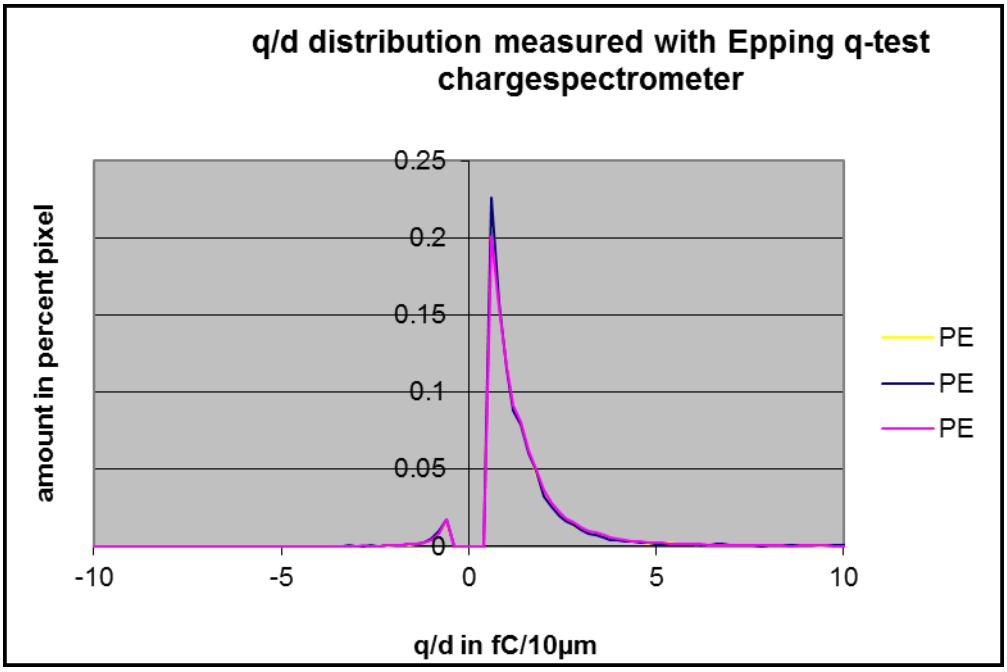

Figure 101 Charge distribution of FA 700 powder (HDPE)

The charging characteristics of the different polymer powders differed significantly. The Nylon, HDPE and polystyrene powder were all positive, with Nylon and Polystyrene demonstrating the greatest and least positive charge characteristics respectively. However, the standard toner (Lexmark 510-yellow) was slightly negatively biased, as would be expected as the majority of desktop laser printers employ negatively charged toner materials. This q-test result is important as it helps to select the correct combination of print engine and material formulation. The results of these trials form an important part of subsequent discussions in this thesis.

4.5 Printing Trials

4.5.1 Magnetic Cartridge of HP LaserJet 4

In these trials Cormier's work (using a HP LaserJet4) was repeated in a structured approach but in this case conventional FCA, rather than carbon black, was applied to the surface of the HDPE.

4.5.2 HDPE (FA 700) Printing trials with HP LaserJet 4

HP LaserJet4 printer is designed for negative charged toner. These printing trials were carried out using HDPE (FA700 material). This HDPE material was selected as Cormier mentioned the feasibility of developing tough toner based on HDPE particles. The toner particle size 20µm is as this higher particle size has advantage for SLP process to produce thicker layer thickness compared to standard toner. Because this material demonstrated a propensity to "cake" (lacks free flowing characteristics) the powder was blended with fumed silica TG308 F (approximately 1% by weight) using lab scale CKL multi-mixer to enhance its flow characteristics. The surface coated fine powder samples where then prepared for printing trials.

The melting point of the HDPE powder is higher than the conventional polystyrene based toners designed for the HP LaserJet 4 and thus it was decided to remove the fusing station from the printer to avoid smudging of the deposited powder image. The fuser unit was connected externally to the printer to avoid flagging any error messages.

Standard paper with blue background of 80 g/ m^2 (with correct dielectric properties) used for printing so that white powder printed on blue background can be easily identified. Paper was fed manually to print the surface coated HDPE powder particles. It was found that this material deposited onto the standard paper but unfortunately, a significant amount of toner leaked from the toner cartridge into the interior of the printer. This leakage contaminated both the OPC drum and the paper substrate (see Figure 102). The larger gap (approximately 100µm) between doctor blade and developing roller of HP LaserJet4 printer allows leakage of the non-magnetic, HPDE toner (in normal use the magnetic core within the developer roller prevents the conventional magnetic toners from leaking by holding it on the developing roller). In addition the thickness of the coating on the developing roller was found

to be lower than for conventional toner as development occurs only as a result of tribo-charging due to particles rubbing against the doctor blade and developing roller. The lack of CCA within the HPDE particles prevents ideal printing conditions from being achieved (as the HDPE is slightly more positive than HP LaserJet 4 standard toner).

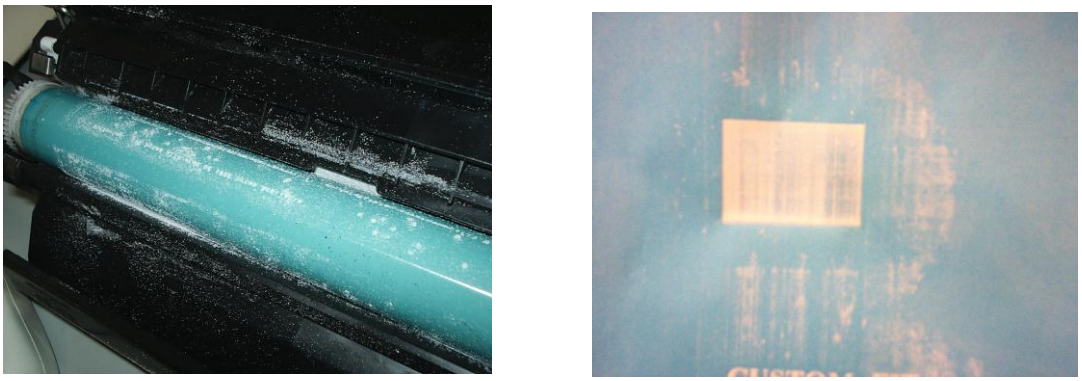

Figure 102 Scattered HDPE powder on OPC roller (left) & printed material on paper (right)

4.5.3 Printing trial with non-magnetic cartridge

The next trials were conducted to investigate the printing performance of HDPE particles with a modern non-magnetic print engine (Lexmark C510), which was designed to print for negatively charged toners. The aim of the experiment was to assess if the deposition efficiency improves and leakage reduces if a non-magnetic print engine is employed. In addition the trials enabled the influence of particle size, charge and flow characteristics (using FCA and a charge conducting agent).

Printing using non-magnetic print engines is more challenging. There is no magnetic force available to hold the toner particles on developing roller for print engines using non-magnetic toners. The non-magnetic print engines require accurate control of charge and flow compared to magnetic toner print engines. The amount of gap between the developing roller and doctor blade is normally less compared to the gap for magnetic print engines (HP LaserJet4). The average particle sizes of conventional nonmagnetic toner is generally lower than magnetic toner.

4.5.3.1 HDPE printing trial (FARD 3718) with FCA

In order to print with the Lexmark C510 it was necessary to use a different HDPE material with a smaller average particle size as this modern non-magnetic print engine is designed for toner with a smaller particle size than the HP LaserJet4. Microthene (FARD 3718) with an average particle size of 12 µms was selected. The top surface of the developer roller of Lexmark C510 cartridge is metallic and non-magnetic. Coating of toner on the developer roller entirely depends on adhesive forces and

tribocharge of the toner whilst in contact with (rubbing against) the doctor blade and developing roller whilst printing. The FARD 3718 powder sample has similar caking characteristics to the FA700 material. Fumed silica HDK20TX was selected, primarily for its flow control characteristics but in addition it is specifically designed to assist with toner charging.

Each sample was prepared using 100g FARD 3718 HDPE powder. Trials were conducted in stages, starting with uncoated HDPE powder and then adding increasing amounts of fumed silica. The printer was allowed to complete its normal 'start-up cycle' prior to sending the print command. After the start-up cycle was completed, the print cartridge was removed and the coating on the developing roller was checked. This quick check was used to ensure that a reasonable amount of toner had been coated onto the developer roller, as there will be no powder transfer onto paper if the developing roller is uncoated.

A very thin layer of powder coating was found on the developing roller with the uncoated FARD 3718 powder samples. The FARD 3718 powder was then coated with fumed silica in different proportions (2% and 4%) using the CKL multi-mix (Eiger Torrance). After the surface coating, sieving was carried out using lab scale Retsch Sieve shaker to remove bigger particles (more than 20 µm) from the powder samples. These large powder particles develop due to localised heat, generated while coating the powder particles. This is an important step prior to printing as the presence of even a small number of larger particles between doctor blade and developing roller can completely stop the printing process.

The fusing unit of the Lexmark C510 printer was removed to avoid any smudging effect on the printed image. The fuser unit was connected externally to the printer hardware as undertaken with the HP LaserJet 4. A standard 80g/m^2 paper with appropriate dielectric property was selected as substrate for printing.

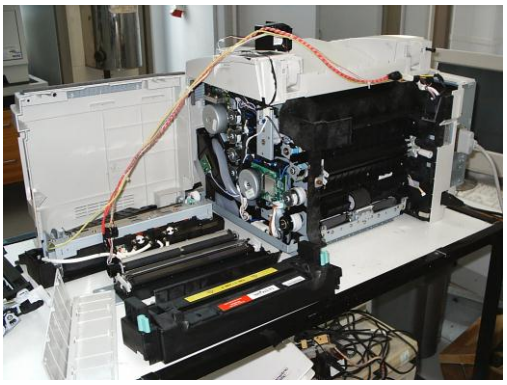

Figure 103 Modified Lexmark C510 Printer for test

The print cartridge was then filled with FARD 3718 powder coated with 2% fumed silica. Prior to printing the start up cycle was commenced and thin coating was noted on developing roller. This thin layer was not sufficient enough to deposit any loose toner on the final substrate/paper. This result demonstrated that further optimisation was required to achieve the desired balance between charge and flow properties for printing.

4.5.3.2 HDPE printing trial (FARD 3718) with FCA and Conductive agents

An appropriate level of electrical conductivity is critical for toner to print effectively. Polyethylene is difficult to charge as it is a non-polar compound (very little intermolecular exists because of carbon-hydrogen bond). To try to overcome this problem it was decided to surface coat the FARD 3718 with several conductive agents (ECTT-1 /Tronox CR 880 /SW340) common to toner industry to improve the conductivity of powder particles.

A new batch of samples was then prepared by surface coating with a small amount of FCA (0.3% HDK20TX by weight) and 1.2 % of ECTT-1 by weight, using the CKL Multi-mix lab scale mixer at 2500 rpm for 30 minutes. The blended material was then passed through a Retsch sieve shake, mesh sizes of 20 and 30μm, to remove any large particles.

As with previous printing trials after the 'warm up cycle' the coating on the developing roller was checked. A slight improvement in layer thickness on the developing roller was noted. This experiment suggests that the conductivity of FARD 3718 powder particles is important and required further optimisation by adjusting the proportion of charging agents.

The amount of conductive agent required for printing can only be established empirically .It was found that the thickness of coating on the developing roller was slightly reduced as the quantity of ECTT-1 was increased from 1.2 to 2%.

A new batch of material was prepared by blending FARD 3718 with a much higher quantity of ECTT-1 (4% by weight). The coated material was then blended with 0.1% fumed silica (HDK20TX). No significant improvement of coating on the developing roller was noticed after executing the warm-up cycle. This shows that the balance between the silica and charge agent is more critical for non-magnetic toner, as any small change in of one of the additives could completely stop the powder deposition due to lack of deposition on the developing roller. Further printing tests were conducted using other conductive agents to check the quality of the coating on the developing roller. A new sample of material was prepared from 100g of FARD 3718 blended with 0.3-0.4% (by weight) of HDK20TX and 1.5% of Tronox CR880 (conductive agent). As with previous trials surface coating was carried out using an Eiger Torrance CKL Multi-mixer and after blending the larger particles were removed by sieving.

Printing trials using the Lexmark C510 were undertaken using the new conductive material and the layer thickness on developing roller was found to be very similar to that for the material blended with the 1.2% ECTT-1. The coating on the developing roller was generally found to be poor for most of the samples using FARD 3718 powder particles (of average particle size 12µm). In addition it was observed that radial lines were present in various locations across the developing roller while printing FARD 3718 powder particles.

Figure 104 Marks on surface of developer roller

The cartridge was then dismantled to investigate the cause of the lines on the developing roller. It was found that larger particles were trapped between the doctor blade and developing roller leading to the absence of powder to form the lines (see Table 15).

FARD 3718 – HDPE - 12 µm				
Sample No	**Fumed silica HDK20Tx (% by weight)**	**Conductive Agent ECTT-1 (% by weight)**	**Conductive Agent Tronox CR880 (% by weight)**	**Results**
1	0	0	0	Very thin coating on roller+ small marks on roller
2	2	0	0	Thin coating on roller+ small marks on roller
3	0.3	4	0	Thin coating on roller +small marks on roller
4	0.3	2	0	Thin coating on roller+ small marks on roller
5	0.4	1.2	0	Reasonable coating on roller +small marks on roller
6	0.4	0	1.5	Better layer and similar to sample #5

Table 15 Printing performance with different surface coating agents

4.5.3.3 HDPE Printing Trial (FARD 3712) with Non-magnetic Cartridge

FARD 3712 with average particle size of 8 µm was selected instead of the FARD 3718 (average particle size of 12 µm) to improve the powder coating on developing roller. New powder samples were prepared using 100g of FARD 3712 blended with 1.5% (by weight) of Tronox CR880 (conductive agent) and 0.4% (by weight) of HDK20TX (fumed silica) using the Eiger Torrance CLK multi-mix lab scale mixer. This formulation was based on Sample 6 (see Table 15).

As with previous trials the samples were sieved again using a Retsch sieve shaker to remove larger sized particles. After printing, a thin layer of coating was also observed on the developing roller, which was free from any straight-line marks.

Although the problem of the lines had been resolved the coating thickness still required further improvement. In order to enhance the transfer efficiency the Tronox CR-880 was replaced by another conductive agent, SW340 (strontium based as it is one of strong conductive agents applied to toner industry as well). A new powder sample was then prepared by blending 1.5% (by wt) of HDK20Tx and 2 % (by wt) of SW-340 with 100g of FARD 3712 powder. As before the sample was sieved after blending to remove any larger particles. There was a clear improvement in the coating on the developing roller, which was also free from radial lines.

To fine-tune the printing characteristics the percentage of fumed silica was increased (from 1.5 to 3%) to improve the flow, as well as maintaining the balance between charge and flow of the powder particles. A material sample was prepared using 100g of FARD 3712 which was blended with 2% (by weight) of SW340 and 3% (by weight) of HDK20TX.

This formation gave a reasonable amount of coating(continuous coating layer without any gap of powder on developing roller)which gave a better deposition onto the substrate (paper) with an average layer thickness of around 5 µm and good edge definition.

FARD 3712 – HDPE - 8 µm				
Sample No	**Fumed silica HDK20Tx (% by weight)**	**Conductive agent Tronox-CR880 (% by weight)**	**Conductive agent SW- 340 (% by weight)**	**Results**
1	0.4	1.5	-	Very thin coating on developing roller
2	1.5	-	2	Better layer than sample 7
3	3	-	1	Better layer than sample 8
4	3	-	2	Best Layer

Table 16 Printing performance with formulation (modified)

Figure 105 Coated developer roller with 8 µm HDPE toner

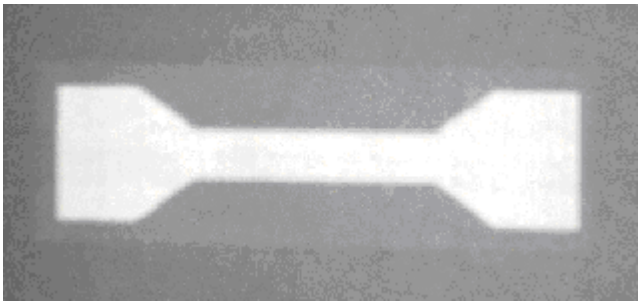

Figure 106 Laser printed T Bone with 8 µm HDPE toner on Lexmark C510

4.5.4 Multiple prints using Lexmark C510

Multiple prints were conducted using Lexmark C510 printer to produce tensile test specimens BS ISO 37: 2005). The objective of the experiment was to assess the mechanical strength of the printed layers using HDPE (FARD 3712) with an average particle size of 8µm, coated with 3% HDK20TX (fumed silica) and 2% SW340 (conductive agents).

Standard (80g/m^2) paper (with appropriate dielectric properties) was selected as the substrate for these trials. The fuser unit of the Lexmark C510 was removed to prevent smudging of the printed images. The printed powder was fused after printing using an external infrared heat source. The process of printing and subsequent fusing was repeated for around 100 layers to produce a sample 0.5mm thick (Figure 107). Unfortunately, accurate registration of the printed layers was difficult to achieve as the process was carried out manually and thus some misalignment of layers was evident on the sample produced. The thin multiple printed HDPE samples showed no evidence of cracks, which was definitely a sign of improvement regarding the mechanical strength compared to the parts produced from standard toner.

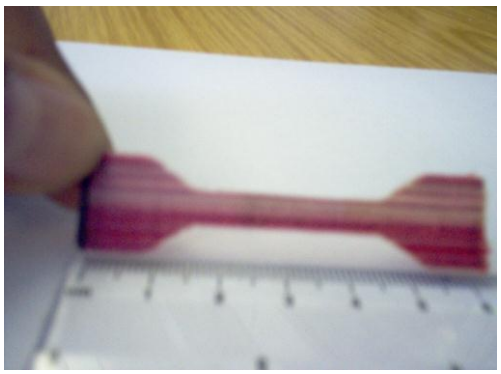

Figure 107 Thickness of 0.5 mm Dog bone with HDPE toner by Lexmark C510 printer

4.5.5 Industrial laser printer (Dual component/non-magnetic)

The next printing trials were conducted using a dual component industrial laser printer (CTG 900) developed for glass coating (For more details see Chapter 6).

The toner normally used for this industrial printer (Figure 86) is negatively charged. As with the earlier trials, HDK20TX fumed silica was selected, as it is a common flow control agent used for negative charged toners. To develop the dual component toner, 1350 g of Ferrite carrier (Fe50Si) of average particle size 50µm was blended with HDPE toner particles (FARD 3712) to achieve 10% toner concentration. The developer (carrier & toner) was then blended with 3% of HDK20TX (by weight) and 2% of SW340 (by weight) using Henschel lab scale mixer. This formulation was selected based on result of the trials described in earlier section.

A ceramic tile (300x 300 and10mm thick) was used as a substrate for these trials. The voltages on the developing station (-1020v), OPC drum surface (-800v) and transfer roller (+500v) were adjusted to maximise the layer thickness (up to 30µm was achieved).

A tackifying method (combination of heat and pressure) was selected to deposit toner from the transfer roller on to the substrate while printing each layer (Bynum 1989). The ceramic tile was heated up to 160-165^{0}C inside oven prior to printing. The temperature on the top surface of the tiles was monitored with IR temperature sensor before printing each layer. The toner was deposited onto the hot ceramic plate (substrate) using a combination of heat (temperature of substrate) and pressure (from the final transfer roller). This high contact pressure was due to decrease in gap between the transfer roller and build platform few microns .

No external voltage was applied to the ceramic tile (substrate). The toner transfer mechanism on substrate was due to mechanical transfer (heat and pressure) rather electrostatic transfer. After printing of each layer, the powder was allowed to fuse inside an oven for 5 minutes. The temperature of top surface was controlled to around 155^{o}C; below this temperature poor transfer occurs and above this temperature there is a risk of back transfer on semi-molten toner on to the final transfer roller.

The deposition process was repeated to give a 1mm high part, after around 30 layers have been deposited, as shown below (see Figure 108 below).

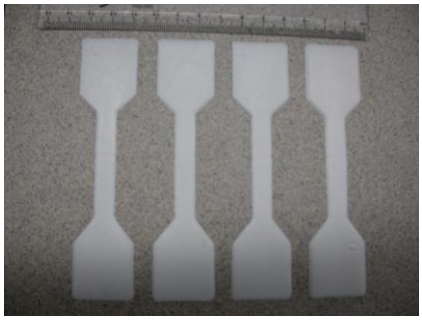

Figure 108 Industrial laser printer (left) & Laser printed HDPE samples (right)

The edge definition of the printed samples started to deteriorate after a few printed layers. This distortion could be due to high contact pressure (between transfer roller and substrate), which might had damaged the edges of the printed layers while printing. It was observed that the toner powder deposited well but there was also evidence of leakage of toner particles within the printed (this is known as 'dusting effect'). This 'dusting effect' could be due to weak adhesive force between the carrier and toner particles which causes the toner particles to be dislodged from carrier before successful transfers onto the substrate.

4.6 Overall Findings of Scoping Trials

Particle size is critical for the success of the process. The architecture of the HP LaserJet 4 is particularly suited to larger toner particle sizes (up to 15-20 µm). For the non-magnetic Lexmark C510 print engine the toner particles need to be less than 8µm in size.

Developing experimental toner based on HDPE has been shown to be feasible however particles must be surface coated with a suitable FCA (in this case fumed silica was used). For these trials of around 1% of FCA by weight was applied by dry mixing, however the amount required depends on the caking (flow) characteristics of the particular material.

To maintain the correct dielectric properties for the experimental HDPE toner it is necessary to apply a conductive agent by dry mixing. In the case of these trials SW340 and Tronox was used in quantities between 0.5-1% by weight. Care must be taken to select the appropriate amount as too much or too little has a detrimental effect on printing performance. Despite the success of the trials the HDPE experimental toner produced significant amounts of dusting due to separation of the coated conductive agents on the surface of the HDPE particles. Based on the results of these trials the main experimental work was conducted using Somos201 particles, this is explained in more detail in the next chapter.

5.0 Chapter 5- Printing with Somos 201 powder

Trials with Thermoplastic Elastomer (TPE)

The results of trials in Chapter 8 showed clearly that although it was possible to generate an experimental toner for the SLP process, significant challenges remain, including problems such as dusting.

Balancing the charge and the flow on toner particle was difficult using only surface coated FCA (such as fumed silica). Normally charge control agent (CCA) is incorporated within the powder particle during manufacture (not applied as a secondary coating process). It was found to be very difficult to hold the CCA particles on the powder surface using only the tribocharge and weak adhesive force (Van der Waals force). This is the likely cause of the "dusting effect" with the HDPE toner, as the CCA is easily dislodged from the toner thus adversely affecting the printing characteristics.

Controlling the charge by introducing CCA inside the powder particles is complex, time consuming process and requires specialist equipment (dual screw extruders, granulators, mechanical grinders etc.), which would preclude the development of a toner within the timeframes of this study. To mitigate the dusting effect it was decided to find a tough engineering polymer, which also has a better charging/electrical characteristics than the HDPE powder used in the scoping trials (ideally charge characteristics similar to standard toner would be a major advantage).

Research was then directed to find 'off-the-shelf' powder which would have charge/electrical characteristics similar to the characteristics of standard toner particles. The electrical properties of conventional powders available within the RP industry were investigated. Tests were conducted on TPE/ Somos 201 powder (commonly used in the 'Selective Laser Sintering' SLS process). This is a Thermoplastic Elastomer (TPE), which has excellent mechanical properties (for example tensile modulus 15.5MPa). The basic polymer for Somos 201 powder is based on a formulated Polybutylene terephthalate **(**PBT) material (See Appendix). The dielectric constant and resistivity of Somos 201 powder was found to be comparable to conventional toner such as PS (unlike the HDPE powder).

Material	Dielectric Constant	Volume ResistivityOhm-cm
Somos 201	2.9	1.5E+13/(1.5x 10^{13})
PE	2.3	1E+15/10^{15}
Non Magnetic Toner (Typical)	3.08-4.10	1E+10/(10^{9})
Magnetic toner (Typical)	3.59-4.36	1E+10/(10^{8})

Table 17 Comparison of Dielectric property/Resistivity/ of Somos 201 compared to standard toner

A q/d test (repeated three times) was also carried out with Somos 201 powder particles (Figure 109). It was found that Somos 201 powder particles are more negatively charged compared to HDPE powder particles which makes this material more compatible for the vast majority of print engines.

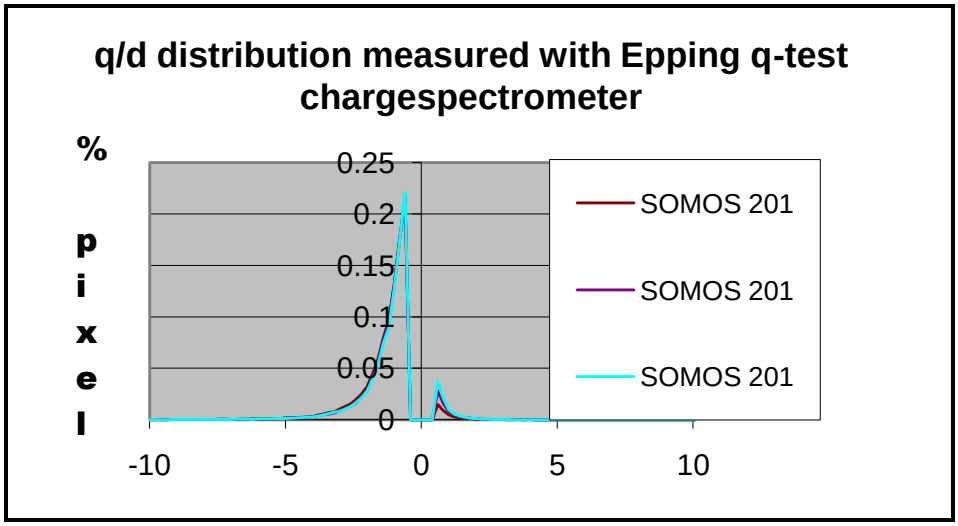

Figure 109 q/d distribution of Somos 201 powder

The tap density of Somos 201 found to be less (0.58gm/cm^3) compared to standard toner particle (0.84gm/cm^3). This indicates that flow characteristic of the off-the-shelf Somos201 powder also needs further improvement for effective laser printing. Fortunately, this does not present a big problem, as powder flow can be controlled various ways as mentioned below:

- Controlling the size distribution (as powder with narrow particle size distributions flow better than powder having wide size distributions (for more information see Chapter 4).

- Applying surface coating of 'Flow Control Agent' such as fumed silica to the particles

- Controlling the shape of powder particles while manufacturing (as powder of regularly shaped particles flow better compared to irregularly shaped particles).

In this particular research the flow of Somos 201 powder controlled selecting the finer particle sizes and degree of coating with fumed silica prior printing.

The same methodology, applied in the earlier scoping trials (for HDPE only) was used for Somos 201 powder.

5.1 Particle Size

The average particle size (d50) of standard Somos 201 powder, based on the manufacturer's data, is around 93µm. Finer particles (average 10 to 30µm) with a narrow size distribution are required to develop effective toners (for more information see Toner under Chapter 2).

Mechanical sieving tests were first conducted to get more information on the particle size distribution of the Somos 201 powder. This was accomplished using a lab scale sieve shaker (Retsch AS -200 unit) with mesh sizes of 20,36,50,100µm respectively. A sample of 150g of powder was sieved using the maximum amplitude of 1.5 mm (this is high amplitude is required to prevent electrostatic charged particles from blocking the sieve). After sieving the samples were collected and the weights were measured.

A wide range of particle size distribution was found for Somos 201 between 10 and 150 µm (with average particle size of 93µm). This average particle size is relatively high, compared to the standard particle size of toners (varies between 10 to 15 µm). After sieving the results were analysed to get an indication of particle size distribution. It was found that more than 50% of the powder was above 114 µm and around 28.4% (by weight) was within 50 and 100 µm (see Figure 110). There was very little powder with a particles less than 20µm. The shape of Somos 201 powder particles was analysed using a Scanning Electron Microscope. It was found that Somos 201 powder particles are very irregular (see Figure 111). The trials suggest that further work is required to produce finer particle size Somos 201 toner.

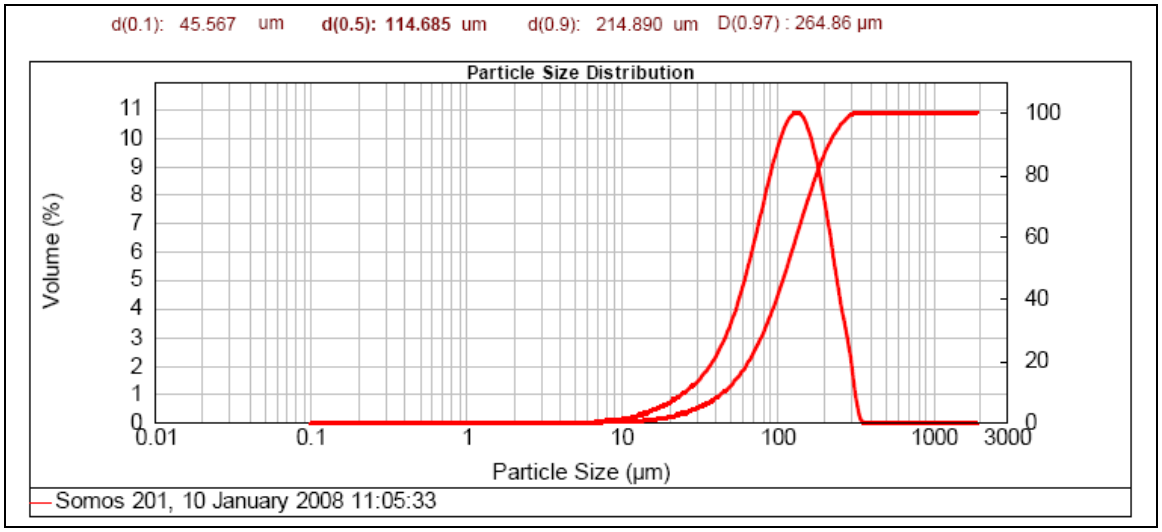

Figure 110 Sieving result with Off-the-Shelf Somos 201 powder

Particle distribution	0.5 mm Rasp screen (µm)	Remarks
d10	45	There are very little amount of material present having particle size less than 20 (µm)
d50	114	
d90	214	
d97	264	

Table 18 Particle size distribution of Typical Somos 201

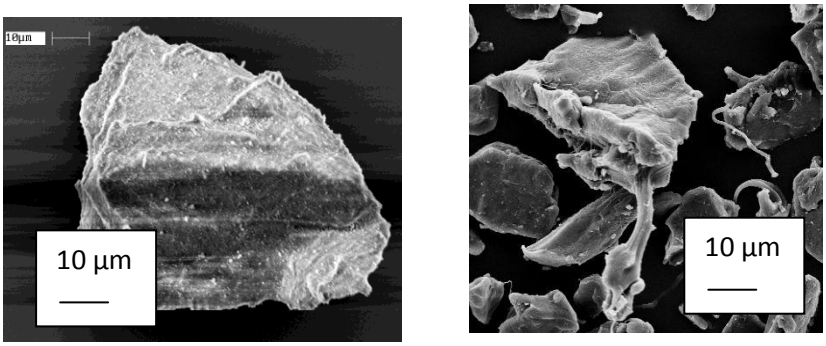

Figure 111 SEM photos of Somos 201 powder

The next stage of activity was to reduce the particle size of Somos 201 with different grinding trials as per the methodology mentioned above.

5.2 Grinding Trial - Somos 20*1*

Somos 201 is elastomeric and therefore difficult to grind. Different milling tests were conducted to assess the grindability of producing fine powders.

5.2.1 Planetary Ball Mill PM 100 CM

Initial grinding tests were carried out using Planetary Ball Mill PM 100 CM. This is a bench-top unit with one grinding station for specimen jars and having a nominal volume from 12 to 500 ml. RETSCH ball mills are designed for pulverising a wide range of materials, including polymers. The PM100 CM (ball mill) was selected, as this is suitable for generating fine particles, down to the submicron range. The grinding jar was filled with Somos 201 powder and the mill was set up to run at 500 rpm for one hour. Ground samples were then sieved using a Retsch Lab scale sieve shaker unit (AS-20). Sieves with a mesh size of 20,36,50,100µm were selected to obtain an overall picture of the particle size distribution. The weight of powder collected in the different sieves was then measured. Unfortunately, no significant particle size reduction of Somos 201 was noted after grinding with the planetary ball mill.

5.2.2 UPZ Impact Mill using Cryogenic atmosphere

The next test was to check the grind-ability of Somos 201 using an impact mill (Hosokawa 100UPZ III) to improve the milling performance. The working principle of impact mill is based on the impact force against hard surfaces while milling. This mill can also run in cryogenic atmosphere, if required. It depends on the embrittlement characteristics of the particular material, which depends on material hardness, and mechanical characteristics (such as Glass Transition Temperature Tg).

Samples were then allowed to cool for 30 minutes using liquid nitrogen prior to grinding. Material (0.9kg) was introduced into the mill through a feeding device (like a rotary air lock or volumetric/gravimetric feeder) at the mill's inlet. The inlet directs the material towards the centre of the grinding chamber. The grinding toll rotates at high speed (14,000 rpm) creating centrifugal force, which propels the powder outwards. The particles impact at high speed against the hard pins/other grinding media within the chamber. Due to this impact the particles breakdown into smaller pieces and the size of the grinding product depends upon the mechanical properties of the powder material.

Three tests were carried out using 2 different screen sizes as shown below(See Table 19) .It was found difficult to grind the particles below 30µm for Somos 201 powder. Less than 10% of the powder was found to be below 30µm (See Figures 112,113). The particle size distribution is found very similar to original feed stock which implies almost no proper grinding has occurred. Each particle sizing characteristics has shown the standard distribution as well as its cumulative in percentage.

Particle distribution	0.5 mm Rasp screen (µm)	0.25 mm Rasp screen	Remarks
d10	58	*	Difficult to grind this material using Impact milling
d50	126	*	
d90	227	*	
d97	275	*	
d100	355	*	

*Material stayed at screen

Table 19 Milling performance using 3 different screen size with Somos 201 powder

This polymer powder material is generally electrostatic in nature and blocks the opening of the mesh particularly when the screen size is smaller than 0.25 mm.

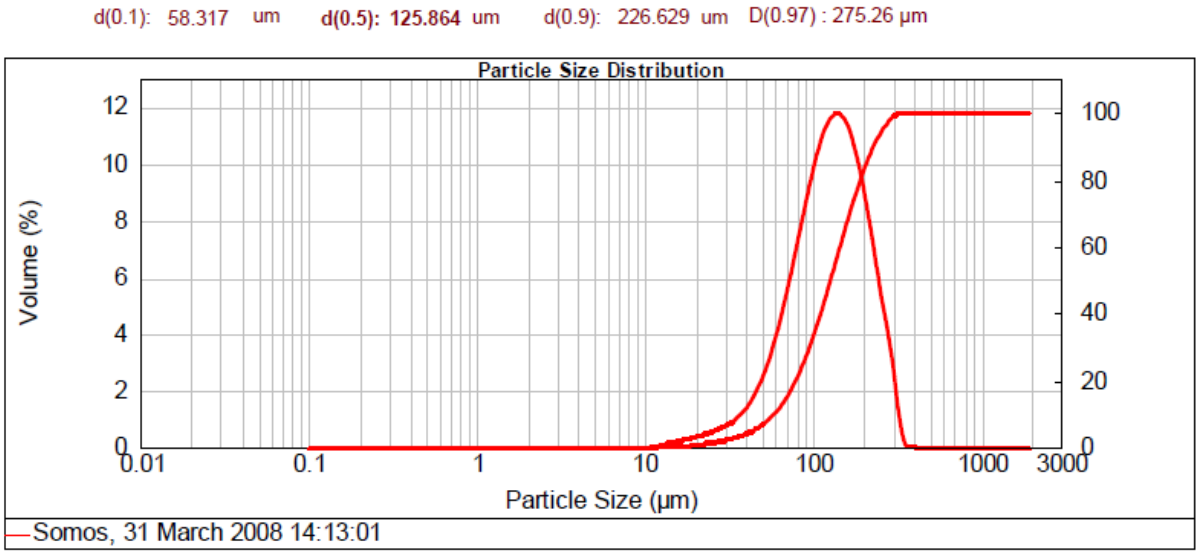

Figure 112 Particle distribution of Somos 201 powder after Impact milling

To confirm these results, the trial was repeated and the results (almost identical) are show below

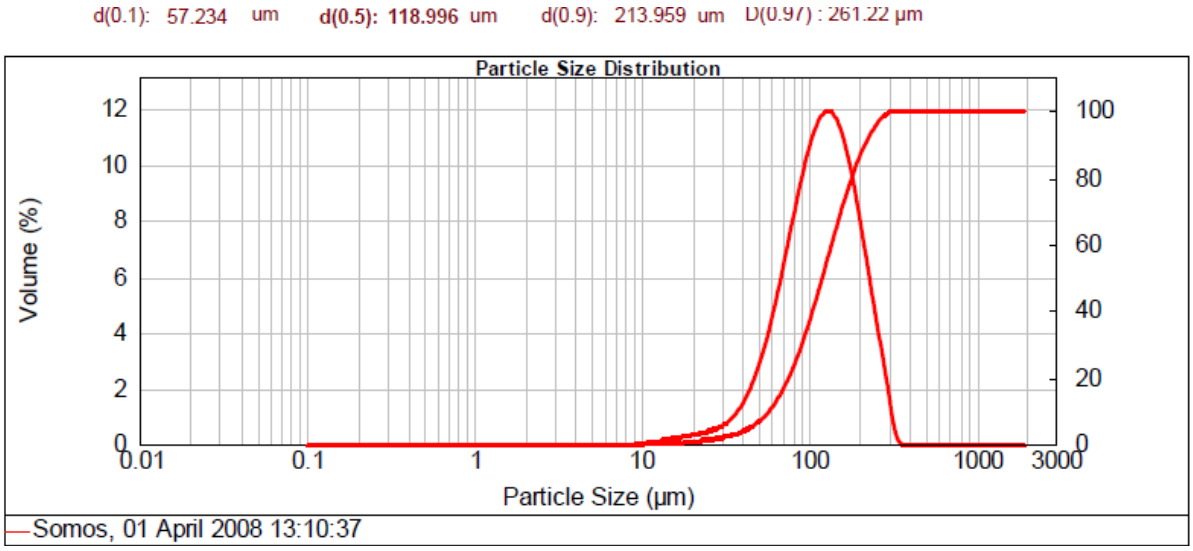

Figure 113 Particle distribution of Somos 201 powder after Impact milling

5.2.3 100 AFG Fluidised Bed Jet Mill

A fluidised jet mill was then selected to check the grindability, as this is a very common type of mill used in the toner industry for producing toner. An Alpine AFG, fluidized-bed jet mill, normally used for fine and ultrafine size reduction, fitted with an internal forced vortex classifier which is capable of controlling the top sizes of the particles (D97) as low as 3µm, was used for the trials.

The working principle of the air-jet mill is based purely on particle-to-particle attrition occurring at the centre of a fluidised bed of material. This is achieved by jetting three or more compressed gas nozzles into the milling chamber which help to accelerate the particles while milling. The accelerated particles will produce collisions and energy is released causing the particles' breakdown in smaller sizes. The key feature is to maintain the consistent particle size is its integral air classifier. By changing the parameter of classifier wheel speed, airflow, and grind pressure, a wide range of particle sizes can be separated.

Using a jet pressure of 6bar and a rotor speed of 4000 rpm the powder was processed for 15 minutes. The particle size range achieved (D97) was found to be between 3 to 60 µm. The material was passed through a 50 ATP classifier and the samples were collected (particle size distribution shown in Figure 114). Only very small amount of material came out from mill. It seems material is absorbing energy while grinding.

Particle distribution	Mean particle size (µm)	Remarks
d10	18.1	Only very small amount of material came out from mill. It seems material is absorbing energy while grinding. Only 15% of the material found below particle size of 20 µm.
d50	36.3	
d90	67.2	
d97	85.1	
d100	120.7	

Table 20 Milling performance using fludized jet mill for Somos 201 powder

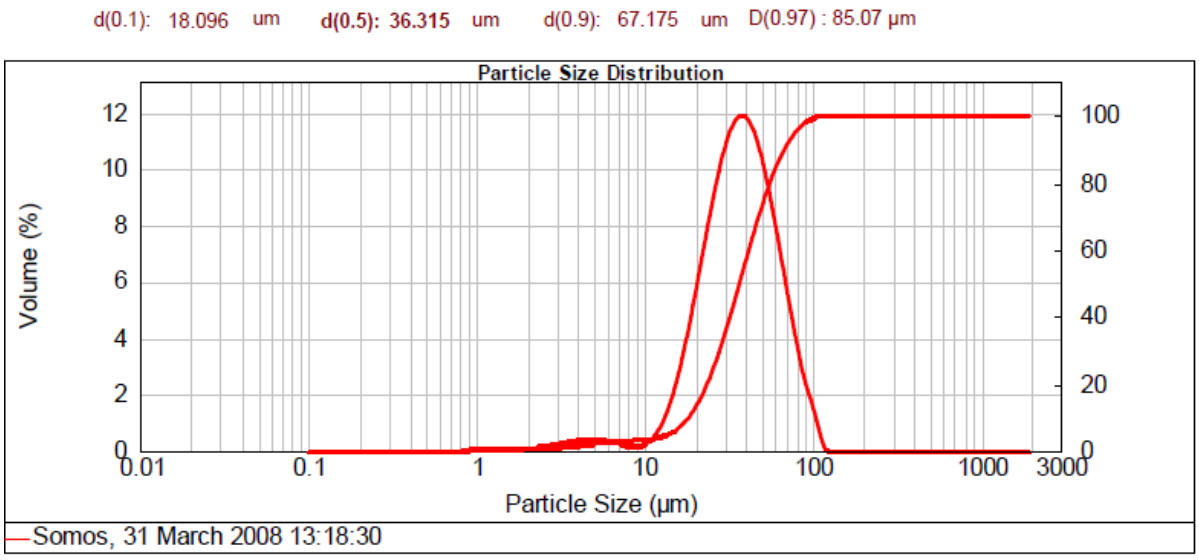

Figure 114 Particle distribution of Somos 201 powder after Impact milling

5.2.4 '50 ZPS' Classifier Mill

As air jet milling was found to have poor efficiency with the Somos 201 powder, the next activity was to introduce mill integrated with classifier to efficiently grind Somos 201 powder particles. This impact mill was integrated with '50 ATP' classifier. The mill was set to run at 18,000 rpm for 1 hour. The process proved to be inefficient and small amount of material (only 12 gm from an initial sample 1kg of material) was collected after 1 hour of grinding. The particle size distribution is shown in Table 21.

Particle distribution	Mean particle size (µm)	Remarks
d10	12.2	Only very small amount of material came out from mill. It seems material is absorbing energy while grinding.
d50	26.4	
d90	52.6	
d97	75.1	
d100	284	

Table 21 Milling performance using 50 ZPS mill for Somos 201 powder

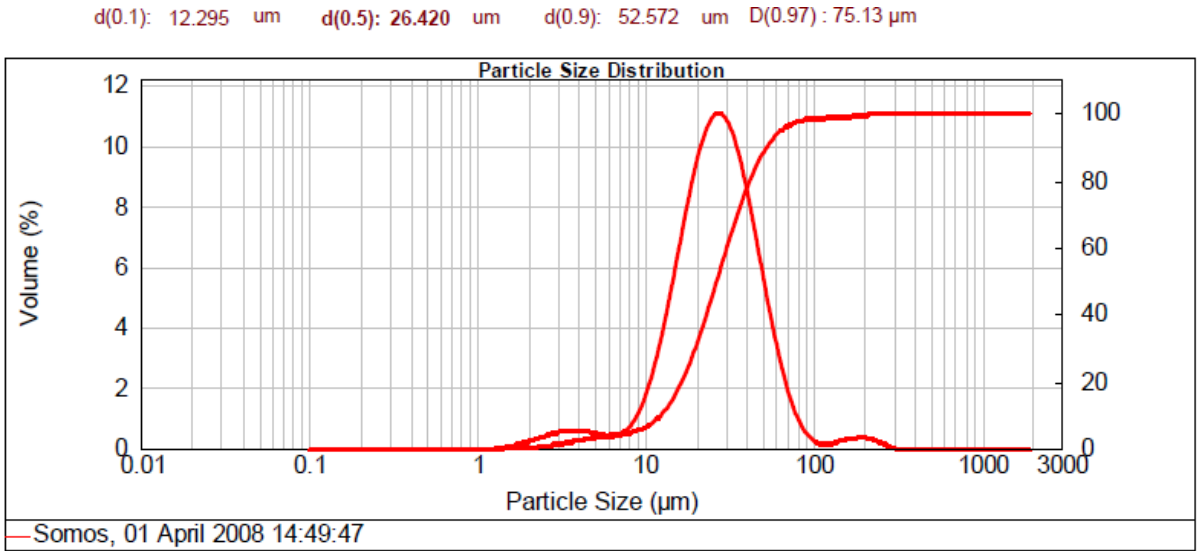

Figure 115 Particle size distribution of Somos 201 powder after milling using 50 ZPS mill

5.2.5 '50 ATP' Turboplex ultrafine classifier

As milling was found to be very difficult for the Somos 201 powder, the next activity was focussed to separate fine powder from the original feedstock using separator/classifier. An air classifier '50ATP' (Hosokawa), ultra fine classifier, was selected to separate larger particles from smaller ones very precisely. This machine can produce fine materials with a precise size limit and free from oversize particles. This machine has an extremely wide range of operation to produce particle sizes within (D97) 2.5 µm to 120 µm. This machine is capable of processing feed rates of approximately 4 to 100 kg/hr and is common used as a laboratory classifier. This machine is also capable of classifying products with good as well as poor (for example materials having a high tendency to agglomerate) flow properties.

The configuration of the machine is shown where (1) represents the material feed screw; (2) horizontally mounted classifier; (3) fine material exit point; (4) coarse material exit and (5) classifying air entry point (6) flow path of fine material (see Figure 116).

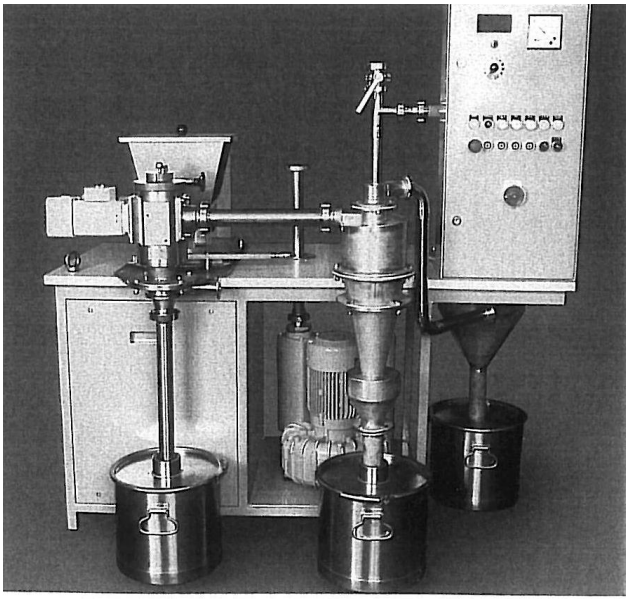

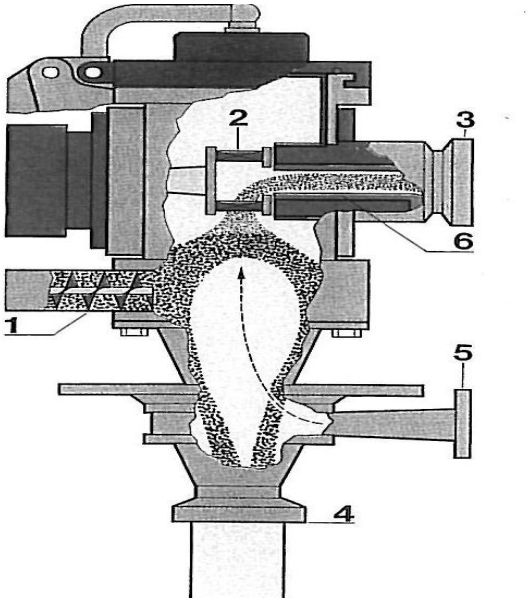

Figure 116(a) Lab Scale 50 ATP Ultrafine classifier & (b) 50 ATP classifier (Process)

Two sets of trials were carried out with a rotor speed fixed at 8,000 rpm and maintaining air flow at 95 m^3/hr. The experiment was carried out running the classifying system around 15 minutes. There was some losses of powder during the classification process. The particle size distribution of the collected samples after the experiment is shown in figure 117.

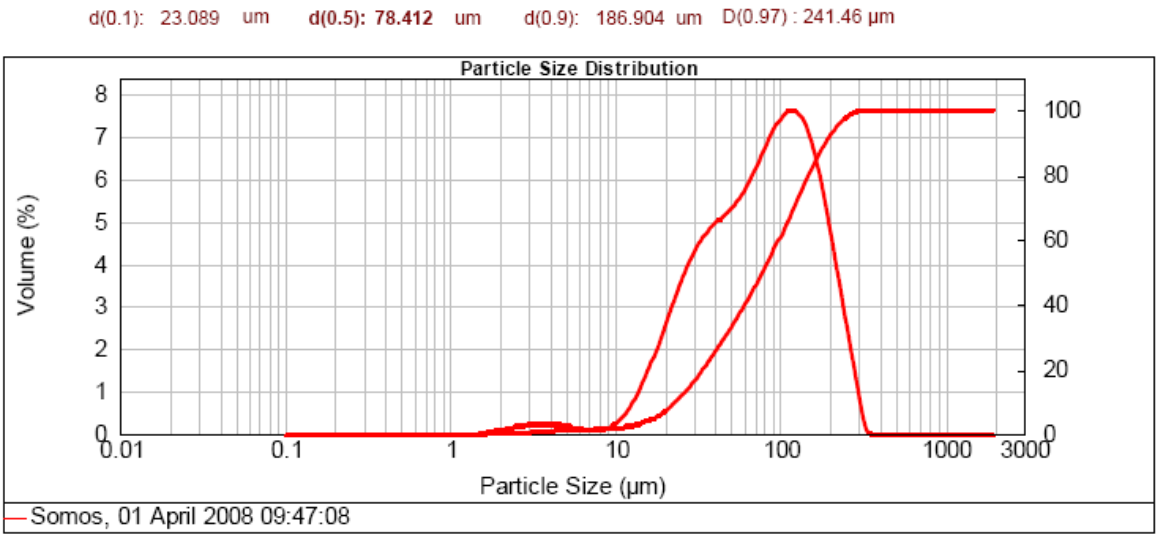

Figure 117 Particle size distribution of Somos 201 powder after classifying

Although this route for the manufacture of toner is far from ideal the classification approach provides the potential to generate enough Somos 201 powder with fine particles for the development of a toner. However, using this approach to generate 1kg of material below 30µm requires a significant quantity of original (off-the-shelf) feed-stock.

5.3 Discussion- Milling Trials

It has been found Somos 201 material would be very difficult to grind below 30 µm using conventional milling techniques due to its elastomeric characteristics. The particle sizes of Somos 201 need to bring down below 25µm for printing. This is very critical for laser printing as this would help to improve the tap density/flow and would help to maintain the right 'charge to mass ratio' required for the printing. Milling of Somos 201 powder particles was very time consuming and ineffective. The alternative quick solution would be the use of classifier to separate larger particles from smaller ones.

A 50-ATP classifier was selected to remove bigger particle sizes for this research to achieve smaller particle sizes below 25µm. As this classifier can produce samples with precise size limit, six different samples were produced for the future trials which are d50 of 17, 30,45 , 60 and 100 µm respectively.

Although this classification process is not cost effective as particles more than 30µm particle size would be of no use for toner development it is a different commercial issue and could be tackled in future. In the meantime this separation of particles using classifier was adapted to achieve fine powder particles for Somos 201.

5.4 Surface Coating Trial-Somos201

After collecting fine powders next activity was to control the charge characteristics by the application of surface additives. TG308F (fumed silica) was selected as the flow control agent for the trials as this is a common 'Flow Control Agent' for negatively charged toner particles as this ensures compatibility with the HP LaserJet 4 and dual component CTG 7000 print engines (negative polarity).

Initial surface coating trials were conducted with 0.5 to 1% of fumed silica using paddle type mixing blades with the Eiger Torrance lab scale mixer. The rotational speed of the mixer was controlled between 1200-2000 rpm and mixing process was closely monitored to ensure that no agglomeration took place due to overheating.

Samples were then tested under electron microscope to check whether the polymer particles are coated with surface coating agents (Fumed silica). It was found that the amount of silica coated on to the Somos 201 particle was slightly less than that for the HDPE particles (see Figure 118 a) & b). This

could be the result of different tribo-charging effect of Somos 201compared to the HDPE powder particles.

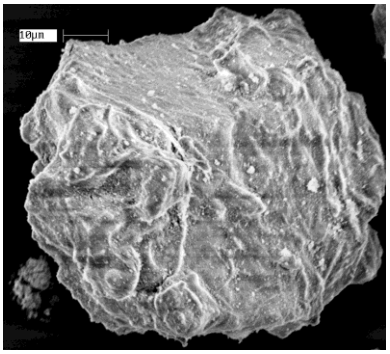

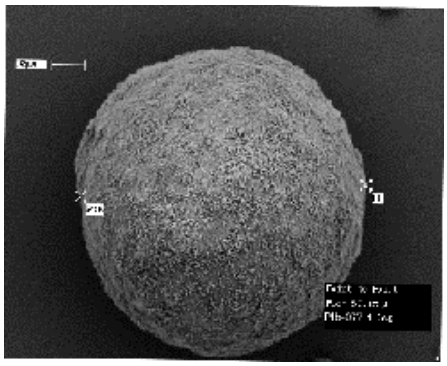

Figure 118(a) Coated TPE & (b) Coated HDPE

5.5 q/d test

A q/d test was carried out on the coated powder particles using an Epping q test charge spectrometer. It was found that the charge distribution of coated TPE/ Somos 201 powder was mostly negative and was similar to the charging characteristics of uncoated powder particles (see Figures 119 and 120).

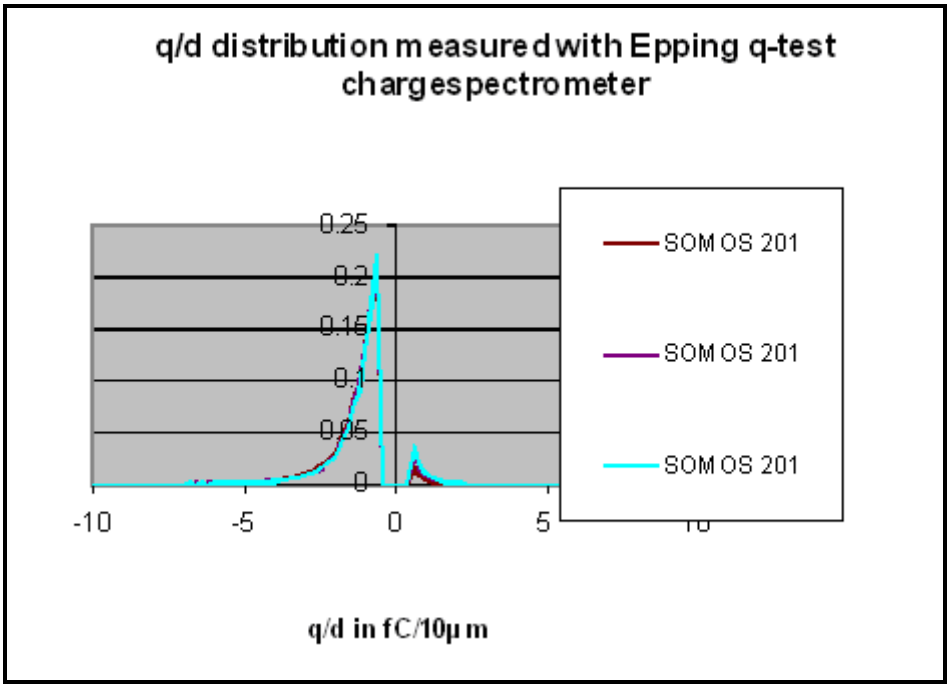

Figure 119 q/d distribution of Somos 201 using Epping q test meter

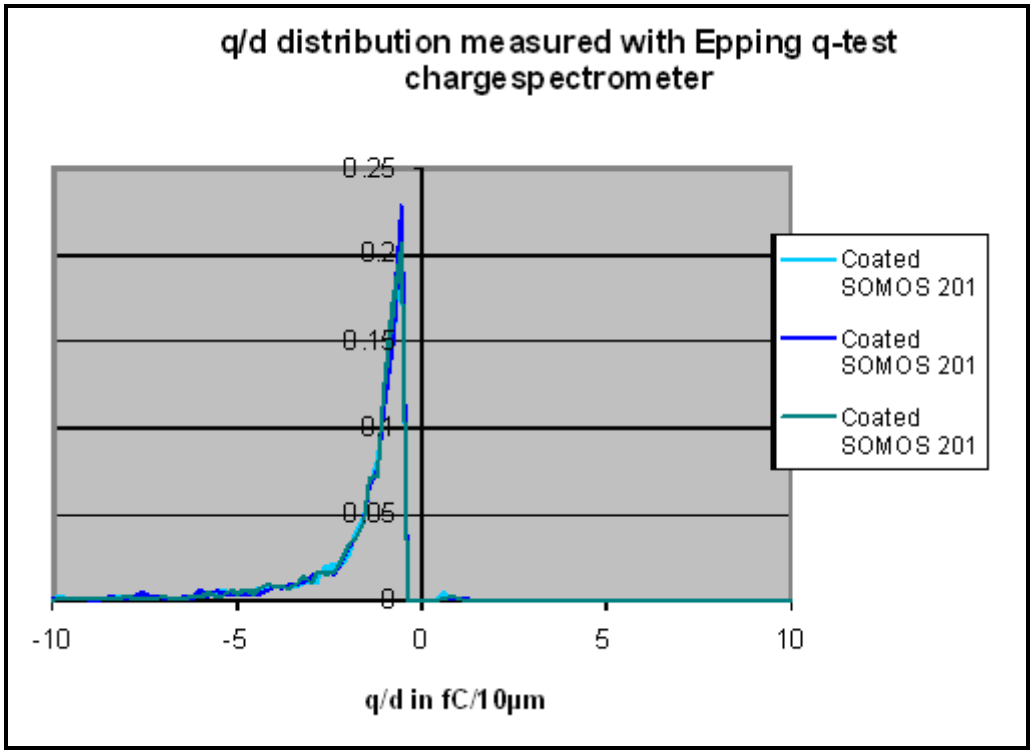

Figure 120 q/d distribution of coated Somos 201 using Epping q test meter

5.6 HP LaserJet 4 Printing Trials

Following a similar approach to earlier trials the coated Somos 201 was initially tested using a HP LaserJet 4 print engine. The magnetic core of the developing roller was removed from the print cartridge (HP LaserJet 92298X) as no magnetic component was present within the coated Somos 201 powder. In addition, the standard fused unit was removed but was still connected with the printer hardware to simulate the presence of the heating unit to avoid generating an error signal, which will interrupt the printing cycle. The print cartridge was then filled with coated Somos 201 powder, with a particle size varying between 50 -75 µm. Standard A4 size paper was manually fed into the printer. The voltages inside the printer were not altered.

In was observed that text images were printed with sharp edge definition on a standard A4 paper (80g/m^2) substrate (see Figure 121). The layer thickness of the loose surface coated Somos 201 powder was estimated to be around 2-3 times the thickness of the printed HDPE. Unfortunately, as with earlier trials there was significant leakage of toner inside the cartridge however this was less than that for HDPE material. This could be due to the better tribocharging characteristic on Somos 201 particles compared to HDPE particles.

Figure 121 Laser printed Somos201(TPE)using HP LaserJet4

5.7 Printing Trials – Dual component CTG Print engine

The next set of printing trials was conducted using the dual component industrial laser printer (CTG 900) as shown below (see Figure 122). Somos 201 powder (150g) was collected from the 50 ATP classifier (d50 of 30 µm) and surface coated with 0.5% (by wt) HDK20TX (fumed silica) using a Henschel lab scale mixer. The formulation was based on the earlier trials carried out using the HP LaserJet4 printer. 1350 g of CB 9011 carrier (particle size 90µm) was blended with the Somos201 toner particles to achieve a 10% toner concentration. This toner concentration selected was based on the requirement for CTG 900 print engine.

Heat was generated inside the mixing chamber while blending and it was found that particles agglomerated and in some cases new fused particles are grew to solid big particles up to 1-2 mm in diameter. Those agglomerated/fused bigger particles were later removed by sieving.

A ceramic tile of dimension 300 x 300 x 10mm (thickness) was selected as a substrate similar to earlier trials. The initial voltages applied on different workstation are as follows; developing station (-1020v), conditioning roller (-600V), OPC drum surface (-800v) and Transfer roller (+500v). Care was taken to avoid subjecting the OPC drum to an excessive voltage, which could damage the photoconductive film.

The printed layer thickness on the ceramic substrate was found to be below 10 µm, which was lower layer thickness than the earlier HDPE trials. It was found that the level of powder coating on top of conditioning roller was very low. It was then decided to adjust the voltages across developing workstation and conditioning rollers to improve the toner transfer. The final optimised voltage across each workstation as follows: developing station (-975V), conditioning roller (-500v), OPC surface (-800V) and transfer roller (+500V).

The ceramic substrate was heat to between 155-160^{o}C in an oven and was then fed into the machine for printing. The temperature on the top surface of the tiles was monitored using IR temperature sensor prior to printing.

After printing, each deposited powder layer was fused inside an oven (160 to 165^{o}C) for 5 minutes. This helps to consolidate the layer as well as keeping the temperature of substrate above 150^{o}C required for the next layer to print. The temperature control of the printed image is critical as powder deposition entirely depends on this temperature and contact pressure between the transfer roller and substrate. This contact pressure could be adjusted by controlling the gap between transfer roller and the substrate. The printing and sintering processes were repeated for 50 layers to produce a multi-layered objects as well as tensile specimen of 120 mm long and 1mm thick (see Figure 123).

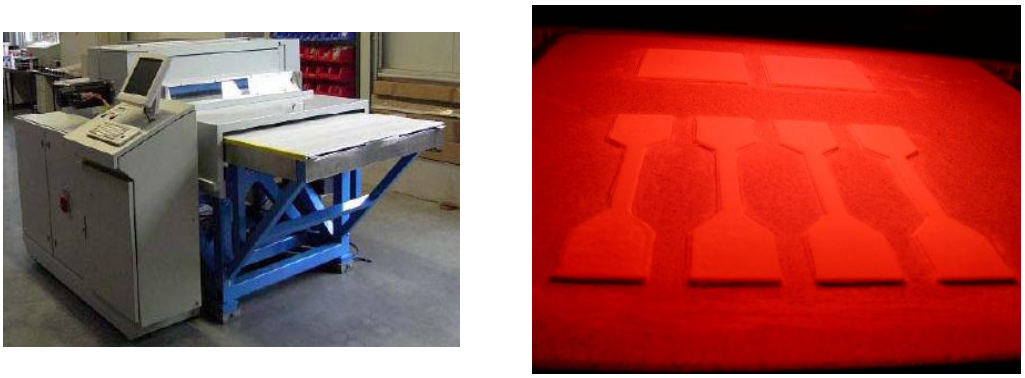

Figure 122 CTG 900 industrial printer (left) and IR sintering of TPE samples (right)

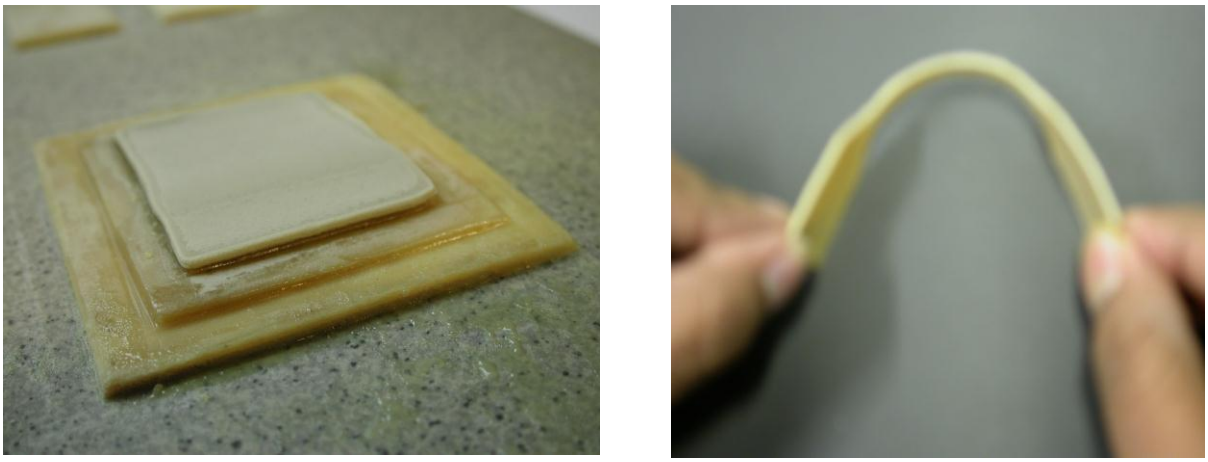

Figure 123 Printed samples with steps of Somos 201 (left) and Laser printed tensile test specimen (right)

5.8 Overall Findings

The mechanical grinding of Somos 201 powder is difficult.It is necessary to use the appropriate particle size and surface coating to produce an effective experimental toner using Somos 201 which can be printed. The next step is to assess how these factors influence mechanical properties of parts produced by the SLP process using Somos201. This is discussed in the following chapters.

6.0 Chapter 6 - IR & Oven sintering of Coated and Uncoated Somos 201 powder

Aim of IR trials was to determine the appropriate distance from the source to the samples to sinter the powder samples without any hot spots from the bulbs. The selected optimised distance would be applied for all the future trials.

6.1 Experimental procedure: Distance between infrared source and powder

1. Off-the-Shelf Somos 201 powders selected for the trials.
2. Aluminium mould plate with 10 cavities having geometry of standard Tensile test specimens (Dog bone samples) with 2 mm depth were prepared (as per BS ISO 37: 2005)
3. Fine layers of release agent (MCP Silicone based release agent S3) then applied to each cavity prior to powder filling so that the sintered parts can be removed without damaging them.
4. Powder deposition was carried out manually on aluminium mould plate to produce 10 tensile test specimens (see Figure 124). The dimension of tensile test specimen was selected as per BS ISO 37:2005 –'Rubber vulcanised or Thermoplastics –Determination of Tensile stress-strain specimen . The total length of the specimen was 115 mm with gauge length of 40 mm and thickness 1 mm.
5. The top surface of the loose powder was levelled moving a roller across the top surface of each sample to remove excess powder and provide a smooth, even top surface.
6. The plate with loose powder then placed under infrared heat source having medium wavelength of radiation (see Figure 125). Although the infrared unit selected for the test rig is designed to emit only medium wavelength radiation but the presence of near infrared radiation cannot be completely ruled out.
7. The temperature of powder bed was measured using non contact type infrared temperature
8. Tensile test samples were produced after 5,10, 20,30,40,50 and 60 seconds exposure times for each of the standoff distances.
9. Exposure time of radiation was controlled using a stopwatch for all tests.
10. Sintered samples then removed from the mould.
11. Samples were then prepared to carry out mechanical test to failure. The cross section each samples and gauge length were measured and stored. Samples were then clamped with the grips properly. Mechanical tests to failure of all samples were then conducted maintaining the crosshead speed 50mm/ min for all tests.

Figure 124 Powder on Aluminium mould plate (Tensile test specimens)

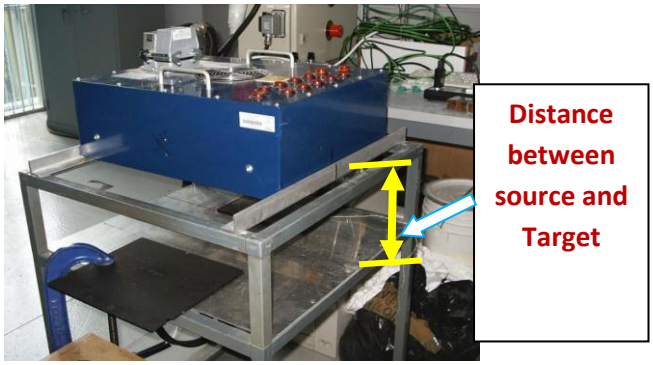

Figure 125 IR source selected for trials

6.2 Experimental Results

6.2.1 Mechanical Properties for 128mm Stand-off Distance

Young's Modulus, UTS and 'Elongation at Break' also recorded for uncoated Somos 201 powder while sintered at 128mm distance from infrared source (see Figures 126,127 and 128). Average Young's Modulus and UTS found increased with the increase of exposure of infrared radiation similar to earlier test results.

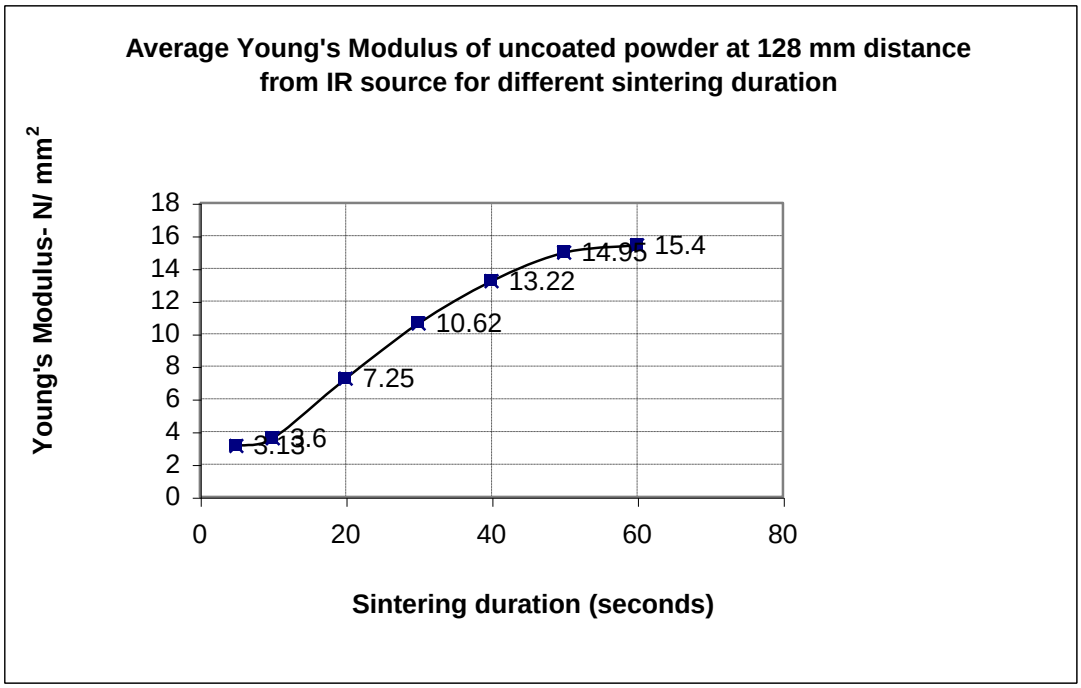

Figure 126 Young's Modulus for uncoated coarse powder vs sintering duration at 128 mm stand-off distance

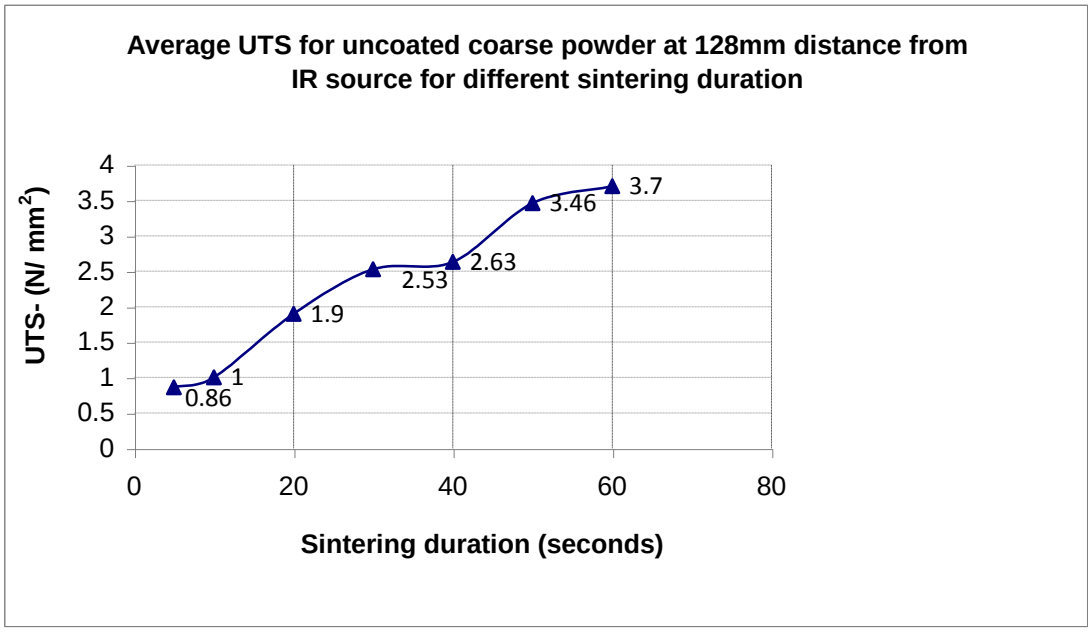

Figure 127 UTS for uncoated coarse powder vs sintering duration at 128 mm stand-off distance

128 mm distance from IR source			
Description/Item	5 seconds IR exposure	60 seconds IR exposure	% increase
Young's Modulus(N/mm^2)	3.13	15.4	79.67
UTS (N/mm^2)	0.86	3.7	76.75

Table 22 Comparison of Young's Modulus and UTS against exposure time under IR for 128 mm stand-off distance

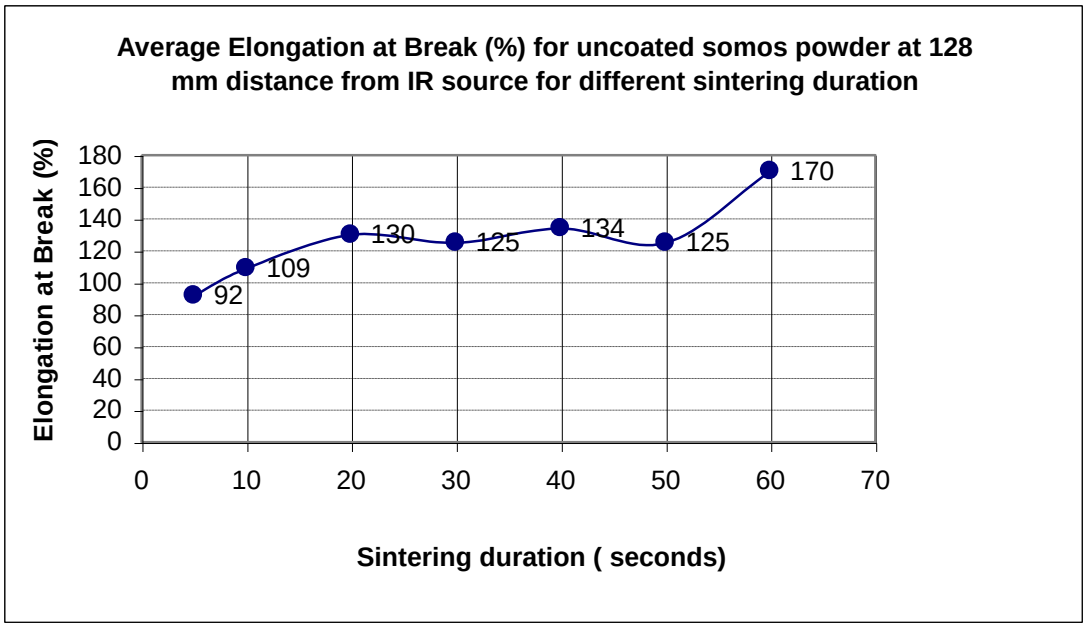

Figure 128 Elongation at Break for uncoated coarse powder vs sintering duration at 128 mm stand-off distance

The 'Elongation at Break' also increased with the duration of IR radiation for powder samples sintered at 128 mm distance from IR source. Moreover this trend was found to be less consistent compared to the trends of Young's Modulus and UTS against the exposure time of infrared radiation.

6.2.2 Results - Mechanical Properties for 178mm Stand-off Distance

Average Young's Modulus, UTS and 'Elongation at Break' are plotted for coarse powder at 178 mm distance for different infrared radiation exposure times as shown in Figures 129, 130 and 131.

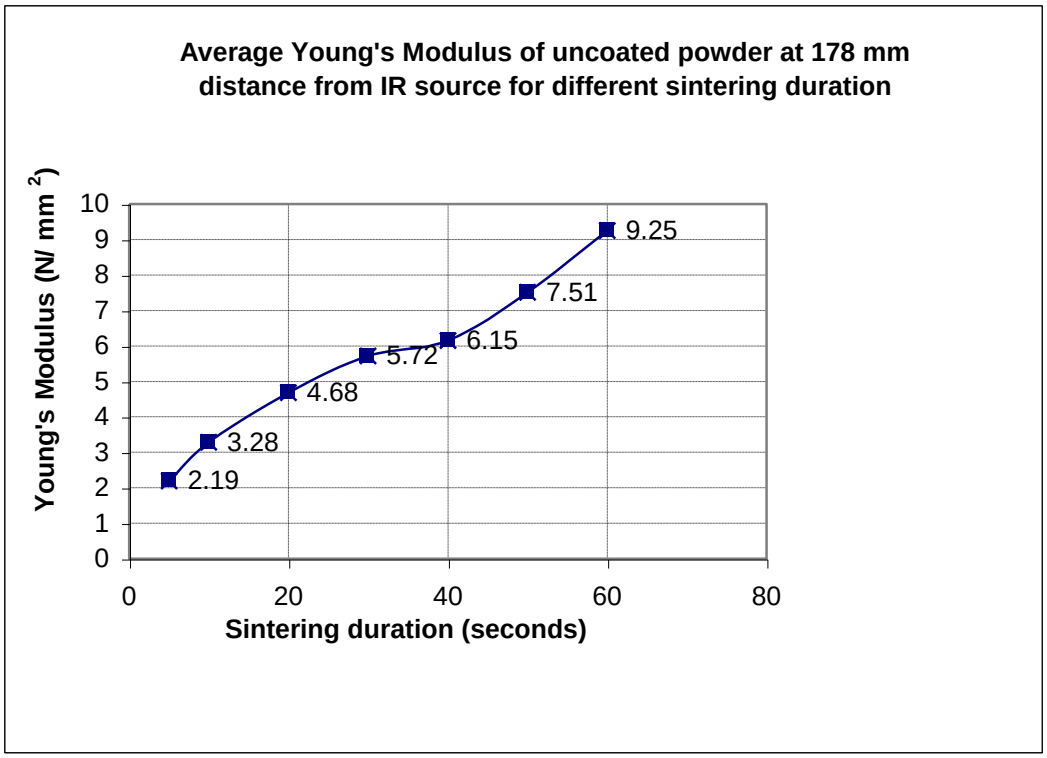

Figure 129 Young's Modulus for uncoated coarse powder vs sintering duration at 178 mm standoff distance

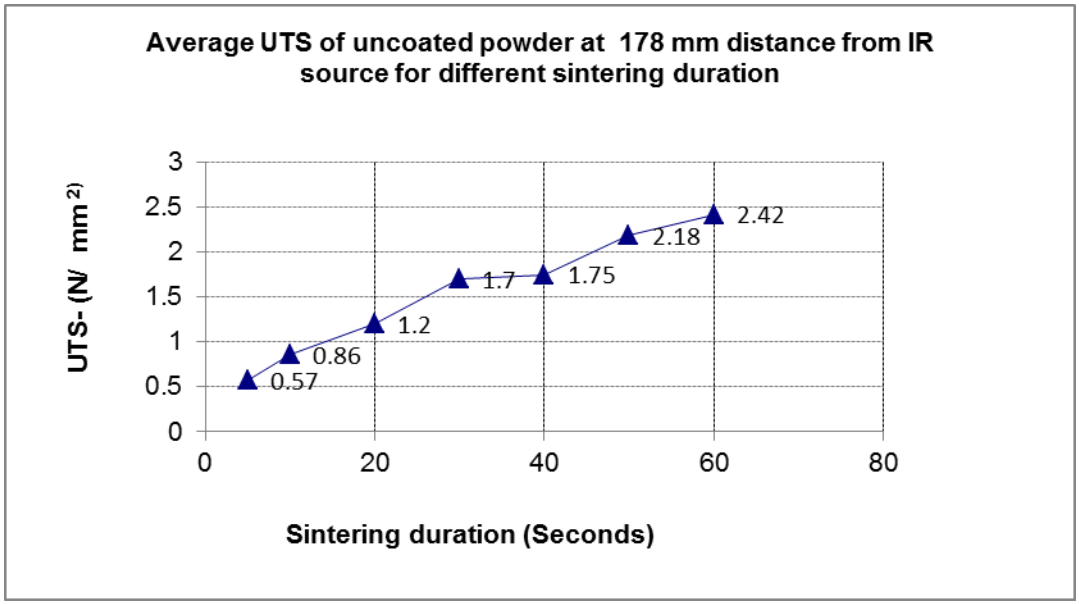

Figure 130 UTS for uncoated coarse powder vs sintering duration at 178 mm standoff distance

The results have shown that Young's Modulus and UTS of tensile specimens increased with the increase of duration of infrared radiation. This enhancement of mechanical strength could be due to improvement in the interparticular bonding because of the increased exposure duration.

Average values of Young's Modulus increased from 2.19 to 9.25 (N/mm^2) as the duration of infrared radiation increased from 5 to 60 seconds. Similarly the average UTS increased from 0.57 to 2.42 (N/mm^2) while the duration of IR increased from 5 to 60 seconds.

178 mm distance from IR source			
Description/Item	5 seconds IR exposure	60 seconds IR exposure	% increase
Young's Modulus((N/mm^2)	2.19	9.25	76.32
UTS((N/mm^2)	0.57	2.42	76.44

Table 23 Comparison of Young's Modulus and UTS against exposure time under IR for 178 mm standoff distance

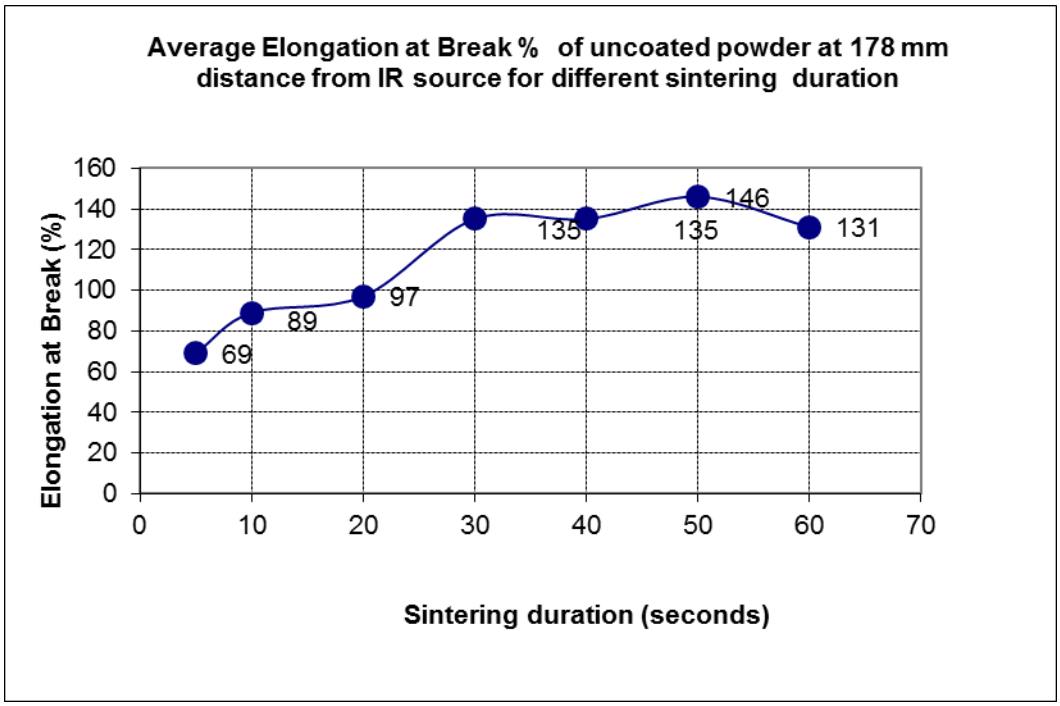

Figure 131'Elongation at Break' for uncoated coarse powder vs sintering duration at 178 mm stand-off distance

Average 'Elongation at Break' increased from 69 up to 131% as the duration of infrared exposure increased from 5 to 60 seconds. The maximum 'elongation at break' was around 146 % after 50 seconds duration of infrared radiation.

6.2.3 Results - Mechanical Properties for 228mm Stand-off Distance

Average Young's Modulus, UTS and 'Elongation at Break' for 228 mm distance between Infrared source and powder samples are measured as shown in figures 132,133,134 respectively.

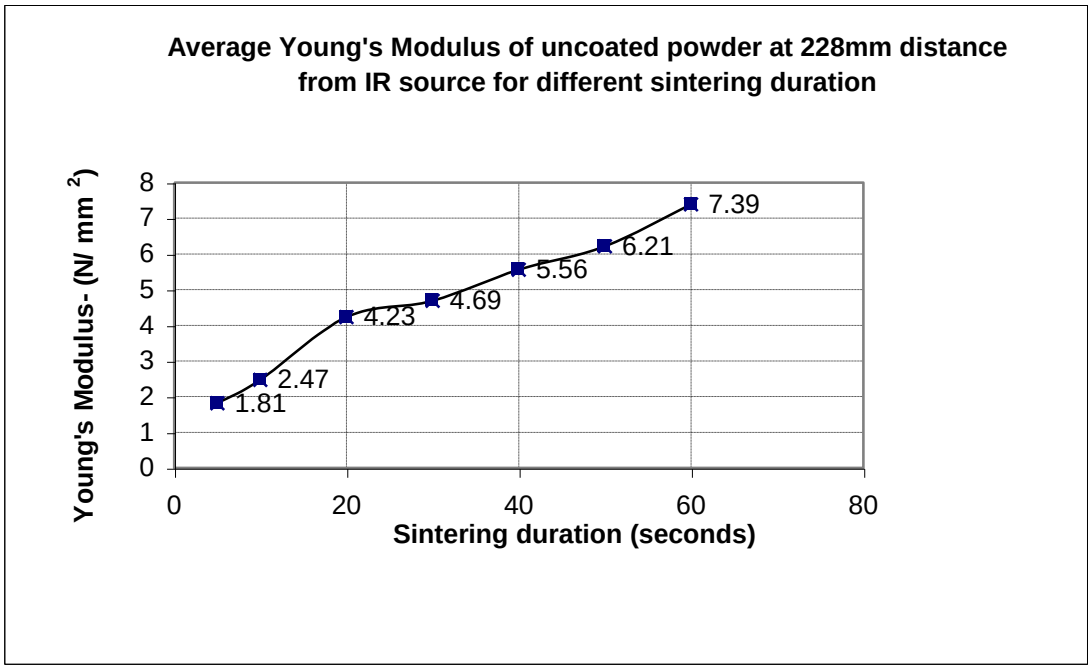

Figure 132 Young's Modulus for uncoated coarse powder vs sintering duration at 228 mm stand-off distance

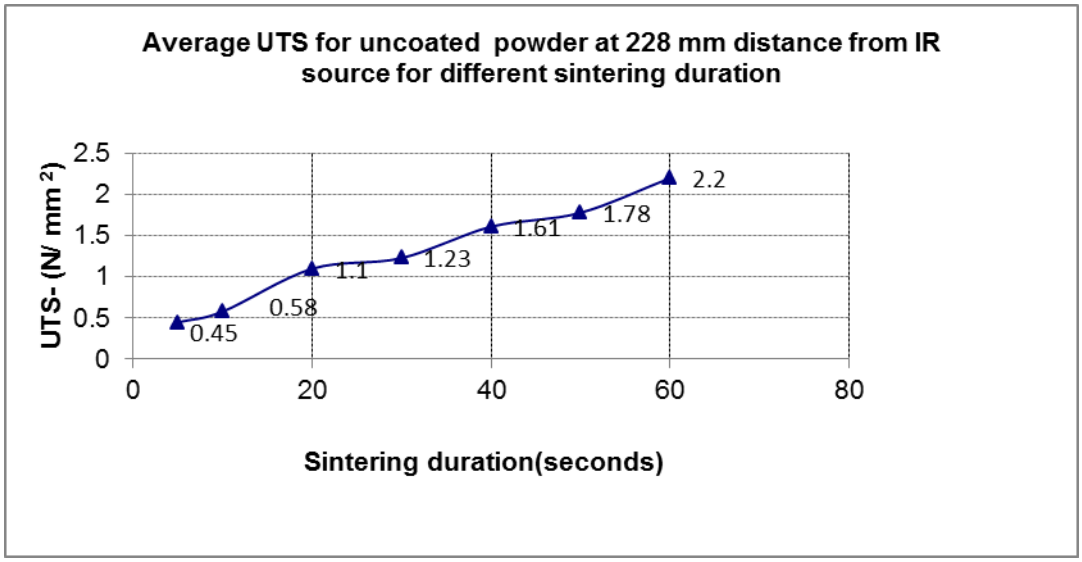

Figure 133 UTS for uncoated coarse powder vs sintering duration at 228 mm stand-off distance

228 mm distance from IR source			
Description/Item	5 seconds IR exposure	60 seconds IR exposure	% Increase
Young's Modulus(N/mm^2)	1.81	7.39	75.50
UTS(N/mm^2)	0.45	2.2	79.54

Table 24 Comparison of Young's Modulus and UTS against exposure time under IR for 228 mm stand-off distance

The average Young's Modulus increased from 1.81 to 7.39 (N/mm^2) as the duration of IR radiation increased from 5 seconds to 60 seconds. Similarly average UTS values increased from 0.45 to 2.2 (N/mm^2) as the duration of IR increased from 5 to 60 seconds.

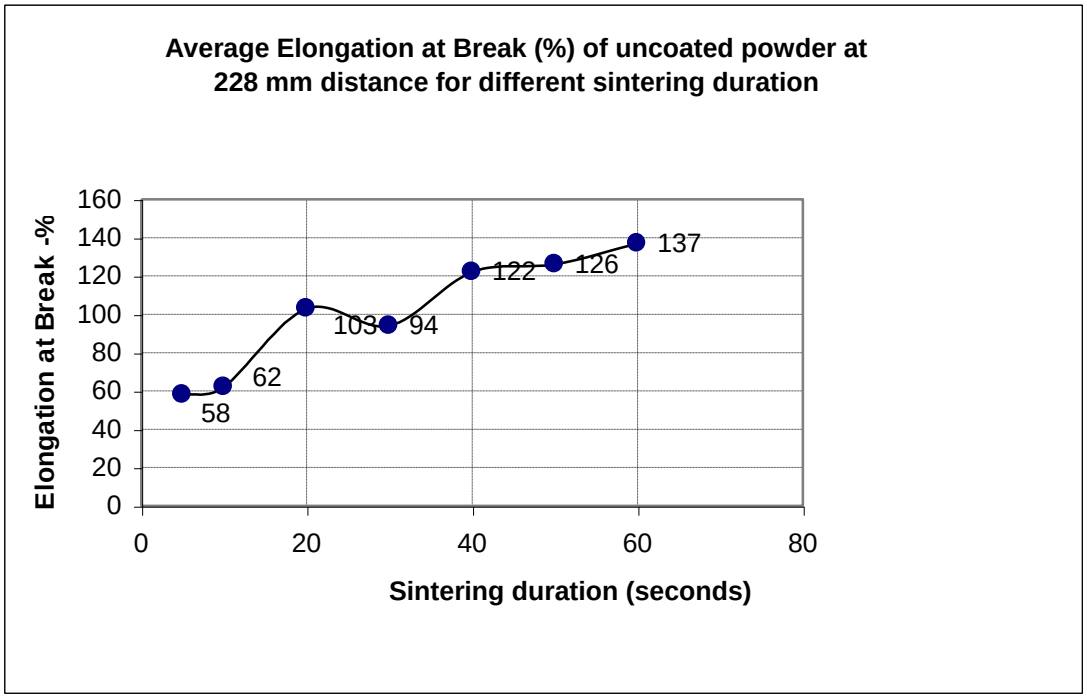

Figure 134 Elongation at Break for uncoated coarse powder vs sintering duration at 228 mm stand-off distance

'Elongation at Break' increased with the increase of exposure of infrared radiation for powder samples sintered at 228 mm distance from infrared radiation. Similar to earlier samples the trend of 'Elongation to Break' found less consistent compared to trend of Young's Modulus and UTS.

6.2.4 Comparison of Mechanical Properties for 128, 178 and 228mm Stand-off Distance

The average values of UTS, Young's Modulus and 'Elongation at break' for 128 mm,178 mm and 228mm distances between infrared and powder particles as shown in the following figures (see Figures 135,136,137 below).

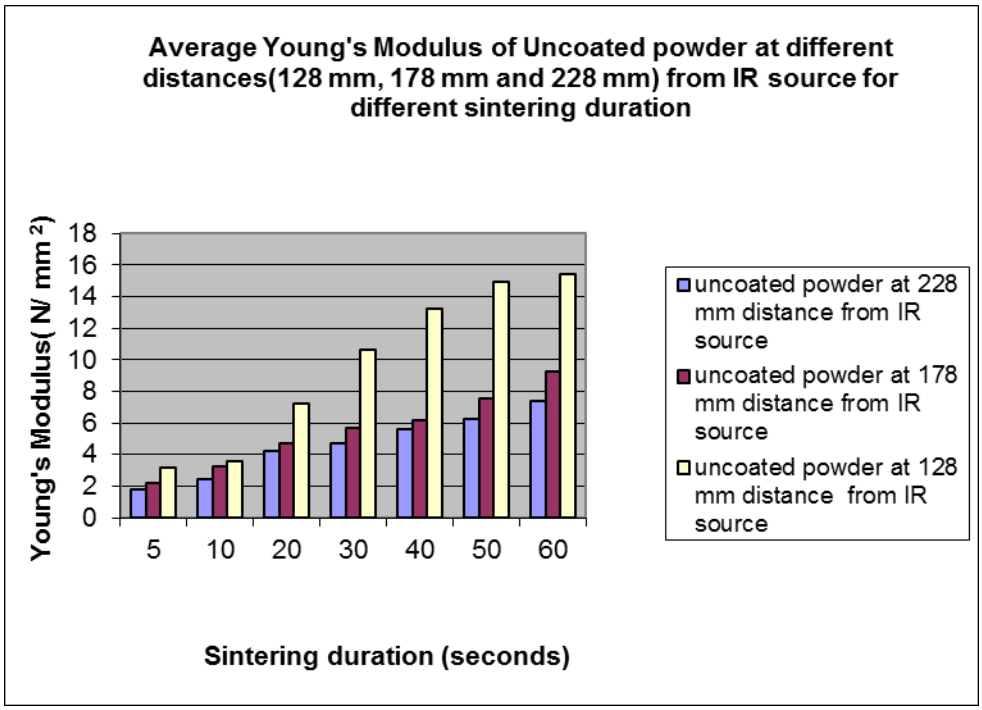

Figure 135 Average Young's Modulus for uncoated coarse powder vs sintering duration at 128,178 and 228 mm stand-off distances

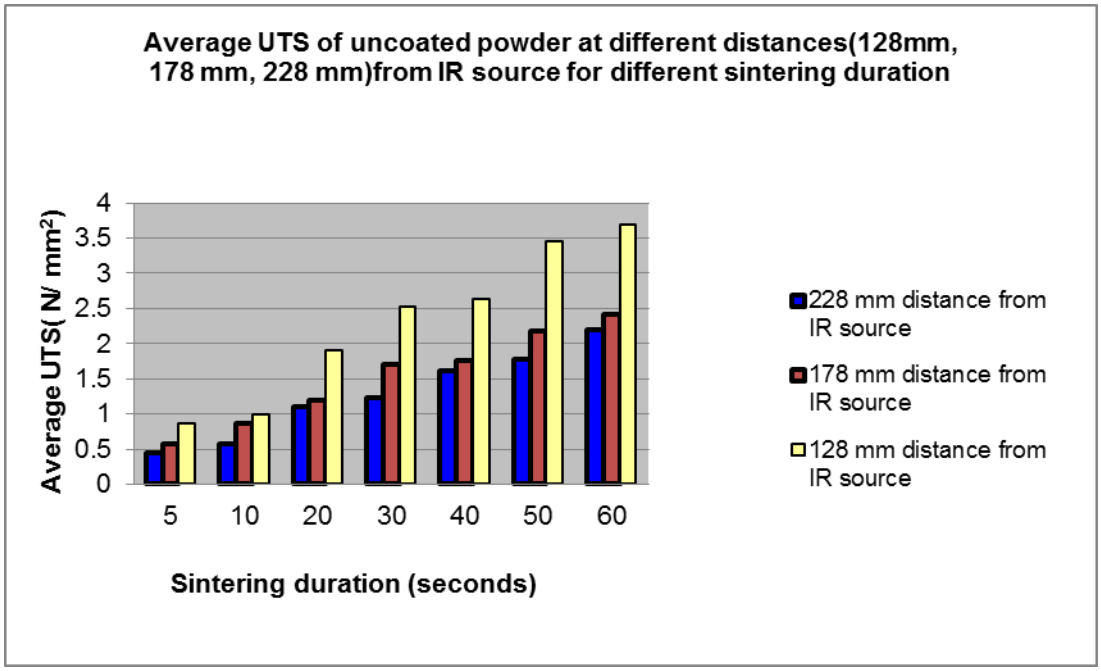

Figure 136 Average UTS for uncoated coarse powder vs sintering duration at 128,178 and 228 mm stand off distances

As expected the Young's Modulus and UTS improved with the increase of exposure time for all powder samples. It is possible to apply a linear regression to the results and thereby calculate the rate of increase of Young's modulus with exposure time. Clearly the 128 mm (5 inch) distance from IR source, had the highest rate of increase of Young's modulus with the duration of exposure of IR radiation.

No significant increase of Young's modulus was noted after 50 seconds duration of infrared radiation for powder particles sintered at 128mm distance from infrared heat source. This could be due to attaining the saturation limit in terms of coalescence of powder particles as beyond that point it is normally difficult to achieve any further improvement of mechanical properties.

Similar to Young's modulus the rate of increase of UTS was also slightly reduced after 50 seconds duration of IR radiation. This could be explained again due to achieving the saturation limit in terms of coalescence of powder particles after 50 seconds duration of infrared radiation.

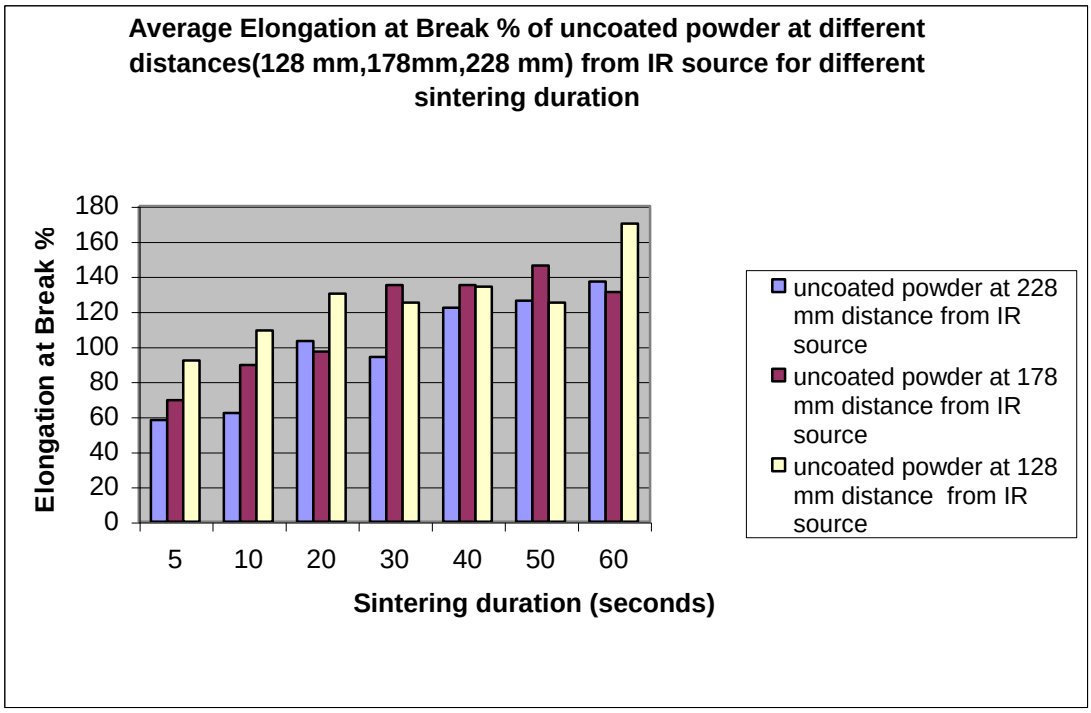

Figure 137 Average Elongation at break for uncoated coarse powder vs sintering duration at 128,178 and 228 mm stand-off distances

As expected 'Elongation at Break' also increased with the increase of exposure time of IR radiation. This could be again due to better inter-particulate bonding. This trend found little less consistent compared to the trend of Young's Modulus and UTS against the exposure time of IR radiation.

6.2.5 Discussion

6.2.5.1 Sintering duration and standoff distance vs. Part's mechanical strength

a) It was found that sintering duration and stand-off distance between powder and heat source have major influence on Young's Modulus and UTS. The maximum Young's modulus achieved during trials at 128 mm standoff distance under 50 seconds of sintering duration (under infrared) was very close to 15.5 MPa(N/ mm^2).This corresponds to published (MSDS of Somos 201) tensile modulus of Laser sintered samples of Somos 201. This demonstrates that mechanical strength of infrared sintered samples of uncoated Somos 201 powder could be comparable for Laser sintered samples. Interestingly, in both cases (IR radiant heating and laser sintering) the powder is melted through liquid phase sintering (as the duration of processing is relatively short < 60 seconds) and moreover, the powder is not subjected to pressure during the sintering process. Processing conditions for laser sintering and IR radiant

heating are in fact very similar .The minimum standoff distance is selected as 128 mm for this research as it was noticed that possibility of having hot spots due to uneven distribution temperature across the powder bed is increased while the standoff distance is reduced (See Appendix C –Thermal survey of IR sintered samples).

b) The increase of Young's modulus could be due to better inter particulate bonding and improved particle densification when the distance between source and target is reduced. This phenomenon directly follows from 'Inverse square law' where intensity of radiation is inversely proportional to the square of the distance between the source and target (see Chapter 2 for more information).

c) Assuming Intensity of radiation 1 unit at 228 mm stand off distance, the intensity of radiation at 178 mm would be $[(1x(228/178)^2$] i.e 1.64 unit. Similarly the intensity at 128 mm would be $[(1x(228/128)^2$] i.e 3 unit. Young's Modulus at 128 mm distance is found approximately 2 and 1.6 times more than the samples sintered at 228 and 178 mm respectively. Similarly UTS at 128 mm distance is found approximately 1.7 and 1.5 times more compared to UTS of the samples sintered at 228 and 178 mm respectively. This shows the effect of 'inverse square law' of intensity of electromagnetic (IR) radiation on Young's Modulus and UTS of the IR sintered samples of Somos 201 powder.

d) 'Elongation at break' is more sensitive to any defect compared to Young's Modulus and UTS. Samples were prepared by manually depositing the powder on the mould as described in the methodology section of the experiment. Any minor inconsistency can introduce some defects within samples which could affect 'Elongation at Break' significantly compared to Young's Modulus and UTS.

e) 110% elongation to failure for laser sintered Somos 201 powder is quoted. For the samples generated by IR radiant heating the elongation to failure was 120-140% and in the case of the 60 second at 128mm it was approximately170%. This may be due to melting of the materials rather than partial melting of particles and sintering as this was indicated by the transition to a shiny compact polymer (melted). This further illustrates the potential at least for uncoated material, that properties of infrared sintered samples could be better than Laser Sintered samples.

f) The maximum value for UTS and Young's modulus for powder samples at 128mm distance from infrared heat source was achieved at 60 seconds sintering duration. This saturation level (maximum value) in terms of Young's Modulus could be equally achieved for powder samples placed at a stand-off distance of 178 mm and 228 mm if the duration of sintering is

increased to 115 seconds and 143 seconds respectively (based on linear extrapolation). Similarly this saturation level in terms of UTS could be equally achieved for powder samples placed at a stand-off distance of 178 mm and 228 mm if the duration of sintering would increase up to 96 and 109 seconds respectively (again based on linear extrapolation).

g) The tensile modulus and UTS for all samples seem to show two distinct phases of sintering (increasing trend of tensile modulus and UTS in 2 steps) . The following figure shows that very loose inter particle bonding takes place at 10 seconds of IR radiation (see Figure 138). At 40 seconds of IR radiation, the improvement of sintering and inter particular bonding were noticed. The global sintering is more feasible after 60 seconds duration of infrared radiation (Figure 138 c).

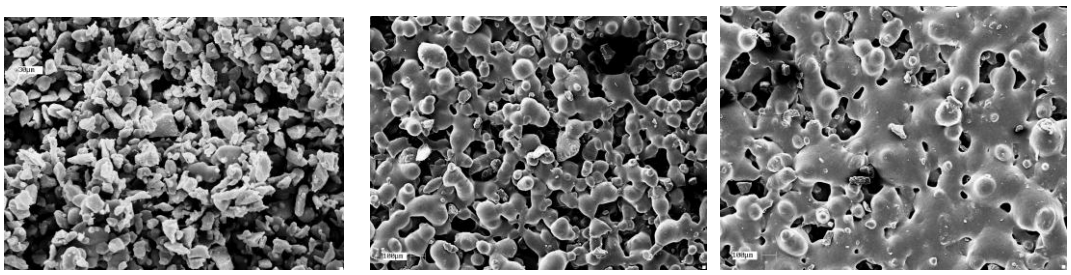

(a) (b) (c)

Figure 138 SEM images of Uncoated powder at 10 ,40 and 60 seconds (a,b and c) exposure of IR radiation

The following figures are also showing the dip (around 40 seconds of infrared radiation) and thereafter a steady increase in Young's Modulus and UTS are noted (see Figures 139 and 140). The first stage may be liquid phase sintering followed by global melting, which can be explained with the following SEM images.

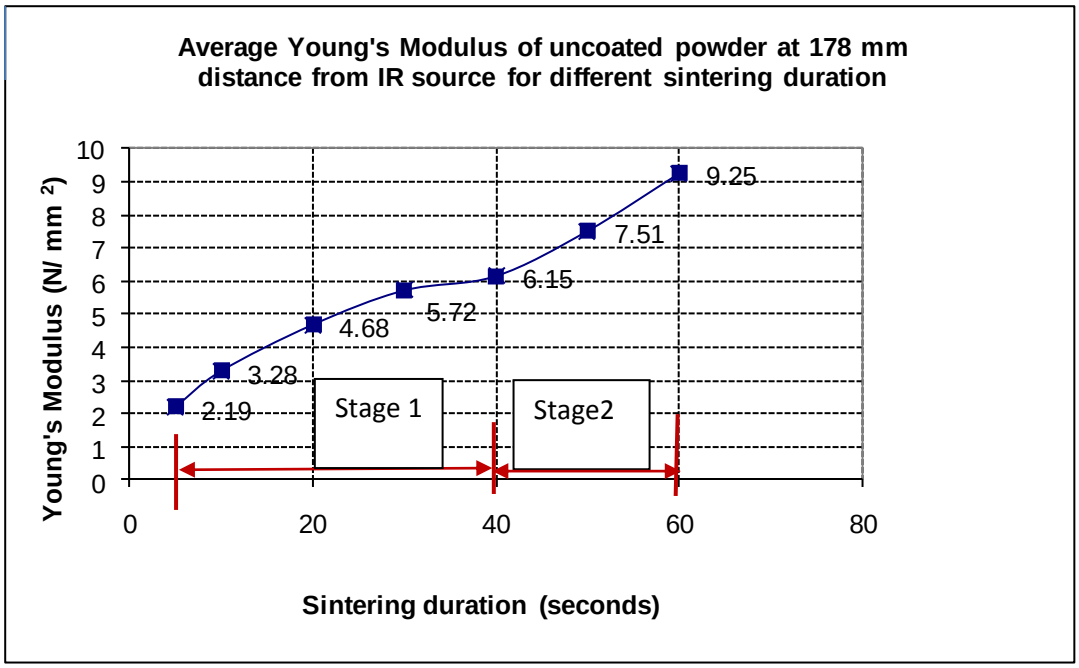

Figure 139 Trend line of Average Young's Modulus for uncoated coarse powder vs sintering duration at 178 mm stand-off distance

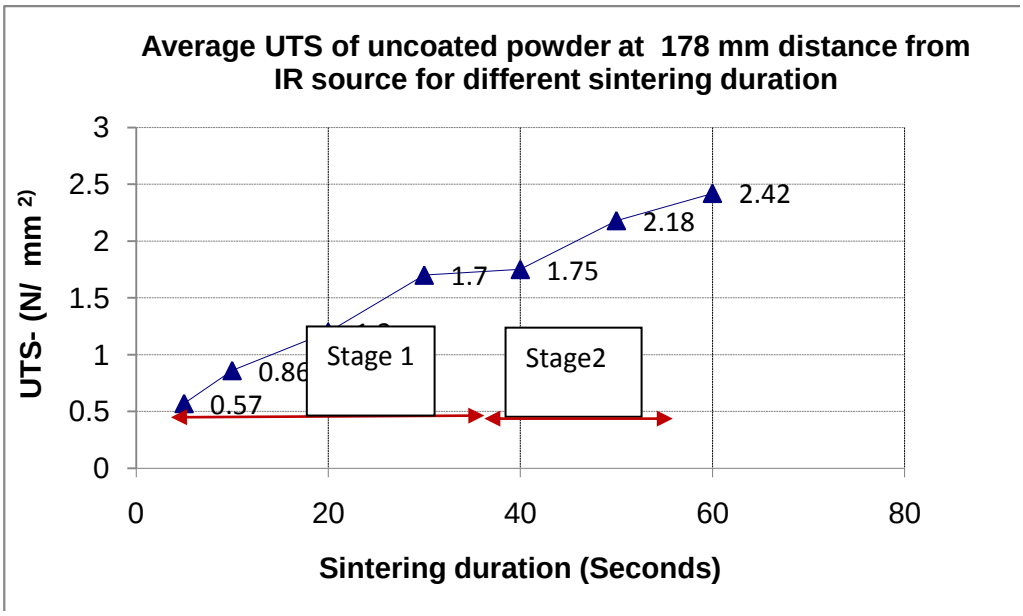

Figure 140 Trend line of Average UTS for uncoated coarse powder vs sintering duration at 178 mm stand-off distance

6.2.5.2 Standard Deviation of Test Results

Although the mechanical strength was found to higher for the tensile samples sintered under 128 mm stand-off distance compared to samples sintered at 178 mm and 228 mm stand-off distance, the standard deviation of Young's Modulus and UTS found to be significantly higher compared to samples sintered using 178 mm and 228 mm stand-off distances respectively (see Figures 142 and 143). The average Coefficient of Variation (CoV) of Young's Modulus for samples sintered at 128 mm stand-off distance found higher (37%) compared to samples sintered at stand-off distance of 178 mm (15%) and 228 mm (15%) respectively (see Figures 144 and 145). The average Coefficient of Variation (CoV) of UTS for samples sintered at 128 mm stand-off distance found higher (27%) compared to samples sintered at stand-off distance of 178 mm(17 %) and 228 mm (CoV 20 %) respectively. This relatively high value of standard deviation and CoV indicates there is inconsistency in the sintering conditions for stand-off distance at 128 mm. This could be the result uneven heating distribution (hot spots) due to the localised affect of individual heating elements (see Figure 141). Moreover, at 128mm even small variations in sintering time (due to experimental procedure) could have a significant effect on the mechanical properties. On the other hand the 228 mm standoff distance takes more time to sinter the sample, which would reduce the process speed for SLP process. To balance between high inconsistencies at 128 mm standoff distance and reduction of process speed due to longer distance at 228 mm, the 178 mm standoff distance was selected for future trials.

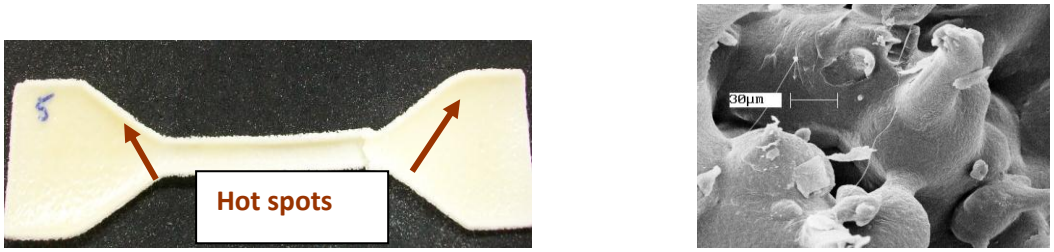

(a) (b)

Figure 141 Hot spots (a) and SEM images (b) of uncoated coarse powder at 128 mm stand-off distance after 60 seconds exposure of IR radiation

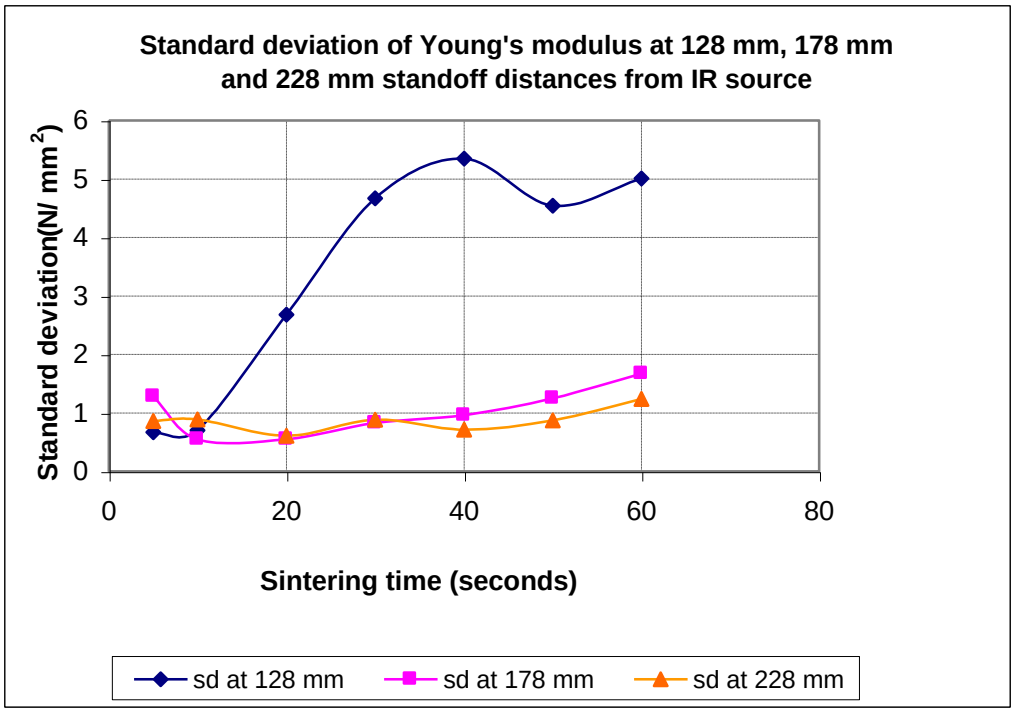

Figure 142 Standard deviation of Young's Modulus for uncoated coarse powder vs sintering duration at 128,178 and 228 mm stand-off distances

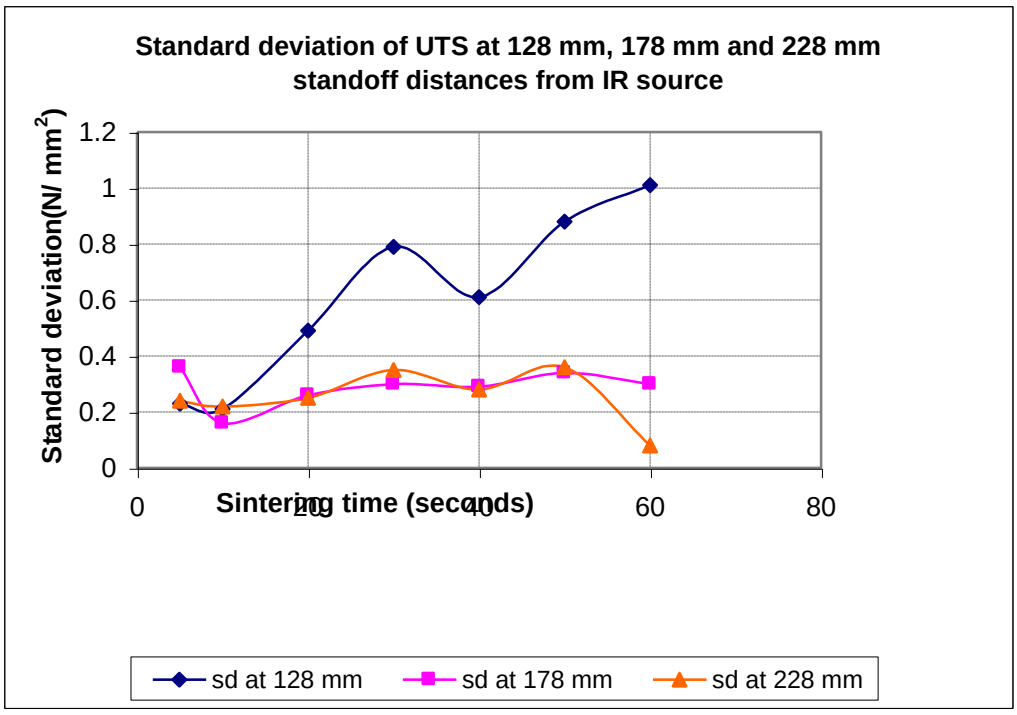

Figure 143 Standard deviation of UTS for uncoated coarse powder vs sintering duration at 128,178 and 228 mm stand-off distances

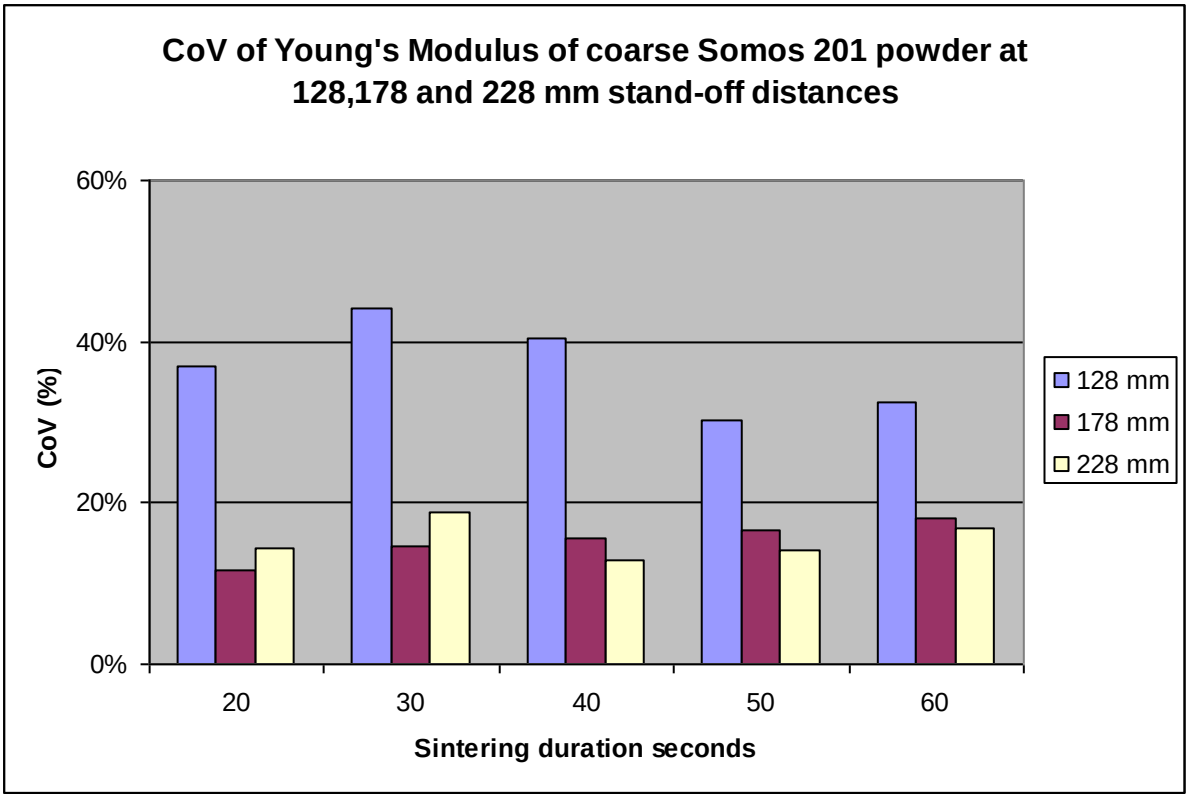

Figure 144 CoV of Young's Modulus for uncoated coarse powder vs sintering duration at 128,178 and 228 mm stand-off distances

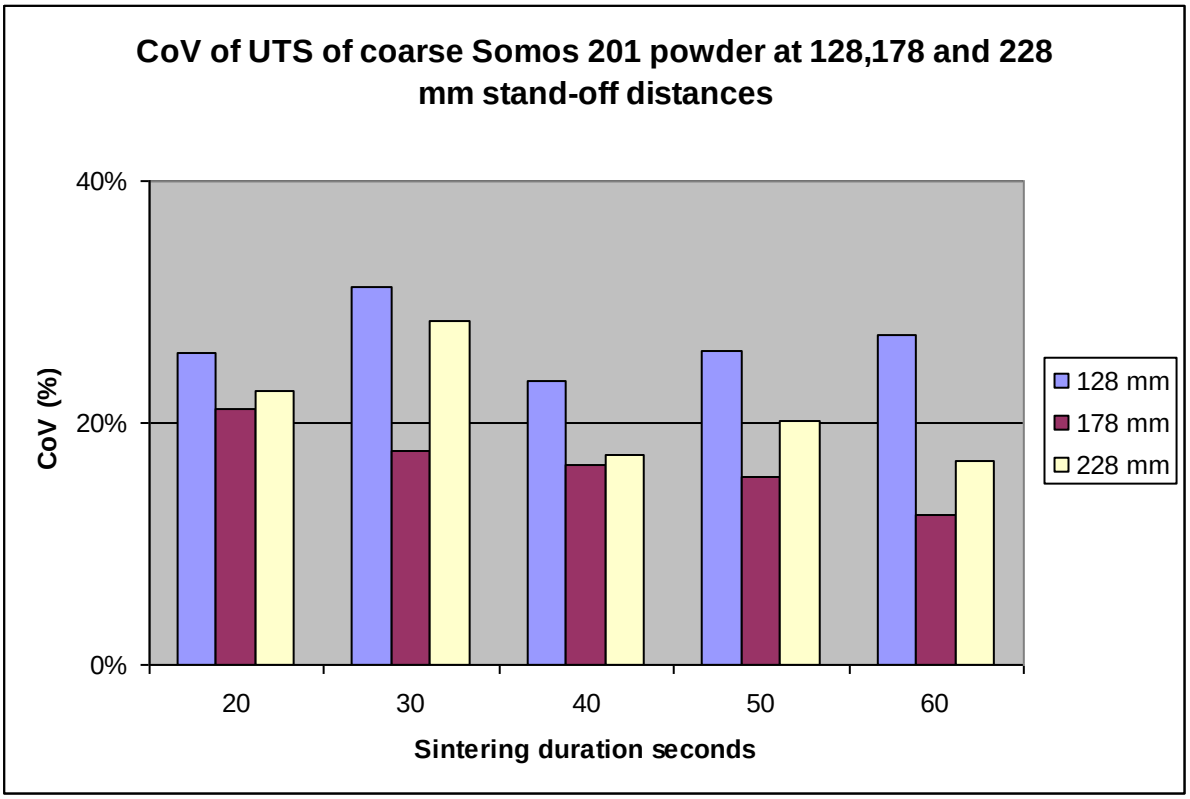

Figure 145 CoV of UTS for uncoated coarse powder vs sintering duration at 128,178 and 228 mm stand-off distances

6.3 Background: Particle size and IR sintering for SLP process

In order to establish the influence of particle size on IR radiation, trials were undertaken to expose 17 and 30µm particle sizes to different exposure duration of IR radiation. These particle sizes were selected, as powder particle more than 30µm are very difficult to print using electrophotography as justified in the methodology section. The experimental methodology was very similar to earlier trials as mentioned below (section 10.1).

6.3.1 Particle size: Experimental procedures

An aluminium mould plate with 10 cavities each having the geometry of tensile test specimen (dog bone shaped) with 2 mm depth was prepared as per tensile test specimen BS ISO 37: 2005 standard– 'Rubber vulcanised or Thermoplastic –Determination of Tensile stress-strain specimen' (see appendix). The experimental procedures used was very similar to that described in the earlier section, using two different sets of powder samples with average particle sizes of 17 and 30µm were prepared.

Serial Number	Particle size (µm)	Standoff distance (mm)	% of coating with Fumed silica
1	17	178	0
2	30	178	0

Table 25 Specific conditions for tests 17 and 30 µm particle size

6.3.2 Results - Mechanical Properties for 17 µm Uncoated Powder

The average Young's Modulus and UTS values for 17µm particle size are plotted against the different exposure time of infrared radiation (see Figures 146 and 147). The average value of Young's Modulus increased from 9 to 12 N/ mm^2 (MPa) when the duration of radiation increased from 20 to 60 seconds. Similarly the average values of UTS increased from 1.75 to 2.19 N/ mm^2 (MPa) when the duration of infrared radiation increased from 20 to 60 seconds. This indicates that increased duration of infrared radiation helps to improve the inter-particle bonding to achieve better mechanical strength.

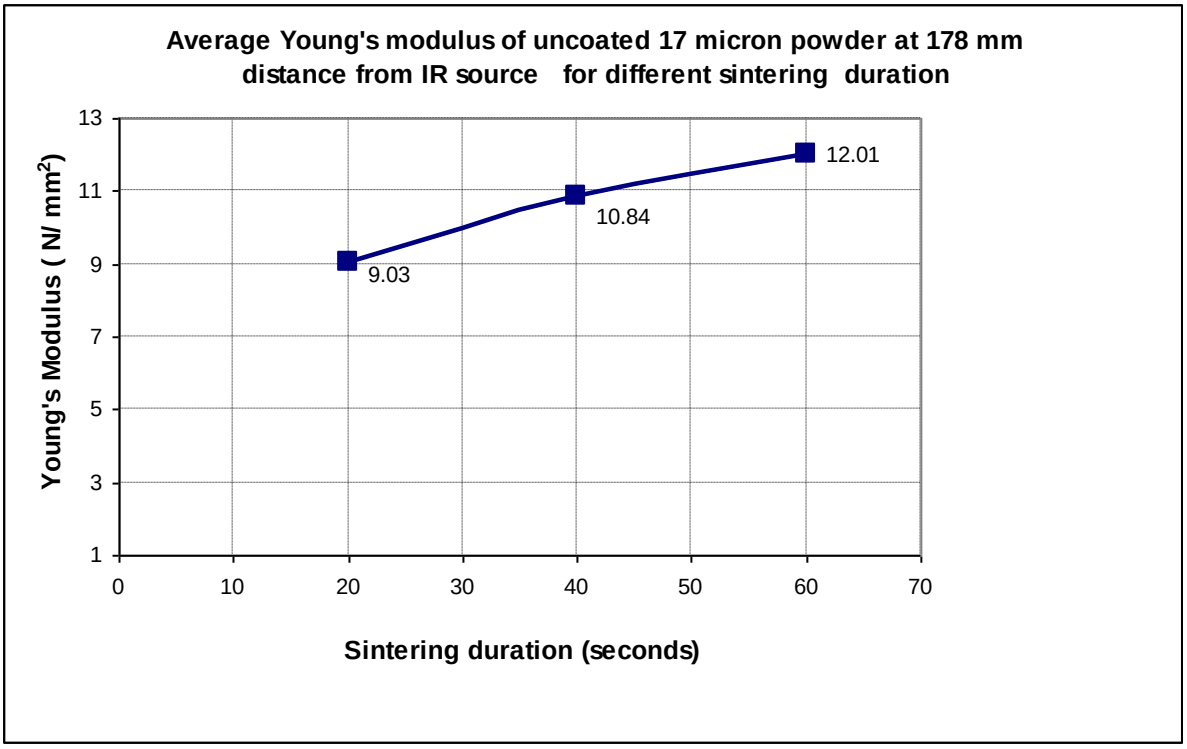

Figure 146 Average Young's Modulus of uncoated 17µm Somos 201 powder particles sintered at 178 mm stand-off distance for 20,40 and 60 seconds exposure of IR radiation

A steady increase of Young's modulus was noted with an increase in exposure of IR radiation. Assuming linear trend line as y= .0745x+7.6467 (and R^2 =0.98) that Young's modulus of approximately 15 N/ mm^2 (MPa) could be achieved if sintering duration is extended up to 100 seconds. Similarly a steady increasing trend between UTS and duration of infrared radiation also noted for uncoated 17µm powder samples as shown below.

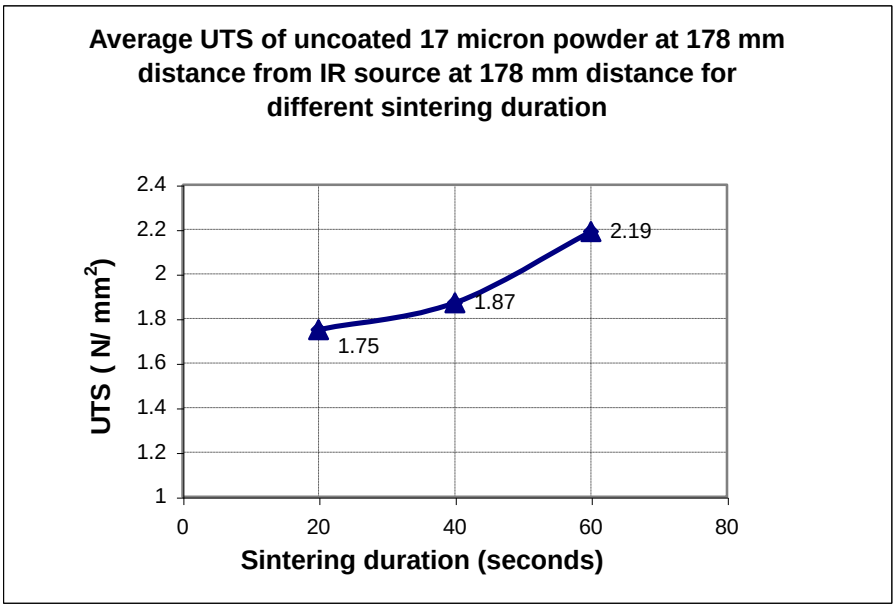

Figure 147 Average UTS of uncoated 17µm Somos 201 powder particles sintered under infrared at 178 mm stand-off distance for 20,40 and 60 seconds exposure of IR radiation

Selecting linear trend between UTS and infrared duration (y= .011x +1.4967) it was found that rate of increase (slope) of UTS against the exposure time was 6.5 degree (θ = tan-1 (0.11).

Similarly 'Elongation at Break' was also measured to determine the relationship with the duration of IR radiation for 17 µm uncoated powder samples. No significant change in 'Elongation at Break' was found with increasing exposure time (as 69% and 61% are not very different in terms of 'Elongation to Break' , particularly when testing a rubberised polymer).

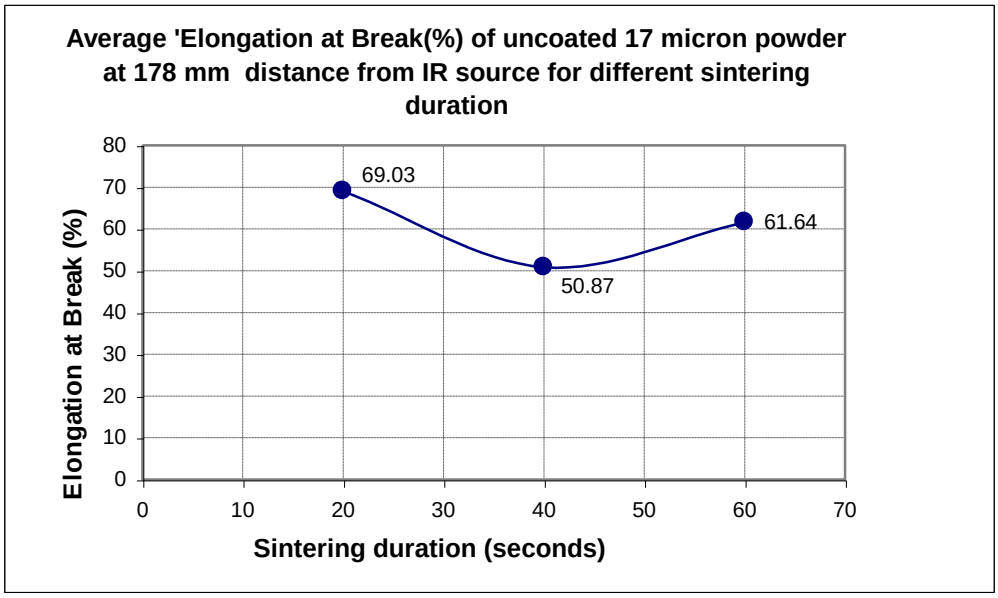

Figure 148 Average 'Elongation at Break' of uncoated 17µm Somos 201 powder particles sintered under infrared at 178 mm stand-off distance for 20,40 and 60 seconds exposure of IR radiation

6.3.3 Results - Mechanical Properties for 30 µm Uncoated powder

The average Young's Modulus and UTS values for 30µm particle size are plotted against the different exposure time of infrared radiation .It was found that average Young's modulus and UTS values increased as the exposure time of infrared radiation increased. This could be due to improved inter particulate bonding, which would occur with increasing duration of exposure time of IR radiation.

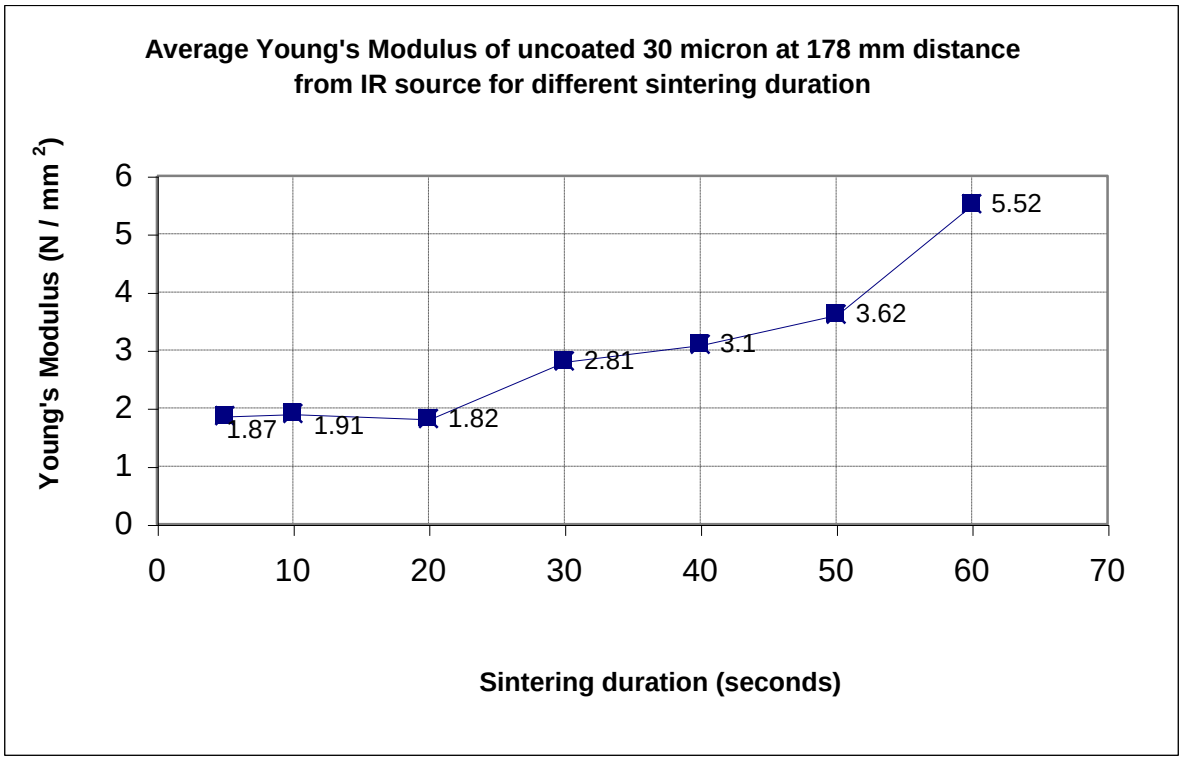

Figure 149 Average Young's Modulus of uncoated 30µm Somos 201 powder particles sintered at 178 mm stand-off distance for 20,40 and 60 seconds exposure of IR radiation

A steady increase in Young's modulus was noted with increasing of exposure of IR radiation. Selecting linear trend line as y=0.0599x+1.1094 (and R^2 =0.8526) it is found that Young's modulus of approximately 15MPa could be achieved if sintering duration is extended up to 120 seconds. Similarly a steady increasing trend between UTS and duration of infrared radiation also noted for uncoated 30µm powder samples as shown in Graph 55.

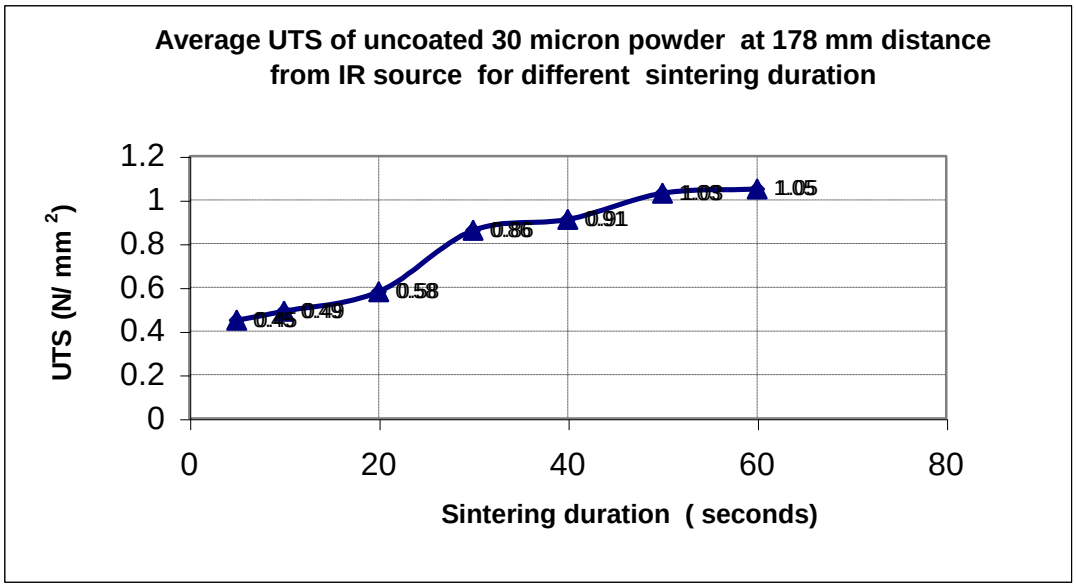

Figure 150 Average UTS of uncoated 30µm Somos 201 powder particles sintered at 178 mm stand-off distance for 20, 40 and 60 seconds exposure of IR radiation

Selecting linear trend between UTS and infrared duration it was found that rate of increase (slope) of UTS against the exposure time was 6.5 degree (θ = tan-1 (0.11). Similarly 'Elongation at Break' was also measured to find out the relationship with the duration of IR radiation for 30µm uncoated powder samples. The saturation limit for 'Elongation to Break' was observed between 40 to 50 seconds of infrared duration, as there was no evidence of a further increase of 'Elongation at Break' beyond that point.

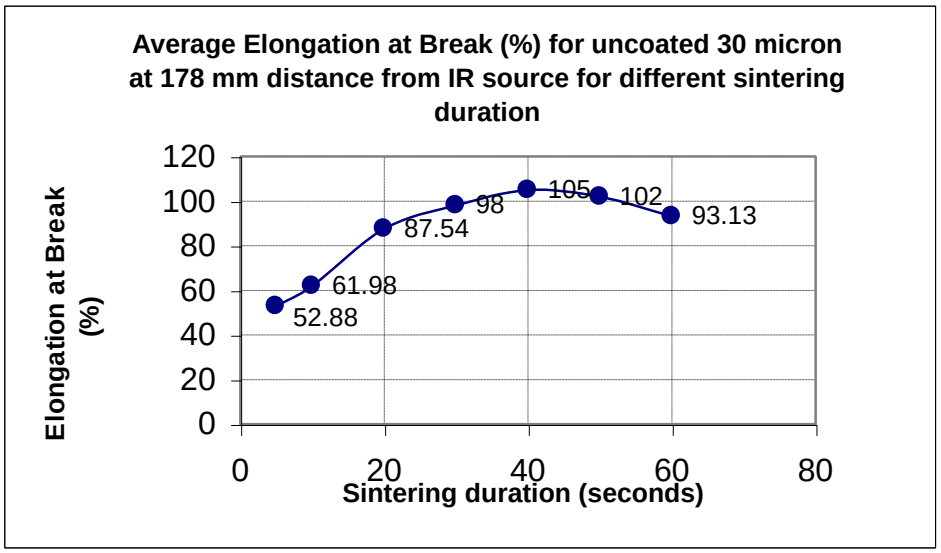

Figure 151 Average UTS of uncoated 30µm Somos 201 powder particles sintered at 178 mm stand-off distance for 20,40 and 60 seconds exposure of IR radiation

6.3.4 Discussion

It has been found that particle size and wavelength of infrared radiation selection are equally important for SLP process as both influence mechanical strength of the parts produced while sintering under infrared radiation. The Somos 201 powder has shown better mechanical strength for average particle size of 17µm for the infrared unit (wavelength of radiation varying within 0.7 to 3 µm comprising both near infrared and medium wavelength) selected for the trials. This could be due to larger surface area is available for 17µm particle sizes compared to 30µm particle sizes.

As per literature survey the IR absorption of polymer powder particle is a complex process which depends not only on particle sizes but also depends on various other factors including shape of the powder particles, compaction strength and infrared sensitivity (Ventura, Papini1999).

This chapter was intended to find out the optimise particle size considering both mechanical properties and ability to print. Finer particle sizes (below 20µm) always help for laser printing with improved resolution and good quality images. The particle sizes above 25 to 30µm are generally very difficult to print for standard laser printers. The improvement of mechanical strength for smaller particle size under the selected infrared unit also helps to go for small particle size as it is equally good for printing and mechanical strength.

The UTS and Young's Modulus have shown linear trend with exposure time of IR radiation for both 17 and 30 µm powder sample. It is expected that rate of increase will be slower as the coalescence of powder particles would reach its highest level because of very little opportunity would be left for further improvement of the inter-particle bonding.

Similar to uncoated powder particles the 17 and 30 µm powder particles have shown increasing trend of UTS and Young's Modulus in 2 steps. This 2 stage of sintering was due to very loose inter-particular bonding in the beginning (approximately 10 to 20 seconds of IR radiation) and thereafter an improved inter-particular bonding occurred after 40 seconds of IR radiation. The global melting is more feasible after 60 seconds duration of infrared radiation.

The average Young's Modulus for 17 and 30µm particle sizes are plotted against the duration of exposure of infrared radiation to understand the effect of particle sizes on mechanical strength as shown below. It was noted that that the values of Young's Modulus and UTS for the 17µm particle size samples is approximately 50% higher than for 30µm particle size samples (see Figures 152 and 153).

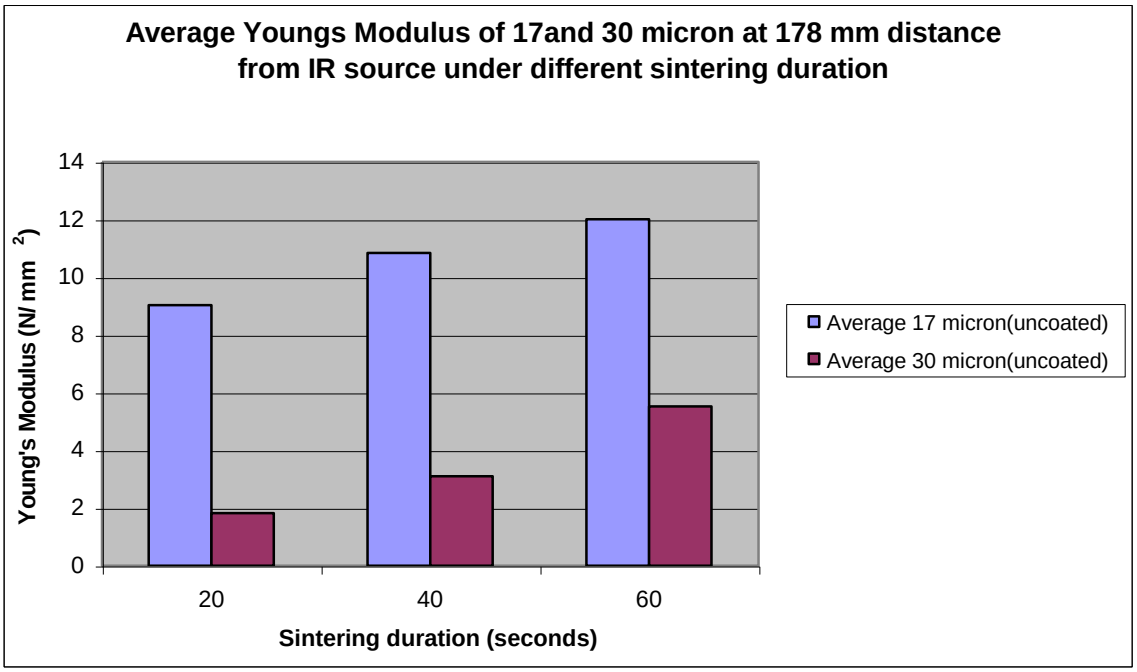

Figure 152 Comparison of Average Young's Modulus of uncoated 17 and 30µm Somos 201 powder particles sintered under infrared radiation at 178 mm stand-off distance for 20,40 and 60 seconds exposure of IR radiation

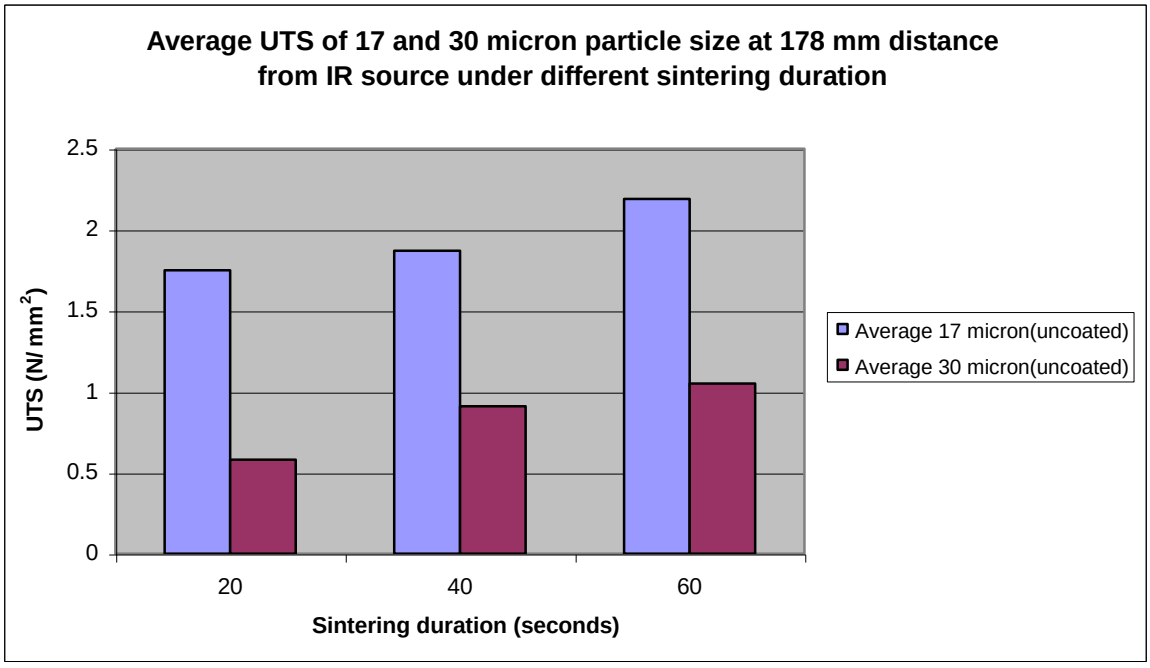

Figure 153 Comparison of Average UTS of uncoated 17 and 30µm Somos 201 powder particles sintered under infrared radiation at 178 mm stand-off distance for 20,40 and 60 seconds exposure of IR radiation

The rate of increase of UTS and Young's modulus of 17 µm powder sample found also higher compared to 30 µm powder sample. Extrapolating the trend line it was mentioned that Young's modulus of 15 MPa could be achieved after 100 and 120 seconds of IR duration for 17 and 30 µm powder samples respectively. This time duration could be reduced either by increasing the intensity of infrared source or by decreasing the stand-off distances below 178 mm. This improved mechanical properties is due to more surface area for the same mass of 17 µm compared to 30 µm powder particles. The following SEM images of 17 and 30 µm powder samples after 60 seconds of infrared duration are indicating better inter-particular bonding for 17 µm compared to 30 µm powder samples (see Figure 154).

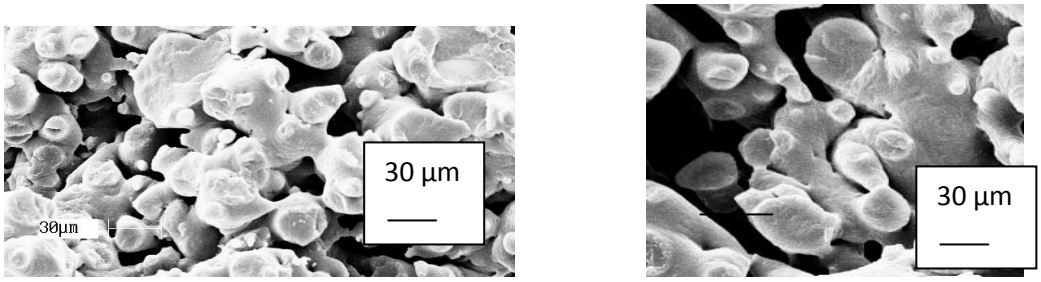

Figure 154 SEM images of (a) 17 µm and (b) 30 µm at 178 mm stand –off distance

6.4 Influence of Surface Additives on the Properties of IR Fused Somos 201 Powder

The trials presented in Chapter 9 show that it is important for particles of Somos 201 to be coated with fumed silica to improve the flow of particles in order to print with the SLP process. Although the effect of surface additives on mechanical strength of a laser printed layer for conventional printing applications is not a significant concern for Additive Manufacturing, where a 3D object is constructed from multiple layers of material, this must be considered. In this chapter a study on the overall effect of fumed silica on the mechanical properties of radiant infrared fused samples is presented.

6.4.1 Experimental Methodology

A similar experimental methodology, as described in earlier sections was applied in this case. Three different levels of silica coatings (0%, 0.3% and 1.2% by weight) are selected based on the industrially accepted level of coating which is normally applied for toner development. 17 and 30 µm particle sizes are selected as these sizes are close to industrially accepted toner sizes for new toner development. The coated Somos201 was exposed to IR radiant heating for different durations (up to 60 seconds) and the tensile test specimens formed samples were subjected to mechanical testing.

Serial Number	Particle size (µm)	Fumed silica(% by wt)	Standoff distance(mm)
1	17	0	178
2	17	0.3	178
3	17	1.2	178
4	30	0	178
5	30	0.3	178
6	30	1.2	178

Table 26 Specific conditions of tests with different level of coatings

6.4.2 Results - Mechanical properties of 0.3% silica coated 17µm powder

The Average Young's Modulus, UTS and 'Elongation at Break' for 0.3% coated of average particle size of 17µm at 178 mm distance from IR source for 20, 40 and 60 seconds exposure is presented in this section.

The average values of Young's modulus for the 0.3% coated samples are plotted against the duration of IR exposure (see Figure 155). As the duration of IR exposure is increased from 20 to 60 seconds it was noted that average value of Young's Modulus increased from 3.92 to 9.78 MPa.

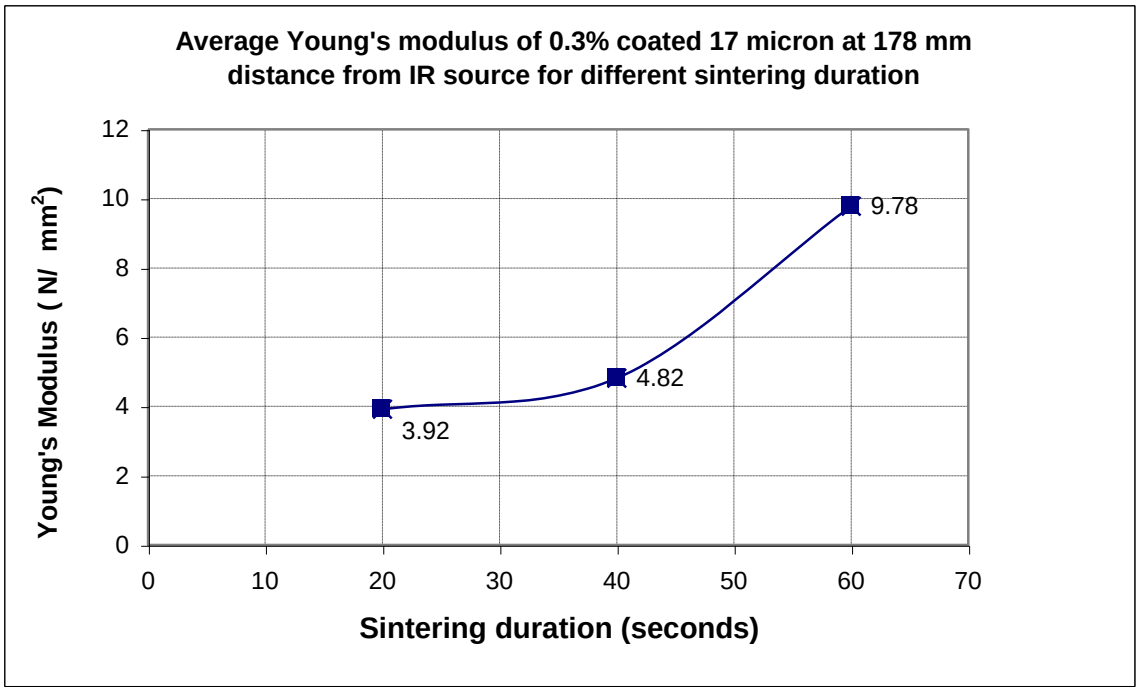

Figure 155 Average Young's Modulus of 17-µm particle size with 0.3% surface coated and sintered under infrared radiation at 178 mm stand-off distance

Similar to uncoated powder particles, the coated (0.3% by weight) has shown the increasing trend of UTS and Young's Modulus in 2 steps. This 2 stage of sintering was due to very loose inter-particular bonding in the beginning (approximately 10 to 20 seconds of IR radiation) and thereafter an improved inter-particular bonding occurred after 40 seconds of IR radiation. The global melting is more feasible after 60 seconds duration of infrared radiation.

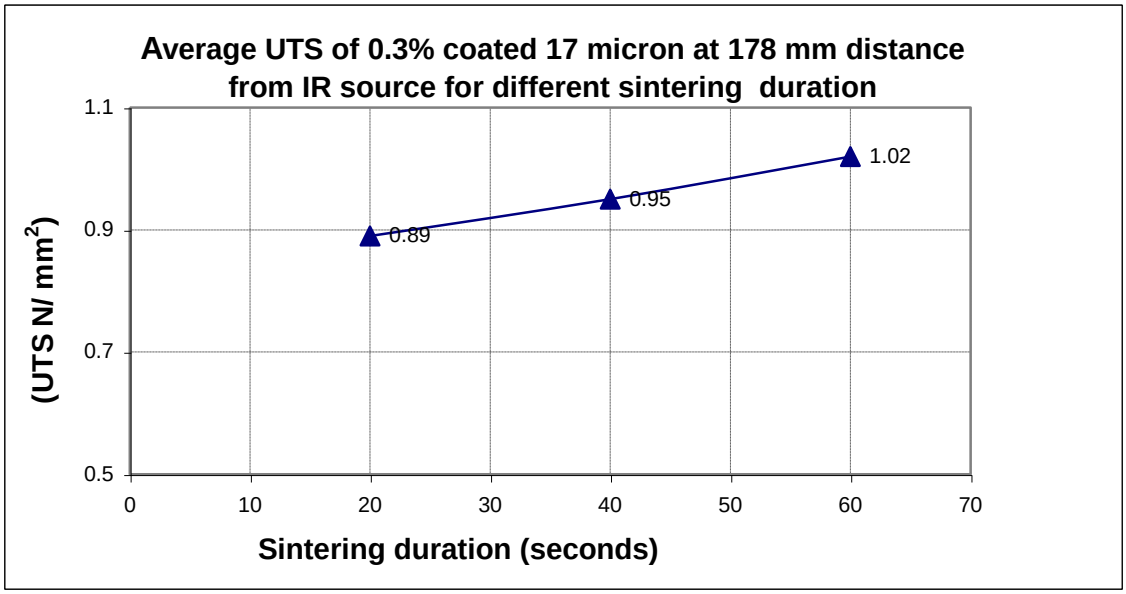

Figure 156 Average UTS of 17-µm particle size with 0.3% surface coated and sintered at 178 mm stand-off distance

The average values of UTS for the 0.3% coated samples are plotted against the duration of IR exposure (see Figure 156). As the duration of IR exposure increased from 20 to 60 seconds it was noted that average value of UTS increased from 0.89 to 1.02 MPa. The rate of increase of UTS with exposure of IR radiation found linear for both uncoated and 0.3% coated powder samples which is similar to uncoated powder samples (Please refer earlier section).

The average values of 'Elongation at Break' were also measured (see Figure 157). It was found that 'Elongation at Break' was 30% for the samples sintered for 60 seconds and 22% for the samples sintered for 20 seconds under the same infrared radiation. This 8 % change in 'Elongation at Break' is comparatively small percentage increase for rubberised polymer.

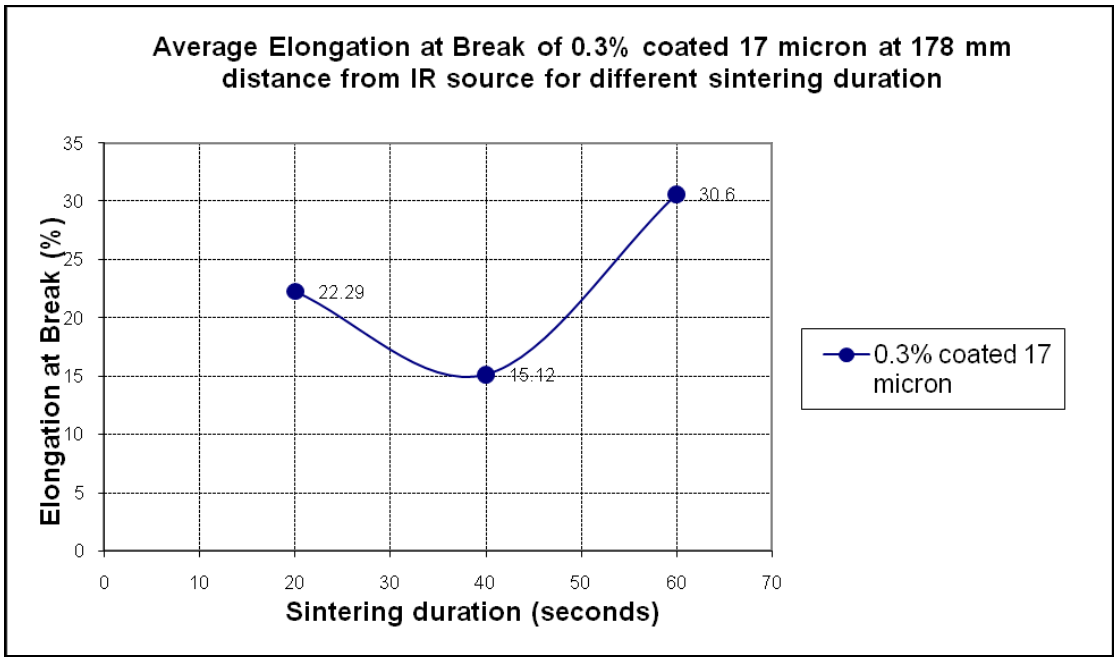

Figure 157 Average 'Elongation at Break' of 17 µm particle size with 0.3% surface coated and sintered under infrared radiation at 178 mm stand-off distance

6.4.3 Mechanical properties of 1.2 % coated 17µm powder sample

Average Young's Modulus, UTS and 'Elongation at Break' for 1.2 % coated of average particle size of 17µm at 178 mm distance from IR source for 20, 40 and 60 seconds exposure.

The average values of Young's modulus for 1.2 % coated 17µm powder samples are plotted against the duration of infrared duration (see Figure 158). It was noticed that average value of Young's Modulus increased from 0.38 to 0.55 MPa when the duration of IR exposure increased from 20 to 60 seconds.

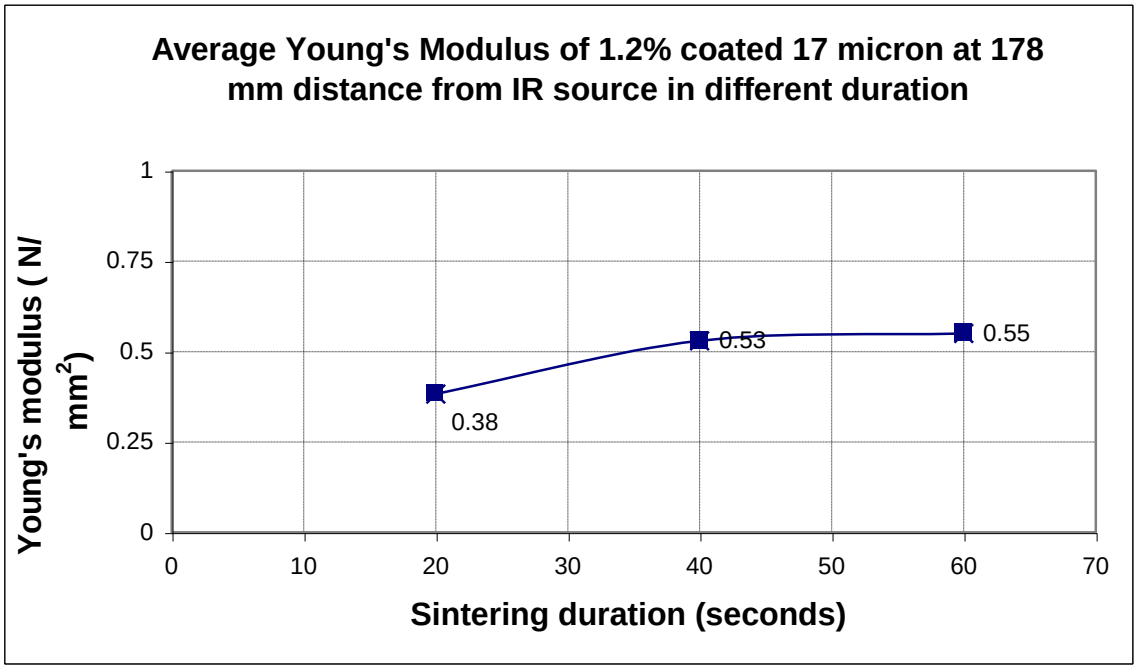

Figure 158 Average Young's Modulus of 17µm particle size with 1.2 % surface coated and sintered under infrared radiation at 178 mm stand-off distance

It was noticed that average value of UTS for 1.2 % coated Somos 201 material increased from 0.06 to 0.12 MPa while the duration of radiation when the duration of IR exposure increased from 20 to 60 seconds (see Figure 159). The trend of both UTS and Young's Modulus against the duration of IR exposure time for 1.2% coated 17 µm powder sample found very similar. Slight increase of UTS and Young's Modulus were noticed as the duration of exposure is increased from 20 to 40 seconds but no further improvement was noticed for UTS and Young's modulus after 40 seconds of exposure time.

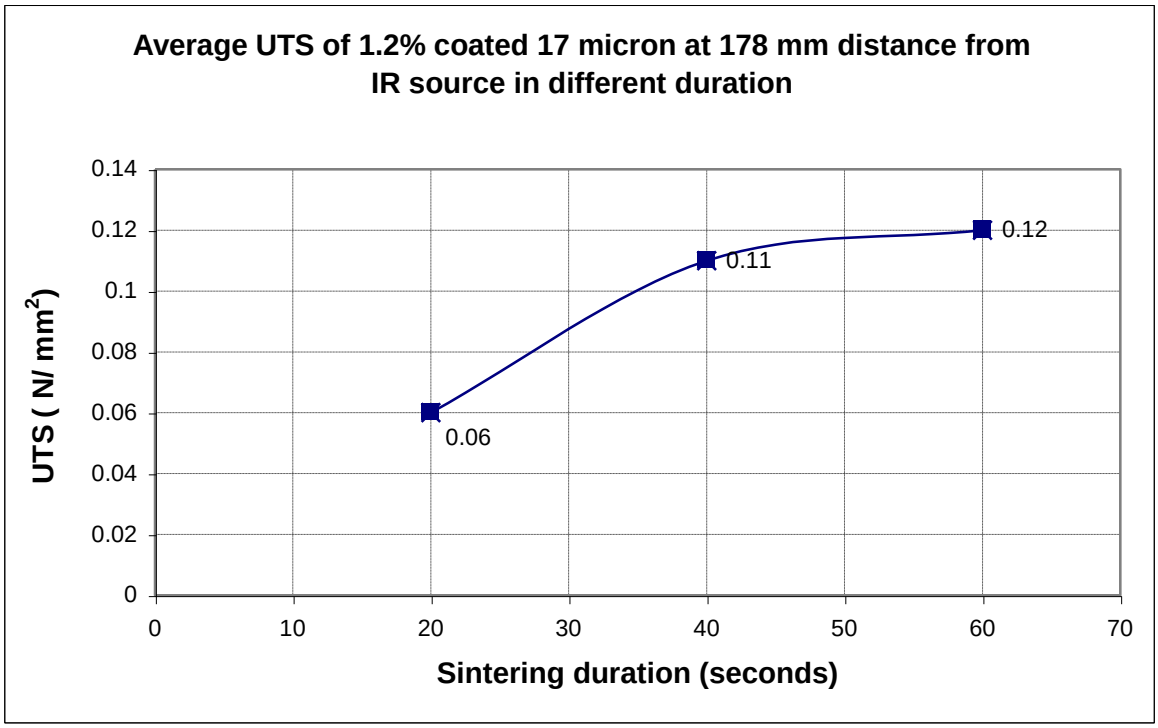

Figure 159 Average UTS of 17 µm particle size with 1.2 % surface coated and sintered at 178 mm stand-off distance

The average values of 'Elongation at Break' were measured at 20, 40 and 60 seconds of exposure time of IR radiation (see Figure 160). It was found that 'Elongation at Break was 22% for the samples sintered for 20 seconds and increased to 30% after 40 seconds and then reduced to just 16% after 60 seconds of infrared exposure. There is a slight increase of Elongation at Break was noticed at 40 seconds of IR radiation But later the 'Elongation of Break' was reduced to 16%as the exposure time increased from 40 to 60 seconds. The +/-10 % change of 'Elongation at Break' is not significant for rubberised material (like Somos 201 which is a Thermoplastic Elastomer).

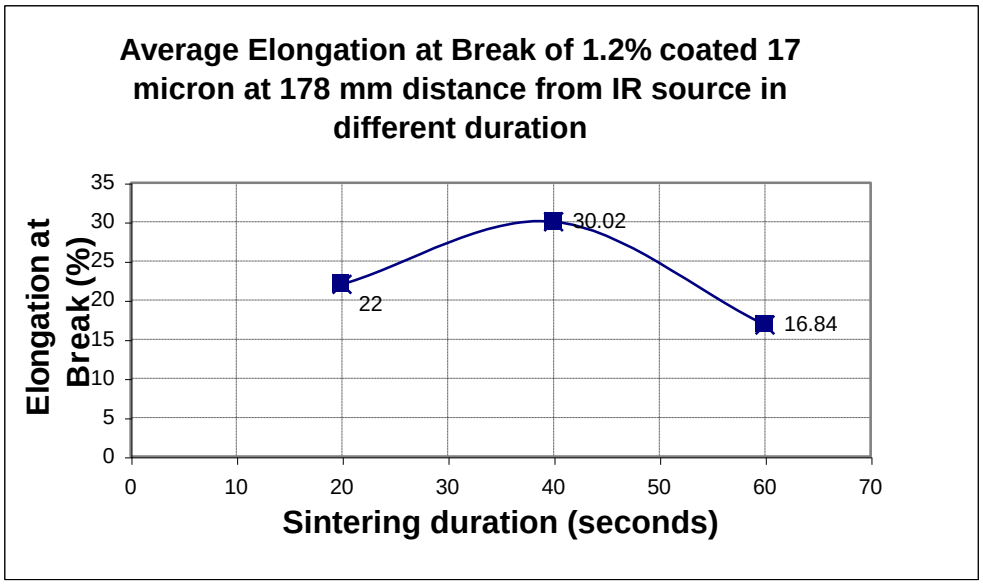

Figure 160 Average 'Elongation at Break' of 17µm particle size with 1.2 % surface coated and sintered at 178 mm stand-off distance

6.4.4 Mechanical properties of 0.3% coated of 30 µm powder sample:

The average Young's Modulus, UTS and 'Elongation at Break' for uncoated 30µm average particle size at 178 mm stand-off distance from IR source for 20, 40 and 60 seconds duration mentioned in the earlier section of the thesis .

The average Young's Modulus, UTS and 'Elongation at Break' for 0.3% coated average particle size of 30µm at 178 mm distance from IR source for 20, 40 and 60 seconds exposure.

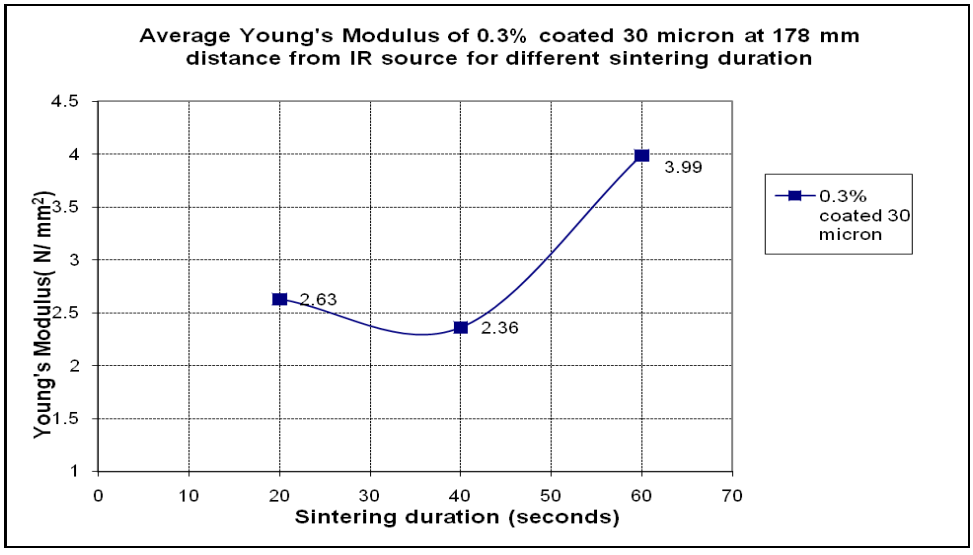

Figure 161 Young's Modulus of 0.3% coated 30 µm particle size IR sintered at 178 mm stand-off distance of 20, 40 and 60 seconds of sintering duration

The average values of Young's modulus for the 0.3% coated 30µm samples are plotted against the duration of IR exposure (see Figure 161). As the duration of IR exposure increased from 20 to 60 seconds, the average value of Young's Modulus increased from 2.63 to 3.99 MPa. The rate of increase of Young's Modulus of 0.3% coated material found 41% which is significantly lower than the 67% rise in Young's Modulus for uncoated material for the same exposure of IR radiation. (Please refer earlier section of uncoated 30 µm powder sample)

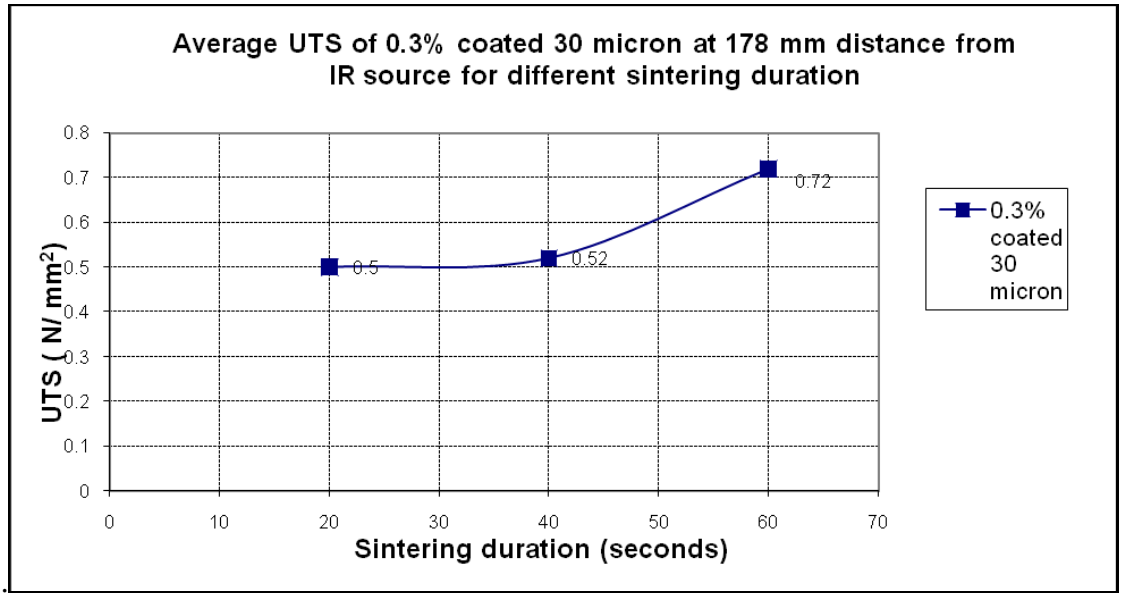

Figure 162 UTS of 0.3% coated 30 µm particle size IR sintered at 178 mm stand-off distance of 20, 40 and 60 seconds of sintering duration

The average values of UTS for the 0.3% coated 30 micron samples are plotted against the duration of IR exposure (see Figure 162). As the duration of IR exposure increased from 20 to 60 seconds it was noted that average value of UTS increased from 0.5 to 0.72 MPa (30 % increase). This rate of increase of UTS was significantly lower compared to uncoated 30 µm powder sample which was 45%.

Similar to uncoated powder particles and 0.3% coated 17 µm powder particle ,the 0.3% silica coated 30µm powder samples have also shown the increasing trend of UTS and Young's Modulus in 2 steps. This 2 stages of sintering was due to very loose inter-particular bonding in the beginning (approximately 10 to 20 seconds of IR radiation) and thereafter an improved inter-particular bonding occurred after 40 seconds of IR radiation. The global melting is more feasible after 60 seconds duration of infrared radiation

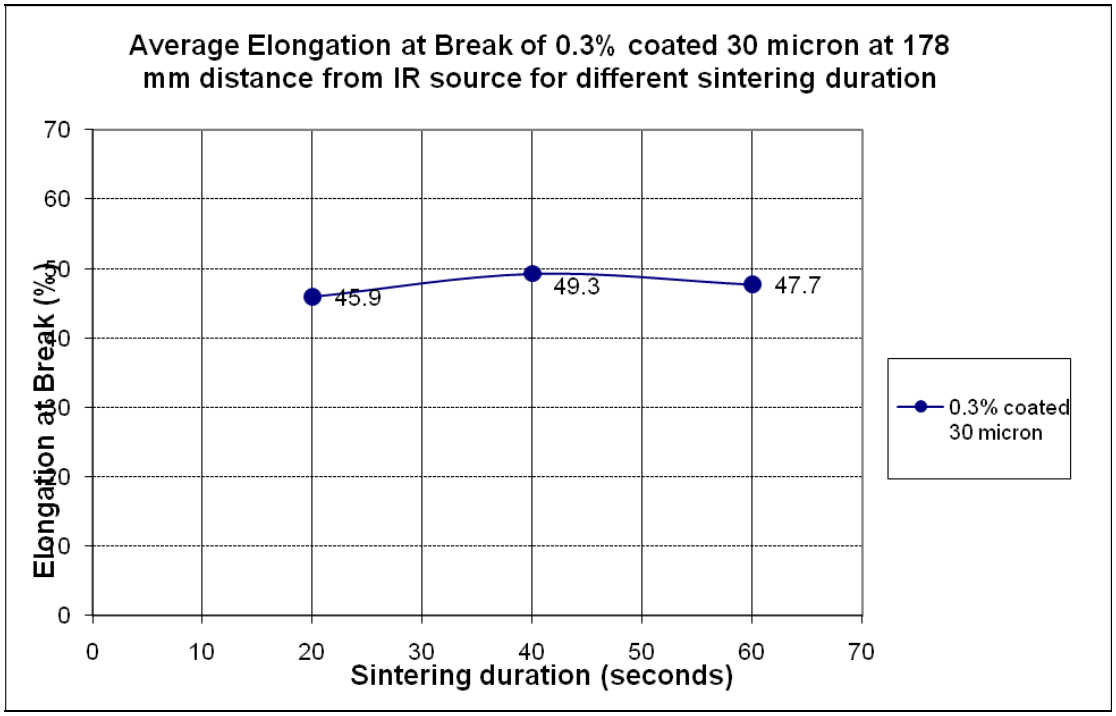

Figure 163: Elongation at Break of 0.3% coated 30 µm particle size IR sintered at 178 mm stand-off distance of 20, 40 and 60 seconds of sintering duration

The 'Elongation at Break' increased from 45 to 49 % when the duration of exposure increased from 20 to 40 seconds and yet fell very slighlty to 47 % when the duration of exposure reached 60 seconds (see Figure 163).This trend has similarity with 'Elongation of Break' of uncoated 30 µm powder sample. The 'Elongation of Break'for uncoated 30 µm powder sample also increased as the duration of IR exposure is increased from 20 to 60 seconds and therafter decreased as the duration of IR exposure increased from 40 to 60 seconds (Please refer earlier section of IR sintering of uncoated 30 µm powder sample).

6.4.5 Discussion

- The measurement of tensile properties for ruberised material (TPE) is always challenging because of its high extensibility and significant change in poission ratio (due to its elastomeric charaterictics while conducting the experiment. The measurement of tensile properties for silia coated tensile properties is more challenging due to following reasons:

- The tensile specimens produced using silica coated Somos 201 were very fragile.The average number of samples successfully tested for coated 17 micron powder varied between 5 and 7 instead of 10 samples for uncoated material .

- The Somos 201 powder particles were prepared using a lab scale mixer (CKL) which makes it difficult to maintain a homogeneous disribution of fumed silica across all of the Somos 201 powder particles. This led to more variation in the properties of the tensile test samples produced.

- The changes in 'Coefficient of Variation' (CoV) for coated and uncoated 17µm powder samples is shown below (see Figures 164,165) . The CoV is used to compare the consistency of the test results for coated powder samples. As the CoV represents the ratio of the standard deviation to the mean, and it is a useful statistic for comparing the degree of variation from one data series to another, if the means are drastically different from each other. As there is a significant difference in mean between coated and uncoated powder samples this CoV is used to compare the results instead of standard deviation alone. 1.2 percent coated 17µm powder samples have more variation in UTS and Young's modulus compared to uncoated and 0.3% coated powder samples for 60 seconds duration of IR exposure.

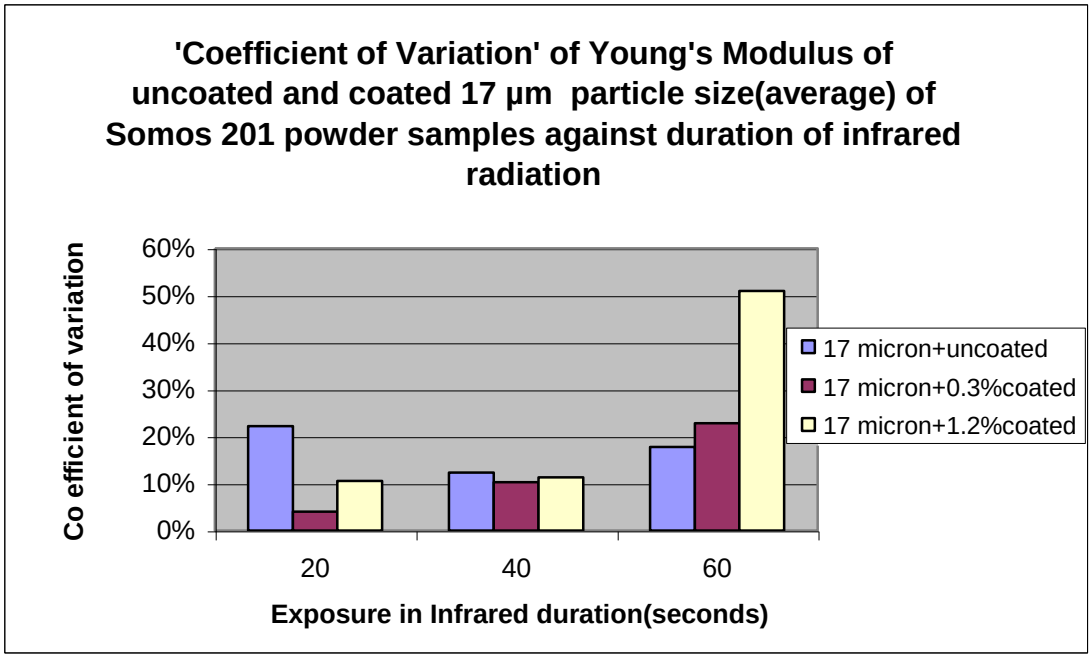

Figure 164 CoV of Young's Modulus of uncoated and coated 17 µm particles size against duration of IR radiation

- The CoV of Young's Modulus of uncoated material found within 10 to 20 % .This represents the typical variation of Young's Modulus for TPE samples. The results represent that the variation of Young's Modulus for 17µm particles due to heat distribution/particle size effect (normal noise level). For coated 17 µm powder particles the CoV is at its lowest value(10%) at the beginning of sintering process and higher(50%) towards the later stage of the sintering process. The reason of variation in result at the beginning of the process is due to less consistency of interparticle bonding. The more CoV towards the end represents the total variation(50%) due to combined efffect temperature distribution of the IR radiation(20%) as well as the effect of silica during sintering(30%).

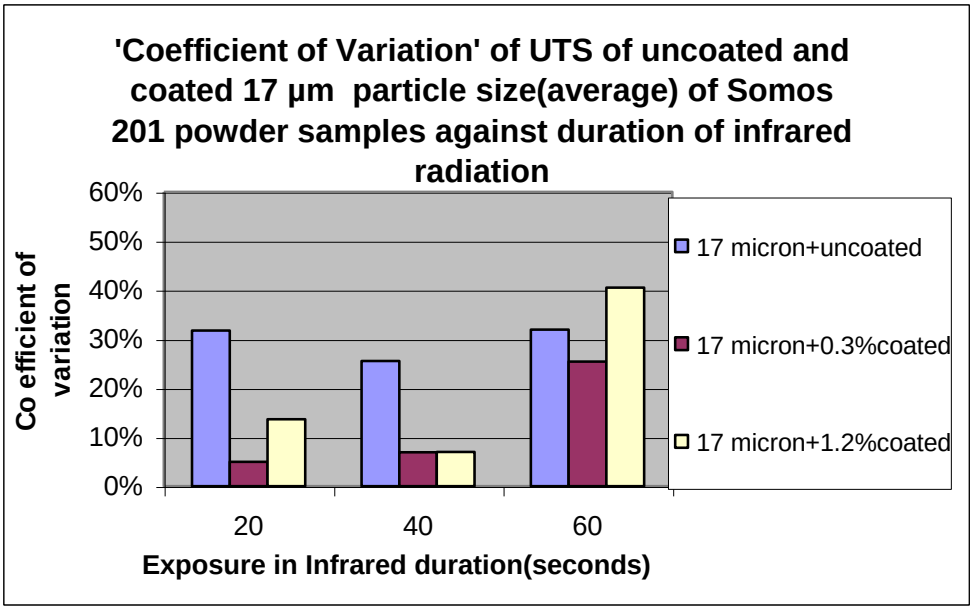

Figure 165 CoV of UTS of uncoated and coated 17 µm particles size against duration of IR radiation

- The CoV of UTS of uncoated material was within 25 to 30 % .This represents typical variation of UTS for TPE samples.The results represent that the variation of UTS for 17µm particles due to heat distribution/particle size effect (noise level).
- For coated 17 µm powder particles, the CoV of UTS is at its lowest value(15%) at the beginning of sintering process and higher(40%) towards the later stage of the sintering process. The reason of variation in result at the beginning of the process is due to less consistency of interparticular bonding. The more CoV towards the end represents the total variation(40%) due to combined efffect temperature distribution of the IR radiation(25%) as well as the effect of silica during sintering(15%).

- The CoV of Young's Modulus of uncoated 30 µm powder samples was within 15 to 20%, which is very similar to uncoated 17µm powder sample. The CoV of Young's Modulus for 0.3% coated 30 µm powder sample was between 10 to 12 %which is very close to 0.3% coated 17 µm powder sample.

- The CoV of UTS of uncoated 30 µm powder samples was within 10 to 15%, which is very similar to uncoated 17µm powder sample (around 20%). The CoV of UTS for 0.3% coated 30 µm powder sample was between 6 to 14 % which is also very similar to 0.3% coated 17 µm powder sample(around 6 to 25%).

- The effect of 1.2% coated 30 µm powder samples could not be carried out as the samples were very fragile.

- The COV of Young's Modulus and UTS for 30 µm powder samples was less in the beginning but and high values of CoV towards the later stage of sintering which perhaps represents the variation in the heat distribution from IR bulbs.

In a nutshell the variation of CoV due to the following reasons;

- High levels of coating clearly interfere with the sintering process
- Sintering of 17 µm coated samples occurs between 40 to 60 seconds of infrared exposure. The variation of CoV is probably due to variation in the IR radiation across the substrate/sintering platform, which leads some samples heating more slowly. This effect is particularly noticeable as the 2^{nd} stage bulk sintering occurs when rapid changes of the mechanical properties takes place.

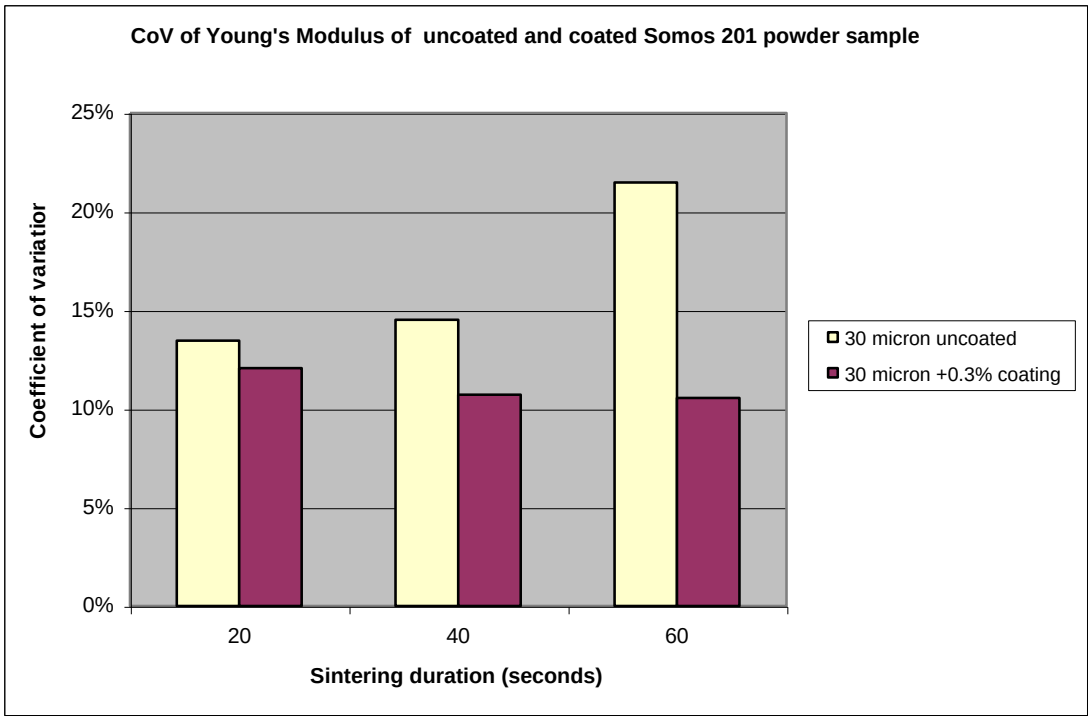

Figure 166 CoV of Young's Modulus of uncoated and coated 30 µm particles size against duration of IR radiation

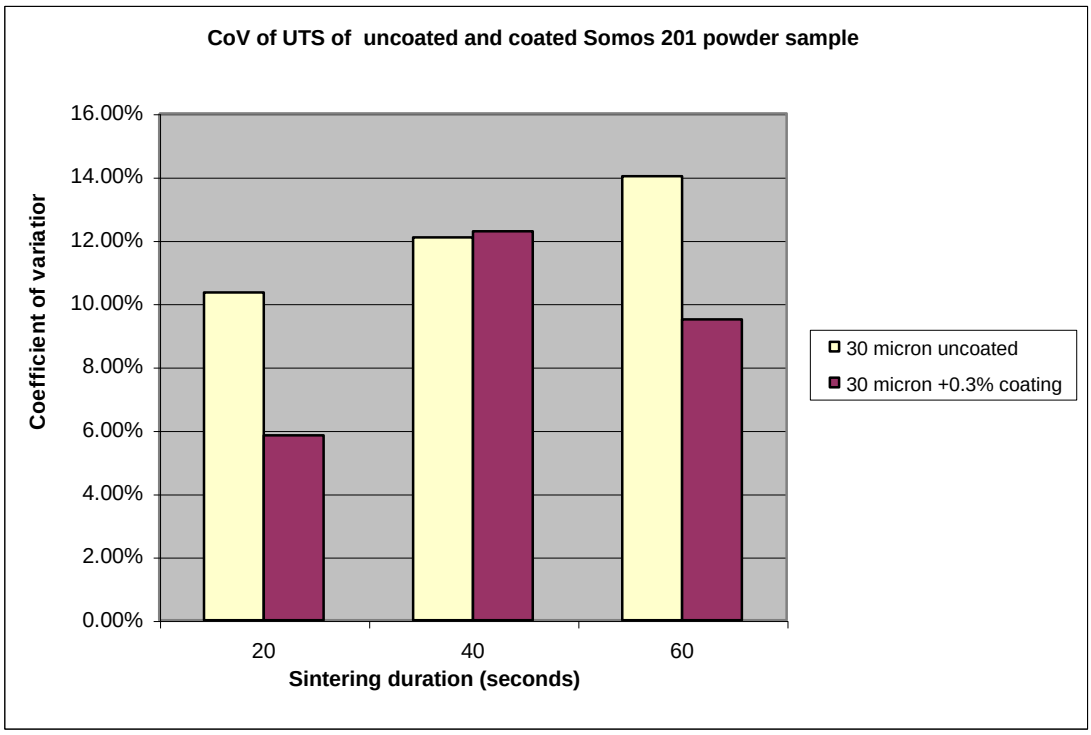

Figure 167 CoV of UTS of uncoated and coated 30 µm particles size against duration of IR radiation

- The effect of coating and IR radiation on the average values of Young's modulus for 17 µm powder sample (for 0.3 and 1.2% coated and uncoated) is shown below (see Figure 168). It is showing that very minimal increase of Young's Modulus would be achieved with the increase in IR duration if the powder sample is coated with 1.2% silica (by weight).This implies that no interparticle bonding would occur for powder samples with surface coated silica even the duration of IR radiation is increased.This could be due to poor coalascenece of powder particle due to silica which would be investigated in the next section.

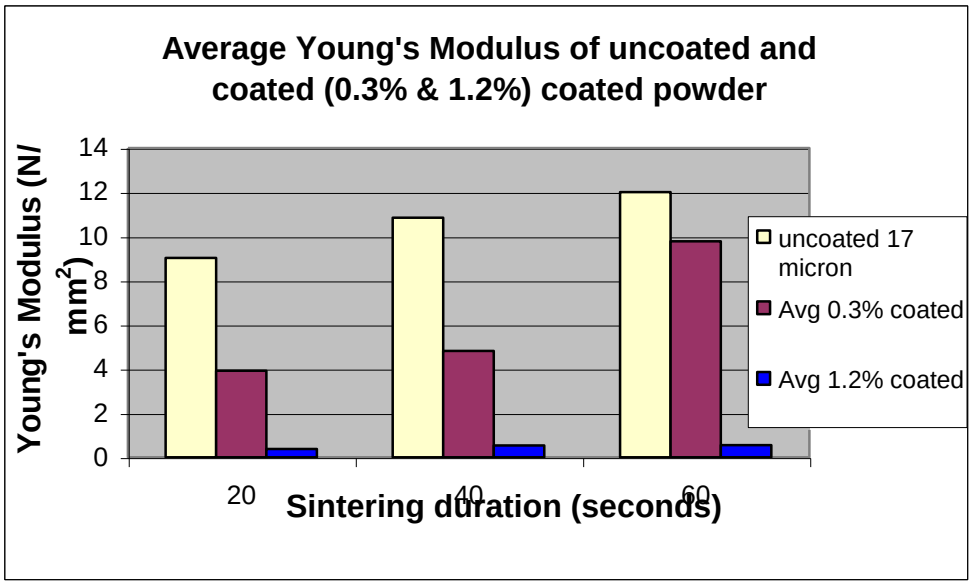

Figure 168 Average Young's Modulus of uncoated 17µm with 0.3% and 1.2% coated surface coated and sintered at 178mm stand-off distance

- Extrapolating the data from the Figure 168 it can be stated that the Young's Modulus similar level of Laser sintered part (i.e 15.5 MPa) could be achieved if the duration of infrared exposure is increased up to 105 seconds. The rate of increase of Young's Modulus of 1.2% coated material is very small (almost horizontal as $\tan^{-1}$ (0.0043) is equal to 0.24 degree). This suggests that 1.2% coated silica does not help to improve the mechanical strength even with the increase of infrared duration.

- Very minimal increase of UTS with the increase in IR duration is found for 1.2% silica coated powder samples (see Figure 169). This is due to weak interparticular bonding for powder samples with 1.2% surface coated silica. The average Young's Modulus and UTS reduced by more than 80% while the amount of silica is increased from 0% to 1.2%.

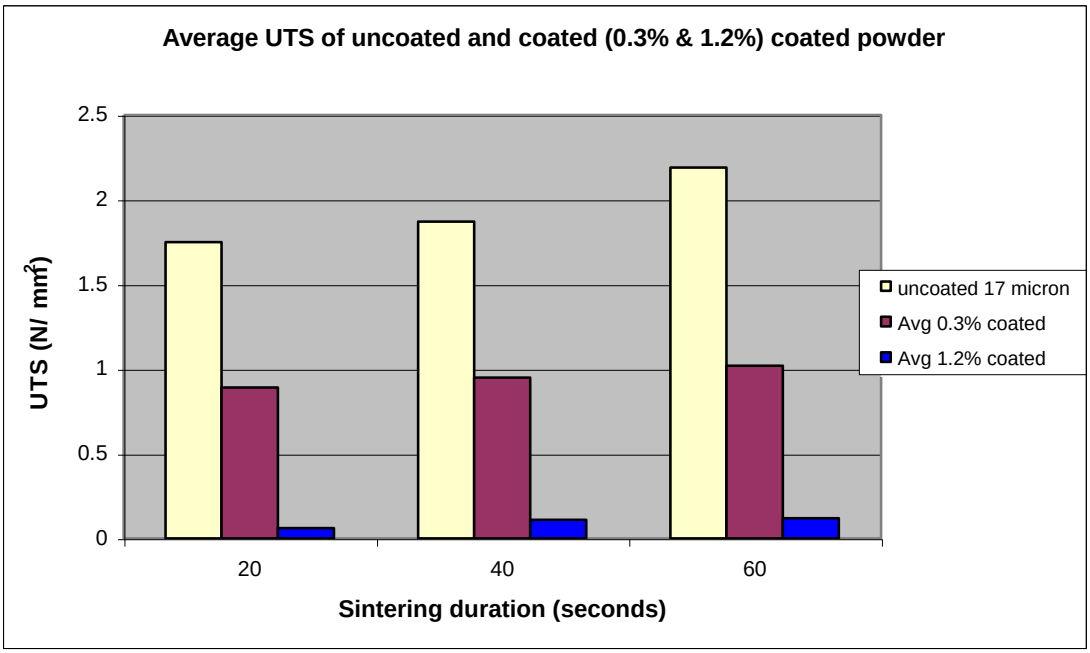

Figure 169 Average UTS of uncoated 17µm with 0.3% and 1.2% coated surface coated and sintered at 178 mm stand-off distance

- Extrapolating the data from the Figure 169 , it can be stated that the UTS of similar level of Laser sintered part (i.e 3 MPa) could be achieved if the duration of infrared exposure is increased up to 130 seconds. Similarly the rate of increase of UTS of 1.2% coated material is also found very small .This suggests that 1.2% coated silica does not help to improve the mechanical strength even with the increase of infrared duration .

- This poor mechanical properties (due to the surface coating with silica) could be due to loose interparticle bonding or poor IR sensitivity, which is would be investigated later. Although the Elongation to Break was not as consistent as expected, the average 'Elongation at break' was generally the highest value for the uncoated powder samples (see Figure 170).

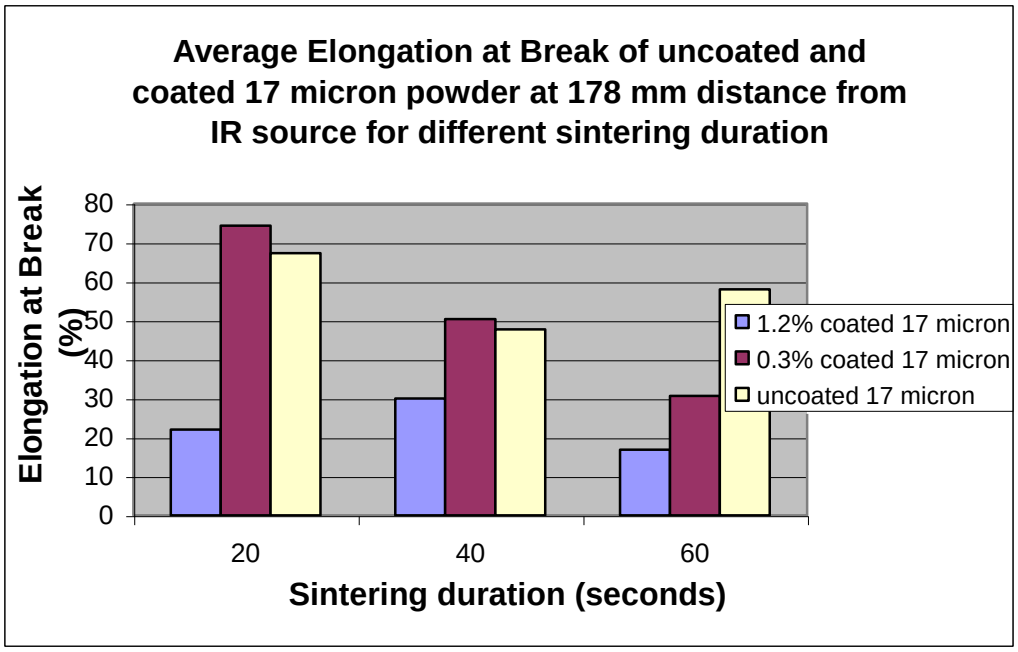

Figure 170 Elongation at Break of uncoated 17 µm with 0.3% and 1.2% coated surface coated and sintered at 178 mm stand-off distance

- The average Young's modulus and UTS for 30µm powder sample (both coated and uncoated) increases with the duration of infrared radiation.The mechanical strength is reduced significantly with the increase in silica coating (see Figure 171).

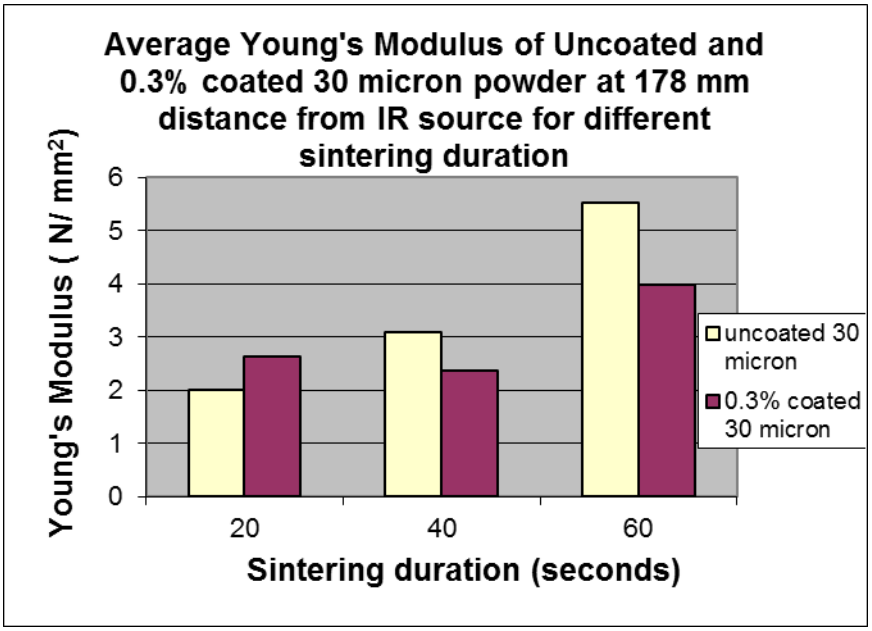

Figure 171 Average Young's Modulus of uncoated 17µm and 0.3% coated samples sintered at 178mm stand-off distance

- The higher Young's modulus value for the 0.3% coated 30µm material, compared to the uncoated material for the 20 seconds. This difference is relatively small and occurs at the very initial stages of sintering (as it is just started) and thus should be regarded with caution.

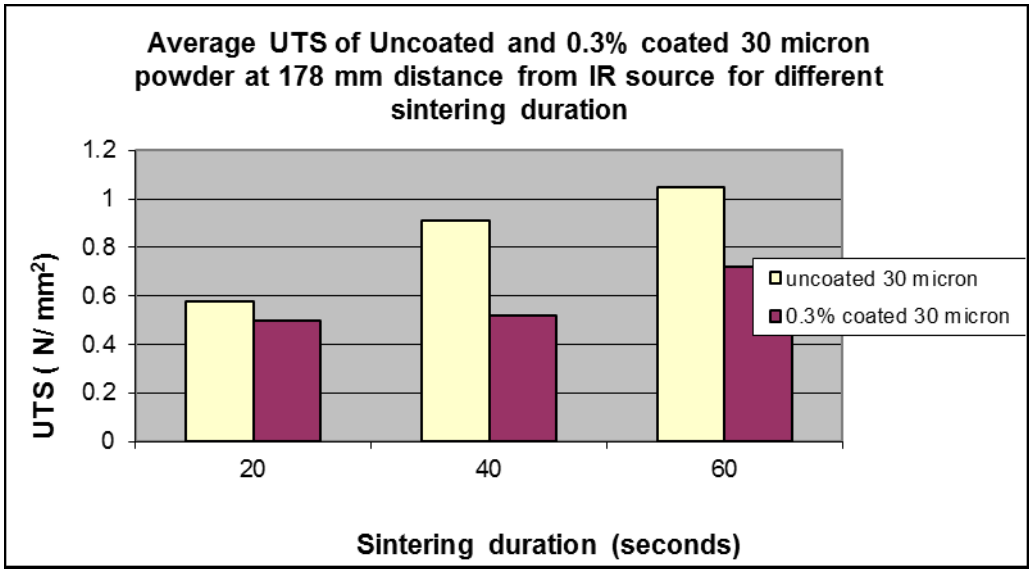

Figure 172 Average UTS of uncoated 17µm and 0.3% surface coated samples sintered at 178mm stand-off distance

Similar to Young's Modulus,very minimal increase of UTS with the increase in IR duration if the powder sample is coated with 1.2% silica (See Figure 172). This is again due to weak interparticular bonding for powder samples with 1.2% surface coated silica. The average Young's Modulus and UTS reduced by more than 80% while the amount of silica is increased from 0% to 1.2%..

- Young's Modulus of uncoated powder of 30 µm particle size is found significantly higher compared to 0.3% coated material when the duration of IR radiation is increased more than 30 seconds. The rate of increase of uncoated material is found higher compared to 0.3% coated material. The slightly lower value of Young's Modulus for uncoated material at 20 seconds duration of infrared radiation is not a major concern as sintering process does not take place below 20 seconds duration for the standoff distance 178 mm between infrared source and the powder particles (both coated and uncoated).

- The UTS of uncoated powder of 30 µm particle size is found higher compared to 0.3% coated material for all the tests. The slope of the linear trend line of UTS values for uncoated material is found higher ($\tan^{-1}$ 0.0118) compared to 0.3% coated material ($\tan^{-1}$ 0.0055) showing that UTS for uncoated material is increasing more rapidly.

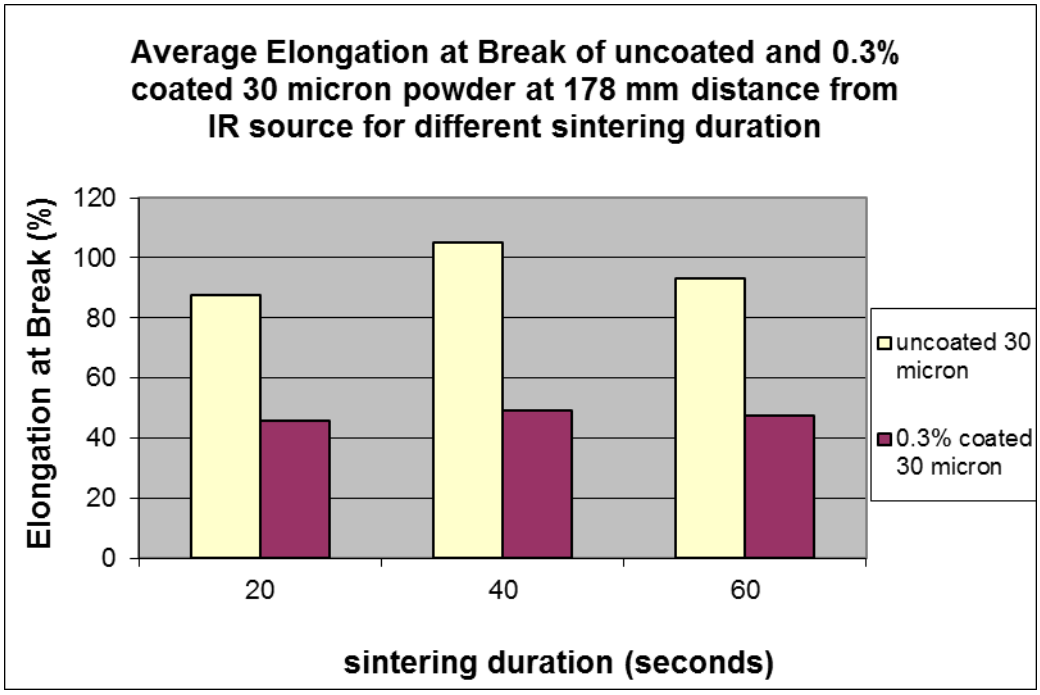

Figure 173 Average Elongation to Break of uncoated 17µm and 0.3% surface coated samples sintered at 178mm stand-off distance

- The 'Elongation at Break' for uncoated 30 micron was high for 0.3% coated 30µm powder sample as shown above. The elongation at Break for 0.3%-coated samples were same for all 3 cases as proper sintering has not occurred for the coated samples after 60 seconds of infrared exposure.

- Although Young's Modulus and UTS increases with the duration of IR exposure for both the coated and uncoated 30 µm particle size samples, the rate of increase of Young's modulus and UTS was found to be much higher for 17 µm particle size material (See Figures 174 and 175 below).The Young's modulus and UTS for 0.3% coated 17 µm found approximately 50% high compared to 0.3% coated 30µm powder sample. This result is following the similar trend as the mechanical strength of uncoated 17 µm found higher compared to 30µm powder sample. This result demonstrates the sensitivity of infrared sintering for the different particle sizes both uncoated and coated Somos 201 powder particles.

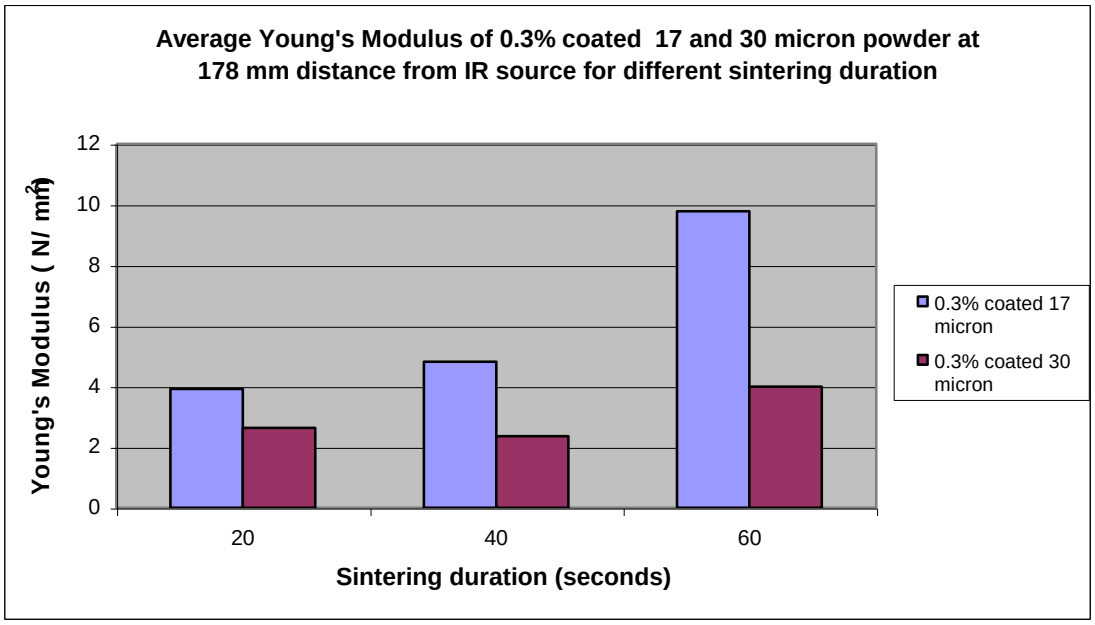

Figure 174 Average Young's Modulus of 0.3% surface coated 17 and 30 µm samples sintered at 178mm stand-off distance

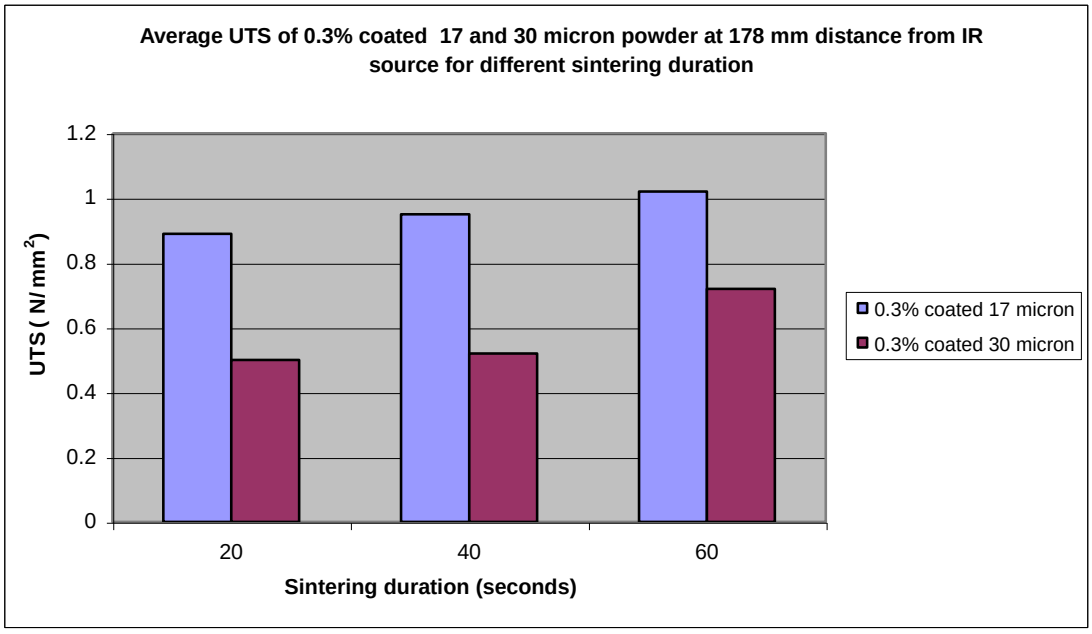

Figure 175 Average UTS of 0.3% surface coated 17 and 30 µm samples sintered at 178mm stand-off distance

- The mechanical strength of 1.2% coated Somos 201 found very weak and not possible to carry out any mechanical test failure test.This implies the 1.2% coated 17 µm particle size are also having better mechanical strength compared to 1.2% coated 30 µm powder samples. The graphs above shown the rapid decrease in mechanical strength of both Young's Modulus and UTS for 1.2 % coated 30 micron powder samples compared to 0.3% coated Somos 201 powder sample.
- The two most important fillers for thermoplastic materials are glass and carbon fibers. Silica is another common reinforcing fillerwhich has become of greater importance for several years. The encapsulation of submicron sizes of fumed silica in polymer particles are well developed which helps to improve the mechanical properties of the basis polymer. But the surface coating of Somos 201 with fumed silica does not help to improve the mechanical properties as the silica particles are weakly adhered to the basic polymer particle . It was found that 1.2% silica coated Somos 201 particles started burning as the duration of IR radiation is increased up to 60 seconds. This would be due to heat absorption by silica and thereafter transferring this heat to underlying polymer by method of heat conduction. This burning also might have caused further degradation of the mechanical properties of the 1.2% silica coated powder samples. Dark brown patches for 0.3 and 1.2% silica coated Somos 201 powder sample were noted as the duration of IR radiation is increased to 60 seconds (see Figures 176 and 177). This is due to burning of powder particles with the increase of sintering duration. The poor mechanical properties (due to the surface coating with silica) could be due to loose inter-particular bonding or poor IR sensitivity, which is would be investigated later

Figure 176 uncoated 17 µm particle size sintered for 60 seconds under IR radiation

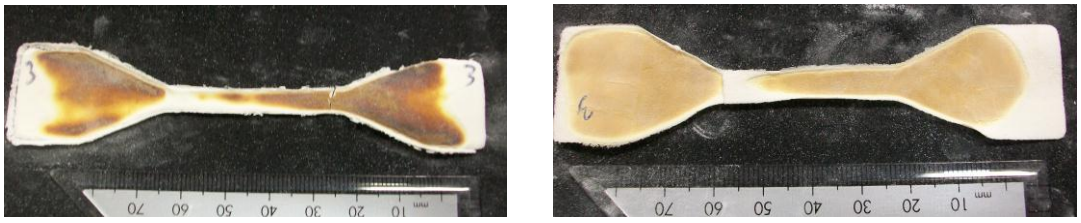

(a) (b)

Figure 177 0.3% (a) and 1.2% coated (b)17 µm powder particle sintered for 60 seconds under IR radiation

6.5 Oven sintering of coated and uncoated Somos 201 powder

Somos 201 powder particles were surface coated with fumed silica to print with dual component industrial laser printer for SLP process (Chapter 3). In earlier section the results of trials to assess the affect of fumed silica on mechanical properties of infrared sintered samples were presented and discussed. It was found that the UTS, Young's Modulus and 'Elongation at Break' of infrared sintered samples decreased as the amount of silica surface coated on the Somos 201 toner particles increased.

There are several potential reasons for the fall in mechanical properties due to the presence of the silica. One potential explanation is that the silica is altering the ability of the particles to absorb IR radiation. Another option is that the silica is acting as a barrier to prevent the molten surface of the toner particles from making contact and thus bonding together. To try to establish the primary role of silica in the IR sintering process further experiments need to be conducted.

It was decided to conduct sintering trials on Somos 201 toner in a conventional fan assisted oven. As heat transfer in the oven does not rely on IR radiation if the silica is found to affect the mechanical properties of the sintered samples produced then this can only be attributed to its forming a barrier to effective sintering rather than any change in IR absorption.

The oven sintering trials were conducted at 3 different temperatures: 160, 170 and 180^{o}C. The melting point of standard Somos 201 powder is 156^{o}C. For SLP process the top surface of the deposited powder needs higher than this melting temperature so that it would be stickier to facilitate the tackification process (Bynum 1989). The results of the oven sintering trials will also be compared with the previous IR sintering trials to identify any key differences in the sintering behaviour.

6.5.1 Experimental Methodology: Oven sintering with different amount of surface coated sample of Somos 201 powder

1. An average particle size of 30 µm was selected for the oven sintering trials. – This was due to limited quantity of 17 µm material and the choice of the higher particle size(30 µm) material does not affect the value of the tests.

2. Powder particles of the desired size (D50 - 30 µm) were separated from standard Somos 201 powder using a Hosokawa 50 ATP (ultrafine) classifier.

3. Powder samples were coated with three different levels of fumed silica 0.3%, 0.6% and 1.2 % (by weight) using CKL Eiger Torrence mixer.

4. Powder deposition was carried out manually into aluminium moulds to produce 10 tensile test specimens (quote BS/ASTM standard for tensile test specimen) per experiment.

5. The top surface of the loose powder was leveled moving a roller across the top surface of each sample to remove excess powder and provide a smooth, even top surface.

6. The rate of heating of oven kept at constant for all trials.

7. The temperature of aluminium plate, powder bed and oven were measured using K type thermocouples connected with Pico data Logger device

8. Trials were conducted for powder bed temperature at 160 ^{0}C, 170 ^{0}C and 180 ^{0}C respectively

It is important to try to mimic the thermal cycle to which the toner in the SLP rig will be subjected during fusing. The powder bed temperature rises to 150^{o}C within 15 to 20 seconds using the infrared heat source in the SLP process. Temperature control of top surface of powder layer is critical as the combined effect of temperature (the hot surface of the earlier printed layer) and pressure (contact force between the transfer roller and build platform) helps to ensure effective transfer and fusing of the powder layers in the SLP process (Bynum 1989).This necessitates a rapid raise in the temperature of the powder until fusing has occurred. The approach should reduce the influence of time on the results and also minimise the level of oxidation, which occurs on the surface of the Somos 201 powder during fusing process. The key parameter for the oven sintering trial was to increase the temperature of the powder bed so that it could be comparable with SLP process. Unfortunately, oven sintering is a slow process compared to heating rate of infrared radiation. Heat transfer primarily takes place due to convection instead of radiation inside oven. The air inside the oven is first heated up and then heat is transferred to powder bed by convection. Secondary heat transfer takes place on powder bed due to heat conduction from the aluminium plate to powder bed.

A series of trials were conducted until a method for rapidly heating the aluminium moulds in the oven was devised. Initially one mild steel plate (MS- I) was selected and preheated inside oven (225^{o}C). The aluminium plate with loose powder was then placed on top of the MS plate (MS- I) inside the oven to enhance the heating rate of the powder bed. The rate of heat transfer was improved due to heat conduction from the MS plate in addition to standard convection normally takes place inside oven. Mild steel was selected due to its relatively high thermal conductivity.

The temperature of the MS plate decreased as the temperature of the Somos201 powder increased as heat transfer taking place from MS plate to the powder via the aluminium mould. The powder bed temperature was raised from ambient temperature (30 ^{o}C) to 160^{o}C in 30 to 35 minutes using one MS Plate -I. This duration of heating cycle was considered too long compared to the infrared sintering process within the SLP process. It was found that the initial rate of heat transfer to the powder bed

was high as the temperature difference between heat source (MS Plate) and heat sink (powder bed) was more than 100 ^{o}C . The rate of heat transfer sharply decreased as the temperature difference between the heat source (MS block) and sink (aluminium mould) decreased below 80 ^{o}C

The next stage of the experimental methodology was to enhance the heat transfer rate to the aluminium mould by employing two MS plates instead of one MS plate. The temperature of powder bed and metal plate were recorded using data logger unit.

The improvised experimental approach using two MS plates is described below;

1) Oven is switched ON at the Maximum RAMP rate (selector switch position12).

2) Powder is deposited manually onto the aluminium mould.

3) Two MS plates are preheated inside the oven to 225 ^{o}C

4) Aluminium plate with loose powder samples (@25 ^{o}C then placed on top surface of MS Plate I (@225 ^{o}C. The temperature of the powder bed rises to 110 ^{o}C within 2 minutes and temperature of the MS Plate I is reduced to 185 ^{o}C

5) Heat transfer rate reduced as temperature of MS Plate -I further decreased below 185 ^{o}C .Aluminium powder bed then placed on top of MS Plate-II

The aluminium tool plate with partly sintered powder then placed on the top of the hot surface of MS plate-II with temperature 225 ^{o}C. In next 4 minutes to 5 minutes the temperature of the powder within the aluminium mould plate raises to around 150 to 160 ^{o}C. This is the normal operating temperature of the top surface of deposited Somos 201 powder layer used for SLP process. The entire sintering process takes around 6-7minutes.

6) The aluminium mould with sintered samples then removed from the oven. The aluminium mould plate is then allowed to cool .The sintered samples were then carefully removed from the mould plate and prepared for tensile testing.

Figure 178(a) oven used for sintering trials (left) & (b) Powder on aluminium mould (right)

6.5.2 Test matrix of oven sintered samples:

Experiments were carried out to sinter the coated and uncoated Somos 201 powder with average particle size of 30 µm of Somos 201 (See Table 26 below) . The samples were held at 1 minute at the maximum temperature.

Amount of fumed silica applied to the Somos 201 powder (%)	Average temp of sintering ^{o}C
0	160
0.3	
0	170
0.3	
0	180
0.3	

Table 27 Percentage of silica coating and sintering temperature selected for oven sintering trials

6.5.3 Comparison of uncoated and 0.3% coated samples sintered at 160 ^{0}C of powder bed temperature

Young's Modulus, UTS and Elongation at Break are compared against uncoated and 0.3% coated of average particle size 30 µm of Somos 201 powder samples sintered at 160 degree c. The average Young's modulus, UTS and Elongation at Break reduced by 20.34%, 47.65% and 38.99% respectively as the percentage of fumed silica increased from 0% to 0.3% (See Table 28 below).

	Uncoated 30 µm powder sample	0.3% coated 30 µm powder sample	Difference	Difference in %
Average Young's Modulus (N/mm^2)	5.75	4.58	1.17	20.34%
Average UTS (N/mm^2)	1.28	0.67	0.61	47.65%
Average Elongation to Break(%)	34.72 %	21.18%	13.54%	38.99%

Table 28 Comparison of uncoated and coated (0.3%) Somos 201 powder at 160 0C sintering temperature

6.5.4 Comparison of Uncoated and 0.3% Coated Samples at 170 ^{0}C of Powder Bed Temperature

Young's Modulus, UTS and Elongation at Break are compared between uncoated and 0.3% coated 30 µm Somos201 powder samples, which were sintered at 170 ^{0}C (see Table 29 below).

Description	Uncoated	0.3% fumed silica	Difference	Difference in %
Average Young's Modulus (N/mm^2)	20.95	4.95	16	76.37 %
Average UTS (N/mm^2)	4.73	0.77	3.96	83.73 %
Average Elongation to Break (%)	71.70	23.47	21.57	67.26 %

Table 29 Comparison of uncoated and coated (0.3%) Somos 201 powder at 170 0 C sintering temperature

The average values of Young's Modulus, Elongation at Break and Ultimate stress decreased significantly while the percentage of fumed silica increased from 0% to 0.3%.

6.5.5 Comparison of uncoated and 0.3% coated samples sintered at 180 ^{0}C of powder bed temperature

Young's Modulus, UTS and Elongation at Break are compared between uncoated and 0.3% coated 30 µm Somos powder samples which were sintered at 180 ^{0} C (see Table 30 below)

	Uncoated 30 µm	0.3% coated 30 µm	Difference	Difference in %
Average Young's Modulus (N/mm^2)	21.61	6.34	15.27	70.61%
Average UTS (N/mm^2)	6.29	0.99	5.3	84.26%
Average Elongation to Break(%)	118.59 %	23.18%	95.41%	80.45%

Table 30 Comparison of uncoated and coated (0.3%)Somos 201 samples at 180 0 C sintering temperature

It has been found that samples coated with 0.3% silica having less mechanical strength compared to uncoated powder samples as shown below. Young's Modulus, UTS and Elongation at Break of 0.3 % coated samples were reduced by 70.61%, 84.26% and 80.45% respectively compared to uncoated samples.

6.5.6 Discussion-oven sintering trials:

Young's Modulus, UTS and Elongation at Break of Somos 201 powder samples (both uncoated and coated) increased with increasing the oven sintering temperature (see 179 , 180 and 181 below).

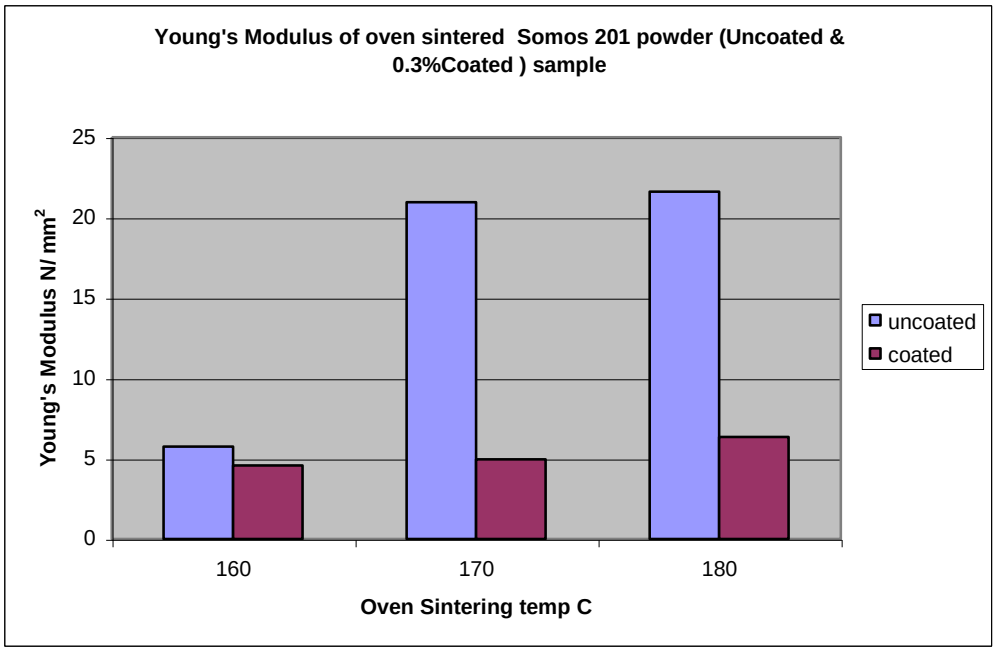

Figure 179 Young's Modulus of oven sintered Somos 201 samples at different sintering temperature

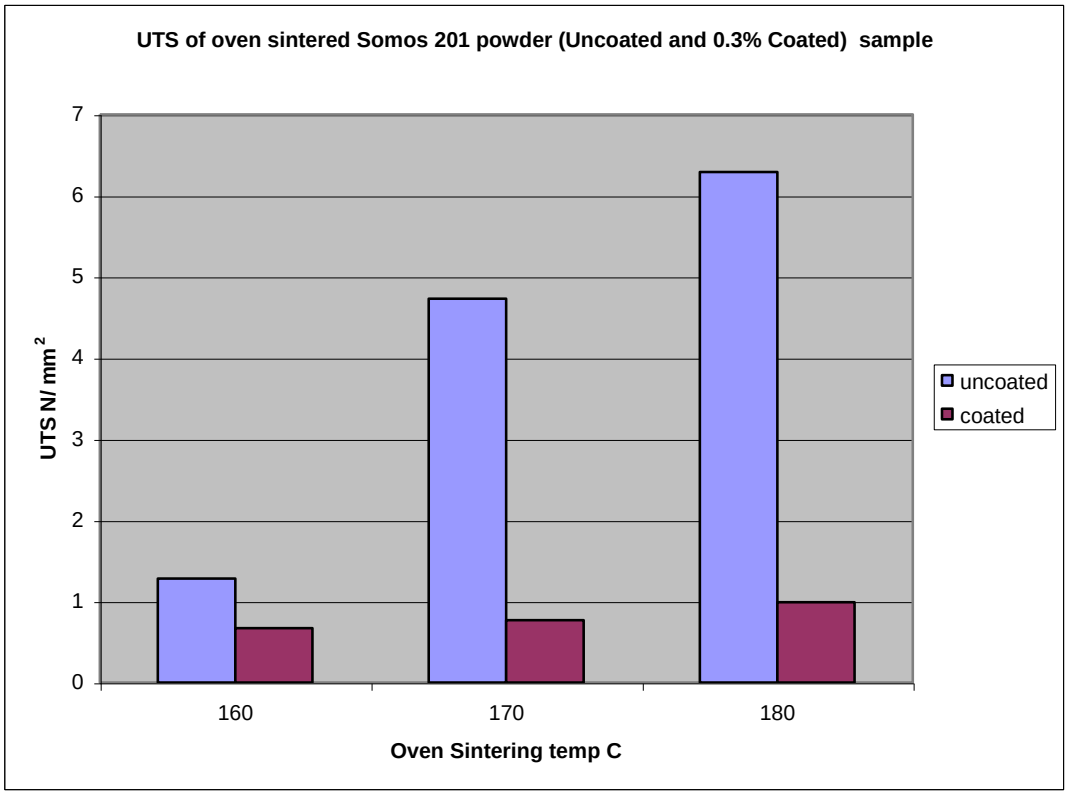

Figure 180 UTS of oven sintered Somos 201 samples at different sintering temperature

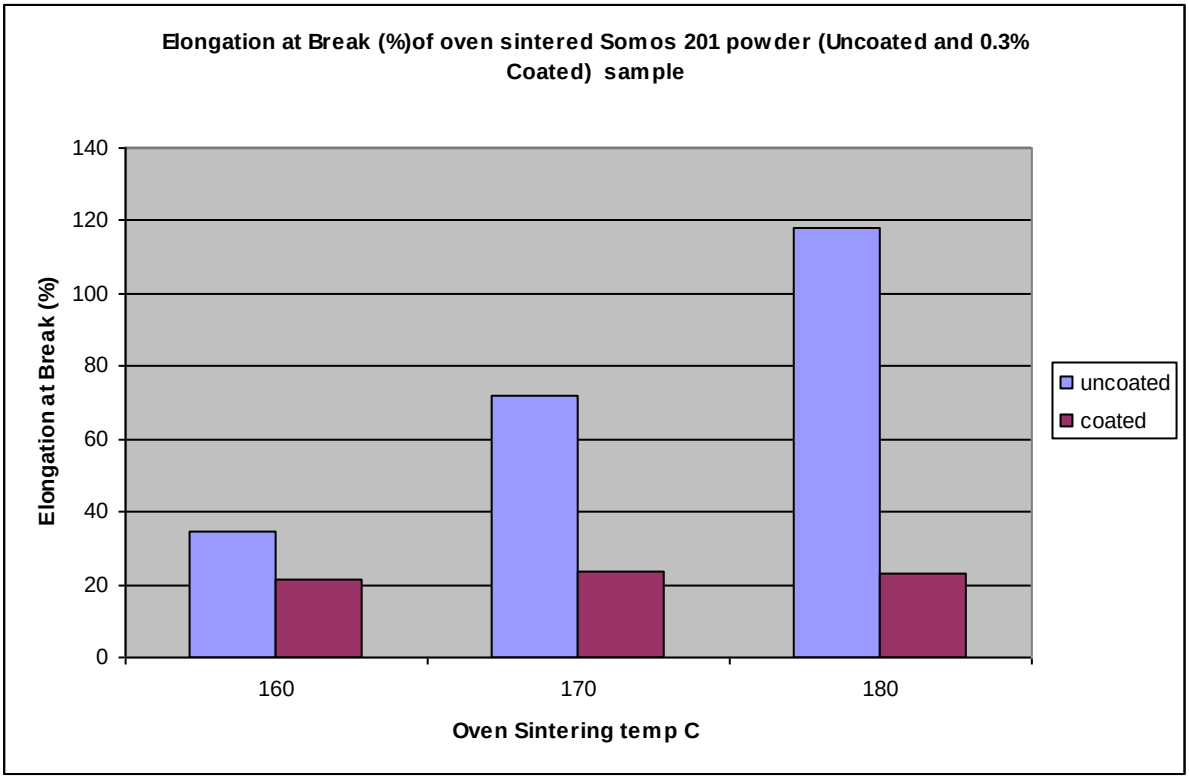

Figure 181 'Elongation at Break' of oven sintered Somos 201 samples at different sintering temperature

Tensile properties of infrared sintered and oven-sintered samples have shown that mechanical properties exponentially decrease with the addition of fumed silica. This degradation of mechanical properties suggests that fumed silica predominantly acts as a sintering inhibitor rather than interfering with the infrared absorption of powder. Figure 182 showing coated and uncoated somos powder samples.

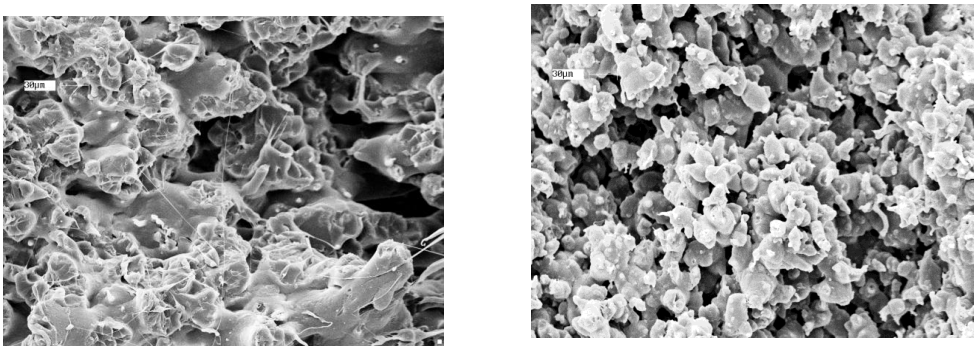

(a) (b)

Figure 182 (a) Uncoated oven sintered 30 micron of Somos 201 & (b) fumed silica coated Somos 201

6.5.7 Comparison between oven and infrared sintered Somos 201 powder samples (uncoated and coated)

Infrared radiation is a faster heat transfer process compared to the convective type of heat transfer in the oven. Therefore a non-contact type infrared sensor was used to measure the powder temperature instead of pico data logger unit (see Appendix-C). The downside of using IR temperature detector is due its high sensitivity to colour and the surrounding hot air for the infrared bulbs. Both parameters found adversely affected the accuracy of the temperature measurement. To minimise the error in temperature measurement infrared temperature detector a was kept near about 20 cm away from heat source (bulbs) and inclined at 20 degree angle from the horizontal (see appendix)level to minimise reflection from powder bed.

Comparing the properties of the uncoated samples produced by IR sintering for 60 seconds at 178mm standoff distance with the properties of uncoated samples by oven sintering – it was found that the results for 160 ^{0}C were very similar (see Table 31 and 32) . The results were then compared the results for 0.3% coated material for both IR and oven sintering processes. The very similar trend for both IR and oven sintering indicates that the oven-sintered samples follow the same pattern thus giving a high probability that the primary role of fumed silica is on interparticle bonding rather than IR absorption.

Description/Item	Uncoated 30 µm 60 seconds of IR exposure (N/mm^2)	0.3% coated 30 µm (60 seconds of IR exposure) (N/mm^2)	Difference (%)
Average Young's Modulus	5.52	3.99	27.71%
Average UTS	1.05	0.72	31.42%

Table 31 Average Young's Modulus and UTS Mechanical properties of IR sintered Somos 201 -30 micron (coated and uncoated) powder sample at 178 mm standoff distance:

The temperature of powder samples was measured using k type thermocouples with 'Pico data logger' unit. Although this datalogger unit was slow in capturing field data but this was used as the temperature change inside the oven generally takes place very slowly. This slow rate of temperature rise inside the oven is due to convective method of heat transfer.

Description	Uncoated 30 micron-160^0 C (N/mm^2)	0.3% coated 30 micron-160^0 C (N/mm^2)	Difference	Difference in (%)
Average Young's Modulus	5.75	4.58	1.17	20.34%
Average UTS	1.28	0.67	0.61	47.65%

Table 32 Mechanical properties of oven sintered Somos 201 - 30 micron (coated and uncoated) powder sample at 160 c

The rate of degradation of mechanical properties (Young's modulus and UTS) for both coated and uncoated powder sample found very similar for both oven and IR sintered powder samples. This indicates that the effect of silica is more likely to be as a result of its role in interfering with inter-particular bonding rather than as a result of changing the infrared sensitivity of the powder.

7.0 Chapter 7 -Final Conclusions:

7. 1 Scoping Trials:

- Mechanical grinding of the engineering thermoplastic powder samples (PE, PP, Nylon) was very inefficient compared to conventional toners

- It is possible to develop an experimental toner based on PE powder which can be printed using both mono-component (HP LaserJet4 and Lexmark C510) and dual component (CTG900) print engines.

- Titanium dioxide can be used to coat powder particles to impart the desirable dielectric properties on the PE powder while printing with nonmagnetic, monocomponent print engine (Lexmark C510). Optimum amount of titanium dioxide must be used as deposition is adversely affected for higher or lower levels of this coating agent.

7.2 Main Trials with Somos 201

7.2.1 Grinding

- Similar to PE, it is impractical to mechanically grind Somos 201 powder particles to form small particle sizes below 30µm.

7.2.2 Coating/printing:

- It is possible to develop an experimental toner based on Somos201 powder, which can be printed using both mono-component (HPLaser jet4) and dual component (CTG900) print engines.
- The q/m of Somos 201 powder revealed that the powder particles are more negatively charged, compared to polyethylene, making it easier to print with the negative print engine.

- The application of Fumed silica is essential to enable Somos 201 powder to print. The level of silica coating should be set at the minimum threshold level to achieve printing (ideally less than 0.3%). If the silica coating is greater than 1% (by weight) there will be virtually no inter particular bonding during subsequent fusing.

7.2.3 Fusing & Mechanical Properties (IR Radiant Sintering) :

- The stand-off distance between the IR radiant heating source and powder particles plays a crucial role in determining the speed of the fusing process, the consistency of sintering and the mechanical properties of the fused material. The stand-off distance must not be too small as, although sintering speed will increase, the consistency of sintering is undermined.

- Sintering duration is critical and a longer processing time will be required to maximise the mechanical properties of parts. Better Young's modulus, UTS of IR sintered samples were obtained while sintering duration is increased.

- It is possible to achieve the same mechanical properties (Young's Modulus, UTS) using IR radiant heating as for Laser Sintering with uncoated Somos201 powder.

- Powder samples under infrared were found to have two distinct stages of sintering , firstly the liquid phase sintering followed by bulk melting.

- Particle size is critical for both printing and sintering. 17 µm particle size of Somos 201 provided the optimum results in terms of printing and sintering.

- The application of fumed silica to the surface of the Somos201 results in a significant reduction in the mechanical properties (Young's modulus, UTS and elongation to break) of fused samples produced by IR radiant heating. The reduction in mechanical properties has an approximately linear relationship with the quantity of fumed silica used.

- Measurement of powder bed temperature is very difficult, thermocouples suffer from significant measurement lag and that IR measurement methods (camera or pyrometers) are affected by the surface characteristics of the material.

7.2.4 Fusing & Mechanical Properties (Oven Sintering)

- The application of fumed silica to the surface of Somos201 powder results in a significant reduction in the mechanical properties (Young's modulus, UTS and elongation to break) of fused samples produced by oven sintering.

- As with the IR radiant sintering trials the mechanical properties of the silica coated Somos 201 powder will never achieve similar properties to the uncoated material irrespective of the oven sintering duration.

- The results from oven sintering shows that the silica acts as a barrier to inter-particular bonding.

7.3 Recommendation

- The feasibility of developing experimental tough toner could carried out using the procedure developed in this project and described in the flow chart below

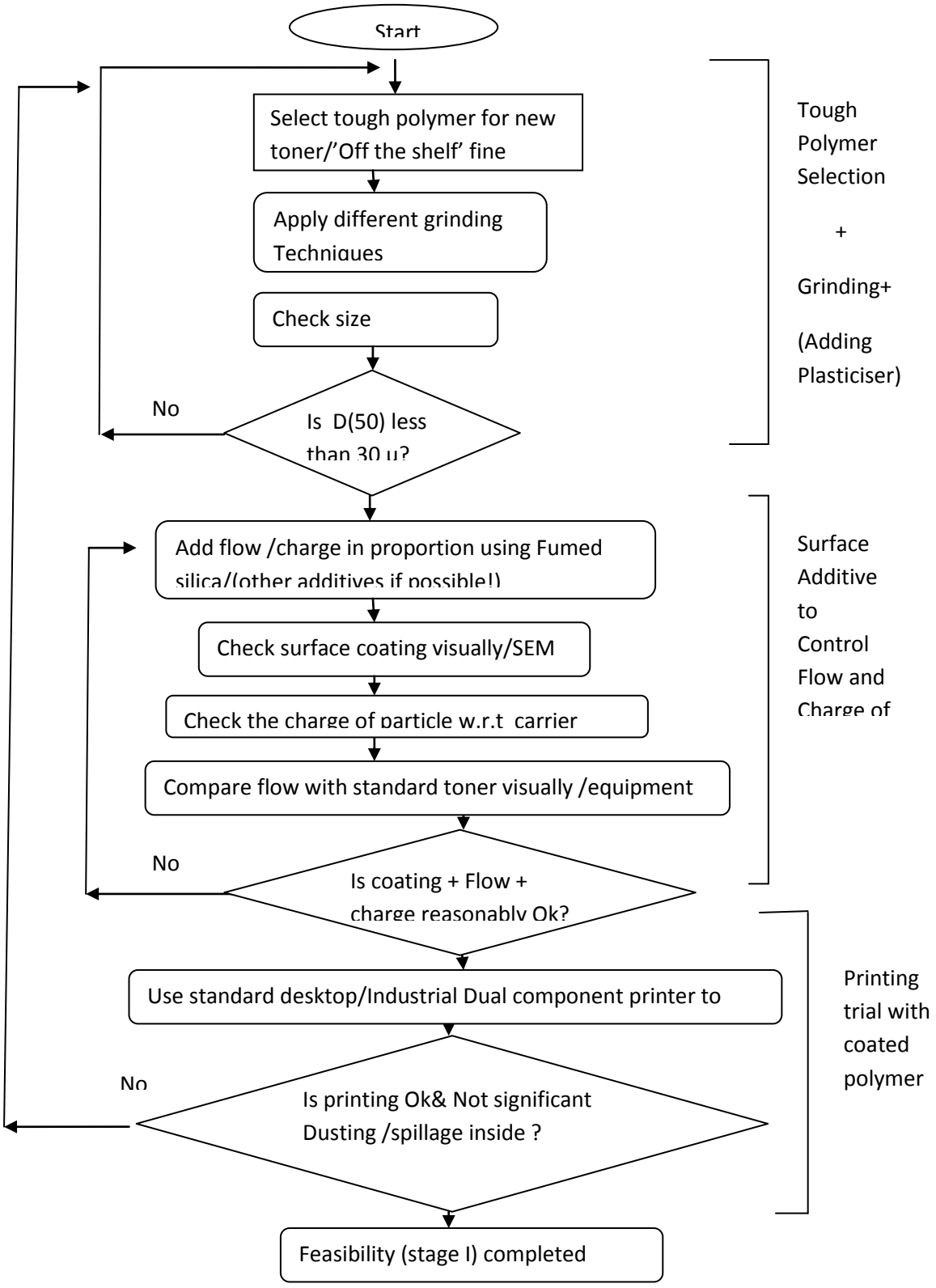

- Mechanical process is better route for developing experimental tough toner as chemical route is more complex and costly. Chemical route can be investigated later if mechanical process found feasible for the same experimental toner

- The q/m characteristics of the powder particles should be measured in the very early stage of toner development. It is difficult to coat polymer particles with 'Charge Control Agent' as this can be dislodged during the toner transfer process inside the printer.

- 'Off the shelf' polymer with right particle size is the best choice while developing tough experimental toner .The industrial scale sieve shaker unit with high throughput is one of the viable options to separate the smaller particles from larger ones. This process will be not economically viable if very small percentage of powder particles are present for the right particle size required for toner development

- The printer hardware would be selected based on the charge, flow and the particle size of the experimental toner.

- The gap between doctor blade and developing roller should be selected based on the particle size of the experimental toner

- A dual component print engine found more suitable for experimental toner compared to mono-component system. The right carrier and the correct tribocharge is very important for dual component toner development

- Temperature measurement of the rotating blade and its surrounding powder particle is critical during surface coating .The heat develop during coating fused the surrounding powder which need to be removed from the final sample size of the experimental toner to get rid of larger fused particles

- The voltage adjustment facility across each workstation (like developing roller, OPC drum, transfer roller, substrate) is one of the important factor while developing printer hardware

- The stand-off distance needs to be optimised for SLP process, as it will affect both process speed and mechanical properties of the parts produced using this process. This standoff distance would depend on melting point and infrared sensitivity and the wavelength and the intensity of infrared radiation

- The temperature measurement of the powder bed is very critical for powder deposition using tackifying approach mentioned earlier. Any non-contact type temperature detector can be used provided it would not very sensitive to the colour, reflectivity of the target and the temperature of the surrounding warm air. Calibration would be required to carry out prior to installation to minimise these disturbances.

- Fumed silica needs to be added to improve the flow of experimental toner. The percentage of silica above 1 %(by weight) is not recommended, as it would severely affect the mechanical properties of the parts produced using this SLP process.

- Medium wavelength of infrared radiation is suitable for most of the polymer as a heat source for powder sintering. Near infrared (NIR) radiation can be selected if pigments are introduced with the experimental toner

- The cushioning facility on powder bed is important as toner deposition takes place for both tackification and electrostatic transfer. This cushioning affect can be introduced underneath the powder bed providing spring (with correct spring constant)/any other spongy substances.

- The speed of the build platform should exactly match with the linear speed of the rotating transfer roller

- The home position of the build platform need to be placed at correct location before each print matching with the layer thickness as small change from the actual value will result no deposition due to larger gap between transfer roller and top surface of the printed layer

- Electrostatic force of repulsion combining with the tackification approach could be a better route for toner transfer mechanism for SLP process

7.4 Future work:

- Improved print quality with less dusting effect (within the printer as well as on substrate) can be possible for Somos 201 powder by improving the tribo-charge of carrier particles. The right carrier with correct triboelectric charge for Somos 201 is required to improve print quality.
- Better method of coating need to be investigated to coat the experimental toner particle (like Somos 201) with Flow Control Agent (fumed silica)
- Better method of coating need to be investigated to coat the experimental toner particle (like Somos 201) with Charge Control Agent
- Development of a better print hardware to print Somos 201 powder more accurately with different formulation and measurement the mechanical strength of the deposited layers. The pressure generated by transfer roller could help to improve the consolidation of the powder particles.
- The average particle size of Somos 201is generally high (93 µm). The original manufacturing route of Somos 201 powder need to be investigated further to produce finer particle size (less than 30 µm), if possible
- The top surface of the printed layer needs to be levelled otherwise high peaks would develop on powder surface and powder would be picked up by only those high points for future prints. The levelling of top surface could be carried out in various ways. One of the potential solutions could be the use of hot roller (non stick type), which would help while levelling of top surface without any smudging of the deposited layer.
- The electrostatic mode of repulsion of powder transfer combined with discharging facility to withdraw charge from the printed layers need to be investigated in future. Discharging would dissipate the accumulated charge from the printed layers otherwise they would repel after few layers of prints and reduce the transfer efficiency later
- The tackification can also be carried out if adhesives can be deposited on the top surface of the powder layer prior to printing of next layer of powder particles. Special care is required so that the adhesive would not damage the transfer roller.
- The non contact type Z height sensor (using laser) can be applied to measure the z height of the printed layer very accurately. This would help to obtain the precise location of home position of build platform before printing

- The orientation of printed part and its affect on mechanical strength while being sintered under infrared also need to studied The effect of heat and contact pressure from transfer roller could help to improve the mechanical properties of the produced part. This would

not only mimic the heat and pressure effect of injection moulding but also can help to dislodge the silica from particles which might help to obtain better mechanical strength

- The uniform pattern of heat distribution across the powder bed is important for any powder sintering process. Control of powder bed temperature using the feedback mechanism with thermal image camera was patented by 3D System for SLS system (US 6815636).

Reference

Aoki, H., Yamuguchi, N., Takubo, C.,2004, 'A Study of Electrophotography process for Manufacturing Printed Circuit Board', *lS&T \ NIP20: 2001 International Conference on Digital printing technologies*

Akihiko, K., Isao, Kato.,Norio, S., 2000, *Electrophotographic apparatus*, US Patent 6157789

Asiabanpour, B.,Cano,R., Lane V.W., McCormick, T., Wasik, F.,2005,'New Design for Conserving Polymer Powder for the SIS Rapid Prototyping Process', *16th International Symposium on Solid Freefrom Fabrication,* Austin, Texas

Asiabanpour, B., Palmer, K., Khoshnevis, B., 2004, 'An Experimental Study of Surface Quality and Dimensional Accuracy for Selective Inhibition of Sintering', *Rapid Prototyping Journal*, vol. 10, No. 3, pp. 181-192

Asiabanpour, B., Wasik, F., Cano, R., Jayapal, V., VanWagner, L., McCormick, T., 2005, 'New waste-saving heater design for the SIS Rapid Prototyping Process', *IIE Conference*, Atlanta, GA

Banerjee, S. and Wimpenny, D.I., 2006, 'Laser Printing of Polymeric Materials', *Seventh Proceedings from the Solid Freeform Fabrication Symposium Austin, Texas*, pp. 366-374

Banerjee, S., Wimpenny, D., 2007, 'Rapid Manufacturing of Thermoplastic Parts by Laser printing', *2nd International conference on Polymers & Moulds Innovations – Belgium*

Banerjee, S., Wimpenny, D.,2007, 'Feasibility study of Laser Printing of Thermoplastic materials for Rapid Prototyping',*ICMR07 conference UK*

Banerjee, S., Wimpenny, D.,2008,Development of a Laser Printing Based Rapid Manufacturing Process for Thermoplastic Elastomers , ICMR conference at DeMontfort University Leicester UK

Banerjee, S. and Wimpenny, D.I., 2008, 'Laser Printing of Soluble Toner for Rapid Manufacturing', *Proceedings from the 2nd International Conference on Additive Technologies* Slovenia'

Bartscher, G., Cormier, S. O., Lyness, R., Schein, L. B., 2001, 'Comparison of the electric fields of electrophotography and contact electrography', *Journal of Electrostatics*, vol. 53, pp. 295-310

Baur,R., Macholdt ,H.-T.,1993, Charge control agents for triboelectric (friction) charging, Jounal of Electrostatatics, vol 30 , pp. 213-222

Baur R, Macholdt,T., 1997, 'Charge control agents and triboelectrically adjusted pigments in electrophotographic toner', *Journal of Electrostatics*, vol. 40 , pp. 621-626

Bombard,I., DaSilva,B., Dufour,P.,Laurent,P.,2010, ' Experimental predictive control of the infrared cure of a powder coating: A non-linear distributed parameter model based approach', *Journal of Chemical Engineering Science* , vol. 65 , pp. 962-975

Bombard,I., Laurent, P., Lieto, L. J.,2008, 'A model of the infrared cure of powder coatings based on surface absorptivities in-situ measurements, *Journal of Coating Technology*, vol. 5, pp. 353-363

Bynum, David K., 1989, *Automated manufacturing system using thin sections*, US Patent 5088047

Carlson, Chester.,1942, *Electrophotography*, US Patent 2297691

Carpos J., German, M.l., Advances in Powder metallurgy & Particulate Materials Sintering, American Powder Metallurgy Institute, vol. 3, NJ, 1992

Chung, M., Allanic, A., 2004, *Sintering using thermal image feedback*, US Patent 6815636

Cormier, D. 2002, 'An investigation of selective colouring with 3-D Laser printing', Journal *of Manufacturing Processes*, vol. 4, no. 2

Deckard, Carl R., 1989, *Method and apparatus for producing parts by selective sintering*, US Patent 4863538

German , M. R.,Sintering theory and practice , John Wiley & Sons Inc, NY, 1996

Greogory , P., Printing and Imaging Systems ,Blackie Academic & Professional , Glasgow, 1994

Grenda, E.P., 2001, *Apparatus of fabricating 3 dimensional objects by means of electrophotography, ionography or similar process*, US Patent 6206672

Güttler,S., Gröning, M., Willems,P.,Biesinger,B., 2008, 'An efficient manufacturing process for highly complex biochips using laser printing technique', *NIP24 and Digital Fabrication*

Hasegawa, J., Yanagida, N., Tamura, M., 1999, 'Toner prepared by the direct polymerization method in comparison with the pulverization method', Journal of Colloids and Surfaces A: Physicochemical and Engineering Aspects, vol. 153,issues 1-3, pp. 215-220

Hays, D. A.,Sheflin, J. C.,2005, 'Electrostatic adhesion of ion and triboelectric-charged particles, Journal of Electrostatics' , vol. 63, pp 687–692

Hopkinson, N., Erasenthiran, P., 2006 , Method and Apparatus for Combining Particulate Material US patent, WO Publication Number 2006/0180957

Hopper, M.,2004, 'Colorants for chemically prepared toner',*7th Annual toner & imaging chemicals conference* ,February 11-13, 2004

Hull, Charles W., 1986, *Apparatus for production of three-dimensional objects by stereolithography*, US Patent 4575330

Iwata, N., Tani, K., Watada, A., Araki, T., Hitchcock AP., 2006, 'Chemical component mapping of pulverized toner by scanning transmission X-ray microscopy', *Journal Micron* , vol. 37, pp. 290-295

Karlsen, R., Bakkelund, J., 2004, *Method and apparatus for rapid manufacturing of metal, ceramic and metal-ceramic products* , World Wide Patent WO 200403746

Karlsen, R.,Olav, A.,2007, 2007, *Method and device for manufacturing a powder layer for in layer production of objects*, Worldwide Patent WO 2007073206

Khoshnevis, B., 2000, *Selective inhibition of bonding of power particles for layered fabrication of 3-D objects*, US Patent 6589471

Khoshnevis, B., 2007, *Methods for reduction of powder waste in selective inhibition of sintering*, US Patent 7291242

Khoshnevis, B., Asiabanpour, B., Mojdeh, M., Palmer, K., 2003, 'SIS – A New SFF Method Based on Powder Sintering', *Rapid Prototyping Journal*, vol. 9 , No. 1, pp. 30-36

Kumar, A.V., 2000, *Solid free form fabrication using powder deposition*, US patent 6066285

Kumar A.V., Dutta A., 2003, 'Investigation of an electrophotography based rapid prototyping Technology', *Rapid Prototyping Journal*, vol. 9, no. 2, pp. 95-103

Kumar A.V., Dutta A., 2004, 'Electrophotographic printing of part and binder powders', *Rapid Prototyping Journal*, vol. 10, no. 1, pp. 7-13

Larsson, R., 2003, *Method and device for manufacturing three-dimensional bodies*, US Patent 6531086

Majewski, C.E., Oduye , D.,Thomas, H.R., Hopkinson, N.,2008, 'Effect of infra-red power level on the sintering behaviour in the high speed sintering process', *Rapid Prototyping Journal*, vol. 14, no. 3, pp. 155–160

Manjooran,J. N., Kumar ,A. V.,Sigmund, W. M., 2006, Development of a liquid toner for electro-photographic solid freeform fabrication, *Journal of the European Ceramic Society* , vol. 26, pp. 2459–2465

McAlea, K. P., Forderhase, P. F., 1998, '*Selective laser sintering of polymer powder of controlled particle size distribution*', US Patent 5817206

Michel,E., Baur ,R., Macholdt, H.-T., 2001, Charge stabilizers: properties and applications, Journal of Electrostatics , vol. 51 , pp. 91-96

Muller, F., Polke, R., Schafer, M., Scholz, N., 2001, Particle System Characterization and Modelling, *WILEY-VCH Verlag GmbH*, pp. 248-253

Papaini,M., 1996, 'Study of radiative properties of powdered and fibrous polymers , Journal of vibrational spectroscopy' , vol. 11, pp. 61-68

Papini, M.,1997, 'Analysis of the reflectance of granular materials in the near infrared wavelength range', *Journal of Quant Spectroscopscopy Radiant Transfer*, vol. 57, nos. 2, pp. 265-274

Pomerantz, I., Cohen-Sabban, J., Bieber, A., Kamir, J., Katz, M., Nagler, M., 1990, *Three dimensional modelling apparatus*, US Patent 4961154

Scharfe M, *Electrophotography principles and optimization*, Research study press ltd UK , UK, 1984

Schien L.B, 1999, 'Recent advances in our understanding of toner charging', *Journal of Electrostatics*, vol. 46, pp.29-36

Schein, L.B., Stanley, W., 2005, 'Electrostatic proximity force, toner adhesion, and atomic force microscopy of insulating particles', *Journal of Electrostatics*, vol. 63, pp. 699–704

Shuji, M.' Hiroaki, M., 2003,'Electrostatics of particles', *Advanced Powder Technol.*, vol. 14, no. 2, pp. 143– 166

Takeuchi,M.,2006, Adhesion forces of charged particles, *Journal of Chemical Engineering Science*, vol. 61, pp. 2279 – 2289

Takagi,K.,Castle,G.S. P.,Takeuchi,M., 2003,'Tribocharging mechanism of mono-component irregular and spherical toners in an electrophotographic development system', *Journal of Powder Technology*, vol. 135–136, pp. 35– 42

Tanaka,M., Kamiya,H., 2006, 'Analysis of the grinding of toner sheets using Vickers hardness as an index of grindability' , *Journal of powder technology*, vol. 164, issue 2, pp. 82-88

Tanaka, M., Kamiya, H., 2008, 'Evaluation of flow properties of toner powder using conical rotor', *Journal of Powder Technology*, pp. 36-44

Taylor,M,D., Sekher, E.P., Industrial Electrostatics, Recent Studies Press Ltd, UK 1994

Thomas, H.R., Hopkinson, N.,Erasenthiran, P.E. , 2006, 'High speed sintering – continuing research into a new rapid manufacturing process', *Proceedings from the 17th SFF Symposium*, Austin, Texas

Ventura, P., 1999 'Analysis of the reflectance of granular materials in the near infrared wavelength range', *Journal of Quant Spectroscopscopy Radiant Transfer*, vol. 61, nos. 2, pp. 185-195

Walker , A.,Baldwin, D.,1999, 'Initial Investigations into Low-Cost Ultra-Fine Pitch Solder Printing Process Based on Innovative Laser Printing Technology' *International Symposium on Advanced Packaging Materials*

Wimpenny D, Banerjee S.,2006, ' Selective Infrared sintering of polymers using Radiant IR heating and Ink-Jet printing ', *Seventh Soild Frreform Fabrication symposium" in University of Texas, Austin , USA*

Wimpenny, D., Banerjee, S.,2007, ' Selective Infrared sintering of polymers using IR heating and Ink-Jet printing ', *8th National conference on 'Rapid Design, prototyping, and Manufacture'*

Wimpenny, D I., Banerjee, S.,2008, '*Rapid Prototyping method using infrared sin*tering', UK Patent Publication 2422344

Zhou,H., Götzinger,M., Peukert, W., 2003, The influence of particle charge and roughness on particle–substrate adhesion Journal of Powder technology , vol. 135-136 , pp. 82-91

Zimmer, M., Waldemar, W.,Auchter , P., Jung , D., 2002,'*Device for applying decors and/or characters on glass, glass ceramics and ceramics products*' US Patent 6487386

Appendix:

A) Tensile test results including Young's Modulus, UTS and Elongation at Break

Figure A1: Mechanical properties of Uncoated Coarse Somos 201 powder at 128 mm stand off distance:

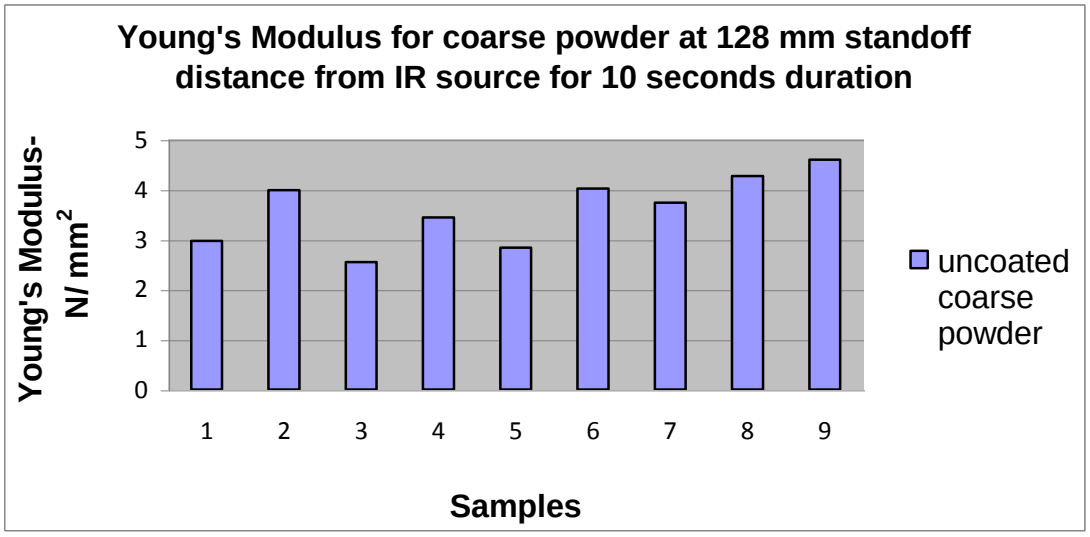

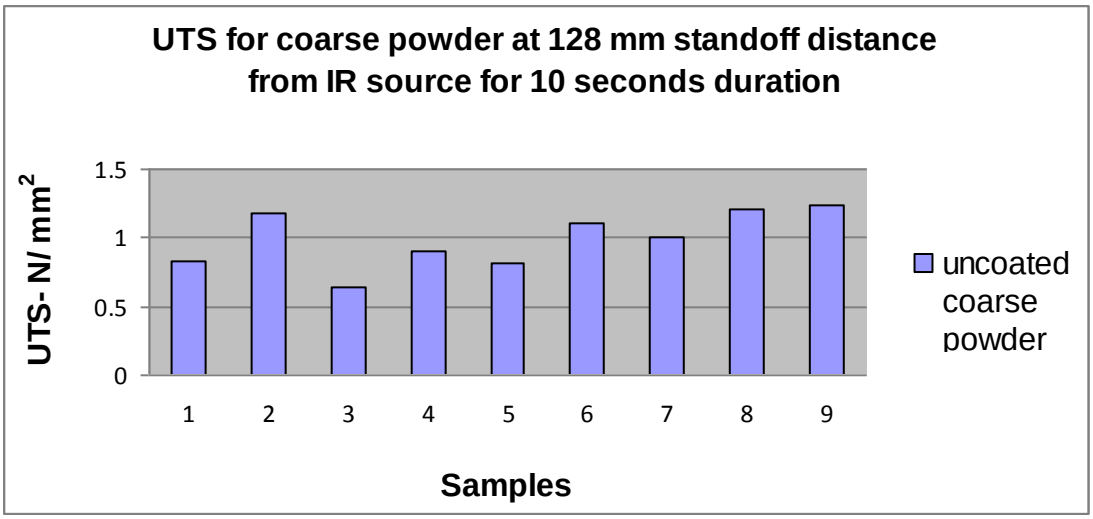

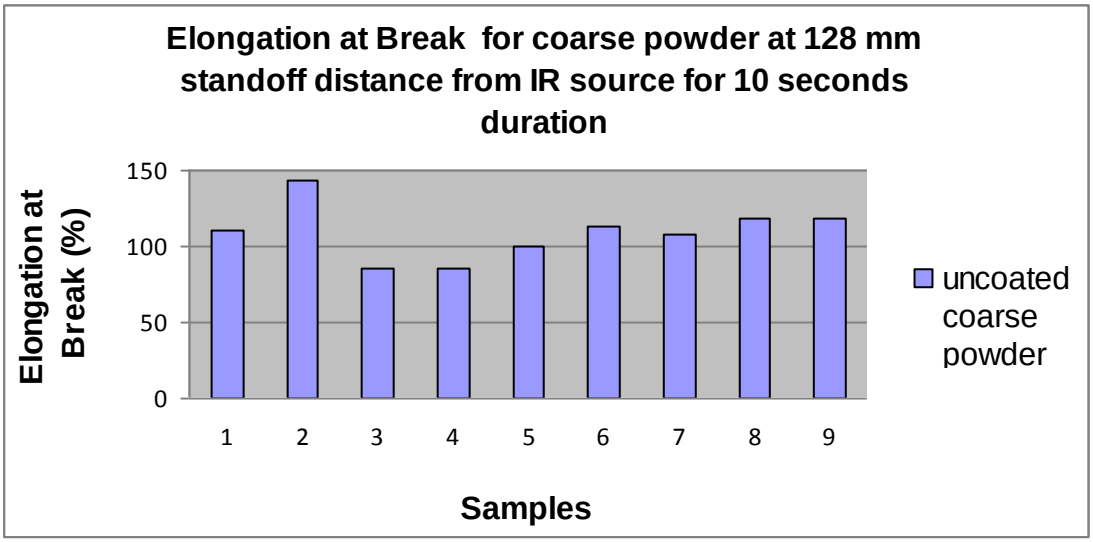

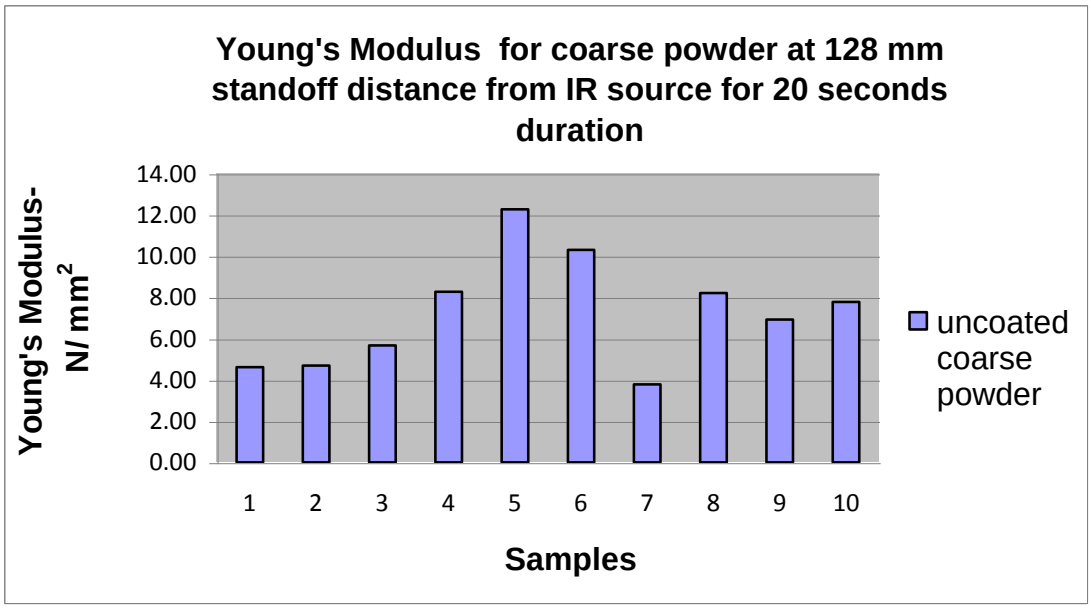
Young's Modulus for coarse powder at 128 mm standoff distance from IR source for 20 seconds duration
Young's Modulus- N/ mm2
14.00
12.00
10.00
8.00
6.00
4.00
2.00
0.00
1 2 3 4 5 6 7 8 9 10
Samples
uncoated coarse powder

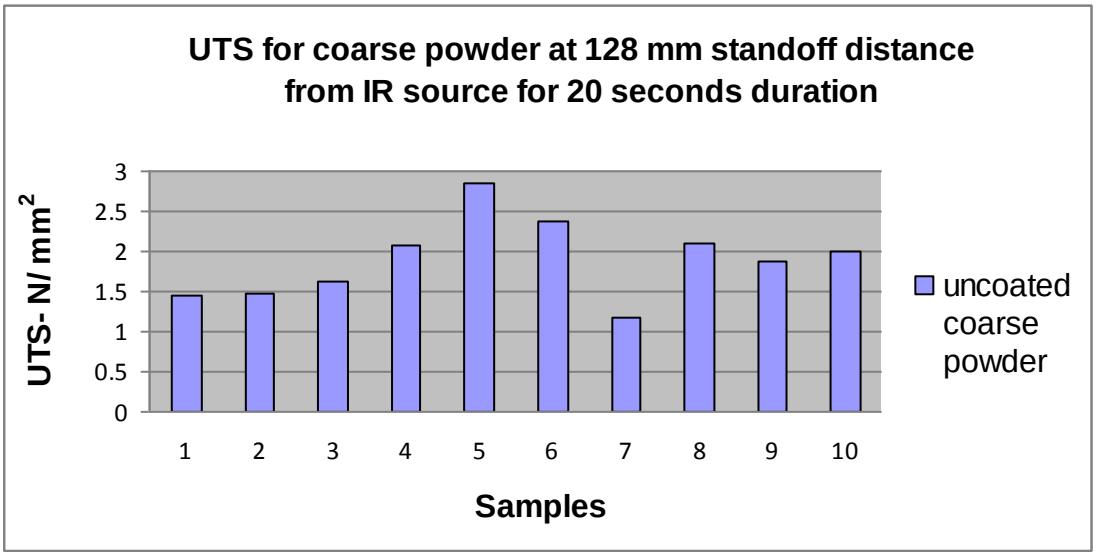
UTS for coarse powder at 128 mm standoff distance from IR source for 20 seconds duration
UTS- N/ mm2
3
2.5
2
1.5
1
0.5
0
1 2 3 4 5 6 7 8 9 10
Samples
uncoated coarse powder

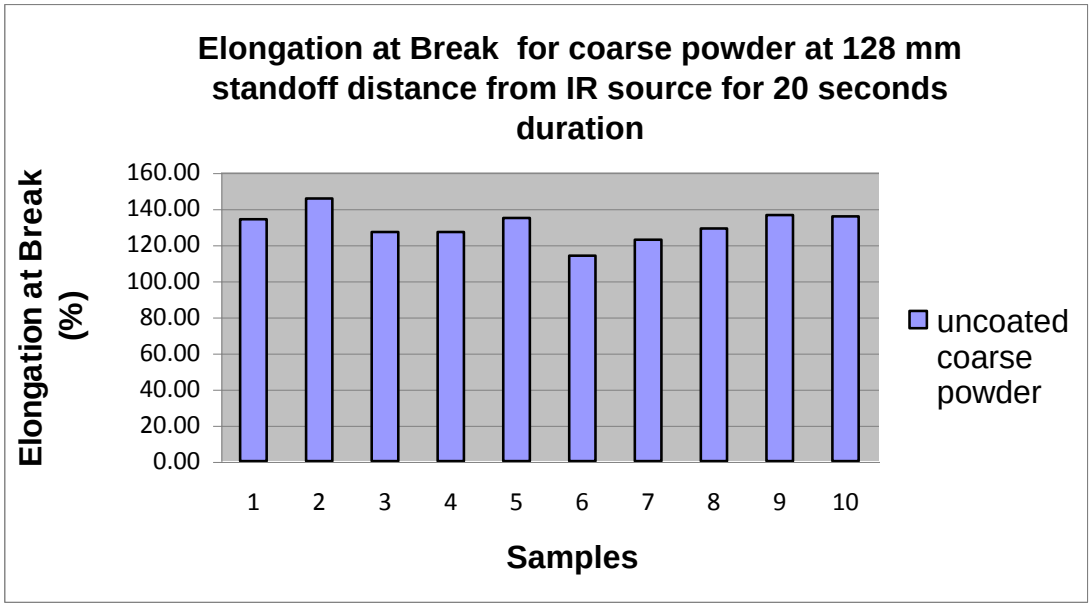
Elongation at Break for coarse powder at 128 mm standoff distance from IR source for 20 seconds duration
Elongation at Break (%)
160.00
140.00
120.00
100.00
80.00
60.00
40.00
20.00
0.00
1 2 3 4 5 6 7 8 9 10
Samples
uncoated coarse powder

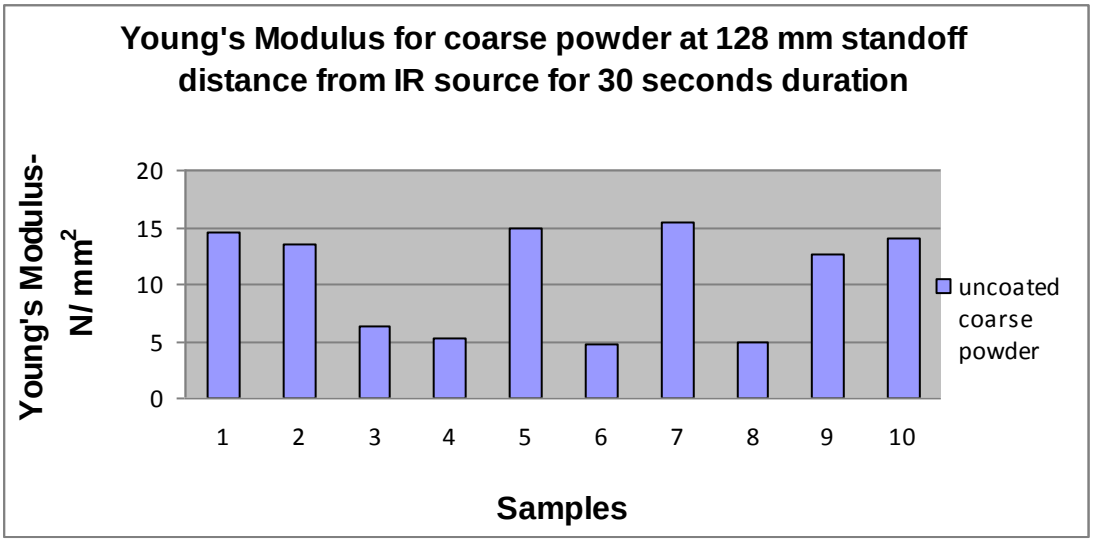
Young's Modulus for coarse powder at 128 mm standoff distance from IR source for 30 seconds duration
Young's Modulus- N/ mm2
20
15
10
5
0
1
2
3
4
5
6
7
8
9
10
Samples
uncoated coarse powder

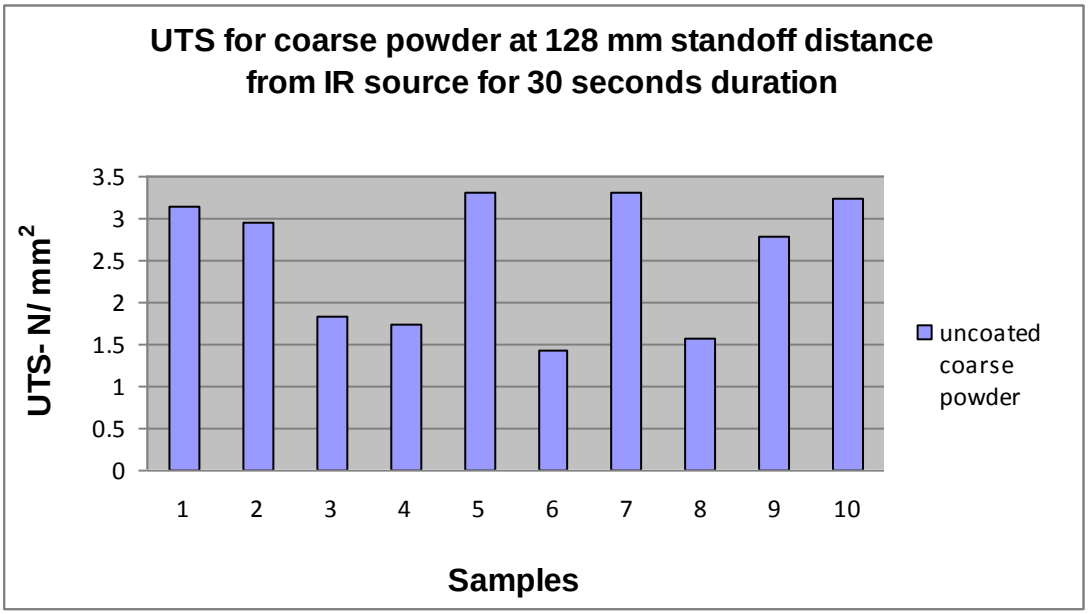
UTS for coarse powder at 128 mm standoff distance from IR source for 30 seconds duration
UTS- N/ mm2
3.5
3
2.5
2
1.5
1
0.5
0
1
2
3
4
5
6
7
8
9
10
Samples
uncoated coarse powder

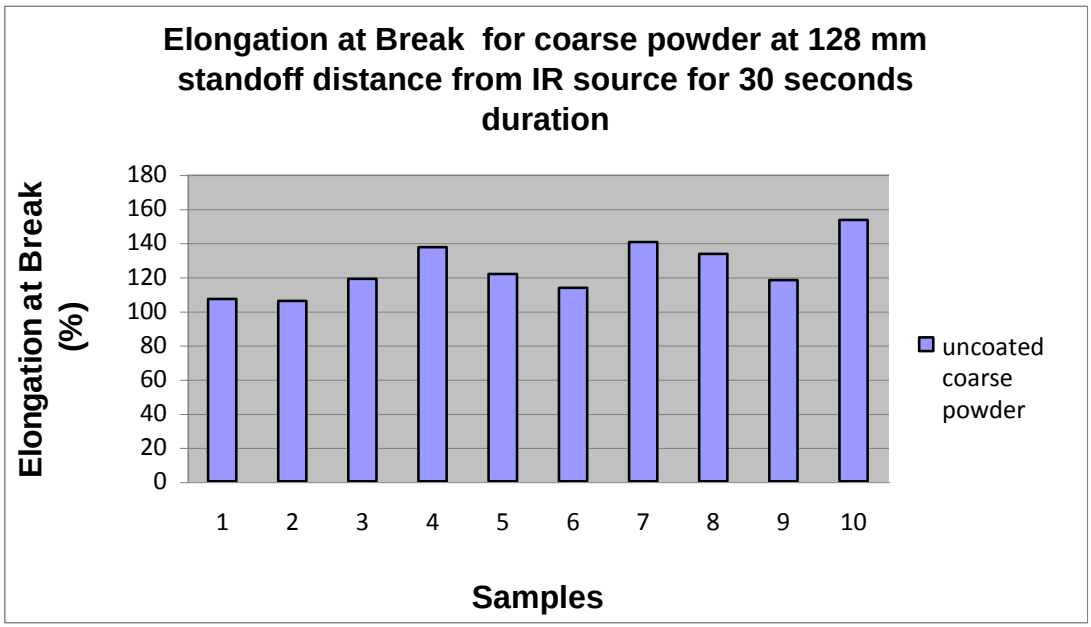
Elongation at Break for coarse powder at 128 mm standoff distance from IR source for 30 seconds duration
Elongation at Break (%)
180
160
140
120
100
80
60
40
20
0
1
2
3
4
5
6
7
8
9
10
Samples
uncoated coarse powder

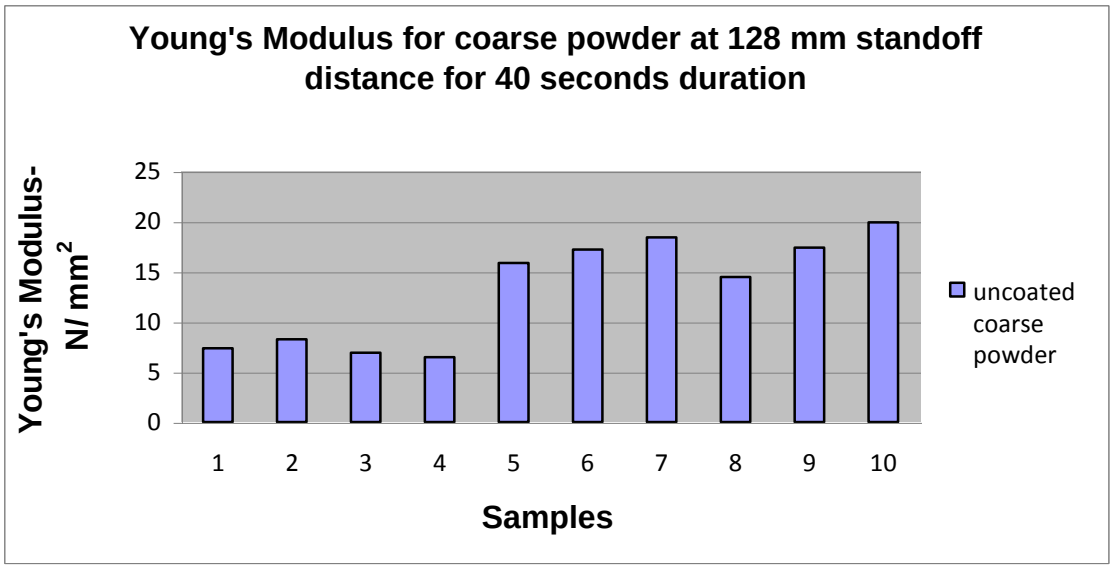
Young's Modulus for coarse powder at 128 mm standoff distance for 40 seconds duration
Young's Modulus- N/ mm2
25
20
15
10
5
0
1
2
3
4
5
6
7
8
9
10
Samples
uncoated coarse powder

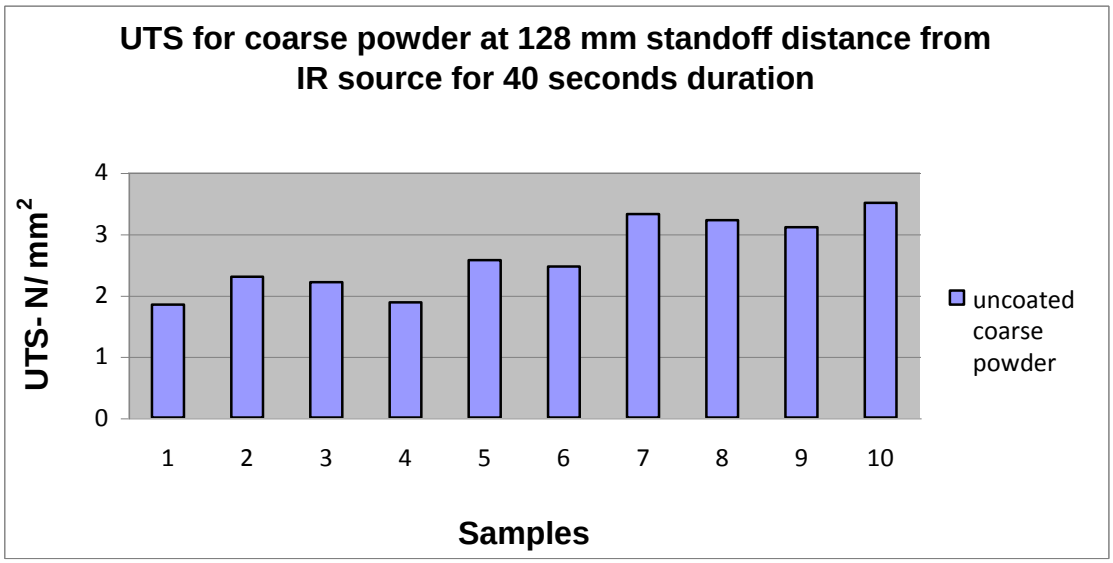
UTS for coarse powder at 128 mm standoff distance from IR source for 40 seconds duration
UTS- N/ mm2
4
3
2
1
0
1
2
3
4
5
6
7
8
9
10
Samples
uncoated coarse powder

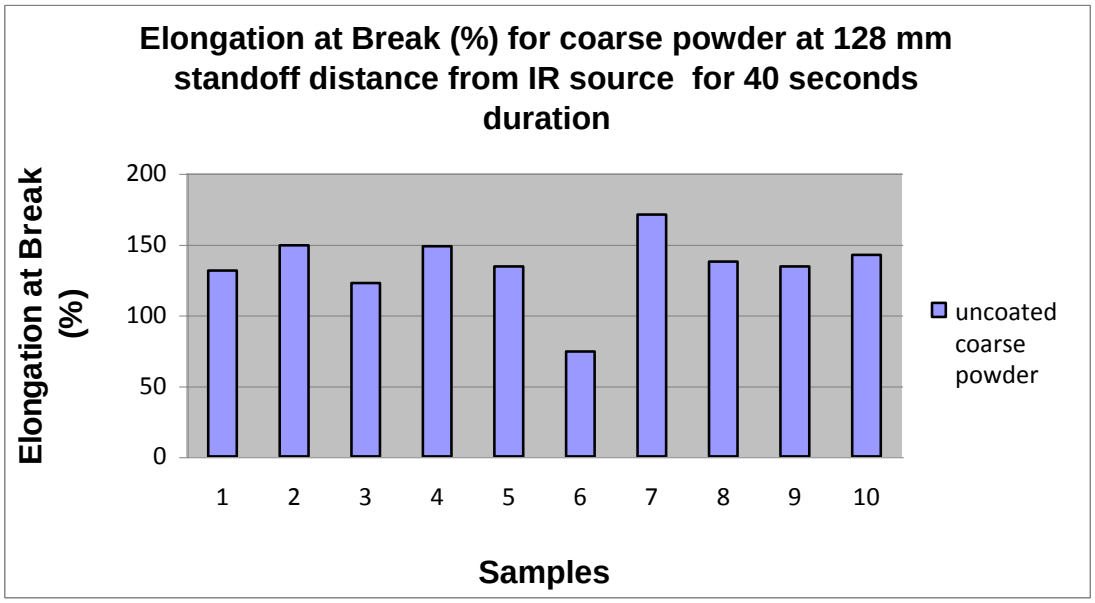
Elongation at Break (%) for coarse powder at 128 mm standoff distance from IR source for 40 seconds duration
Elongation at Break (%)
200
150
100
50
0
1
2
3
4
5
6
7
8
9
10
Samples
uncoated coarse powder

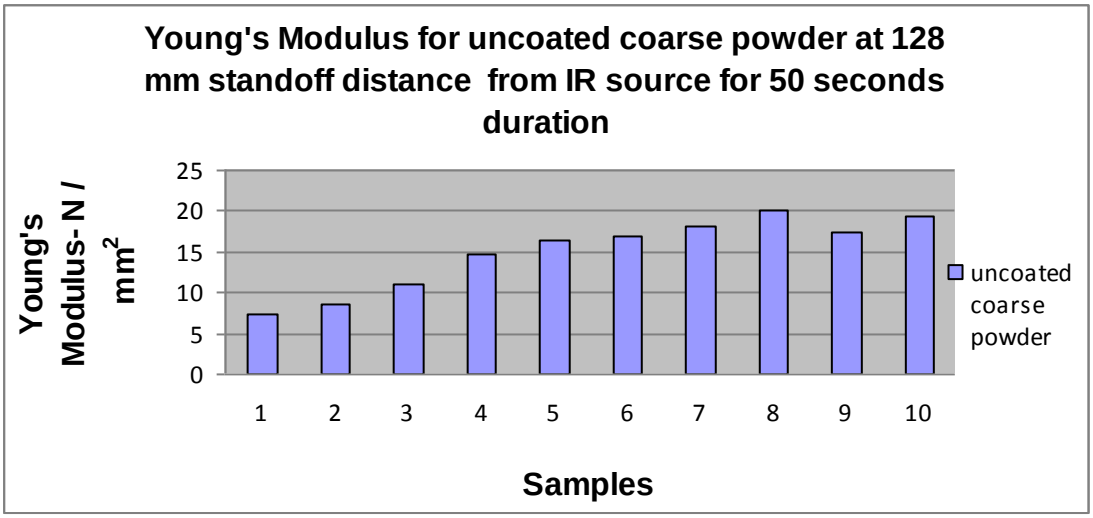
Young's Modulus for uncoated coarse powder at 128 mm standoff distance from IR source for 50 seconds duration
Young's Modulus- N / mm2
25
20
15
10
5
0
1
2
3
4
5
6
7
8
9
10
Samples
uncoated coarse powder

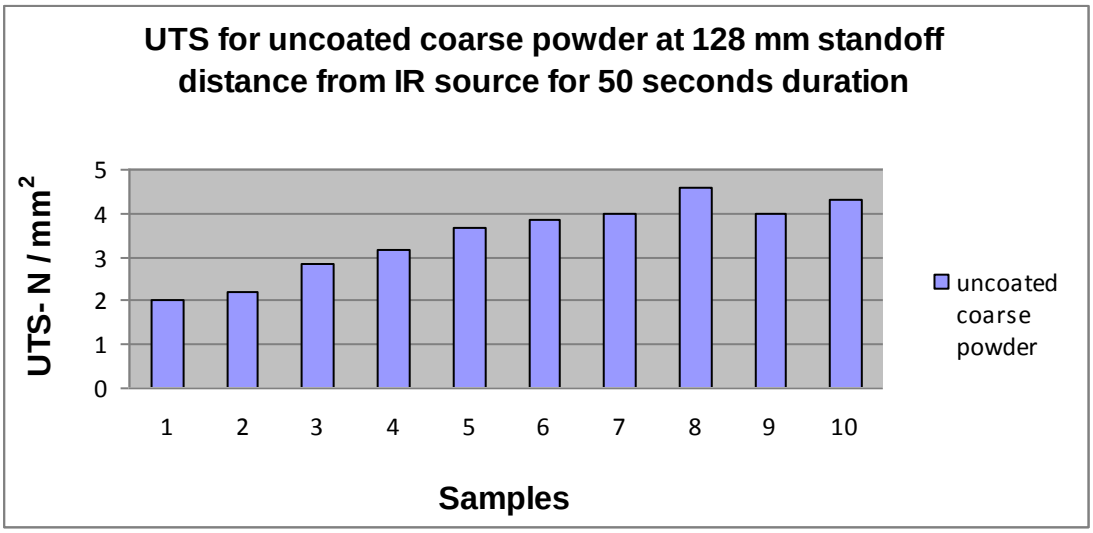
UTS for uncoated coarse powder at 128 mm standoff distance from IR source for 50 seconds duration
UTS- N / mm2
5
4
3
2
1
0
1
2
3
4
5
6
7
8
9
10
Samples
uncoated coarse powder

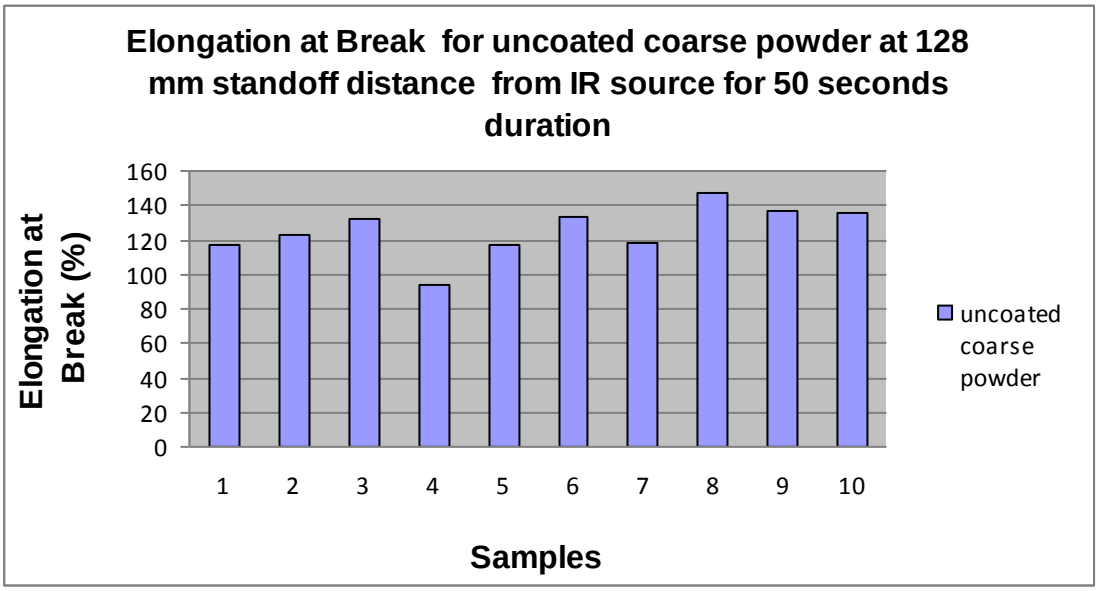
Elongation at Break for uncoated coarse powder at 128 mm standoff distance from IR source for 50 seconds duration
Elongation at Break (%)
160
140
120
100
80
60
40
20
0
1
2
3
4
5
6
7
8
9
10
Samples
uncoated coarse powder

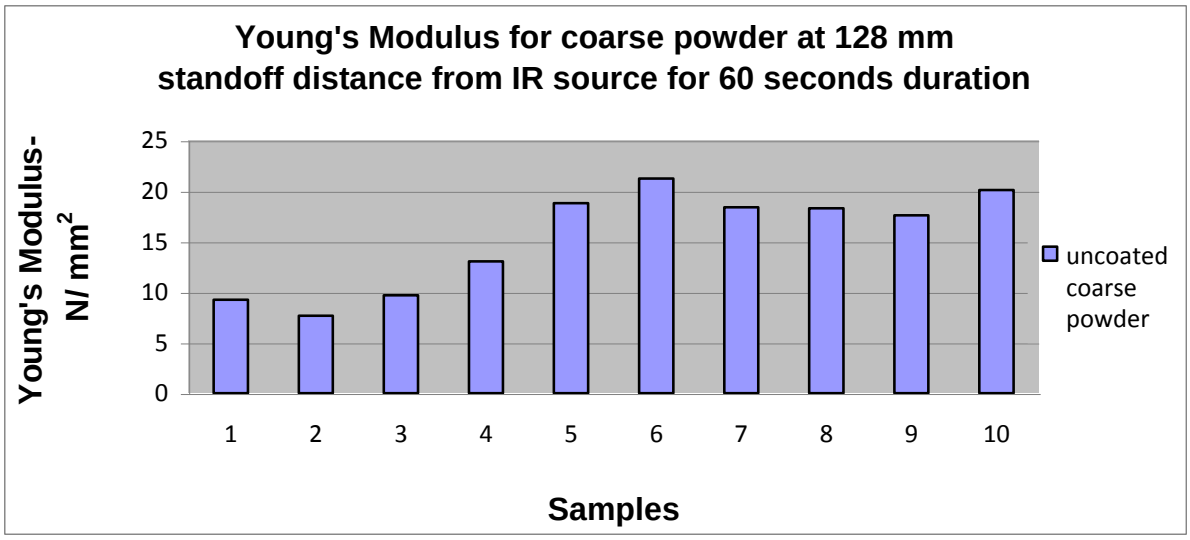
Young's Modulus for coarse powder at 128 mm standoff distance from IR source for 60 seconds duration
Young's Modulus- N/ mm2
25
20
15
10
5
0
1
2
3
4
5
6
7
8
9
10
Samples
uncoated coarse powder

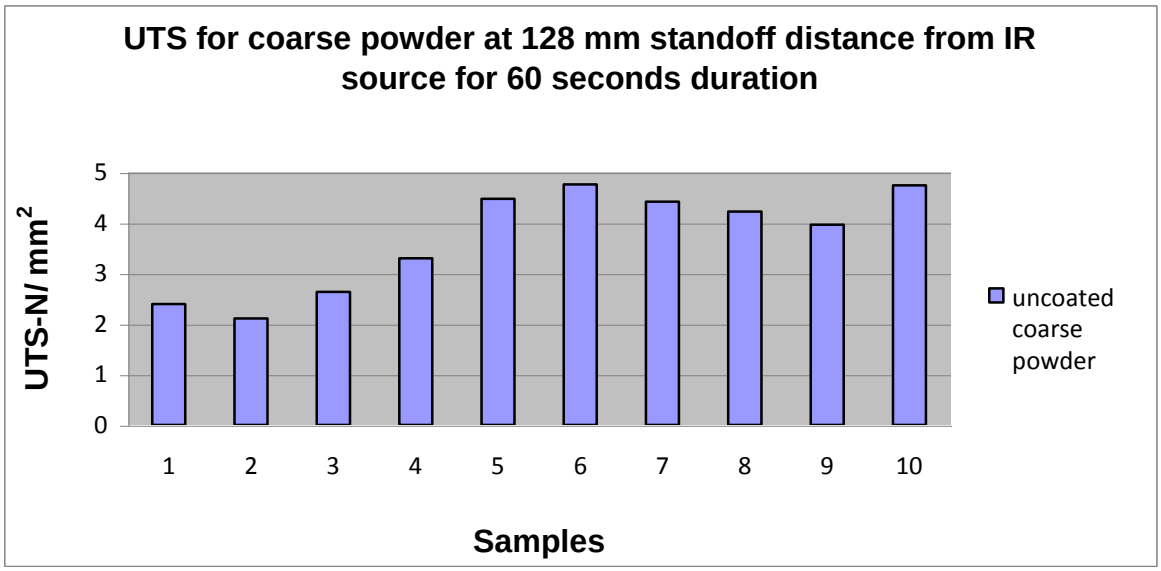
UTS for coarse powder at 128 mm standoff distance from IR source for 60 seconds duration
UTS-N/ mm2
5
4
3
2
1
0
1
2
3
4
5
6
7
8
9
10
Samples
uncoated coarse powder

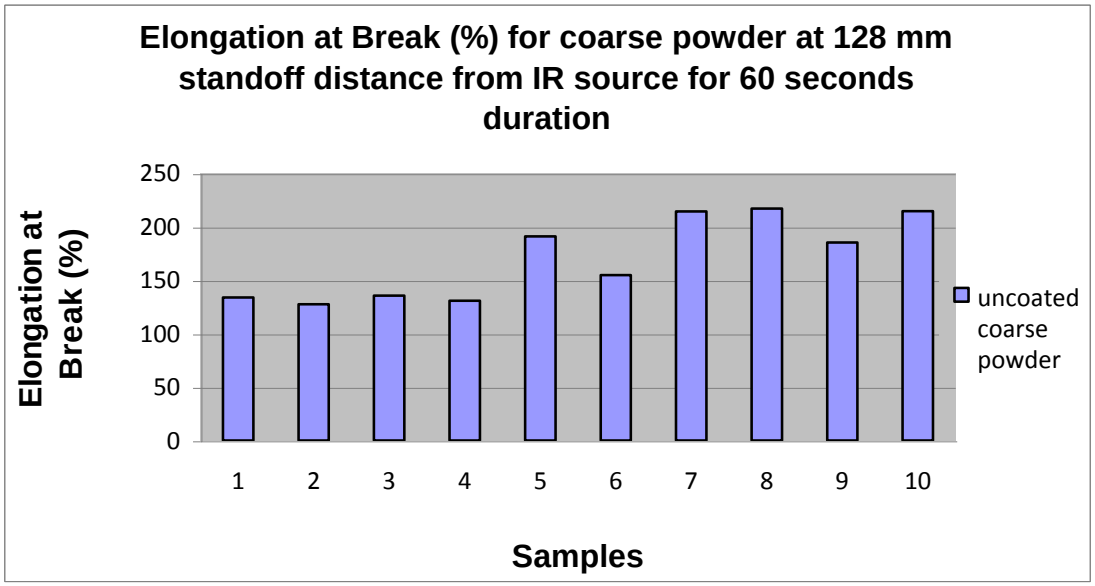
Elongation at Break (%) for coarse powder at 128 mm standoff distance from IR source for 60 seconds duration
Elongation at Break (%)
250
200
150
100
50
0
1
2
3
4
5
6
7
8
9
10
Samples
uncoated coarse powder

Figure A2: Mechanical properties of Uncoated coarse Somos 201 powder at 178 mm stand off distance:

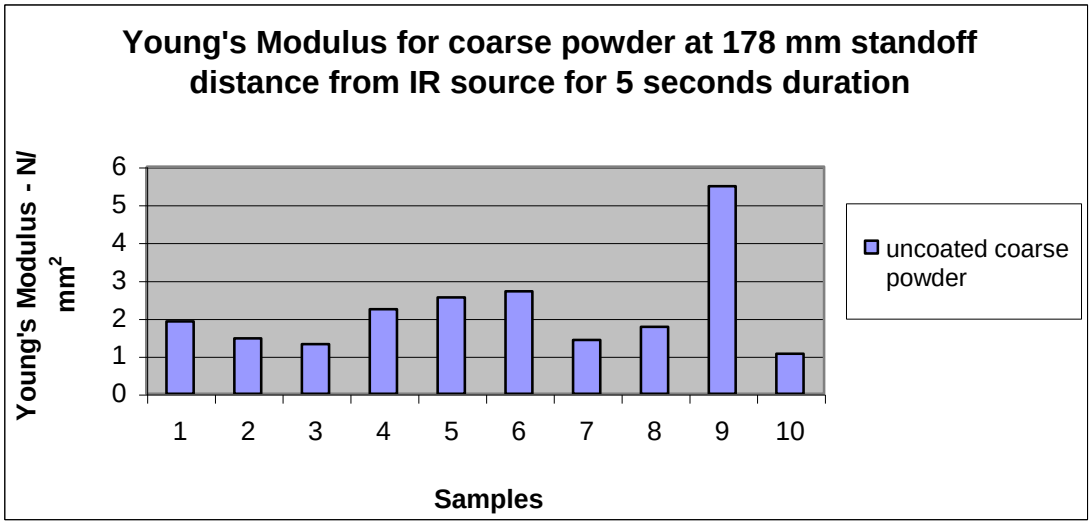

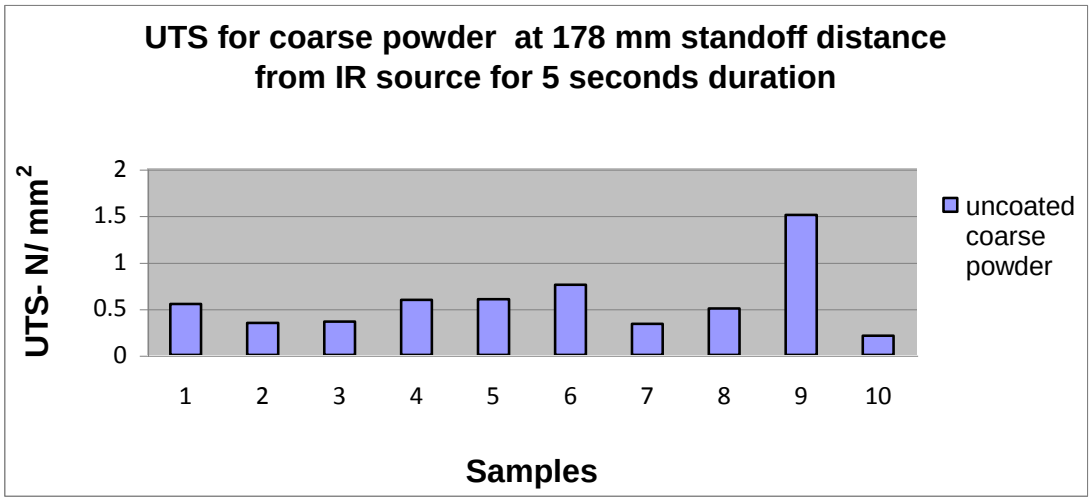

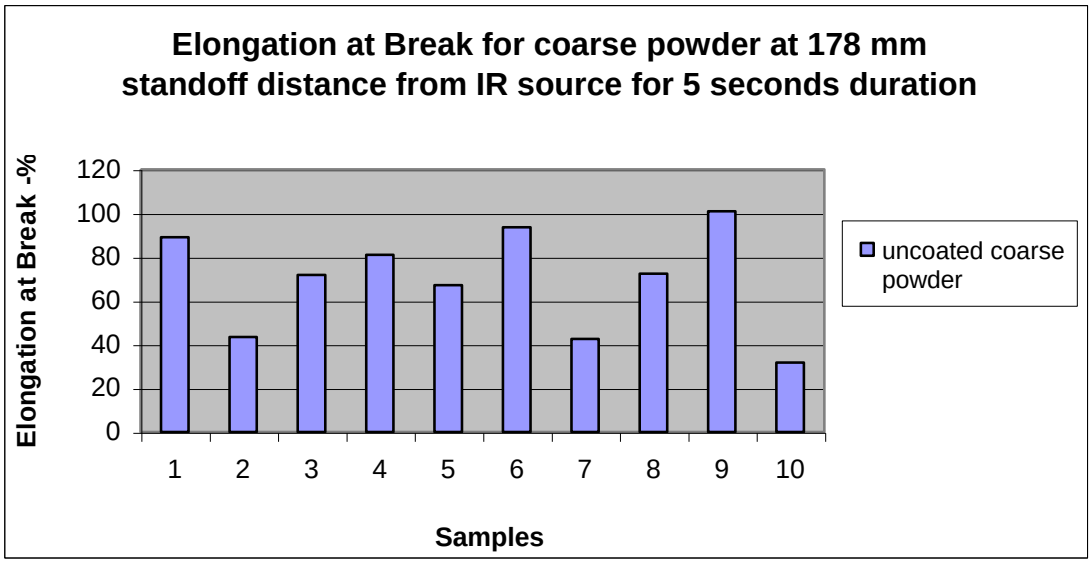

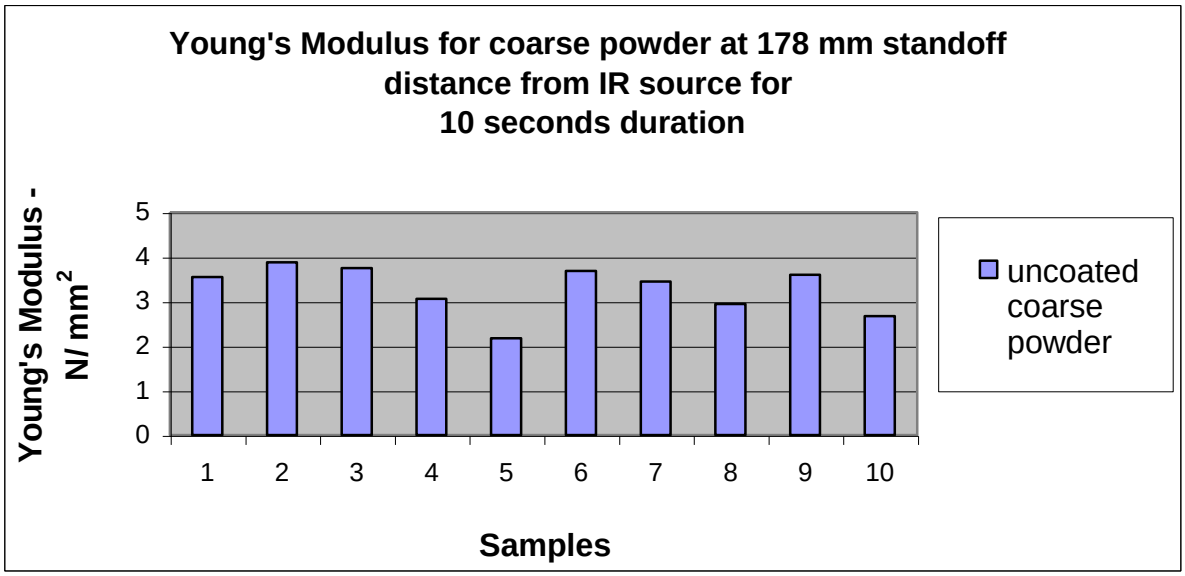
Young's Modulus for coarse powder at 178 mm standoff distance from IR source for 10 seconds duration
Young's Modulus - N/ mm2
0
1
2
3
4
5
1
2
3
4
5
6
7
8
9
10
Samples
uncoated coarse powder

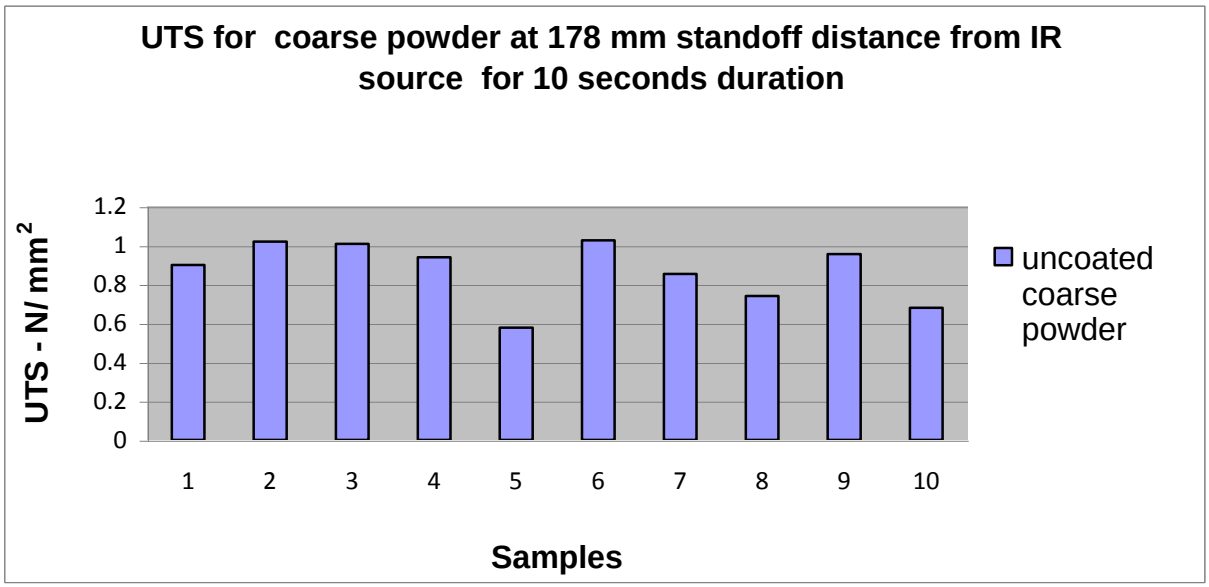
UTS for coarse powder at 178 mm standoff distance from IR source for 10 seconds duration
UTS - N/ mm2
0
0.2
0.4
0.6
0.8
1
1.2
1
2
3
4
5
6
7
8
9
10
Samples
uncoated coarse powder

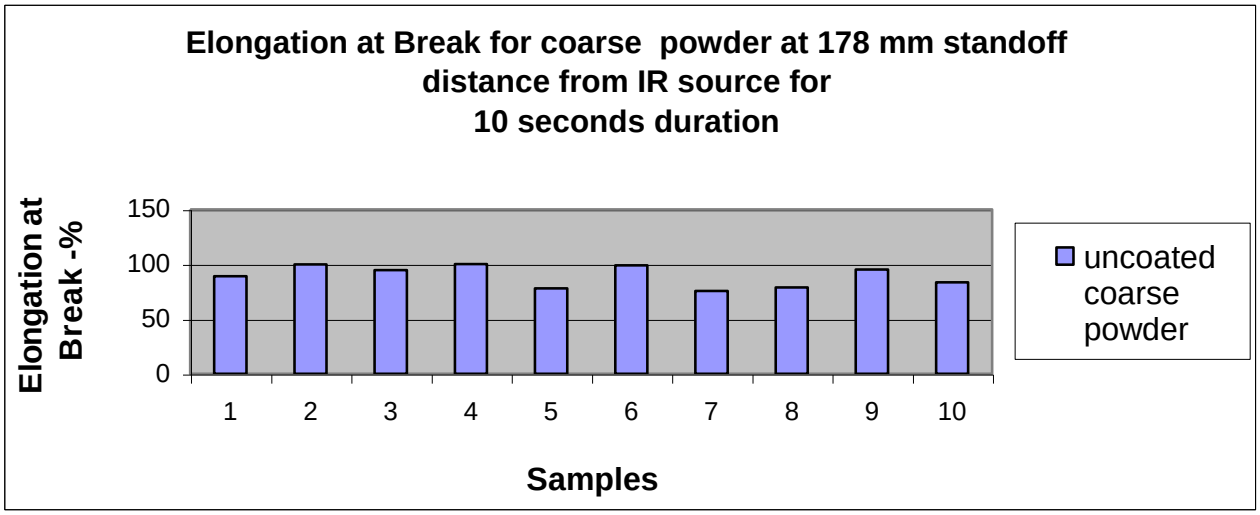
Elongation at Break for coarse powder at 178 mm standoff distance from IR source for 10 seconds duration
Elongation at Break -%
0
50
100
150
1
2
3
4
5
6
7
8
9
10
Samples
uncoated coarse powder

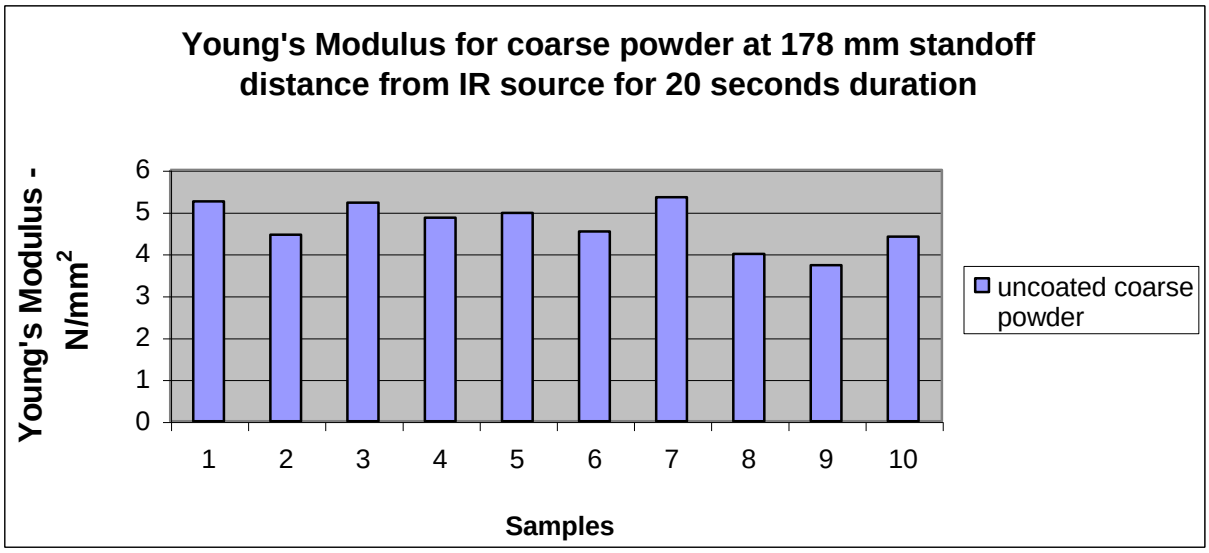
Young's Modulus for coarse powder at 178 mm standoff distance from IR source for 20 seconds duration
Young's Modulus - N/mm2
0
1
2
3
4
5
6
1 2 3 4 5 6 7 8 9 10
Samples
uncoated coarse powder

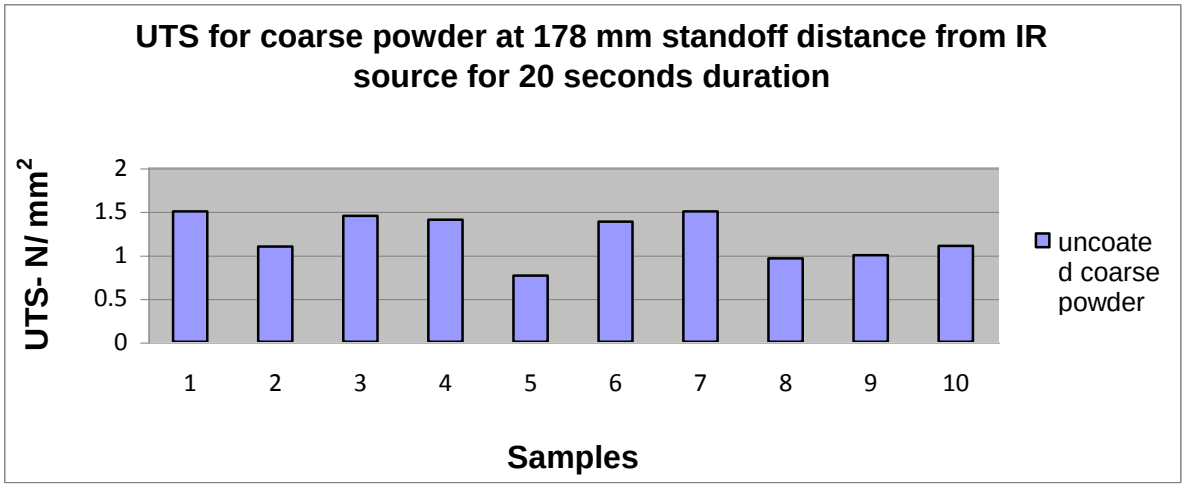
UTS for coarse powder at 178 mm standoff distance from IR source for 20 seconds duration
UTS- N/ mm2
0
0.5
1
1.5
2
1 2 3 4 5 6 7 8 9 10
Samples
uncoated coarse powder

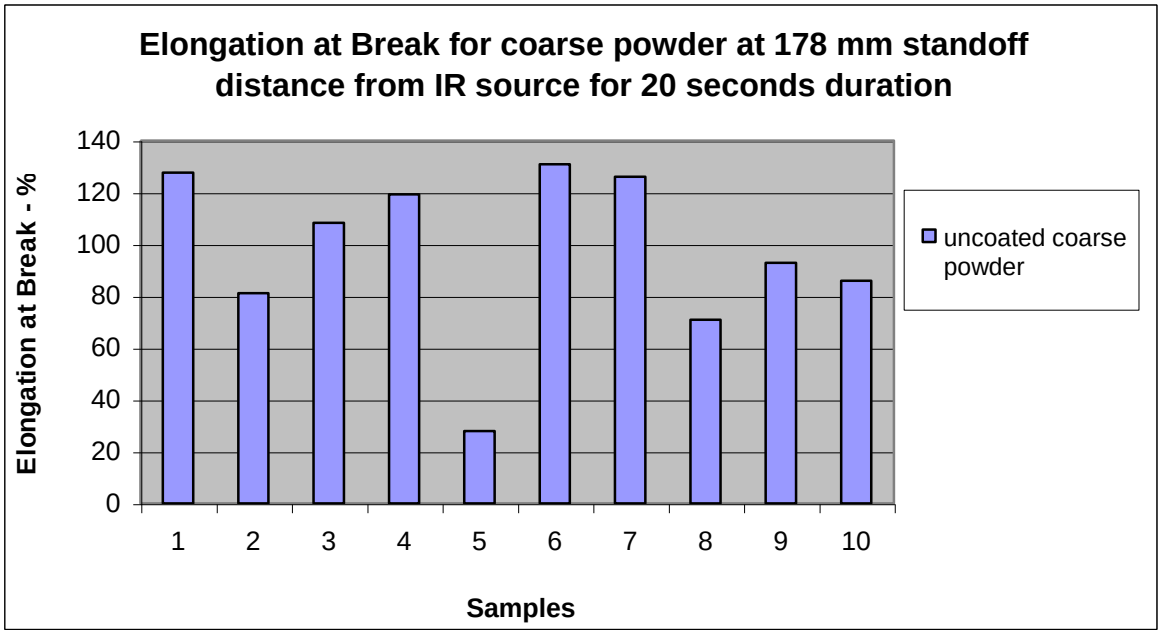
Elongation at Break for coarse powder at 178 mm standoff distance from IR source for 20 seconds duration
Elongation at Break - %
0
20
40
60
80
100
120
140
1 2 3 4 5 6 7 8 9 10
Samples
uncoated coarse powder

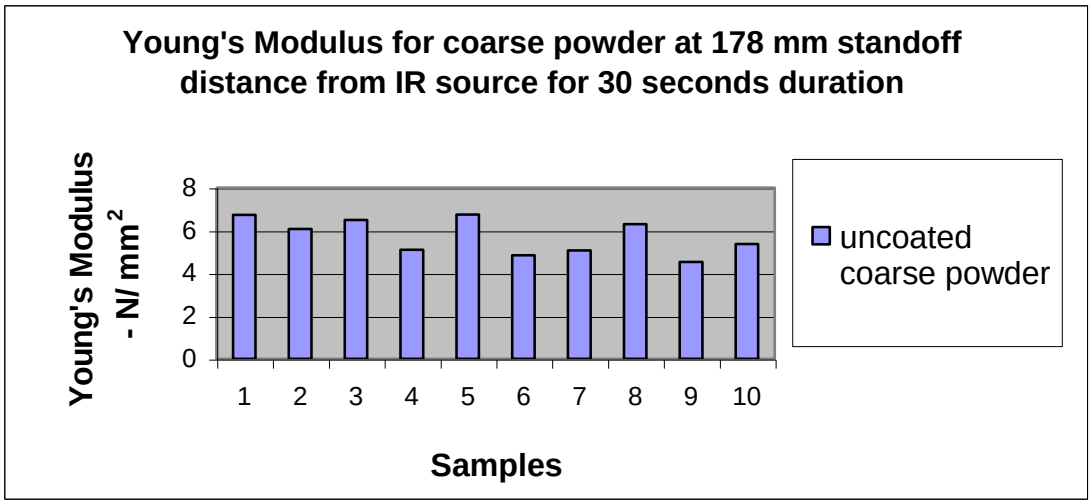
Young's Modulus for coarse powder at 178 mm standoff distance from IR source for 30 seconds duration
Young's Modulus - N/ mm2
8
6
4
2
0
1 2 3 4 5 6 7 8 9 10
Samples
uncoated coarse powder

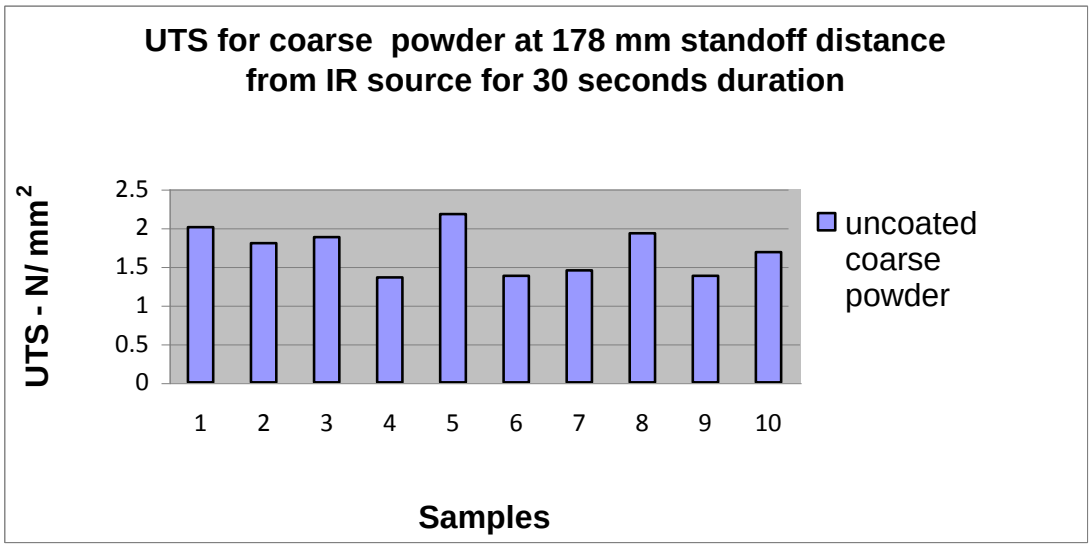
UTS for coarse powder at 178 mm standoff distance from IR source for 30 seconds duration
UTS - N/ mm2
2.5
2
1.5
1
0.5
0
1 2 3 4 5 6 7 8 9 10
Samples
uncoated coarse powder

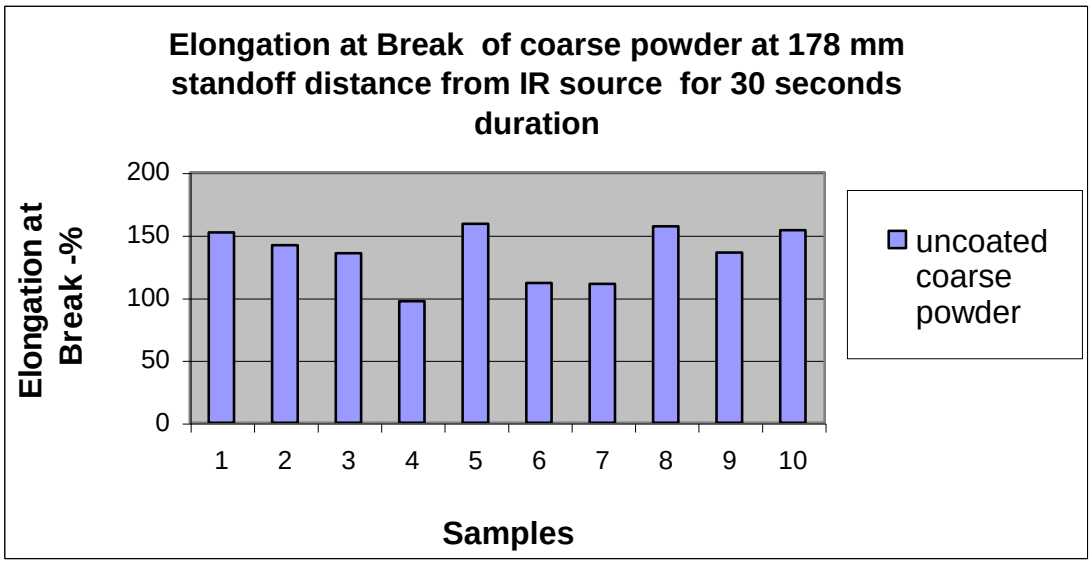
Elongation at Break of coarse powder at 178 mm standoff distance from IR source for 30 seconds duration
Elongation at Break -%
200
150
100
50
0
1 2 3 4 5 6 7 8 9 10
Samples
uncoated coarse powder

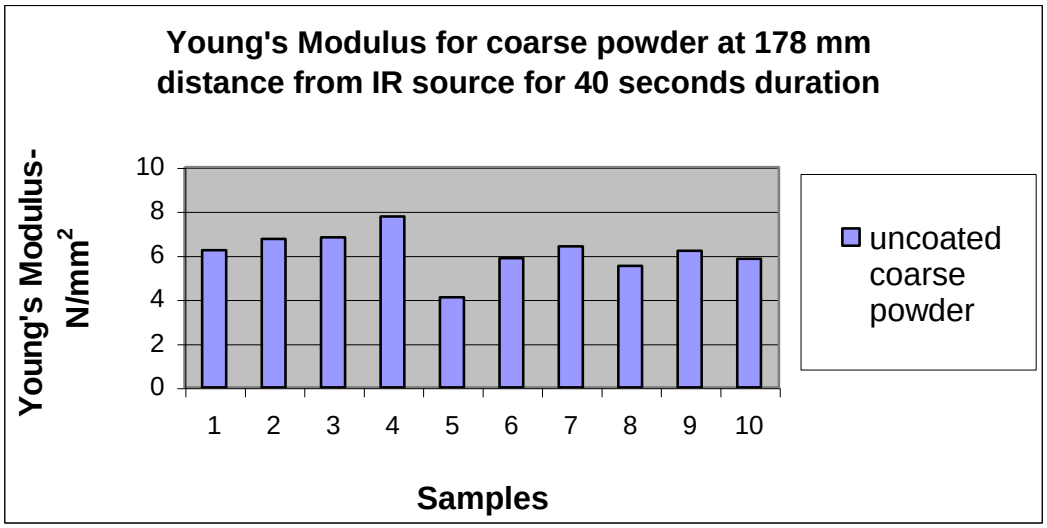
Young's Modulus for coarse powder at 178 mm distance from IR source for 40 seconds duration
Young's Modulus- N/mm2
10
8
6
4
2
0
1 2 3 4 5 6 7 8 9 10
Samples
uncoated coarse powder

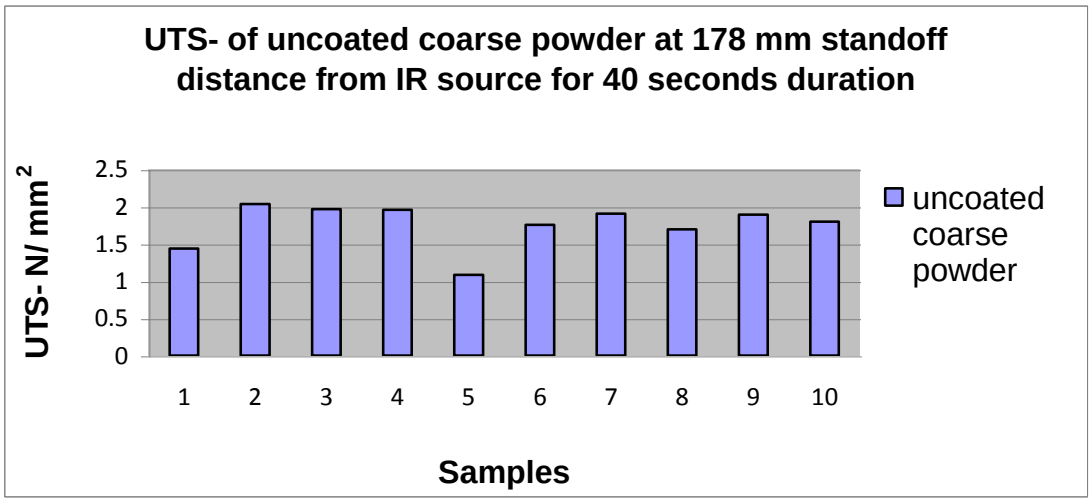
UTS- of uncoated coarse powder at 178 mm standoff distance from IR source for 40 seconds duration
UTS- N/ mm2
2.5
2
1.5
1
0.5
0
1 2 3 4 5 6 7 8 9 10
Samples
uncoated coarse powder

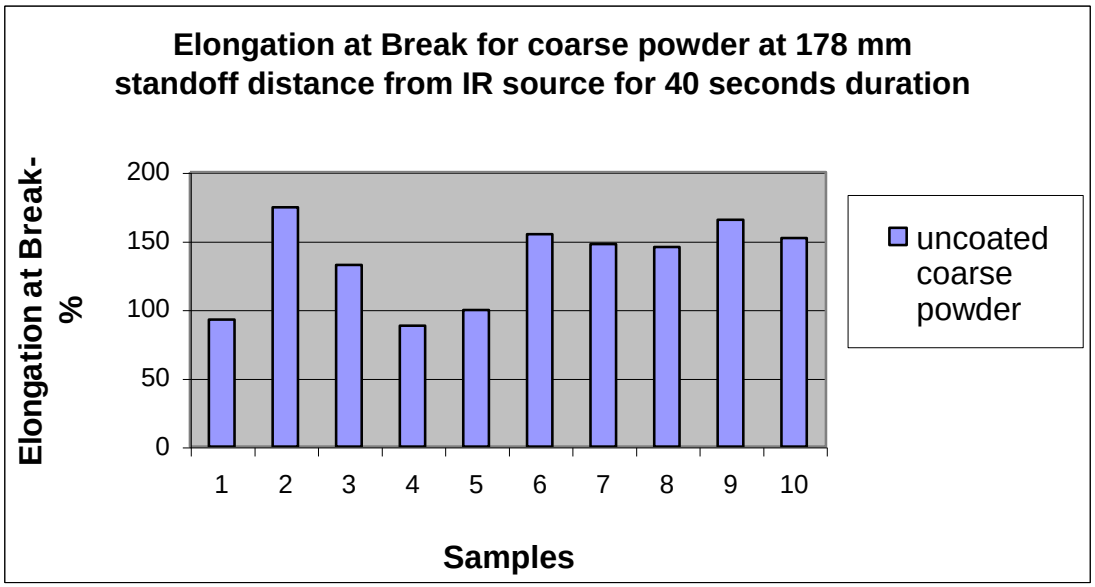
Elongation at Break for coarse powder at 178 mm standoff distance from IR source for 40 seconds duration
Elongation at Break- %
200
150
100
50
0
1 2 3 4 5 6 7 8 9 10
Samples
uncoated coarse powder

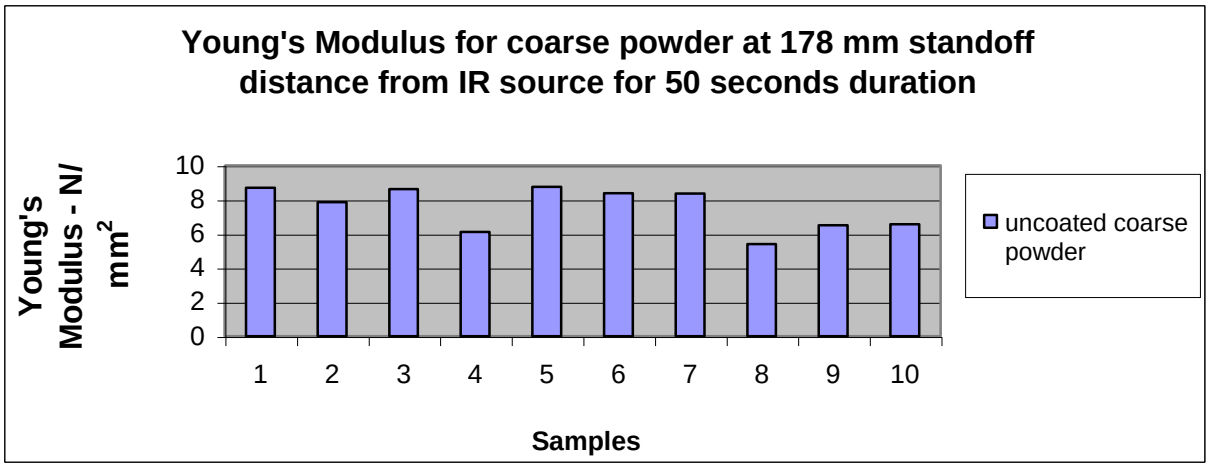
Young's Modulus for coarse powder at 178 mm standoff distance from IR source for 50 seconds duration
Young's Modulus - N/ mm2
10
8
6
4
2
0
1
2
3
4
5
6
7
8
9
10
Samples
uncoated coarse powder

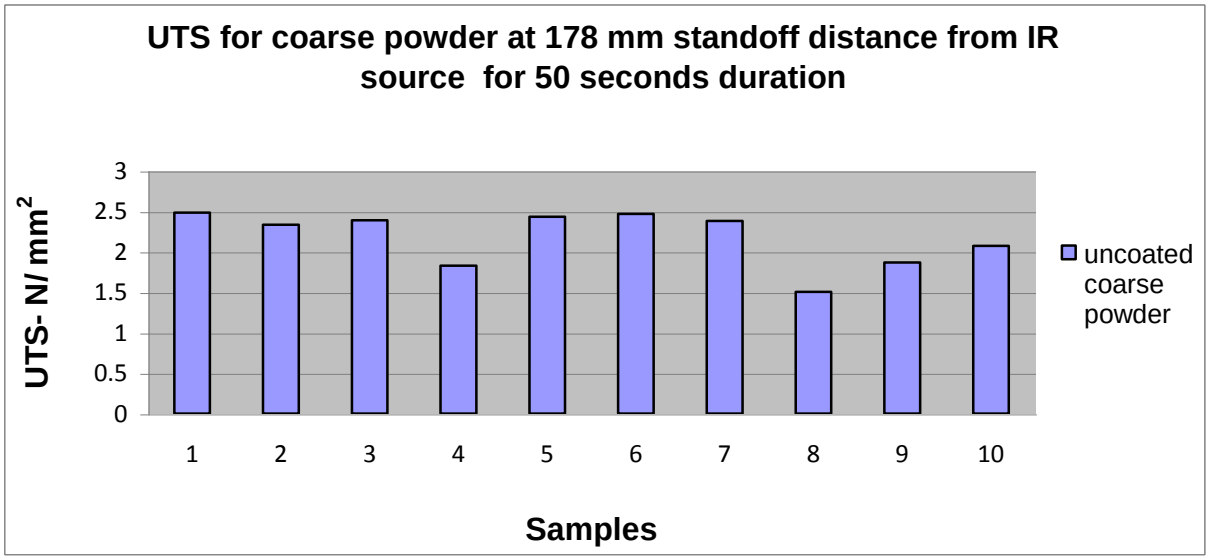
UTS for coarse powder at 178 mm standoff distance from IR source for 50 seconds duration
UTS- N/ mm2
3
2.5
2
1.5
1
0.5
0
1
2
3
4
5
6
7
8
9
10
Samples
uncoated coarse powder

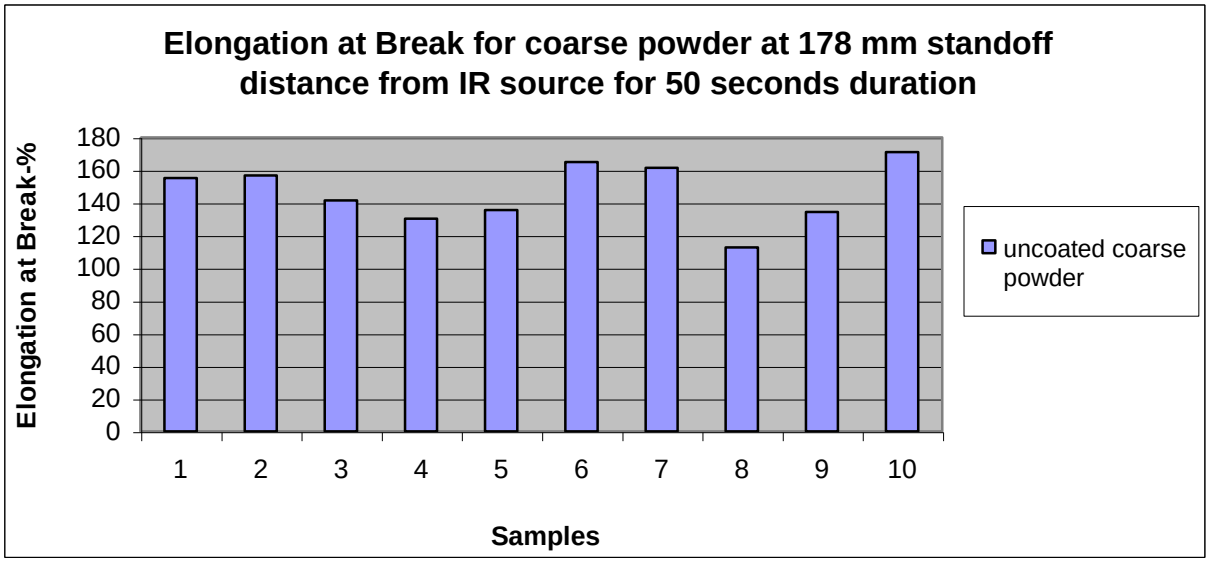
Elongation at Break for coarse powder at 178 mm standoff distance from IR source for 50 seconds duration
Elongation at Break-%
180
160
140
120
100
80
60
40
20
0
1
2
3
4
5
6
7
8
9
10
Samples
uncoated coarse powder

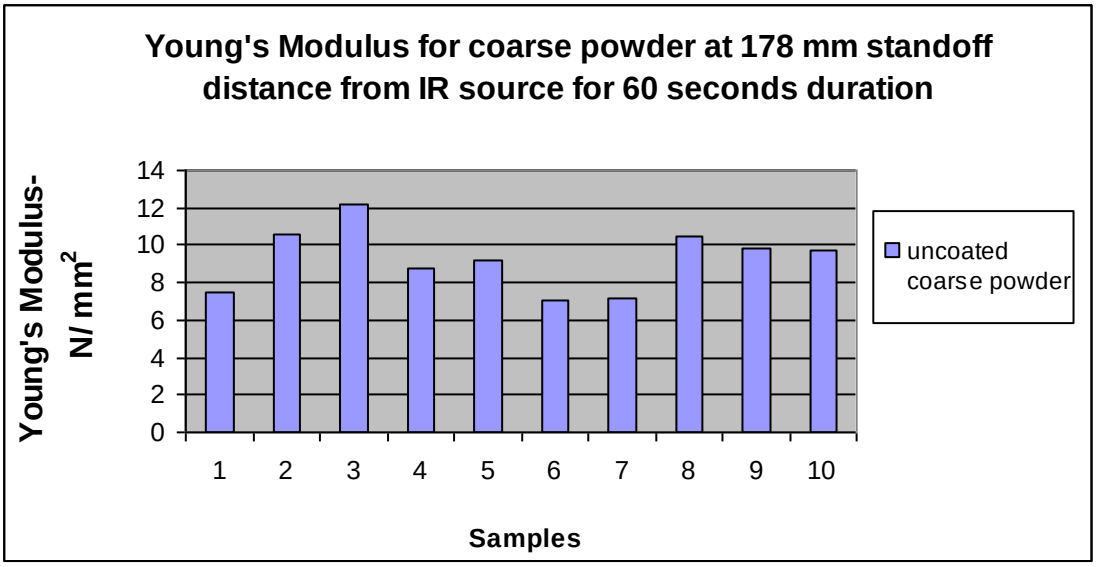
Young's Modulus for coarse powder at 178 mm standoff distance from IR source for 60 seconds duration
Young's Modulus- N/ mm2
14
12
10
8
6
4
2
0
1 2 3 4 5 6 7 8 9 10
Samples
uncoated coarse powder

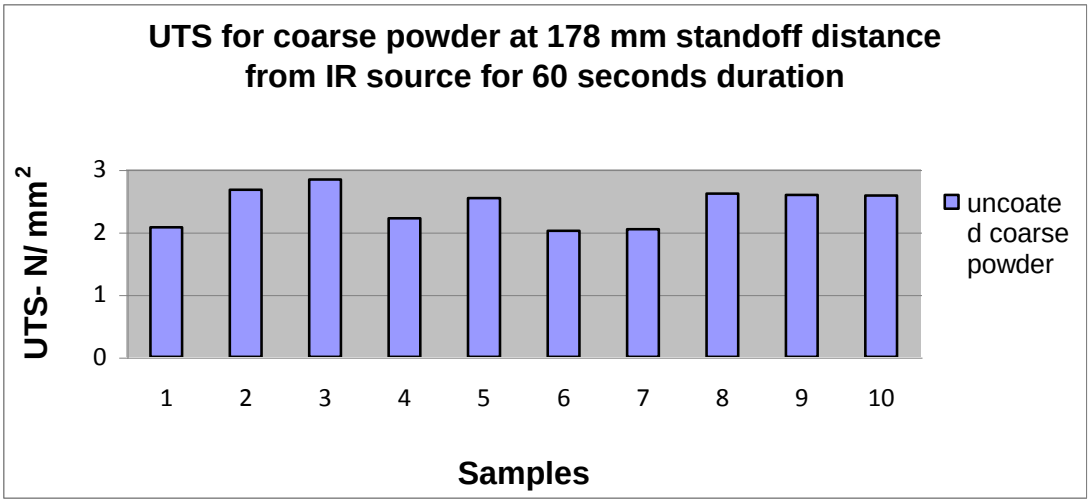
UTS for coarse powder at 178 mm standoff distance from IR source for 60 seconds duration
UTS- N/ mm2
3
2
1
0
1 2 3 4 5 6 7 8 9 10
Samples
uncoated coarse powder

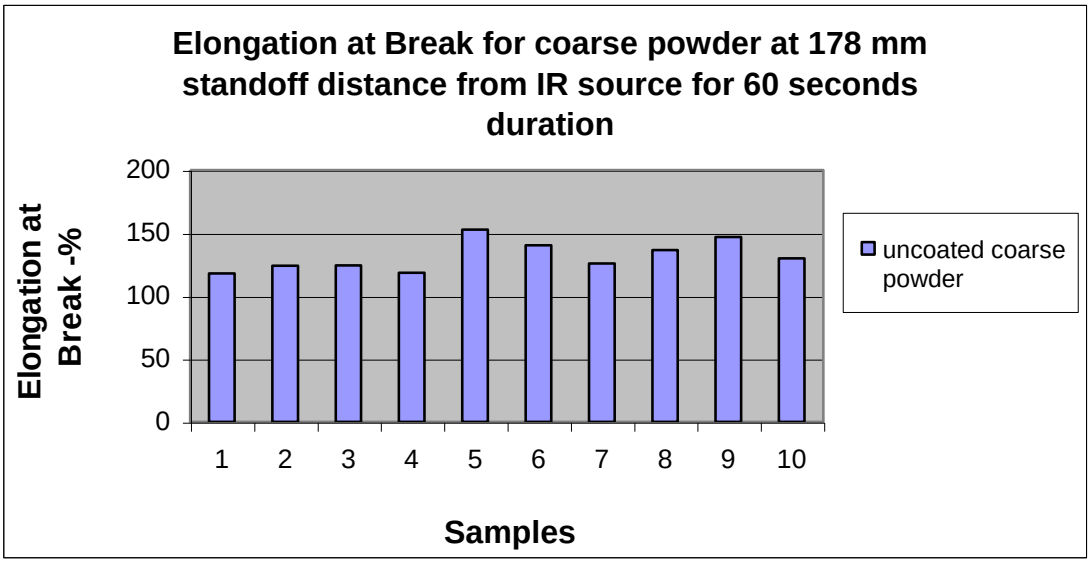
Elongation at Break for coarse powder at 178 mm standoff distance from IR source for 60 seconds duration
Elongation at Break -%
200
150
100
50
0
1 2 3 4 5 6 7 8 9 10
Samples
uncoated coarse powder

Figure A3: Mechanical properties of Uncoated Somos 201 powder at 228 mm standoff distance:

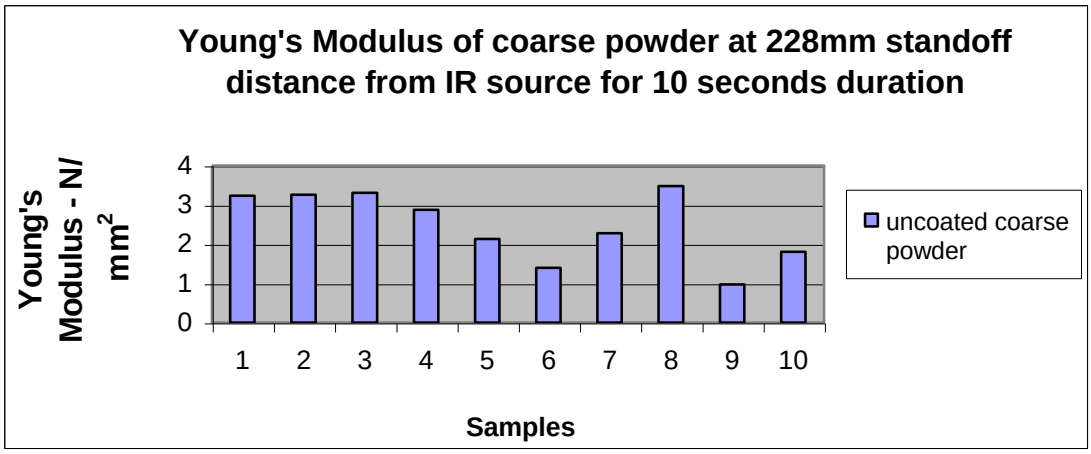

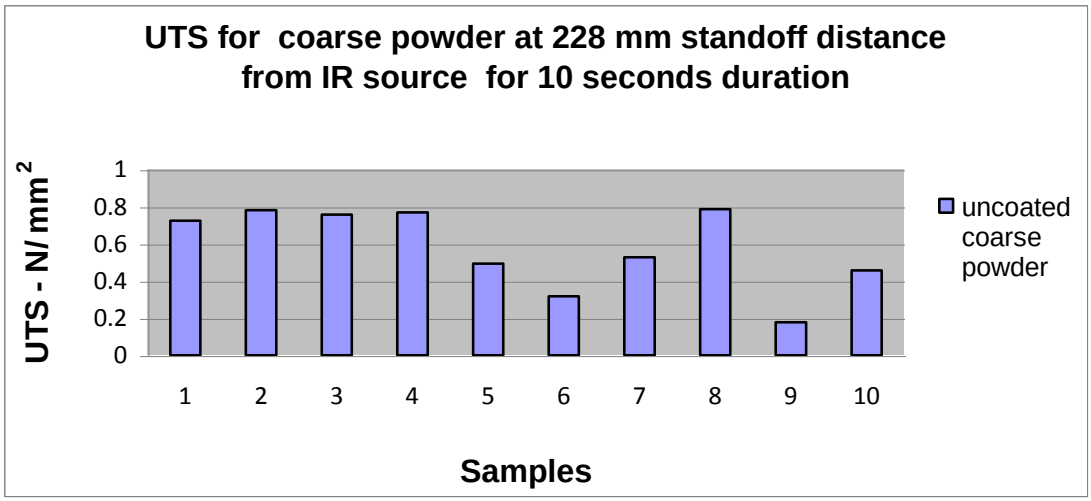

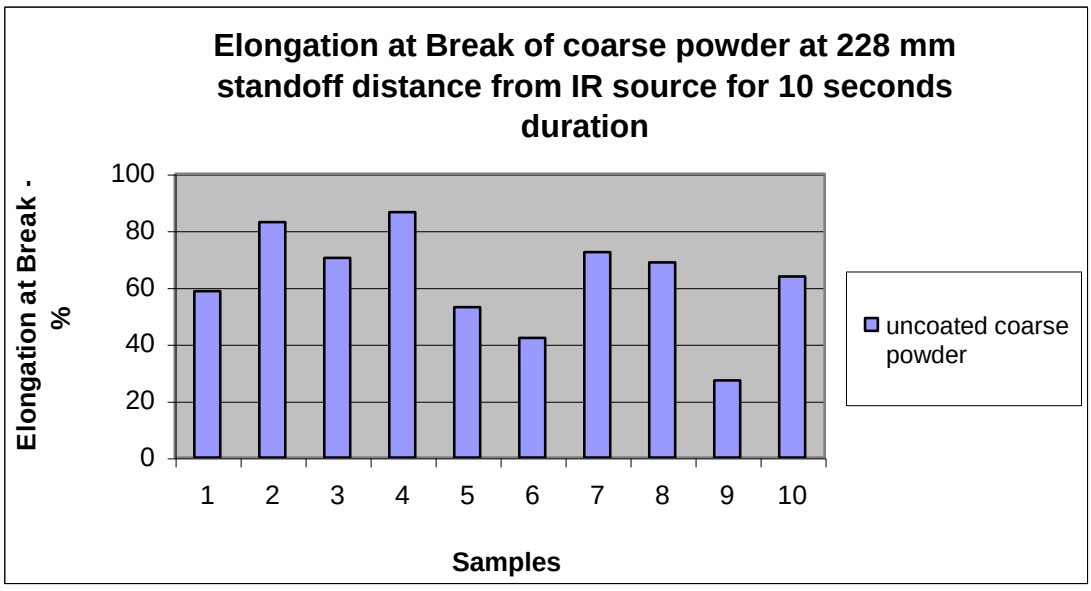

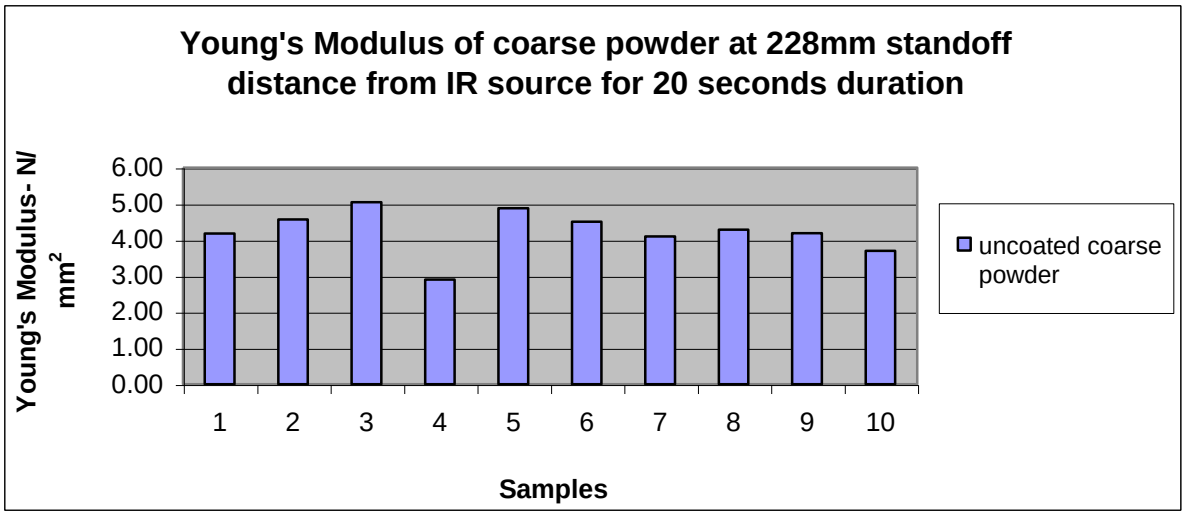
Young's Modulus of coarse powder at 228mm standoff distance from IR source for 20 seconds duration
Young's Modulus- N/ mm2
6.00
5.00
4.00
3.00
2.00
1.00
0.00
1
2
3
4
5
6
7
8
9
10
Samples
uncoated coarse powder

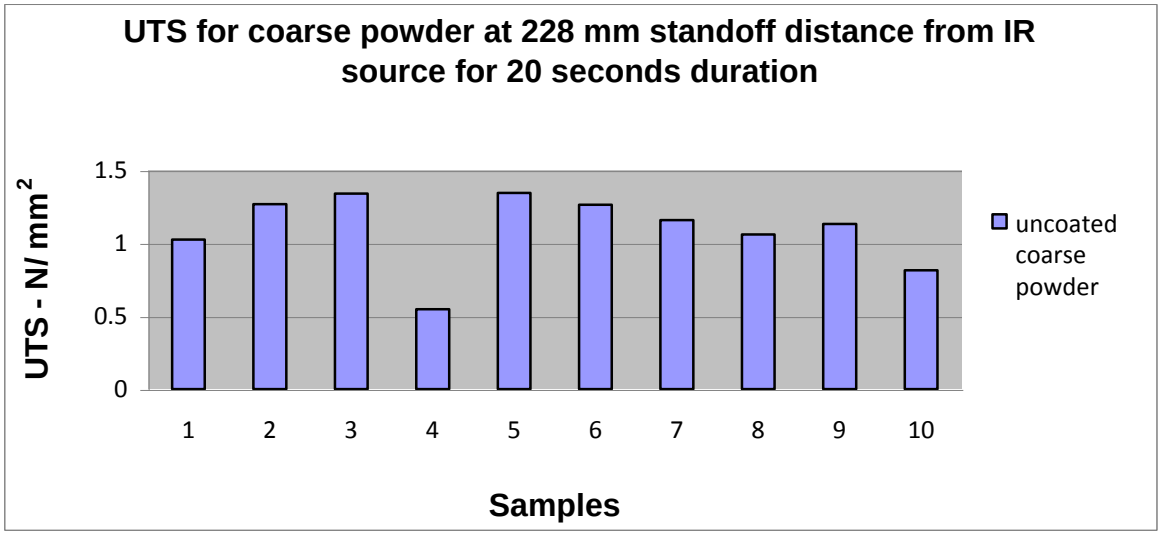
UTS for coarse powder at 228 mm standoff distance from IR source for 20 seconds duration
UTS - N/ mm2
1.5
1
0.5
0
1
2
3
4
5
6
7
8
9
10
Samples
uncoated coarse powder

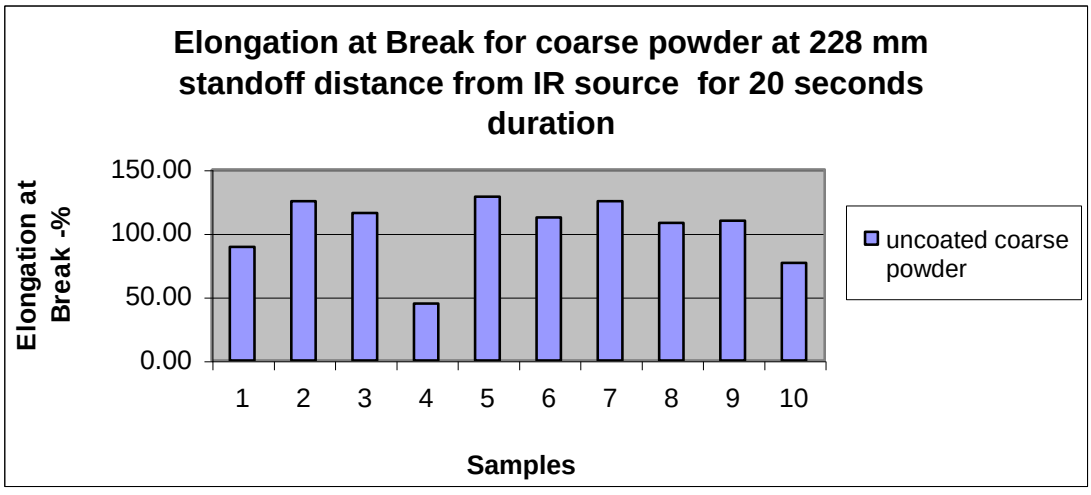
Elongation at Break for coarse powder at 228 mm standoff distance from IR source for 20 seconds duration
Elongation at Break -%
150.00
100.00
50.00
0.00
1
2
3
4
5
6
7
8
9
10
Samples
uncoated coarse powder

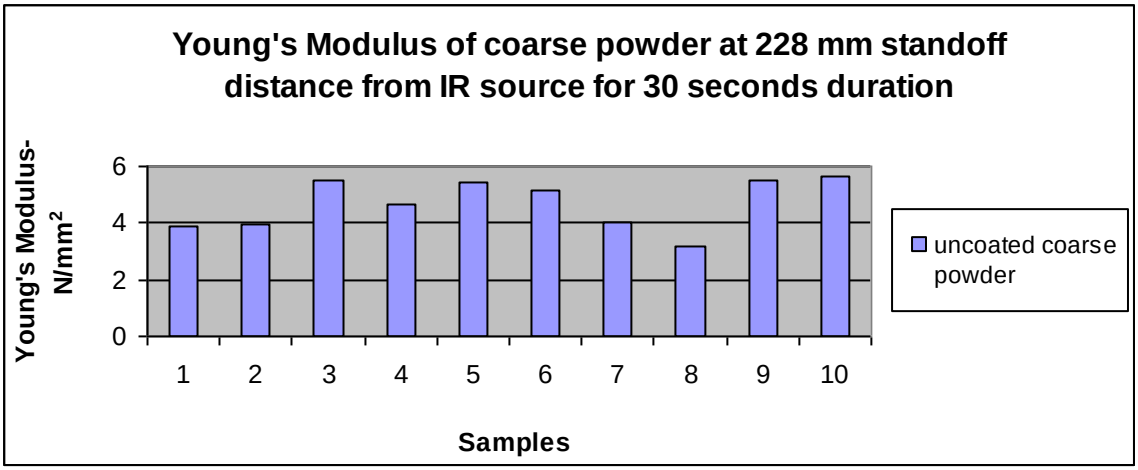
Young's Modulus of coarse powder at 228 mm standoff distance from IR source for 30 seconds duration
Young's Modulus- N/mm²
0
2
4
6
1
2
3
4
5
6
7
8
9
10
Samples
uncoated coarse powder

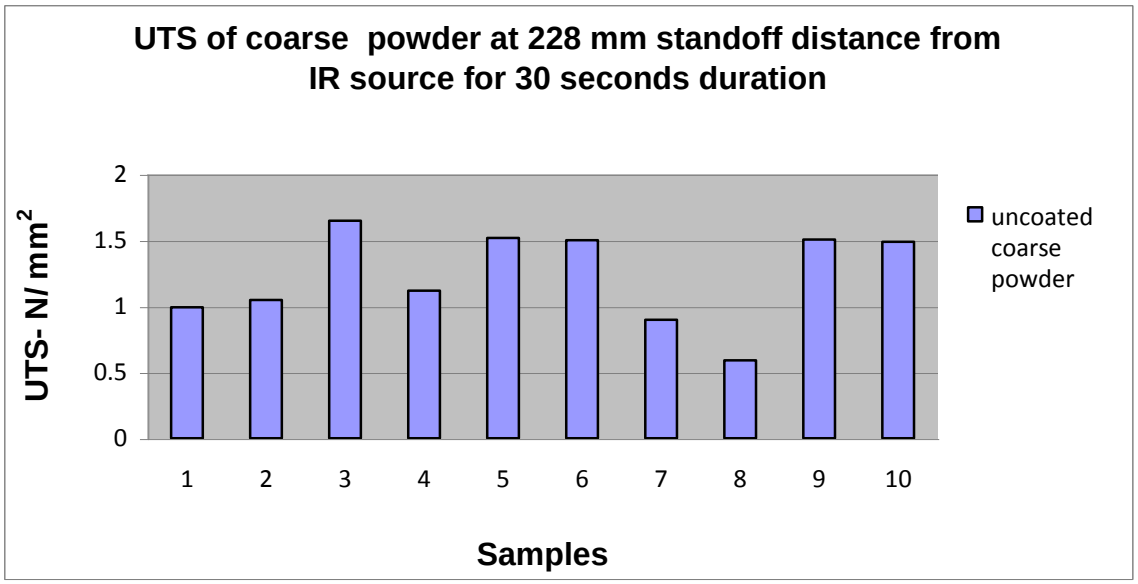
UTS of coarse powder at 228 mm standoff distance from IR source for 30 seconds duration
UTS- N/ mm²
0
0.5
1
1.5
2
1
2
3
4
5
6
7
8
9
10
Samples
uncoated coarse powder

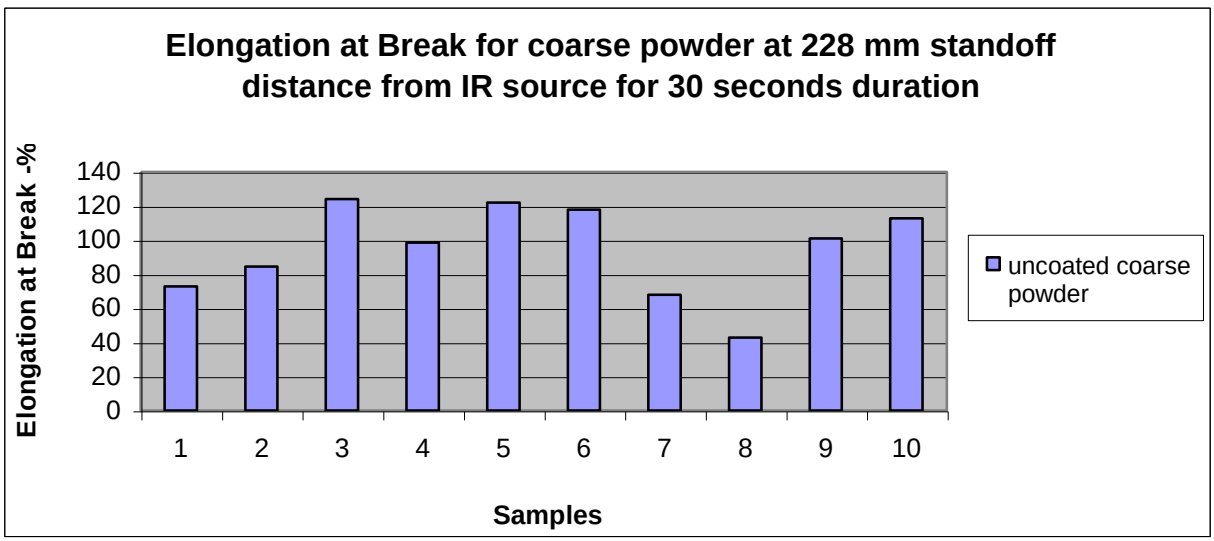
Elongation at Break for coarse powder at 228 mm standoff distance from IR source for 30 seconds duration
Elongation at Break -%
0
20
40
60
80
100
120
140
1
2
3
4
5
6
7
8
9
10
Samples
uncoated coarse powder

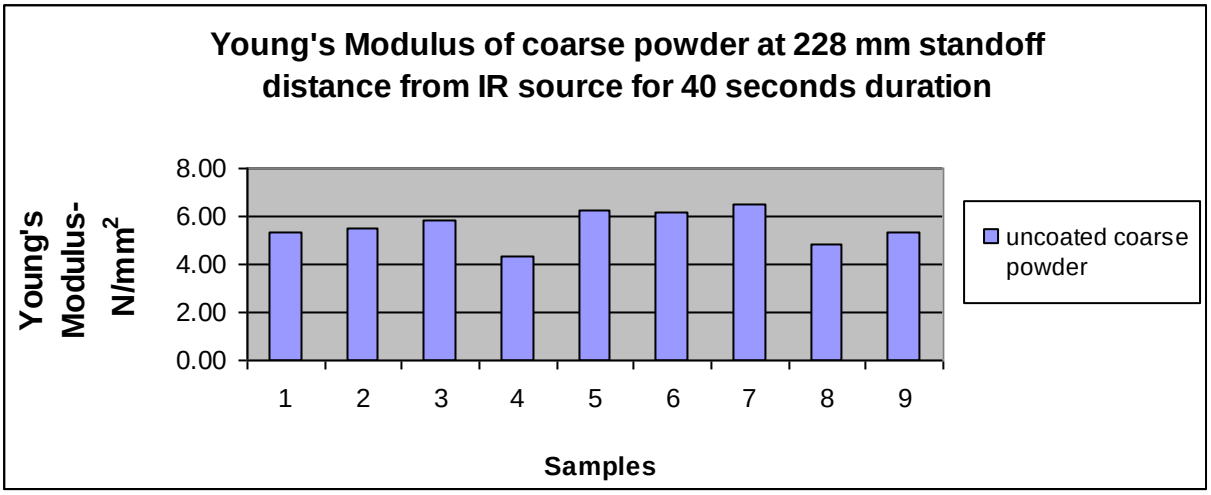
Young's Modulus of coarse powder at 228 mm standoff distance from IR source for 40 seconds duration
Young's Modulus- N/mm2
8.00
6.00
4.00
2.00
0.00
1 2 3 4 5 6 7 8 9
Samples
uncoated coarse powder

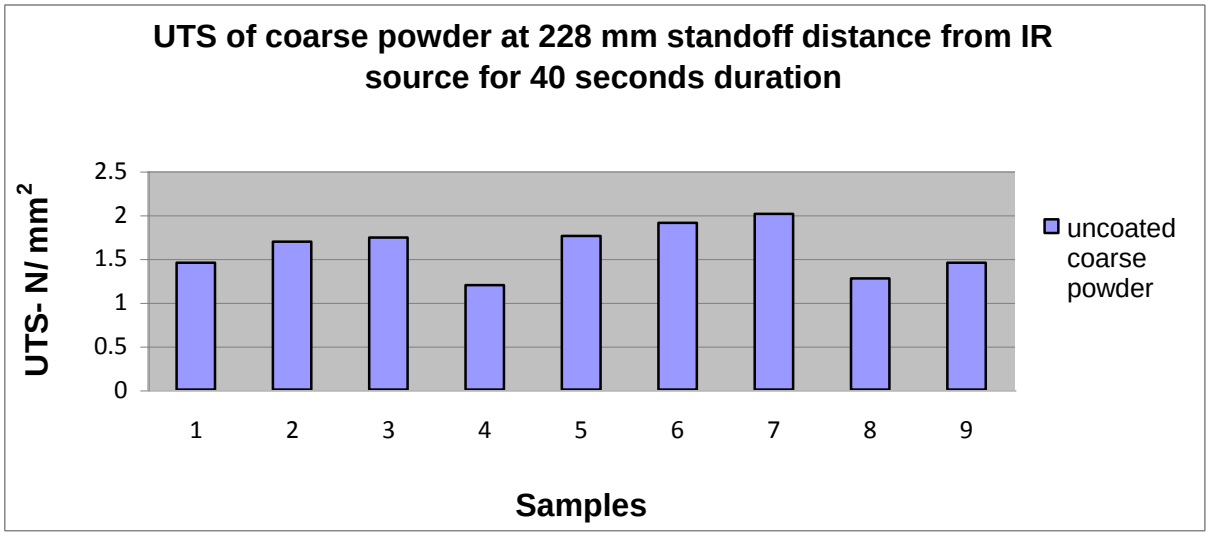
UTS of coarse powder at 228 mm standoff distance from IR source for 40 seconds duration
UTS- N/ mm2
2.5
2
1.5
1
0.5
0
1 2 3 4 5 6 7 8 9
Samples
uncoated coarse powder

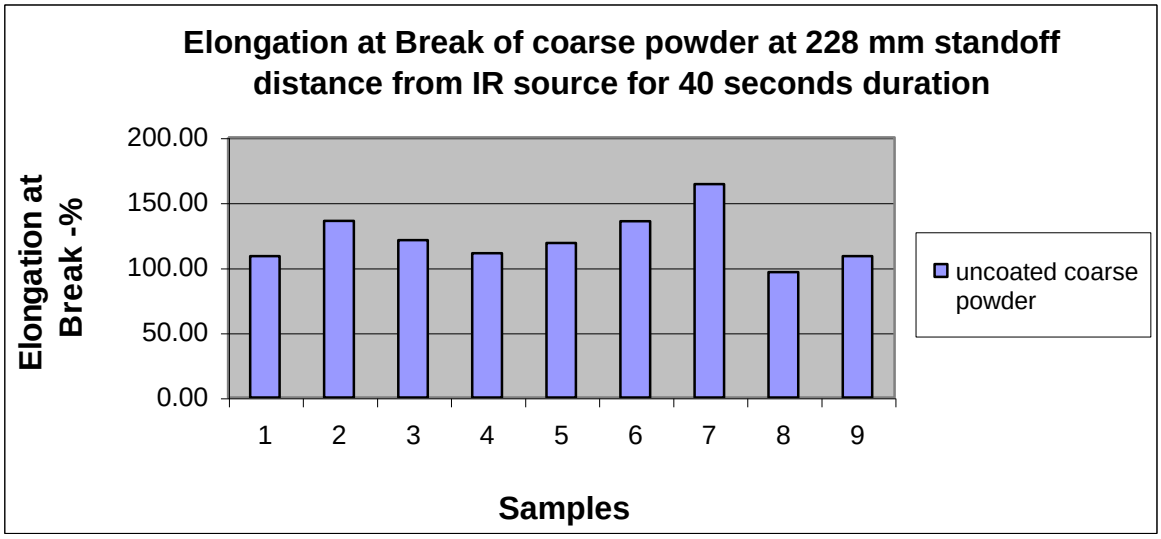
Elongation at Break of coarse powder at 228 mm standoff distance from IR source for 40 seconds duration
Elongation at Break -%
200.00
150.00
100.00
50.00
0.00
1 2 3 4 5 6 7 8 9
Samples
uncoated coarse powder

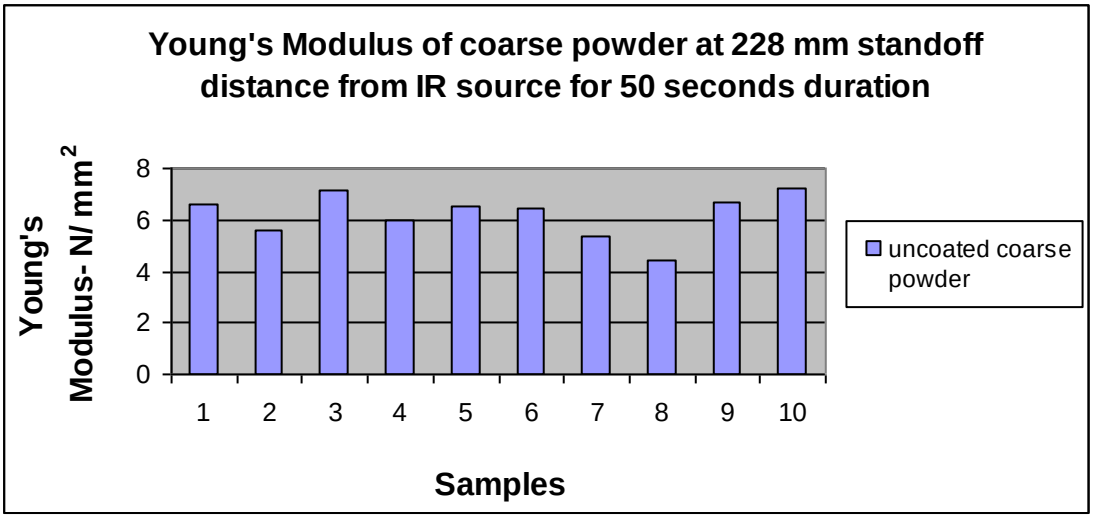
Young's Modulus of coarse powder at 228 mm standoff distance from IR source for 50 seconds duration
Young's Modulus- N/ mm2
8
6
4
2
0
1
2
3
4
5
6
7
8
9
10
Samples
uncoated coarse powder

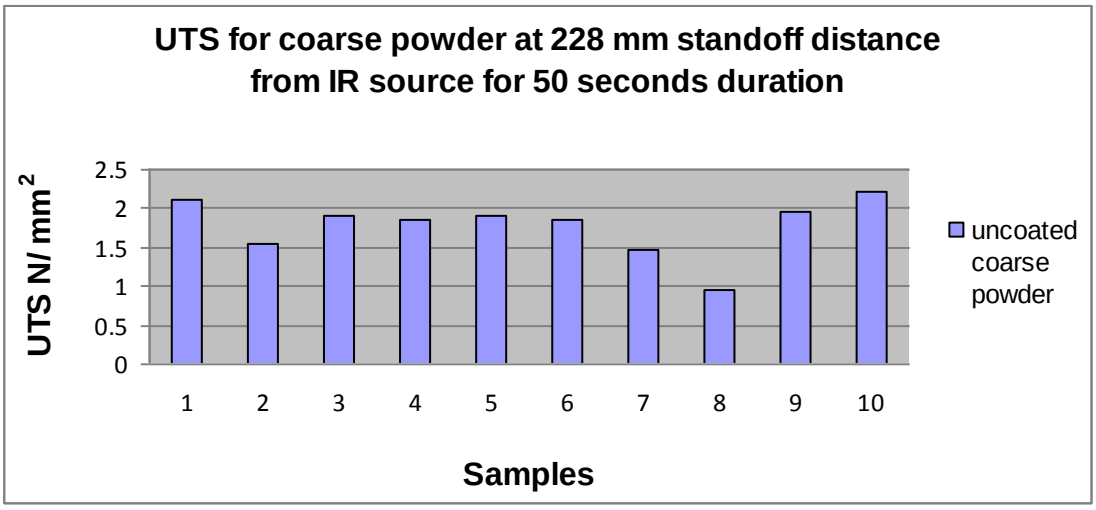
UTS for coarse powder at 228 mm standoff distance from IR source for 50 seconds duration
UTS N/ mm2
2.5
2
1.5
1
0.5
0
1
2
3
4
5
6
7
8
9
10
Samples
uncoated coarse powder

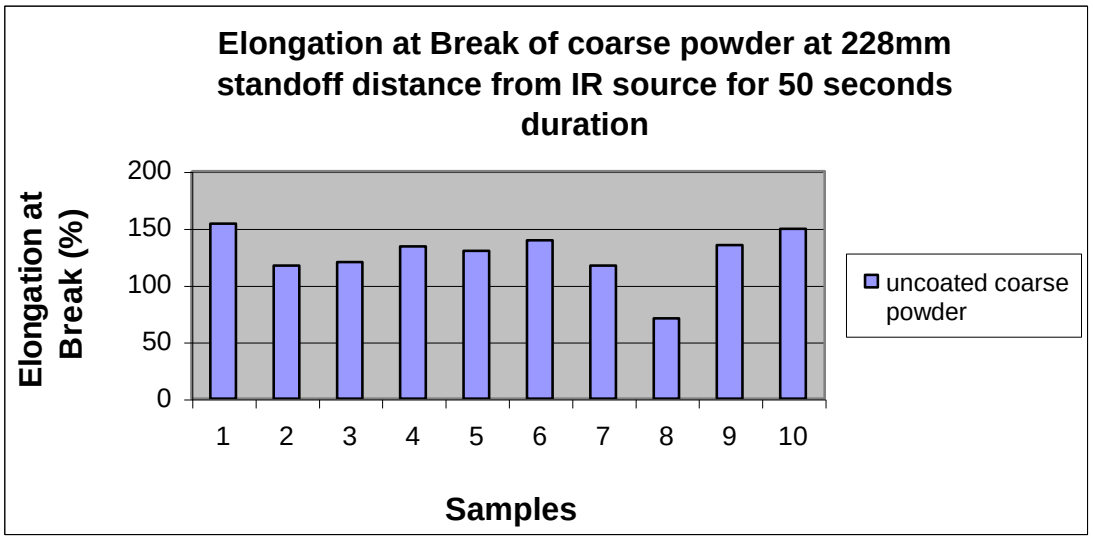
Elongation at Break of coarse powder at 228mm standoff distance from IR source for 50 seconds duration
Elongation at Break (%)
200
150
100
50
0
1
2
3
4
5
6
7
8
9
10
Samples
uncoated coarse powder

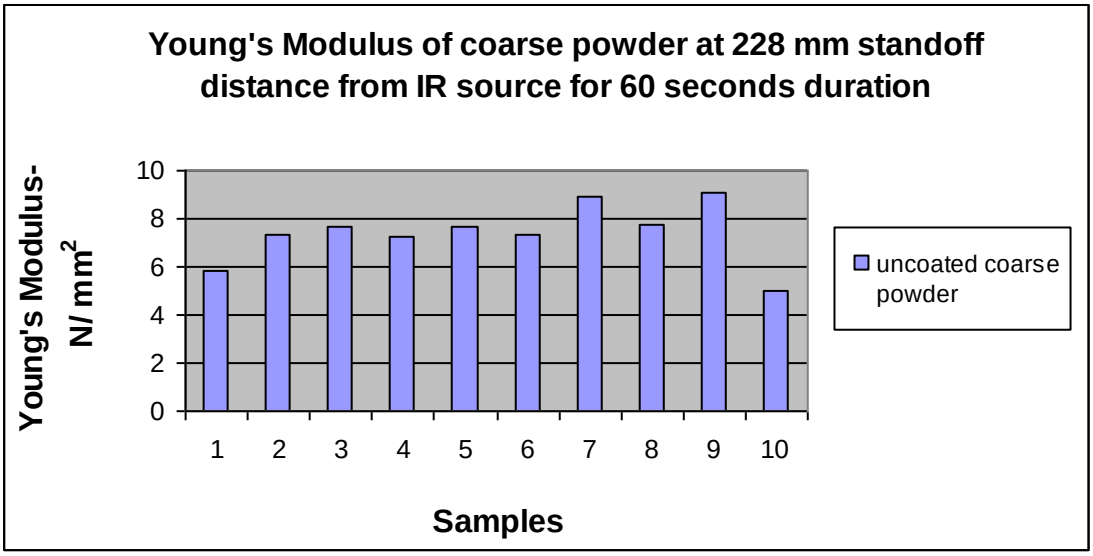
Young's Modulus of coarse powder at 228 mm standoff distance from IR source for 60 seconds duration
Young's Modulus- N/ mm2
10
8
6
4
2
0
1 2 3 4 5 6 7 8 9 10
Samples
uncoated coarse powder

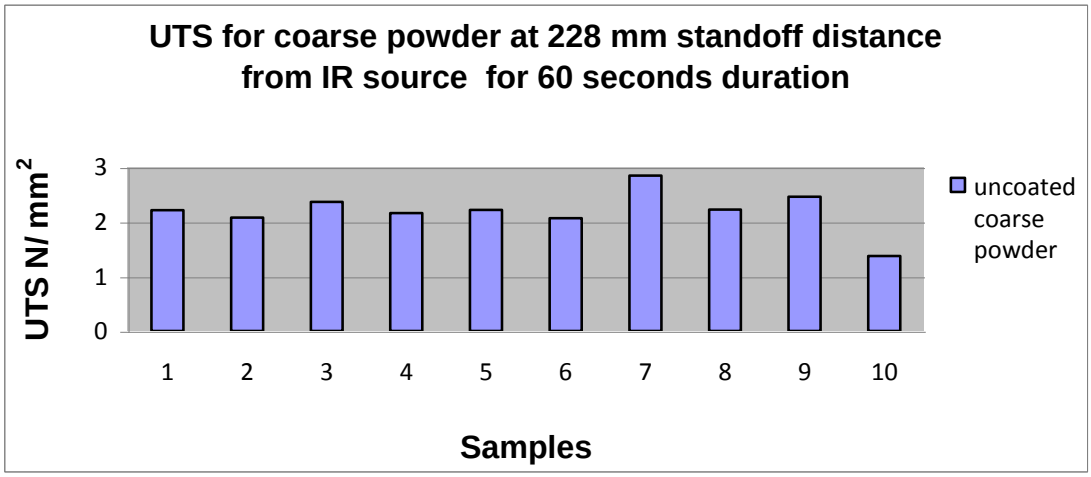
UTS for coarse powder at 228 mm standoff distance from IR source for 60 seconds duration
UTS N/ mm2
3
2
1
0
1 2 3 4 5 6 7 8 9 10
Samples
uncoated coarse powder

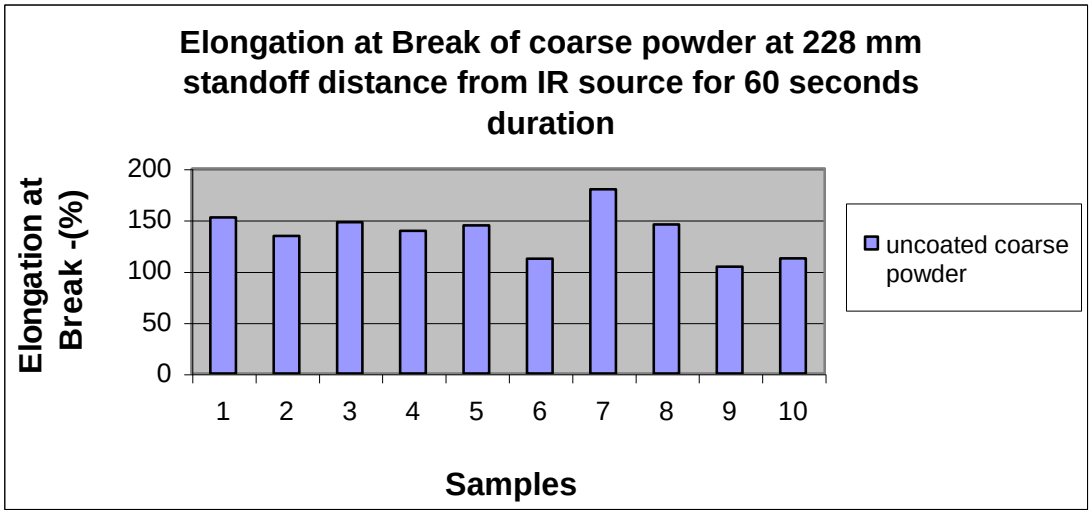
Elongation at Break of coarse powder at 228 mm standoff distance from IR source for 60 seconds duration
Elongation at Break -(%)
200
150
100
50
0
1 2 3 4 5 6 7 8 9 10
Samples
uncoated coarse powder

Figure A4: Mechanical properties of uncoated 30 μm Somos 201 powder at 178 mm stand off distance:

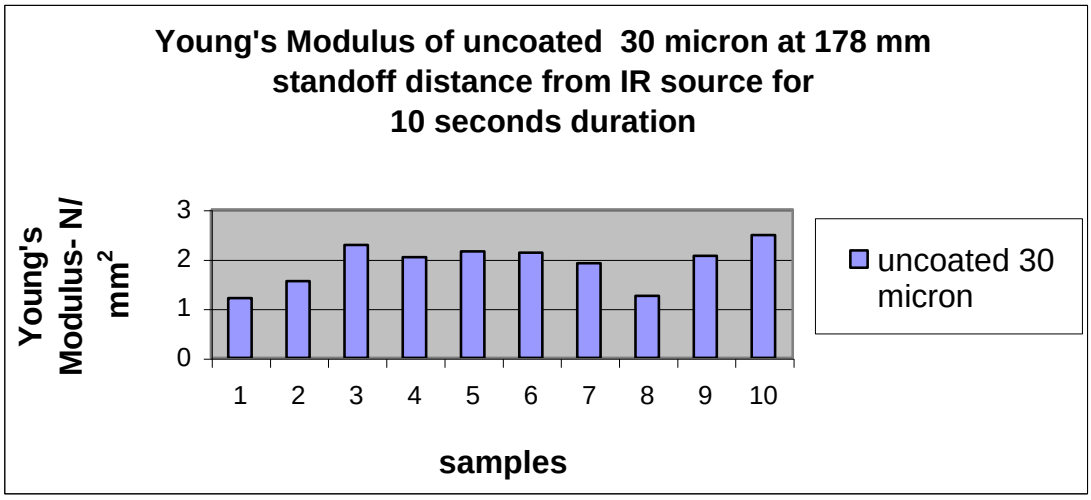

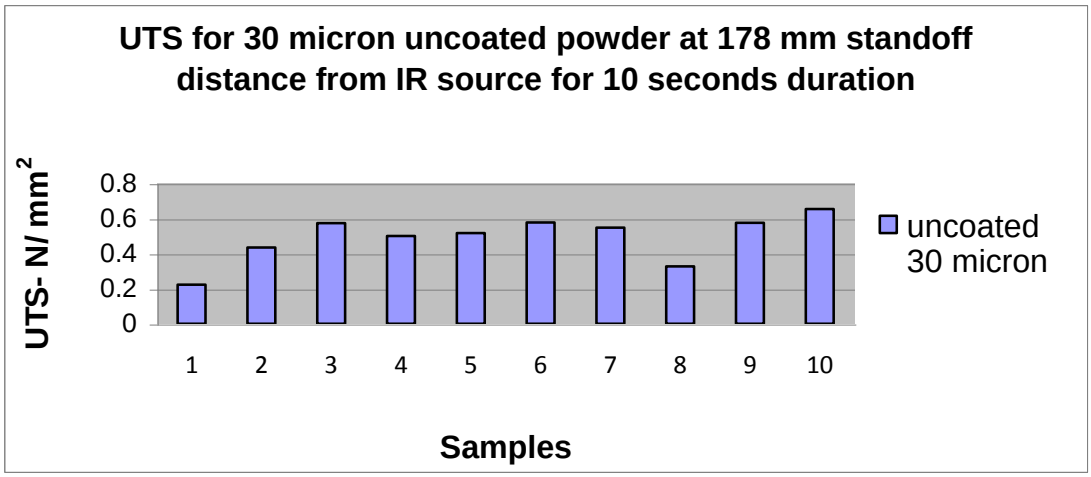

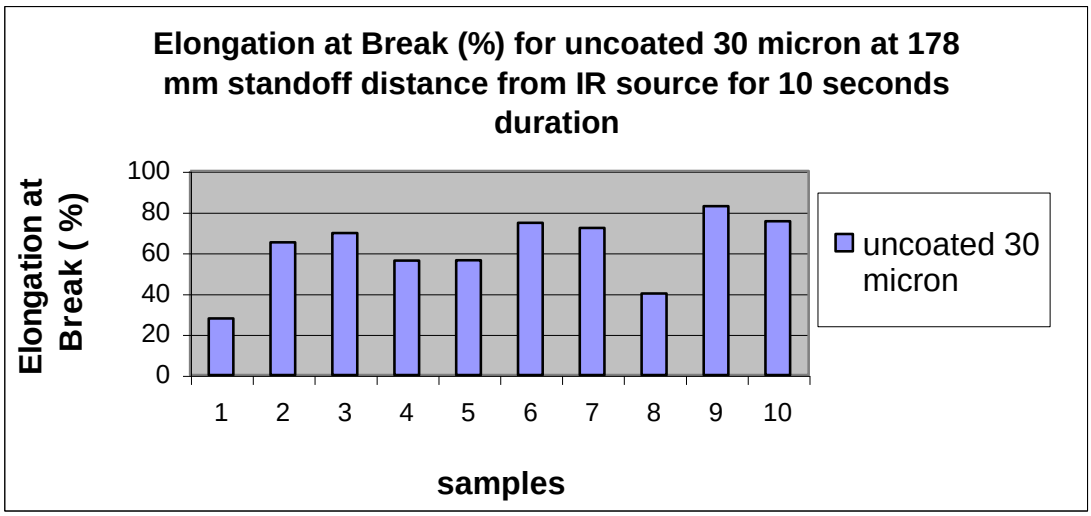

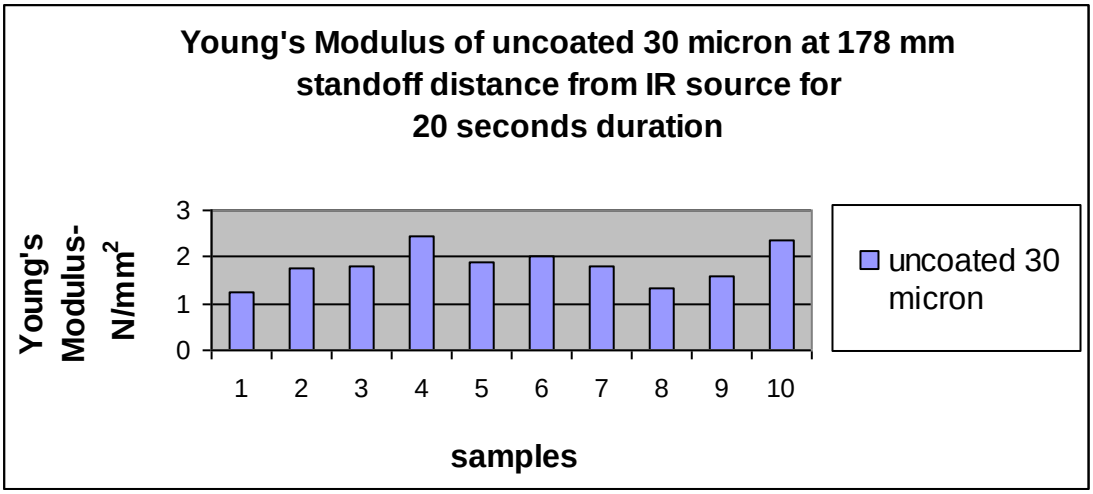
Young's Modulus of uncoated 30 micron at 178 mm standoff distance from IR source for 20 seconds duration
Young's Modulus- N/mm2
3
2
1
0
1 2 3 4 5 6 7 8 9 10
samples
uncoated 30 micron

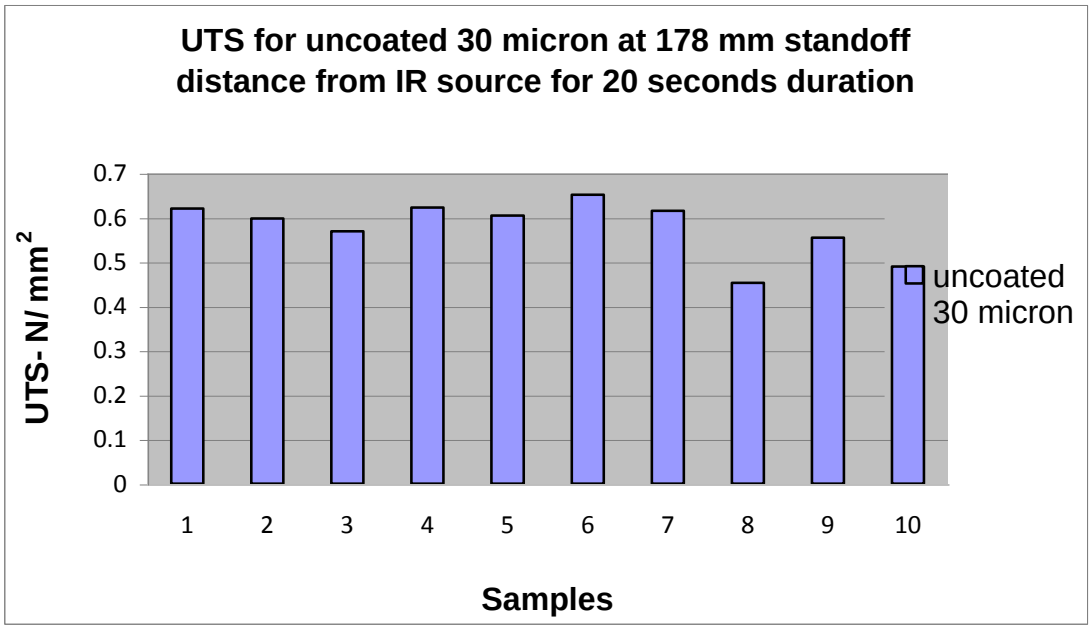
UTS for uncoated 30 micron at 178 mm standoff distance from IR source for 20 seconds duration
UTS- N/ mm2
0.7
0.6
0.5
0.4
0.3
0.2
0.1
0
1 2 3 4 5 6 7 8 9 10
Samples
uncoated 30 micron

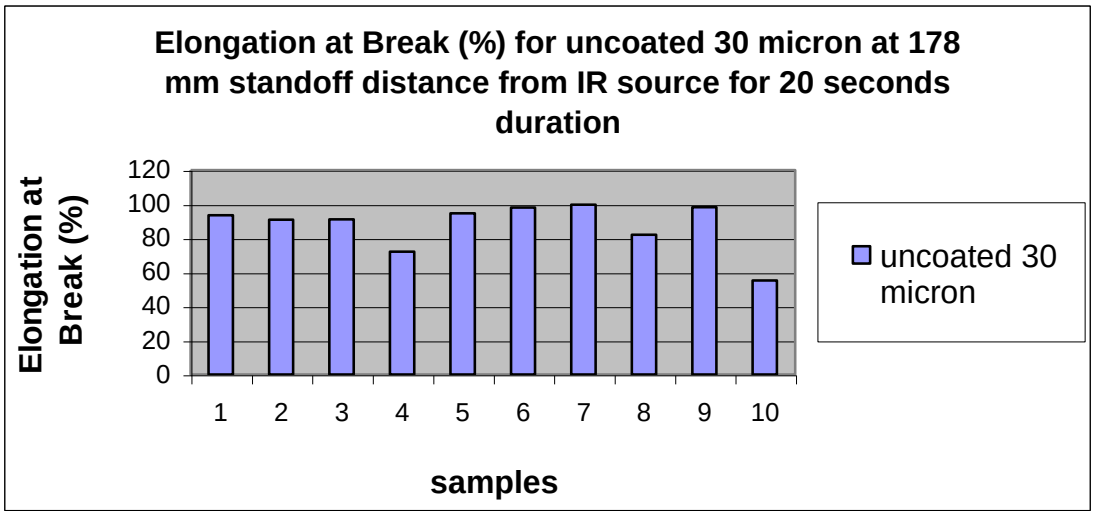
Elongation at Break (%) for uncoated 30 micron at 178 mm standoff distance from IR source for 20 seconds duration
Elongation at Break (%)
120
100
80
60
40
20
0
1 2 3 4 5 6 7 8 9 10
samples
uncoated 30 micron

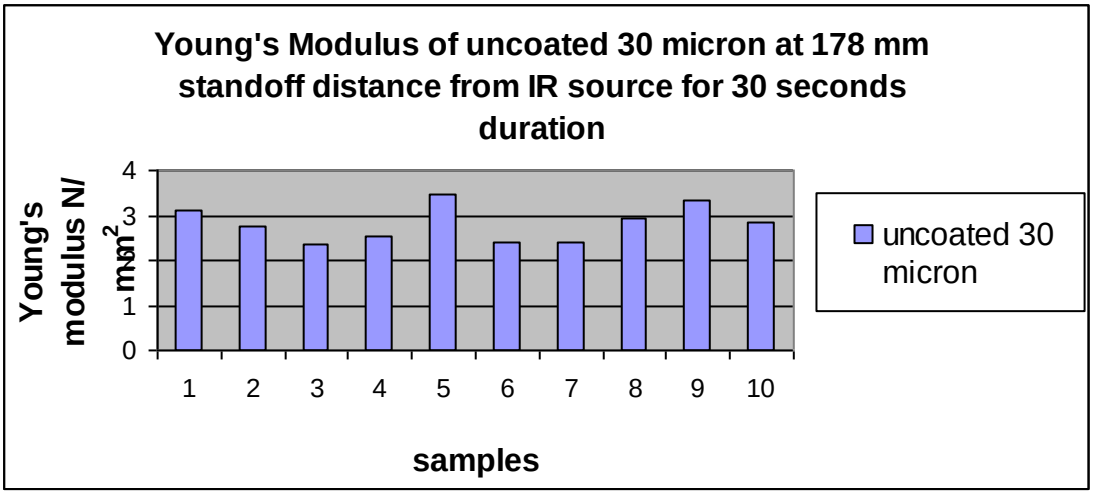
Young's Modulus of uncoated 30 micron at 178 mm standoff distance from IR source for 30 seconds duration
Young's modulus N/ mm2
0
1
2
3
4
1 2 3 4 5 6 7 8 9 10
samples
uncoated 30 micron

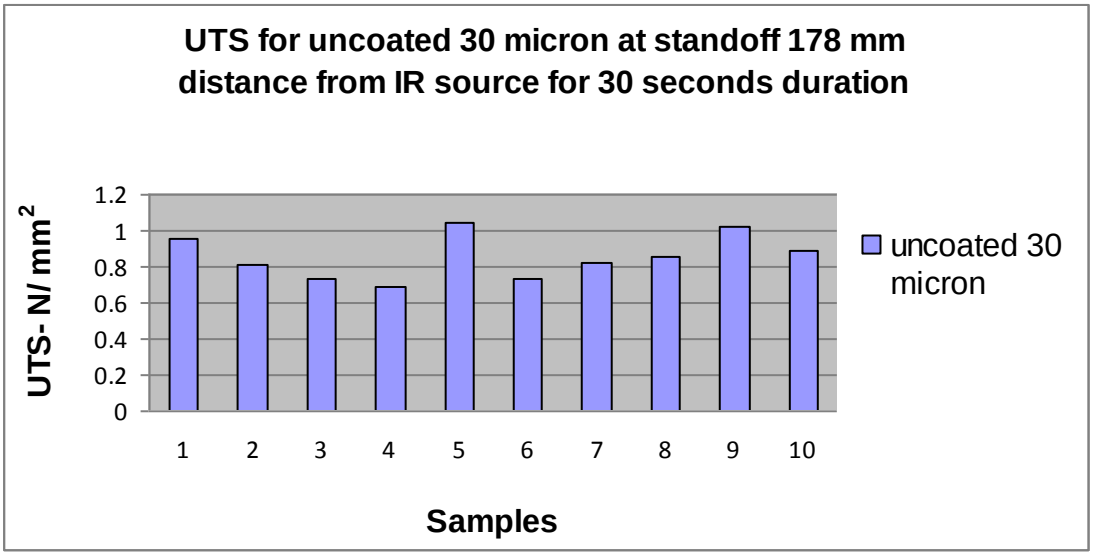
UTS for uncoated 30 micron at standoff 178 mm distance from IR source for 30 seconds duration
UTS- N/ mm2
0
0.2
0.4
0.6
0.8
1
1.2
1 2 3 4 5 6 7 8 9 10
Samples
uncoated 30 micron

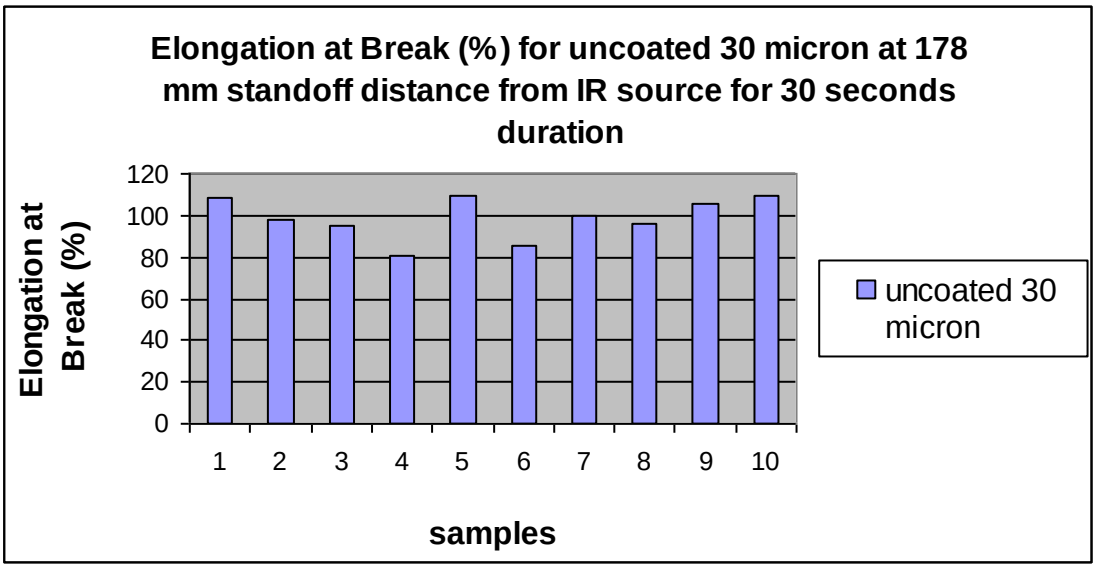
Elongation at Break (%) for uncoated 30 micron at 178 mm standoff distance from IR source for 30 seconds duration
Elongation at Break (%)
0
20
40
60
80
100
120
1 2 3 4 5 6 7 8 9 10
samples
uncoated 30 micron

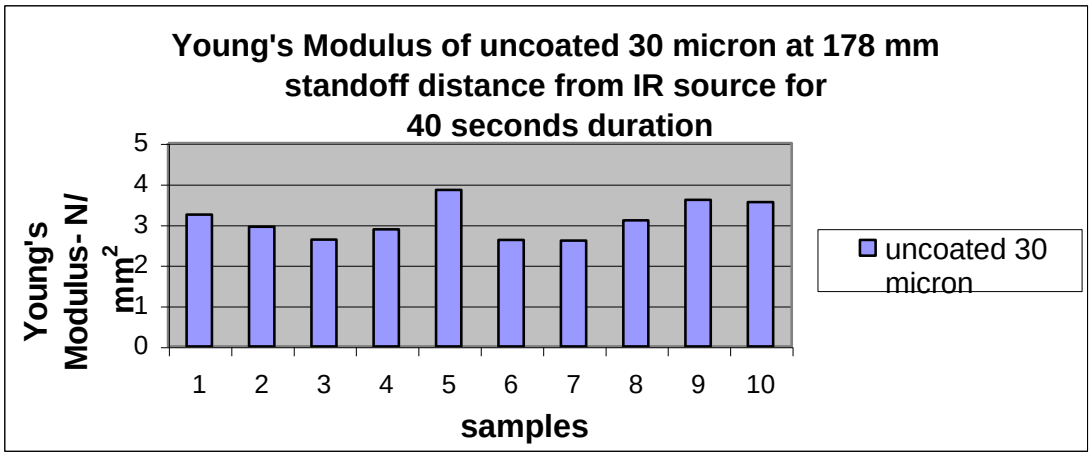
Young's Modulus of uncoated 30 micron at 178 mm standoff distance from IR source for 40 seconds duration
Young's Modulus- N/ mm2
0
1
2
3
4
5
1 2 3 4 5 6 7 8 9 10
samples
uncoated 30 micron

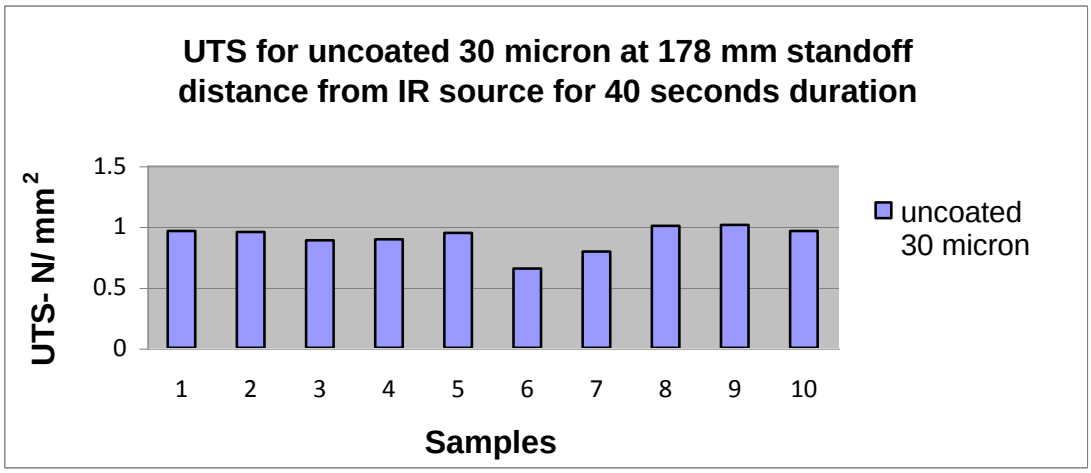
UTS for uncoated 30 micron at 178 mm standoff distance from IR source for 40 seconds duration
UTS- N/ mm2
0
0.5
1
1.5
1 2 3 4 5 6 7 8 9 10
Samples
uncoated 30 micron

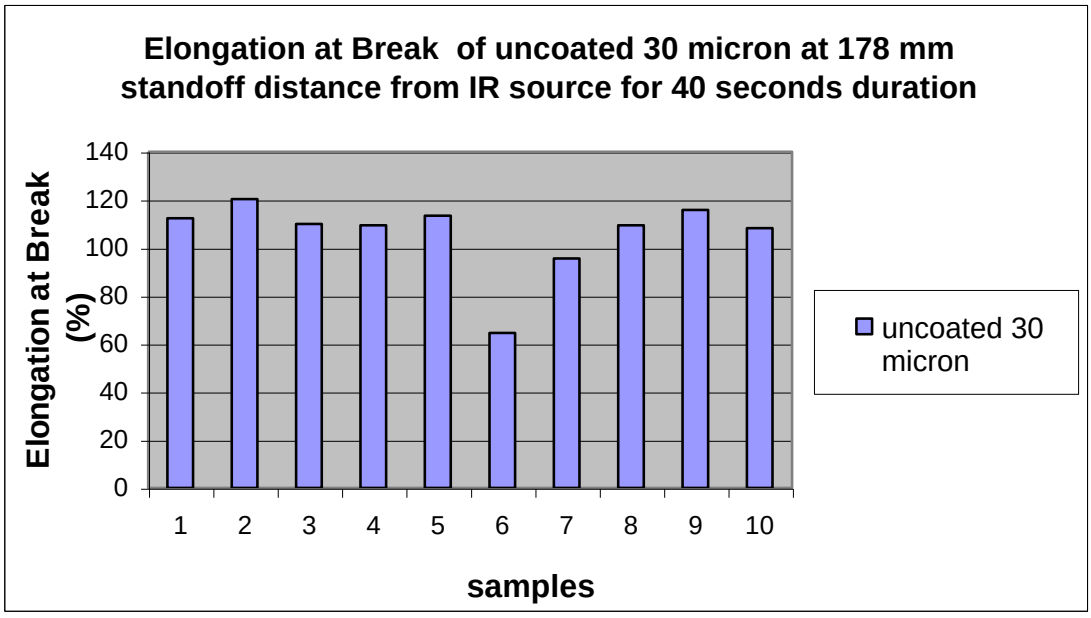
Elongation at Break of uncoated 30 micron at 178 mm standoff distance from IR source for 40 seconds duration
Elongation at Break (%)
0
20
40
60
80
100
120
140
1 2 3 4 5 6 7 8 9 10
samples
uncoated 30 micron

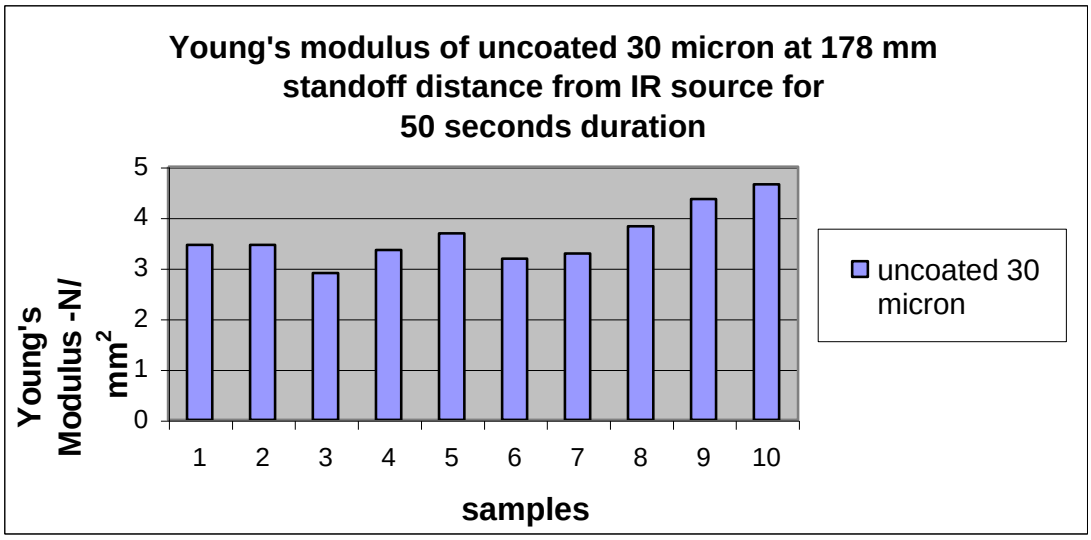
Young's modulus of uncoated 30 micron at 178 mm standoff distance from IR source for 50 seconds duration
Young's Modulus -N/ mm2
0
1
2
3
4
5
1 2 3 4 5 6 7 8 9 10
samples
uncoated 30 micron

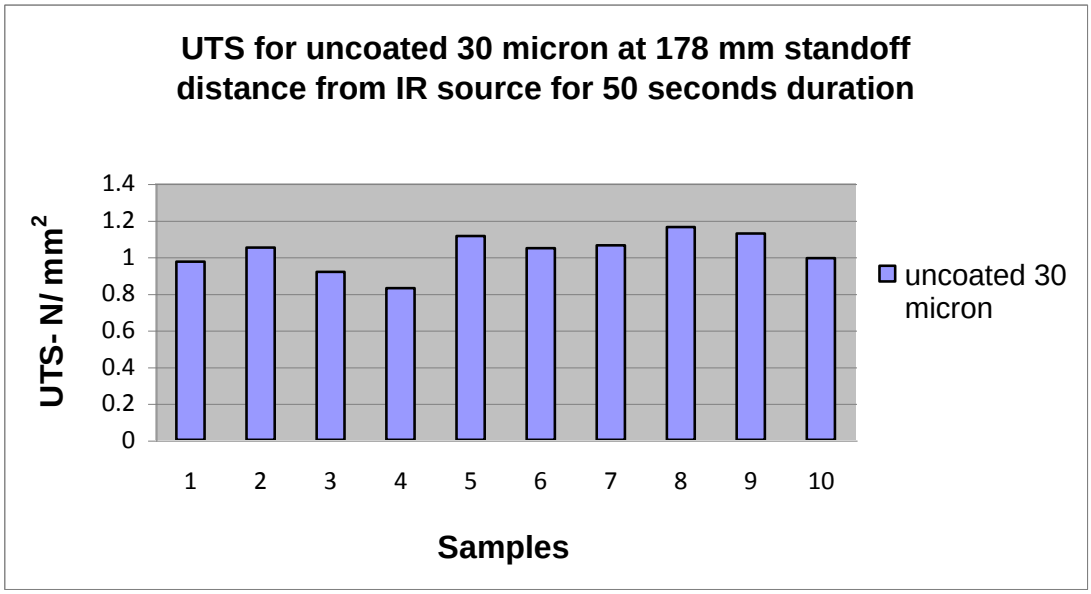
UTS for uncoated 30 micron at 178 mm standoff distance from IR source for 50 seconds duration
UTS- N/ mm2
0
0.2
0.4
0.6
0.8
1
1.2
1.4
1 2 3 4 5 6 7 8 9 10
Samples
uncoated 30 micron

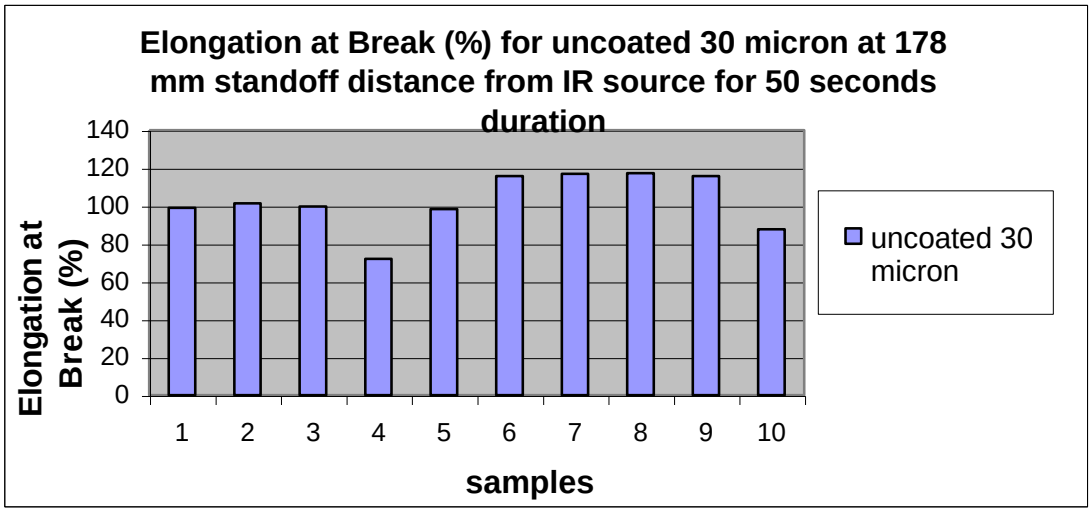
Elongation at Break (%) for uncoated 30 micron at 178 mm standoff distance from IR source for 50 seconds duration
Elongation at Break (%)
0
20
40
60
80
100
120
140
1 2 3 4 5 6 7 8 9 10
samples
uncoated 30 micron

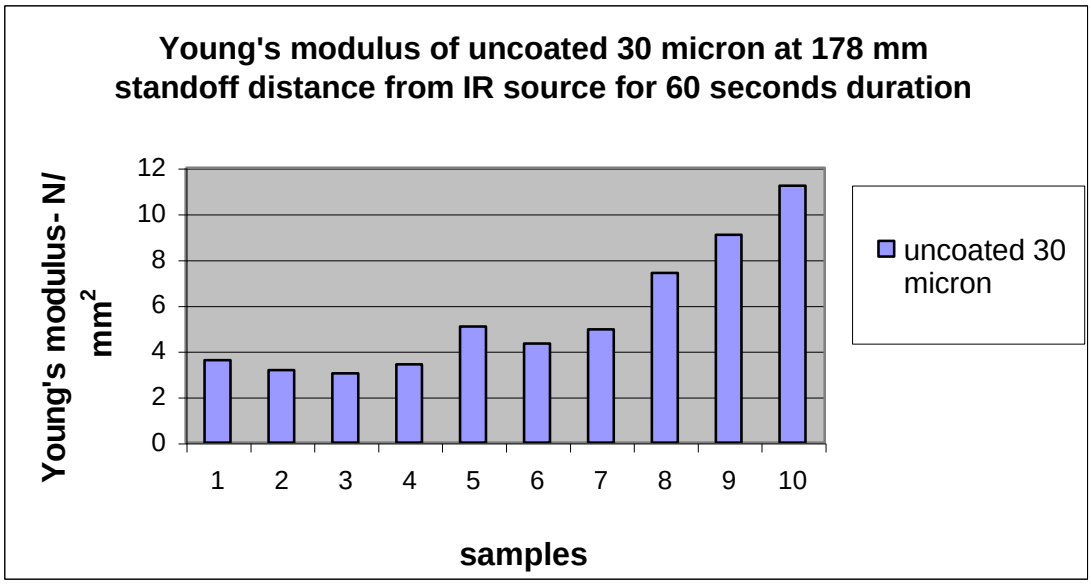
Young's modulus of uncoated 30 micron at 178 mm standoff distance from IR source for 60 seconds duration
Young's modulus- N/ mm2
12
10
8
6
4
2
0
1 2 3 4 5 6 7 8 9 10
samples
uncoated 30 micron

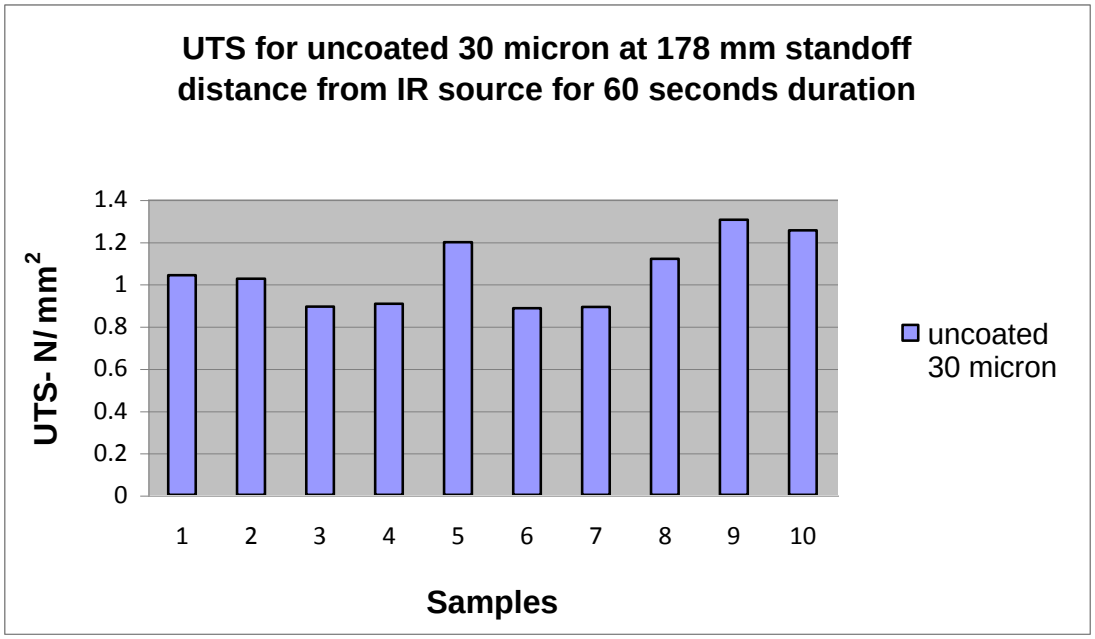
UTS for uncoated 30 micron at 178 mm standoff distance from IR source for 60 seconds duration
UTS- N/ mm2
1.4
1.2
1
0.8
0.6
0.4
0.2
0
1 2 3 4 5 6 7 8 9 10
Samples
uncoated 30 micron

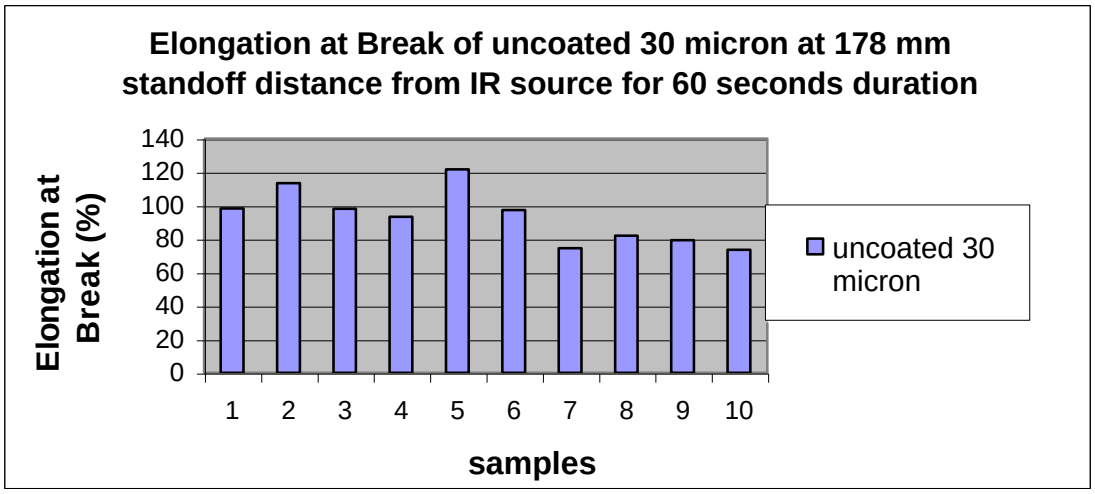
Elongation at Break of uncoated 30 micron at 178 mm standoff distance from IR source for 60 seconds duration
Elongation at Break (%)
140
120
100
80
60
40
20
0
1 2 3 4 5 6 7 8 9 10
samples
uncoated 30 micron

Figure A5: Mechanical properties of 0.3% silica coated 30 μm Somos 201 powder at 178 mm stand off distance:

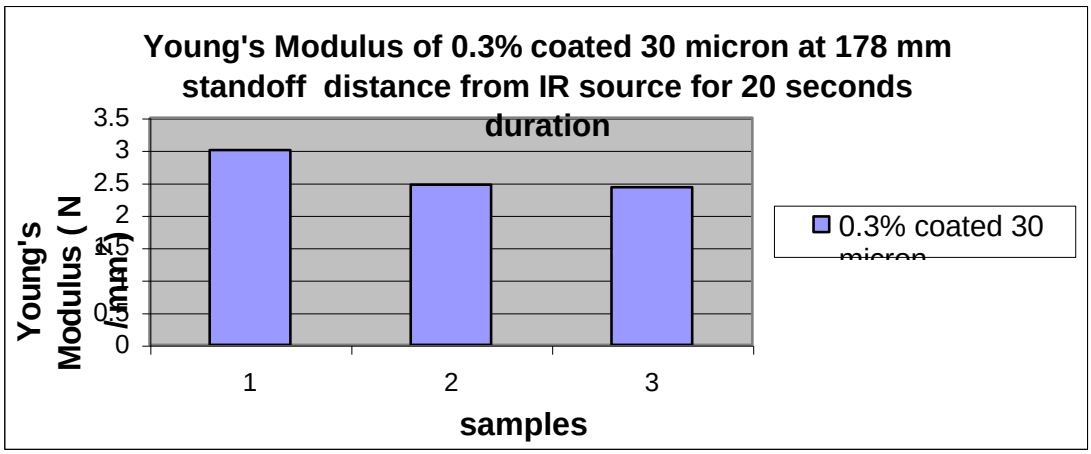

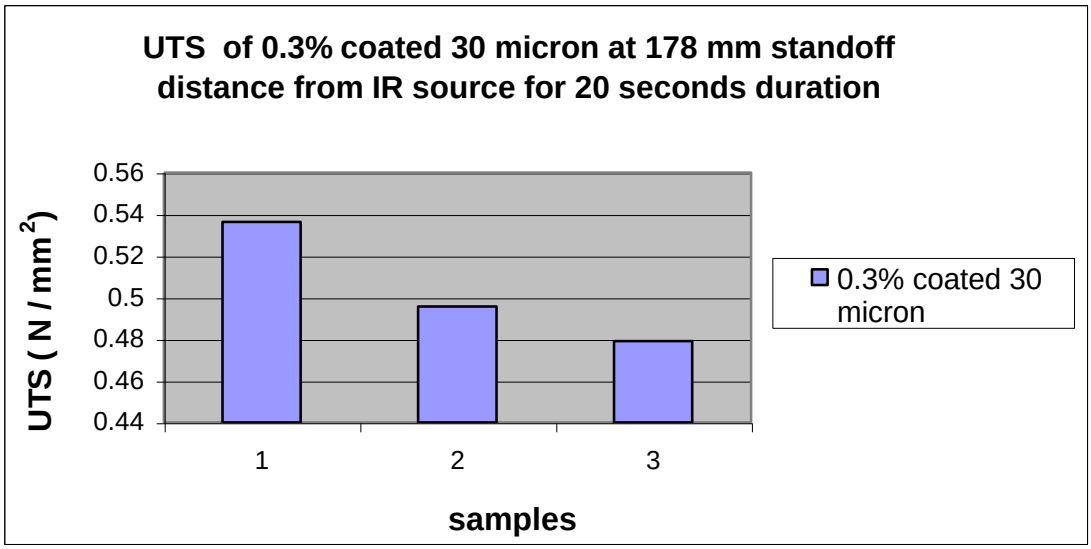

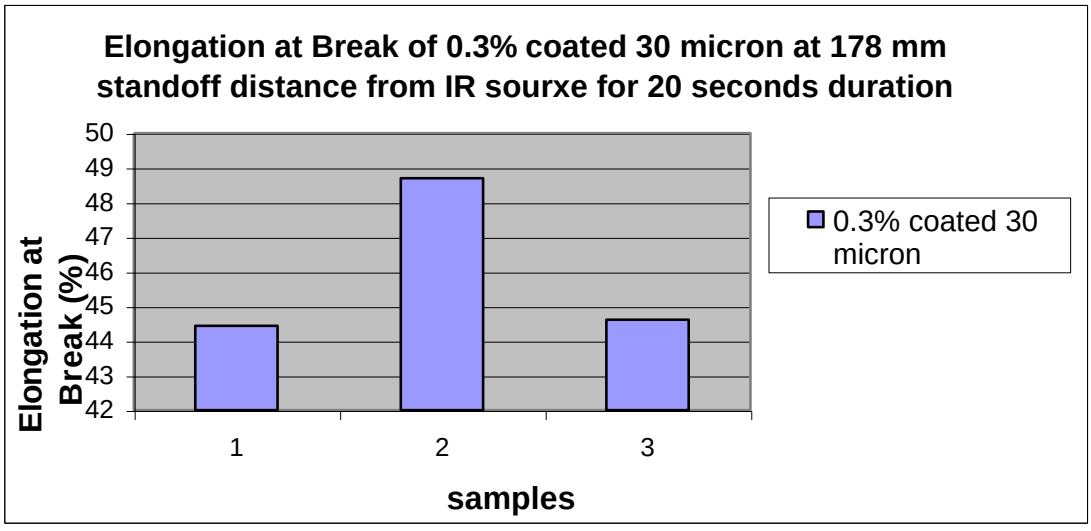

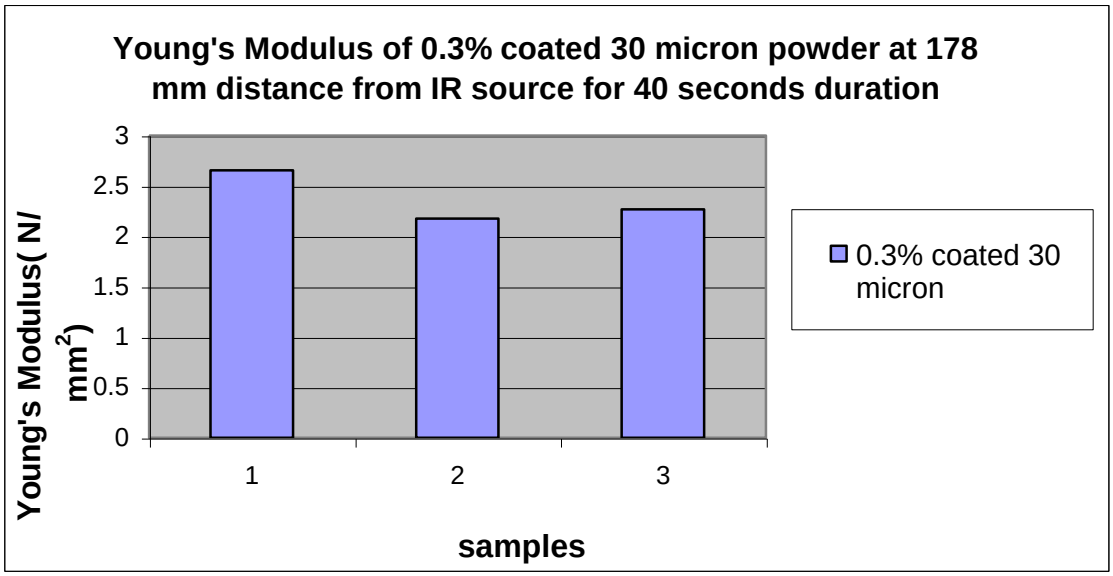
Young's Modulus of 0.3% coated 30 micron powder at 178 mm distance from IR source for 40 seconds duration
Young's Modulus(N/ mm2)
3
2.5
2
1.5
1
0.5
0
1
2
3
samples
0.3% coated 30 micron

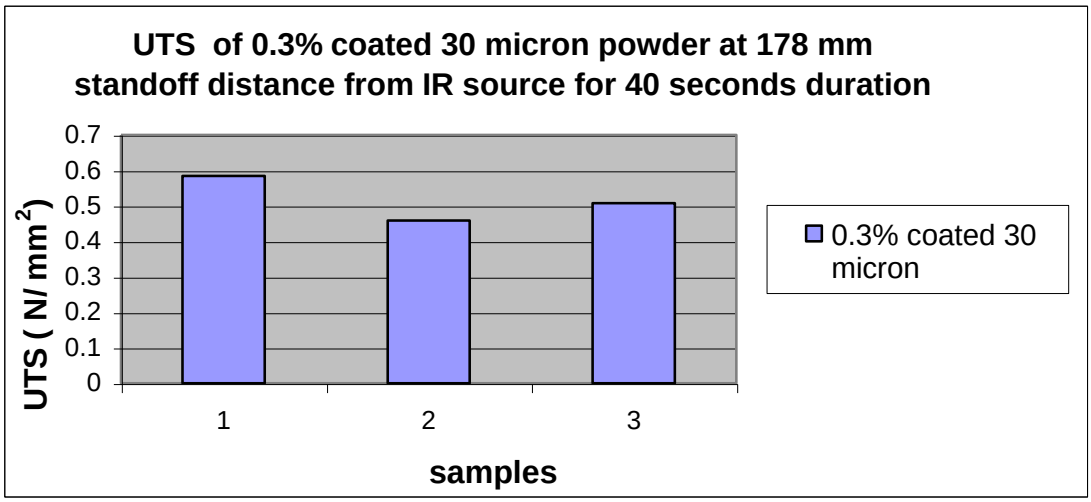
UTS of 0.3% coated 30 micron powder at 178 mm standoff distance from IR source for 40 seconds duration
UTS (N/ mm2)
0.7
0.6
0.5
0.4
0.3
0.2
0.1
0
1
2
3
samples
0.3% coated 30 micron

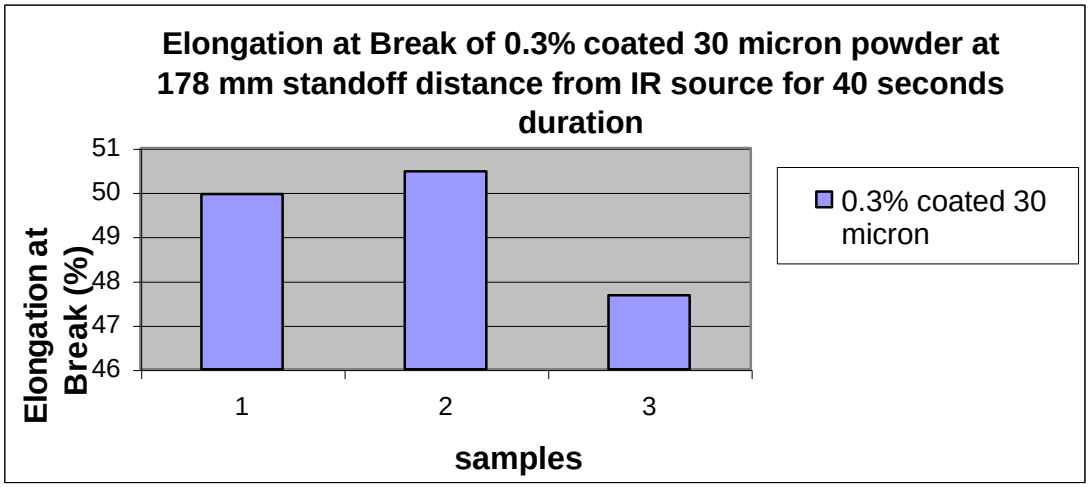
Elongation at Break of 0.3% coated 30 micron powder at 178 mm standoff distance from IR source for 40 seconds duration
Elongation at Break (%)
51
50
49
48
47
46
1
2
3
samples
0.3% coated 30 micron

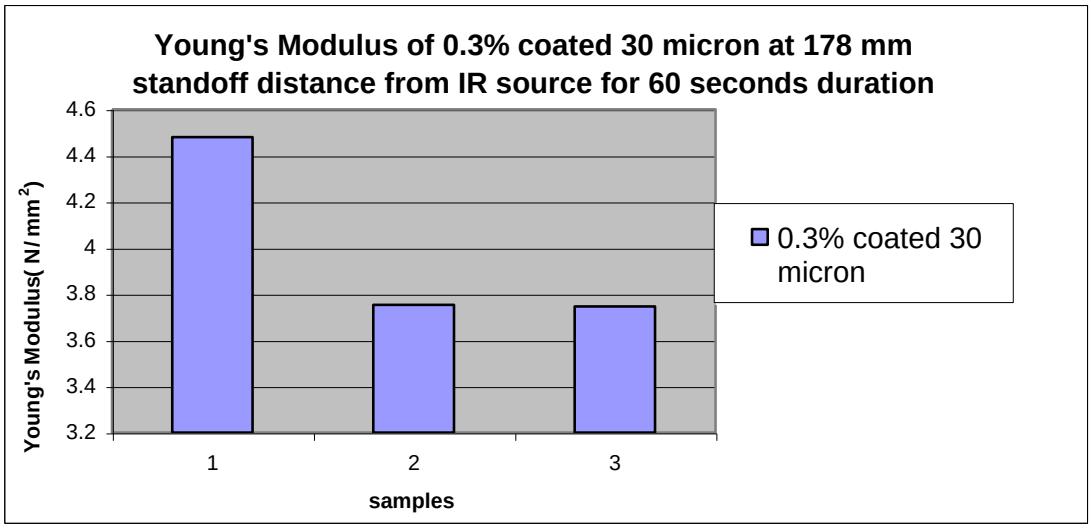
Young's Modulus of 0.3% coated 30 micron at 178 mm standoff distance from IR source for 60 seconds duration
Young's Modulus(N/ mm2)
4.6
4.4
4.2
4
3.8
3.6
3.4
3.2
1
2
3
samples
0.3% coated 30 micron

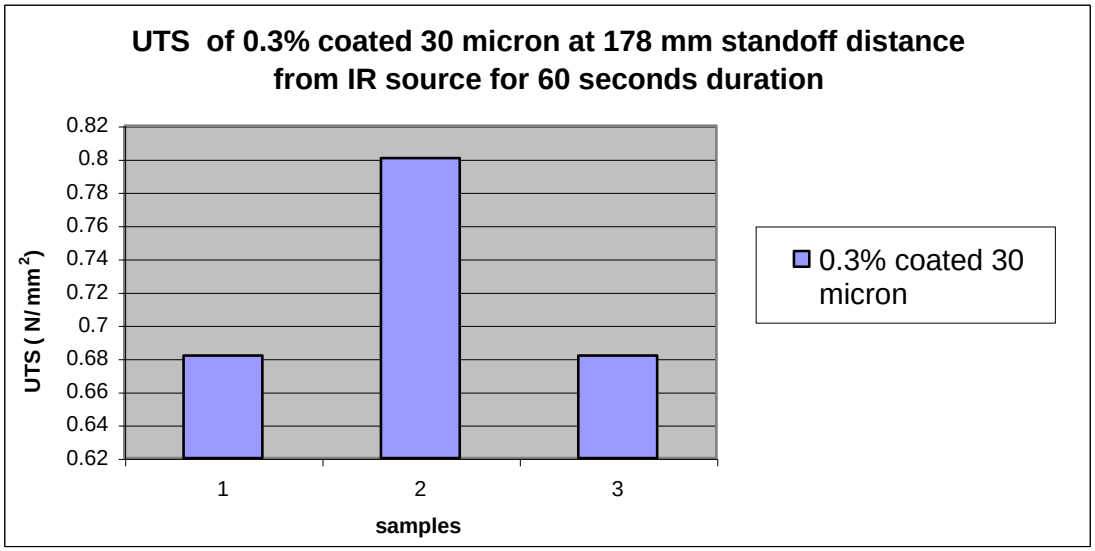
UTS of 0.3% coated 30 micron at 178 mm standoff distance from IR source for 60 seconds duration
UTS (N/ mm2)
0.82
0.8
0.78
0.76
0.74
0.72
0.7
0.68
0.66
0.64
0.62
1
2
3
samples
0.3% coated 30 micron

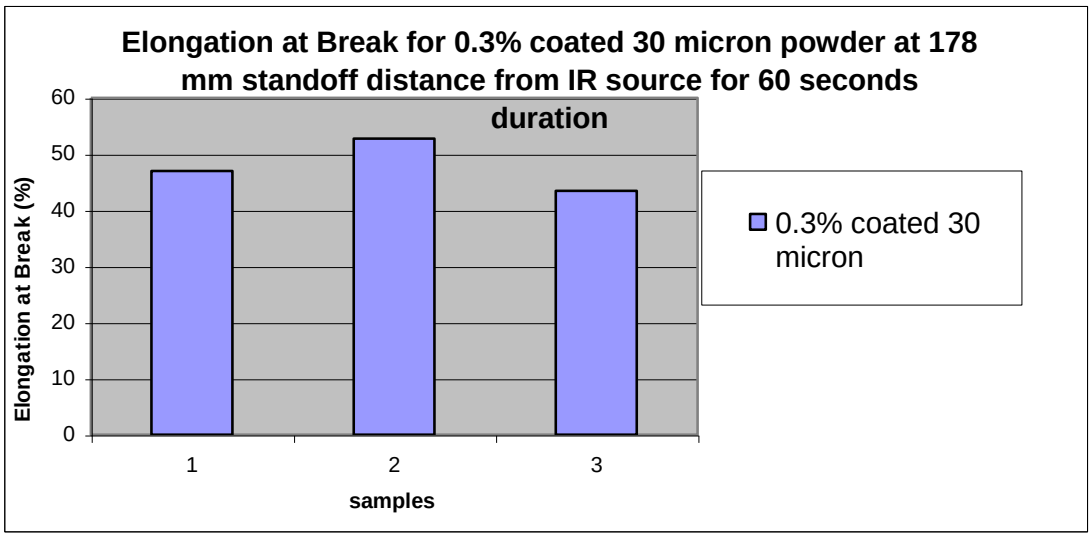
Elongation at Break for 0.3% coated 30 micron powder at 178 mm standoff distance from IR source for 60 seconds duration
Elongation at Break (%)
60
50
40
30
20
10
0
1
2
3
samples
0.3% coated 30 micron

Figure A6: Mechanical properties of 17 μm Somos 201 powder at 178 mm stand off distance:

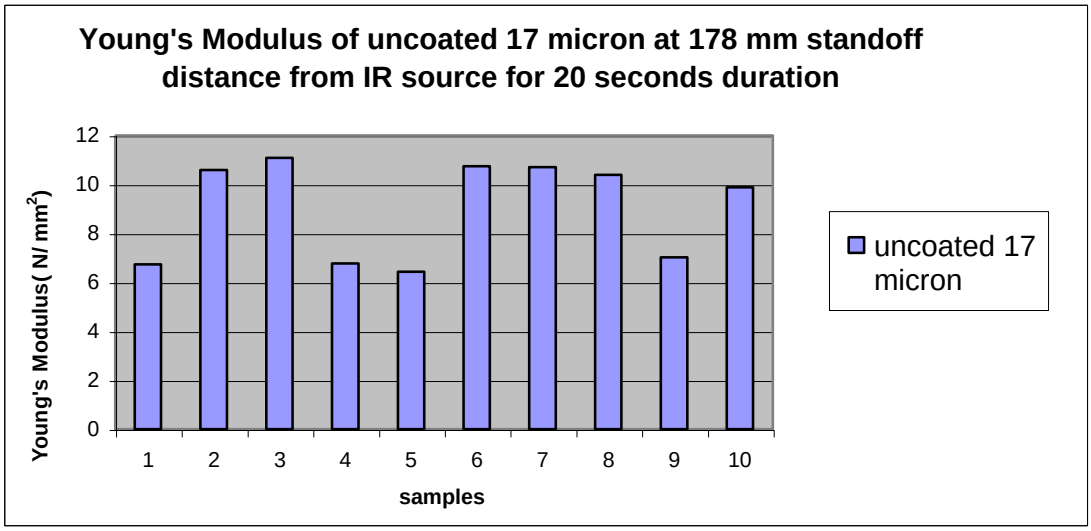

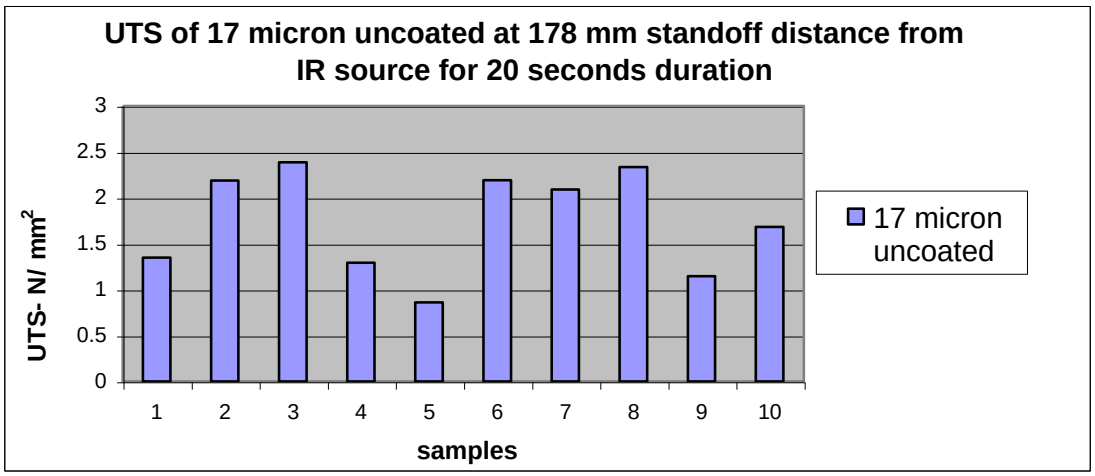

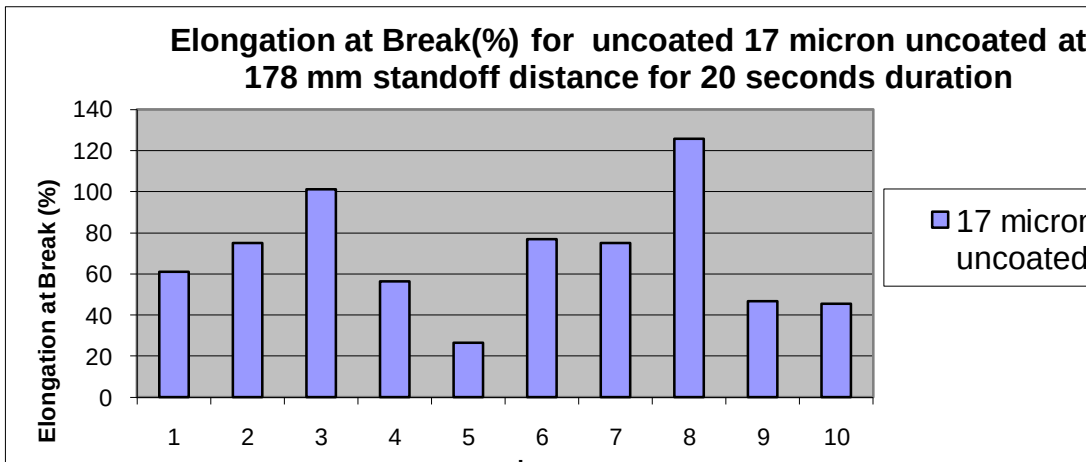

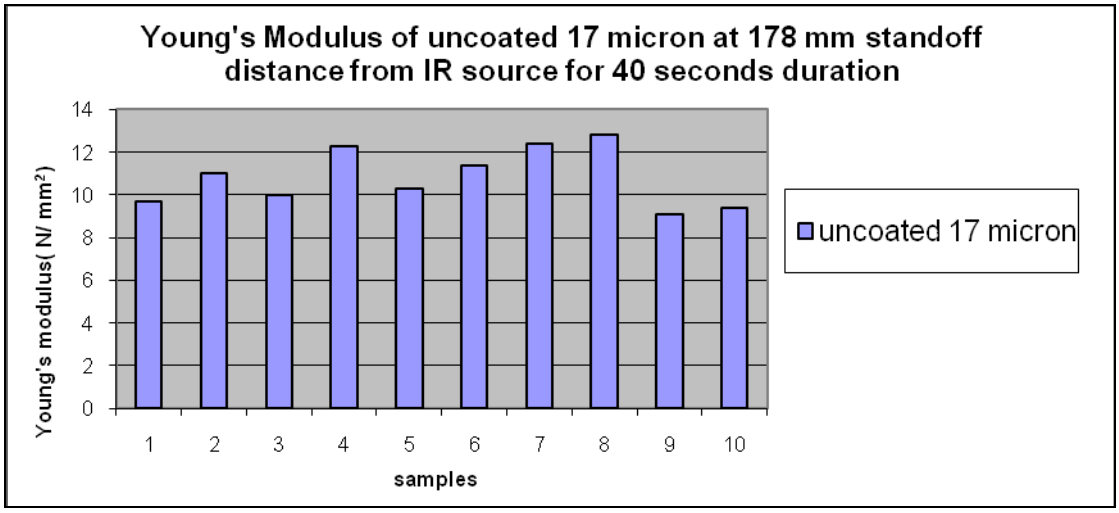
Young's Modulus of uncoated 17 micron at 178 mm standoff distance from IR source for 40 seconds duration
Young's modulus(N/ mm²)
14
12
10
8
6
4
2
0
1 2 3 4 5 6 7 8 9 10
samples
uncoated 17 micron

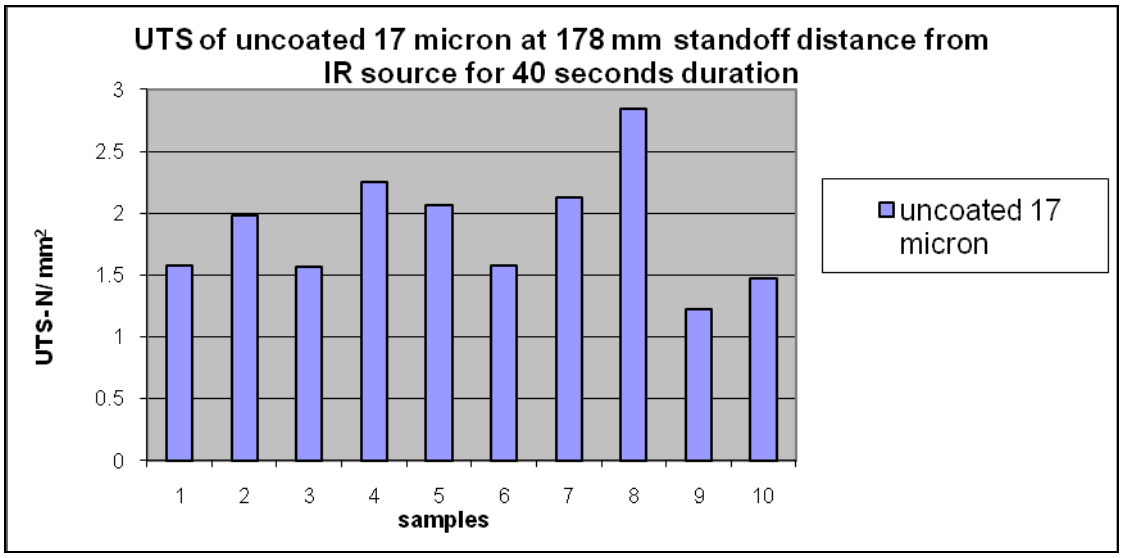
UTS of uncoated 17 micron at 178 mm standoff distance from IR source for 40 seconds duration
UTS-N/ mm²
3
2.5
2
1.5
1
0.5
0
1 2 3 4 5 6 7 8 9 10
samples
uncoated 17 micron

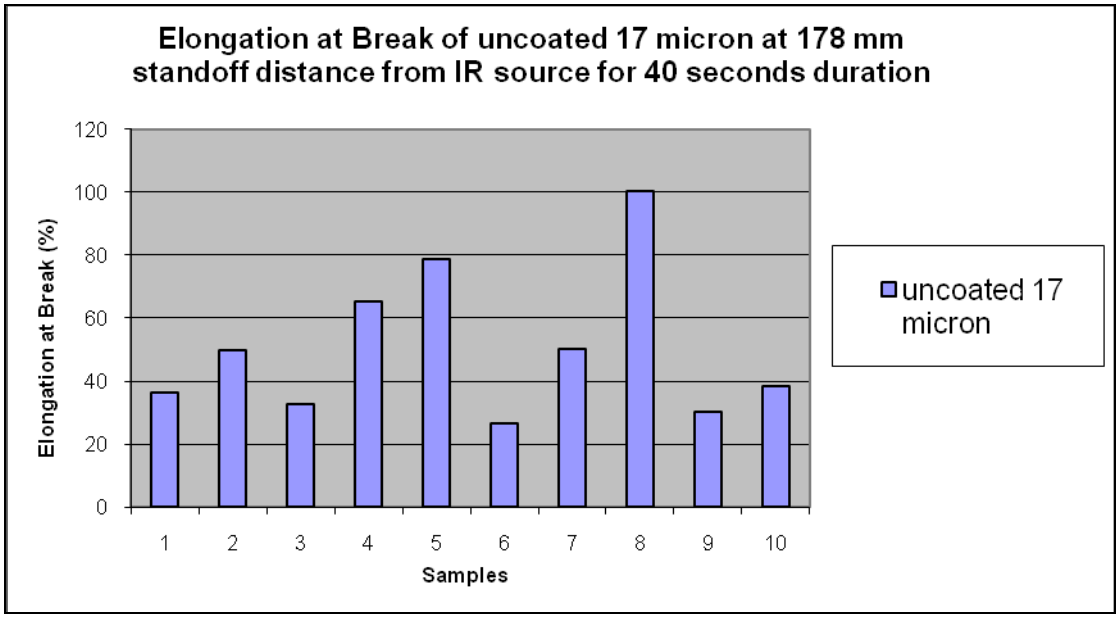
Elongation at Break of uncoated 17 micron at 178 mm standoff distance from IR source for 40 seconds duration
Elongation at Break (%)
120
100
80
60
40
20
0
1 2 3 4 5 6 7 8 9 10
Samples
uncoated 17 micron

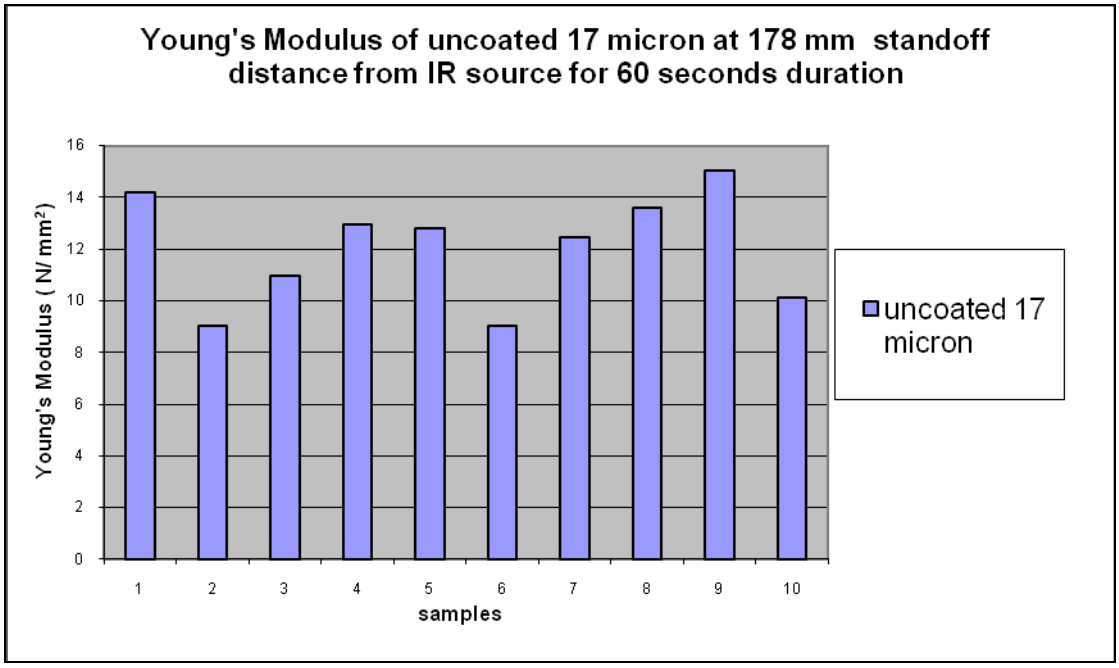
Young's Modulus of uncoated 17 micron at 178 mm standoff distance from IR source for 60 seconds duration
Young's Modulus (N/ mm²)
16
14
12
10
8
6
4
2
0
1
2
3
4
5
6
7
8
9
10
samples
uncoated 17 micron

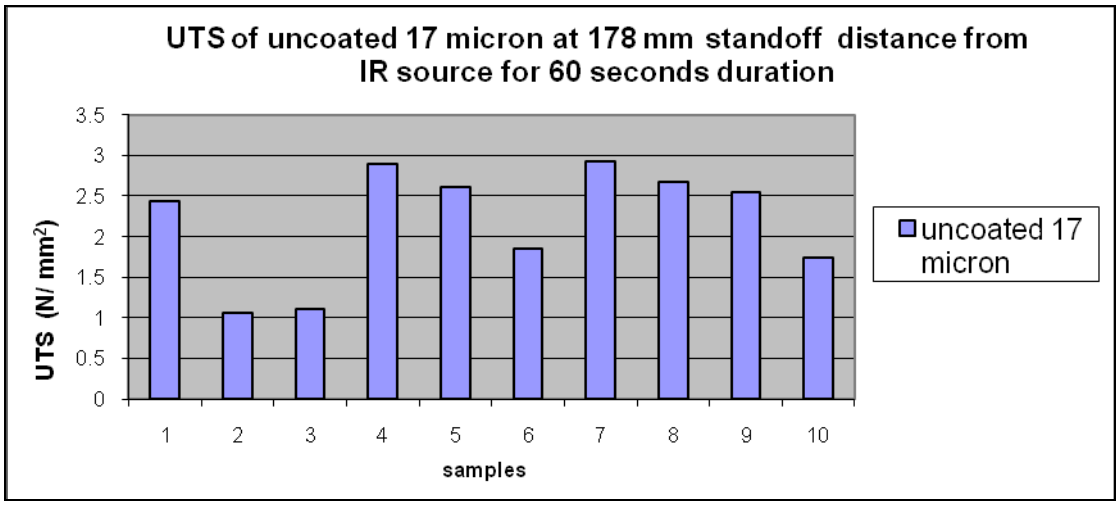
UTS of uncoated 17 micron at 178 mm standoff distance from IR source for 60 seconds duration
UTS (N/ mm²)
3.5
3
2.5
2
1.5
1
0.5
0
1
2
3
4
5
6
7
8
9
10
samples
uncoated 17 micron

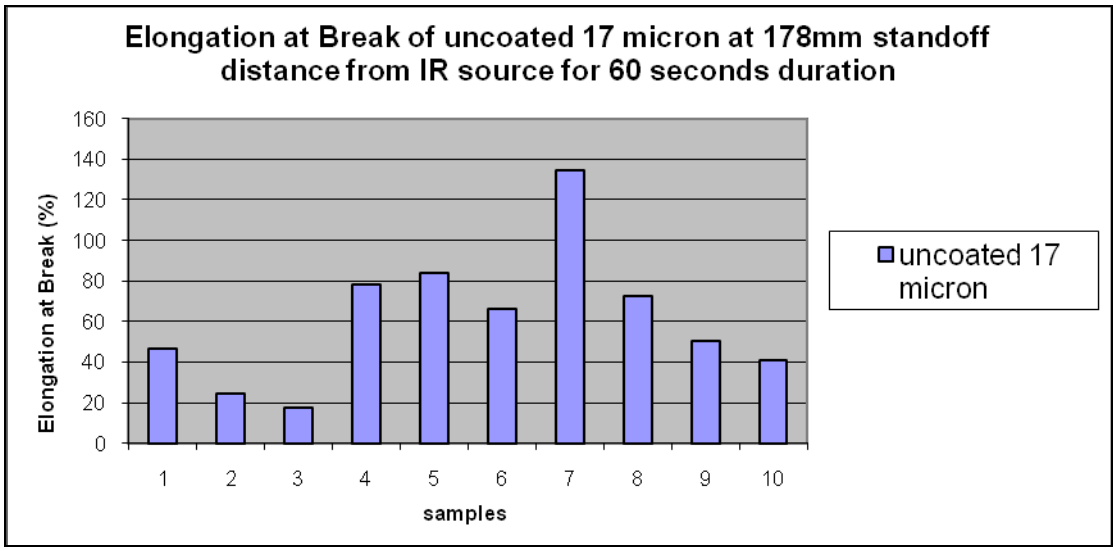
Elongation at Break of uncoated 17 micron at 178mm standoff distance from IR source for 60 seconds duration
Elongation at Break (%)
160
140
120
100
80
60
40
20
0
1
2
3
4
5
6
7
8
9
10
samples
uncoated 17 micron

Figure A7: Mechanical properties of 0.3% silica coated 17 μm Somos 201 powder at 178 mm stand off distance:

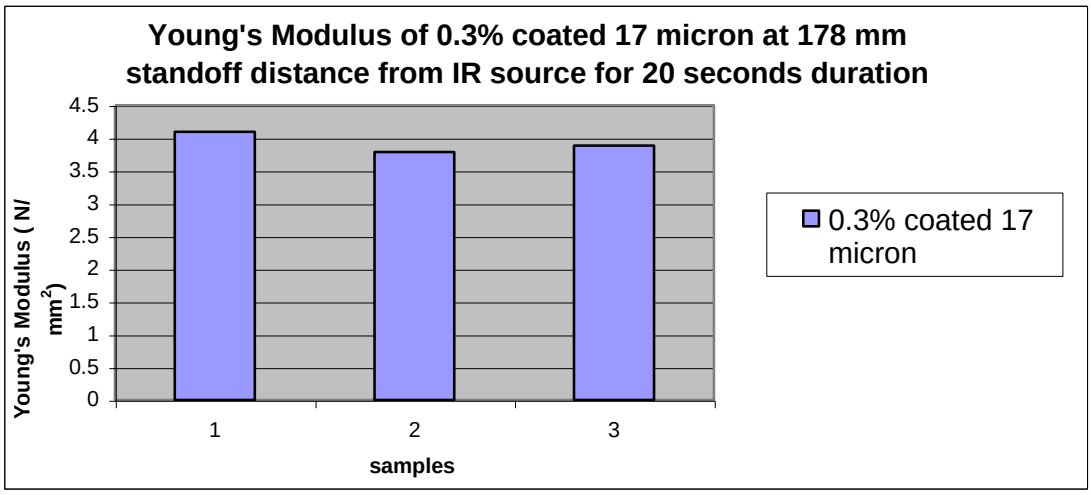

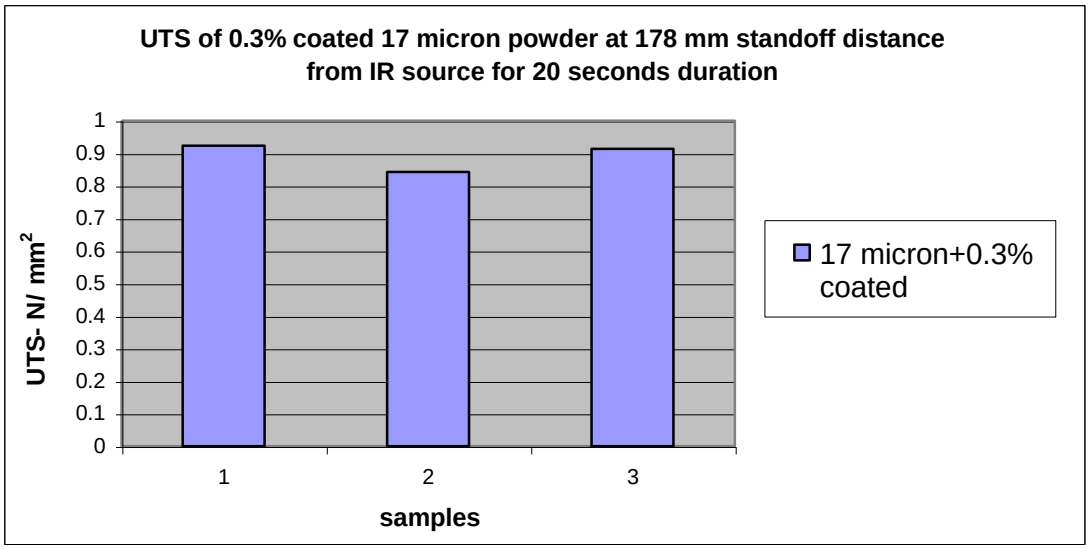

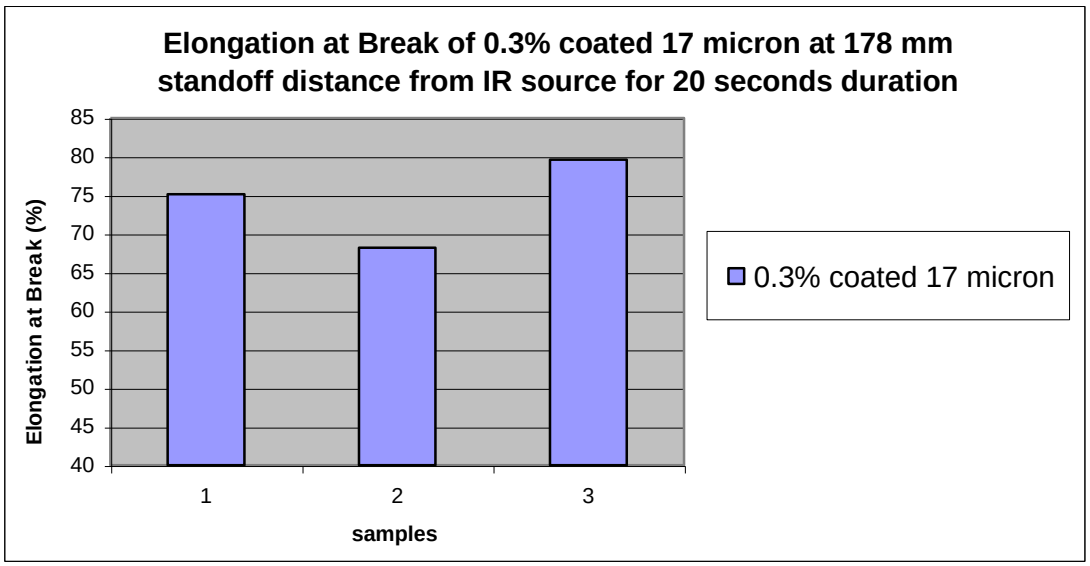

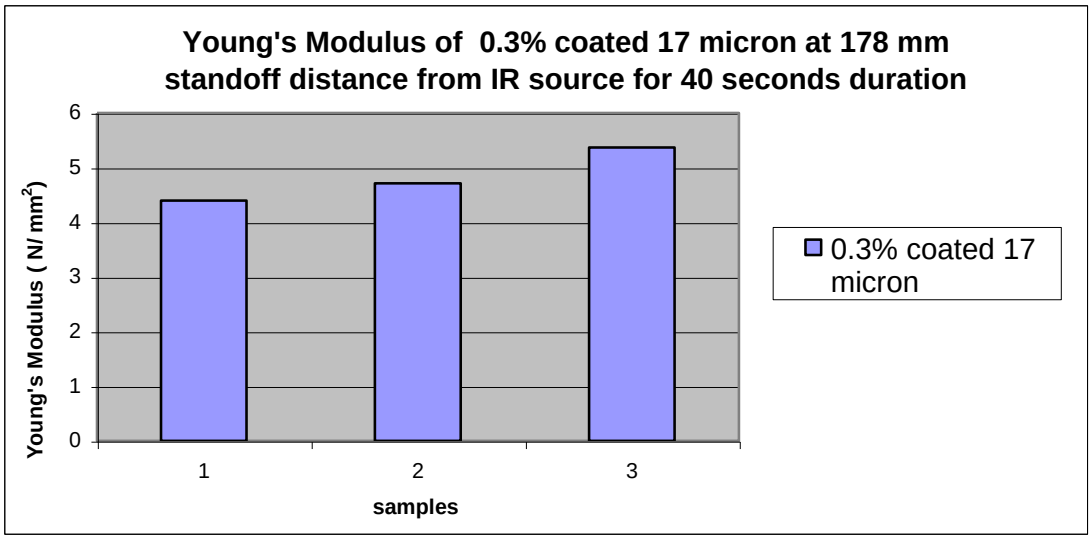
Young's Modulus of 0.3% coated 17 micron at 178 mm standoff distance from IR source for 40 seconds duration
Young's Modulus (N/ mm2)
0
1
2
3
4
5
6
1
2
3
samples
0.3% coated 17 micron

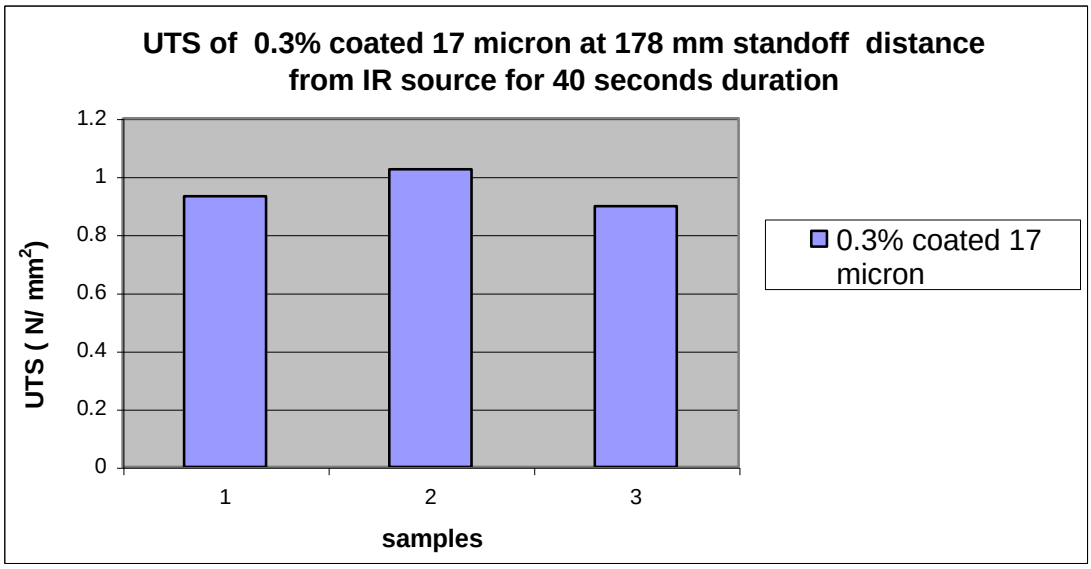
UTS of 0.3% coated 17 micron at 178 mm standoff distance from IR source for 40 seconds duration
UTS (N/ mm2)
0
0.2
0.4
0.6
0.8
1
1.2
1
2
3
samples
0.3% coated 17 micron

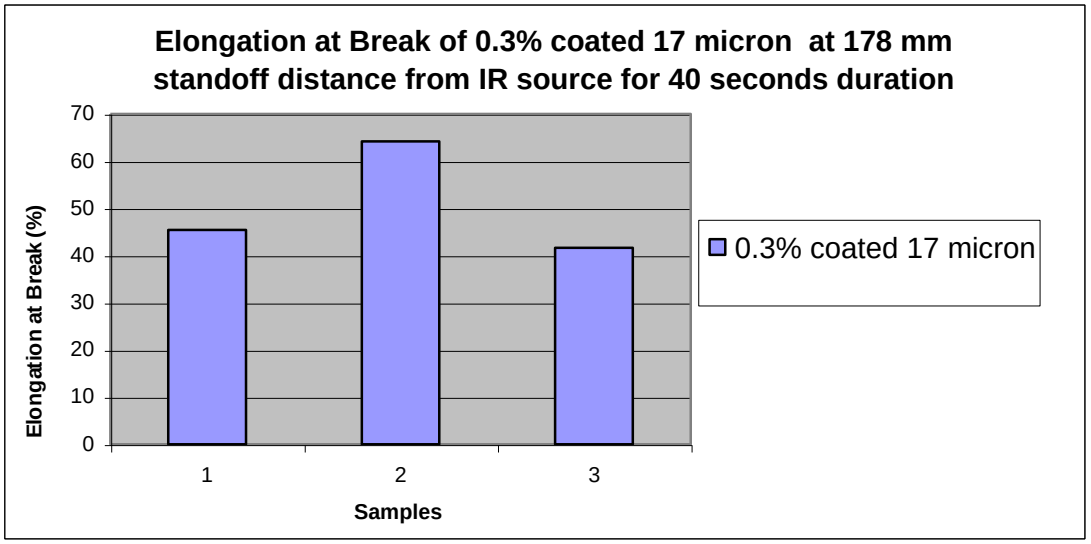
Elongation at Break of 0.3% coated 17 micron at 178 mm standoff distance from IR source for 40 seconds duration
Elongation at Break (%)
0
10
20
30
40
50
60
70
1
2
3
Samples
0.3% coated 17 micron

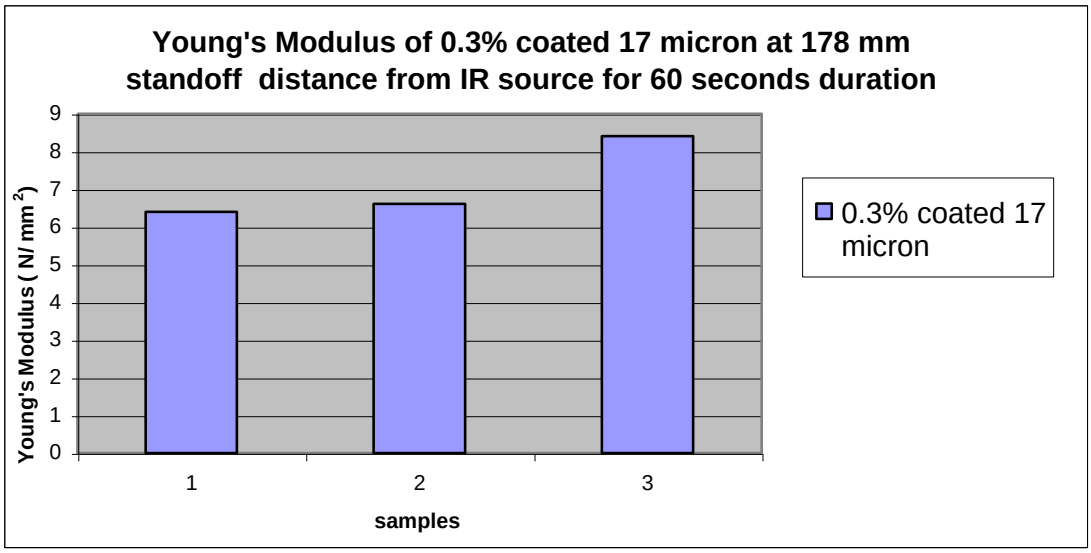
Young's Modulus of 0.3% coated 17 micron at 178 mm standoff distance from IR source for 60 seconds duration
Young's Modulus (N/ mm 2)
0
1
2
3
4
5
6
7
8
9
1
2
3
samples
0.3% coated 17 micron

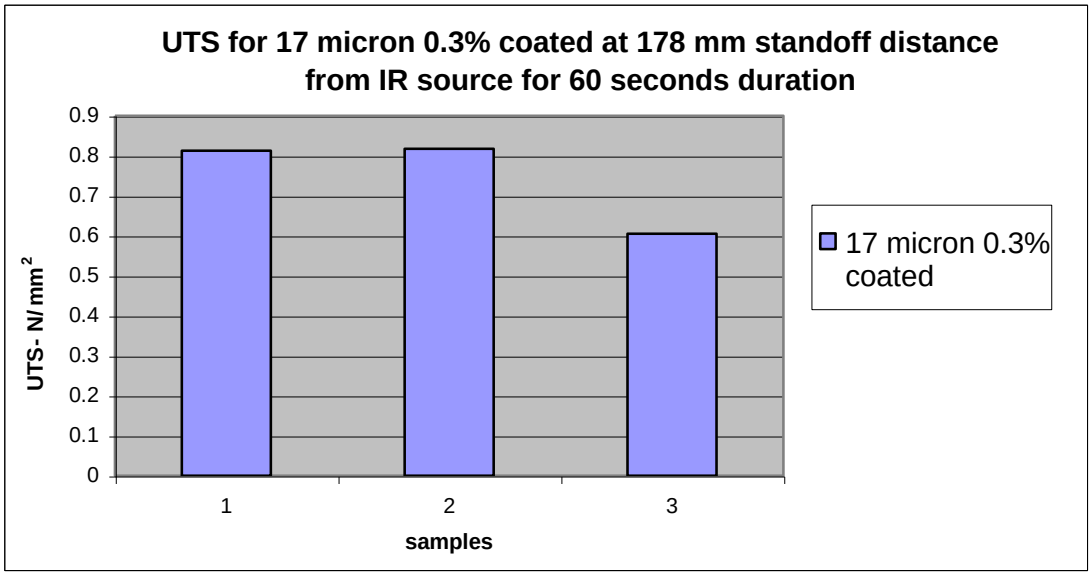
UTS for 17 micron 0.3% coated at 178 mm standoff distance from IR source for 60 seconds duration
UTS- N/ mm 2
0
0.1
0.2
0.3
0.4
0.5
0.6
0.7
0.8
0.9
1
2
3
samples
17 micron 0.3% coated

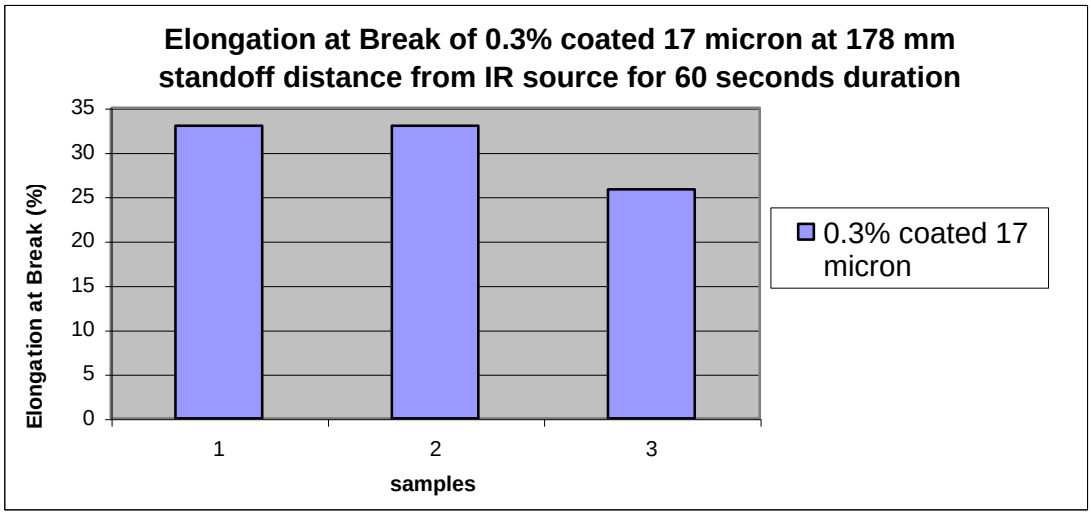
Elongation at Break of 0.3% coated 17 micron at 178 mm standoff distance from IR source for 60 seconds duration
Elongation at Break (%)
0
5
10
15
20
25
30
35
1
2
3
samples
0.3% coated 17 micron

Figure A8: Mechanical properties of 1.2 % silica coated 17 μm Somos 201 powder at 178 mm stand- off distance:

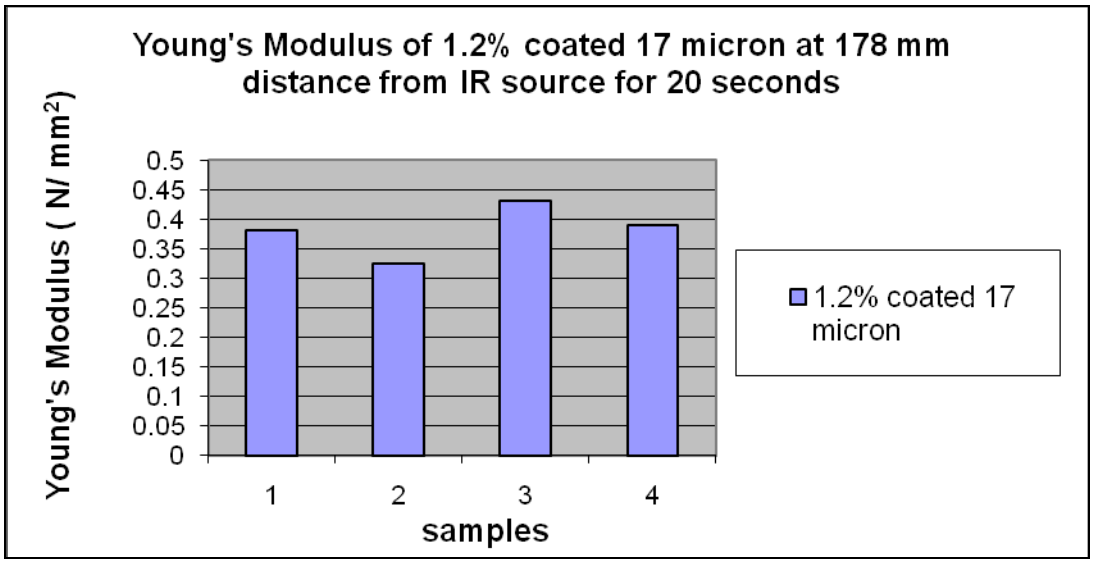

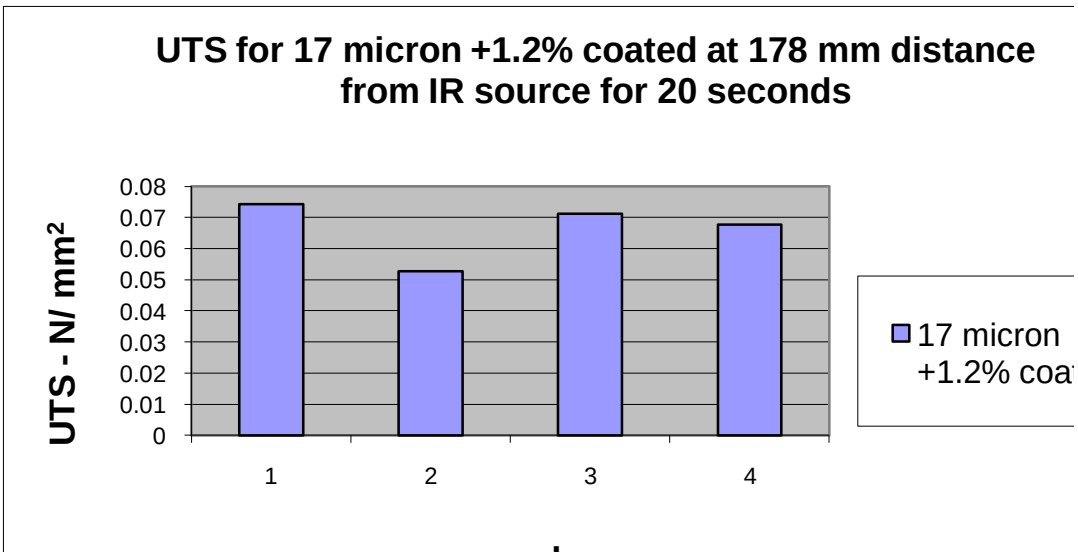

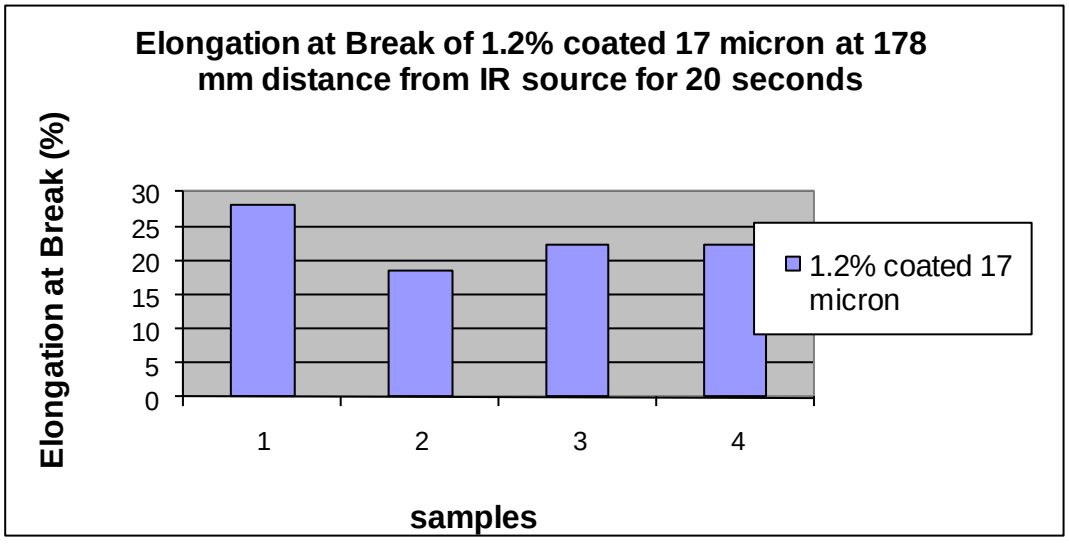

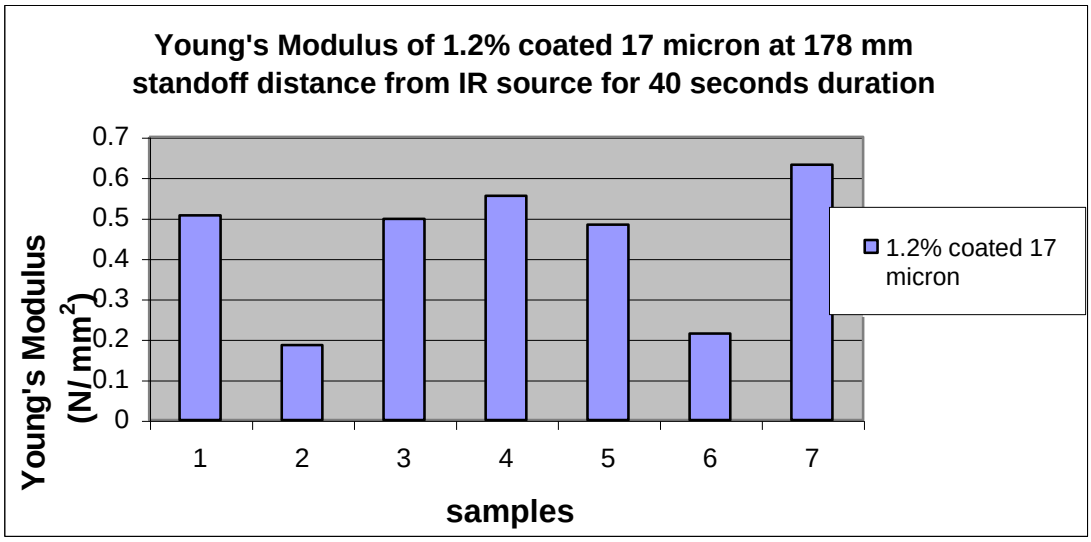
Young's Modulus of 1.2% coated 17 micron at 178 mm standoff distance from IR source for 40 seconds duration
Young's Modulus (N/mm2)
0.7
0.6
0.5
0.4
0.3
0.2
0.1
0
1
2
3
4
5
6
7
samples
1.2% coated 17 micron

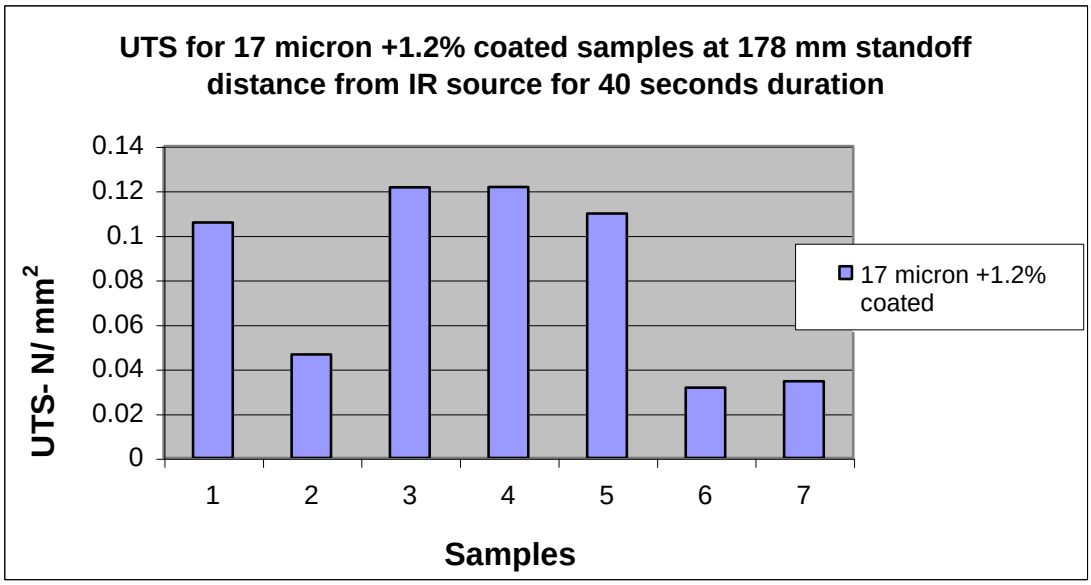
UTS for 17 micron +1.2% coated samples at 178 mm standoff distance from IR source for 40 seconds duration
UTS- N/ mm2
0.14
0.12
0.1
0.08
0.06
0.04
0.02
0
1
2
3
4
5
6
7
Samples
17 micron +1.2% coated

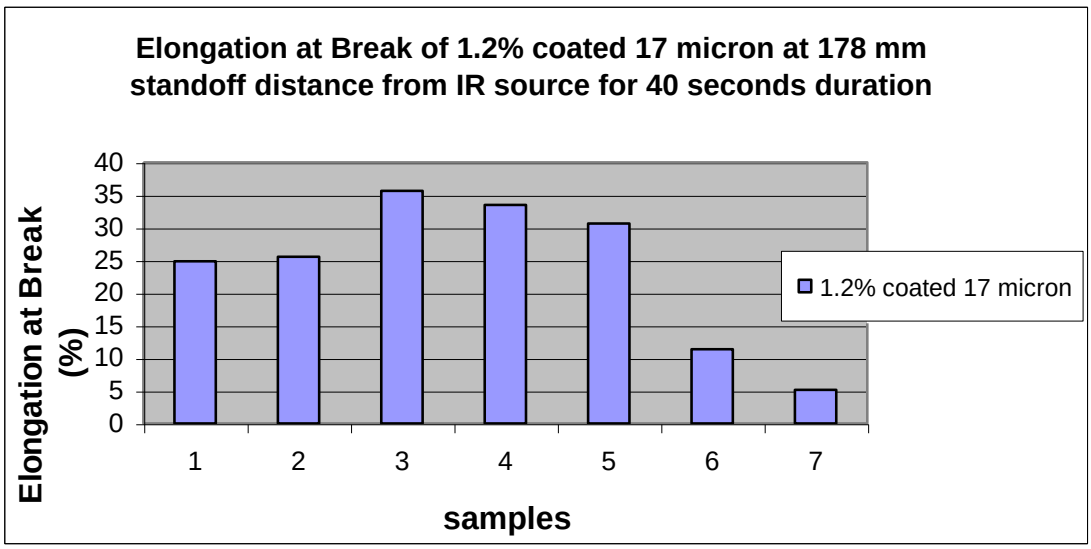
Elongation at Break of 1.2% coated 17 micron at 178 mm standoff distance from IR source for 40 seconds duration
Elongation at Break (%)
40
35
30
25
20
15
10
5
0
1
2
3
4
5
6
7
samples
1.2% coated 17 micron

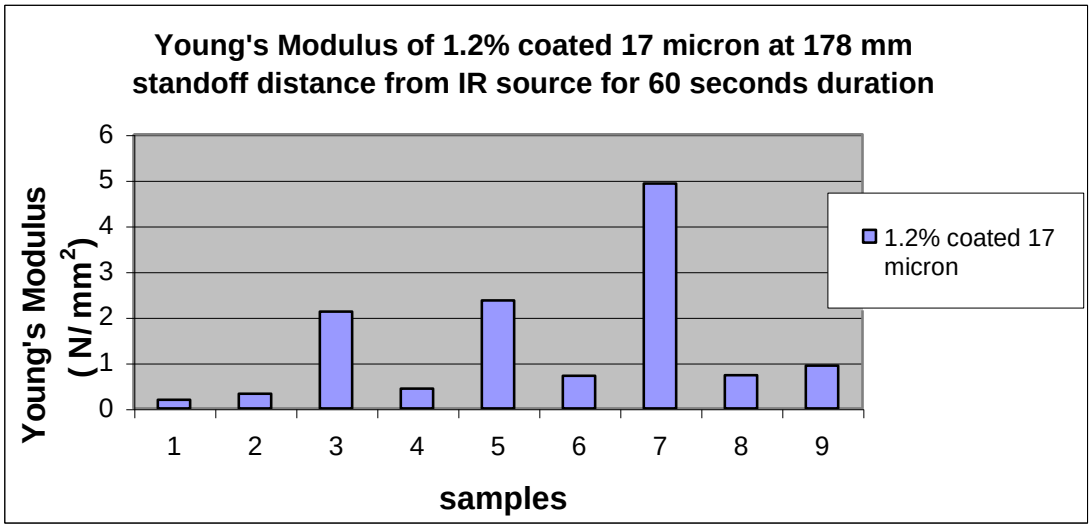
Young's Modulus of 1.2% coated 17 micron at 178 mm standoff distance from IR source for 60 seconds duration
Young's Modulus (N/ mm2)
6
5
4
3
2
1
0
1 2 3 4 5 6 7 8 9
samples
1.2% coated 17 micron

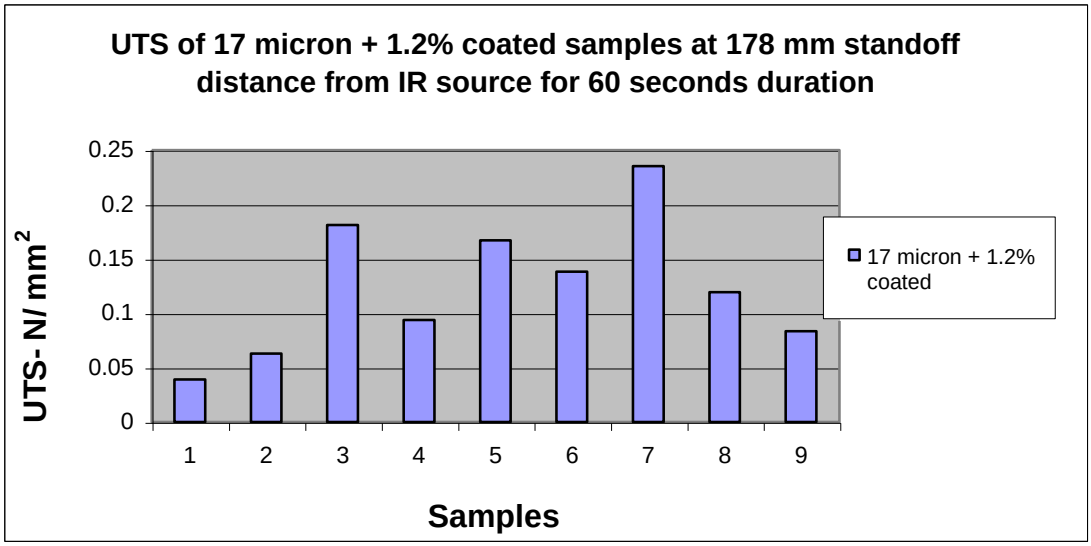
UTS of 17 micron + 1.2% coated samples at 178 mm standoff distance from IR source for 60 seconds duration
UTS- N/ mm2
0.25
0.2
0.15
0.1
0.05
0
1 2 3 4 5 6 7 8 9
Samples
17 micron + 1.2% coated

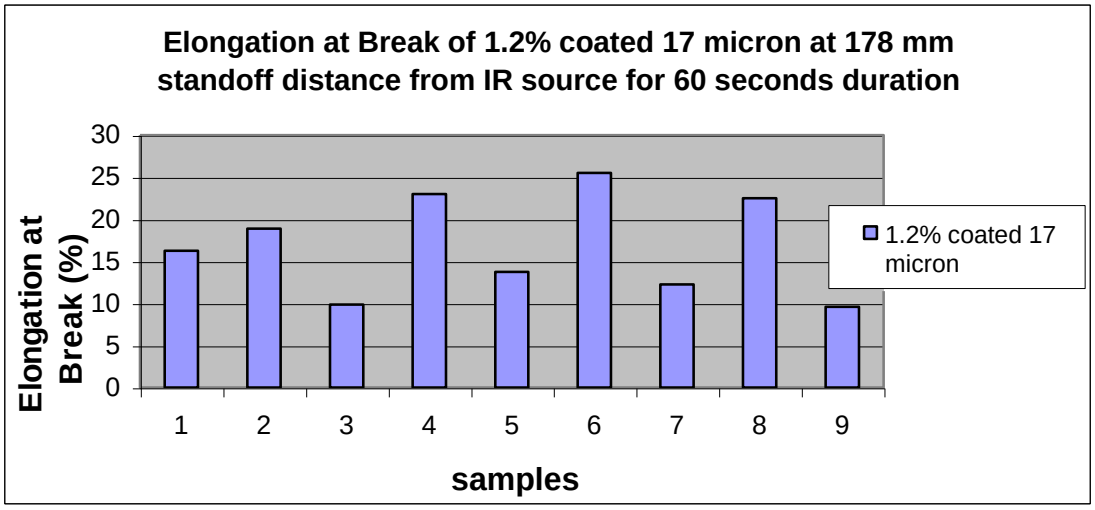
Elongation at Break of 1.2% coated 17 micron at 178 mm standoff distance from IR source for 60 seconds duration
Elongation at Break (%)
30
25
20
15
10
5
0
1 2 3 4 5 6 7 8 9
samples
1.2% coated 17 micron

B) Tensile test Graphs generated from Tensile test machine

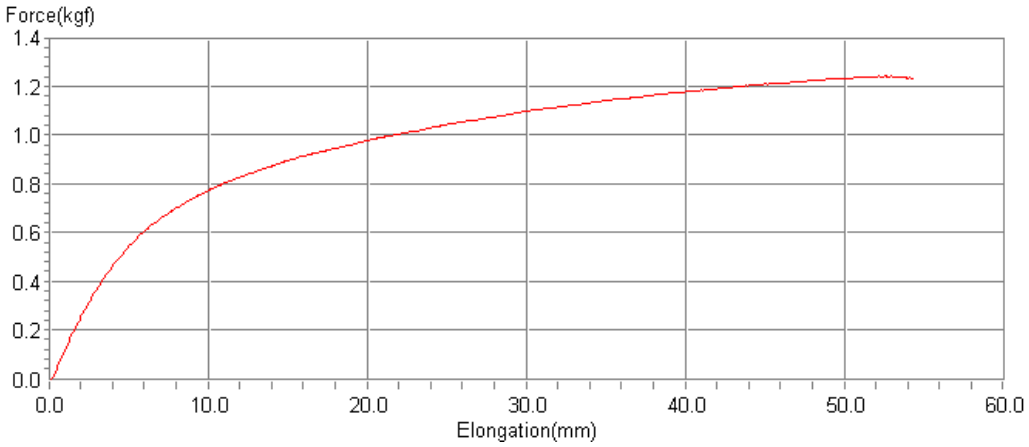

Figure B1 : Uncoated coarse Somos 201 powder at 128 mm standoff distance for 20 seconds duration under IR radiation

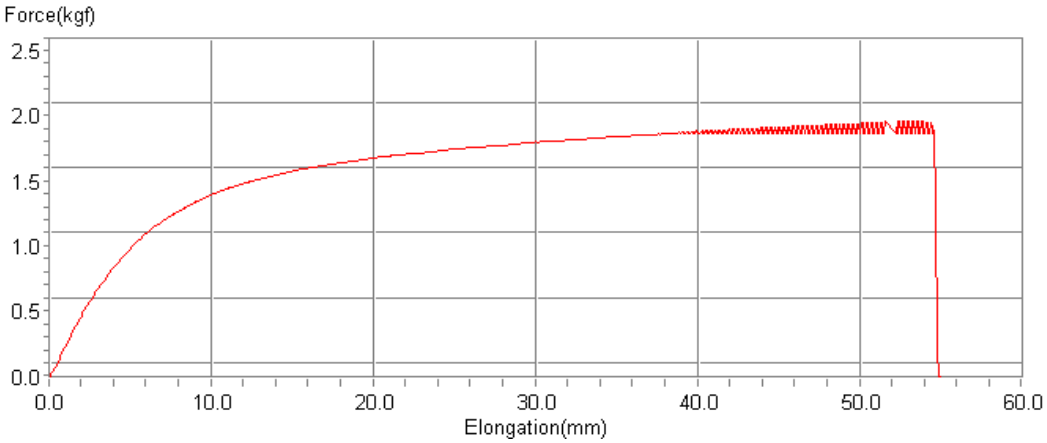

Figure B2: Uncoated Coarse Somos 201 powder at 128 mm standoff distance for 40 seconds duration under IR radiation

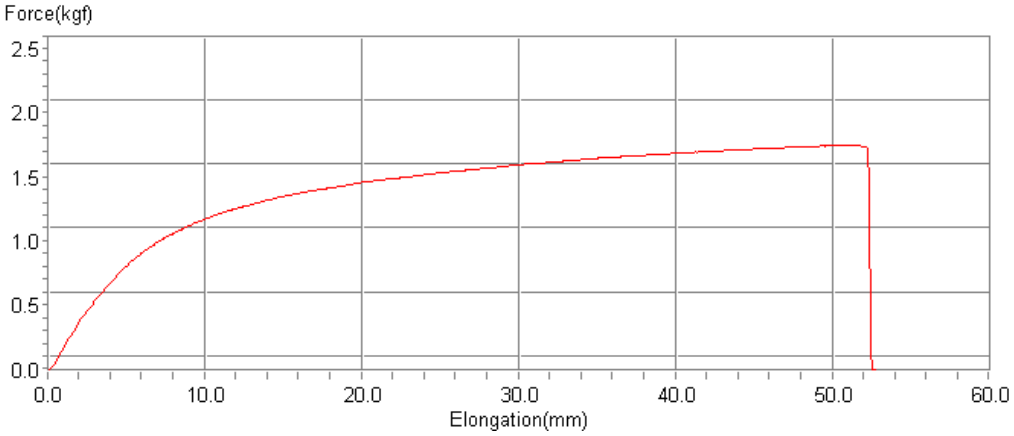

Figure B3: Uncoated Coarse Somos 201 powder at 128 mm standoff distance for 60 seconds duration under IR radiation

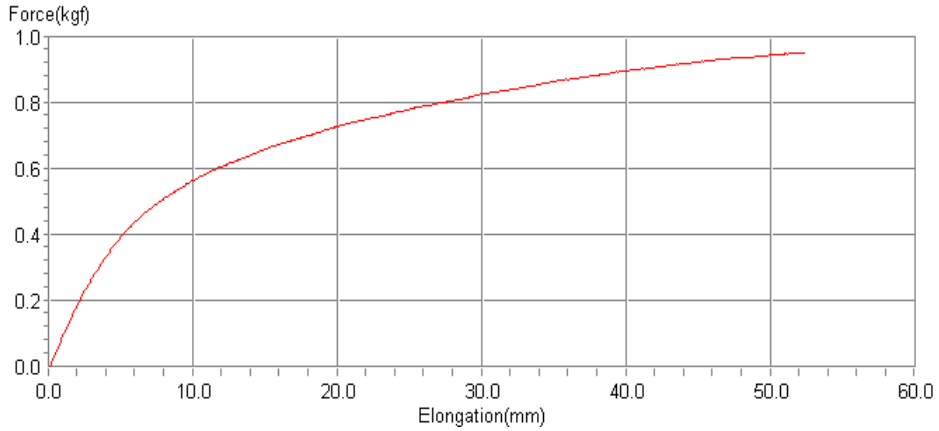

Figure B4: Uncoated Coarse Somos 201 powder at 178 mm standoff distance for 20 seconds duration under IR radiation

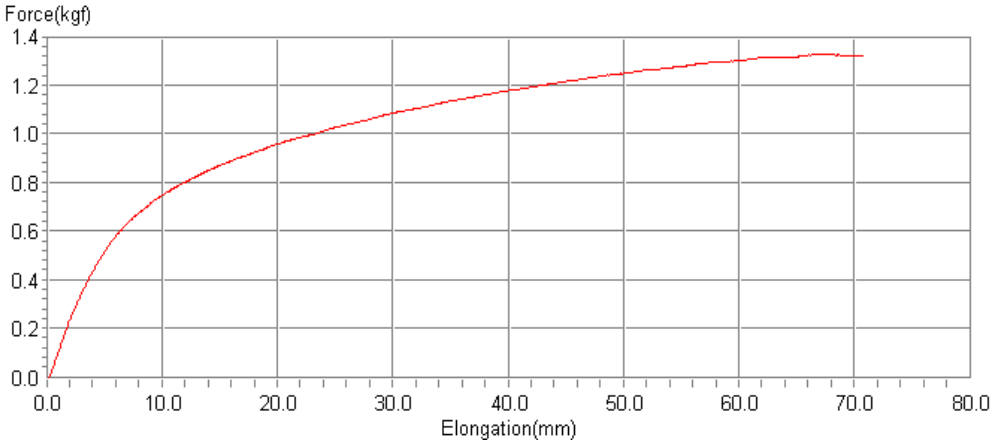

Figure B5: Uncoated Coarse Somos 201 powder at 178 mm standoff distance for 40 seconds duration under IR radiation

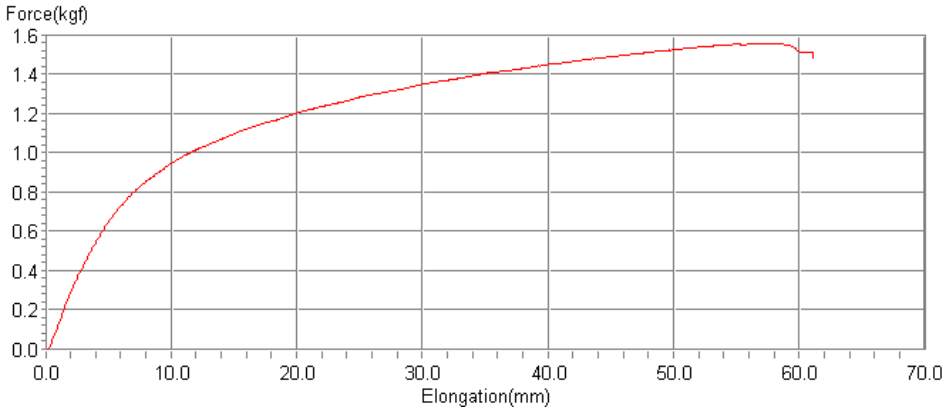

Figure B6: Uncoated Coarse Somos 201 powder at 178 mm standoff distance for 60 seconds duration under IR radiation

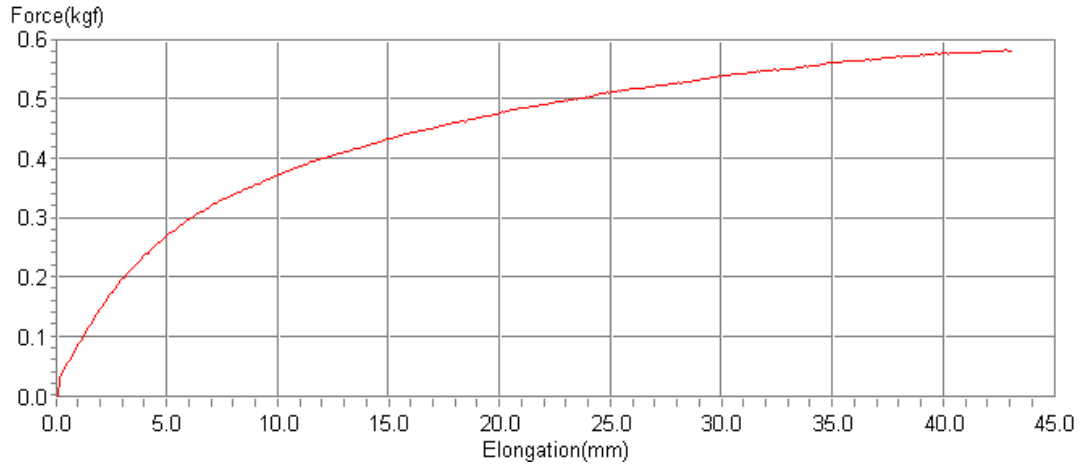

Figure B7: Uncoated Coarse Somos 201 powder at 228 mm standoff distance for 20 seconds duration under IR radiation

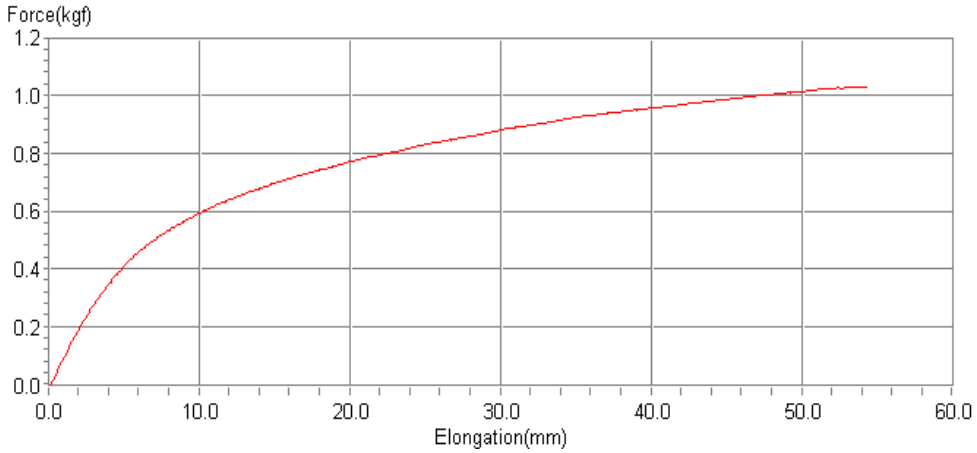

Figure B8: Uncoated Coarse Somos 201 powder at 228 mm standoff distance for 40 seconds duration under IR radiation

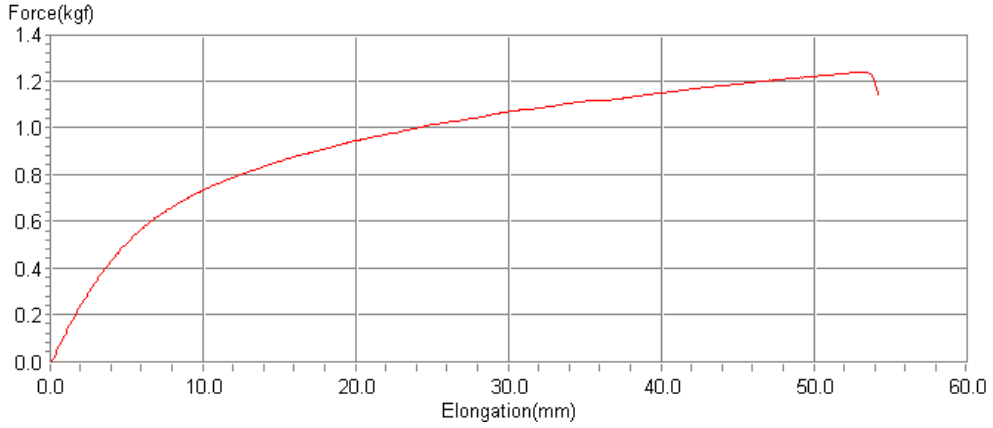

Figure B9: Uncoated Coarse Somos 201 powder at 228 mm standoff distance for 60 seconds duration under IR radiation

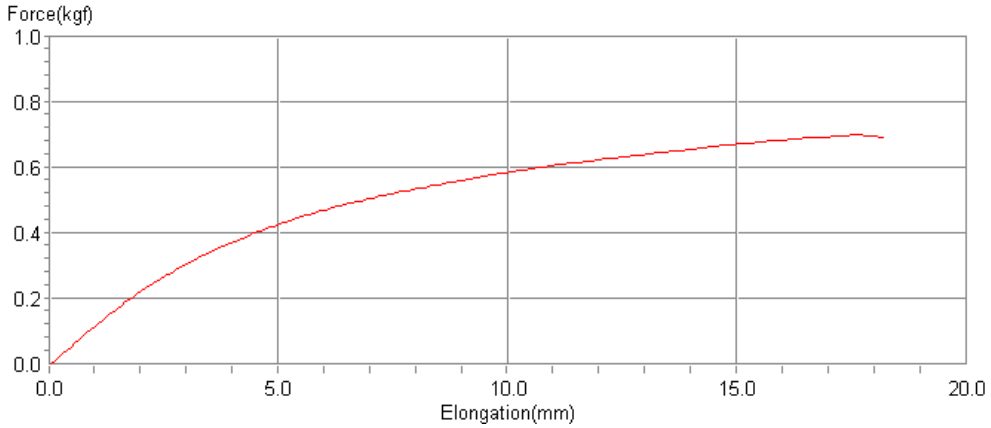

Figure B10: Uncoated 17 μm Somos 201 powder at 178 mm standoff distance for 20 seconds duration under IR radiation

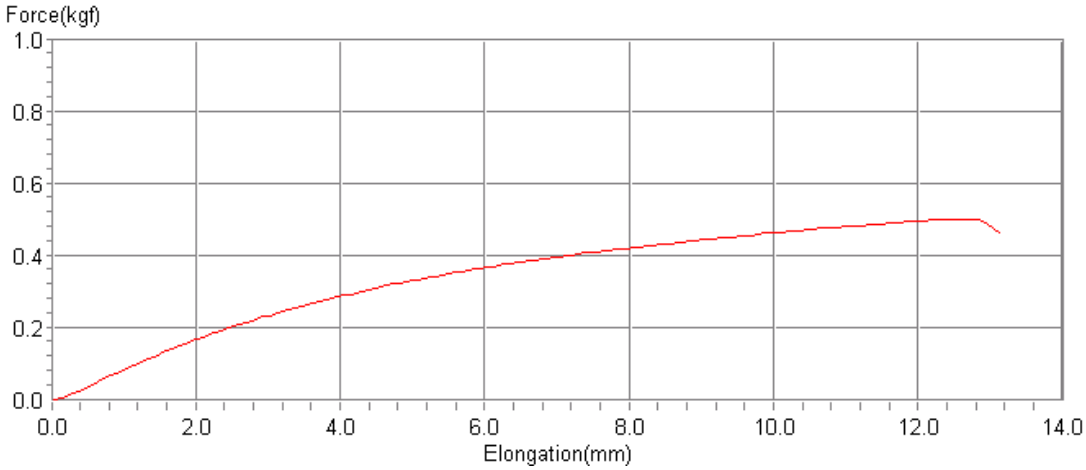

Figure B11: Uncoated 17 μm Somos 201 powder at 178 mm standoff distance for 40 seconds duration under IR radiation

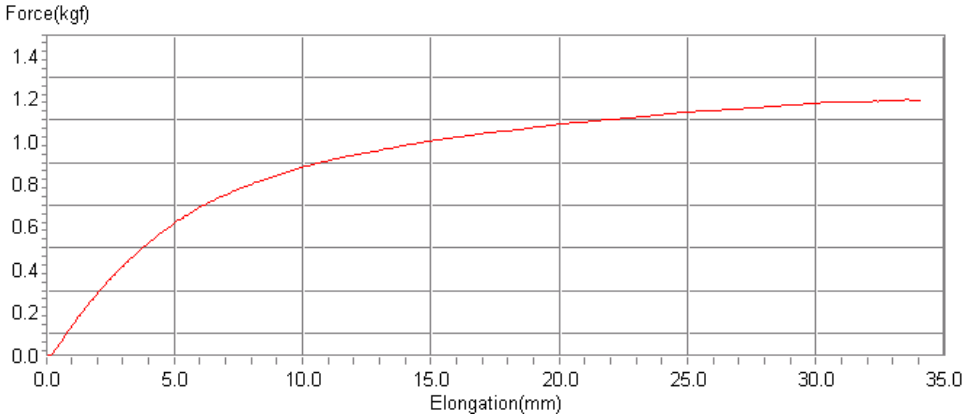

Figure B12: Uncoated 17 μm Somos 201 powder at 178 mm standoff distance for 60 seconds duration under IR radiation

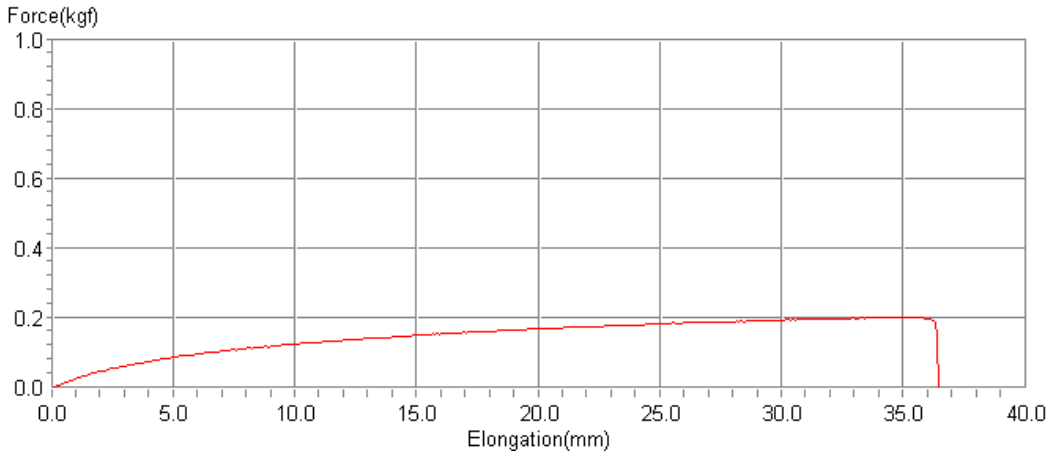

Figure B13: Uncoated 30 μm Somos 201 powder at 178 mm standoff distance for 20 seconds duration under IR radiation

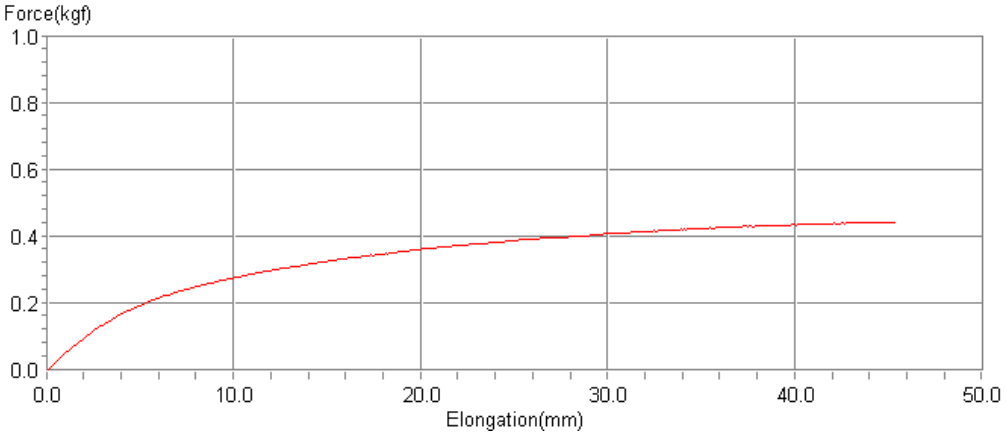

Figure B14: Uncoated 30 μm Somos 201 powder at 178 mm standoff distance for 40 seconds duration under IR radiation

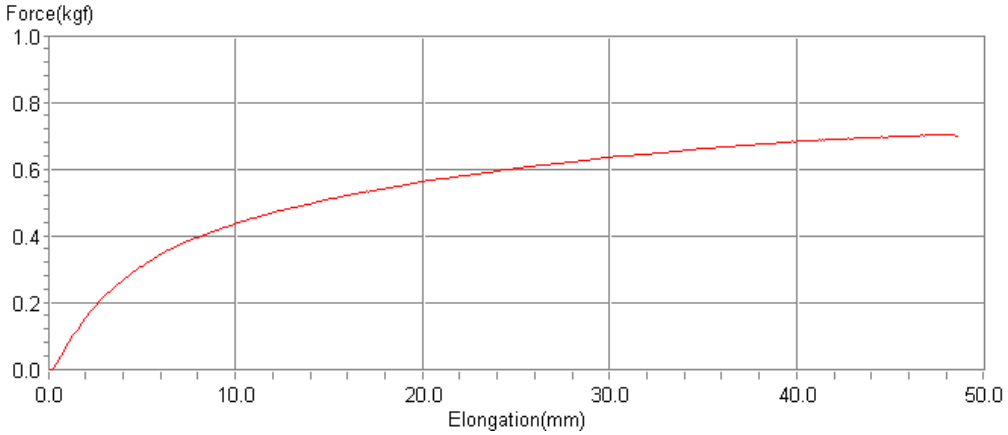

Figure B15: Uncoated 30 μm Somos 201 powder at 178 mm standoff distance for 60 seconds duration under IR radiation

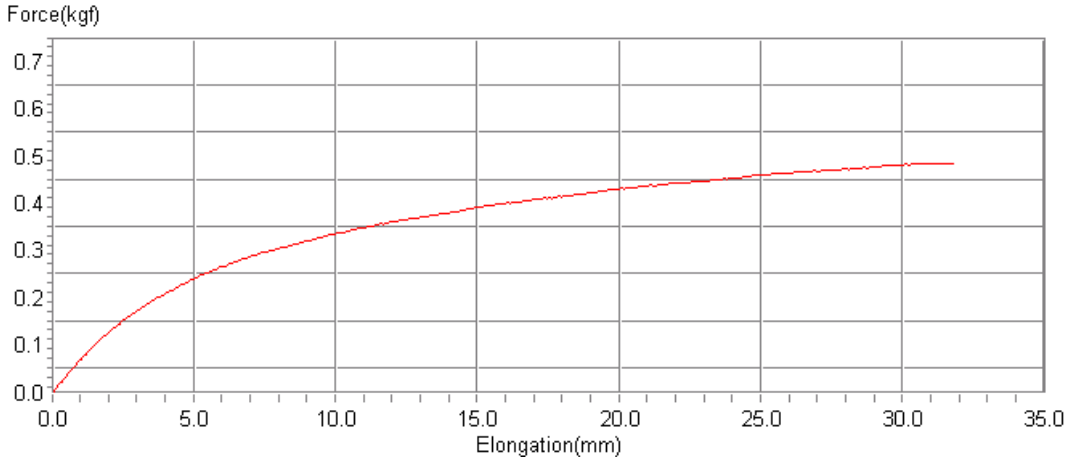

Figure B16: Coated(0.3%) 17 μm Somos 201 powder at 178 mm standoff distance for 20 seconds duration under IR radiation

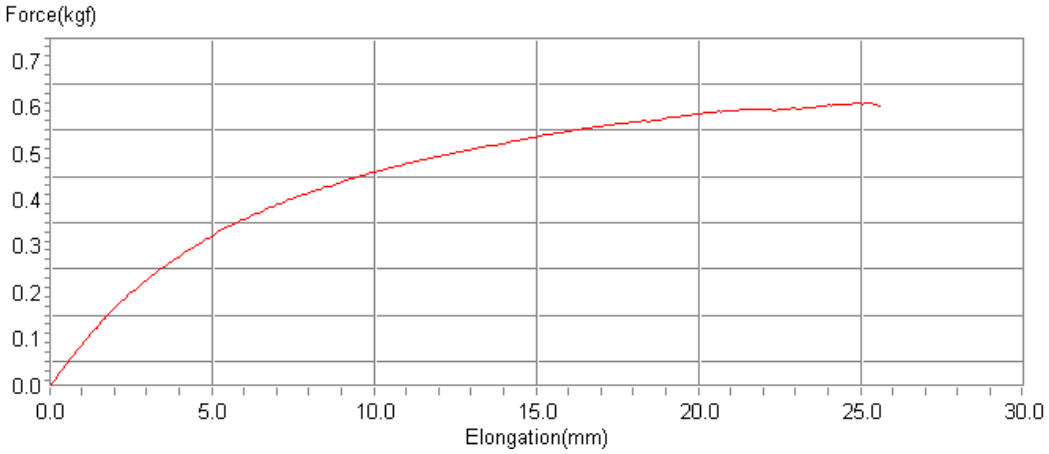

Figure B17: Coated(0.3%) 17 μm Somos 201 powder at 178 mm standoff distance for 40 seconds duration under IR radiation

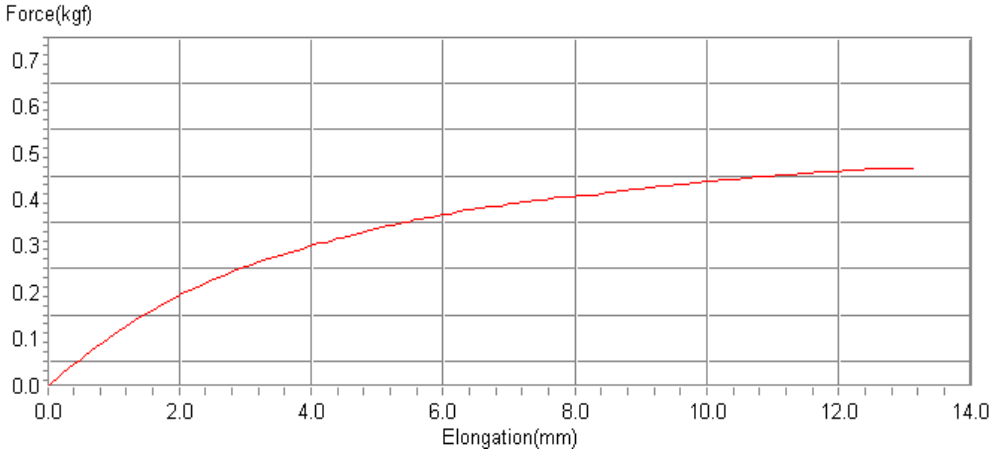

Figure B18: Coated(0.3%) 17 μm Somos 201 powder at 178 mm standoff distance for 60 seconds duration under IR radiation

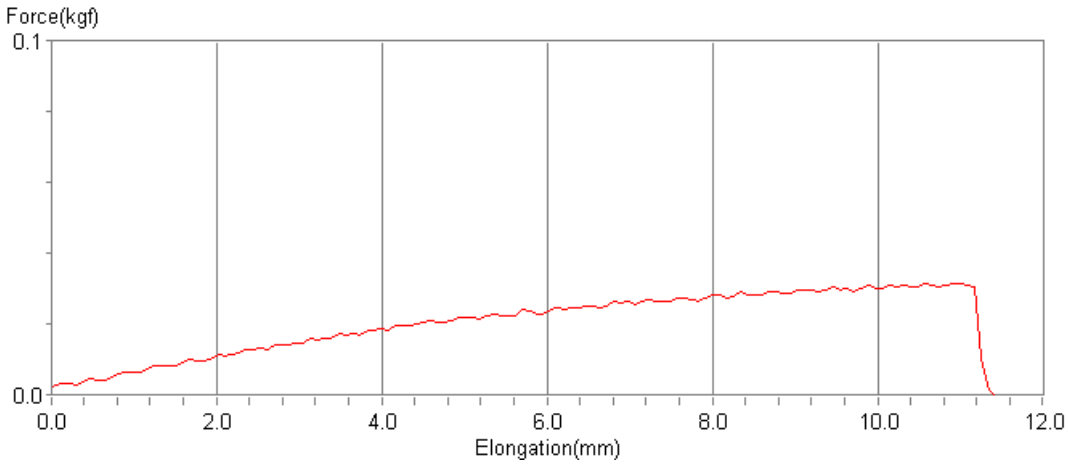

Figure B19: Coated (1.2%) 17 µm Somos 201 powder at 178 mm standoff distance for 20 seconds duration under IR radiation

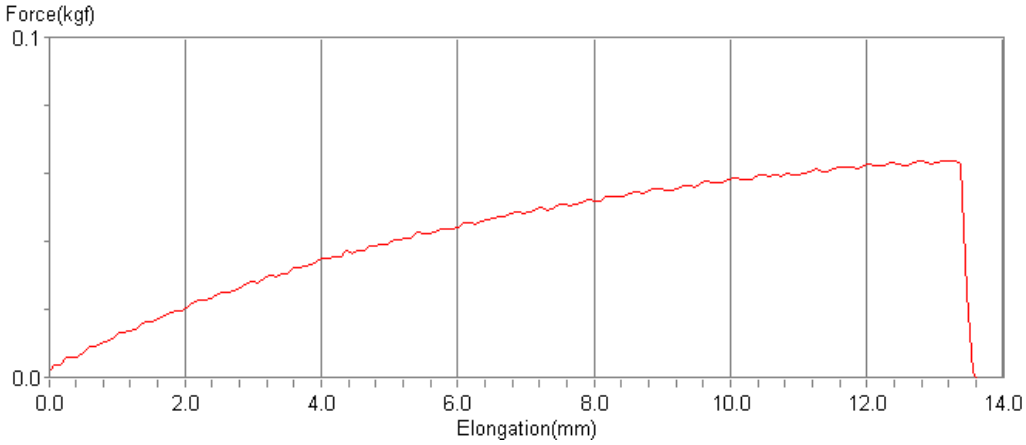

Figure B20: Coated(1.2%) 17 µm Somos 201 powder at 178 mm standoff distance for 40 seconds duration under IR radiation

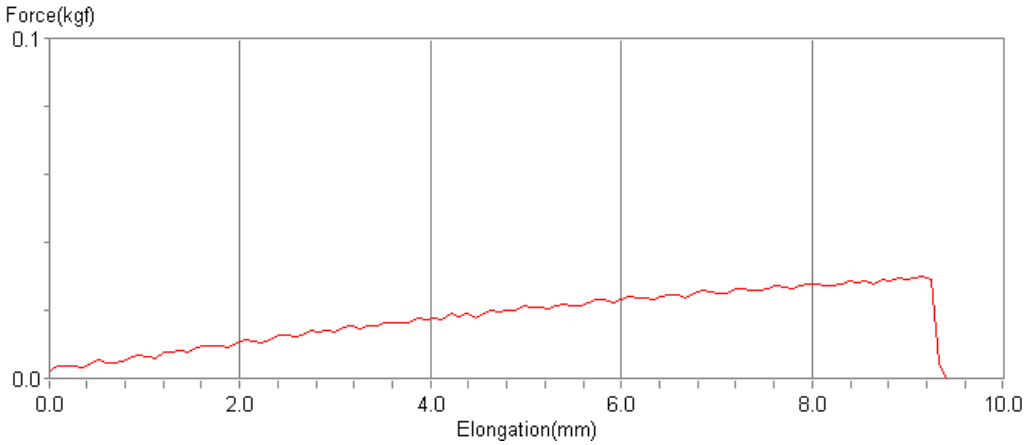

Figure B21: Coated(1.2%) 17 µm Somos 201 powder at 178 mm standoff distance for 60 seconds duration under IR radiation

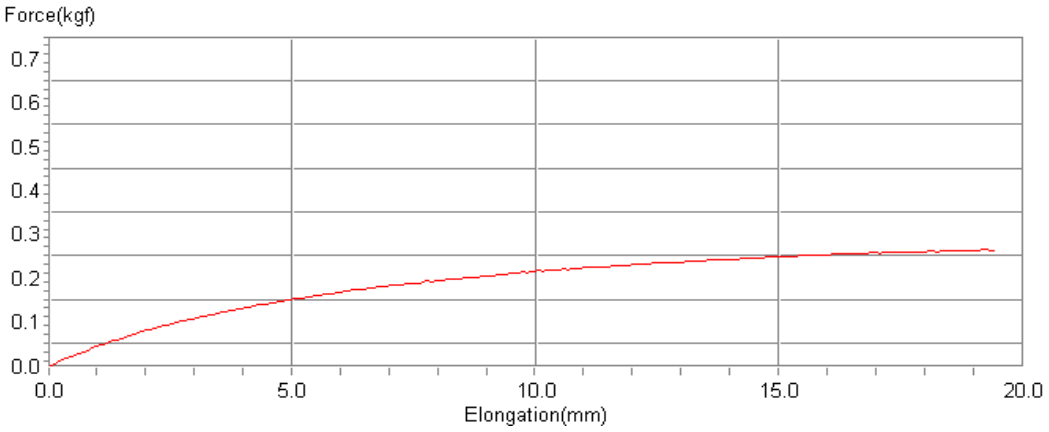

Figure B22: Coated(0.3%) 30 μm Somos 201 powder at 178 mm standoff distance for 20 seconds duration under IR radiation

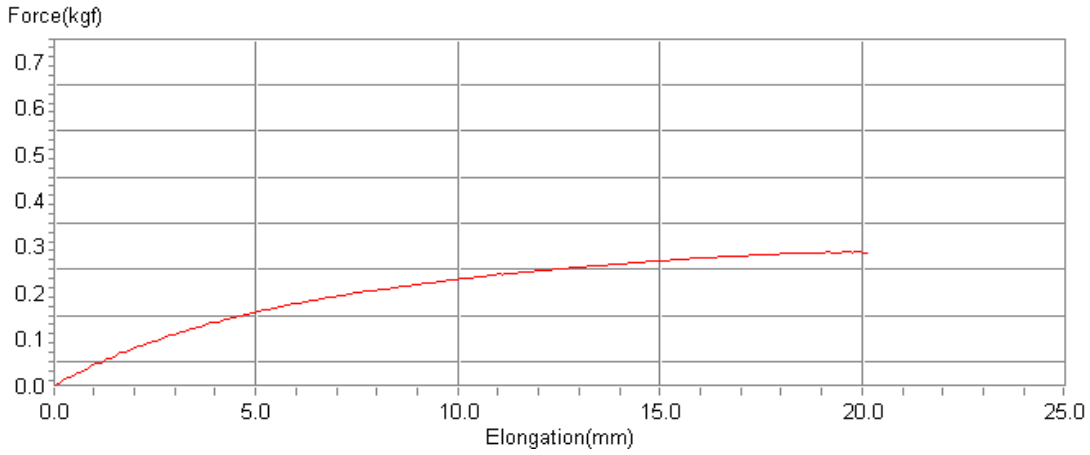

Figure B23: Coated(0.3%) 30 μm Somos 201 powder at 178 mm standoff distance for 40 seconds duration under IR radiation

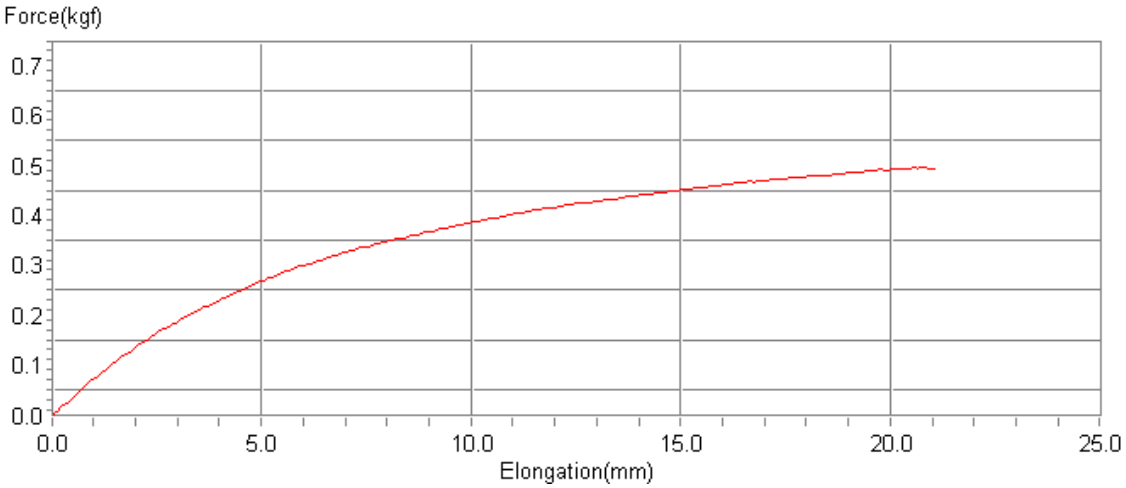

Figure B24: Coated(0.3%) 30 μm Somos 201 powder at 178 mm standoff distance for 60 seconds duration under IR radiation

C) Thermal Survey –IR sintered samples

Test Log 11th Aug – 15th Aug-2008

Problem with camera in that it appears to take 1 –2 hours to properly cool down. Also the calibration files seem to need be re-loaded after carrying out the black body zero image routine, in order to get a clear un-pixilated image.

Initial images taken at 600mm distance at an angle of approx. 70 deg. This allowed three dogbone specimens into the field of view. Plinth to heater height 230mm.

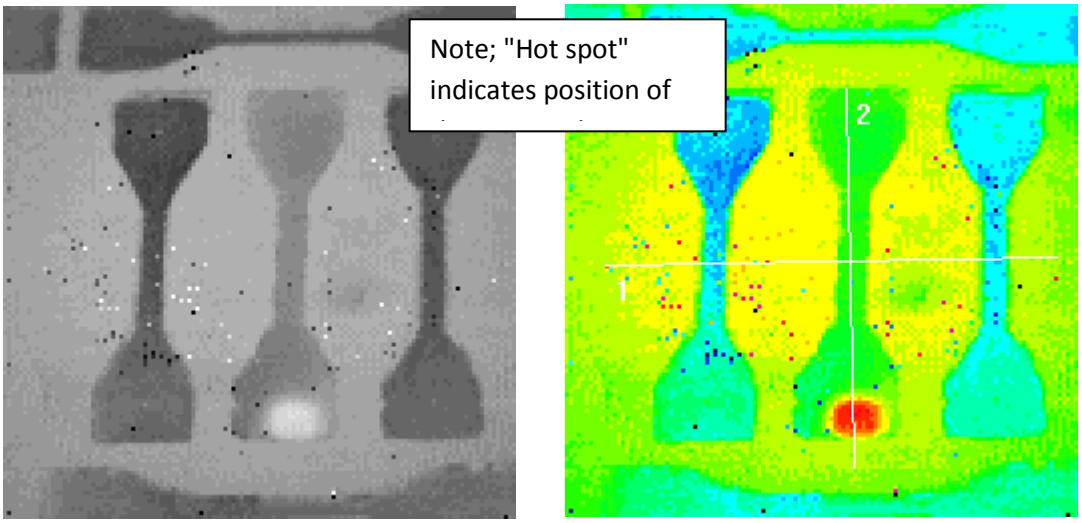

Fig C1 Initial image room temp

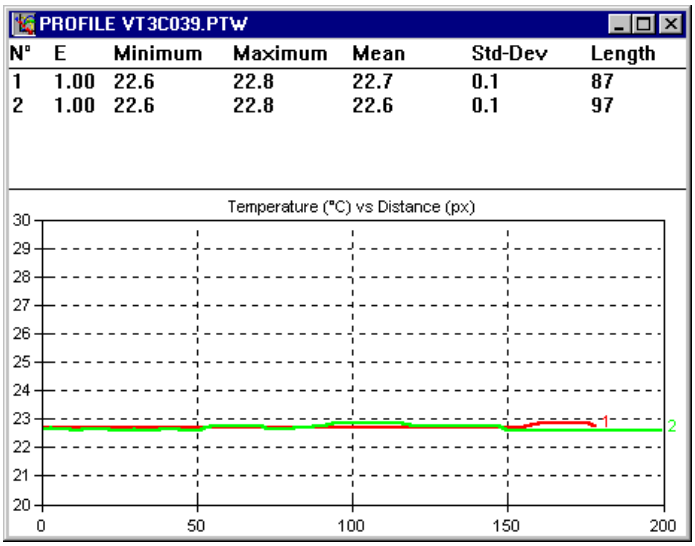

Fig C2 Temperature plot from Fig 1

Initial temperature readings agreed with thermocouples and IR thermomerter, i.e 22.8 deg C room temp. There is a problem with the temperature range as this camera is restricted to a maximum digital level (DL) of 4 so the tests will have to be done with 2 calibration settings i.e.21 to 90 deg C , 90 – 200 deg C.

Test 1

Heaters set on 0.7 max power and only 4 central element batches activated. Thermal images taken every 10secs. After 2 mins thermocouple reding No.2 34.6 deg C and corresponding IR thermometer reading 67.5 deg C. The No.2 sample slot had an old sample placed in to reduce reflections – hence the lower temp readings.

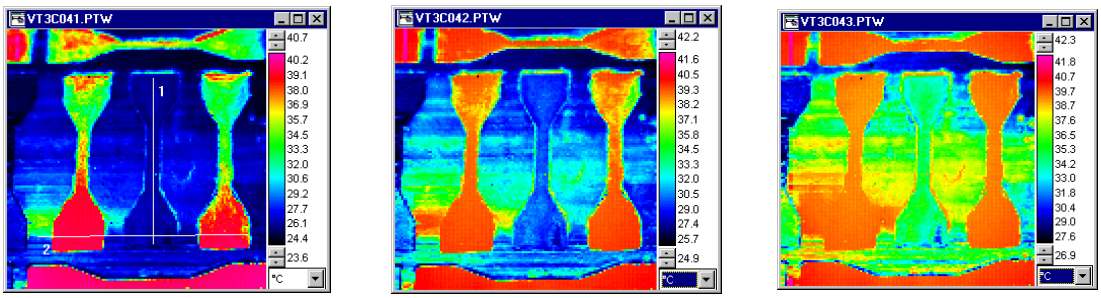

Fig C3 10 – 20 - 30 secs

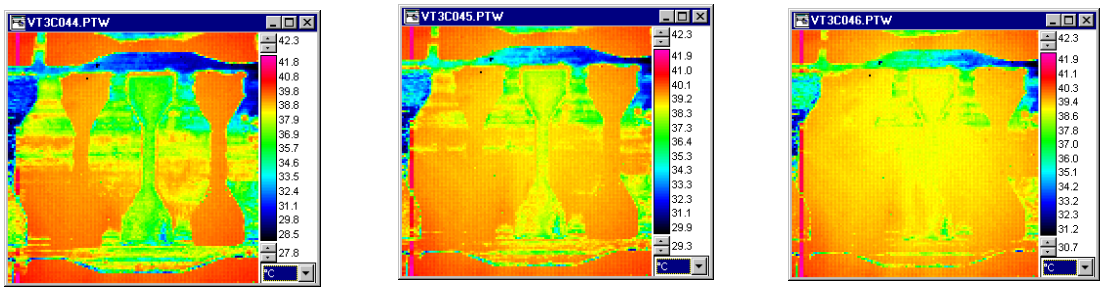

Fig C4 40 – 50 – 60 secs

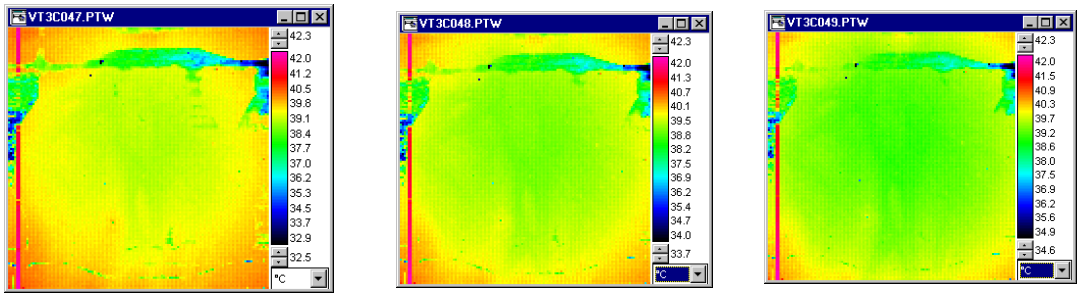

Fig C5 70 – 80 – 90 secs

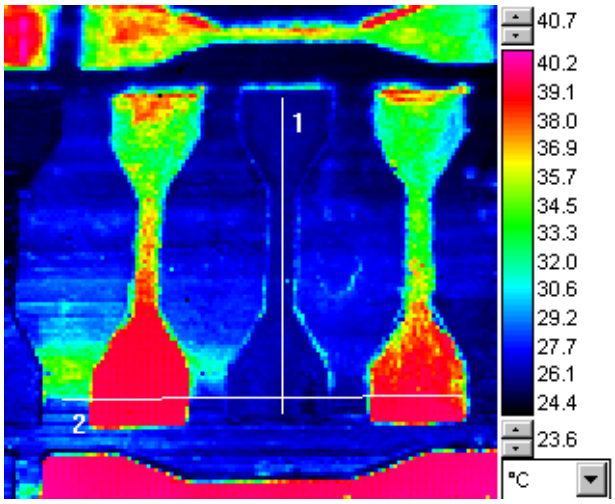

Fig C6 10 sec image

Note: Plot 1 (red) is along the length of spec 2

Plot 2 (green) is across the bottom of the 3 specimens and the temperature

N°	E	Minimum	Maximum	Mean	Std-Dev	Length
1	1.00	25.2	26.6	26.0	0.3	83
2	1.00	25.0	39.9	32.8	6.5	105

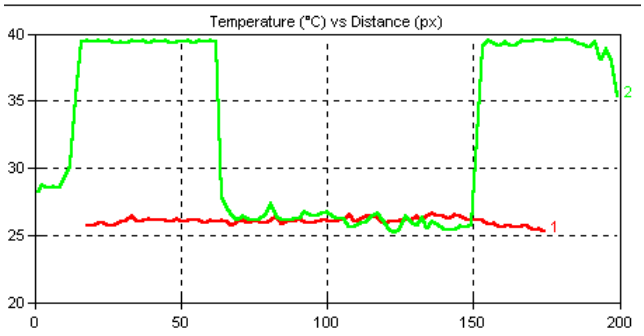

Fig C7 Line plots from 10 sec image

Calibration temperature peaked early at 40 deg C plus after 50 – 60 secs. see fig 8 below:

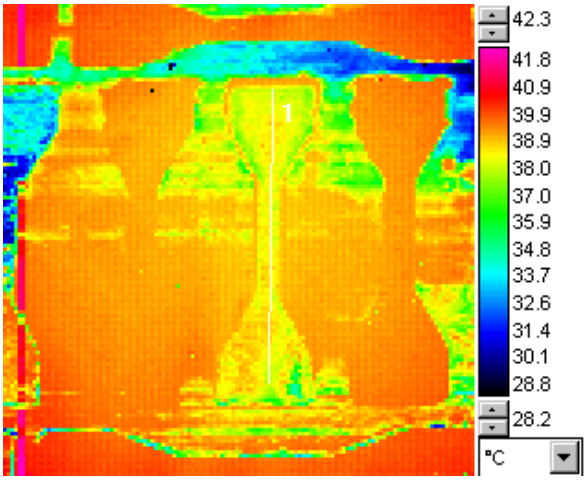

Fig C8 50 sec image

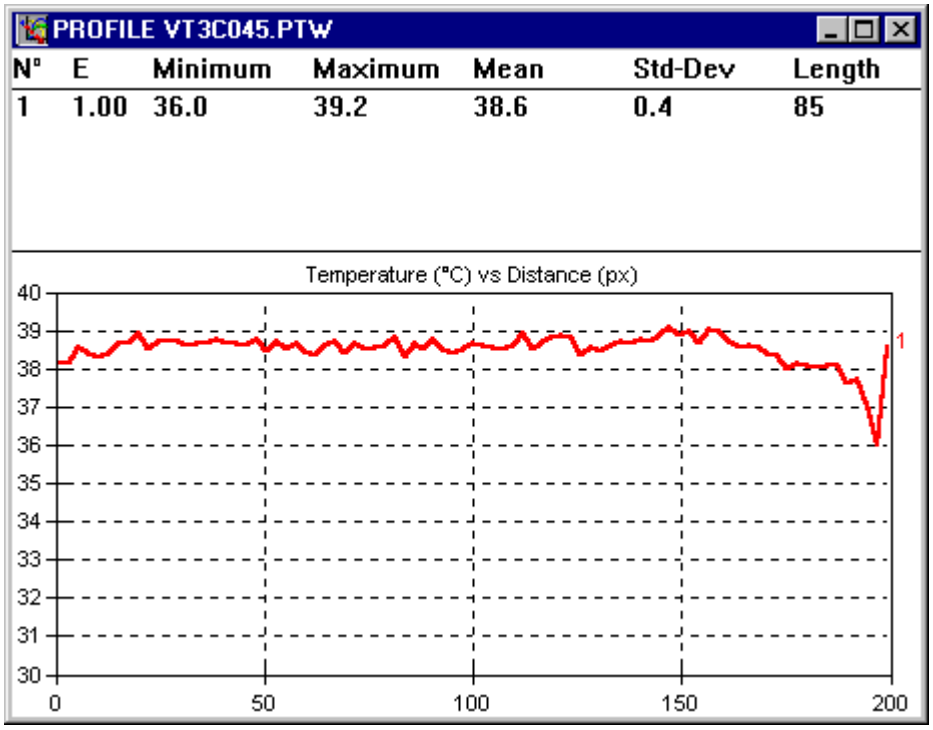

Fig C9 Polt along spec 2

Thermocouple 29 deg C IR thermometer 40 deg C.

Test 1 conclusions

The problem with the camera scaling can only be resolved by doing the test in two stages, a high and a low temp imaging. The problem of fast temperature saturation of the image is however, more likley to be reflections on the mould from the IR heating elements. this would account for the large difference in temperature between the empty mould and the mould no.2 filled with an old specimen. Situating the camera at a more oblique angle may reduce this effect and test 2 utilised the hand held IR thermometer to test this theory.

Test 2

Heaters still on 70% power 4 elements used and IR thermometer pointed at spec 2 at varying angles to determine any reflection effects. From an ambient of approx 27 deg C the heaters were switched on and tenps recorded after 1 min.

Specimen in mould – thermocouple temp 32.2 deg C after 1 min

Angle	Temp
80	47
60	46
45	44
20	37

Specimen out of mould – thermocouple temp 31.7 after 1 min

Angle	Temp
80	181
60	62
45	57
20	38

A trial with the IR camera at 80 degs and 25 degs confirmed the reflection problem, as shown n the thermal image results below. Fig 10 at an 80 degree angle gave a reading peaking out at 110 deg C and fig 11 shows the same test avoiding reflections by using a 25 degree angle, hence getting more accurate results and agreeing with the 38 deg C obtained by the IR thermometer.

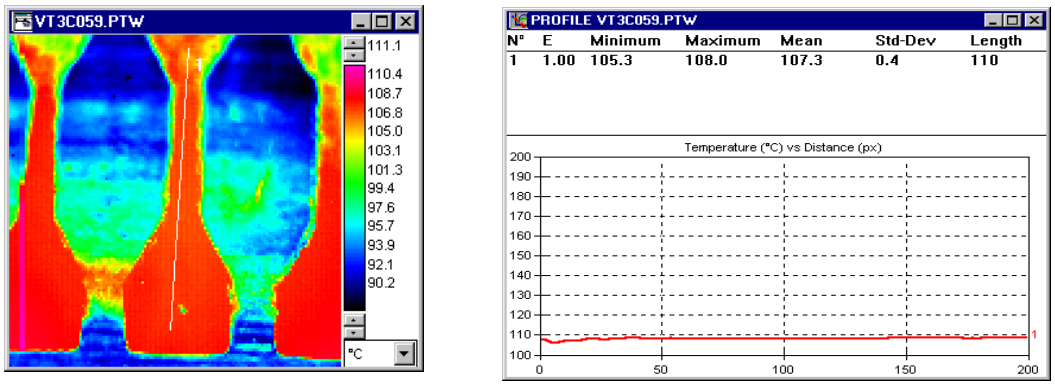

Fig C10 IR Camera Image after 1 min 80 degree angle

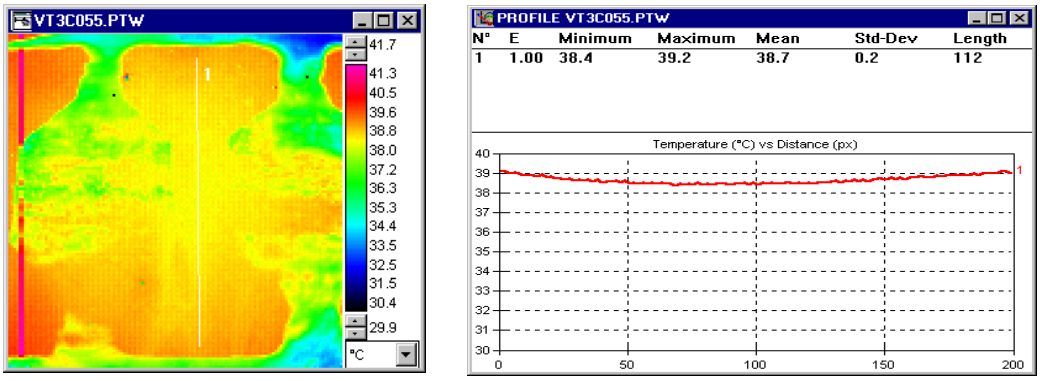

Fig C11 IR Camera Image after 1 min 25 dgeree angle

Test 2 Conclusions

Encouraging results as it not only shows that the angle of view is indeed critical to avoid reflections, but also shows that the specimen material is a poor reflector of IR so less critical on the angle than the basic aluminium mould face. Trials with the camera showed the same effect as seen with the IR thermometer, so an oblique angle is essential to avoid reflections, although with the powder in the mould the effect is not as great. Obviously accuracy is lost if the angle becomes too oblique but an optimum angle of 20 – 25 deg should eliminate most reflections and still provide realistic temperature readings.

Test 3

Now that an optimum viewing angle for the IR camera and the IR thermometer has been established, confidence in the accuracy of the temperature readings is high. The following test therefore will investigate the uniformity of temperature across the mould platform delivered by the IR heaters.

Fig 12 below still shows a slight issue with reflections, the image on the left showing the IR heater reflection effects at initial switch on, although on the specimen itself there was only a 0.5 deg C increase at the nearest end (see fig C13). The "red" area at the far end of the specimen is a reflection from the end face of the mould recess so would not affect the results and in any case is again only a 1.5 deg C difference .

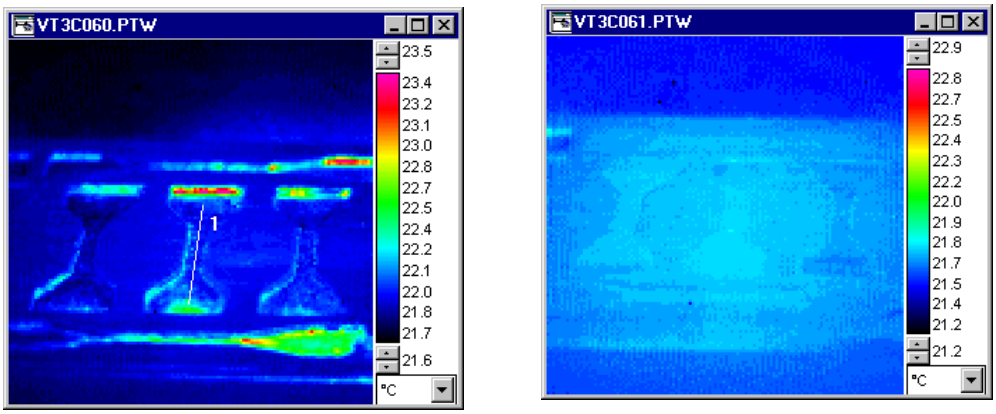

Fig C12 Left image – heater on – right image - heater off

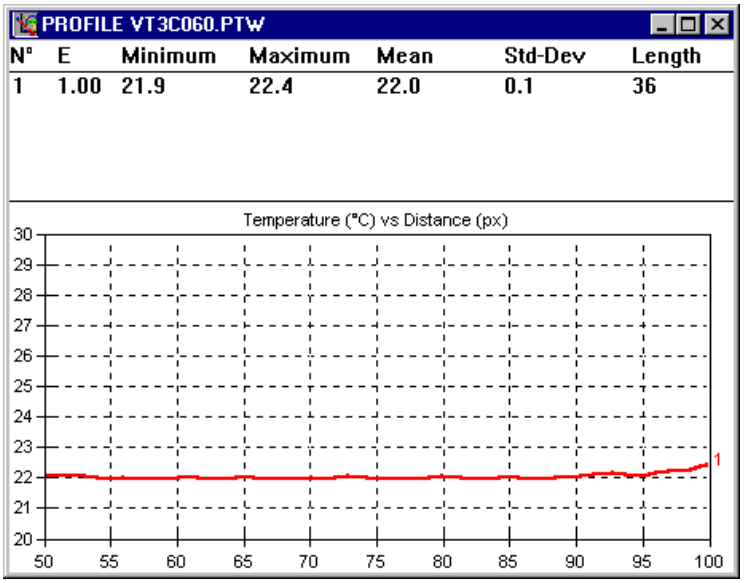

Fig C13 Plot from left hand image Fig 12 showing small 0.5 deg C increase due to IR reflection

The following images were taken from a new CEDIP IR camera imaging the plinth area under the IR cameras, firstly (Fig C14) with just a uniformly painted matt black metal plate to minimise any reflection issues and secondly with the mould in place (Fig C15). The images were taken before and after heating at 70% power for a period of 1 minute.

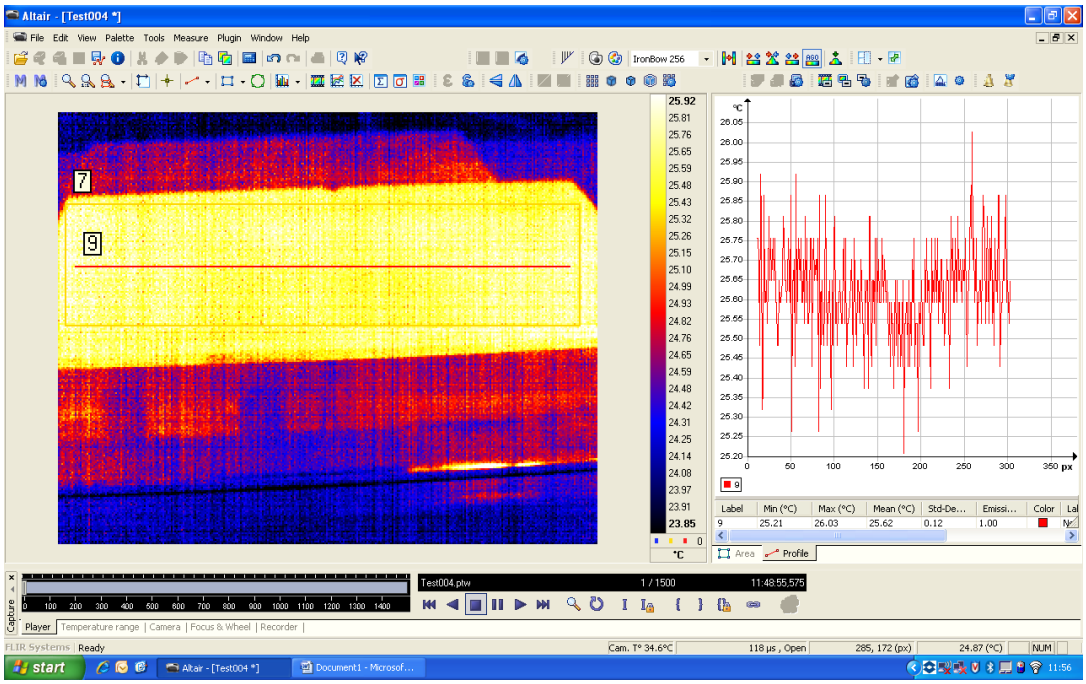

Fig C14 Uniform matt black plate – before heating

Note that the apparently noisy image is due to the very low temperature differences in the image, i.e. approx only 0.25 deg C therefore there is little information for the camera to differentiate.

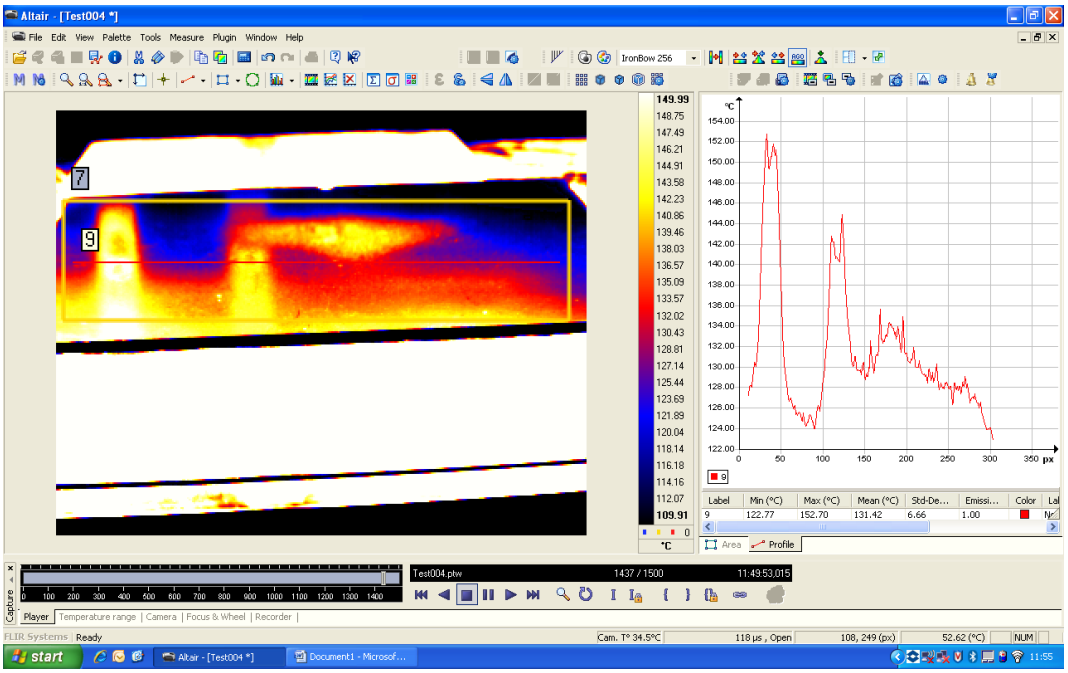

Fig C15 Uniform matt black plate – after heating

Over the majority of the plate the temperature differences are only 2 – 4 deg C however significant areas showing differences of over 20 degs C were present at the left hand end of the plate and it is not certain whether these are reflections or an additional heating effect from the power input cables which are above the left hand side. An identical test was carried out with the hand held IR thermometer, values ranging from 139 deg C to 122 deg C left to right so also showing an uneven heating effect.

The mould plinth was then put under the heaters, with specimens in the moulds and the test repeated but on only 70% power.

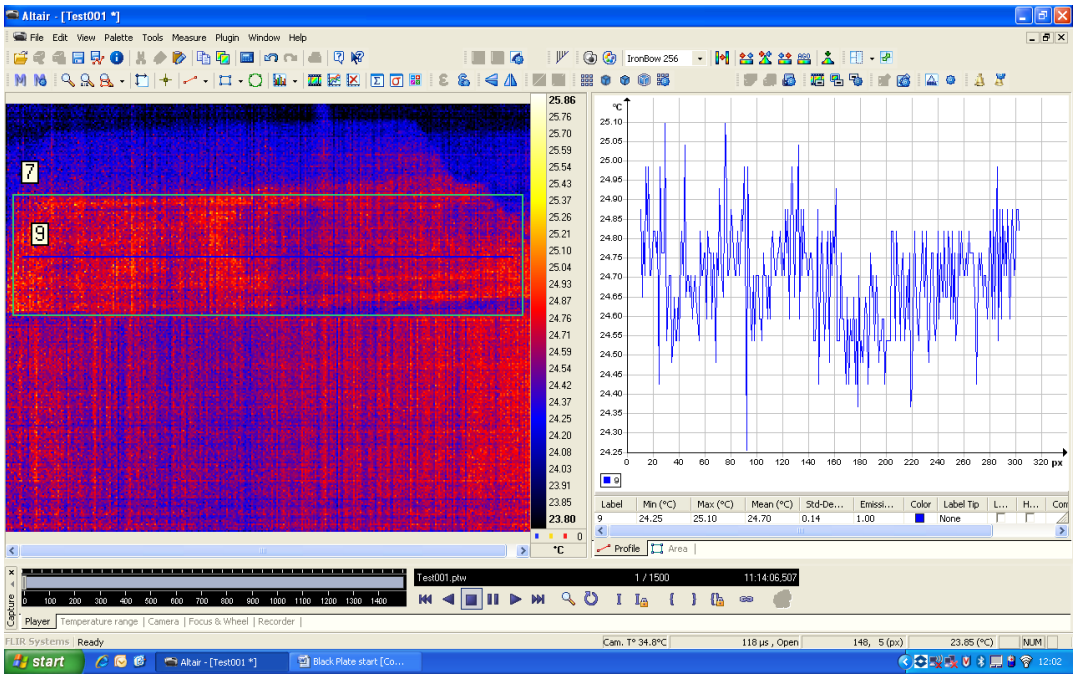

Fig C16 Mould plinth – before heating

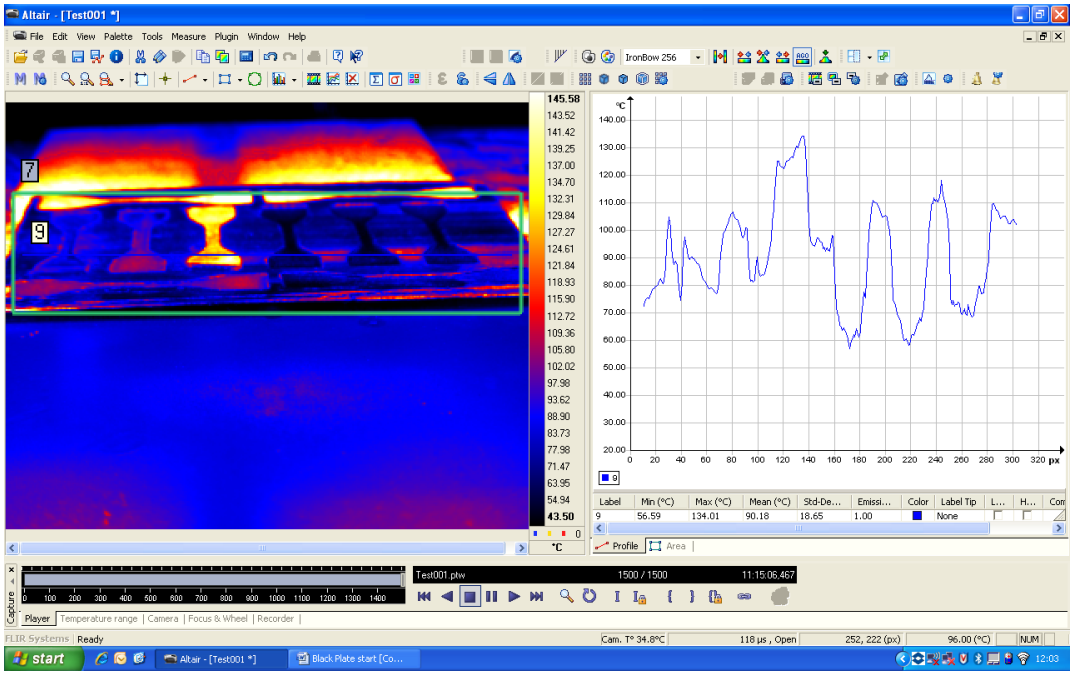

Fig C17 Mould plinth – after heating

The difference between temperatures on and off specimens is more likely due to the difference in emissivity of the differing materials, however there is also a very noticeable difference in emissivity on specimen 3 which is clearly not due to uneven heating from the heaters.

Test 3 Conclusions

It is difficult to establish exactly what the temperature distribution differences under the heater elements are due to and indeed whether they are real or due to reflections or some other IR radiation effect, i.e. from the power input. Probably the distribution of heat is within 5 to 10 degs C across the area of the plinth as the images with the mould in place show less differences on the specimens. So point temp measurements across the 6 centre specimens after 30 secs of heating on full power were proposed for the next set of tests. The question is how critical is the curing of the specimens once they reach melt temperature so a range of tests moulding specimens at different maximum temps is also proposed for later investigation.

Test 4

Without the IR camera an attempt was made to investigate the use of the IR thermometer instead to determine individual specimen temps during curing. Initially the work was carried out on empty mould.

Specimen	Initial Temp	Temp + 30 secs	Temp + 60 secs	Temp + 120 secs
1	23.4	62	81	
2	23.4	64	84	
3	23.4	69	86	
4	23.4	71	91	
5	23.4	75	93	
6	23.4	75	96	

NB: specimens 1 – 6 refer to middle specimens in mould from left to right. (see fig C18). The above test was carried out with all elements on full power and no powder in mould. Temps taken using the handheld IR thermometer, hence the differences as heating was too rapid. Test repeated at 70% power (see below) to see if it was easier to take temp readings.

Specimen	Initial Temp	Temp + 30 secs	Temp + 60 secs	Temp + 120 secs
1	32	41	58	74
2	32	41	58	75
3	32	42	59	78
4	32	45	61	79
5	32	46	62	77
6	32	47	59	78

The rapid rise in temperatures made it difficult to get meaningful comparisons of temperature between specimens, but the previous IR camera work had indicated that temperatures were reasonably uniform on the mould plinth between specimens, so for the first test with powder in the moulds just one specimen No. 5 was chosen to obtain temperatures from.

Test 5

Specimens prepared in mould with 30 micron powder as shown in Fig 18 below.

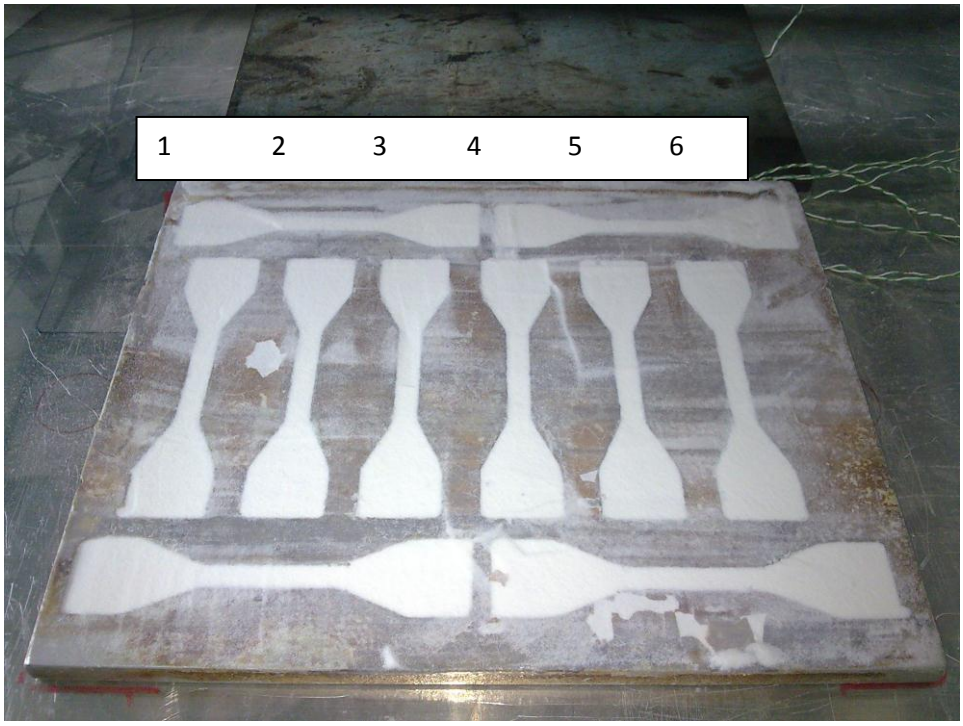

Fig C18 Specimen layout on mould plinth

With heaters still at 70% power but all switched on the mould was heated until melting of the material could be observed. The temperature and time at which melting took place (on specimen 5) was recorded below:

Specimen	Initial Temp	Temp + 60 secs	Temp + 120 secs	Final Temp
5	24.8	63.9`	94.8	157

At 70% power the heating elements were insufficient to get up to the required temperature, i.e. around 185 deg C. Temperature started to peak out at 158 – 161 deg C. Thermocouple reading 105 degC on specimen 5.

Test repeated with full power

Specimen 5	Initial Temp	Temp + 60 secs	Temp + 120 secs	Final Temp 3min 25 sec
IR	31.9	63.5	138	199
Thermo No.2	34.4	46.4	61.8	158

Difficult to observe exact melting point so future tests should be stopped at peak temps and the specimens assessed for correct curing. Also the IR thermometer body warmed up during the test which resulted in high readings when used directly afterwards on ambient temperature objects. Body therefore will need to be protected from heat as it obviously affects the detector.

Thermocouple graph shown below in fig C19.

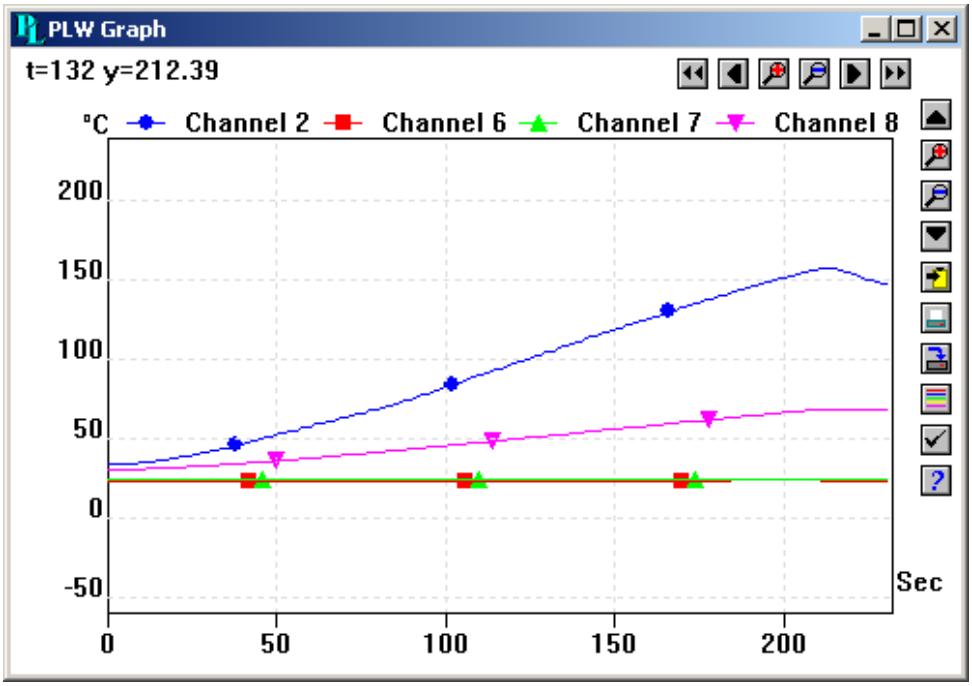

Fig C19 Thermocouple output Test 5

Test 6

As above, i.e full power but heaters cut off at 180 deg C

Specimen 5	Initial Temp	Temp + 60 secs	Temp + 120 secs	Final Temp 183C @ 145 secs
IR	26.6	133		183
Thermo No.2	28.5	48		85

These tests demonstrate the time lag in the thermocouples so confirming that as a precise temperature measurement for controlling the process they are not adequate.

Note: specimens not cured right through – some powder left in mould.

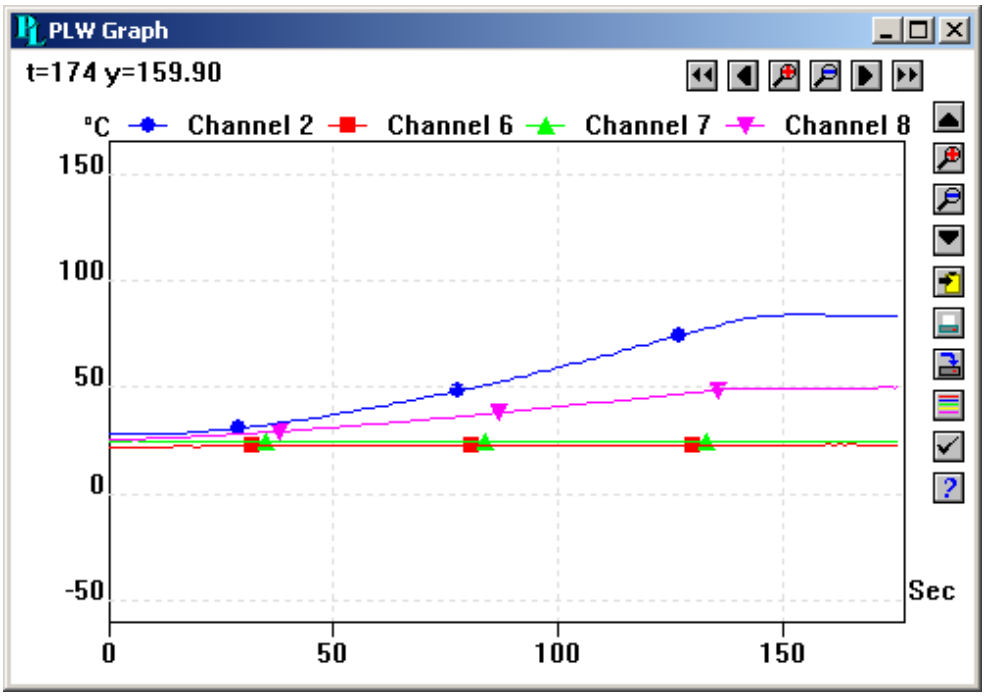

Fig C20 Thermocouple output Test 6

Test 7

100 micron powder

Specimen 5	Initial Temp	Temp + 60 secs	Temp + 120 secs	Final Temp 200C @ 3 mins
IR	25	120	167	201
Thermo No.2	23	43	74	

Thermocouple logger did not record data – powder still not cured on underside.

Test 8

4 min cycle

100 micron powder

Specimen 5	Initial Temp	Temp + 60 secs	Temp + 120 secs	Final Temp 4 mins
IR	35	132	202	222
Thermo No.2	37	55	89	157

Some evidence of light powder on back of some specimens but mostly cured right through. Obviously the time exposure to the heater is now also relevant in order to cure through the entire thickness. Two factors have to be taken into account here, one the distance from the moulding plinth and two the time left at full heat after the surface has started to melt at the

185 deg C mark. So the next tests were set up to determine the differences caused by altering the plinth height.

Test 9

Plinth height reduced from 230mm to 180mm

Specimen 5	Initial Temp	Temp + 30 secs	Temp + 60 secs	Final Temp 120 secs
IR	27	106	177	228
Thermo No.2	27	32	50	103

Mould removed after a further 60 secs under the switched off heaters
Powder on the back so specimens not fully cured right through.

Test 10

Plinth height reduced from 230mm to 180mm

Specimen 5	Initial Temp	Temp + 30 secs	Temp + 60 secs	Final Temp 90 secs
IR	35	141	201	230
Thermo No.2	37	44	64	87

Mould removed after a further 120 secs
Powder on back

Specimens returned to heater for a further 2 mins on full power then left to stand for 2 mins. Max temp after additional heating 258 deg C. Specimens fully cured.

Test 11

Plinth height reduced from 180mm to 110mm

Specimen 5	Initial Temp	Temp + 30 secs	Temp + 60 secs	Final Temp 90 secs
IR	29	134	190	210
Thermo No.2	27	37	63	104

Specimens 1 and 2 still powdery at one end so not fully cured

Test 12
Plinth height reduced from 180mm to 110mm

Specimen 5	Initial Temp	Temp + 30 secs	Temp + 60 secs	Final Temp 120 secs
IR	31	121	190	273
Thermo No.2	31	39	64	137

Left for 120 secs after heater switched off – fully cured.

Temperature monitoring

A standard off the shelf IR thermometer should be capable of monitoring the temperature of the powder in the mould, provided reflections are eliminated or at least minimised and that the body of the IR thermometer is kept in a cool airstream to avoid the detector heating up and possibly increasing temperature readings.

The optimum angle for avoiding reflections with this heater set up is 20 – 25 degrees and the thermometer should be placed between 335 and 330 mm away from the specimen on the plinth. At that length an 8mm dia measuring area is possible on one of the specimens grip areas. A possible way to insulate it from the radiant heat would be to surround it with polystyrene but also mount a cooling fan drawing ambient air in and pushing it past the detector towards the heat source. An old computer fan could be adapted for this purpose. A thermocouple on the casing to monitor the temperature would be useful as confidence in the accuracy of results would be greater if it was known that the IR thermometer was kept at a constant ambient temperature.

D) Description of Experiment Inside Oven:

Temperature measurement during Tests:

Powder bed temperature monitoring is critical for oven sintering. K type thermocouples were used to measure the temperature of powder bed, aluminium plate and MS plate and numbered to measure the temperature with data logger as shown below:

Thermocouples numbering	Location
Channel 1 (TC1) Channel 2 (TC2)	On 2 intermediate moulds (second from each side of the plate)
Channel 6 (TC6)	Oven temperature (upper section)
Channel 7 (TC7)	MS plate placed at bottom inside oven
Channel 8 (TC8)	MS plate placed at Top inside oven

Table D1: Location of Thermocouples on Aluminium mould for oven sintering trials

Heating of MS Plates I & II:

The two MS plates are placed inside oven to increase the temperature near about 200 ^{o}C One MS plate was placed near about 10 cm above the other MS Plate. After 10 minutes of heating the temperature of the plates measured as mentioned below:

Temperature of Oven : 222 ^{o}C

MS Plate I placed on bottom shelf: 210 ^{o}C

MS Plate II placed on Bottom shelf: 210 ^{o}C

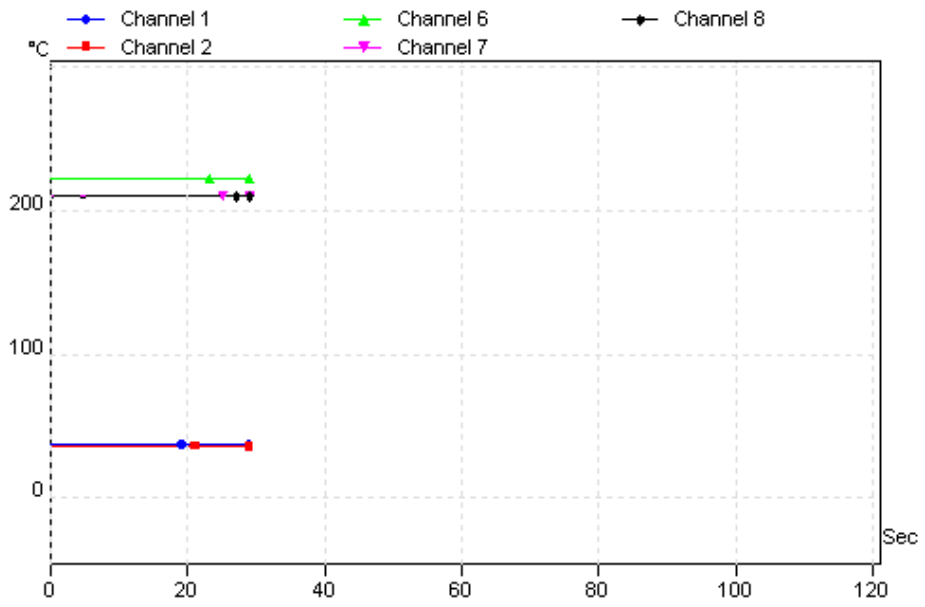

Graph D2: The snapshots from online data collection just before the experimentBlue and red lines (channel #1 & #2) powder bed near ambient(outside the oven) and 2 MS plates (inside the oven) heated near about (210 C) and Chanel 6 is showing the Oven temperature

Heat transfer from MS Plate-I:

The aluminium plate with powder bed then placed on MS plate-I inside oven. After 4 minutes of heating it was found that powder bed temperature increased from ambient temperature to 104 ^{o}C and temperature of MS Bottom plated was reduced to 181 ^{o}C from 210 ^{o}C as shown below

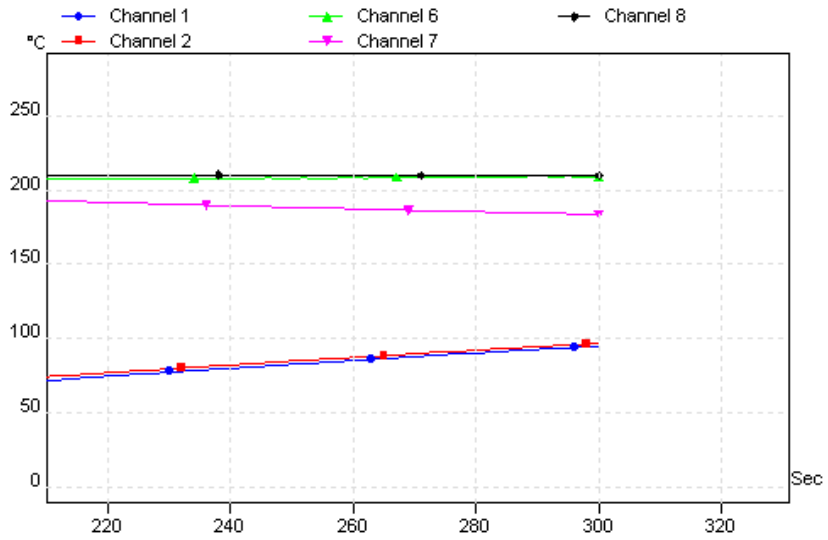

Graph D3 Temperature profile of powder bed with mould plate

(Channel 1 and 2 showing temperature increase of powder bed after 300 sec)

Heat transfer from MS plate-II:

To improve the rate of heat transfer oven door was opened to place the aluminium plate on another MS plate II which was already preheated at 210 ^{o}C. After 2 minutes it was found that powder bed temperature was raised from 104 ^{o}C to 132 ^{o}C.

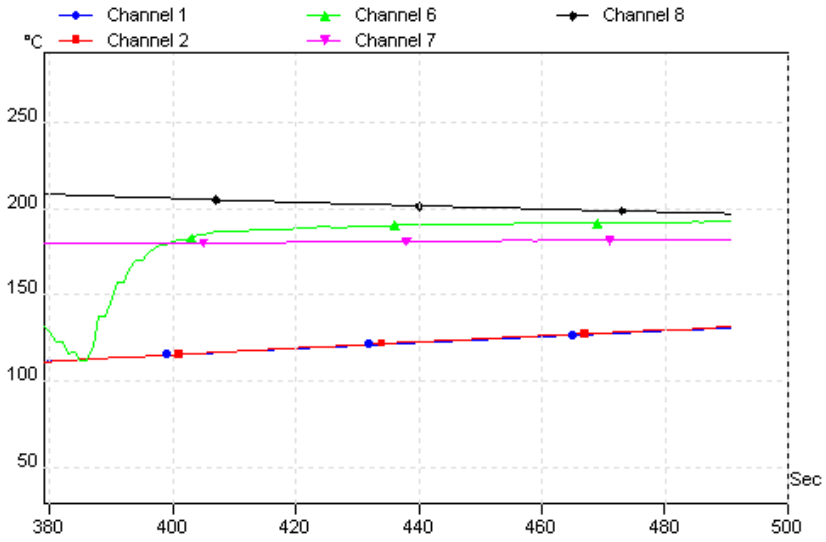

Graph D4 Powder bed (Channel 1 and 2)temperature increasing while placed on MS plate II (Temperature of MS Plate II (Channel 8)was decreasing due to heat transfer)

After 5 min of total heating on MS Plate -II the powder bed temperature was raised to 160 ^{o}C and temperature of MS Plate II reduced to 183 ^{o}C due to heat transfer from MS Plate II to powder bed.

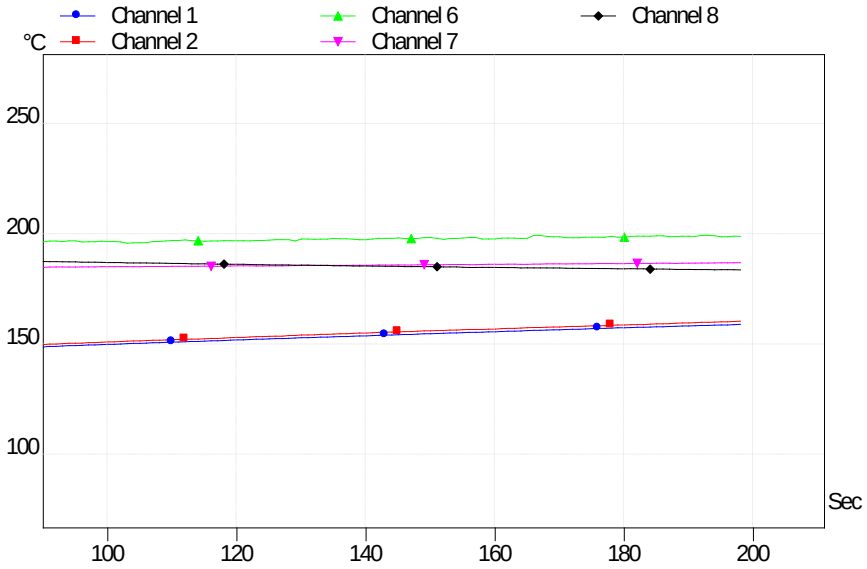

Graph D5 Red and Blue (Channel 1 and 2) showing temperature of powder bed increased around 160 ^{o} C

Removing samples from Aluminium mould:

The sintered T bone powder samples were removed from oven and placed outside at ambient temperature for natural cooling. After 2 to 3 minutes the temperature of powder on aluminium mould reduced to126 ^{o}C and samples were released from mould when the aluminium plate temperature reduced to near about 50 ^{o}C.

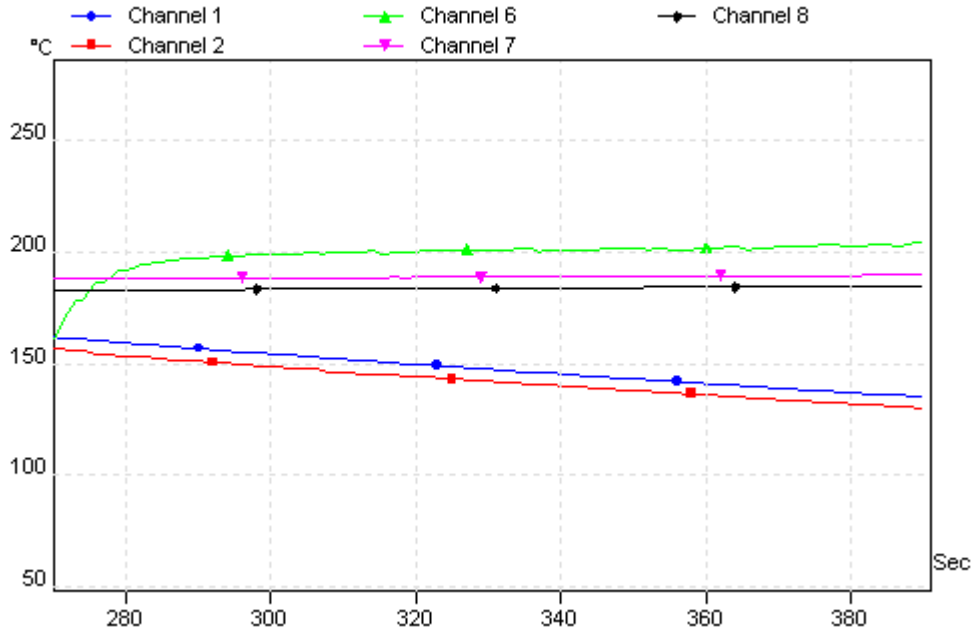

Graph D6 Red and Blue lines (Channel 1 and 2) -Temperature of powder bed decreasing due to natural cooling

The total heating cycle was around 8 minutes with the two MS plate set up (significantly faster than the 30 minutes heating cycle using a single MS plate). The rate of heating was almost maintained at constant rate as shown below .

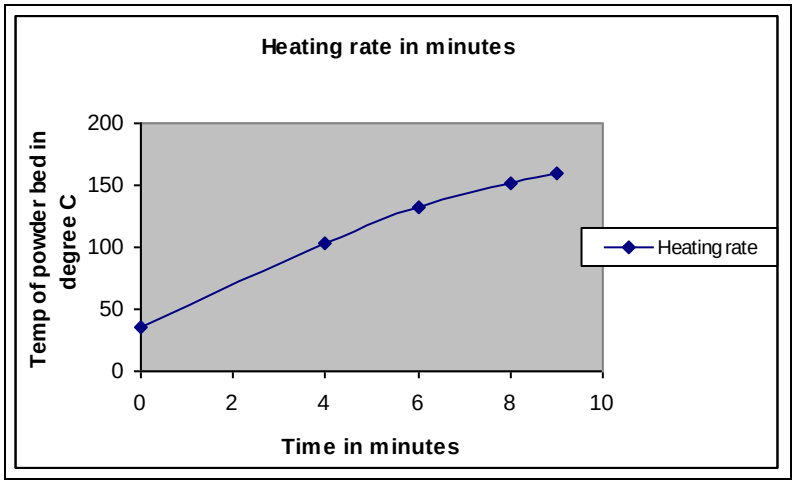

Graph D7 Rate of heating of Somos 201 powder particles during test

E) Study on Somos 201 powder :

(- Basic information- Polybutylene terephtalate (PBT)

The polymer is synthesized by reaction of terephtalic acid and 1, 4-butane diol. The only structure difference between PBT and more commonly used PET is the substitution of four methylene repeat units in PBT in stead of two methylene units which are present in chemical structure of PET. This feature imparts better flexibility to the PBT macromolecule and reduces its polarity. PBT is a semicrystalline thermoplastic polyester with rapid crystallization rate.

Owing to polar character, PBT should be dried before processing. Recommended conditions are 2-4 hours at 120 ^{0} C. The moisture content should be less than 0.05%. PBT has a better processibility than PET, the melt viscosity is low enough to prepare very thin sections. Recommended melt temperatures are 235 – 265 ^{0}C. A rapid processing speed is also recommended, material's fast crystallization rate enables short cycle processing time.

Unreinforced PBT is available in several types differing in molar mass, depending on

processing requirements. Most PBT is compounded with a variety of additives to produce resins with a wide range of end-use properties. PBT is often blended with other polymers or copolymerized with co-monomers.

Modification of PBT based on copolymerization reactions has been used to prepare

biodegradable variants, e.g. PBT co-polyesters, PBT-polyethylenglycol multiblock

copolymers, PBT-polycaprolactone copolymers etc. The general objective of these

modifications is to make degradation processes easy and to accelerate degradation with the support of water, microbial and enzymatic attack. The co-monomers provide weak linkages with butyleneterephtalate chains. These linkages are susceptible to biodegradation through hydrolysis.

Degradation processes of polyesters like PET and PBT are in principle based on hydrolytical reactions. Hydrolysis is a form of degradation resulting from contact with water, more precisely said with the hydrogen ions or hydroxyl ions present in water. Hydrolysis also means similar degradation mechanism resulting from contact with other water containing fluids such as acids (higher concentration of hydrogen ions) and alkalis (higher concentration of hydroxyl ions). Hydrolysis invariably leads to chain scission and thus to reduction of molar mass. In polyesters the COO group is the point of hydrolysis, very simple top say, this ester group is attacked by water. Water cleaves the ester groups to produce carboxylic acids and alcohols and polymer chain is interrupted by such a way.

Basic properties of PBT:

Good dimensional stability, favorable friction and wear characteristics, good insulating properties, crystallinity 40-50%. density 1300-1320 kgm-3, modulus of elasticity in tension 2500-2800 MPa , yield stress 50-60 MPa, yield strain 3.5-7 %, fracture strain in tension 20->50%, glass transition temperature 45-60 ^{0} C, melting temperature 220-230 $^{\circ}$ C.

SOMOS 201 analysis Solid Imaging Powder

The goal of the analysis was to determine the composition of given material. Moreover the blend components were also taken into account. For the components identification Fourier transform infrared spectroscopy (FTIR), elementary analysis (C, H, N and other components) and GC-MS analysis after the alkali hydrolysis was used.

FTIR spectroscopy Perkin Elmer Paragon 1000PC + Golden Gate diamond ATR. The spectrum record is given in Figure E1.

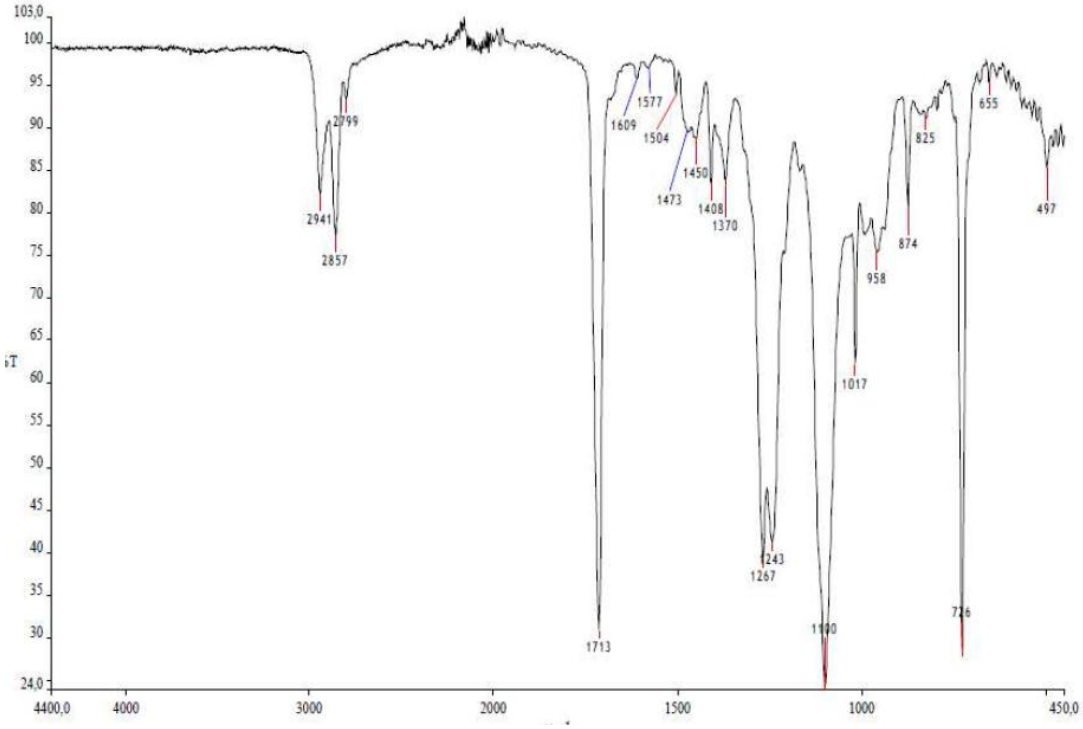

Figure E1: FTIR analysis.

After the analysis and comparison with the infrared spectrum, the polyester of terephtalate acid and diol is the resulted composition of material.

Elementar analysis:

Perkin Elmer Elementar analyzer 2400 CHNS (II)

Results:

C 65,5%

H 7,8%

N 0%

P 0% (mineralization and photometric evaluation of P)

Analysis of hydrolysis:

GC-MS Perkin Elmer Autosystem + Turbo Mass, colone PE5MS 20m, id. 0,18 mm, film thickness 0,18um, temperature program 60°C – 300°C

Alternative 1

C. 50 mg of polymer + 20 mg NaOH + 1 ml deionized water in sealed test tube for 10 hrs at 110°C. Non-reacted polymer was filtered off after the cooling (PTFE filter). Alkalic water solution was neutralized by HCl (1:10). After centrifugization the water solution was analyzed by GC-MS. In water solution 1,4-butandiol was found.

Alternative 2

Cca 50 mg of polymer + 20 mg KOH + 0,5 ml deionized water in sealed test tube heated for 8 hrs at 110°C. After the test tube was opened, the content was evaporated (infrared lamp + N_2).Than 1ml of

acetanhydride (ACN) was added and the suspension was put in ultrasonic bath for 15 min. After centrifugization the volume was reduced to 100 µl and the solution was further analyzed by the GC-MS method (see Figure E2).

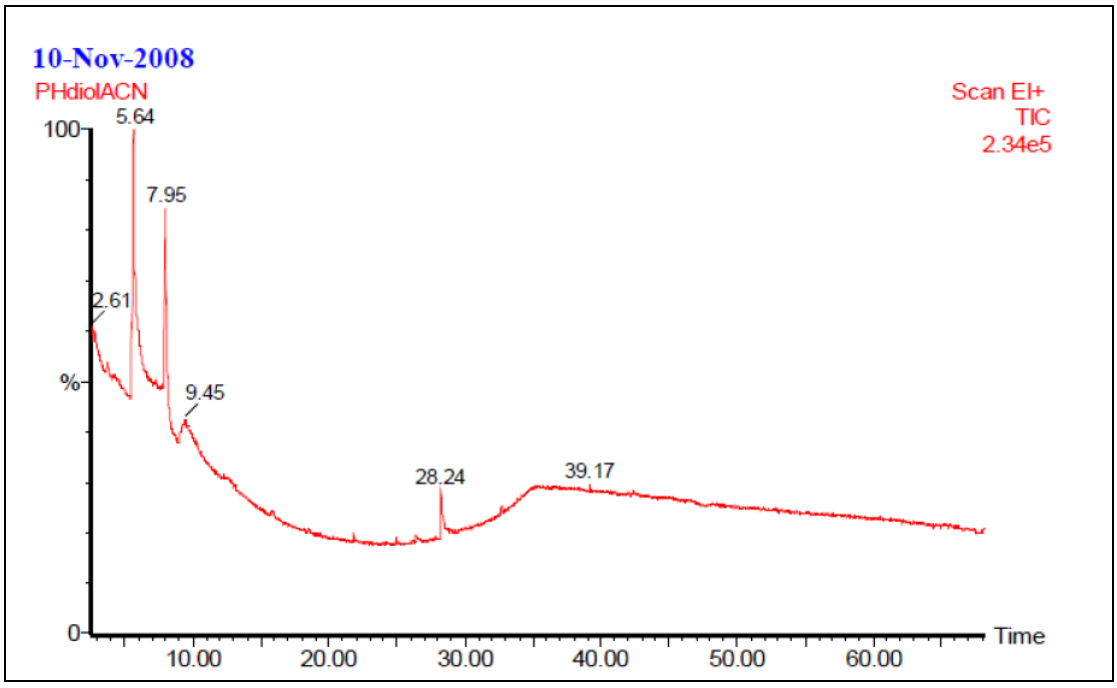

Figure E2:

5,64 min – 1,4-butandiol

Other peaks – aramides

1 ml of demonized water was added to the remainder after the ACN extraction. The

suspension was inserted into the ultrasonic bath for 15min. After that 20 µl of concentrated HCl was added the clot was created out of the solution (terephtalate acid and anorganic part). Suspension was evaporated and to the rest 1ml of acetone was added. The whole mixture was inserted into ultrasonic bath once more for 15 min. The acetone solution was filtered, dried under the infrared lamp (in presence of N2) and forwarded to further GC-MS analysis.

The remainder was derivatized BSTFA (10mg of sample + 0,5ml derivatization reagent heating for 15min to 60°C). The GC-MS analysis was performed on derivatized sample (Figure E3).

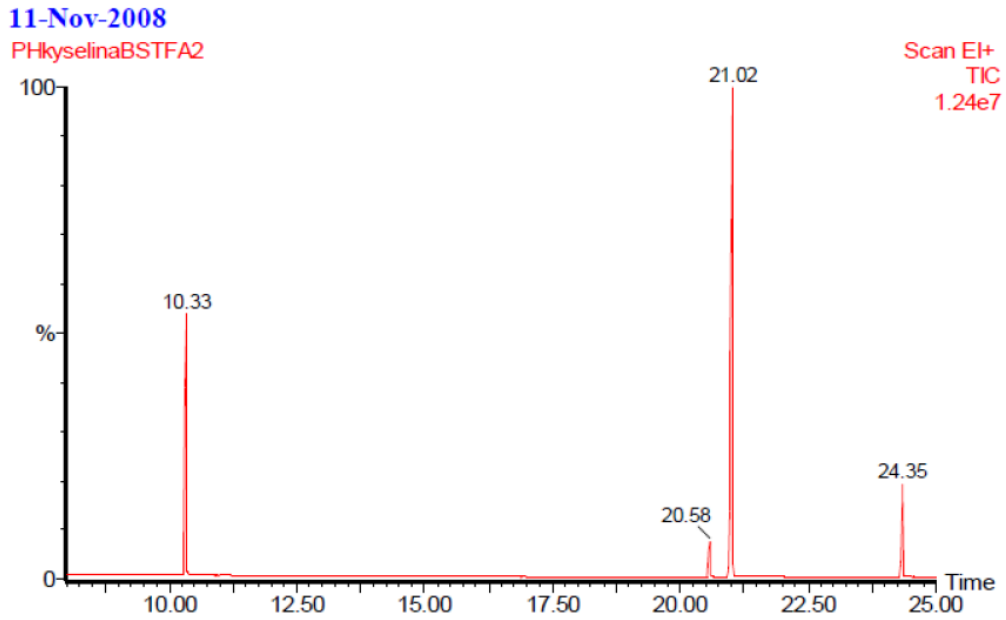

Figure E3: Part of record

Rt 10,33 min TMS 1,4 butandiol

21,02 TMS terephtalate acid

Conclusion

Applied methods didn't allow to fully analyze the polymeric sample. Most probably the main component is polyester like terephtalate acid – 1,4 butandiol. Further the presence of diol (polyol) with longer chain is probable. Acetic acid can reflect the presence of polymeric acetates in the sample. Because no presence of nitride was found out by the elementary analysis, the presence of amides after the hydrolysis is not possible to be clarified.

F) Conclusion from Hardware for SLP development

In addition to main trials, the following conclusions have also been drawn from the tests carried out under hardware development section

- The contact force between the transfer roller and top surface of build platform found very critical. The cushioning effect of build platform offers some flexibility and adjustments while powder being deposited on a movable build platform from a rotating transfer roller.

- The dielectric property of substrate is critical while powder is deposited as the deposition process is governed by electrostatic force for standard laser printing. Somos 201 /standard toner deposited well on standard A4 size paper compared to plastic/metallic substrate.

- The voltage applied on OPC drum should not exceed the maximum limit otherwise the high voltage would damage the photoconductive property of the OPC layer.

- The gap between the transfer roller and top surface of the printed layer need to adjusted accurately matching with the layer thickness as any small change from the correct gap would result no deposition on powder bed. The layer thickness would depend on particle size and would be in the range between 15 to 25 µm layer thickness for 30 µm average particle size of Somos 201.

- The powder deposition always found highest across the edges of the printed layers for both standard toner and experimental toner (like PE/ Somos 201 powder particles). This is due to the electrostatic charge distribution of the printed image.

- The voltage on top surface of the printed layer found reduced sharply after few layers of prints while printing nonconductive, polymeric toner when voltage is applied from underneath the build platform for standard toner transfer mechanism. Earlier scoping trial suggested that electrostatic force of repulsion could be a potential solution to overcome the z-height problem. The combined process including tackification and repulsion could be the best possible solution to overcome z height problem.

- For tackfication toner transfer mechanism, the temperature of the top surface of the deposited layer would be maintained very close to 150 to 155 ^{0} C for Somos 201 powder so that Somos 201 powder can be deposited with the help of combined heat and pressure. This temperature selection would depend on the melting point of powder particles.

  The temperature control on the top surface of the deposited layer found critical otherwise no toner deposition can take place .Furthermore higher temperature than 160^{0}C can develop hot spots on top of surface of transfer roller which would damage the top surface the transfer roller which could adversely affect the toner deposition for future layers. If the temperature is not maintained properly the transfer roller could also pick up the powder particles from powder bed instead of depositing powder on the build platform.

- The powder found deposited more towards the edge of the printed surface. This is due to the electrostatic nature of powder particles while printing with laser print engines.
  The top surface of the printed layer needs to be levelled otherwise high peaks would develop on top surface of the deposited layer and powder would be thereafter picked up by only those high peaks /points of the surface from the transfer roller. The levelling of top surface could be carried out in various ways. One of the potential solutions could be the use of hot roller (non stick type), which would help while levelling of top surface without any smudging of the deposited layer.

G) Material Data Sheet – Somos 201

SOMOS 201 Typical Properties for the SLS systems

Powder Properties	Units	Test Method	SOMOS 201 (1)	Infiltrated (2)
Density Tap	g/cm^3	ASTM D4164	0.58	
Particle Size Average (1) d_{50} (3)	µm	Laser Diffraction	93	
Particle Size Range (1) 90%	µm	Laser Diffraction	23-190	
Specific Gravity 20°C		ASTM D792	0.91	1.07

Thermal Properties	Units	Test Method	SOMOS 201 (1)	Infiltrated (2)
Melting Point: T_m	°C	DSC	156	

Mechanical Properties	Units	Test Method	SOMOS 201 (1)	Infiltrated (2)
Tensile Modulus	MPa	ASTM D638	15.5	17.3
Tensile Elongation at Break	%	ASTM D638	110	130
Stress at 5% strain	MPa	ASTM D638	1.8	2.2
Stress at 10% strain	MPa	ASTM D638	2.0	2.6
Flexural Modulus at -40°C	MPa	ASTM D790	23	37.3
at 23°C	MPa	ASTM D790	13.4	14.1
at 100°C	MPa	ASTM D790	3	7
Initial Tear Resistance				
Die C at 23°C	kN/m	ASTM D624	6	23.1
Die C at 100°C	kN/m	ASTM D624	5.2	6
Abrasion Resistance				
Taber, CS-17 wheel, 1kg load	mg/1000/cycles	ASTM D4060	520	0.3
Taber, H-18 wheel, 1kg load	mg/1000/cycles	ASTM D4060	870	0.5
Bursting Strength (Straight) 23°C 25mm ID x 2 mm thick x 300 mm long hose	kPa	ASTM D380	0	>160
Shore A Hardness 23°C		ASTM D2240	74	75

Electrical Properties	Units	Test Method	SOMOS 201 (1)
Volume Resistivity 22°C, 50% RH, 500V	ohm x cm	ASTM D257-93	1.5E + 13
Surface Resistivity 22°C, 50% RH, 500V	ohm x cm	ASTM D257-93	1.9E + 13
Dielectric Constant 22°C, 50% RV, 5V 1000Hz		D150-95	2.9
Dielectric Strength 22°C, 50% RH, under oil, 500V/sec	v/mm	D149-95a	4.1E + 3
Comparative Tracking Index	V	D5288-92 and/or IEC Standard 112	315, TI-Cu <3mm depth

(1) Data was generated from the testing of parts produced with the SOMOS 201 material the Materials Guide processing conditions.

(2) Data was generated from the testing of parts produced with the SOMOS 201 material the Materials Guide processing conditions and then infiltrating using the BJB ST-1040 polyurethane.

(3) Results are based upon the volume distribution of particles.

Detailed test conditions are available upon request. Expected shelf life of this material is at least twelve months, when stored in dry conditions at ambient temperatures.

Warranty/Disclaimer: The performance characteristics of these products may vary according to product application, operating conditions, material combined with, or with end use. 3D Systems makes no warranties of any type, express or implied, including, but not limited to, the warranties of merchantability or fitness for a particular use.

3D Systems
26081 Avenue Hall
Valencia, CA 91355 USA
telephone 661.295.5600, ext. 2882
fax 661.294.8406
toll free 888.337.9786
email moreinfo@3dsystems.com

www.3dsystems.com
Nasdaq: TDSC

France
telephone +33 1 69 35 17 17

Germany
telephone +49 6151 357 303

Hong Kong
telephone +852 2923 5077

Italy
telephone +39 039 68 904 00

Japan
telephone +03 5288 5951

Spain
telephone +34 93 751 49 49

UK
telephone +44 1442 282600

P/N 70457